University of Strathclyde

Department of Mechanical Engineering

Division of Mechanics of Materials

EXPERIMENTAL AND ANALYTICAL STUDIES OF COLD-FORMED THIN-WALLED FRAMEWORKS WITH SEMI-RIGID CONNECTIONS

Thesis presented for the

Degree of Doctor of Philosophy

by

S. H. TAN, B.Eng.

Jan. 1991

ABSTRACT

The behaviour of symmetrical single and double storey frameworks, constructed with cold-formed thin-walled plain channel members and semi-rigid connections, is investigated both analytically and experimentally in this thesis.

A method of analysis, which is based on the matrix stiffness method, is developed and written into a computer programme. Generalized relationships between forces and displacements at the ends of an element with semi-rigid connections are derived and presented in a matrix form. The analysis takes account of local and torsional flexural buckling, connection strength and full moment-rotation behaviour, axial load effects, member plasticity, initial imperfection and shortening due to flexure. Using the theoretical analysis, the full loading history of the framework can be traced up to the final failure load. Results are finally presented graphically and in tabulated form.

Details of an experimental investigation, which was undertaken to obtain the moment-rotation relationship of connections of various stiffnesses, are given. From the experimental data, a standardized theoretical model capable of representing the full moment-rotation behaviour of the connections is developed. Results from the model are compared with the experimental data and the agreement is generally very good. The theoretical model is incorporated into the theoretical analysis to account for the change in stiffness of the connection during loading.

For the frameworks, an extensive experimental investigation was undertaken to ascertain the accuracy of the theoretical analysis. Details of the fabrication of the specimens, construction of the frameworks, testing equipment and procedures are also presented.

Results of the framework experimental investigation are compared with the theoretical predictions. The agreement between theory and experiment is shown to be very close in general. Some wholly theoretical numerical results are also presented and discussed.

The findings of the investigation are summarized and the main conclusions are listed.

ACKNOWLEDGEMENTS

I wish to thank Professor John Spence, Chairman and Head of the Department of Mechanical Engineering and Head of the Division of Mechanics of Materials, University of Strathclyde, for the use of the laboratory, workshop, computing and photocopying facilities.

Special gratitude goes to Dr. James Rhodes, Reader in the Mechanics of Materials Division, for his unceasing guidance, invaluable suggestions and thoughtful criticism that brought the research to this stage.

Thanks are also extended to the laboratory staff for the skilful workmanship displayed in the fabrication of the test rig, assistance in the use of machineries and advice on various practical aspects of the research.

To Janet Harbidge, Secretary of the Mechanics of Materials Division, for her assistance in various administrative matters.

Acknowledgement is also due to the Committee of Vice-Chancellors and Principals of the Universities of the United Kingdom and the University of Strathclyde for the financial support given.

Finally, to my beloved wife, Karen, whose constant emotional support and continuing encouragement kept my morale high, especially in times of despair and depression.

TABLE OF CONTENTS

NOMENCLATURE

A	Cross sectional area or Elemental area
ACC	Accuracy
b	Full flat width of an element
b_e, b_{eu}	Effective width of stiffened and unstiffened element respectively
b_1, b_2	Full flat width of stiffened and unstiffened element of a plain channel respectively
C_o	Initial imperfection amplitude
C_w	Warping constant of a cross section
c	Stability function
$\mathbf{D}$	Nodal displacement vector of a structure in the structure axes system
D	Plate flexural rigidity [$= E t^3/12(1-\nu^2)$]
$\mathbf{d}, \mathbf{d}'$	Nodal displacement vector of an element in the element and structure axes system respectively
d	Diameter of a bolt
d_e	Theoretical displacement of free end of cantilever
d_r	Theoretical displacement of free end of beam due to column rotation
d_t	Total theoretical displacement of free end of beam when the connection is fully rigid

d_{ex}	Experimental displacement of free end of beam
d_{xi}, d_{yi}	Linear displacement at end i along the x and y axes respectively
E	Diagonal matrix
E	Young's modulus of elasticity [$= 205\ KN/mm^2$]
F	Non dimensional stiffness coefficient constant $[= 1 + 4(\alpha_1 + \alpha_2) + 12\alpha_1\alpha_2]$
$\overline{F}$	Non dimensional stiffness coefficient constant $[= 1 + s(\alpha_1 + \alpha_2) + s^2(1 - c^2)\alpha_1\alpha_2]$
G	Shear modulus of steel [$= 79\ KN/mm^2$]
H	Position of zero strain axis
h	Non dimensional constant [$= b_2/b_1$]
I	Second moment of area about the critical axis or Number of iterations
INC	Load increment
I_b, I_c	Second moment of area of beam and column about the critical axis respectively
I_x, I_y	Second moment of area about the x and y axes respectively
J	St. Venant torsion constant of a cross section
K	Structure stiffness matrix in the structure axes system

K	Buckling coefficient of an element
$\mathbf{k}, \mathbf{k}'$	Element stiffness matrix in the element and structure axes system respectively
$\mathbf{L}$	Lower triangular matrix
L	Length of a member
LF	Load factor
l	Effective length of a member
M	Bending moment in general
M_i	Bending moment at end i
M_p, M_{pa}	Plastic moment without and with axial load respectively
M_x	Bending moment at a section of distance x along the x axis
M_{cu}	Ultimate bending moment capacity of connection
m_{zi}	Bending moment about the z axis at end i
N	Number of loading cycles
n	Structure matrix size or Curve fitting constant
$\mathbf{P}$	Nodal load vector of structure in the structure axes system
P	Axial force in general
PE	Potential energy

P_E	Euler load of a column about the critical axis
P_s	Squash load
P_x	Euler load of a column about the x axis
P_y	Design strength of steel or Euler load of a column about the y axis
P_y'	Effective design strength of steel
P_z	Torsional buckling load of a column
P_{bs}	Bearing capacity of a bolt
P_{cl}, P_{cn}	Collapse load with and without consideration of local buckling respectively
P_{cr}	Critical buckling load
P_{el}, P_{en}	Elastic critical load with and without consideration of local buckling respectively
P_{ex}	Experimental failure load
P_{sh}	Shear capacity of a bolt
$\mathbf{p}, \mathbf{p}'$	Nodal load vector of an element in the element and structure axes system respectively
$\mathbf{p}_f'$	Element fixed end force vector in the structure axes system
p_s	Design shear strength of a bolt
p_{xi}, p_{yi}	Force at end i along the x and y axes respectively

Q_{ij}	Cross rotation-translation coefficient
$\mathbf{R}$	Rotation matrix
R_i	Connection stiffness at end i
R_o	Connection initial stiffness
r_o	Polar radius of gyration of a section about the shear centre
SE	Strain energy
S_a	Axial shortening
S_b	Shortening due to bending
$S_{ij}, \overline{S}_{ij}$	Pure rotation coefficient of a rigid and semi-rigid jointed element respectively
s	Stability function
$\mathbf{T}$	Transformation matrix
T_c	Thickness of connection
T_{ij}	Pure translation coefficient
t	Material or element thickness
$\mathbf{U}$	Upper triangular matrix
U	Change in energy
u, v	Translation in the direction of the x and y axes respectively
V, V_i	Shear force and shear force at end i respectively

W	Uniform distributed loading
W_i	Distributed loading at end i
WD	Work done
x, y, z	Generally used to denote axes system
x_o, y_o	Distance from the shear centre to the centroid measured along the x and y axes respectively
Y	Position of centroid
y	Displacement in general or Position of centroid of an elemental area
y_o	Initial imperfection displacement
Z	Connection factor
Z_p	Plastic section modulus
α	Effective length multiplier for torsional flexural buckling
α_i	Non dimensional connection constant [$= EI/R_iL$]
β	Non dimensional constant [$= \sqrt{1 + 15h^3}$]
γ_i	Slope at end i of a semi-rigid jointed element
ν	Poisson's ratio [= 0.3]
μ	$\sqrt{P/EI}$

ρ	Non dimensional constant [$= P/P_E$]
ω	Non dimensional constant [$= 1-(x_o/r_o)^2$]
θ	Rotation in general
θ_i, θ_{zi}	Rotation at end i and about the z axis respectively
ϕ	Relative angle change of member centre lines at connection or Angle of twist about the shear centre
$\lambda_c, \lambda_f, \lambda_p$	Elastic critical load, actual failure load and simple plastic collapse load factor respectively
σ_c	Compressive stress on an element
σ_y	Yield stress of steel
σ_{cr}	Critical local buckling stress of an element
σ_{max}	Maximum compressive edge stress

CHAPTER 1

INTRODUCTION

AND

REVIEW OF RELEVANT LITERATURE

1.1 INTRODUCTION

The determination of the actual behaviour of even a simple structure is extremely complex and also time consuming even in this modern age of computerization. This is due to the complex interaction of loading on the actual structure. There will also be interaction between individual members of the structure. The actual loading on individual members will always be highly variable and difficult to predict in advance.

For analysis purposes, the actual structure will in most cases be idealized as a two dimensional framework structure. The members of the structure are furthermore assumed to be connected either by frictionless pins or by fully rigid connections. Such framed structures are usually known as plane trusses and plane or rigid frameworks respectively.

Like plane trusses, rigid frameworks are loaded only in their own plane and are extensively used in the civil industry. Examples include storage racks, offshore structures and all types of building frameworks. For a framework where the members are assumed to be rigidly connected at the joints, the angles between members meeting at a joint remain unchanged as the framework deforms under loading. Consequently, the members of rigid frameworks transmit load, not only axially, but also by bending and shear. Rigid frameworks are also often designed to carry loads both at the joints and along the lengths of the members.

Although the above two idealized models corresponding to the two extreme cases are simple to use and easy to implement in analysis and design, their validities are not corroborated by experiments. Experiments carried out over the past decades have shown convincingly that actual joint behaviour generally falls between the two extremes of perfectly pinned and fully rigid. In addition, the moment-rotational deformation behaviour of the connections is usually non-linear and always irreversible almost for the entire range of rotations. This effect will alter the internal

force distribution in the members of the framework and the framework overall behaviour. The above type of joint is known as semi-rigid connection and frameworks having such connections are known as semi-rigid frameworks.

In the elastic-linear analysis of plane frameworks, both rigid and semi-rigid, the material properties are assumed to be constant and displacements are assumed to be small. This type of analysis is usually straightforward and quite simple. However, when non-linear effects are present, the analysis can be very complex. Non-linearity is caused by geometrical and material effects. The main factor that contributes to the former effect is the influence of axial force on member flexural stiffness. Another major cause is the horizontal displacements, commonly known as the P-Delta effect. Changes in members chord length and initial imperfections also cause non-linearity. The non-linear stress-strain relationship of the material and residual stresses present in members prior to loading are the main causes of material effects.

As mentioned above, the most significant non-linear influence in the elastic behaviour of frameworks is the influence of the axial forces on the flexural stiffness of the members. Tensile forces can be considered as increasing the flexural stiffness while compressive forces decrease the flexural stiffness. If a set of compressive forces is increased to the extent that the bending stiffness of the framework as a whole reduces to zero, the framework becomes unstable. This is known as the elastic critical load.

When the material of the framework is stressed beyond the limit of proportionality, the elastic critical load does not give an accurate representation of the actual failure load. At collapse, large regions of the framework may be inelastic. Hence, a collapse load analysis is required, i.e., plastic hinges can developed wherever the bending moment is sufficiently large. In a collapse load analysis, the load may be obtained through rigid - plastic, elastic - perfectly - plastic or elasto - plastic analysis.

With the widespread and increasing use of cold-formed, thin-walled structures as main components of plane frameworks, the tendency for local buckling to occur is inevitable, especially when the walls of the section are very thin compared with their widths.

Local buckling is characterised by distortion of the shape of the cross-section. The walls depart from their original plane and form waves, or buckles, along the length of the member. After local buckling, there is a radical alteration of the stress system within the section, causing a reduction in the stiffness of the member and a subsequent lowering of the ultimate moment carrying capacity.

The problem of local buckling, coupled with the non-linear behaviour of the connections and other non-linear effects lead to a rather complex but nevertheless much required analysis. In the investigation of the behaviour of such frameworks, a knowledge of several relevant topics are essential.

The following review of the literature, therefore consists of the following sections:

1.2 Rigid frameworks

1.3 Connections

1.4 Semi-rigid frameworks

Due to the wealth of literature, especially on the first subject mentioned above, only those papers considered by the author to be most relevant are reviewed in this thesis and are listed in part one of the bibliography. Part two of the bibliography contains references which have not been mentioned in the review but are nevertheless informative in this and allied field.

1.2 RIGID FRAMEWORKS

In a survey conducted by Lu (1), it was mentioned that the first systematic method of analysis of plane frameworks was presented by Bleich (2,3). Although further

investigations followed, it was not until in the mid fifties that Merchant and his associates (4,5,6,7) made a significant contribution. They proposed an analytical method of stability analysis suitable for the examination of tall buildings.

Lundquist (8) applied the principles of the moment distribution method to stability computations and devised the fundamental stiffness criteria for structures. A rigorous proof of the uniqueness of the results was given by Hoff (9,10,11). Modifications of the basic moment distribution method have been proposed by Masur and Cukurs (12) and Livesley and Chandler (13). The modifications included the use of stability functions as illustrated in figure 1.2.1.

The above mentioned methods involved the setting up of a system of simultaneous equations and solving them manually. For complex structures the numerical computations required in the analysis is sometimes prohibitive. However, with the advent of computers, more factors affecting the stability of frameworks could be added.

Zweig (14) generalized the slope-deflection method used by Bleich (3). He applied the method to multi-storey frameworks. A design method and tables were also presented permitting a simplified solution for some intricate framework problems.

The moment distribution method of solution was further developed by Porter (15) in 1970. His modification involved the introduction of the successive over-relaxation method whereby convergence is never a problem. Limiting conditions for the critical load of a framework with identical storeys were obtained and shown in figure 1.2.2.

The displacement matrix method of analysing the stability of frameworks has received attention in recent years. This method involves the solving of the equation

$$\mathbf{K}\ \mathbf{D} = 0 \qquad (1.2.1)$$

Numerically, this requires the determination of the load, such that K becomes singular. Using this principle, Korn (16) devised a method for converting framework stability calculations into a form of a low order, non-linear eigenvalue problem. The solution to this problem was obtained by repetitive solutions of tentatively linearized eigenvalue problems.

In 1984, Zweig (17) presented the force matrix method for stability analysis, which was not very popular among researchers. He outlined the advantages and disadvantages of both the displacement and force matrix methods. A detailed design procedure was included to facilitate the practical application of this method. Numerical examples also showed that the results agreed very well with those obtained using the displacement method.

The finite element approach became very popular due to the advance in computer technology. It was proposed by Gallagher and Padlog (18) in 1963. Beskos (19) analysed various framework stability problems using the above method. He pointed out that the error of the critical load computed may be greater than about 80% if each member of the framework is taken as a single element. In 1986, Long (20) used a high precision element to analyse various framework stability problems, including those analysed by Beskos (19). It was found that the accuracy obtained was very much higher when compared with those obtained from conventional finite element method.

The theoretical developments in the stability analysis outlined above are limited to frameworks whose members are stressed primarily by axial forces at the instant of instability. Several investigators have studied the effects of primary bending moment in the members on the instability of rigid frameworks.

Chwalla (21) was the first researcher to investigate the effects of primary bending moment on framework stability. He considered a portal framework with

symmetrical loads applied transversely on the beam and used the classical approach of integrating a system of differential equations which defined the equilibrium of various members in the buckled state. The bending moments present in the members and their increments after buckling were taken into account in establishing the basic equations. From the results, he showed theoretically the existence of the point of bifurcation on the load- deformation curve of the framework. He also determined the exact buckling load of several frameworks with uniform member sizes and subjected to two concentrated loads at various points on the beam. His results indicated that the presence of bending deformation causes only a small reduction of the elastic buckling loads and for simple frameworks the deformation effect may be disregarded.

Masur et al (22) succeeded in modifying Bleich's slope deflection and moment distribution methods (3) so as to include the effects of bending moment and the associated deformations. By using this modification, various instability problems of this type could be investigated in a systematic manner. A limited number of experiments on model frameworks have been conducted by Lu (23) for the verification of the theoretical solutions mentioned above.

In late 1964, Moses (24) modified the method used by Lu (23). He applied an iterative numerical procedure to find the load verses deflection curve, and hence, the buckling load of inelastic frameworks subject to primary bending moments and lateral forces. To use this procedure, it is necessary to have experimental or analytical expressions for the curvature of the cross section of the framework members as a function of bending moment and axial force.

The displacement matrix method of solving a series of equations became very popular and received plenty of attention since the early sixties because of the rapid formulation of stiffness matrices using computers. Hartz (25) applied this method to perform elastic analysis on various frameworks. Krueger et al (26) proposed a

design programme for multi-storey frameworks whereby member sizes can be computed. Connor et al (27) presented a non-linear analysis of elastic frameworks. They employed the Newton-Raphson iteration process for convergence. This method can detect the equilibrium position in very few cycles of iterations. The matrix method leading to an eigenvalue problem of solution was employed by Awadalla (28) to study multi-storey frameworks. Numerical results obtained were found to be very close to those obtained from stability function solutions.

Chu and Rampetsreiter (29) used the matrix method to take into account large deflection. Toridis and Khozeimeh (30) and Mahendra (31) developed a general method of inelastic analysis of plane and space frameworks. The method employed by the former investigators could also cater for dynamic analysis.

In 1986, Rankovic and Kanjeric (32) presented a non-linear stability analysis of frameworks, taking into account the non-linear stress-strain relationship of the material. The flexibility method of solution was used in place of the displacement matrix method. The criterion used in establishing the critical load was by equating the determinant of the structure stiffness matrix to zero. Only theoretical results for a portal framework loaded by uniform distributed load on the beam and a horizontal concentrated load on the side were obtained.

Simitses and his associates (33,34) investigated stability problems of asymmetrically loaded portal framework and symmetrically loaded multi-storey framework. The former study was a non-linear analysis taking into account the effects of member slenderness ratio, load eccentricities and the support rotational restraint stiffness. It was established that the effect of member slenderness ratio on the load verses displacement characteristic was negligible. The portal framework is not imperfection-sensitive for the load eccentricity type of imperfection.

Rotational restraint at the support increases the buckling load. In the latter investigation, the parameters considered were similar to the former except that loading was symmetrical. Rather similar findings were established.

Again, because of the rapid computation of solutions by computers, the finite element method of approach was proposed by several investigators. Akkoush et al (35) included incremental numerical solution techniques to analyse the non-linear behaviour of plane and space frameworks. Remseth (36) also studied the non-linear behaviour of space frameworks but he included initial imperfections and dynamic effects. Wen and Rahimzadeh (37) also studied plane and space frameworks. They took into account the effects of large translation and rotation of the chord. In all the above investigations, it was concluded that the accuracy of the results increases as the number of elements was increased. Large errors may occur if a one element one member analysis is adopted.

The P-Delta effect, which reduces the load carrying capacity of sway frameworks, have received a great deal of attention. In 1986, Scholz (38) presented an approximate method to account for the P-Delta effect coupled with the Load and Resistance Factor Design of various frameworks in general. He proposed that the method be used as a check against the other conventional designs. In the same year, Kanchanalai (39) made a theoretical investigation to determine the strength of columns in symmetrical portal frameworks and frameworks with some columns having pinned connections. Besides the P-Delta effect, he also considered the slenderness ratio and relative column to beam stiffnesses. He proposed a modification to the column design according to the allowable stress. The applicability of the modification was verified by experiments.

Gaiotti and Smith (40) investigated the P-Delta effect on multi-storey frameworks using a new method which was rather similar to the iterative method, but based on analyses using the actual gravity loading applied to successive deflected shapes.

They also compared the results with several other methods used by previous researchers. It was found that the results obtained were identical to those given by the iterative method but the new analysis took only about one third of the time.

In 1989, Ekhande et al (41) applied the stability functions type of solution to derive the stiffness matrix of three dimensional element. Although several numerical examples were presented, no experimental verification were undertaken.

In recent years, the plastic method of structural analysis has been rapidly developed and extensive applications have been made in the design of building frameworks. Much of design was based on the major contribution made by Merchant (42) as early as 1954. In that year, he pointed out the effects of overall instability on the load-carrying capacity of rigid frameworks. Although his paper dealt only with some fundamental concepts of instability, it has stimulated many investigators to study various plastic instability problems, particularly those related to multi-storey building frameworks. Among his findings, it was shown that for columns of intermediate length, the failure load may be expressed empirically in terms of the Euler load, the yield load and some arbitrary parameters representing the initial imperfections. He also suggested that it might be possible to consider the elastic critical load and the simple plastic load of a framework as the basic parameters for the determination of its true ultimate load.

A few years later, Merchant et al (43) presented a summary of the results obtained from a large number of experiments conducted on model triangular trusses and rigid portal frameworks. The tests were performed for obtaining experimental evidence of the empirical approach proposed by Merchant (42). The investigators made statistical analyses on the test results with the hope that some simple relationship might be obtained for expressing the observed ultimate load in terms of a few theoretical parameters mentioned above. Unfortunately, after testing numerous combinations of the parameters in the regression analyses, it was not

possible to find a definite relationship which might be used to compute the inelastic instability load with a known degree of accuracy. The authors also presented statistical correlations of a large number of theoretically calculated instability loads with some selected parameters. The theoretical loads were determined for one and two storey frameworks using the idealized elastic-plastic moment-curvature relations so that all yielding was concentrated at the hinges. It was found that nearly all the theoretical points fell within the bounds established by the analysis of the experimental results.

Low (44) tested several series of model steel frameworks to investigate the magnitude of the framework instability effect on the load-carrying capacity. The results obtained from the experiments were plotted non-dimensionally in the form suggested by Merchant (42). The plots seem to indicate that, for most cases, Merchant's simple formula

$$\frac{1}{\lambda_f} = \frac{1}{\lambda_p} + \frac{1}{\lambda_c} \qquad (1.2.2)$$

for estimating the inelastic instability load of frameworks is rather conservative. The above equation is known as the Merchant-Rankine formula. The tests also indicated that the reduction of the ultimate load due to instability was higher for taller frameworks. The average reductions for three, five and seven storeys frameworks were found to be around 10%, 30% and 35% of the simple load respectively.

In 1958, Salem (45) carried out experimental test for one and two storey frameworks. One of his objectives was to verify the Merchant-Rankine formula. The results obtained were plotted as points as illustrated in figure 1.2.3. Lines corresponding to various ratios of λ_p/λ_c have been drawn, and it can readily be seen that the Merchant-Rankine formula is most successful when λ_p/λ_c is small and the collapse

load is close to the rigid-plastic collapse value. When $\lambda_p/\lambda_c > 0.3$, the scattering of the points away from the Merchant-Rankine formula is considerable. Merchant suggested the formula as a safe limit for the collapse load as pointed out by Low (44)

In 1960, Lu (23) presented an analytical solution to the buckling of portal frameworks in the plastic range. The method takes into account the effects of axial force, yielding, deformation and residual stresses. Tests conducted by Yen et al (46) have verified the theoretical solution.

Morris and Fenves (47) used an elastic-plastic analysis to study the load verses displacement behaviour of a fixed base symmetrically portal framework loaded beyond the elastic range up to the ultimate load. An incremental analysis procedure was employed and structural forces, displacement and reactions were determined at various load levels. The concept of the classical yield hinge was extended to included cross sections deforming plastically under combinations of flexural and torsional moment and axial force.

Due to the great demand and popularity of high-rise buildings, the period beginning from the sixties saw a rapid increase in the investigation into this class of buildings. Korn and Galambos (48) investigated the full load verses displacement path of several multi-storey frameworks by means of first order and second order elastic-plastic theory. They concluded that frameworks lacking sufficient working load deflection and stability controls are subject to a catastrophic early instability at large losses in potential load-carrying capacity. Such frameworks are also highly non-linear at working loads due to the second order amplification of sway. For frameworks having reasonably linear behaviour at working loads, at least 86% of the first order load-carrying capacity was obtained.

About two years later in England, Wood (49) made an important contribution to the design of framework. He suggested a modification of the Merchant-Rankine load to allow for the minimum beneficial effects that must always be present from strain-hardening and restraint provided by cladding. He suggested that provided

$$\frac{\lambda_c}{\lambda_p} > 10$$

then

$$\lambda_f = \lambda_p \qquad (1.2.3)$$

and when

$$10 \geqslant \frac{\lambda_c}{\lambda_p} \geqslant 4$$

then

$$\lambda_f = \frac{\lambda_p \lambda_c}{\lambda_p + 0.9\lambda_c} \qquad (1.2.4)$$

When expressed graphically, these proposals are represented by the lines ACD of figure 1.2.4, and may be compared with the Merchant-Rankine formula given by the straight line AB. When applying condition (1.2.3) to derive the design requirements, it can be seen that the required minimum value of λ_f is that corresponding to the required factored loading. λ_p can be derived by using the design strength, P_y, of the steel. Supposing the required minimum final load factor of the structure, λ_f, is expressed as a plastic load factor, using, instead of the specified design strength, P_y, an effective design strength P'_y, so that

$$\frac{\lambda_f}{\lambda_p} = \frac{P'_y}{P_y}$$

whence

$$\frac{\lambda_c}{\lambda_p} = \alpha \frac{P'_y}{P_y}$$

where

$$\alpha = \frac{\lambda_c}{\lambda_f}$$

On substituting the above value of

$$\frac{\lambda_f}{\lambda_p} = \frac{A}{\lambda_p}$$

where A is λ_f of equation (1.2.2), and λ_c/λ_p into equation (1.2.3), it is found that, in design, it can be assumed that

$$P'_y = P_y$$

when

$$\lambda_c/\lambda_f > 10$$

and

$$P'_y = P_y\left(\frac{\alpha-1}{0.9\alpha}\right) \qquad (1.2.5)$$

when

$$10 \geqslant \lambda_c/\lambda_f \geqslant 4.6$$

This proposal is the basis for the adoption of plastic design for continuous low-rise framework in the BS 5950: Part 1. When $\lambda_c/\lambda_f < 4.6$, it is recommended that, if elastic- plastic methods of ultimate load design are to be employed, then a special analysis allowing for elastic-plastic behaviour and change of geometry effects should be undertaken. It will, of course, also be necessary to satisfy the deflection limits imposed by the provisions of the appropriate clauses in the standard. It should be noted that, if the more conservative modified Merchant-Rankine load, equation (1.2.2), is used in design rather than equations (1.2.3) and (1.2.4), then a modified yield stress must always be used, i.e.,

$$P'_y = P_y\left(\frac{\alpha-1}{\alpha}\right) \qquad (1.2.6)$$

Chi and Lin (50) presented a paper on the elastic-plastic analysis of multi-storey frameworks. The elastic slope defection method was modified and generalized. The plastic strain was treated as a set of additional moments. The method was applicable to frameworks of work hardening as well as ideally plastic materials. The method employed reduces the problem to the solution of a system of simultaneous equations and no iteration was required.

A numerical procedure for large deformation analysis of elastic-plastic frameworks was presented by Kassimali (51). The procedure utilised an incremental load approach with Newton-Raphson iteration to satisfy joint equilibrium equations. Changes in member chord length due to axial strains and flexural bowing was considered. Analysis was performed on the frameworks used by Korn and Galambos (48) whereby bowing effect was neglected. The results obtained were very similar and thus it was concluded that the consideration of large deformation and flexural bowing effects complicates the problem of non-linear analysis of frameworks considerably.

With the recent introduction of cold-formed thin-walled structures, more building frameworks are using these members as main components. The following reviews are on frameworks composed of thin-walled members.

In 1977, McIvor et al (52) presented a structural theory for the large plastic deformation of space frameworks composed of thin-walled members. The framework, which was composed of several square tubings, was considered to consist of an arbitrary number of beam elements connected at node points. The analysis assumed that plastic deformation is confined to idealized hinges located at node points. To generalize the analysis for computer programming, the equations of a beam element were derived as a relationship between generalized force and deformation rates. The structural theory employed for the plastic hinges included bi-axial bending, torsion and axial extension. Reduction in the load carrying capacity of the hinge due to local deformation was accounted for. An experiment was carried out on a space framework which was constructed by welding thin square tubings together. The predicted force-deformation curve was found to be in good agreement with the experimental results.

The effects on the member end moment of a framework due to local buckling was investigated by Wang (53). In the analysis, the matrix stiffness method was adopted. The effective width concept was used to account for local buckling. The expression, which was introduced by Winter (54), is as follows:

When

$$\frac{b}{t} \geq 1.288\left(\frac{E}{\sigma_{max}}\right)^{1/2}$$

then

$$\frac{b_e}{t} = 1.9\left(\frac{E}{\sigma_{max}}\right)^{\frac{1}{2}}\left\{1 - 0.415\left(\frac{t}{b}\right)\left(\frac{E}{\sigma_{max}}\right)^{\frac{1}{2}}\right\} \qquad (1.2.7)$$

When

$$\frac{b}{t} < 1.288\left(\frac{E}{\sigma_{max}}\right)^{1/2}$$

then

$$b_e = b \qquad (1.2.8)$$

As the compressive edge stress, σ_{max}, is not uniform along the member, application of equation (1.2.7) will result in a non-prismatic member. This was accounted for by dividing individual member into several segments.

As a follow-up, Wang and Blandford (55) proposed a method of stability analysis of locally buckled frameworks. The procedure was based on the finite element approach and the method of solution was by equating the stiffness matrix of the framework to zero. To take into the account of local buckling, the following expression (56) was used :

When

$$\frac{b}{t} \geq 0.64A$$

then

$$\frac{b_e}{t} = 0.95A\left[1 - 0.95A\, C\left(\frac{t}{b}\right)\right] \qquad (1.2.9)$$

where $A = \sqrt{KE/\sigma_{max}}$ and C is a modification factor based on experimental evidence and engineering judgement.

When

$$\frac{b}{t} < 0.64A$$

then

$$b_e = b \qquad (1.2.10)$$

Theoretical analyses, with and without local buckling, were performed on various frameworks and it was found that the critical load with local buckling taken into consideration was always lower than if local buckling is neglected. Unfortunately, no experimental verification was undertaken.

Baigent and Hancock (57,58,59,60) and Hancock (61) investigated the behaviour of low-rise portal frameworks composed of cold-formed members extensively used in the recent years. The analysis method was based on the matrix stiffness approach. Effects such as warping torsion, cross section monosymmetry, progressive yielding, inelastic local buckling in the thin-walled sections and cross section distortion were considered. The collapse load was predicted using an inelastic finite strip local buckling analysis. Experimental investigations were carried out on several pitched-roof portal frameworks constructed from cold-formed channels. The frameworks were loaded to failure in three different patterns as shown in figure 1.2.5. Although the theoretical and experimental failure loads were in good agreement, it was found that all the experimental apex deflection indicated a more flexible response from the frameworks as shown in figure 1.2.6. The explanation given was that the greater flexibility could lie in the behaviour of the joint, which

was assumed to be rigid. Another conclusion drawn was that all the frameworks have a considerable inelastic reserve capacity as the collapse load was about twenty percent higher than the load at first yield.

The torsional flexural buckling of rigid plane frameworks composed of I section members and subjected to planar loading was investigated theoretically by Vacharajittiphan and Trahair (62). The generalized method, which can be used for planar rigid frameworks with various planar loading, was based on the formation of differential equations for bending and torsional flexural buckling. These equations were solved using the finite integral method with the aid of computers. The accuracy of the method was studied by comparing the results for beams and simple portal frameworks with known solutions. It was established that to achieve accuracy sufficient for engineering purposes, nine nodes were required for each member. Solutions for various low-rise frameworks were also obtained but no comparison of results were made.

In 1985, Nethercot (63) presented a paper on the analysis of portal frameworks with the effects of torsional flexural buckling. The method comprised of the formulation of stiffness matrices, the coefficients of which were obtained using the energy method proposed by Barsoum and Gallagher (64). In the analysis, the element ends were assumed to be restrainted from warping. The eigenvalue of solution was used to obtain the critical load of isolated members. Two numerical examples on portal frameworks were given. It was concluded that careful use of the results of isolated members will lead to acceptable estimate of the framework critical load. In cases where published results of isolated members are inadequate, it was suggested that a finite element programme be used.

Alwis and Usami (65) proposed a finite element method of analysis to determine the elastic lateral torsional buckling of rigid frameworks. The effects of in-plane deformations on lateral torsional buckling were included in the analysis, where

in-plane and out of plane deformations were treated separately. The critical load was obtained by equating the determinant of the overall stiffness matrix to zero. Numerous examples were performed on simple frameworks and from the results obtained, it was shown that the number of elements needed to produce a desired accuracy increases with increasing length of the members.

1.3 CONNECTIONS

Research into the behaviour of connections and their moment-rotation characteristics was first carried out in 1917 by Wilson and Moore (66). Although some interesting results were obtained, the paper only touched on the fringes of the subject.

In 1929, the Steel Structures Committee of Great Britain initiated a programme of theoretical and extensive experimental research (67) in various aspects of building behaviour that had a great influence on later studies. Under the combined leadership of J. F. Baker and C. Batho, the committee advanced understanding as to how building frameworks actually behave under load and it set forth principles whereby the influence of connection flexibility and framework behaviour could be studied and analysed. After various tests on riveted connections, a linear expression was proposed to model the connection behaviour. The connection factor, Z, which is the inverse of the initial tangent of the connection moment-rotation plot, takes the form :

$$Z = \frac{\phi}{M} \qquad (1.3.1)$$

The above expression was also employed to model the connection behaviour by Rathbun (68) about the same period in America.

In 1951, Lothers (69) proposed a method of representing the moment-rotation relationship of angle-plate connection, which was very popular during that period, in a linear form. The stiffness was expressed in terms of the connection critical bending moment and rotation, which through elastic analysis, could be computed using size parameters of the angle-plate connection. From tables provided, the approximate linear stiffness of various sizes of angle-plate connections investigated could be established.

Munse et al (70) studied the behaviour of standard double web angle flexible connection which was very popular during that period. The connections were assembled with rivets and high strength bolts and completely with rivets in order to study the behaviour of the effect of the type of fasteners upon the behaviour of the connections. The main findings arrived at were that although assumed for design purposes to behave as simple supports, the connections provided some end restraint. This restraint increases when high strength bolts were used.

To further improve the representation of the connection behaviour, Sommer (71) fitted experimental moment-rotation data to standardized moment-rotation curves in the form of non dimensional polynomial series. The form of the polynomial function is

$$\phi = C_1(KM) + C_2(KM)^3 + C_3(KM)^5 \qquad (1.3.2)$$

where K is the standardization factor dependent on the connection type and geometry, and C_1, C_2 and C_3 are curve fitting constants. The standardized moment-rotation function is applicable to all connections of the same type, the influence of different sizes and dimensions is accounted for by the factors. The above model can only be used provided sufficient experimental data are available.

To improve the model used by previous investigators, Romstad and Subramanian (72) developed a method of representing the moment-rotation curve of double-angle connections. Using this method, the actual curve is bi-linearised as shown in figure 1.3.1. By using the connection size parameters, the slopes of the bi-linear approximation could be obtained as illustrated in figure 1.3.2. This information could then be used to account for semi-rigid joints.

Frye and Morris (73) extended Sommer's method (72) to seven different connection types shown in figure 1.3.3. The standardized polynomial expression of these connections are tabulated and shown in table 1.3.1 and typical moment-rotation curves are illustrated in figure 1.3.4. The accuracy of the standardization procedure can be seen in figure 1.3.5, which shows the moment-rotation curves generated by the standardized equation and the corresponding experimentally obtained curves for two double web angle connections. The main drawback of this method is that the nature of a polynomial is to peak and trough within a certain range. The connection stiffness, which is represented by the slope of the moment-rotation curve, may become negative at some values of moment and this is physically unacceptable.

To overcome this, Jones et al (74,75,76,77) developed a method of representing the actual moment-rotation curves of connections more accurately. This method is known as the B-spline method. The method requires the division of the range of connection rotations into a finite number of smaller ranges. Within each range, a cubic function is fitted in turn with the first and second derivatives, continuity being maintained between adjacent ranges. Numerical description resulting from the curve fitting can then be used directly within numerical differentiation procedures. This method has been found to produce close and smooth representation of

experimental results as illustrated in figure 1.3.6, which also shows the comparison of the polynomial fit. The disadvantage of the B-spline model is the large number of data required for the curve fitting process.

Richard et al (78) presented a method of modelling the moment-rotation characteristics of single plate connections. This method involves the experimental determination of the load-displacement relationship for a single bolt connecting two plates in shear. In this manner, all linear and non-linear deformations occurring in the bolt and the connected plates were lumped together. The connection was then analysed using finite element method whereby the non-linear behaviour of the bolts and connected plates was modelled as a shear connector with load-deformation properties obtained previously. The moment-rotation curves obtained were then compared with experimental data and reasonable agreements were achieved.

In the early seventies, a series of tests on various beam-to-column connections were carried out by Chen and his associates (79,80,81). The connections consisted of various commonly used type and were either welded or bolted with high strength bolts. The results obtained were intended to be used as a basis for the design of beam-to-column connections for multi-storey buildings.

In order to enable the designer to anticipate the connection stiffness during the designing phase, Ackroyd and Gerstle (82) proposed a method of relating the connection stiffness to the required connection strength. This relation takes the form:

$$R \propto \frac{M_{cu}\, d}{\sigma_y} \qquad (1.3.3)$$

This relationship between the strength and stiffness, as inferred from available experimental results for several connection types, is shown in figure 1.3.7, which allows estimation of connection stiffness once the required moment and girder depth, d, are known.

In the year 1983, Colson and Louveau (83) presented a model which uses a power function of the form :

$$\phi = \frac{|M|}{R_o\left[1-\left(|\frac{M}{M_{cu}}|\right)^n\right]} \qquad (1.3.4)$$

The curvature of the moment-rotation relationship is accounted for by the parameter n. Since the model has only three parameters R_o, M_{cu} and n, as illustrated in figure 1.3.8, it is not as accurate as the B-spline model. However, the number of data required is drastically reduced.

Ang and Morris (84) replaced the polynomial function by a form of the function given by Ramberg and Osgood (85) in the development of standardized moment-rotation expression for connection types shown in figure 1.3.9. The latter function, which is illustrated in figure 1.3.10, has the form :

$$\frac{\phi}{\phi_o} = \frac{KM}{(KM)_o}\left\{1+\left(\frac{KM}{(KM)_o}\right)^{n-1}\right\} \qquad (1.3.5)$$

where ϕ_o, $(KM)_o$ and n are coefficients evaluated in the curve fitting process and K is defined in equation (1.3.2). Depending on the value of the coefficient n, equation (1.3.5) can represent any of a family of curves passing through point 1 of figure 1.3.10. Thus, it can model a moment-rotation curve with a sharp "knee", or one with a long gradual decrease in slope. Standardized expression of the

connections can be found in table 1.3.2. The Ramberg-Osgood function has the advantage that its derivative, hence the slope of the moment-rotation curve, does not fluctuate.

In order to reduce the costs of carrying out experiments to determine the moment-rotation characteristics of connections, Yee (86) developed a new approximate method to model the connection behaviour. The expression used in the method, which is known as the exponential and correction model, is expressed in terms of certain functions as shown in equation (1.3.6).

$$M = M_{cu}\{1 - exp\left[-\frac{(K_i - K_p + C\phi)\phi}{M_{cu}}\right]\} + K_p\phi \qquad (1.3.6)$$

where K_i and K_p are constants dependent on the connection stiffening and failure mode as can be seen from tables 1.3.3 and 1.3.4. The value of C is obtained empirically from the test data. It should be noted that the model is valid only for bolted extended end-plate eave connection as shown in figure 1.3.11. When compared with available experimental results, the model predicted the curves within acceptable limits. Some of the comparisons are shown in figures 1.3.12 and 1.3.13.

In 1985, Nethercot (87) discussed the various connection moment-rotation curves obtained by previous investigators using experimental rigs as shown in figure 1.3.14. After careful examination, he commented that only about 50% of the 700 individual test were considered to be useful. Comments were also made on the various models used to represent the connection moment-rotation curve. A summary of the comments is listed in table 1.3.5. The feasibility of organising the available moment-rotation curves of various connections into a computerized data bank system was also demonstrated and found to be encouraging.

Due to the advancement in computer technology, the finite-element approach of analysis became very popular with researchers. Among them, Krishnamurthy and Battles (88), Krishnamurthy (89), Maxwell et al (90), Jenkins et al (91) and Kukreti et al (92) employed the method to study the behaviour of connections. The connections studied by them included top-angle, tee-stub and end-plate connections.

To overcome the disadvantage of requiring large amount of data as in the B-spline model, Lui and Chen (93) presented a method to model the non-linear moment-rotation relationship of connections. The model is expressed in an exponential function of the form :

$$M = \sum_{j=1}^{m} C_j[1 - exp(-|\phi|/2j\alpha)] + R_{kf}|\phi| + M_o \qquad (1.3.7)$$

where

R_{kf} is the strain hardening stiffness of the connection.

M_o is the initial moment at which the curve is fitted.

α is a scaling factor.

C_j is a curve fitting constant.

The model, which is known as the exponential model, is a multi-parameter model. The number of parameter required is $(m + 3)$, where m is the number of curve fitting constants, C_j. The above model has been shown to represent the non-linear behaviour of connections very well. The limitation of this model is that it may not completely represent the moment-rotation curve that consists of a few linear components.

Kishi and Chen (94,95) refined the exponential model to accomodate linear components of moment-rotation curves of connections. This model is represented by the form :

$$M = M_o + \sum_{j-1}^{m} C_j[1 - exp(-|\phi|/2j\alpha)] \quad +$$

$$\sum_{k=1}^{n} D_k(|\phi| - |\phi_k|) H[|\phi| - |\phi_k|] \qquad (1.3.8)$$

where

D_k is a curve fitting constant.

ϕ_k is the starting rotation of kth linear component taken from experimental moment-rotation curve.

$H[\ \ ]$ is the Heaviside's step function given by :

$$H[\phi] = 1 \qquad \text{for} \qquad \phi \geq 0 \qquad (1.3.9)$$

$$H[\phi] = 0 \qquad \text{for} \qquad \phi < 0 \qquad (1.3.10)$$

Like the exponential model, also known as the Chen-Lui model, this modified exponential model deals with connection loading and unloading for the full range of rotation in a second order analysis. The comparison between the Chen-Lui exponential model and the modified exponential model for numerical example test data including a linear component is shown in figure 1.3.15.

While the modified exponential model is a curve fitting equation obtained by using the least mean square technique for the test data, Kishni and Chen (96,97) and Kishni et al (98) developed the power model from a different point of view. In this procedure, the initial elastic stiffness and ultimate moment capacity of the connection are determined by a simple analytical model. Using those values so obtained, a three parameter power model given by Richard and Abbot (99) was adopted to represent the connection behaviour. The generalized form of this model is :

$$M = \frac{R_o \phi}{\left[1 + \left(\frac{\phi}{\phi_o}\right)^n\right]^{1/n}} \qquad (1.3.11)$$

where

ϕ_o is a reference plastic rotation $= M_{cu}/R_o$

n is the shape parameter.

Figure 1.3.16 shows the comparison of the power model with various values of n to the experimental data. A comparison of the Chen-Lui model and the power model can be seen in figure 1.3.17.

Morris and Packer (100) presented a paper which described the factors influencing the force-deformation behaviour of various connections. Procedures for modelling various connection moment-rotation characteristics were discussed, a summary of which is tabulated and shown in table 1.3.6. The effects of connections were also described generally and illustrated with examples.

The normal approach in static calculation and analysis is to assume that the joint, which has defined dimensions, of a structure is contracted to a point at the intersection of the member lines. Tschemmernegg and Hunter (101) proposed a new method of representing the moment-rotation curve of connection, whereby the joint is looked at in a macroscopic view and a distinction is made between the panel zone and the connection as illustrated in figure 1.3.18. In this approach, the panel zone is modelled as a load introduction spring and a shear spring, which accounts for the panel shear deformation. The connection itself is represented by the connection spring. The final connection moment-rotation curve is obtained by totalling the individual spring model moment. This is illustrated in figure 1.3.19, which also shows the schematic diagram of the spring models.

1.4 SEMI-RIGID FRAMEWORKS

Modifications to the slope deflection and moment distribution methods were both applied to frameworks with semi-rigid connections in the 1930's by Baker (67,103) and Pippard and Baker (102) in England and Rathbun (68) in United States. In their analysis, the linear connection factor, Z, was employed. According to the final report (67), savings as much as 20% could be achieved on the design of beams in frameworks by taking advantage of end restraints, which could be predicted by the beam-line method proposed by Batho and Rowan (67) and later developed by Batho (67).

To increase the accuracy of the analysis, Johnston and Mount (104) refined Baker's method by considering the effect due to the widths of the members. The various joint moments computed were found to be in good agreement with results from experimental tests.

In 1947, Stewart (105) applied the traverse method to analyse frameworks with semi-rigid connections. The traverse, which expresses the joint rotation and the flexure angle due to the moment at each end of a member, is basically a representation of the deflected framework. In the analysis, the rotation of a joint due to a moment was expressed as a percentage of the elastic curvature caused by the same moment in a connecting member. The disadvantage of this method lies in the fact that numerous traverse lines are required to be drawn when a complex framework is to be analysed.

Instead of using the connection factor, Maugh (106) represented the stiffness of the connection by the initial slope of the moment-rotation curve in his analysis of semi-rigid frameworks. Using this approach, analyses were performed on frameworks studied by previous researchers. Comparison of the results showed very little difference in solutions.

In 1961, Lightfoot and Baker (107) refined the method of analysis employed by Johnston and Mount (104). The refinement came in the form of a computer solution to the problem of plane frameworks with elastic connections, using the generalized slope deflection equations in matrix form. The semi-rigid connection restraint was incorporated into the analysis by the use of correction matrices to amend the initial assumption of fully rigid connections.

Monforton and Wu (108) incorporated the effects of semi-rigid connections into the matrix stiffness analysis in a general manner in 1963. Similar procedures were proposed by Livesley (109) and Gere and Weaver (110) at about the same time. The linear semi-rigid connection factor was used to modify the member stiffness matrices and the fixed end force vector. The stiffness matrices were modified by correction matrices and the resulting linear equations were solved as in normal stiffness method. The advantages of this method are that relatively large frameworks can be analysed with ease and the interactive techniques employed would permit the inclusion of improvements in the end restraint representation.

Although the twisting degree of freedom was introduced into Monforton and Wu's analysis (108), a linear torque-twist relationship was assumed and axial deformation was neglected. These were taken into account by Lightfoot and Le Messurier (111).Several numerical examples were performed on three dimensional problems. However, due to the lack of experimental results available, no comparison was carried out.

Frye and Morris (73) presented an iterative analysis procedure for planar rectangular steel frameworks incorporating the non-linear behaviour of any of the seven beam-to-column connection types shown in figure 1.3.3. The analysis procedure involved repeated cycles of analysis to determine a set of connection secant stiffness that could then be used to predict the displacements and internal forces in the real

non-linear structure. In a numerical example, it was found that using an analysis which assumed pinned beam-to-column connections, a reduction of up to 20% in the column axial load capacity would be ignored.

To shed more light on the subject, Moncarz and Gerstle (112) employed the matrix displacement method of analysis to several semi-rigid frameworks. To represent the connection moment-rotation behaviour, a tri-linearized model was used. In their investigation, it was established that the assumption of fully rigid joints is inadvisable for frameworks with field-bolted or lightly welded connections. It will result in an under estimation of the bare-frame drift and may lead to inaccurate prediction of critical member forces.

With rather similar objectives, especially on the design aspects, Ackroyd and Gerstle (82) used a purely elastic analysis to study semi-rigid frameworks. The connection was modelled using the expression shown in equation (1.3.3). Several frameworks were analysed numerically and general outlines pertaining to design procedures were suggested.

Ang and Morris (84) generalized the Frye and Morris procedure (73) to permit the analysis of three dimensional rectangular frameworks with non-linear connections. They assumed all floors to act as rigid in-plane diaphragms, thus eliminating the in-plane degrees of freedom at all columns. Accordingly, they considered only one non-linear connection moment-rotation relationship which took the form of equation (1.3.5). Examples carried out demonstrated that connection deformation sometimes has a very significant effect on the internal force distribution in, or the deflection of, a structure.

Employing the tri-linearized connection model of Moncarz and Gerstle (112), Stelmack et al (113) provided an analysis which also included the connection

stiffness during unloading. From the verifications through experimental works, the shakedown of the connections to their elastic state was evident and a linear analysis was sufficient to predict framework behaviour under service conditions.

The papers reviewed above dealt mainly with the analysing of semi-rigid frameworks for displacement and member internal forces only. In 1970, Romstad and Subramanian (72) assumed a bi-linear model of the connection moment-rotation curve (figure 1.3.1) in their elastic critical load analysis, which used computational procedures for locating eigenvalues and eigenvectors. They analysed the stability problem using a bifurcation approach and so were unable to find the effect of a non-linear moment-rotation curve on the buckling capacity of frames.

In a paper by Gerstle (114), detailed descriptions and discussions on connection behaviour, linear and non-linear approach to semi-rigid framework analysis were presented. The elastic stability analysis, which assumed linear connection behaviour, was employed by Ackroyd and Gerstle (115). Modified slope deflection equations were used to account for the effects of the flexible end connections on girders. From numeral examples on a simple portal framework, it was found that as the connection stiffness increases, the drift decreases for a given load, and the buckling capacity of the framework is increased. Furthermore, a small increase in connection stiffness results in a substantial increase in framework capacity, while for very stiff connections, extra connection stiffness results in only nominal increase in framework capacity.

The non-linear approach was employed by Ackroyd and Gerstle (116). Material effects such as residual stress and elasto-plastic member behaviour were accounted for. Geometric non-linearities of members and connections were also included in their analysis. The Frye and Morris polynomial function of equation (1.3.2) was used to represent connections non-linear behaviour. A number of subassemblages representing existing portions of typical multi-storey frameworks, each with three

different flexible connections, were analysed. Results showed that in most cases, increased connection stiffness leads to an increase of framework strength, but in exceptional cases of low-rise buildings, it may result in a slight loss of strength. This finding removed the usual assumption or expectation that increase in stiffness of connections in a framework always lead to an increase in the framework strength.

In 1983, Melchers and Yee (117) studied the effects of connection behaviour on the deflections of practical frameworks. Numerical analysis of rigid and near-rigid (assumed to be rigid in design) portal frameworks were carried out, the connection behaviour of the latter being modelled by a quad-linear curve. It was established that the maximum increase in deflection due to connection flexibility was of the order of 20% at service load. The amount of increase was proportional to the degree of flexibility of the connections.

Numerous numerical studies on semi-rigid frameworks were conducted very recently by Simitses and his associates (118,119,120,121). The types of framework studied were two-bar, simple portal and gabled frameworks. The non-linear analysis involved the formation of equilibrium and buckling equations and satisfaction of boundary and joint conditions. Both linear and non-linear connection behaviour were considered , the former being represented by the connection factor and the latter by polynomial function. Included in the intensive study were parameters such as slenderness ratio and effects of load eccentricities. With the intention of shedding more light into the subject, many general conclusions were drawn.

In 1985, Poggi and Zandonini (122) presented a non-linear analysis which accounted for geometrical changes and spreading of plastic zones in members. Connection non-linear relationship was tri-linearized and stiffness during unloading was also considered. To account for the finite dimensions of the joints, the normal beam element was considered to be composed of three sub- elements. Various

parameters, including modelling the connection behaviour by bi-linear and piecewise linear models, were employed in several analyses carried out. The findings were to be used as preliminary studies for a major research.

Yu and Shanmugam (123) proposed a modified stiffness matrix method for finding the elastic critical load of simple semi-rigid frameworks. Besides accounting for the partial rigidity of the joints, the method also considered the effects of flexure on axial stiffness and geometric changes. A linear connection behaviour was assumed. Including the computation of the elastic critical load, a parametric study was also undertaken to study the effects of rigidity of various joints on single bay double storey frameworks.

In very recent years, intensive investigations on the behaviour of semi-rigid frameworks were performed in the United States by Chen and his associates (93,124,125,126,127). Their studies covered T and I shaped assemblage, two-bar, simple portal and multi-storey frameworks. In all the cases, the analysis employed was non-linear and except for the investigation by (127), the true non-linear connection behaviour modelled in the form of equation (1.3.7) was employed. This model can cater for the connection stiffness during its unloading. The formation of plastic hinges in the member was included in the analysis by both (126) and (127). The effects of loading pattern was also accounted for by the latter. The extensive research was undertaken in view of the AISC/LRFD Specification (128), which specifically identifies the need for the inclusion of connection behaviour in the analysis and design procedures.

Driscoll (129) presented an elastic-plastic analysis of frameworks with seat and top-angle semi-rigid connections. In this method, the connection was modelled as a series of fictitious rigid beam elements. The whole framework was then analysed as a rigid framework. An elastic analysis identifies the locations where stress is greatest and therefore plastic hinges may form. After changes in boundary

conditions, additional steps of elastic analysis can give increments in the elastic-plastic load-deformation curve of the entire framework up to the point where a mechanism defining ultimate load is defined.

Most non-linear analysis of semi-rigid frameworks are either too complex or time-consuming to be considered for design use. With the aim of providing a tool for designers, Goto and Chen (130) presented a computer-based method that can be easily applied to design practice for steel building frameworks with flexible connections using computers. Real connection behaviour along with various types of available analytical curves or simplifications were included in the analysis. In the development, special attention was paid to the efficient use of computer capacity, and to the simplicity in formulation of the analytical procedures without losing the numerical stability and accuracy of a rigorous solution.

After thoroughly evaluating the normal procedures used in the design of semi-rigid frameworks, Ackroyd (131) suggested modification to the limit of drift of buildings. A modified design procedure was included in his proposal. This procedure approximates the influence of connection flexibility on force distributions within the framework, so that girders size could be reduced at the expense of increases in the exterior columns. It was demonstrated that the net effect is an overall reduction in steel tonnage for members on the order of 4% to 11%.

In 1988, Jaspart (132) proposed a hand calculation procedure for the evaluation of the collapse load of semi-rigid frameworks based on the generalization of the modified Merchant-Rankine formula (42). Numerical examples were performed and the results compared with those from a conventional non-linear analysis. The agreement was found to be excellent. At the time of writing, further calculations and comparisons were being made at the main research centre to verify the validity of the proposed method.

Conventional structural analysis of frameworks are usually carried out with the postulation that the joint panel zone deformation is negligible. In actual structures, the joint panel may deform to such an extent as to affect the overall behaviour of a framework. This effect has received attention only very recently by Lui and Chen (93), Kato et al (133) and Tschemmernegg and Hunter (101). The effects of joint panel deformation on the seismic response were investigated by Popov (134) and Krawinkler and Mohasseb (135)

1.5 SUMMARY

The literature showed that there is an immense wealth of information available and a great deal of work has been done concerning the analysis of rigid frameworks. A great amount of effort has also been concentrated on the inclusion of the various non-linear effects. The introduction of the limit state design saw a sudden rise in the plastic analysis of rigid frameworks.

Realising the non-linear connection stiffness effects on the behaviour of frameworks, numerous experimental investigations were carried out on commonly used connections. Both linear and non-linear models of the connection moment-rotation characteristics were obtained. These models were then incorporated into the analysis of frameworks with the objective of obtaining more information as to the effects of semi-rigid connections.

Before the development of the computer-based stiffness matrix method of analysis , designers would not even consider the use of semi-rigid connections due to the tedious and complex analysis involved, not to mention the insufficient investigations and validified data on connections. Intensive studies, both theoretical and experimental, were undertaken only rather recently, especially in the United States, in order to arrive at expressions simple and yet safe enough for design use.

In the design of cold-formed thin-walled structures, the behaviour of the individual members under load has been the subject of much research. The overall structural behaviour depends not only on the member behaviour in isolation, but also on how the members interact. Although some work has been carried out on frameworks composed of cold-formed thin-walled members, the study of the combined effects of semi-rigid connections and the problems associated with thin-walled members on their behaviour is relatively very little compared to frameworks constructed from hot-rolled members. Hence, it is felt that there is a need to provide further insight into the study of cold-formed thin-walled framework with semi-rigid connections. The work carried out and compiled in this thesis has been performed to fulfil this need.

In this thesis the behaviour of symmetrical single and double storey frameworks, constructed with cold-formed thin-walled plain channel members and semi-rigid connections, as shown in general form in figure 1.5.1, is investigated both analytically and experimentally.

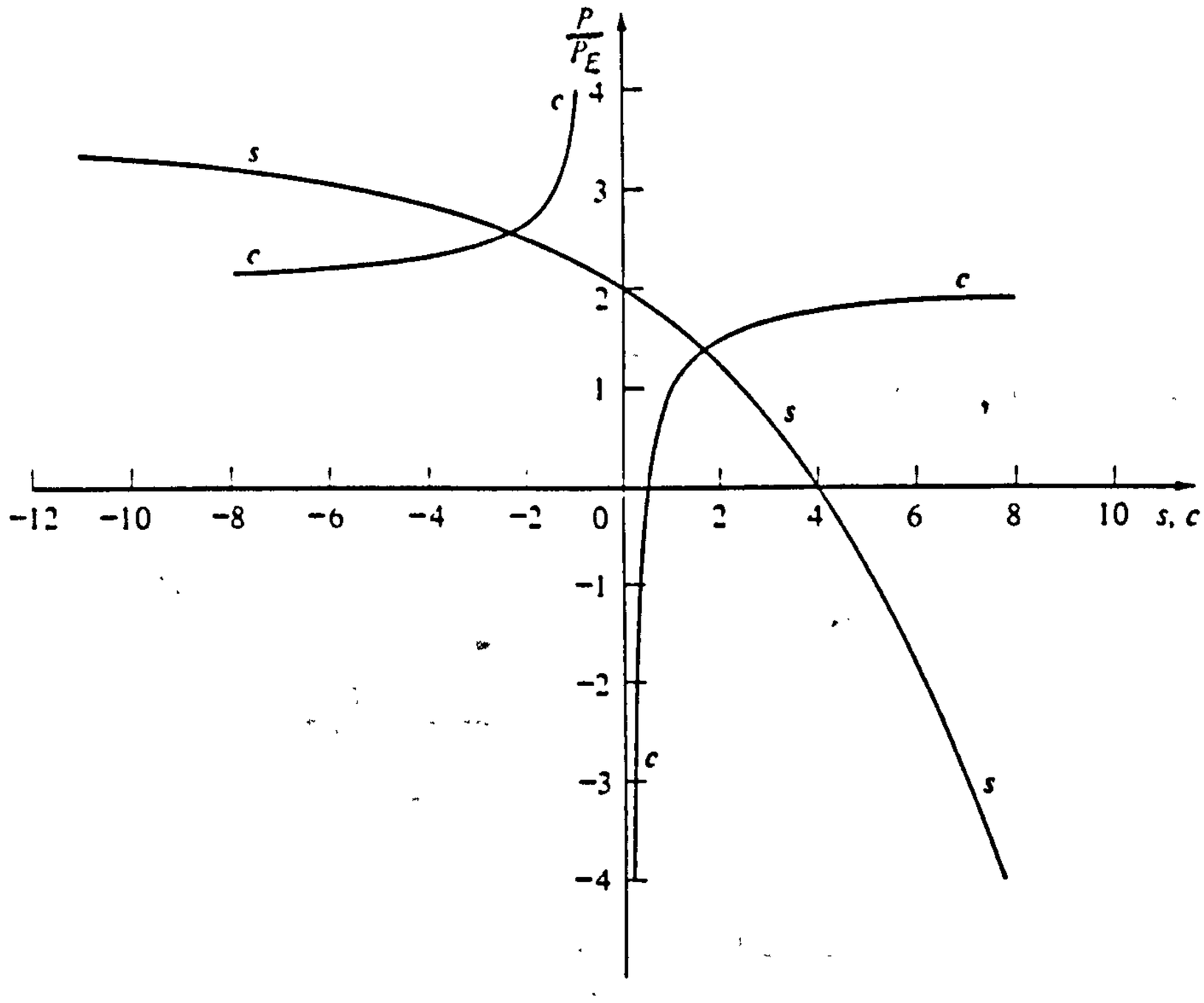

Fig. 1.2.1 Stability Functions (s and c).

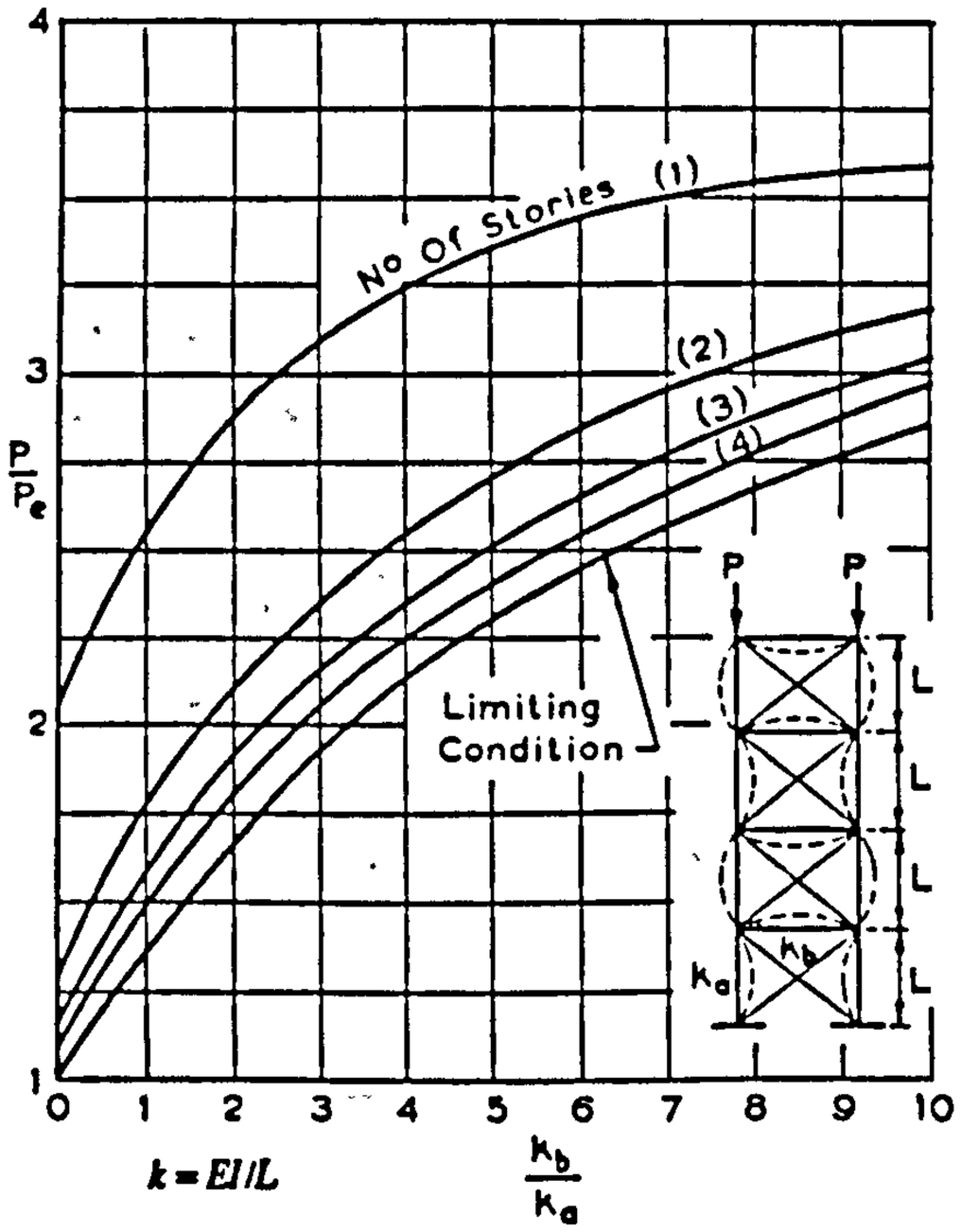

Fig. 1.2.2 Critical Load Limiting Condition.

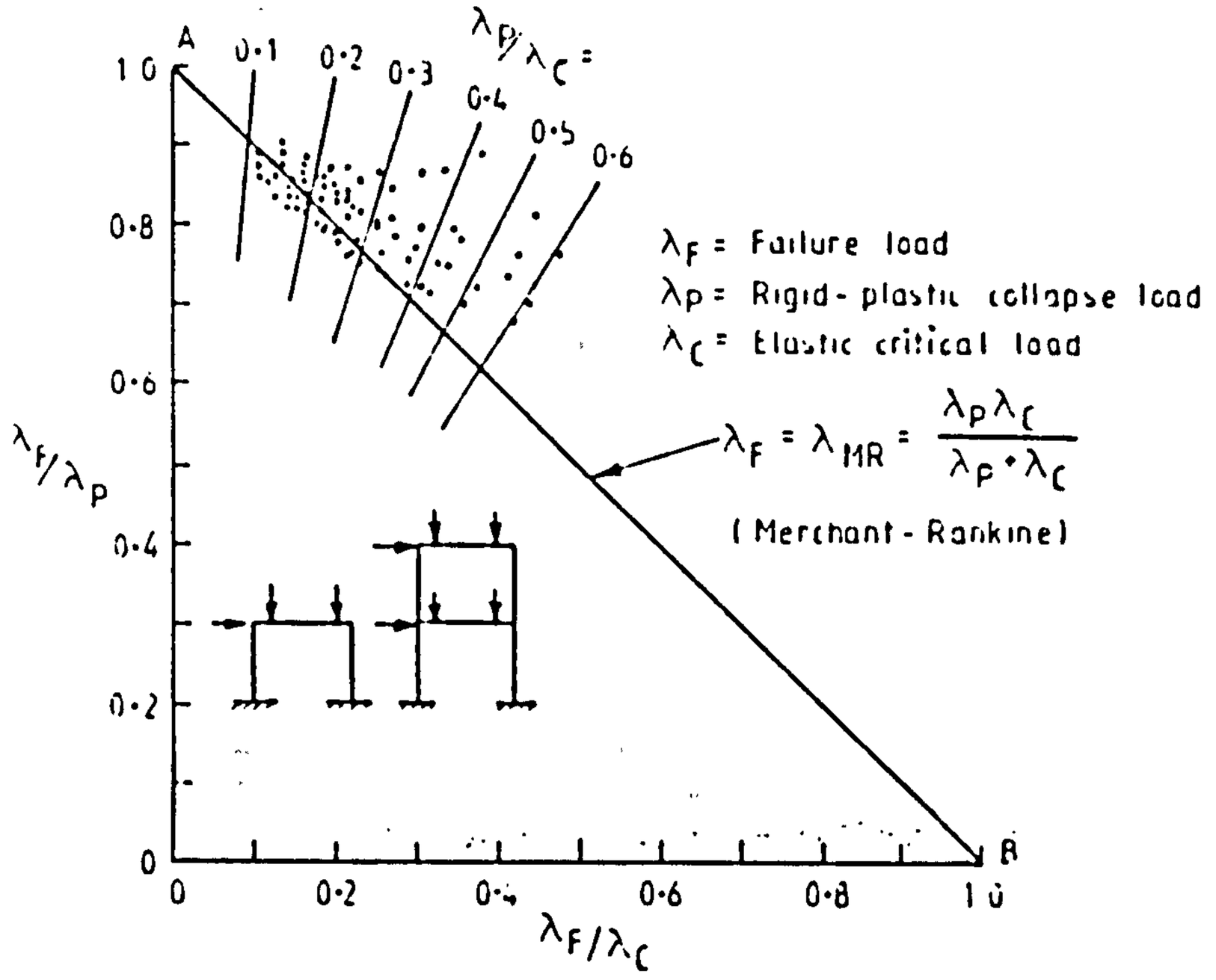

Fig. 1.2.3 The Merchant-Rankine Load compared with the Theoretical Load.

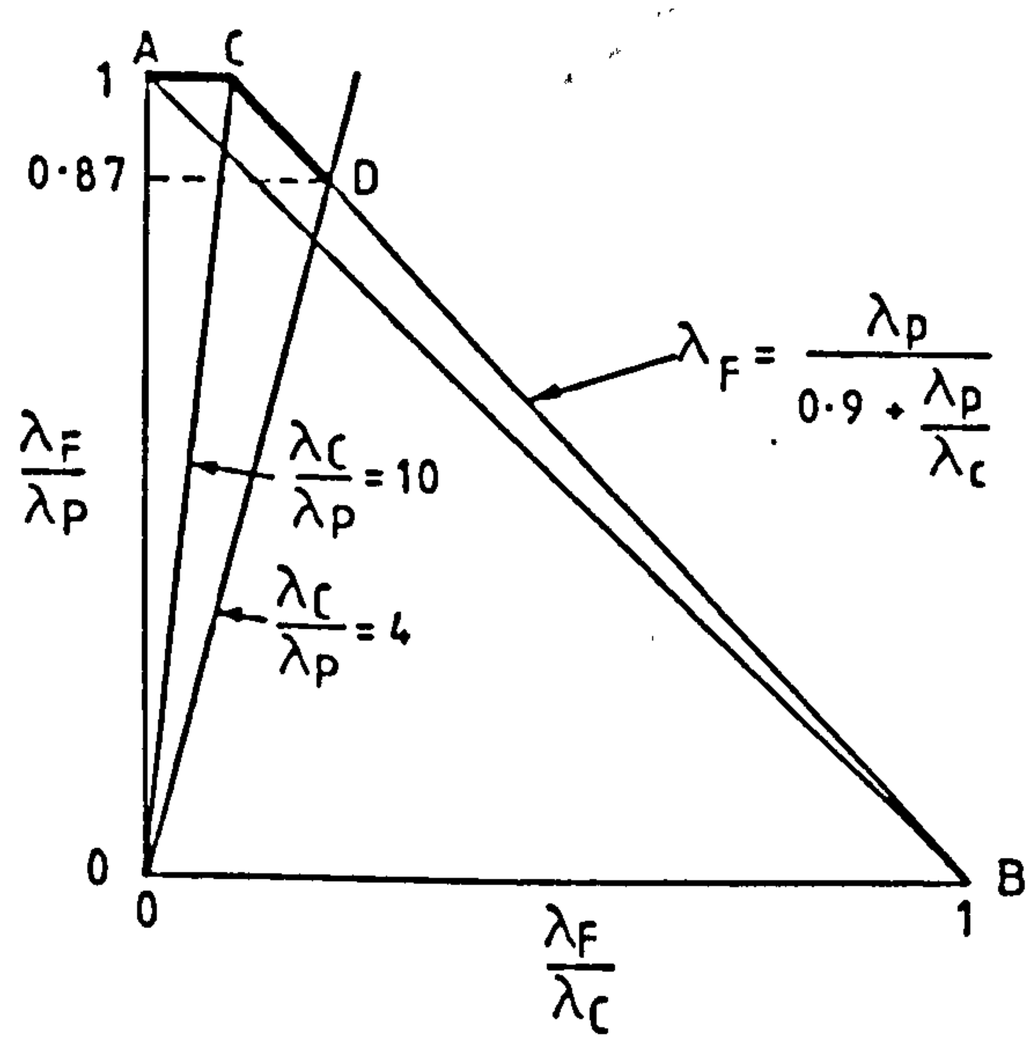

Fig. 1.2.4 Modified Merchant-Rankine Formula.

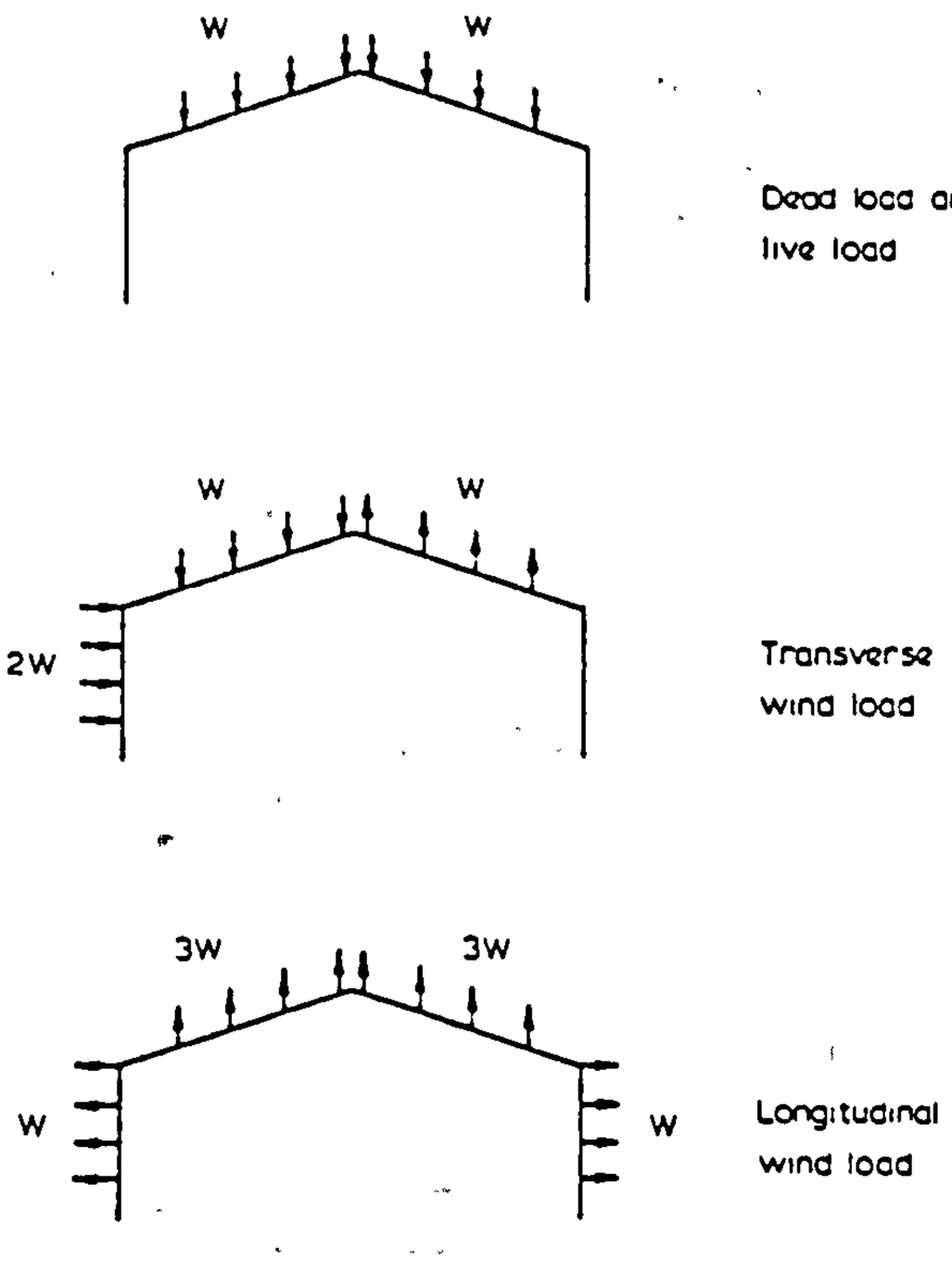

Fig. 1.2.5 Loading Patterns.

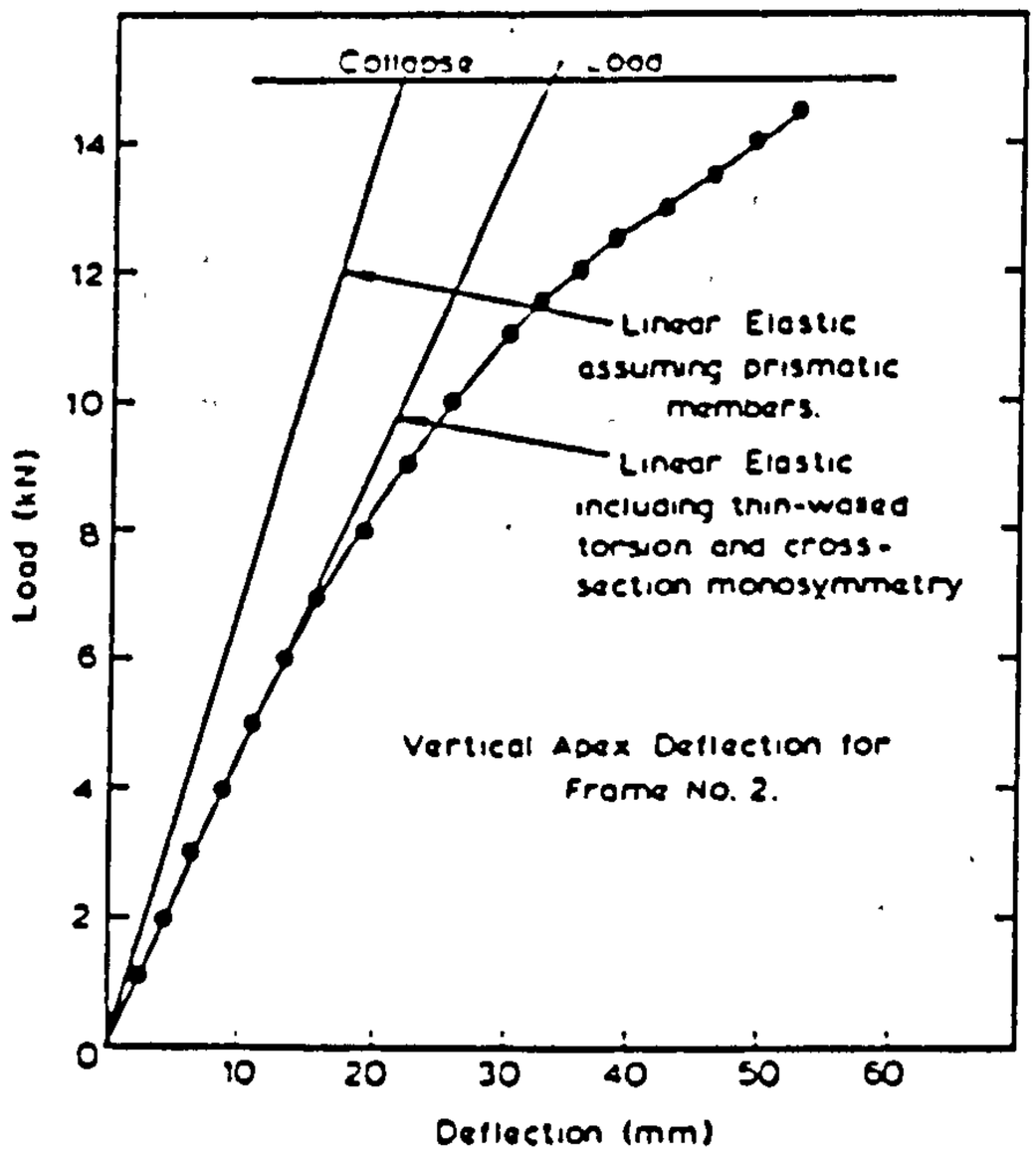

Fig. 1.2.6 Comparison between Theoretical Model and Frame Test Result.

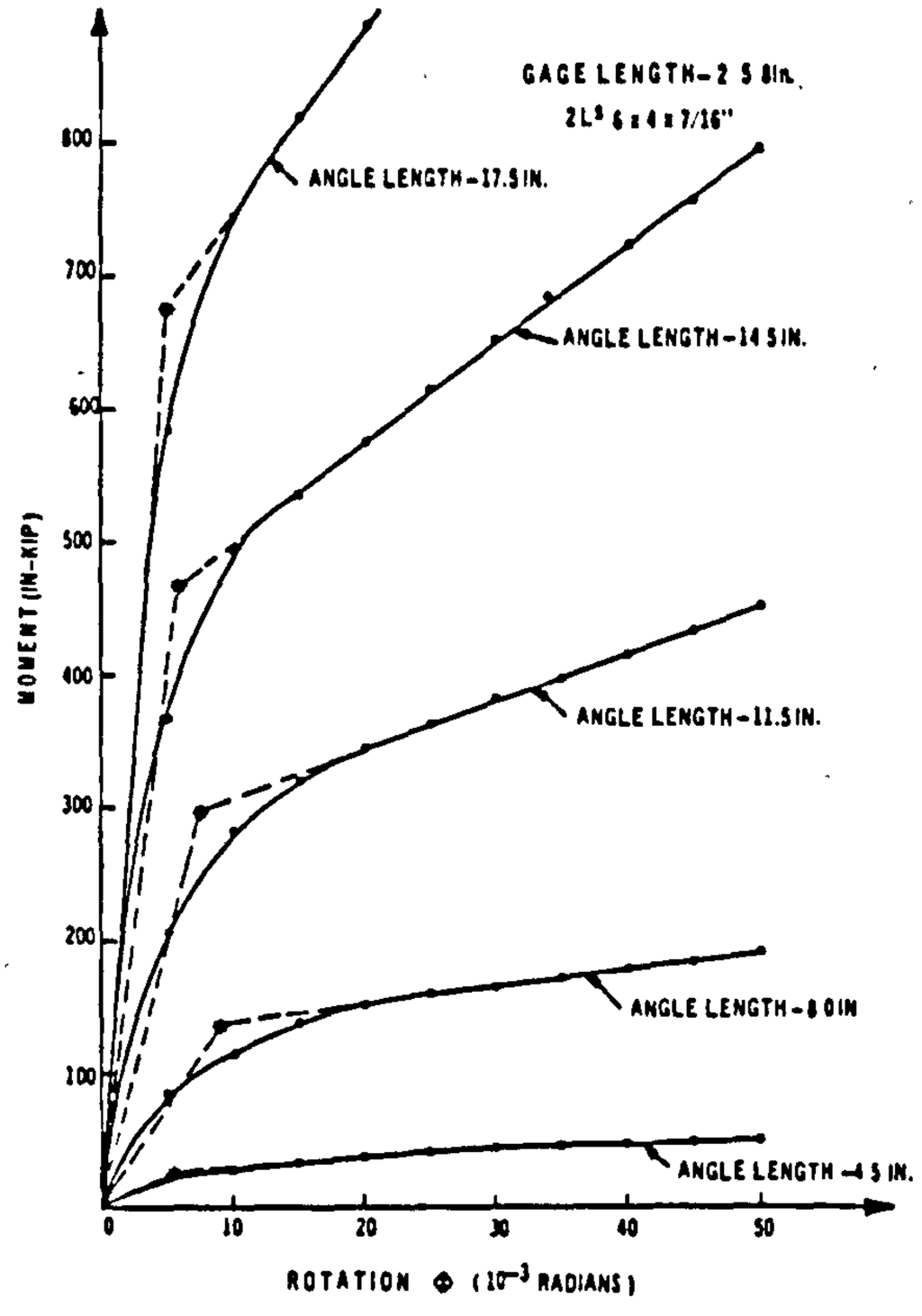

Fig. 1.3.1 Typical Moment-Rotation Curves for Range of Angle Lengths.

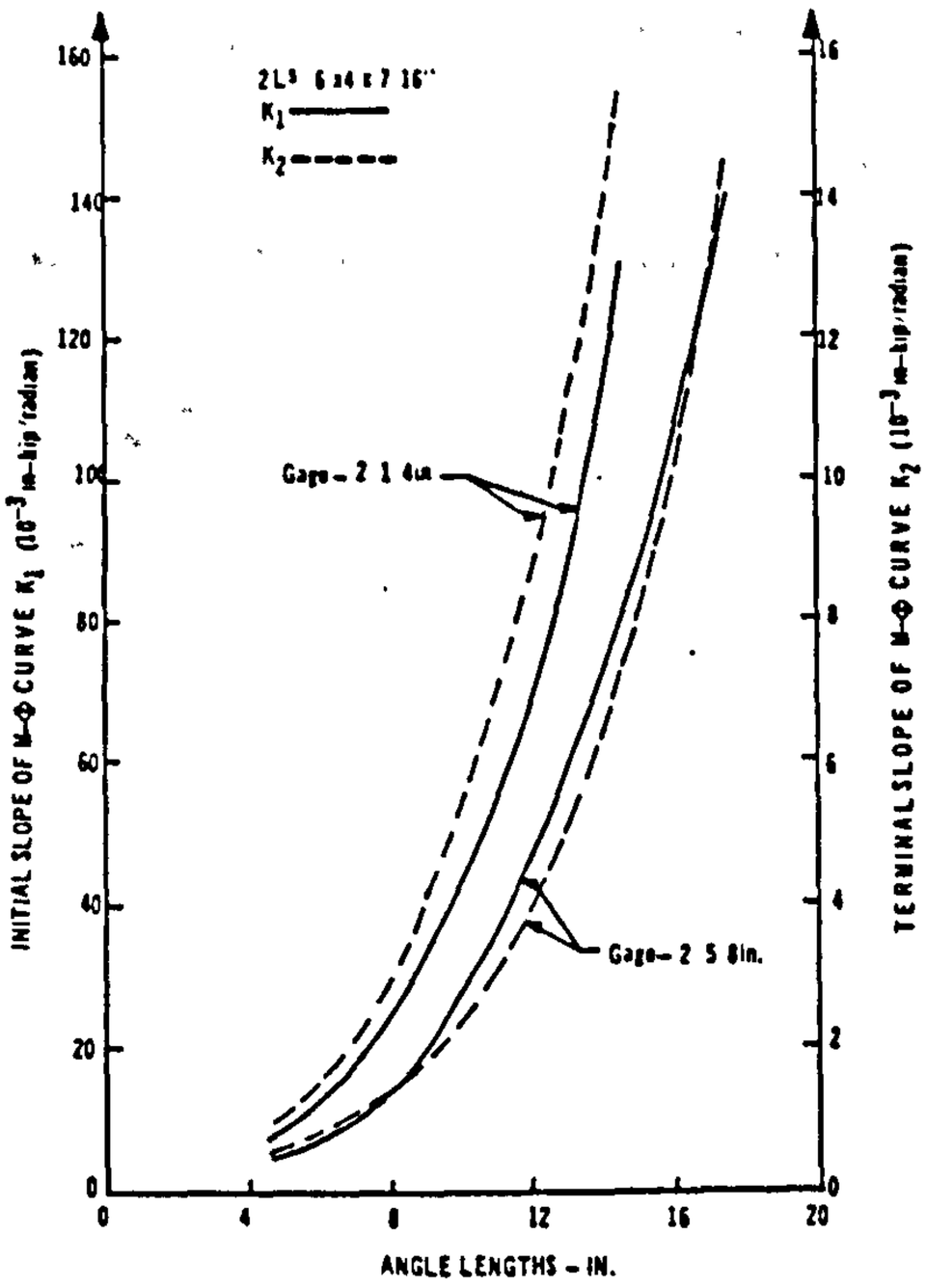

Fig. 1.3.2 Slopes on Bi-Linear Model as Function of Angle Lengths.

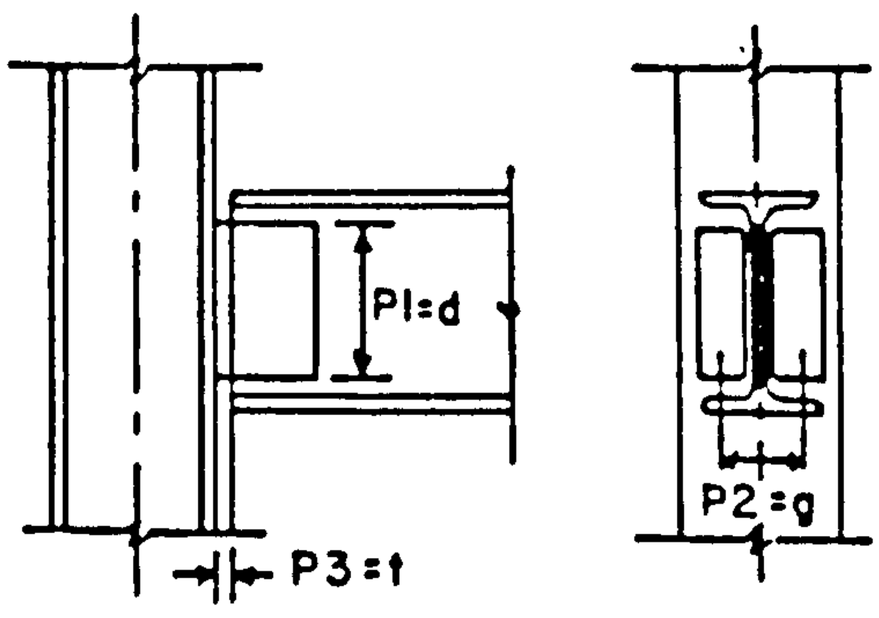

DOUBLE WEB ANGLE

(a)

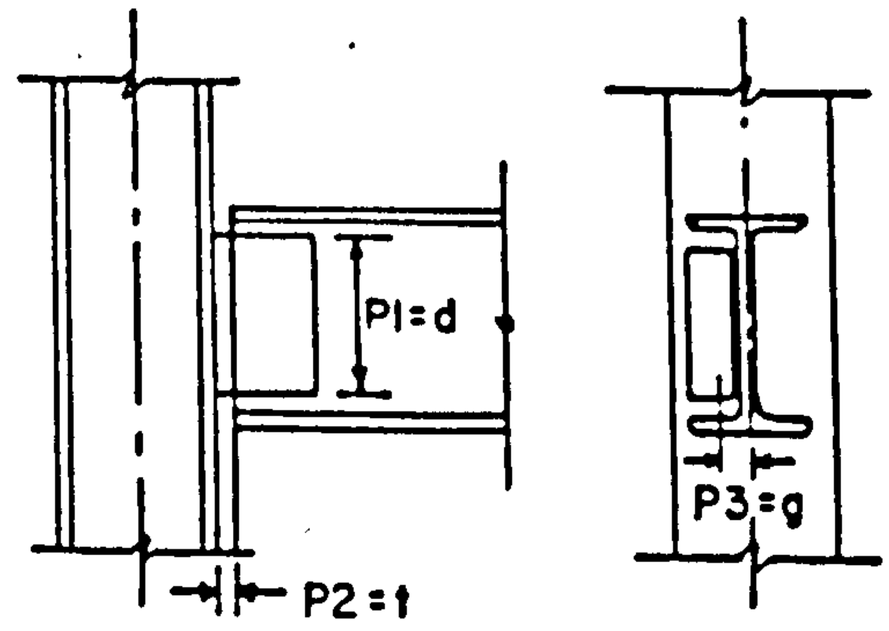

SINGLE WEB ANGLE

(b)

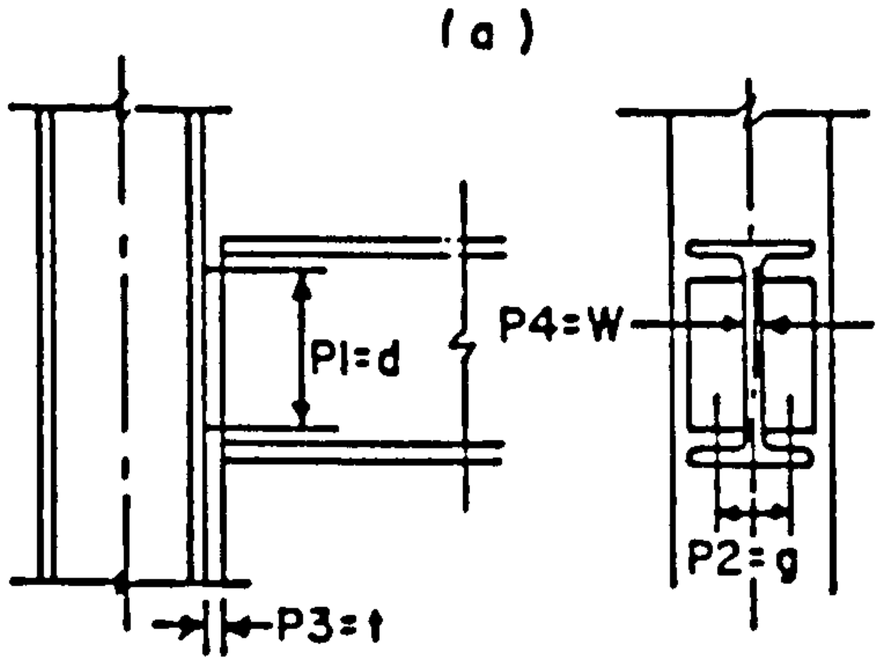

HEADER PLATE

(c)

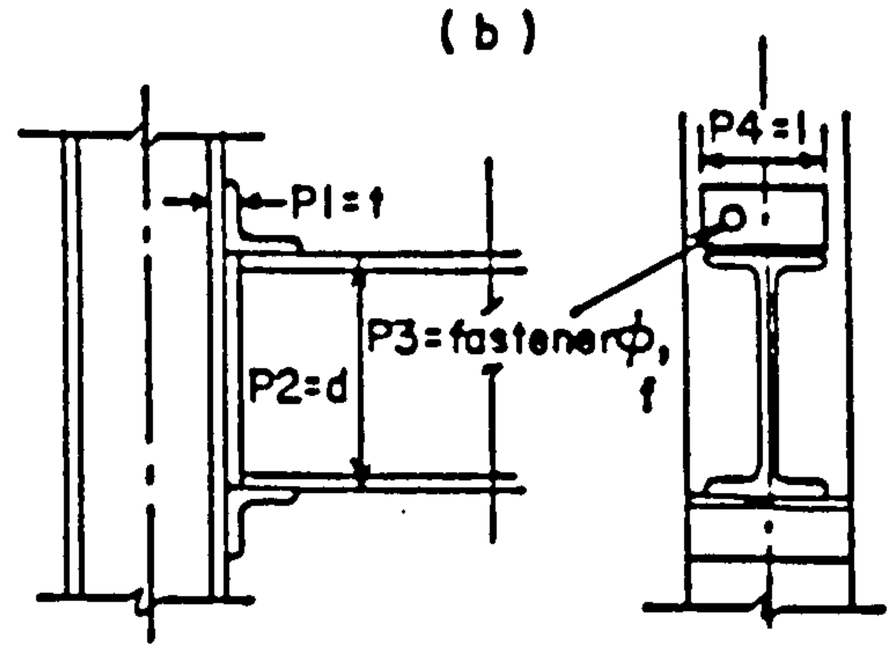

TOP AND SEAT ANGLE

(d)

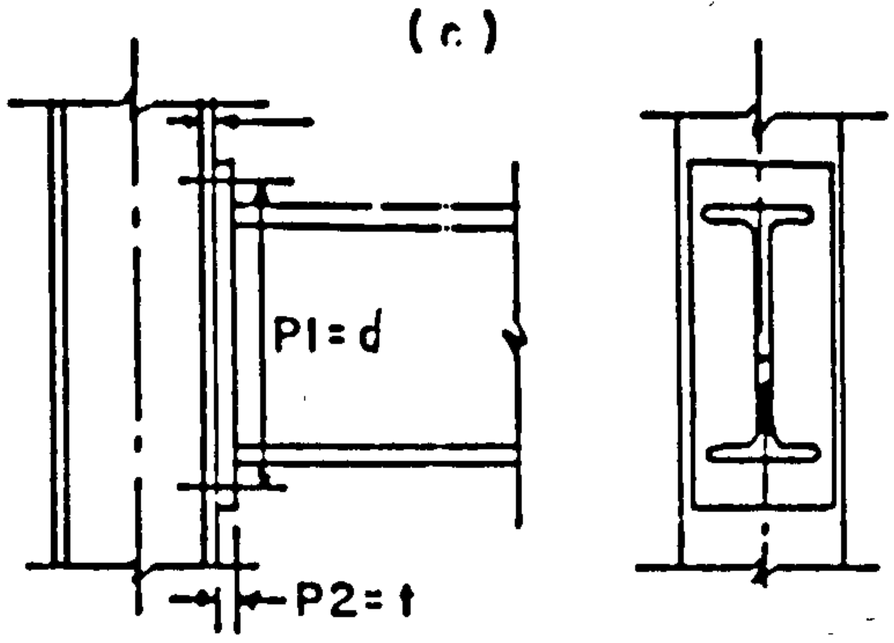

END PLATE NO COLUMN STIFFENERS

(e)

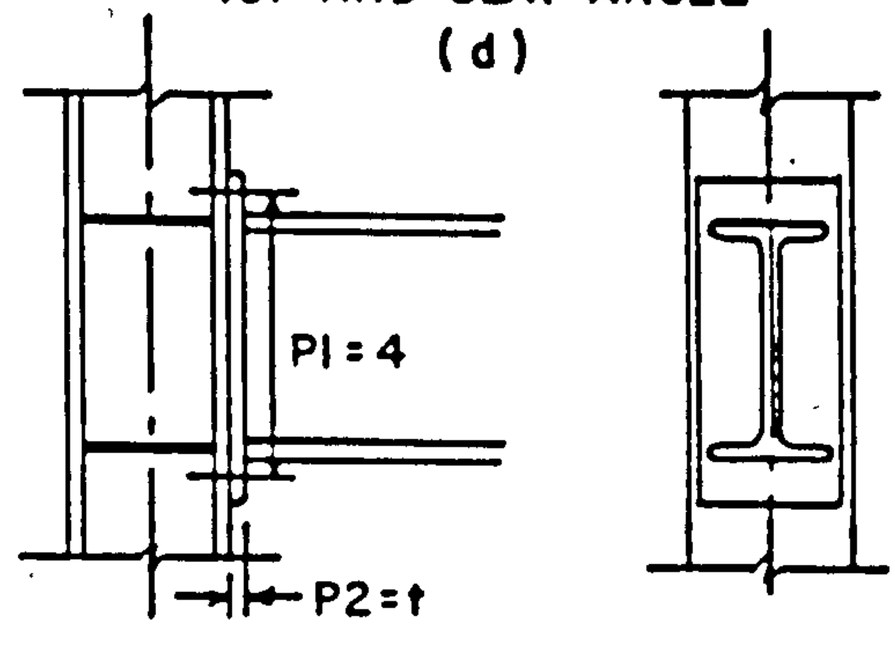

END PLATE COLUMN STIFFENERS

(f)

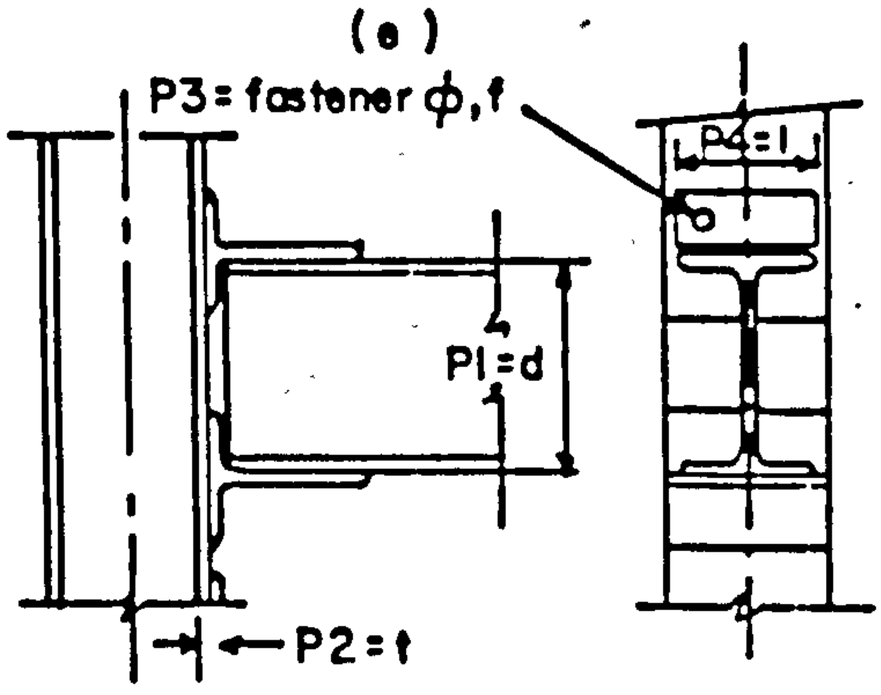

T-STUB

(g)

Fig. 1.3.3 Connection Types and Standardization Parameters.

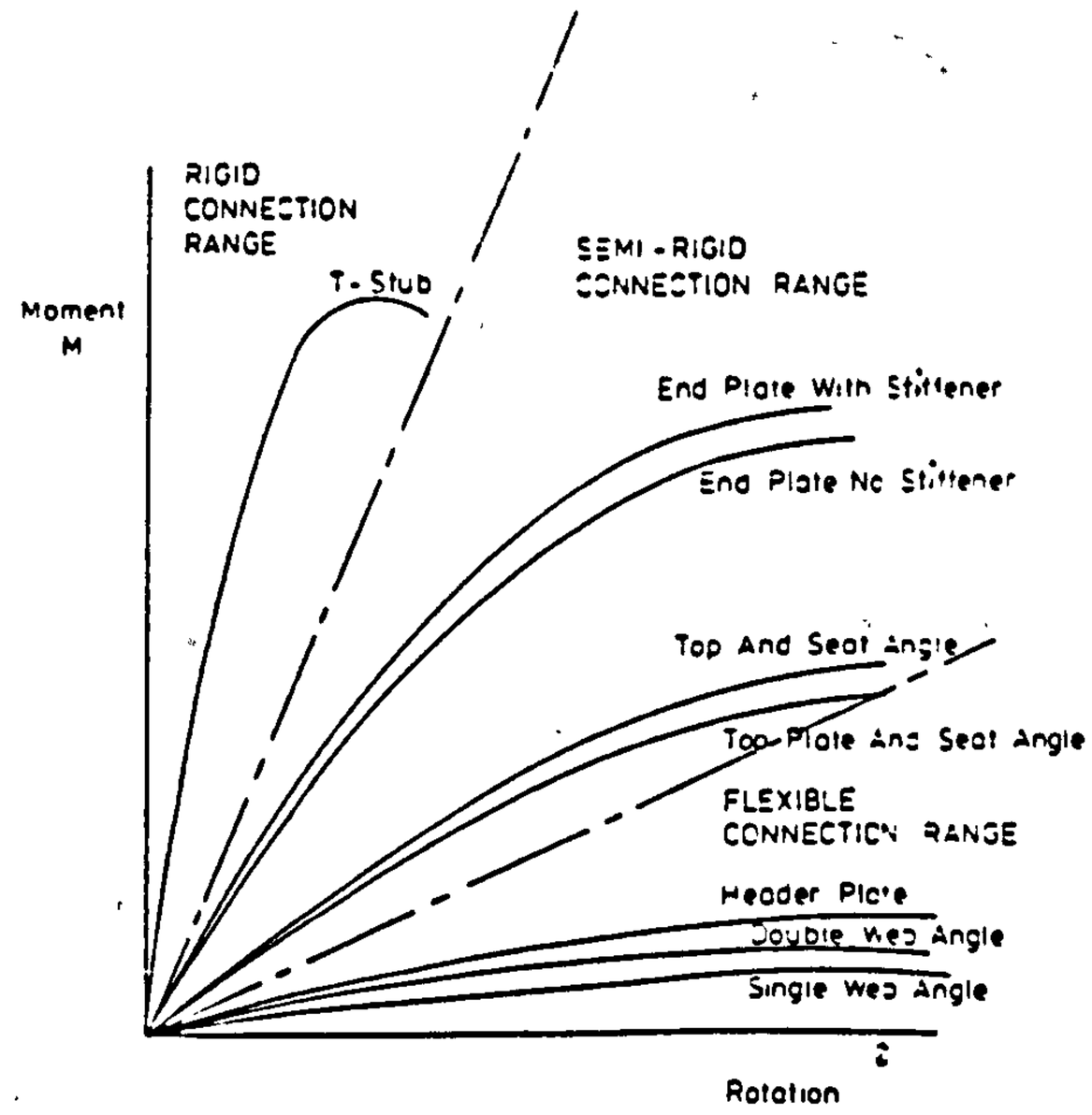

Fig. 1.3.4 Typical Moment-Rotation Curves.

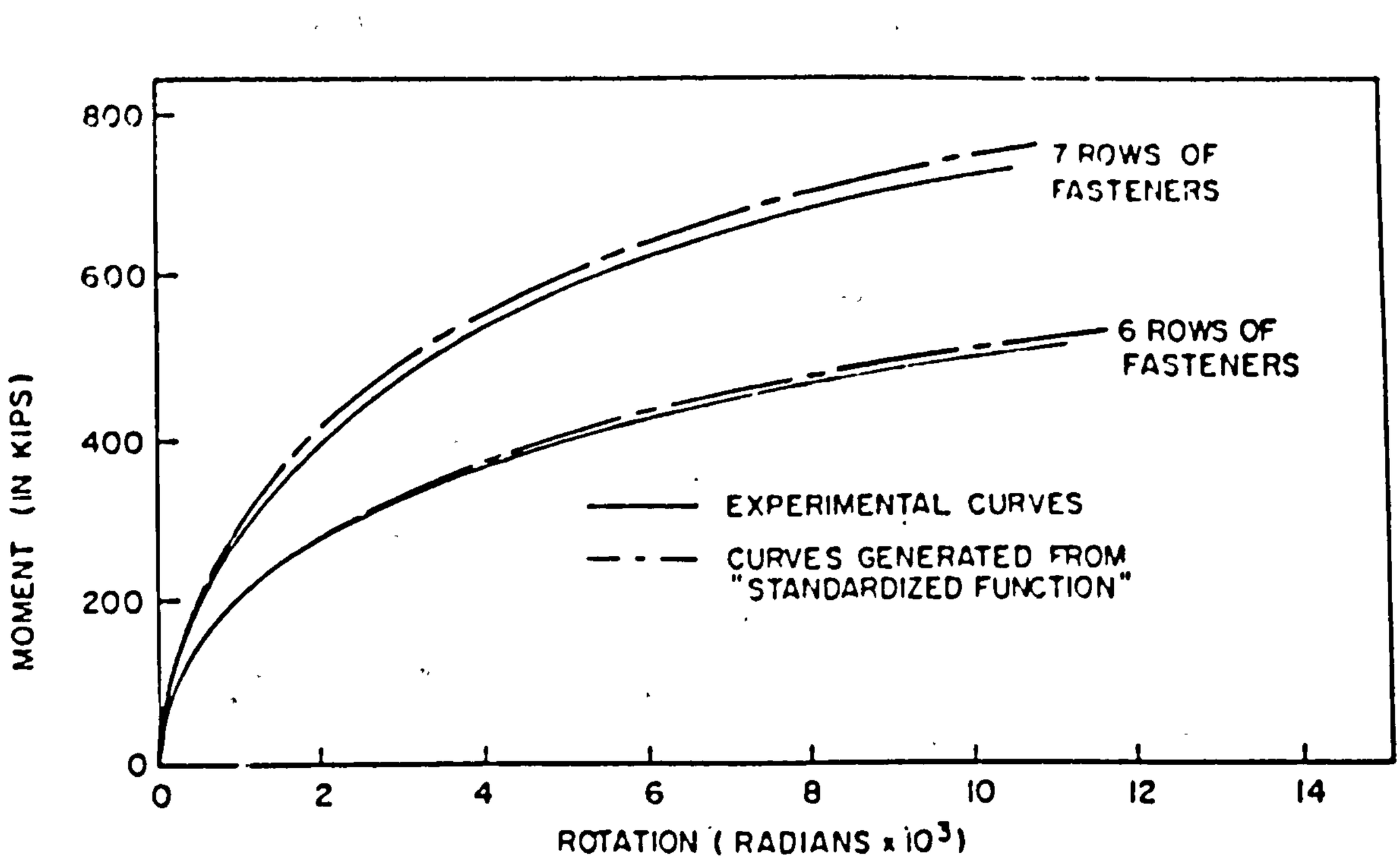

Fig. 1.3.5 Comparison of Moment-Rotation Curves for Double Web Angle Connections.

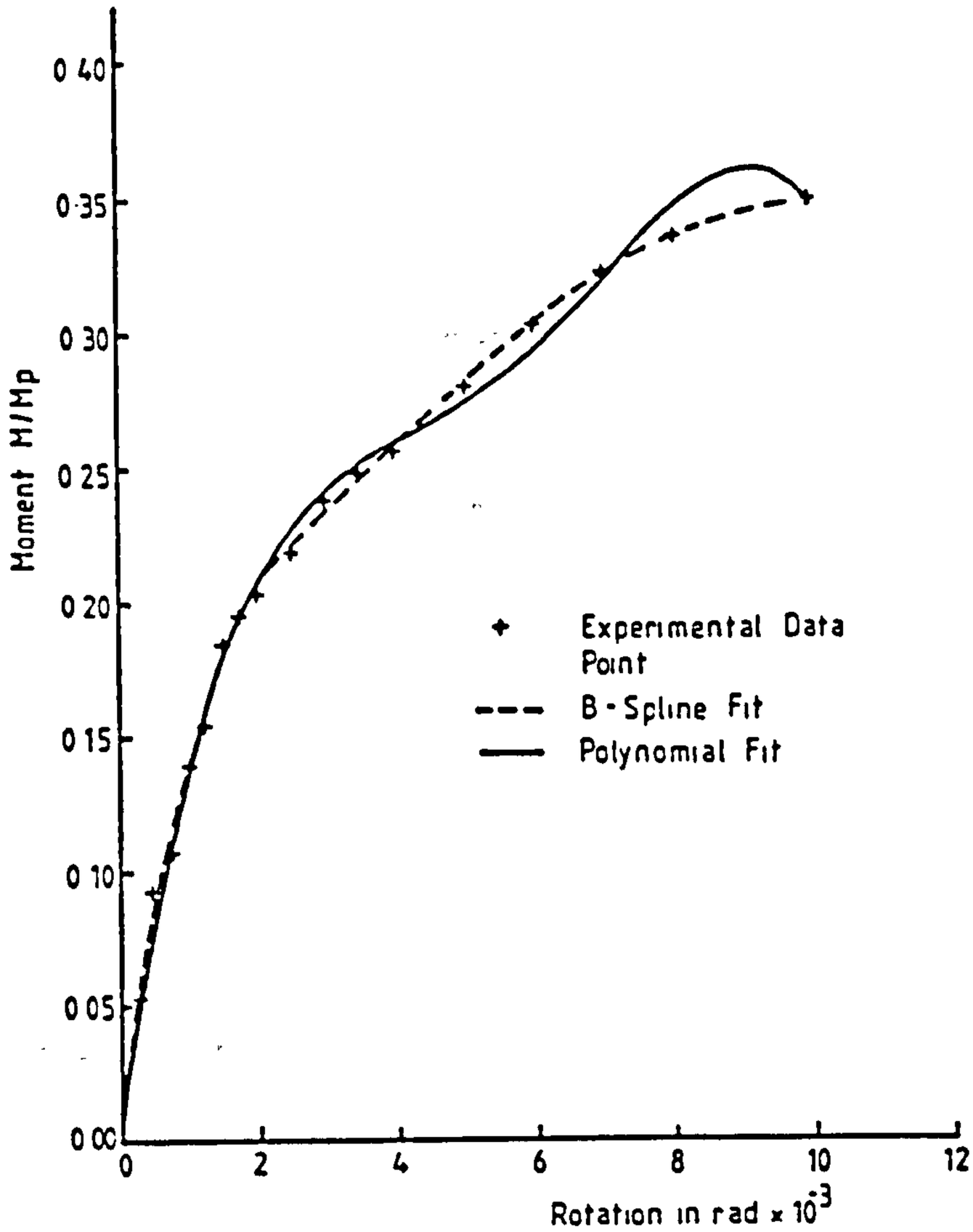

Fig. 1.3.6 B-Spline and Polynomial Curve Fits Comparison.

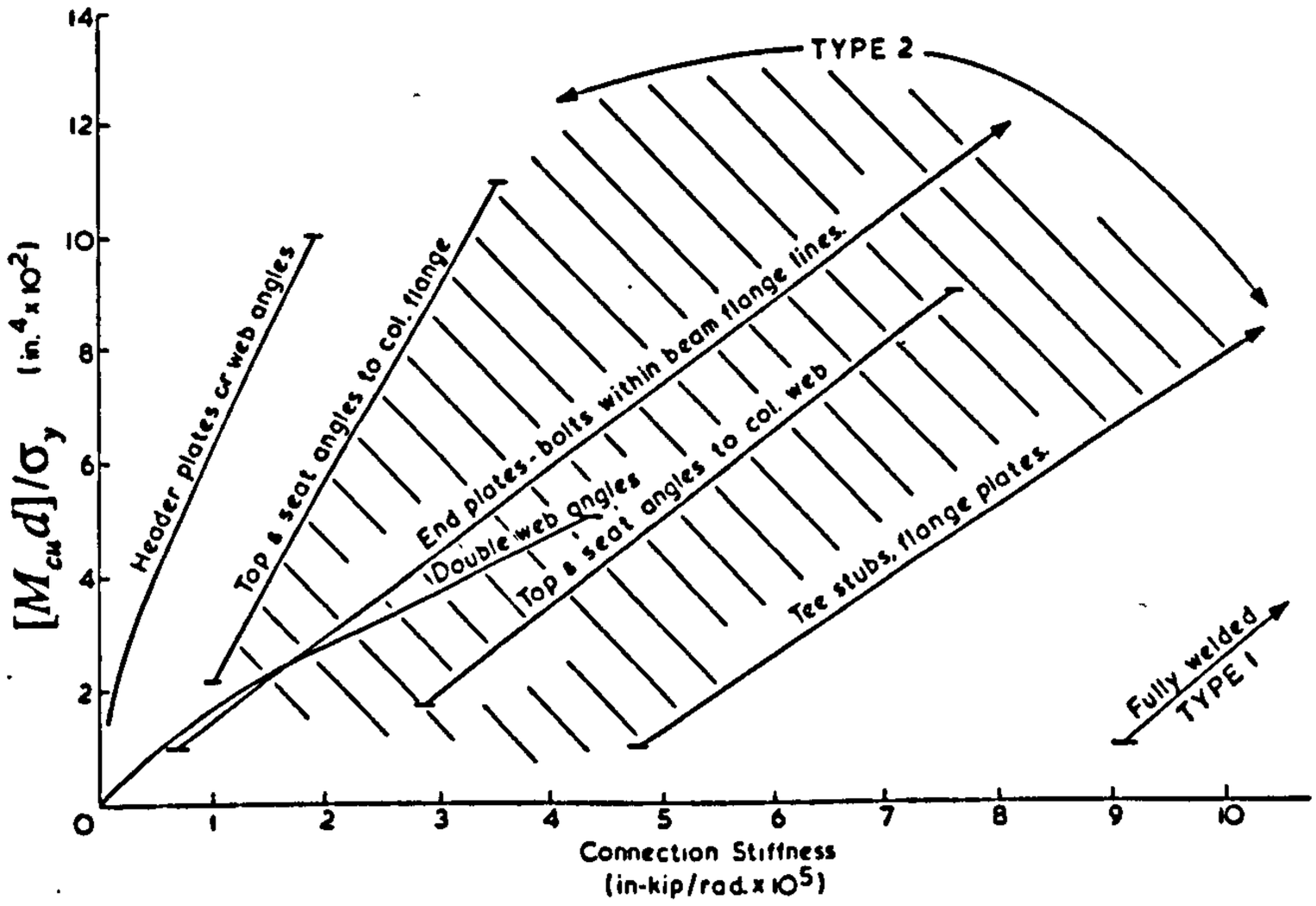

Fig. 1.3.7 Relation between Connection Strength and Stiffness.

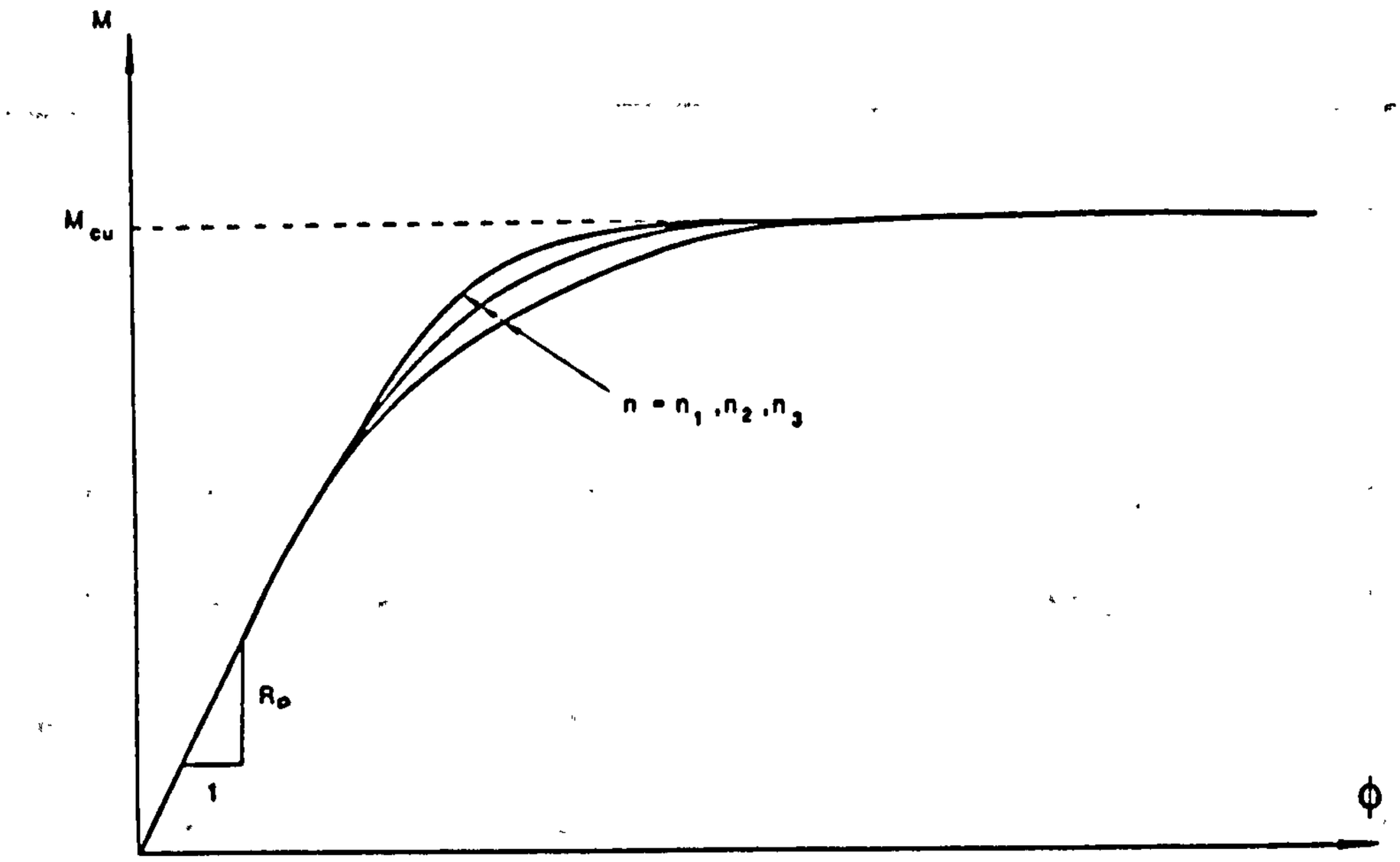

Fig. 1.3.8 Parameters of the Colson's Power Model.

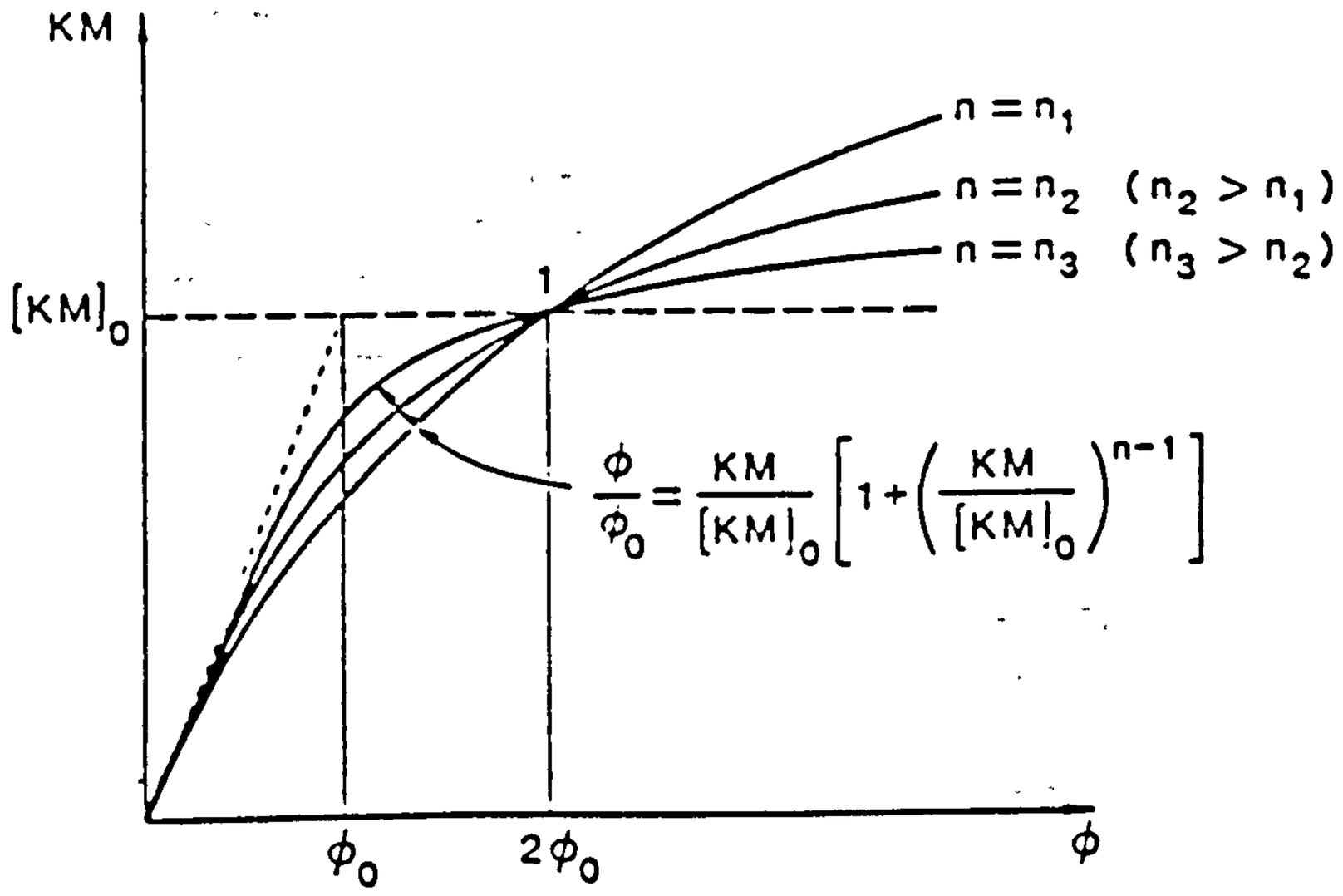

Fig. 1.3.10 Ramberg-Osgood Function for Moment-Rotation Curves.

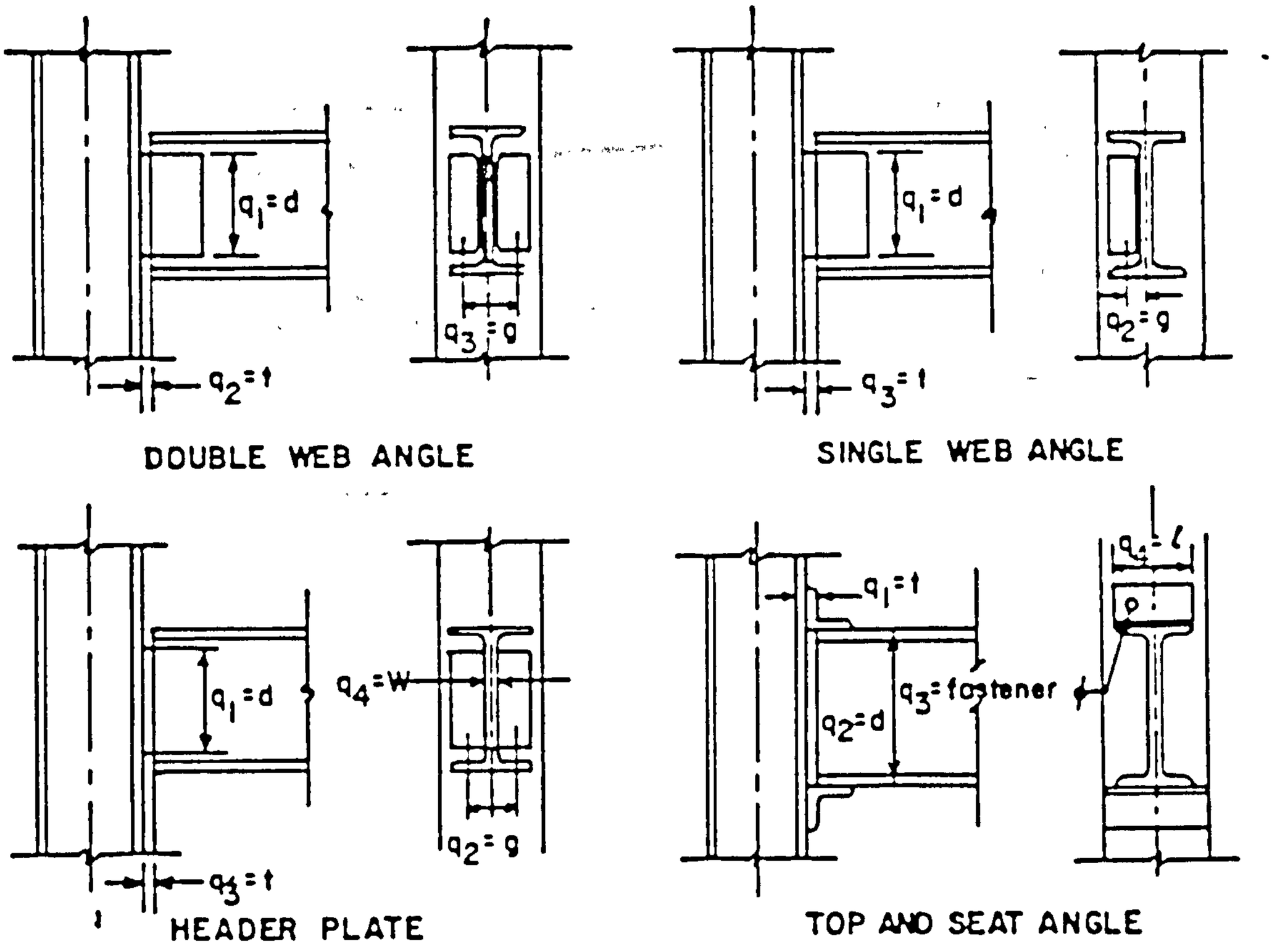

Fig. 1.3.9 Connection Types and Standardization Parameters.

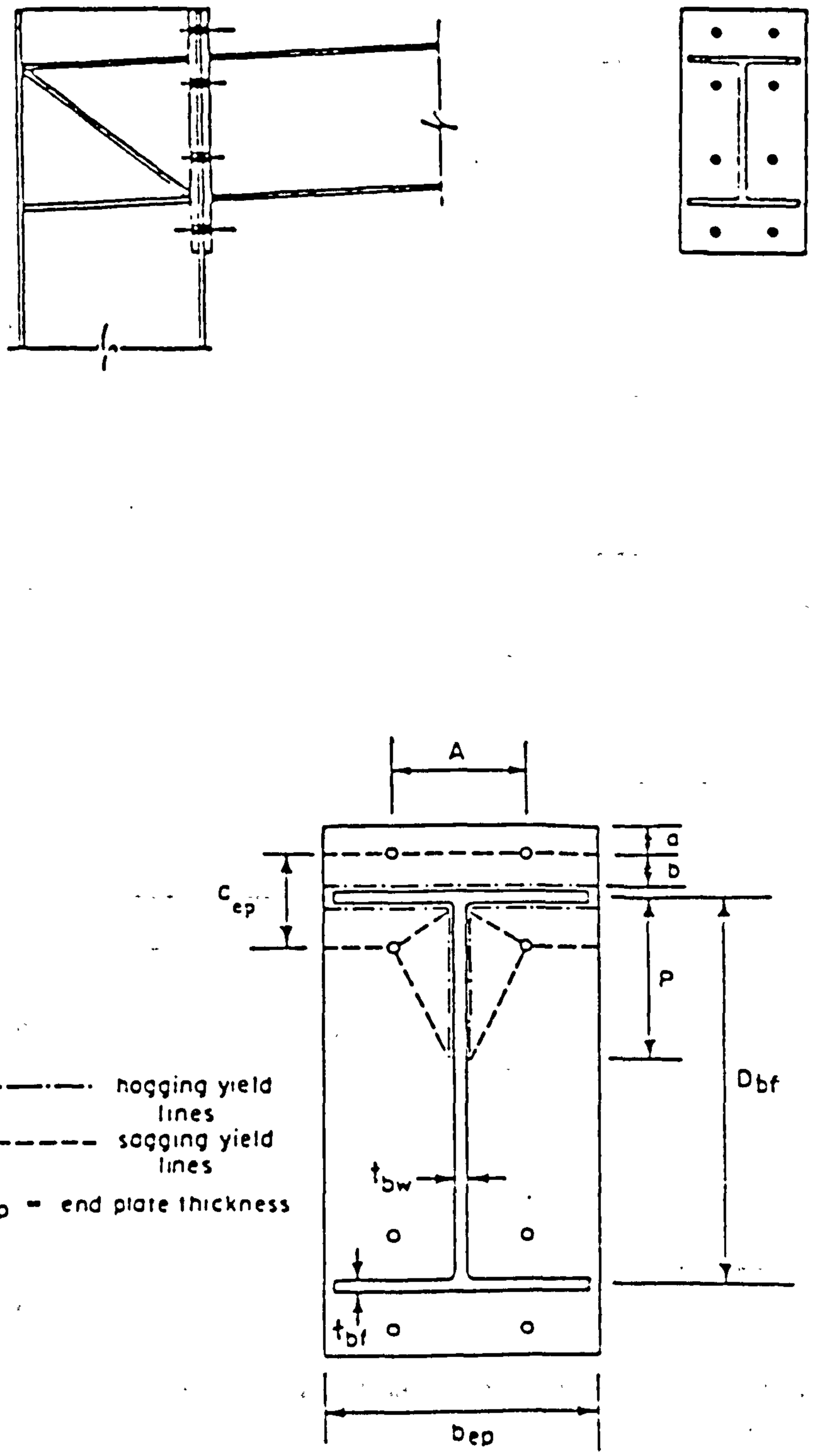

Fig. 1.3.11 Bolted Extended End Plate Eave Connection-Column Stiffened.

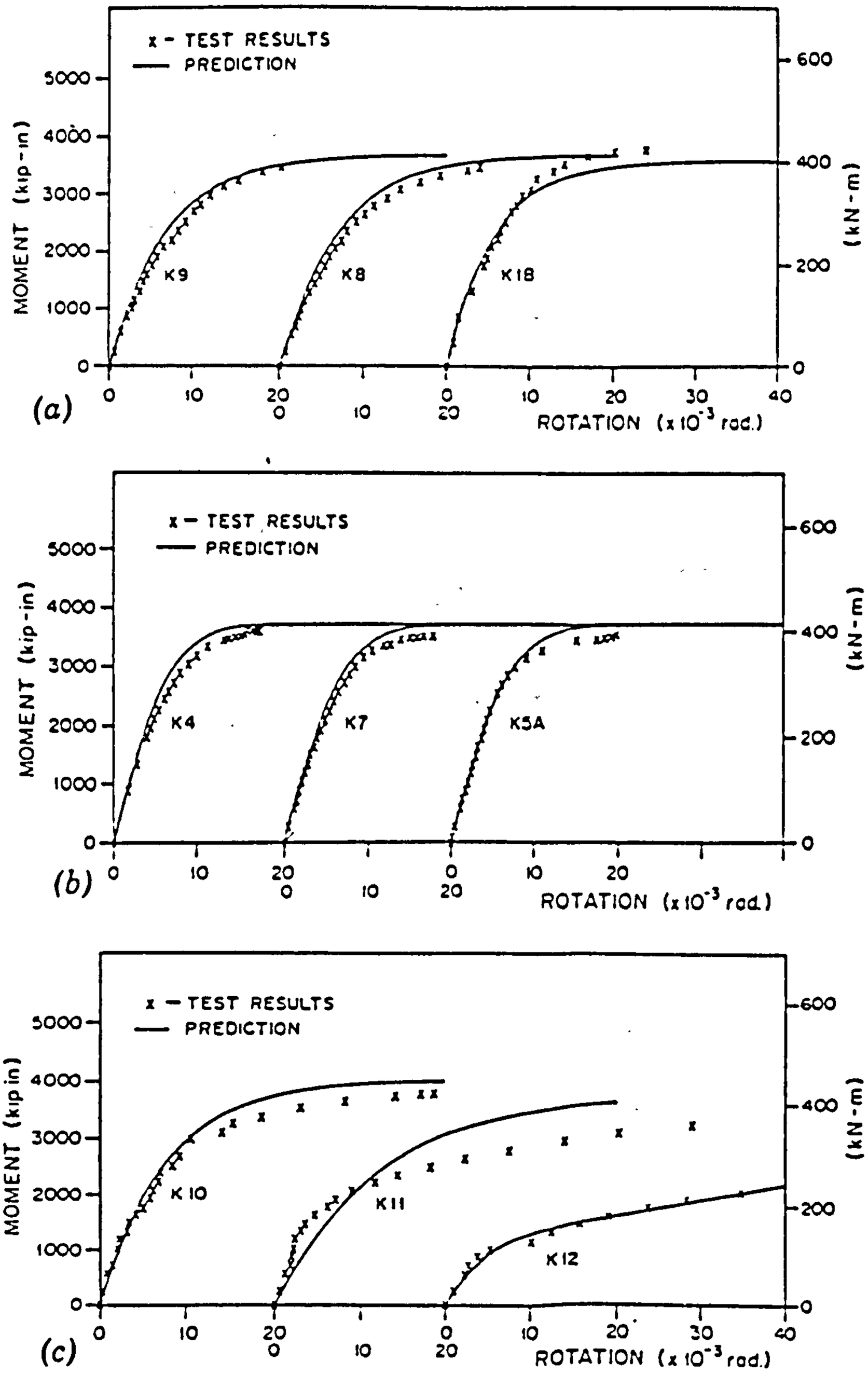

(*a*) Comparison between Test and Prediction Results of Specimens K9, K8 and K1B; (*b*) Comparison between Test and Prediction Results of Specimens K4, K7 and K5A (Fully Tensioned Bolts); (*c*) Comparison between Test and Prediction Results of Specimens K10, K11 and K12

Fig. 1.3.12

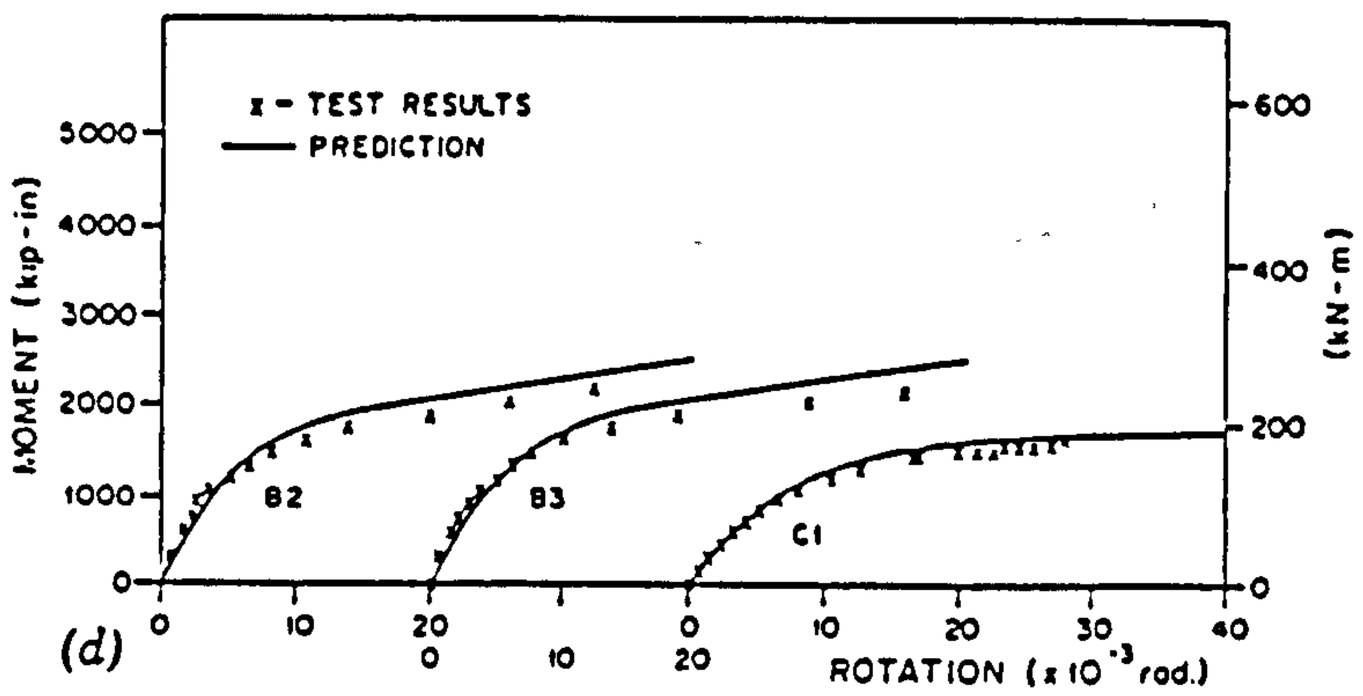

(*d*) Comparison between Test and Prediction Results of Specimens B2, B3 and C1; (*e*) Comparison between Test and Prediction Results of Specimens D2, D1 and C2 (No Stiffeners)

Fig. 1.3.13

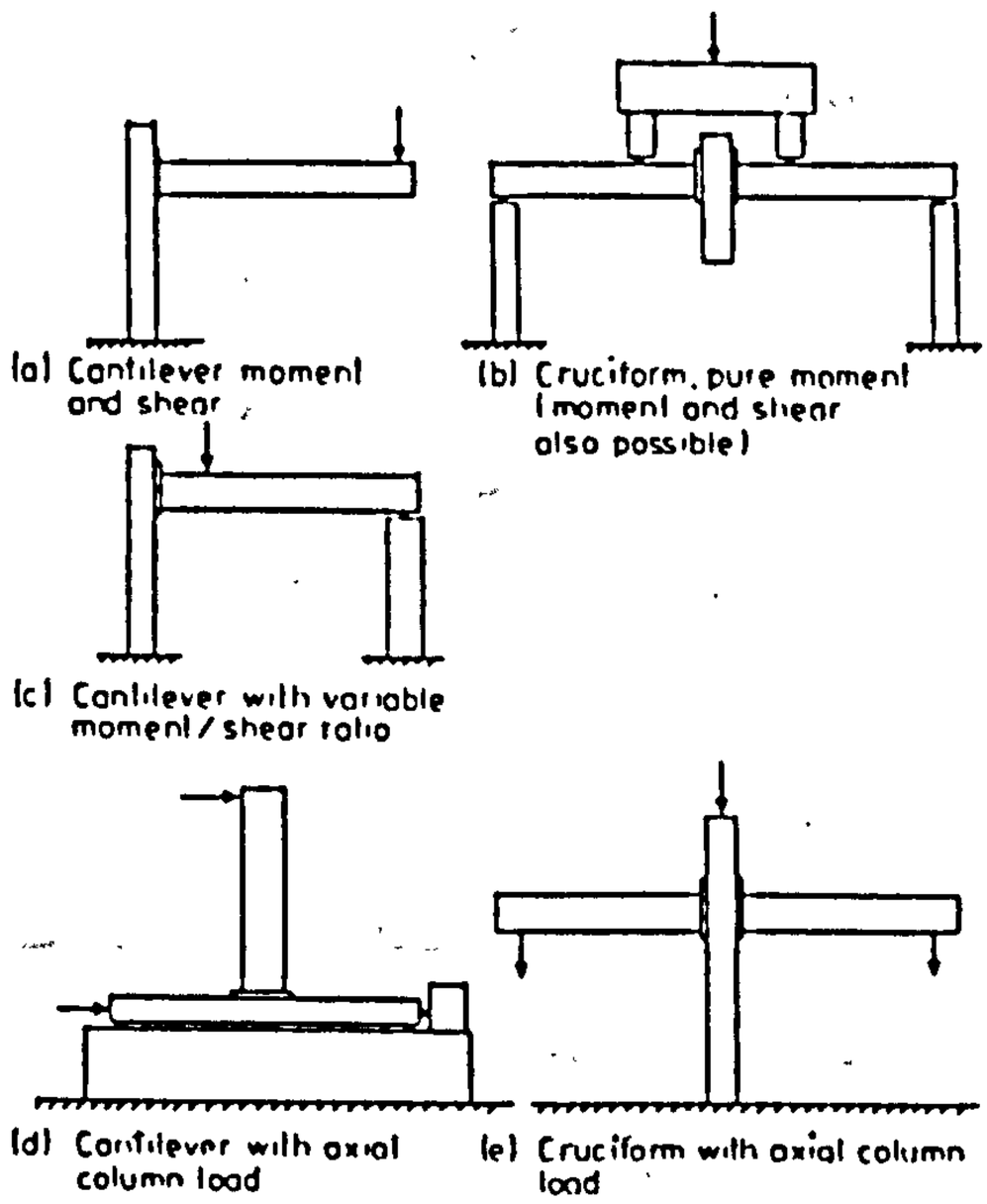

Fig. 1.3.14 Joint Tests Arrangements.

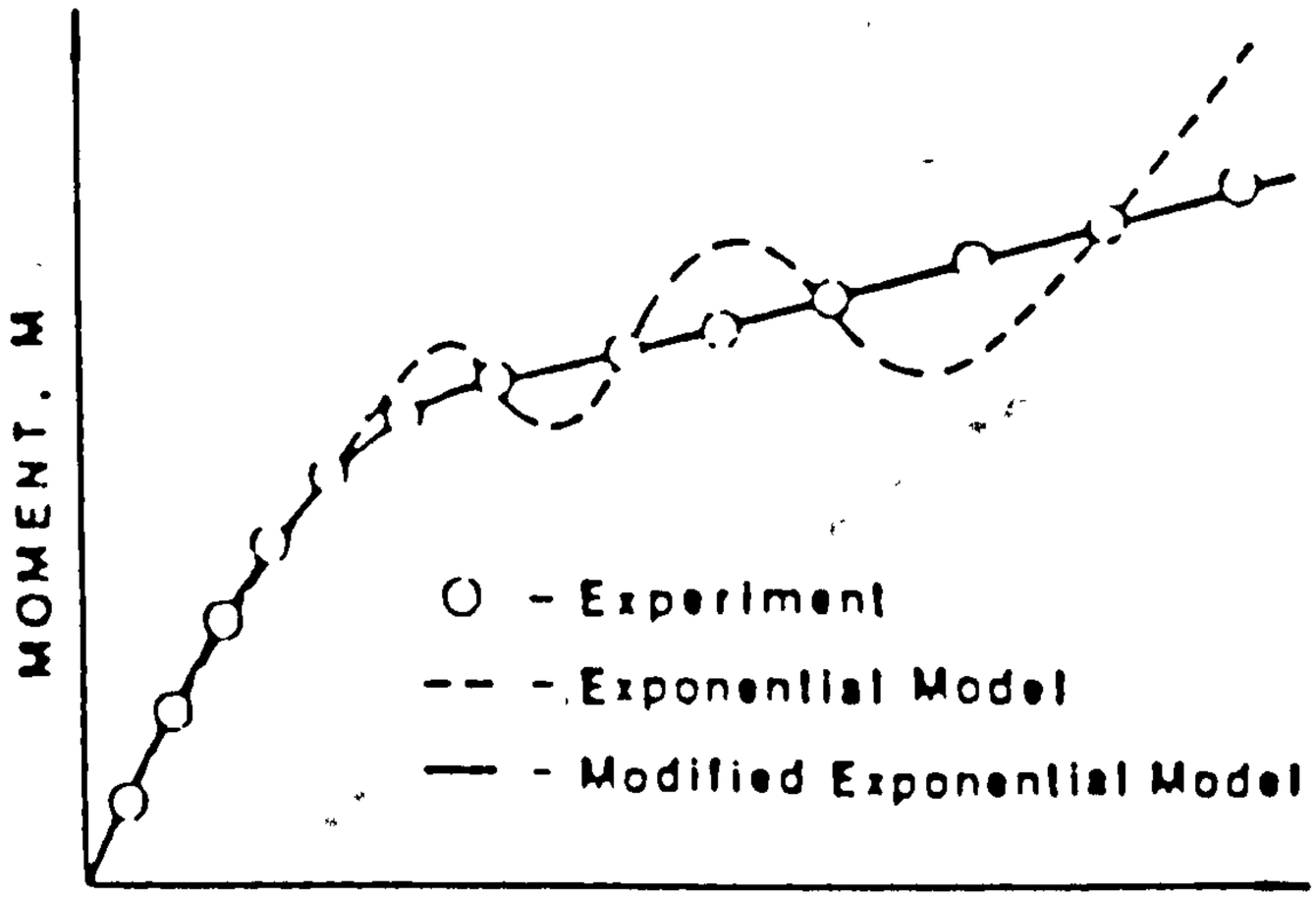

Fig. 1.3.15 Comparison between Results by Exponential and Modified Exponential Models for Moment-Rotation Data including a Linear Term.

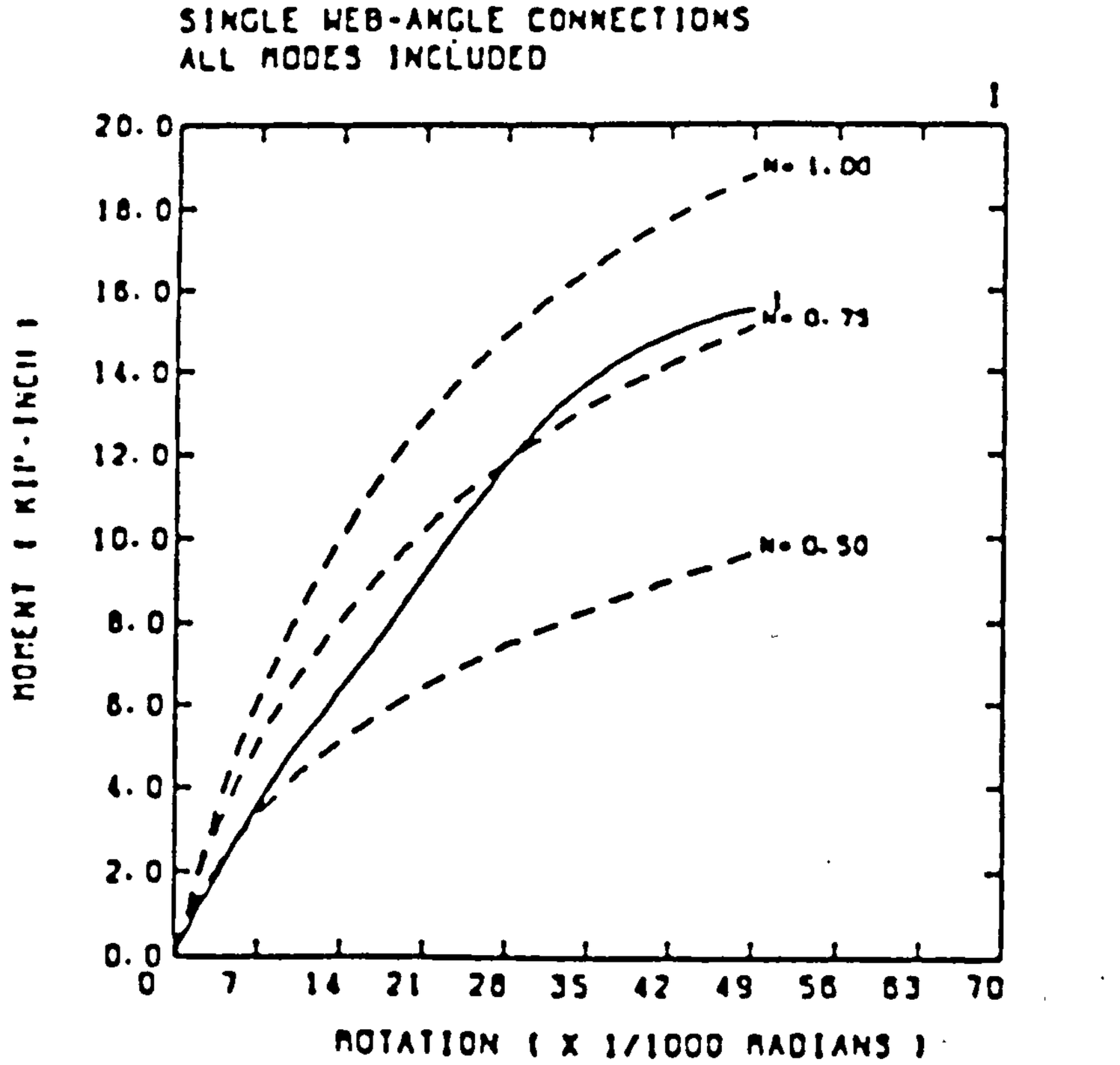

Fig. 1.3.16 Comparison Figures to Determine Appropriate Value of n of Power Model.

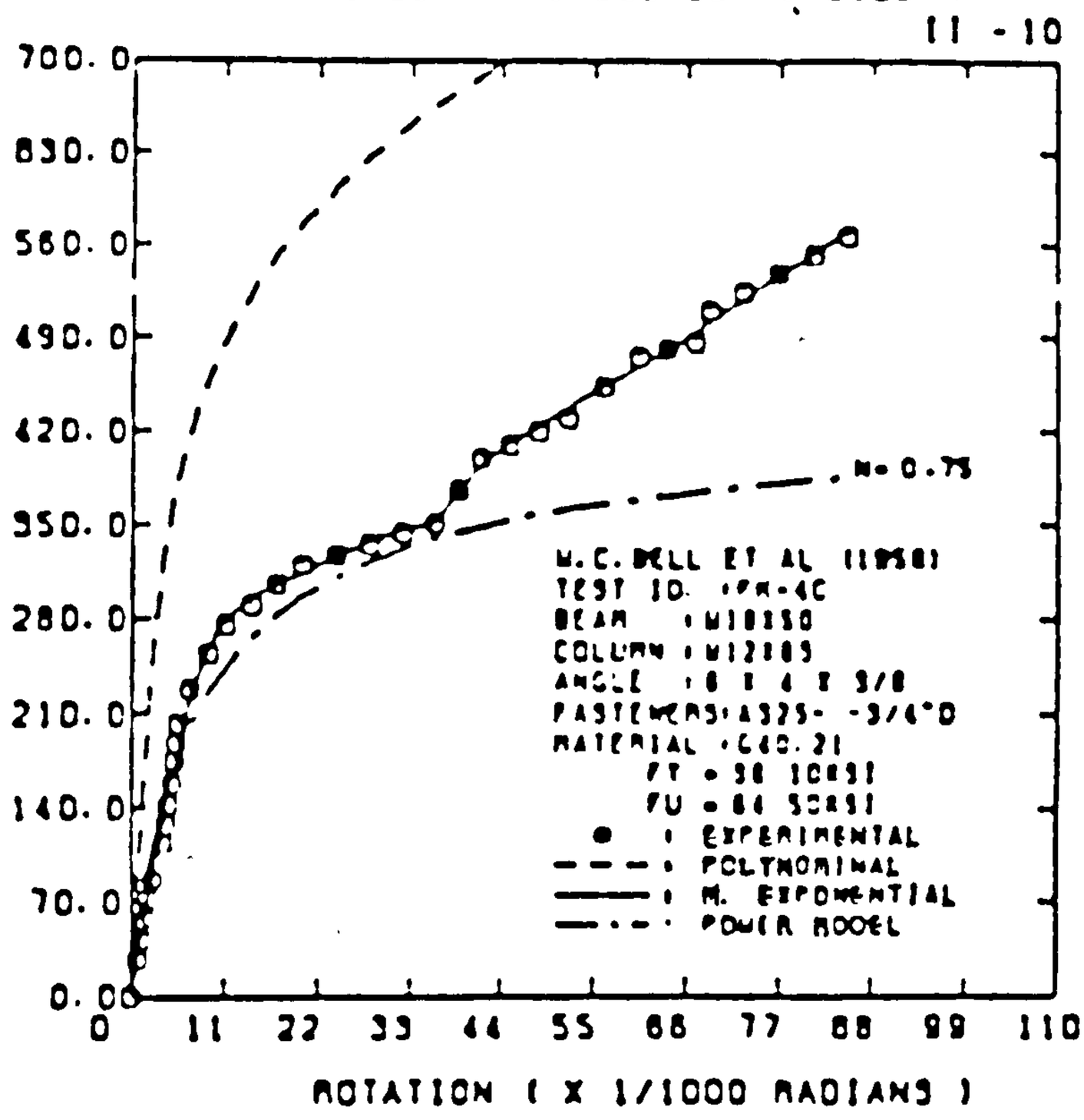

Fig. 1.3.17 Comparison of Experimental and Theoretical Results.

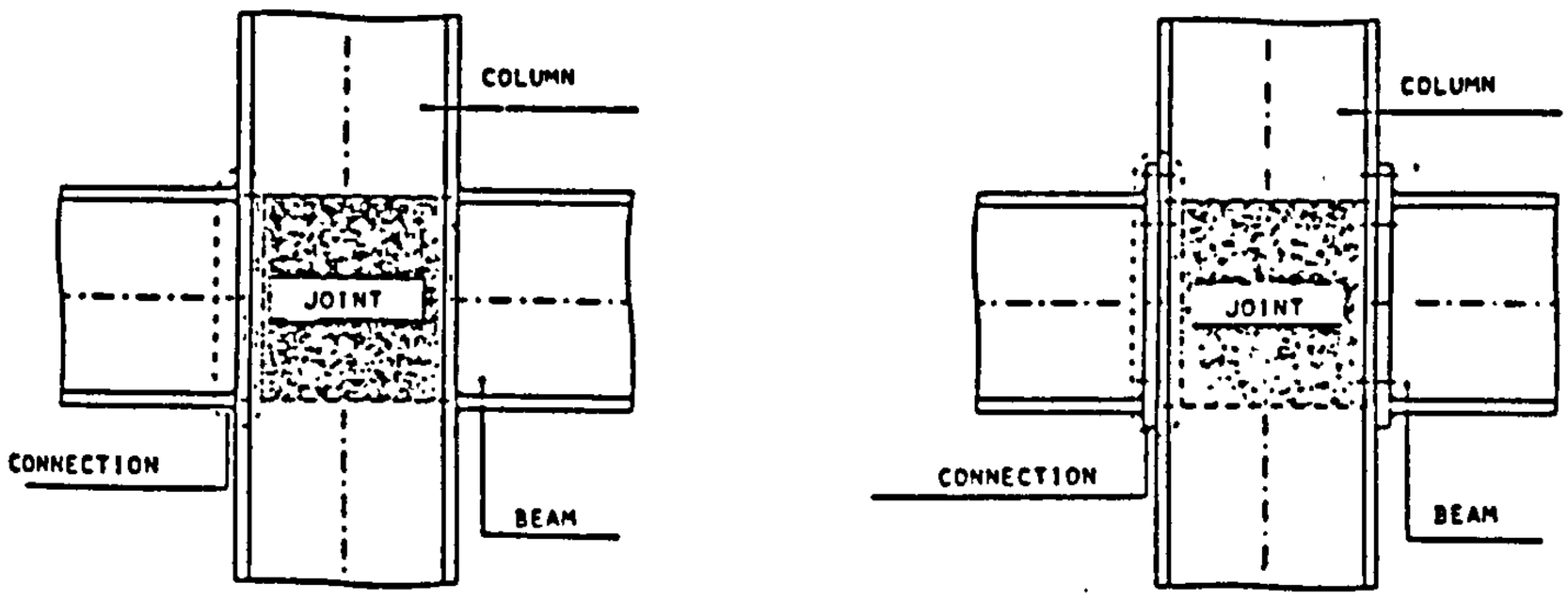

Fig. 1.3.18 Macroscopic View of Joint.

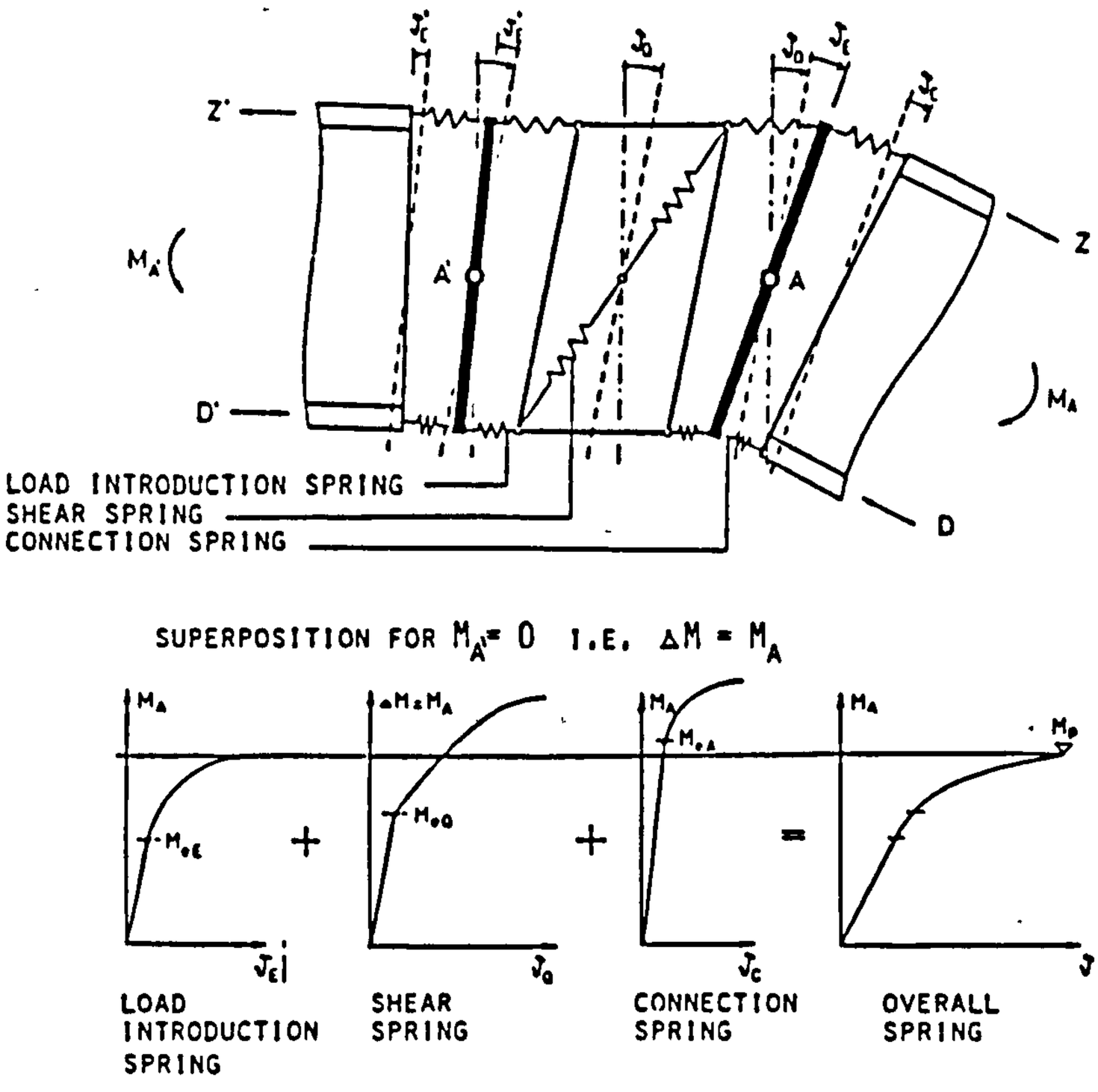

Fig. 1.3.19 Spring Model

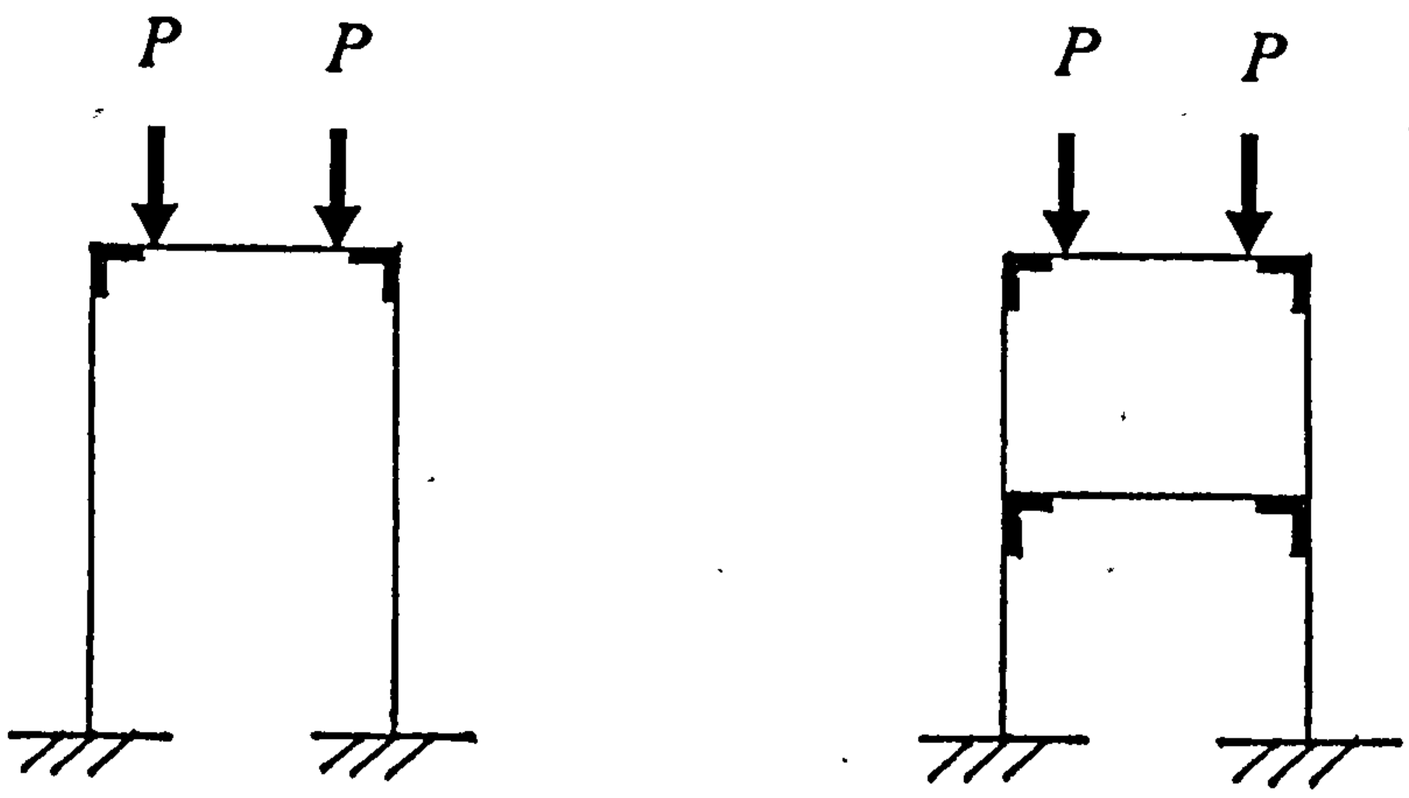

Fig. 1.5.1 Single and Double Storey Frameworks.

CONNECTION TYPE	STANDARDIZED MOMENT-ROTATION FUNCTION	STANDARDIZATION CONSTANT	MAXIMUM DEVIATION OF STANDARDIZED CURVE FROM EXPERIMENTAL CURVE	REFERENCES FOR EXPERIMENTAL CURVES	NUMBER OF TESTS
Double Web Angle Connection	$\phi = 3.66(KM)\times10^{-4}+1.15(KM)^3\times10^{-6}$ $+4.57(KM)^5\times10^{-8}$	$K=d^{-2.4}{}_t{}^{-1.81}{}_g 0.15$	6%	Munse, Bell and Chesson (1959) Rathbun (1936) Sommer (1969)	8 7 4/19
Single Web Angle Connection	$\phi = 4.28(KM)\times10^{-3}+1.45(KM)\times10^{-9}$ $+1.51(KM)\times10^{-16}$	$K=d^{-2.4}{}_t{}^{-1.81}{}_g 0.15$	10%	Lipson (1968)	8
Header Plate Connection	$\phi = 5.1(KM)\times10^{-5}+6.2(KM)^3\times10^{-10}$ $+2.4\times(KM)^5\times10^{-13}$	$K=t^{-1.6}{}_g 1.6_d{}^{-2.3}{}_w 0.5$	4%	Sommer (1969)	16
Top and Seat Angle Connection	$\phi = 8.46(KM)\times10^{-4}+1.01(KM)^3\times10^{-4}+1.24(KM)^5\times10^{-8}$	$K=t^{-0.5}{}_d{}^{-1.5}{}_f{}^{-1.1}{}_l{}^{-0.7}$	11%	Batho and Rowan (1934) Hechtman and Johnston (1947) Rathbun (1936) Brandes and Mains (1944)	11 18 5 21/55
End Plate Connection Without Column Stiffeners	$\phi = 1.83(KM)\times10^{-3}-1.04(KM)^3\times10^{-4}+6.38(KM)^5\times10^{-6}$	$K=d^{-2.4}{}_t{}^{-0.4}{}_f 1.1$	3%	Ostrander (1970) Sherbourne (1948)	11 1/12
End Plate Connection with Column Stiffeners	$\phi = 1.79(KM)\times10^{-3}+1.76(KM^3\times10^{-4}$ $+2.04(KM)^5\times10^{-4}$	$K=d^{-2.4}{}_t{}^{-0.6}$	6%	Ostrander (1970) Sherbourne (1948) Johnson, Cannon and Spooner (1960)	13 4 1/18
T-Stub Connection	$\phi = 2.1(KM)\times10^{-4}+6.2(KM)^3\times10^{-6}$ $-7.6(KM)^5\times10^{-9}$	$K=d^{-1.5}{}_t{}^{-0.5}{}_f{}^{-1.1}{}_l{}^{-0.7}$	12%	Batho and Rowan (1934) Bannister (1966) Rathbun (1936) Douty (1964)	3 5 6 3/17

Table 1.3.1 Standardized Connection Moment-Rotation Functions.

Connection type	Dimensionless factor	Standardized moment–rotation equations	Maximum deviation of standardized curves from experimental curves (%)	Reference for experimental curves	Number of experimental curves produced
Single web angle connection	$K = d^{-2.09} t^{-1.64} g^{2.06}$	$\frac{\phi}{1.03 \times 10^{-2}} = \frac{K \times M}{32.75}\left[1 + \left(\frac{K \times M}{32.75}\right)^{2.93}\right]$	−11	Lipson (1968)	6
Double web angle connection	$K = d^{-2.2} t^{0.08} g^{0.28}$	$\frac{\phi}{3.98 \times 10^{-3}} = \frac{K \times M}{0.63}\left[1 + \left(\frac{K \times M}{0.63}\right)^{4.94}\right]$	−18	Batho and Rowan (1934) Lewitt *et al.* (1966) Somner (1969)	7
Header plate connection	$K = d^{-2.41} t^{-1.54} g^{2.42} w^{-0.45}$	$\frac{\phi}{7.04 \times 10^{-3}} = \frac{K \times M}{186.77}\left[1 + \left(\frac{K \times M}{186.77}\right)^{5.32}\right]$	−12	Somner (1969)	7
Top and seat angle connection	$K = d^{-1.06} t^{-0.54} l^{0.85} f^{-1.28}$	$\frac{\phi}{5.17 \times 10^{-3}} = \frac{K \times M}{745.94}\left[1 + \left(\frac{K \times M}{745.94}\right)^{4.61}\right]$	−4	Hechtman and Johnston (1947)	7
Strap angle connection	$K = h^{-0.059} t^{-0.85} \left(\frac{H}{p}\right)^{-1.06}$	$\frac{\phi}{4.58 \times 10^{-5}} = \frac{K \times M}{753.26}\left[1 + \left(\frac{K \times M}{753.26}\right)^{4.98}\right]$	−5	Brun and Picard (1976) Beaulieu and Giroux (1974)	5

Table 1.3.2 Standardized Connection Moment-Rotation Functions.

Connection type (1)	Equation for: K_i; $\frac{E\Delta_{cp}}{F}$ (2)	$\frac{E\Delta_{cf}}{F}$ (3)	$\frac{E\Delta_s}{F}$ (4)	$\frac{E\Delta_{wc}}{F}$ (5)
Stiffened	$\frac{(D_b - t_w)^2 E}{\frac{E\Delta_{cp}}{F} + \frac{E\Delta_{cf}}{F} + \frac{E\Delta_s}{F}}$ or (31)P	(28)S or (32)P	(20)S (43)	—
Unstiffened	$\frac{(D_b - t_w)^2 E}{\frac{E\Delta_{cp}}{F} + \frac{E\Delta_{cf}}{F} + \frac{E\Delta_s}{F} + \frac{E\Delta_{wc}}{F}}$ or (31)P Note (34); (35) and (37)	(28)S or (32)P Note (34); (51) and (37)	(29)S (39)	(44)

Note: S = Snug tightened bolts; P = Pretensioned bolts.

Table 1.3.3 Expressions for K_i.

Failure mode (1)	K_p (2)	$\frac{E\Delta_{cp}}{F}$ (3)	$\frac{E\Delta_{cf}}{F}$ (4)	$\frac{E\Delta_{wc}}{F}$ (5)	$\frac{E\Delta_{cp}}{F}$ (6)	$\frac{E\Delta_{wcp}}{F}$ (7)
Shear yielding	$\frac{(D_b - t_w)^2 E}{\frac{E\Delta_{cp}}{F} + \frac{E\Delta_{cf}}{F} + \frac{E\Delta_{wc}}{F} + \frac{E\Delta_{sp}}{F}}$ or (31)P Note (34); (35) and (37)	(28)S or (32)P Note (34); (35) and (37)	(29)S (44)	(47)	—	
Web buckling (in compression flange level)	$\frac{(D_b - t_w)^2 E}{\frac{E\Delta_{cp}}{F} + \frac{E\Delta_{cf}}{F} + \frac{E\Delta_{wcp}}{F} + \frac{E\Delta_{sp}}{F}}$			—	(47)	(51)

Note: S = Snug tightened bolts; P = Pretensioned bolts.

Table 1.3.4 Expressions for K_p for Unstiffened Connections.

Type of Model	References	Year	Advantages	Disadvantages
1. Linear	Baker Rathbun	1933	Simple to use Stiffness matrix only requires initial modification	Inaccurate at high rotation values
2. Bilinear	Lionberger & Weaver Romstad &	1969 1970	Simple to use Curve follows M-ϕ curve more closely than linear model	Inaccurate at some rotation values
3. Polynomial	Sommer Frye & Morris Radziminski et al	1970 1975 1982	Produces a close approximation to the shape of the M-ϕ data	Can produce inaccurate (even negative) connection tangent stiffness values Nonlinear requires iterative evaluation
4. Cubic B-Spline	Jones, Kirby & Nethercot	1980	Produces a very close approximation to any M-ϕ data set Produces accurate values of connection stiffness	Nonlinear ∴ requires iterative evaluation Requires special numerical procedures for evaluation
5. Exponential	Richard et al	1980	Produces a good fit to the test data for single angle connecec-tions; untried for other types but should be suitable	Nonlinear requires iterative evaluation Requires weighted least squares evaluation
6. Ramberg-Osgood (exponential)	Ang & Morris	1984	Produces a good fit to a variety of test data. Similar to type	Nonlinear requires iterative evaluation. Requires weighted least squares evaluation.
7. Exponential + correction	Yee	1984	Produces a good fit to Author's own data Has a semi-analytical	Nonlinear requires iterative evaluation Untried outside range of original data

Table 1.3.5 Representation of Connection Moment-Rotation Curves.

Connection	Reference	Description of model	$M-\phi$ curve
Single web angle	—	—	—
Web side angle	Richard *et al.* (1980)	Dimensionless, equation based upon nonlinear finite-element analysis of several connections	
Double web angle	Lothers (1951)	Linear equations for initial stiffness and connection moment capacity, based upon elastic analysis of web angles	
	Lewitt *et al.* (1969)	Two equations based upon elastic and plastic analyses, with intermediate transition. Equations contain factor evaluated empirically	
Header plate	—	—	—
End plate	Tarpy and Cardinal (1981)	Equations for initial $M-\phi$ curve (almost linear) and ultimate moment capacity, based on parametric study using finite-element program	
	Krishnamurthy *et al.* (1979)	Equation for initial $M-\phi$ curve (almost linear), based on parametric study using two-dimensional elastic-plastic finite-element program	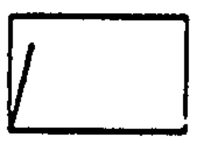
	Johnson and Law (1981)	Linear equations for initial stiffness and plastic moment capacity, based upon elastic and yield line analyses, respectively	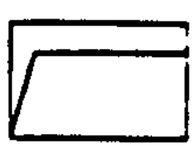
Top and seat angle	Lothers (1951)	Linear equations for initial stiffness and connection moment capacity, based on elastic analysis	
	Maxwell *et al.* (1981)	Linear equations for initial stiffness and ultimate moment, based on finite-element analysis of several connections	

Table 1.3.6 Mathematical Modelling of Connection Moment-Rotation Behaviour.

CHAPTER 2

STIFFNESS MATRIX METHOD

2.1 INTRODUCTION

The advent of electronic computer has removed the problem of forming and solving large sets of equations. In the stiffness matrix method of analysis, which is solely a computer based method, the structure is represented as an assemblage of discrete elements interconnected at joints or nodes i.e., points at which two or more members meet. The relaxation of this definition will be discussed later.

In the stiffness matrix method, the nodal displacements are selected as unknowns. The elements are represented by stiffness matrices that relate the element end displacements to element end forces. The element models are assembled into a system model by imposing conditions of compatibility and equilibrium. The system model relates the nodal displacements to applied nodal forces through the system stiffness matrix. Once the system model is solved for the nodal displacements, any measure of response can be determined. In this study, the structure is idealized as a two dimensional or plane framework.

2.2 NOTATION AND AXES

A typical element is shown in figure 2.2.1. Associated with the element is a set of element axes, which will not, in general, coincide with the axes of other elements of the structure. The right-handed element axis system is adopted and the $x-y$ plane coincides with the plane of the structure.

There is a possibility of two linear displacements and one rotation at the each end of the element as illustrated in figure 2.2.1. Associated with each displacement there is a corresponding force or moment and these are shown in figure 2.2.2. The above mentioned figures also show the positive sense of displacements and forces.

The forces and associated displacements at the ends of the element, in the element axes system, are related by the well known element stiffness matrix equation

$$\mathbf{p} = \mathbf{k}\ \mathbf{d} \tag{2.2.1}$$

where

$$\mathbf{p} = [p_{x1}, p_{y1}, m_{z1}, p_{x2}, p_{y2}, m_{z2}]^T$$

$$\mathbf{d} = [d_{x1}, d_{y1}, \theta_{z1}, d_{x2}, d_{y2}, \theta_{z2}]^T$$

and **k** is a six by six element stiffness matrix.

2.3 COORDINATE TRANSFORMATION

Equation (2.2.1) shows how the element end forces are related to the end displacements, both in the element axes system. Elements meeting at a node will in general lie at different angles. Consequently, the element axes will be inconveniently oriented, which precludes their use when considering equilibrium and compatibility. This can be overcome by transforming the element force and displacement vectors to the structure or global axes system using the transformation matrix,

$$\mathbf{T} = \begin{bmatrix} \mathbf{R} & 0 \\ 0 & \mathbf{R} \end{bmatrix} \tag{2.3.1}$$

where the rotation matrix is

$$\mathbf{R} = \begin{bmatrix} \cos\theta & \sin\theta & 0 \\ -\sin\theta & \cos\theta & 0 \\ 0 & 0 & 1 \end{bmatrix} \tag{2.3.2}$$

where θ is the clockwise rotation of the element about node 1 that will make the element axes coincide with the structure axes.

By expressing the force and displacement vectors in the structure axes system, equation (2.2.1) becomes

$$\mathbf{T}\ \mathbf{p}' = \mathbf{k}\ \mathbf{T}\ \mathbf{d}'$$

The prime denotes reference to the structure axes system. Premultiplying both sides by $\mathbf{T}^T$ gives

$$\mathbf{p}' = (\mathbf{T}^T \quad \mathbf{k} \quad \mathbf{T}) \quad \mathbf{d}'$$

or

$$\mathbf{p}' = \mathbf{k}' \quad \mathbf{d}' \qquad (2.3.3)$$

$\mathbf{k}'$ is the element stiffness matrix in the structure axes system, and

$$\mathbf{k}' = \mathbf{T}^T \quad \mathbf{k} \quad \mathbf{T} \qquad (2.3.4)$$

2.4 LOAD BETWEEN JOINTS OR NODES.

When an element carries load along its span, the forces developed must be taken into account. Such forces can be dealt with using the concept of fixed end forces, equivalent joint forces and superposition. As the name implies, fixed end forces are forces developed at the ends of the element when fully fixed. Equivalent joint forces are the negative of the fixed end forces. The fixed end forces are an artificial system of applied loads that serve to hold the nodal displacements to zero. To return to the true structural behaviour, it is necessary to superimpose the equivalent joint forces. The element end forces and the structural displacements are obtained by the superposition of the effects of the fixed end forces and the final nodal forces, which will include any nodal loads.

For an element carrying point loads along its span, the fixed end forces concept can be discarded by putting nodes at the loading points. Hence, the fixed end forces are only required when the element is carrying distributed loading.

2.5 STRUCTURE STIFFNESS MATRIX

Once the individual element stiffness matrix in the structure axes system of a structure has been formed according to equation (2.3.4), the stiffness matrix of the structure, **K**, can be obtained by assembling of the element stiffness matrices in the conventional manner. The structure nodal load vector, **P**, consists of the nodal applied forces and equivalent joint forces, if any. Hence, the final form of equation (2.3.3) is

$$\mathbf{P} = \mathbf{K}\ \mathbf{D} \tag{2.5.1}$$

To solve for the structure nodal displacements, there are several standardized procedures available. The procedure employed here is the Choleski Triangular Decomposition method of solution. A detailed description can be found in Appendix I.

Once the structural displacements are known, as stated before, the element end forces can be determined from

$$\mathbf{p}' = \mathbf{k}'\ \mathbf{d}' + \mathbf{p}_f' \tag{2.5.2}$$

where $\mathbf{p}_f'$ is the element fixed end force vector in the structure axes system.

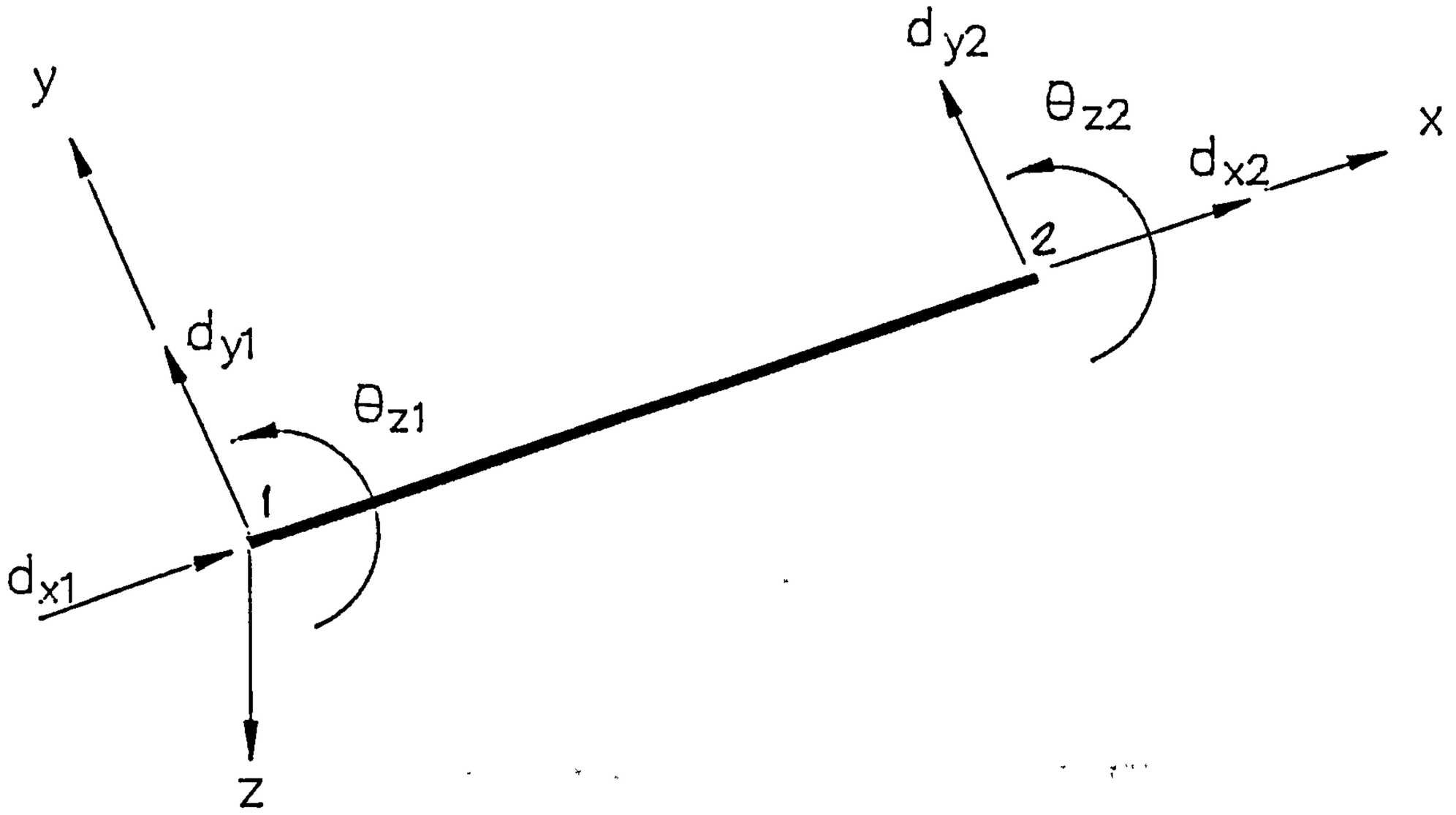

Fig. 2.2.1

General Element Axes System and Associated Displacements.

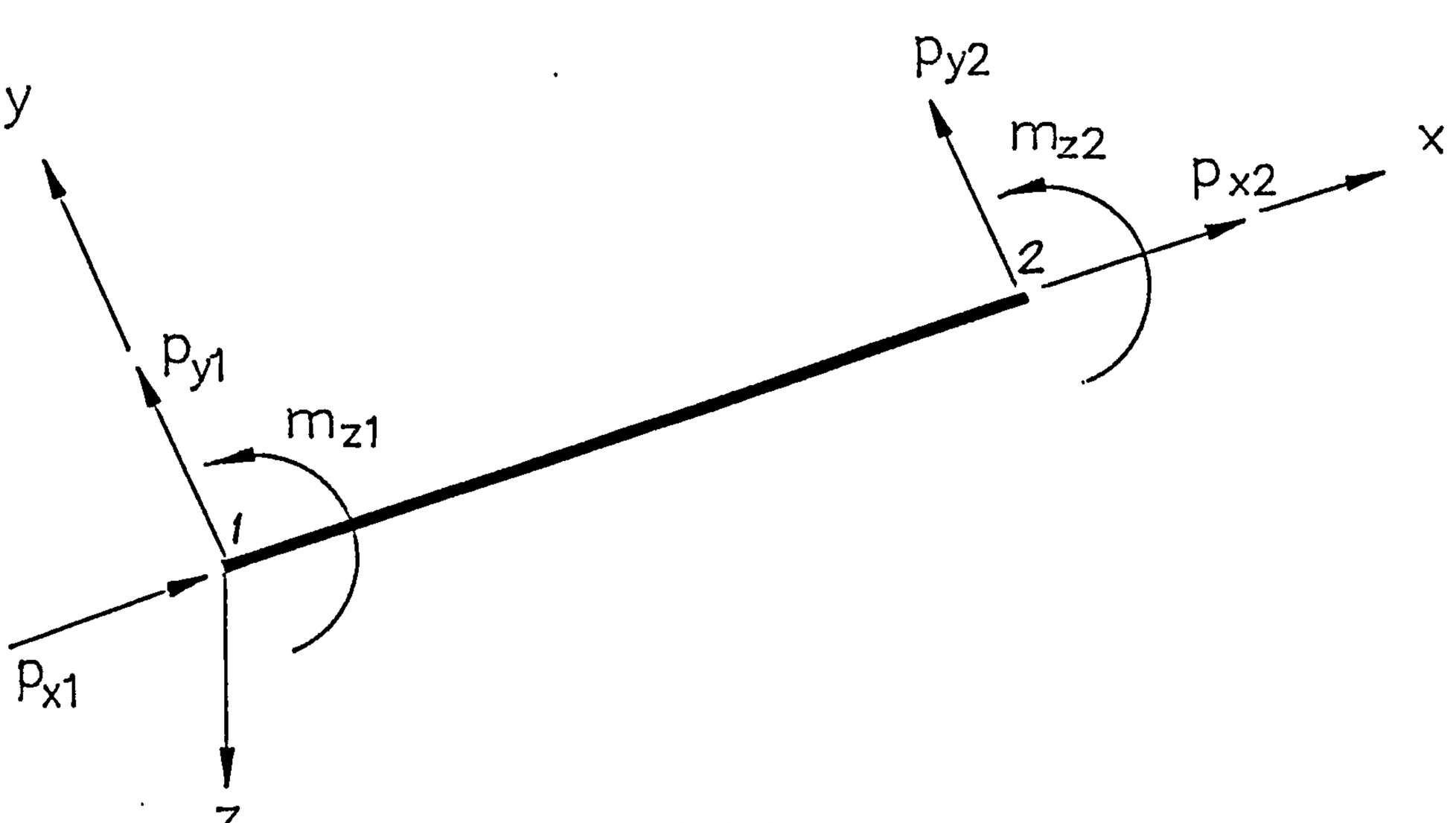

Fig. 2.2.2

General Element Axes System and Associated Forces.

CHAPTER 3

ELEMENT STIFFNESS MATRIX

AND

FIXED END FORCES

3.1 INTRODUCTION

It has been shown in the previous chapter that once the individual element stiffness matrix is known, the structure stiffness matrix can be formed. This chapter deals with the derivation of the element stiffness matrix and fixed end forces for both the rigid jointed and semi-rigid jointed element. In the derivation, the following assumptions are made.

1) Displacements are small.
2) Plane cross sections remain plane after bending.
3) The element material behaves in a linear elastic manner.
4) The element is straight and prismatic.
5) All loads act in the plane of the structure i.e. planar loading.
6) Shear deformation is neglected.
7) Effects of axial load are neglected.

3.2 RIGID JOINTED ELEMENT

3.2.1 ELEMENT STIFFNESS MATRIX

The element stiffness matrix consists of stiffness influence coefficients. These are the actions imposed by the supporting medium when unit displacements occur in isolation at each end of the element in turn. These unit displacements are assumed to occur one at a time, while all other displacements are held zero. They are indicated in figure 3.2.1. The resulting forces are always in equilibrium, and therefore three general equations may be drawn up :

$$p_{x1} + p_{x2} = 0 \qquad (3.2.1a)$$

$$p_{y1} + p_{y2} = 0 \qquad (3.2.1b)$$

$$m_{z1} + m_{z2} = p_{y1} L \qquad (3.2.1c)$$

Consider displacement d_{x1} of figure 3.2.1a ,

$$p_{x1} = \frac{EA}{L} d_{x1} \tag{3.2.2}$$

From equation (3.2.1a),

$$p_{x2} = -\frac{EA}{L} d_{x1}$$

By treating in a similar manner for displacement d_{x2} of figure 3.2.1b,

$$p_{x1} = -\frac{EA}{L} d_{x2}$$

and

$$p_{x2} = \frac{EA}{L} d_{x2}$$

The influence coefficients involving θ_z and d_y will be determined using the strain energy method according to Castigliano's Theorem which is detailed in Appendix II.

Considering the rotation θ_z of figure 3.2.2, the element is given an end rotation θ_{z2}.

The moment at a section of distance x from end 1 is

$$M = -m_{z1} + p_{y1} x \tag{3.2.3}$$

The strain energy due to bending is

$$SE = \int_0^L \frac{M^2}{2EI} dx \tag{3.2.4}$$

Substituting equation (3.2.1c) into equation (3.2.3) and then into equation (3.2.4) and using Castigliano's theorem

$$\frac{\partial SE}{\partial p_{y1}} = d_{y1} = 0$$

yields

$$p_{y1} = \frac{3m_{z2}}{2L}$$

Again using Castigliano's theorem,

$$\frac{\partial SE}{\partial m_{z2}} = \theta_{z2}$$

yields

$$m_{z2} = \frac{4EI}{L}\theta_{z2} \tag{3.2.5}$$

and

$$p_{y1} = \frac{6EI}{L^2}\theta_{z2} = -p_{y2} \tag{3.2.6}$$

From equation (3.2.1c),

$$m_{z1} = \frac{2EI}{L}\theta_{z2} = \frac{m_{z2}}{2} \tag{3.2.7}$$

Similar expressions to equations (3.2.5) to (3.2.7) can be set up for rotation θ_{z1} by careful transposition of the suffices.

Now, considering displacement d_{y2} of figure 3.2.3, the bending moment at x is

$$\begin{aligned} M &= -m_{z1} + p_{y1}x \\ &= -m_{z1} - p_{y2}x \end{aligned} \tag{3.2.8}$$

Substituting into equation (3.2.4) and using

$$\frac{\partial SE}{\partial m_{z1}} = \theta_{z1} = 0$$

yields

$$p_{y2} = -\frac{2m_{z1}}{L}$$

and

$$\frac{\partial SE}{\partial p_{y2}} = d_{y2}$$

yields

$$m_{z1} = -\frac{6EI}{L^2} d_{y2} \qquad (3.2.9)$$

From equation (3.2.1 c),

$$m_{z2} = -\frac{6EI}{L^2} d_{y2} \qquad (3.2.10)$$

hence,

$$p_{y2} = \frac{12EI}{L^3} d_{y2} \qquad (3.2.11)$$

and

$$p_{y1} = -\frac{12EI}{L^3} d_{y2} \qquad (3.2.12)$$

Again, similar expressions to equations (3.2.9) to (3.2.12) can be set up for a displacement d_{y1} by careful transposition of the suffices.

From the above, the full element stiffness matrix can be set up as shown in equation (3.2.13) below :

$$\mathbf{k} = \begin{bmatrix} \frac{EA}{L} & 0 & 0 & \frac{-EA}{L} & 0 & 0 \\ & \frac{12EI}{L^3} & \frac{6EI}{L^2} & 0 & \frac{-12EI}{L^3} & \frac{6EI}{L^2} \\ & & \frac{4EI}{L} & 0 & \frac{-6EI}{L^2} & \frac{2EI}{L} \\ & & & \frac{EA}{L} & 0 & 0 \\ & sym & & & \frac{12EI}{L^3} & \frac{-6EI}{L^2} \\ & & & & & \frac{4EI}{L} \end{bmatrix}$$

.....(3.2.13)

Note that the matrix is symmetric as required by the Betti-Maxwell's Theorem, a detail of which is given in Appendix III. Equation (3.2.13) can be expressed in a more general form which will be used later in the derivation of the stiffness matrix of a semi-rigid jointed element.

Figure 3.2.4 shows the independent bending displacements at the ends of an element and the associated forces. S_{11}, S_{12} and S_{22} are pure rotation coefficients, T_{11}, T_{12} and T_{22} are pure translation coefficients and Q_{11}, Q_{12}, Q_{21} and Q_{22} are cross rotation-translation coefficients.

The generized element stiffness matrix expressed in terms of the above coefficients is shown in equation (3.2.14).

$$\mathbf{k} = \begin{bmatrix} \frac{EA}{L} & 0 & 0 & \frac{-EA}{L} & 0 & 0 \\ & \frac{T_{11}EI}{L^3} & \frac{Q_{11}EI}{L^2} & 0 & \frac{-T_{12}EI}{L^3} & \frac{Q_{21}EI}{L^2} \\ & & \frac{S_{11}EI}{L} & 0 & \frac{-Q_{12}EI}{L^2} & \frac{S_{12}EI}{L} \\ & & & \frac{EA}{L} & 0 & 0 \\ & sym & & & \frac{T_{22}EI}{L^3} & \frac{-Q_{22}EI}{L^2} \\ & & & & & \frac{S_{22}EI}{L} \end{bmatrix}$$

.....(3.2.14)

From figure 3.2.4, equilibrium gives

$$Q_{11} = Q_{12} = S_{11} + S_{12} \qquad (3.2.15a)$$

$$Q_{22} = Q_{21} = S_{22} + S_{12} \qquad (3.2.15b)$$

$$T_{11} = T_{12} = Q_{11} + Q_{21} \qquad (3.2.15c)$$

$$T_{22} = T_{12} = Q_{22} + Q_{12} \qquad (3.2.15d)$$

For a rigid jointed element , because of "symmetry" of the two ends, the properties at the two ends must be the same. Therefore

$$S_{11} = S_{22}$$

and

$$T_{11} = T_{22}$$

Hence, from equation (3.2.15),

$$Q_{11} = Q_{12} = Q_{21} = Q_{22} = S_{11} + S_{12} = Q \qquad (3.2.16a)$$

$$T_{11} = T_{12} = T_{22} = 2Q \qquad (3.2.16b)$$

Thus, it can be seen that the stiffness influence coefficients can be expressed in terms of S_{11} and S_{12}, which are given by :

$$S_{11} = 4 \qquad \text{and} \qquad S_{12} = 2$$

Substitution into equation (3.2.14) will produce a matrix similar to that of equation (3.2.13), i.e., for a rigid jointed element.

The element stiffness matrix in the structure axes system can easily be obtained by using equation (2.3.4) of Chapter 2.The final result is as shown in equation (3.2.17).

$$\mathrm{k}' = \begin{bmatrix} A_{11} & A_{12} & A_{13} & A_{14} & A_{15} & A_{16} \\ & A_{22} & A_{23} & A_{24} & A_{25} & A_{26} \\ & & A_{33} & A_{34} & A_{35} & A_{36} \\ & sym & & A_{44} & A_{45} & A_{46} \\ & & & & A_{55} & A_{56} \\ & & & & & A_{66} \end{bmatrix} \qquad (3.2.17)$$

where

$m = \cos\theta$ $\qquad$ $n = \sin\theta$

$$A_{11} = \frac{T_{11}EIn^2}{L^3} + \frac{EAm^2}{L} \qquad A_{12} = \left(-\frac{T_{11}EI}{L^3} + \frac{EA}{L}\right)mn$$

$$A_{13} = -\frac{Q_{11}EIn}{L^2} \qquad A_{14} = -\left(\frac{T_{12}EIn^2}{L^3} + \frac{EAm^2}{L}\right)$$

$$A_{15} = \left(\frac{T_{12}EI}{L^3} - \frac{EA}{L}\right)mn \qquad A_{16} = -\frac{Q_{21}EIn}{L^2}$$

$$A_{22}=\frac{T_{11}EIm^2}{L^3}+\frac{EAn^2}{L} \qquad A_{23}=\frac{Q_{11}EIm}{L^2}$$

$$A_{24}=\left(\frac{T_{12}EI}{L^3}-\frac{EA}{L}\right)mn \qquad A_{25}=-\left(\frac{T_{12}EIm^2}{L^3}+\frac{EAn^2}{L}\right)$$

$$A_{26}=\frac{Q_{21}EIm}{L^2} \qquad A_{33}=\frac{S_{11}EI}{L}$$

$$A_{34}=\frac{Q_{12}EIn}{L^2} \qquad A_{35}=-\frac{Q_{12}EIm}{L^2}$$

$$A_{36}=\frac{S_{12}EI}{L} \qquad A_{44}=\frac{T_{22}EIn^2}{L^3}+\frac{EAm^2}{L}$$

$$A_{45}=\left(-\frac{T_{22}EI}{L^3}+\frac{EA}{L}\right)mn \qquad A_{46}=\frac{Q_{22}EIn}{L^2}$$

$$A_{55}=\frac{T_{22}EIm^2}{L^3}+\frac{EAn^2}{L} \qquad A_{56}=-\frac{Q_{22}EIm}{L^2}$$

$$A_{66}=\frac{S_{22}EI}{L}$$

3.2.2 ELEMENT FIXED END FORCES

Figure 3.2.5 shows a typical rigid jointed element with both ends fully fixed and the span subjected to distributed loading W_1 at node 1 and increasing proportionally to W_2 at node 2. At the section of distance x from the origin, the bending moment is

$$M_x=V_1x-M_1-\frac{W_1x^2}{2}-\frac{(W_2-W_1)x^3}{6L}$$

Applying simple bending theory and integration gives

$$EI\frac{dy}{dx}=-\frac{V_1x^2}{2}+M_1x+\frac{W_1x^3}{6}+\frac{(W_2-W_1)x^4}{24L}+A$$

Integrating again results in

$$EIy=-\frac{V_1x^3}{6}+\frac{M_1x^2}{2}+\frac{W_1x^4}{24}+\frac{(W_2-W_1)x^5}{120L}+Ax+B$$

Applying the boundary conditions

$$y=0 \quad \text{and} \quad \frac{dy}{dx}=0 \quad \text{at} \quad x=0 \quad \text{and} \quad x=L$$

yields

$$V_1=\frac{7}{20}L\,W_1+\frac{3}{20}L\,W_2 \tag{3.2.18}$$

From equilibrium,

$$V_2=\frac{3}{20}L\,W_1+\frac{7}{20}L\,W_2 \tag{3.2.19}$$

$$M_1=L^2\left(\frac{W_1}{20}+\frac{W_2}{30}\right) \tag{3.2.20}$$

$$M_2=-L^2\left(\frac{W_1}{30}+\frac{W_2}{20}\right) \tag{3.2.21}$$

Equations (3.2.18) to (3.2.21) are also valid when W_1 is greater than W_2. Expressions for cases when $W_1=0$ or $W_2=0$ or $W_1=W_2$ can easily be obtained by substitution into the above equations and these are tabulated and shown in table 3.2.1.

3.3 SEMI-RIGID JOINTED ELEMENT

3.3.1 ELEMENT STIFFNESS MATRIX

This type of element is often used to simulate the deformations at the joints in bolted steel structures. The flexibility of joints is modelled by including rotational springs at the ends of the element. In addition to the general assumptions mentioned earlier, it is also assumed that the joint is contracted to a point at the intersection of the element centre lines and panel zone deformation is neglected.

The stiffness coefficients relationships from equation (3.2.15) are still applicable to the stiffness matrix in the structure axes system (equation 3.2.17). Because the springs at the two ends of the semi-rigid jointed element may not be the same, the element lacks "symmetry", i.e., S_{11} is not equal to S_{22}. It can be seen from equation (3.2.15) that once the coefficients S_{11}, S_{12} and S_{22} are determined, all the stiffness influence coefficients can be obtained.

Consider the semi-rigid jointed element shown in figure 3.3.1. When moments M_1 and M_2 are applied at the two ends, the joint at 1 and 2 rotate by θ_1 and θ_2 respectively. For the element, the moments at ends 1 and 2 respectively are

$$M_1 = \frac{EI}{L}(S_{11}\gamma_1 + S_{12}\gamma_2) \tag{3.3.1}$$

$$M_2 = \frac{EI}{L}(S_{12}\gamma_1 + S_{22}\gamma_2) \tag{3.3.2}$$

where $S_{11} = S_{22} = 4$ and $S_{12} = 2$.

If the rotational stiffness at the ends 1 and 2 are R_1 and R_2 respectively, and assuming that they behave in a linear elastic manner, then

$$M_1 = R_1(\theta_1 - \gamma_1) \tag{3.3.3}$$

$$M_2 = R_2(\theta_2 - \gamma_2) \tag{3.3.4}$$

By eliminating γ_1 and γ_2 from the above equations, the stiffness relationship between M_1 and M_2 and the joint rotations θ_1 and θ_2 are

$$M_1 = \frac{EI}{L}(\overline{S}_{11}\theta_1 + \overline{S}_{12}\theta_2) \tag{3.3.5}$$

$$M_2 = \frac{EI}{L}(\overline{S}_{12}\theta_1 + \overline{S}_{22}\theta_2) \tag{3.3.6}$$

where

$$\overline{S}_{11} = \frac{(4 + 12\alpha_2)}{F}$$

$$\overline{S}_{22} = \frac{(4 + 12\alpha_1)}{F}$$

$$\overline{S}_{12} = \frac{2}{F}$$

where

$$F = 1 + 4(\alpha_1 + \alpha_2) + 12\alpha_1\alpha_2$$

$$\alpha_1 = \frac{EI}{LR_1}$$

$$\alpha_2 = \frac{EI}{LR_2}$$

Hence, by treating S_{11}, S_{12} and S_{22} of equation (3.2.15) as $\overline{S}_{11}, \overline{S}_{12}$ and $\overline{S}_{22}$ respectively, and then substituting into equation (3.2.17), the element stiffness matrix of the semi-rigid jointed element in the structure axes system can be determined.

3.3.2 ELEMENT FIXED END FORCES

Consider the element shown in figure 3.3.2. The span is subjected to distributed loading W_1 at joint 1 and increasing proportionally to W_2 at joint 2. The stiffness of the springs are R_1 and R_2 as before. Because of the action of the distributed loading and the end moments, the net rotation of the beam are γ_1 and γ_2 at ends 1 and 2 respectively. For the element, using the slope and deflection expressions from Section 3.2.2 and applying the boundary conditions

$$y = 0 \qquad \text{at} \qquad x = 0 \qquad \text{and} \qquad x = L$$

results in

$$\gamma_1 = \frac{L}{EI}\left(-\frac{M_1}{3} + \frac{M_2}{6} + \frac{8W_1L^2}{360} + \frac{7W_2L^2}{360}\right) \tag{3.3.7}$$

$$\gamma_2 = \frac{L}{EI}\left(\frac{M_1}{6} - \frac{M_2}{3} - \frac{7W_1L^2}{360} - \frac{8W_2L^2}{360}\right) \tag{3.3.8}$$

For the two springs, the moment-rotation relationship is given by

$$M_1 = R_1\gamma_1 \tag{3.3.9}$$

$$M_2 = R_2\gamma_2 \tag{3.3.10}$$

Eliminating γ_1 and γ_2 from the above equations, the expressions for M_1 and M_2 are of the form :

$$M_1 = \frac{L^2}{60F}\{W_1(3+16\alpha_2)+2W_2(1+7\alpha_2)\} \qquad (3.3.11)$$

$$M_2 = -\frac{L^2}{60F}\{2W_1(1+7\alpha_1)+W_2(3+16\alpha_1)\} \qquad (3.3.12)$$

From equilibrium,

$$V_1 = \frac{L}{6}(2W_1+W_2)+\frac{M_1+M_2}{L} \qquad (3.3.13)$$

$$V_2 = \frac{L}{6}(W_1+2W_2)-\frac{M_1+M_2}{L} \qquad (3.3.14)$$

Expressions for various cases of W value can easily be obtained by substitution and these are shown in table 3.3.1. By substituting $\alpha_1 = \alpha_2 = 0$, i.e., $R_1 = R_2 = \infty$, which is the case of a rigid jointed element, expressions for the fixed end forces will be similar to those as shown in table 3.2.1.

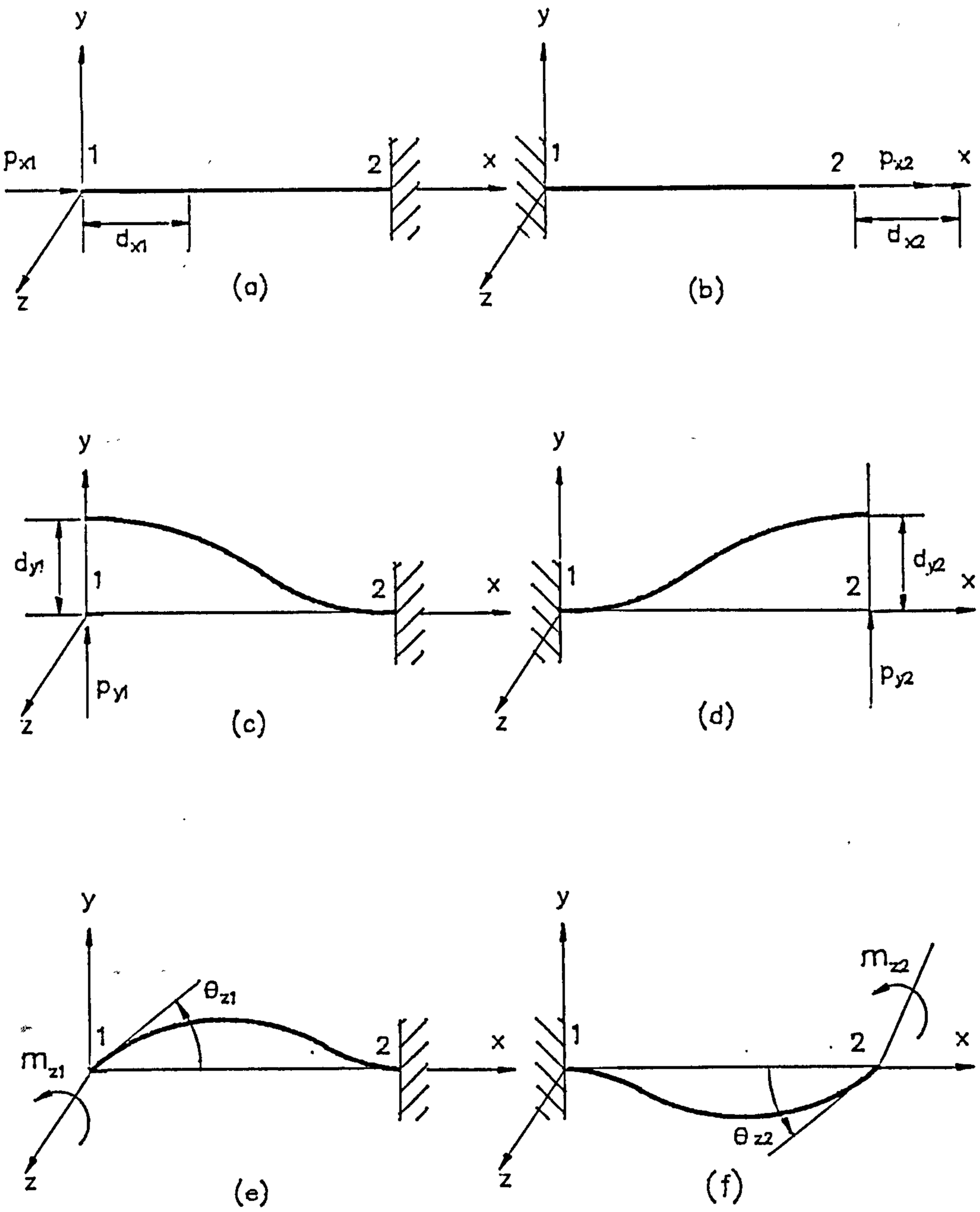

Fig. 3.2.1

Independent Displacements at the Ends of a Rigid Jointed Element and the Associated Forces.

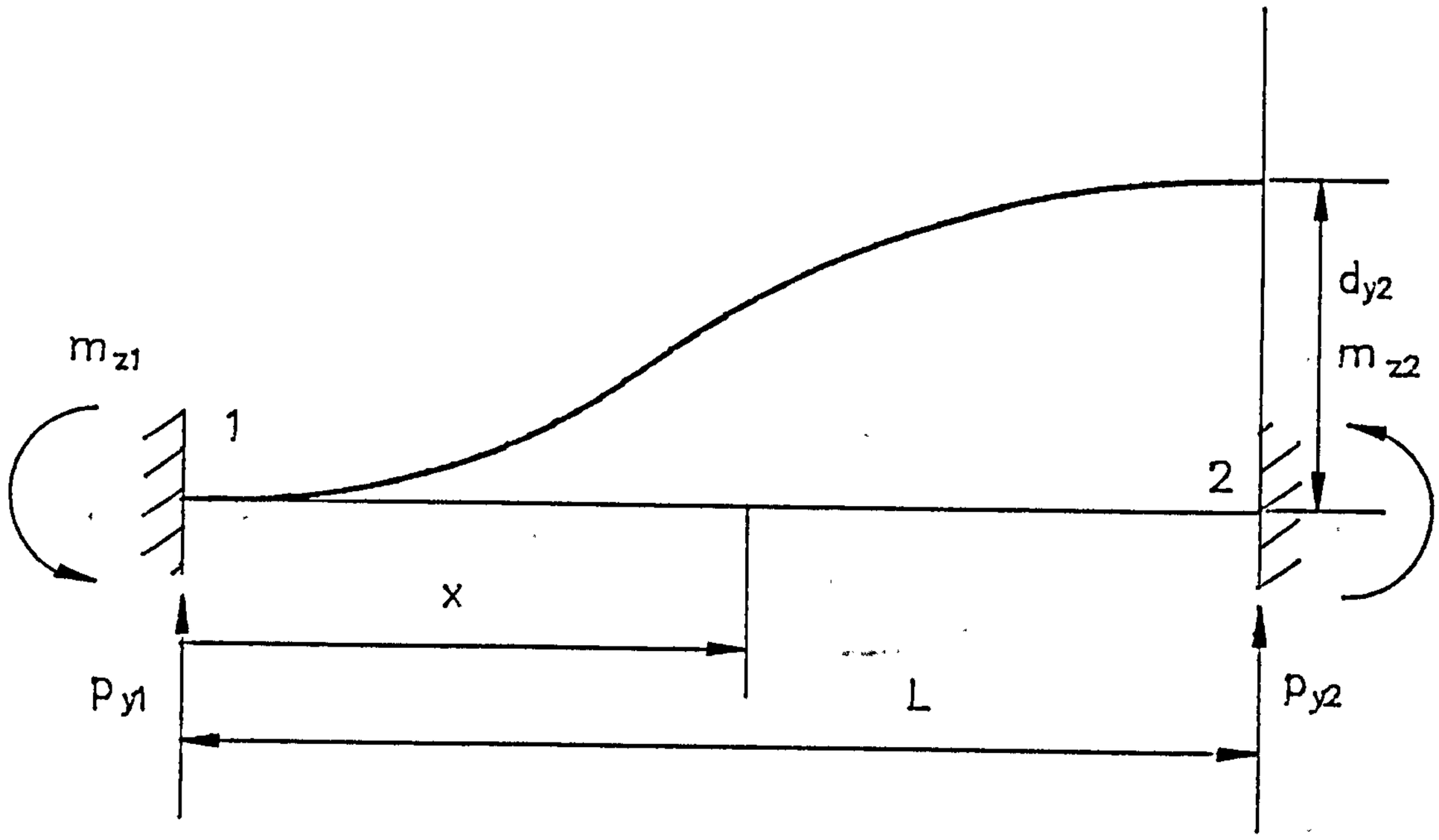

Fig. 3.2.3

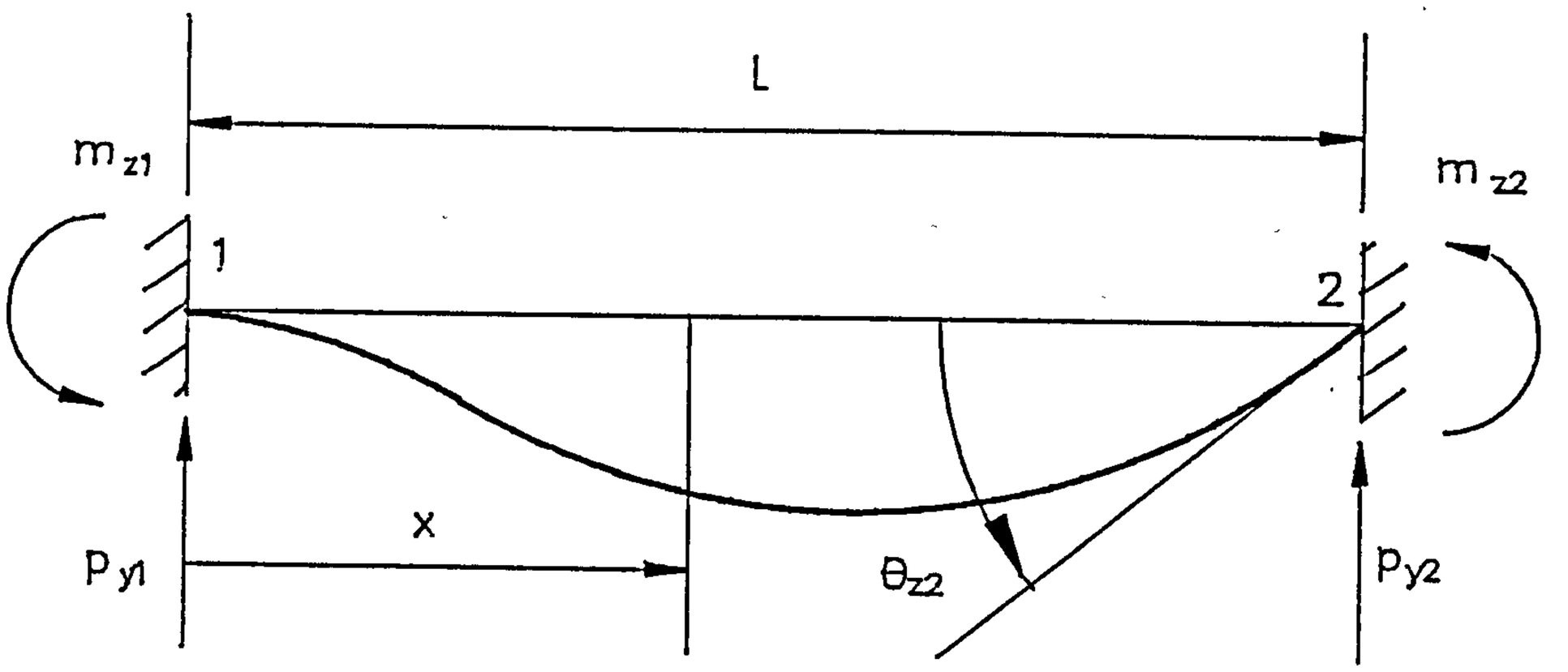

Fig. 3.2.2

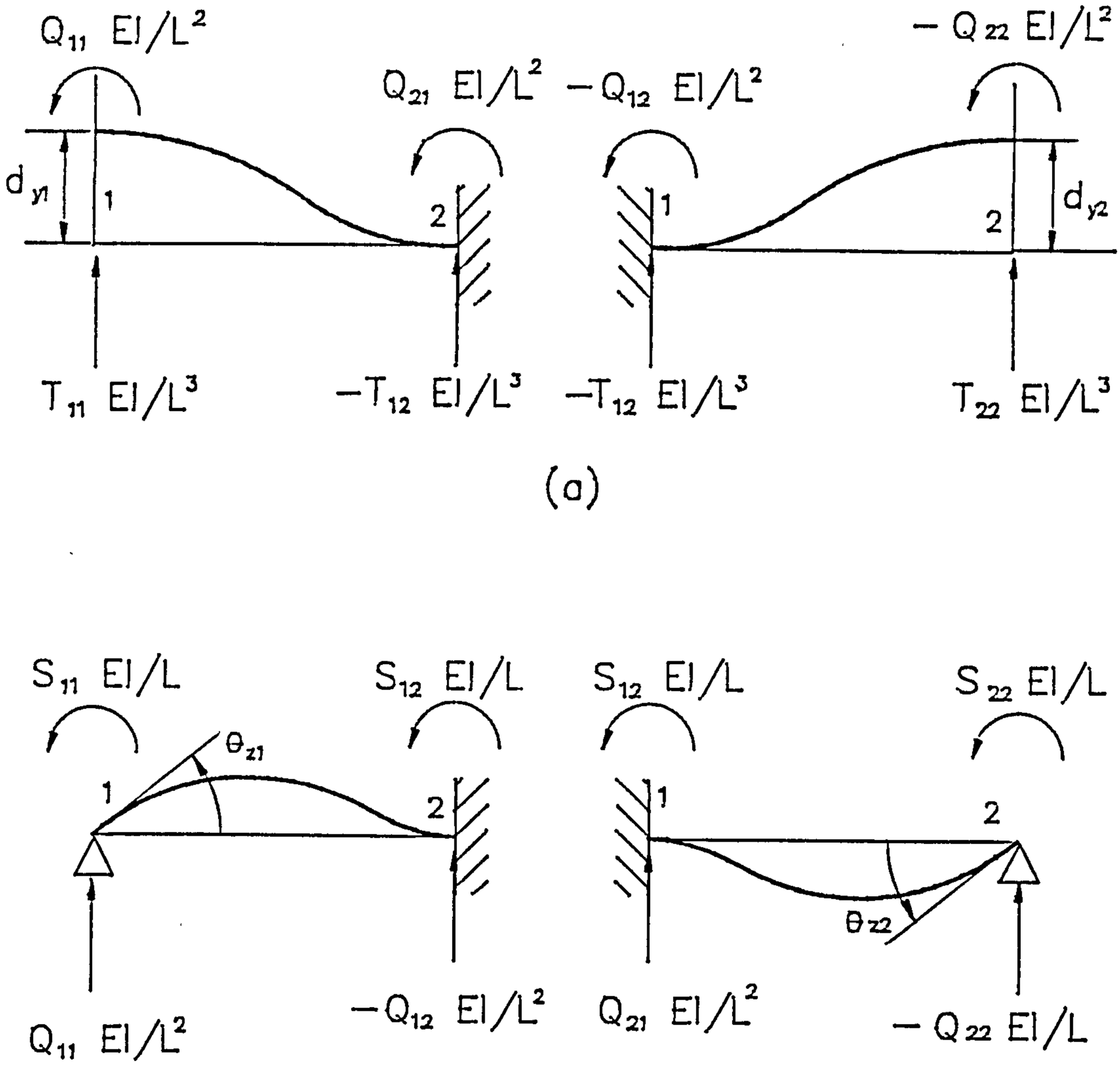

Fig. 3.2.4

Independent Displacements at the Ends of an Element and the Associated Forces.

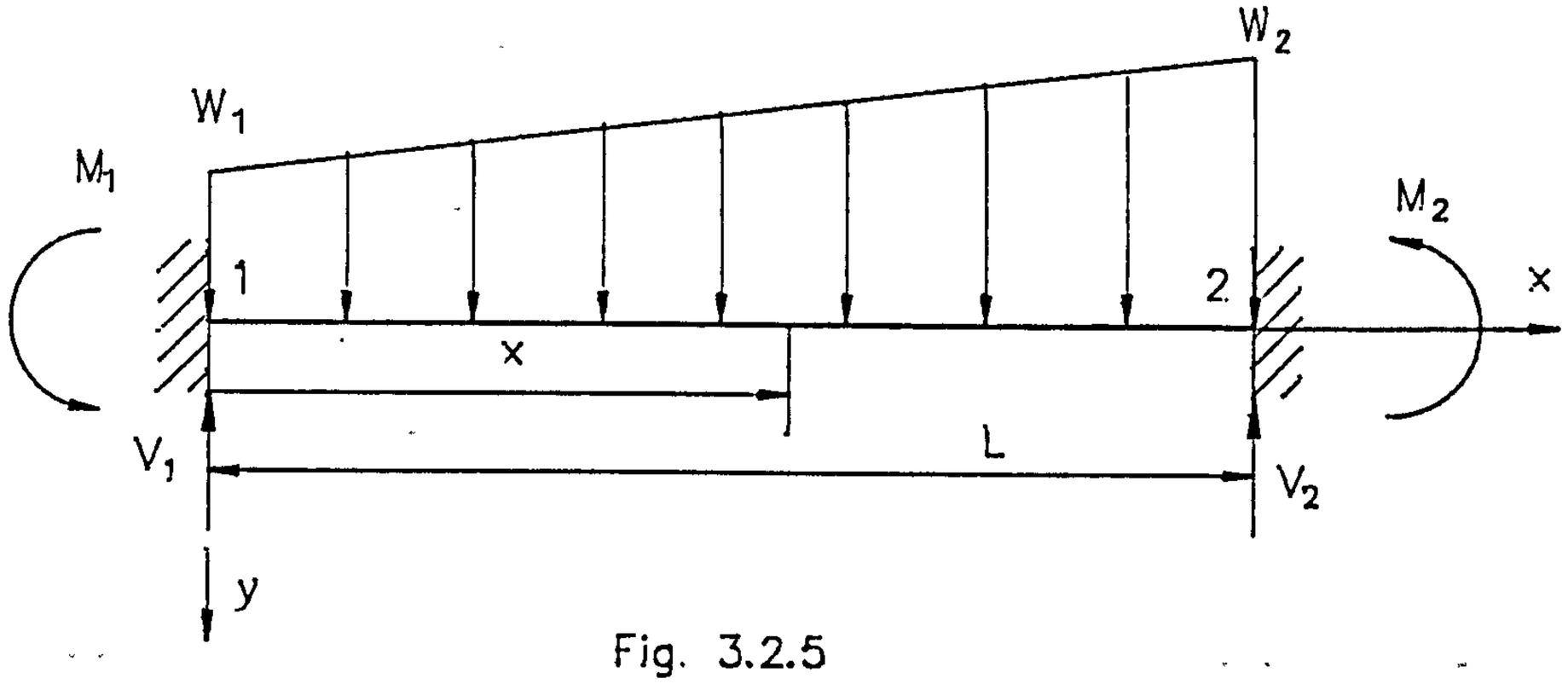

Fig. 3.2.5

Rigid Jointed Element with Linearly Varying Distributed Load.

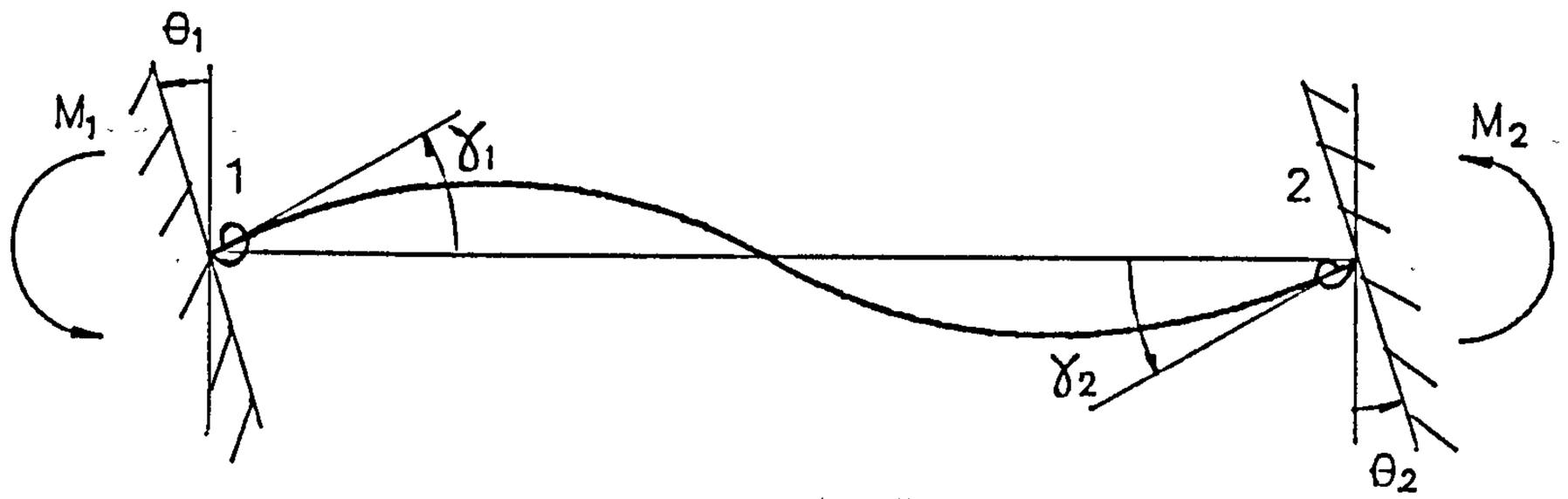

Fig. 3.3.1

Semi–rigid Jointed E;ement.

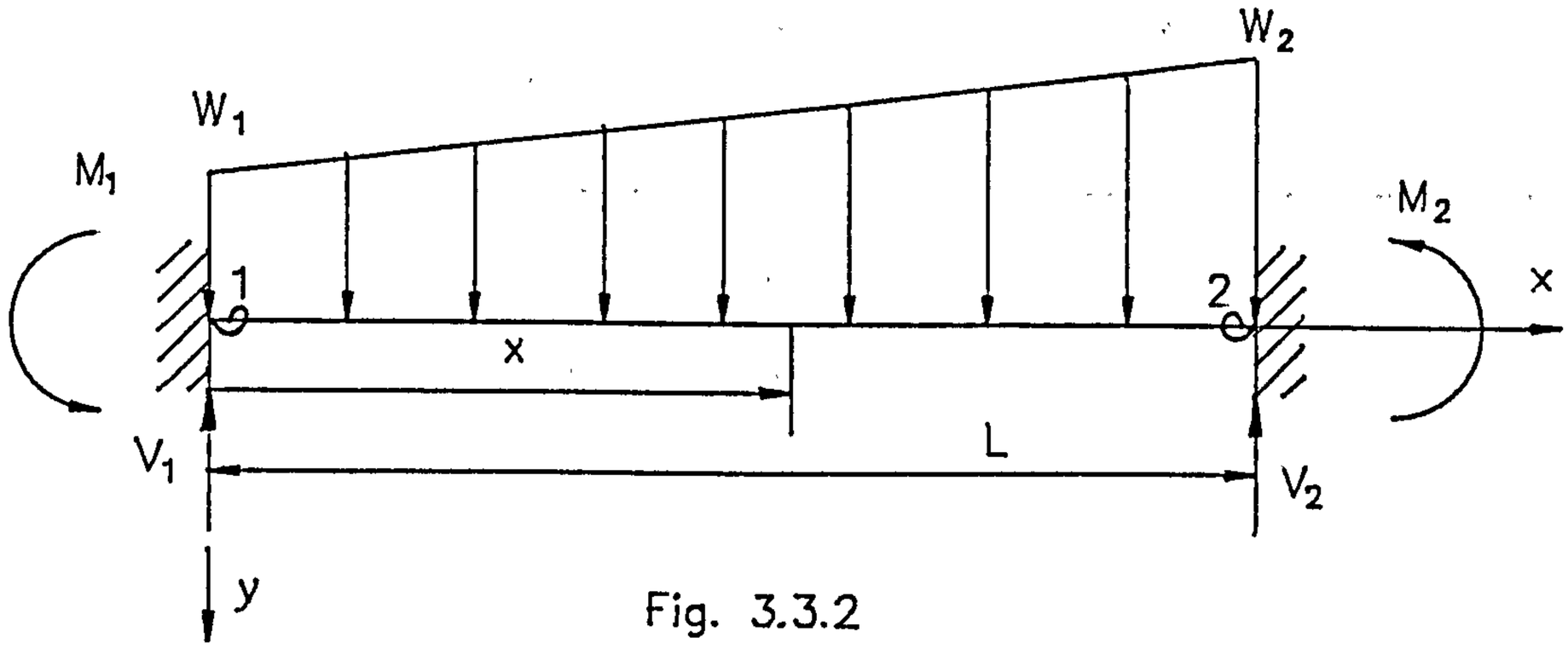

Fig. 3.3.2

Semi–Rigid Jointed Element with Linearly Varying Distributed Load.

W_1	W_2	M_1	M_2	V_1	V_2
0	W_2	$\frac{W_2L^2}{30}$	$-\frac{W_2L^2}{20}$	$\frac{3W_2L}{20}$	$\frac{7W_2L}{20}$
W_1	0	$\frac{W_1L^2}{20}$	$-\frac{W_1L^2}{30}$	$\frac{7W_1L}{20}$	$\frac{3W_1L}{20}$
W	W	$\frac{WL^2}{12}$	$-\frac{WL^2}{12}$	$\frac{WL}{2}$	$\frac{WL}{2}$

Table 3.2.1 Fixed End Forces of a Rigid Jointed Element due to Distributed Loading

W_1	W_2	M_1	M_2	V_1	V_2
0	W_2	$\frac{W_2L^2(1+7\alpha_2)}{30F}$	$-\frac{W_2L^2(3+16\alpha_1)}{60F}$	$\frac{W_2L}{6}+\frac{M_1+M_2}{L}$	$\frac{W_2L}{3}-\frac{M_1+M_2}{L}$
W_1	0	$\frac{W_1L^2(3+16\alpha_2)}{60F}$	$-\frac{W_1L^2(1+7\alpha_1)}{30F}$	$\frac{W_1L}{3}+\frac{M_1+M_2}{L}$	$\frac{W_1L}{6}-\frac{M_1+M_2}{L}$
W	W	$\frac{WL^2(1+6\alpha_2)}{12F}$	$-\frac{WL^2(1+6\alpha_1)}{12F}$	$\frac{WL}{2}+\frac{M_1+M_2}{L}$	$\frac{WL}{2}-\frac{M_1+M_2}{L}$

Table 3.3.1 Fixed End Forces of a Semi-Rigid Jointed Element due to Distributed Loading

CHAPTER 4

ELEMENT STIFFNESS MATRIX

AND

FIXED END FORCES

(WITH AXIAL LOAD EFFECT)

4.1 INTRODUCTION

The derivations of the element stiffness matrix and fixed end forces performed in Chapter 3 were based on the assumption of no axial force acting on the element. As such, they are only applicable in analysis where axial loading is very small or negligible. In the study of stability, the axial loading plays an important role.

This chapter deals with the derivation of the element stiffness matrix and fixed end forces of both the rigid and semi-rigid jointed element taking into account axial loading on the element. The assumptions are similar to those mentioned in the previous chapter, except for the axial loading.

4.2 RIGID JOINTED ELEMENT

4.2.1 ELEMENT STIFFNESS MATRIX

Figure 4.2.1 shows a prismatic element 1-2 of constant flexural rigidity EI and of span L. End 1 is acted upon by moment M_1 and rotates through an angle θ_1, while end 2 is rigidly held in position and direction. The restraining moment at end 2 is M_2. The element carries an axial compressive load P. When the influence of axial load is considered,

$$M_1 = s\frac{EI}{L}\theta_1$$

and

$$\frac{M_2}{M_1} = c$$

Substituting the first equation into the second gives

$$M_2 = s\,c\,\frac{EI}{L}\theta_1 \qquad (4.2.1)$$

s is a factor modifying stiffness EI/L while c is a carry-over factor. s and c are called stability functions and depend on the axial load. Taking moment about end 2,

$$V_1 = \frac{(M_1 + M_2)}{L} \tag{4.2.2}$$

At the section of distance x from the origin, the bending moment is

$$M_x = -Py + V_1 x - M_1$$

Using simple bending theory and substitution of the bending moment equation result in the differential equation of the form :

$$\frac{d^2y}{dx^2} + \mu^2 y - \frac{1}{EI}(V_1 x - M_1) = 0 \tag{4.2.3}$$

The solution of the above equation is

$$y = A \sin \mu x + B \cos \mu x + \frac{1}{\mu^2 EI}\left\{\frac{(M_1 + M_2)x}{L} - M_1\right\} \tag{4.2.4}$$

Applying the boundary conditions

$$y = 0 \qquad \text{at} \qquad x = 0 \qquad \text{and} \qquad x = L$$

the integration constants obtained are

$$A = -\frac{1}{\mu^2 EI}(M_1 \cot \mu L + M_2 \operatorname{cosec} \mu L)$$

$$B = \frac{M_1}{\mu^2 EI}$$

Differentiating equation (4.2.4) gives the slope

$$\frac{dy}{dx} = A\mu\cos\mu x - B\mu\sin\mu x + \frac{(M_1 + M_2)}{\mu^2 EIL} \tag{4.2.5}$$

Applying the boundary condition

$$\frac{dy}{dx} = 0 \qquad \text{at} \qquad x = L$$

results in

$$c = \frac{M_2}{M_1} = \frac{\mu L - \sin\mu L}{\sin\mu L - \mu L\cos\mu L} \tag{4.2.6}$$

Applying the boundary condition

$$\frac{dy}{dx} = \theta_1 \qquad \text{at} \qquad x = 0$$

and using

$$s = \frac{M_1 L}{EI\theta_1}$$

from equation (4.2.1) results in

$$s = \frac{\mu L(1 - \mu L\cot\mu L)}{2\tan\frac{\mu L}{2} - \mu L} \tag{4.2.7}$$

From equations (4.2.1) and (4.2.2),

$$V_1 = \frac{EI}{L^2} s(1+c)\theta_1 \qquad (4.2.8)$$

Expressions equivalent to the above can be set up for the moments and shears arising when end 1 is held and end 2 rotates.

Now, considering the displacement d_y,, figure 4.2.2 shows the element 1-2 initially carrying end loads P, deflected to position 1'-2' without end rotations. The deflections can be conveniently thought of as having taken place in two stages:

a) A rigid body movement of 1-2 to the position 1'-2' indicated by the thinner line. No end moments result from this movement.
b) Equal rotations through angles $-\theta$ at each end to bring 1-2 to its final configuration.

Provided that P is constant during the two stages, the final result can be obtained by superposition. Hence,

$$M_1 = M_2 = -s\frac{EI}{L}\theta - s\ c\frac{EI}{L}\theta$$

or

$$M_1 = M_2 = -\frac{EI}{L^2} s(1+c)\,(d_{y2} - d_{y1}) \qquad (4.2.9)$$

Taking moments about 2',

$$V_1 = \frac{M_1 + M_2}{L} + \frac{P}{L}(d_{y2} - d_{y1})$$

or

$$V_1 = \left\{-2\frac{EI}{L^2} s(1+c) + P\right\}\left\{\frac{d_{y2} - d_{y1}}{L}\right\} \qquad (4.2.10)$$

When $P = 0$ then $M_1 = M_2 = V_1 L/2$.

Considering the axial displacement, d_x ,

$$P = \frac{EA}{L}(d_{x1} - d_{x2}) \tag{4.2.11}$$

The element stiffness matrix in the element axes system (equation (3.2.14)) and in the structure axes system (equation (3.2.17)) are still valid except that the coefficients S_{ij}, T_{ij} and Q_{ij} must be redefined.

Figure 3.2.4 of Chapter 3 shows the independent displacements at the ends of the rigid jointed element and the associated forces at the ends (neglecting axial effect). Figure 3.2.4a is substituted by figure 4.2.3 when axial effect is considered. From figures 3.2.4b and 4.2.3,

$$Q_{11} = Q_{12} = S_{11} + S_{12} \tag{4.2.12a}$$

$$Q_{21} = Q_{22} = S_{12} + S_{22} \tag{4.2.12b}$$

$$T_{11} = T_{12} = Q_{11} + Q_{21} - \frac{PL^2}{EI} \tag{4.2.12c}$$

$$T_{22} = T_{12} = Q_{12} + Q_{22} - \frac{PL^2}{EI} \tag{4.2.12d}$$

Again, for a rigid jointed element, because of "symmetry" of the two ends, the properties at the two ends must be the same. Therefore

$$S_{11} = S_{22}$$

and

$$T_{11} = T_{22}$$

Hence, equation (4.2.12) becomes

$$Q_{11} = Q_{12} = Q_{21} = Q_{22} = S_{11} + S_{12} = Q \qquad (4.2.13a)$$

$$T_{11} = T_{12} = T_{22} = 2Q - \mu^2 L^2 \qquad (4.2.13b)$$

where

$$\mu^2 = \frac{P}{EI}$$

$$S_{11} = s$$

$$S_{12} = s\ c$$

If the axial load is tensile, the term y in equation (4.2.3) becomes negative. This leads to a solution in terms of hyperbolic functions, i.e.

$$s = \frac{\mu L(1 - \mu L \coth \mu L)}{2\tanh\frac{\mu L}{2} - \mu L} \qquad (4.2.14a)$$

and

$$c = \frac{\mu L - \sinh \mu L}{\sinh \mu L - \mu L \cosh \mu L} \qquad (4.2.14b)$$

4.2.2 ELEMENT FIXED END FORCES

Figure 4.2.4 shows an element with both ends fully fixed and the span subjected to uniform distributed loading W. The bending moment at the section of distance x from the origin is

$$M_x = V_1 x + P y - M_1 - \frac{W x^2}{2}$$

Using simple bending theory and substitution of the moment gives

$$\frac{d^2y}{dx^2} + \frac{Py}{EI} - \frac{1}{EI}\left(M_1 + \frac{Wx^2}{2} - \frac{WLx}{2}\right) = 0 \qquad (4.2.15)$$

The solution is

$$y = A\sin\mu x + B\cos\mu x + \frac{1}{\mu^2 EI}\left(M_1 + \frac{Wx^2}{2} - \frac{WLx}{2} - \frac{W}{\mu^2}\right) \qquad (4.2.16)$$

Applying the boundary conditions

$$y = 0 \quad \text{and} \quad \frac{dy}{dx} = 0 \quad \text{at} \quad x = 0 \quad \text{gives}$$

$$A = \frac{WL}{2\mu^3 EI}$$

$$B = \frac{1}{\mu^2 EI}\left(\frac{W}{\mu^2} - M_1\right)$$

Applying the boundary condition $y = 0$ at $x = L$ gives

$$M_1 = \frac{W}{\mu^2}\left(1 - \frac{\mu L}{2}\cot\frac{\mu L}{2}\right) = -M_2 \qquad (4.2.17)$$

If the axial load is tensile, the trigonometry function of equation (4.2.17) should be replaced by the hyperbolic function.

4.3 SEMI-RIGID JOINTED ELEMENT

4.3.1 ELEMENT STIFFNESS MATRIX

The approach used in deriving the element stiffness matrix is similar to the case without axial load. From figure 3.3.1 of the previous chapter, the moments for the element at ends 1 and 2 respectively are

$$M_1 = \frac{EI}{L}(S_{11}\gamma_1 + S_{12}\gamma_2) \qquad (4.3.1)$$

$$M_2 = \frac{EI}{L}(S_{12}\gamma_1 + S_{22}\gamma_2) \tag{4.3.2}$$

where

$$S_{11} = S_{22} = s$$

and

$$S_{12} = s\ c$$

For the springs,

$$M_1 = R_1(\theta_1 - \gamma_1) \tag{4.3.3}$$

$$M_2 = R_2(\theta_2 - \gamma_2) \tag{4.3.4}$$

Eliminating γ_1 and γ_2 from the above equations results in

$$M_1 = \frac{EI}{L}(\overline{S}_{11}\theta_1 + \overline{S}_{12}\theta_2) \tag{4.3.5}$$

$$M_2 = \frac{EI}{L}(\overline{S}_{12}\theta_1 + \overline{S}_{22}\theta_2) \tag{4.3.6}$$

where

$$\overline{S}_{11} = \frac{s + s^2(1-c^2)\alpha_2}{\overline{F}} \tag{4.3.7a}$$

$$\overline{S}_{22} = \frac{s + s^2(1-c^2)\alpha_1}{\overline{F}} \tag{4.3.7b}$$

$$\overline{S}_{12} = \frac{s\ c}{\overline{F}} \tag{4.3.7c}$$

$$\overline{F} = 1 + s(\alpha_1 + \alpha_2) + s^2(1-c^2)\alpha_1\alpha_2 \tag{4.3.7d}$$

Hence, by treating S_{11}, S_{12} and S_{22} of equation (4.2.12) as $\overline{S}_{11}$, $\overline{S}_{12}$ and $\overline{S}_{22}$ respectively,

and then substituting into equation (3.2.17), the element stiffness matrix of a semi-rigid jointed element in the structure axes system can be established.

It is worth mentioning that when both α_1 and α_2 tend to zero, i.e., a rigid jointed element, then

$$F = 1$$

From equations (4.3.7 a,b,c),

$$\overline{S}_{11} = \overline{S}_{22} = s$$

and

$$\overline{S}_{12} = s \quad c$$

These are exactly similar to the pure rotation coefficients for a rigid jointed element with axial loading.

Furthermore, when the axial effect is neglected, i.e., $P = 0$, then figure 1.2.1 of Chapter 1 gives $s = 4$ and $c = 0.5$. These are in fact the values similar to, and for determining, the coefficients of the rigid jointed element without axial effect.

If only $P = 0$ and then the pure rotation coefficients of equations (4.3.7 a,b,c) will be similar to those of the semi-rigid jointed element without axial loading.

4.3.2 ELEMENT FIXED END FORCES

Figure 4.3.1 shows a semi-rigid jointed element subjected to an uniform distributed load W. The stiffness of the springs at ends 1 and 2 are R_1 and R_2 respectively. Because of the distributed loading, axial load and the end moments, the net rotations at the ends are γ_1 and γ_2 respectively.

For the element, from equation (4.2.15),

$$\frac{d^2y}{dx^2}+\frac{Py}{EI}-\frac{1}{EI}\left(M_1+\frac{Wx^2}{2}-\frac{WLx}{2}\right)=0$$

The solution of the differential equation is

$$y=A\sin\mu x+B\cos\mu x+\frac{1}{\mu^2 EI}\left(M_1+\frac{Wx^2}{2}-\frac{WLx}{2}-\frac{W}{\mu^2}\right) \qquad (4.2.16)$$

Applying the boundary conditions

$y=0$ at $x=0$ and $x=L$ gives

$$A=-B\tan\mu L-\frac{M_1}{P\sin\mu L}+\frac{W}{P\mu^2\sin\mu L}$$

$$B=\frac{W}{p\mu^2}-\frac{M_1}{P}$$

By differentiating equation (4.2.16), the slope at the ends are

$$\gamma_1=\frac{M_1}{PL\sin\mu L}(\mu L\cos\mu L-\sin\mu L)+\frac{M_2}{PL\sin\mu L}(\mu L-\sin\mu L)$$

$$+\frac{WL}{2\mu PL\sin\mu L}(2-2\cos\mu L-\mu L\sin\mu L) \qquad (4.3.8)$$

$$\gamma_2=\frac{M_1}{PL\sin\mu L}(\mu L-\sin\mu L)+\frac{M_2}{PL\sin\mu L}(\mu L\cos\mu L-\sin\mu L)$$

$$-\frac{WL}{2\mu PL\sin\mu L}(2-2\cos\mu L-\mu L\sin\mu L) \qquad (4.3.9)$$

For the springs

$$M_1 = R_1\gamma_1 \tag{4.3.10}$$

$$M_2 = R_2\gamma_2 \tag{4.3.11}$$

Eliminating γ_1 and γ_2 results in

$$M_1 = \frac{W\left(2\tan\frac{\mu L}{2} - \mu L\right)\quad\left(\mu^2 L^2\alpha_2 - \mu L\cot\frac{\mu L}{2} + 2\right)}{2\mu^2 F_1} \tag{4.3.12}$$

$$M_2 = \frac{-W\left(2\tan\frac{\mu L}{2} - \mu L\right)\quad\left(\mu^2 L^2\alpha_1 - \mu L\cot\frac{\mu L}{2} + 2\right)}{2\mu^2 F_1} \tag{4.3.13}$$

where

$$F_1 = 2\tan\frac{\mu L}{2} - \mu L - \mu L(\alpha_1 + \alpha_2)\,(\mu L\cot\mu L - 1) + (\alpha_1\alpha_2\mu^3 L^3)$$

The shear forces are

$$V_1 = \frac{WL}{2} + \frac{M_1 + M_2}{2} \tag{4.3.14}$$

$$V_2 = \frac{WL}{2} - \frac{M_1 + M_2}{2}$$

When the spring stiffnesses are equal to infinity, i.e., rigid jointed ends, equations (4.3.12) and (4.3.13) become

$$M_1 = \frac{W}{\mu^2}\left(1 - \frac{\mu L}{2}\cot\frac{\mu L}{2}\right) \tag{4.3.16}$$

$$M_2 = -M_1 \tag{4.3.17}$$

respectively. Notice that they are similar to equation (4.2.17).

As before, if the axial load is tensile, all trigonometric functions are replaced by hyperbolic equivalents.

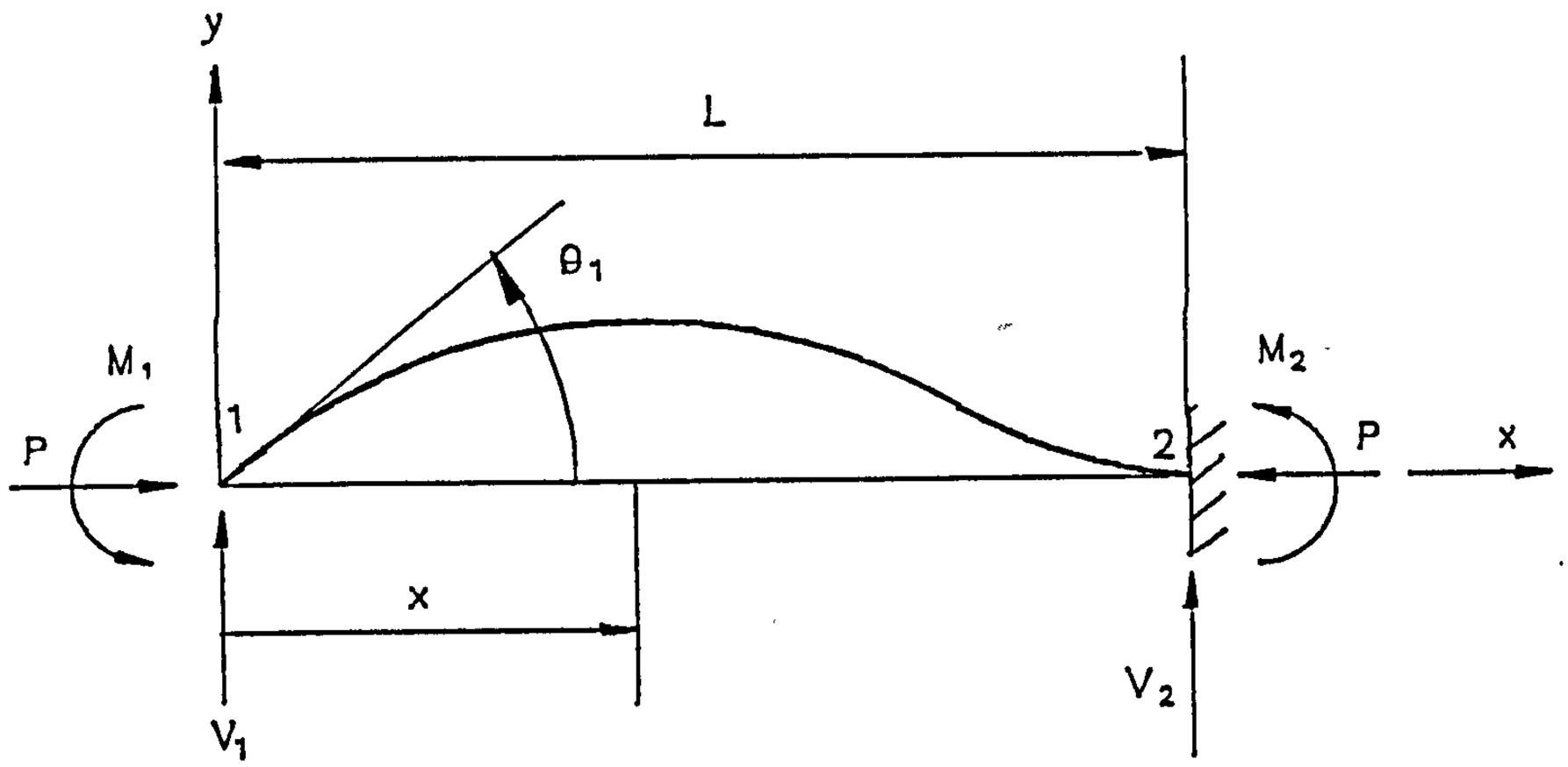

Fig. 4.2.1

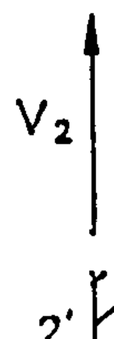

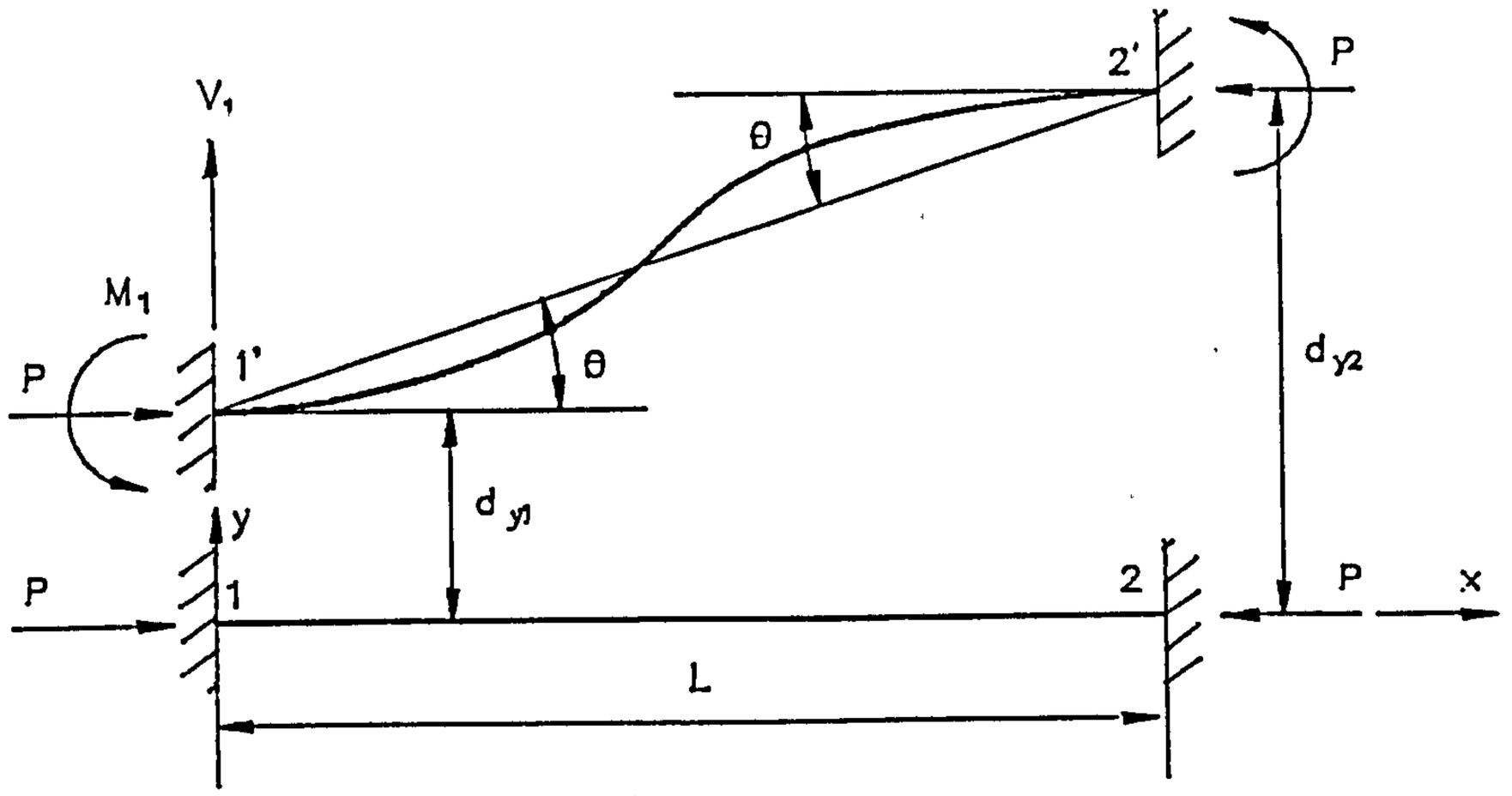

Fig. 4.2.2

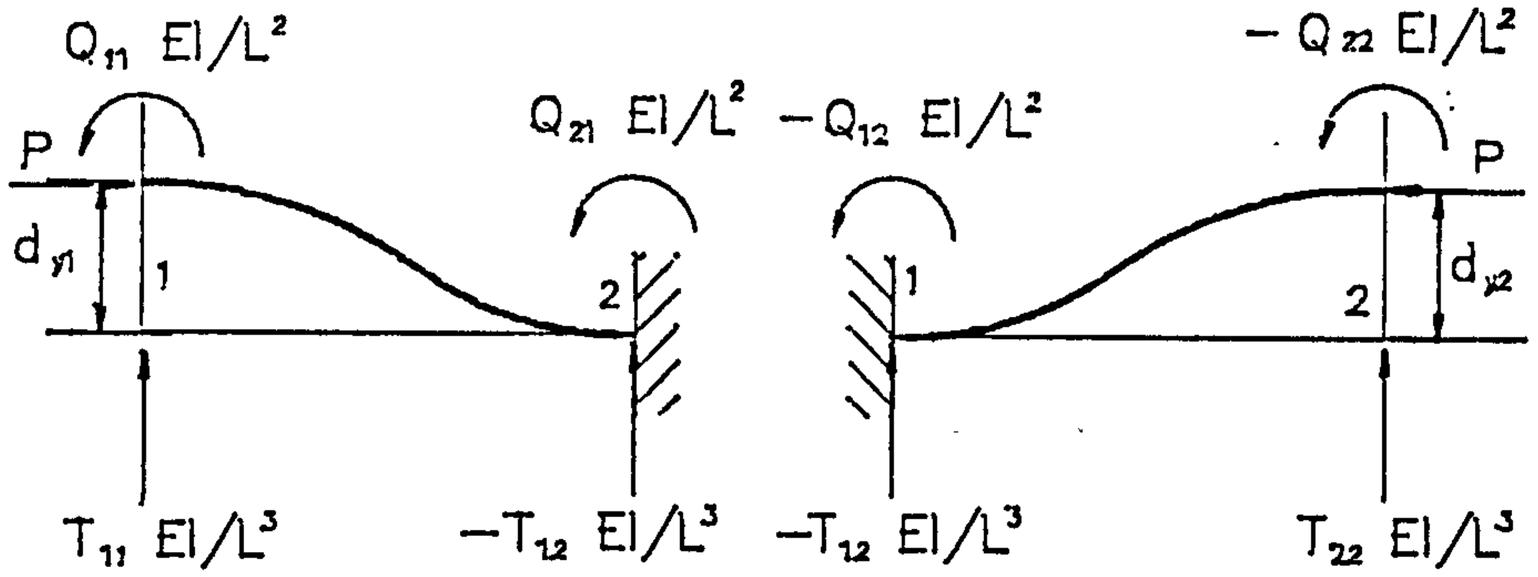

Fig. 4.2.3

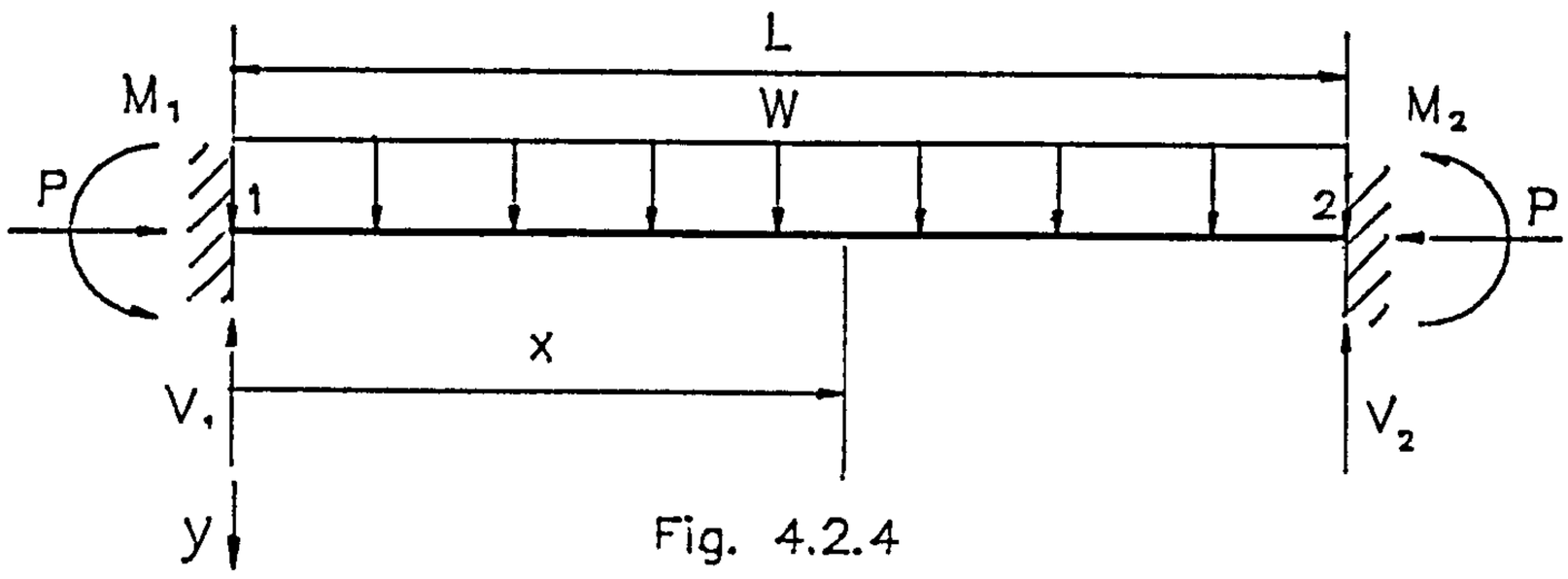

Fig. 4.2.4

Rigid Element with UDL

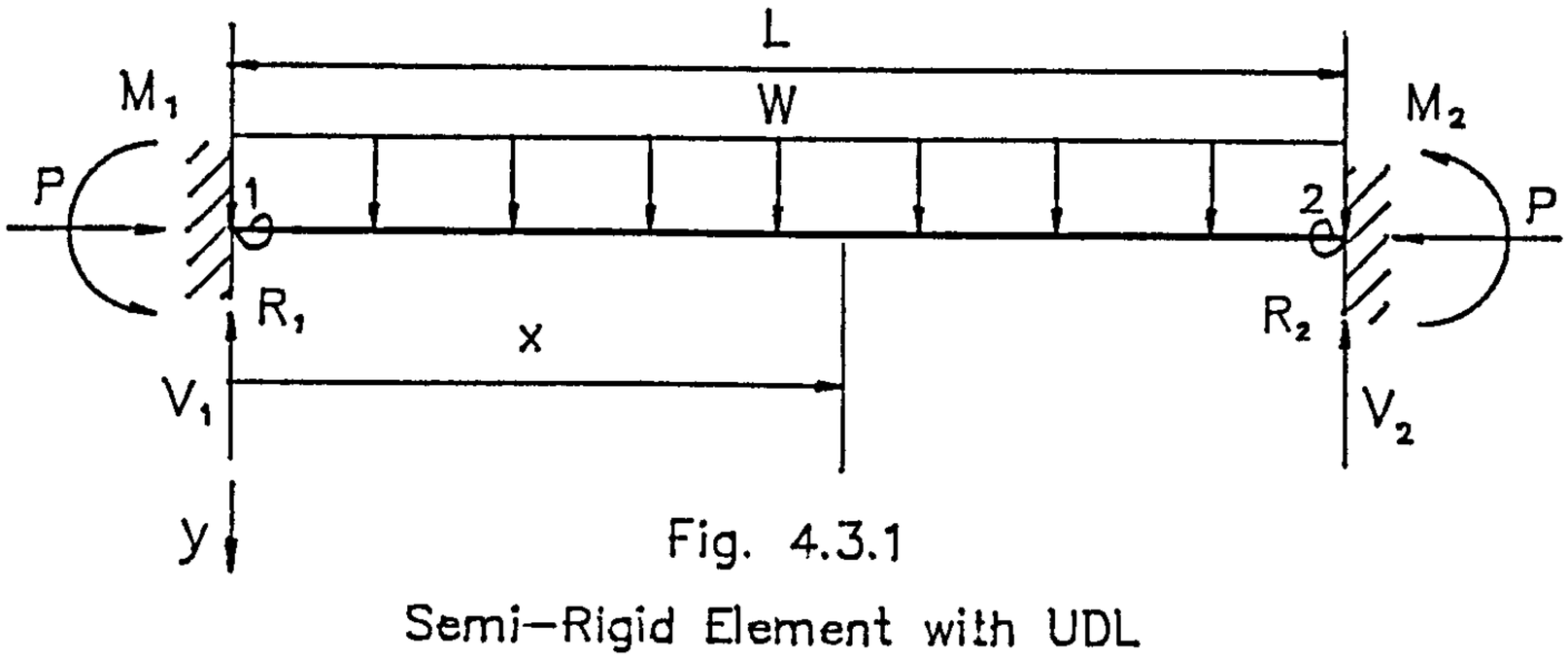

Fig. 4.3.1

Semi–Rigid Element with UDL

CHAPTER 5

LOCAL BUCKLING

5.1 INTRODUCTION

Cold-formed steel sections have been used as structural members for a great many years now. The wide variety of different shapes and the high strength- to- weight ratios combine to make cold-formed steel sections highly competitive for a range of structural applications. One major factor which often gives such sections significant advantages over their hot-rolled counterparts is to be found in the wall thicknesses which can be used. The thickness of the material from which cold-formed sections are manufactured can be very small, and this permits much more economical use of material in many cases than can be obtained using corresponding hot-rolled sections. However, the relative thinness of cold-formed sections, which can be so beneficial to economic range, is also the source of many phenomena which must be considered if advantage is to be taken of the potential economies. Perhaps the most important of these phenomena is local buckling.

Local buckling in a structural member is characterised by a number of ripples or buckles along the walls of a section as illustrated in figure 5.1.1 (a). The buckled shape of the cross section is shown in figure 5.1.1 (b). It is well known that the occurrence of local buckling in a compressed thin-walled structural member, while not necessarily causing immediate failure, radically reduces the stiffness of the member against further compression and hastens the ultimate failure.

Although the effects of local buckling have been extensively investigated, performing the post-buckling in a rigorous manner is extremely complex and tedious. The complication of large deformations combined with inelastic behaviour in the later stages of post-buckling makes a widely applicable solution difficult. Most solutions which do exist are limited to specific sections or are limited to the earlier stages of post-buckling. Fortunately, a much simpler, generally applicable means exists for incorporating the effects of local buckling. This is the effective width concept.

5.2 EFFECTIVE WIDTH CONCEPT

In the use of the effective width concept, it is necessary to differentiate the plate elements of the structural member. Stiffened elements are flat elements with both edges parallel to the direction of stress stiffened by a web, flange or stiffener which supplies sufficient rigidity to prevent out of plane distortion at the edges. Unstiffened elements are flat elements with only one edge stiffened and the other free. These elements are illustrated in figure 5.2.1.

In the effective width approach, the most severely buckled portions of an element are assumed to be ineffective in resisting load, and the applied compression is resisted by effective portions situated adjacent to the supported edges. This is illustrated in figure 5.2.2, which shows a typical buckled plain channel section under an axial load. The compressive stress distributions in both the stiffened and unstiffened elements is non-uniform. This is idealized by an uniform stress distribution which acts only on the effective portion of the buckled plate element based on the effective width concept. Also shown in the figure are parts of the buckled plate elements that have been deleted. Depending upon the width-to-thickness ratios of the individual elements, typical buckled channel sections columns are illustrated in figure 5.2.3.

After the evaluation of the effective widths, the new sectional properties like area, second moment of area, neutral axis position, etc., are used for further computation. A detailed description is given in Chapter 9. Figure 5.2.4 shows a typical effective section of a plain channel with the new neutral axis position.

For the works reported herein, the computation of the effective width is based on the design specifications on local buckling of BS 5950, Part 5. Only sections relevant to and required for the determination of effective width of the elements of plain

channel are extracted and detailed. For cases not covered by the design specifications, approximations are made and will be mentioned as and when encountered.

5.3 ELEMENT UNDER UNIFORM COMPRESSION

5.3.1 STIFFENED ELEMENT

The effective width, b_e, of a stiffened element under uniform compression is as follows :

For

$$\frac{\sigma_c}{\sigma_{cr}} < 0.123$$

then

$$\frac{b_e}{b} = 1 \qquad (5.3.1)$$

For

$$\frac{\sigma_c}{\sigma_{cr}} \geq 0.123$$

then

$$\frac{b_e}{b} = \left\{1 + 14\left[\sqrt{\frac{\sigma_c}{\sigma_{cr}}} - 0.35\right]^4\right\}^{-0.2} \qquad (5.3.2)$$

Equation (5.3.2) is the basic effective width expression. σ_{cr} is the local buckling stress of the element given by :

$$\sigma_{cr} = 185000K\left(\frac{t}{b}\right)^2 \qquad (5.3.3)$$

For this case, the local buckling coefficient is given by :

$$K = \frac{2}{\beta} + \frac{2 + 4.8h}{\beta^2} \tag{5.3.4}$$

where

$$\beta = (1 + 15h^3)^{1/2}$$

$$h = \frac{b_2}{b_1}$$

For a beam element,

$$K = 7 - \frac{1.8h}{0.15 + h} - 0.091h^3 \tag{5.3.5}$$

The value of K for the column and beam element can also be obtained graphically from figures 5.3.1 and 5.3.2 respectively. Note that if K is less than 4, then a value of 4 can be used and this applies to any case of stiffened element.

5.3.2 UNSTIFFENED ELEMENT

The effective width, b_{eu}, of an unstiffened element under uniform compression is:

$$b_{eu} = 0.89b_e + 0.11b \tag{5.3.6}$$

where b_e is determined from Section 5.3.1.

For this case, assuming constant thickness for b_1 and b_2 ,

$$K = h^2\left(\frac{2}{\beta} + \frac{2 + 4.8h}{\beta^2}\right) \tag{5.3.7}$$

If K is less than 0.425, then a value of 0.425 may be used. This applies to any case of unstiffened element.

5.4 ELEMENT UNDER COMBINED BENDING AND AXIAL LOAD

Only the unstiffened element is mentioned here as this is the only relevant case for the members examined here. If the loading is such as to cause compression of the free edge, the effective width may be determined from Section 5.3.2 with σ_c replaced by the stress at the free edge and the buckling coefficient for this case is

$$K = \frac{3.4}{\left(2+\frac{h}{1+h}\right)} \qquad (5.4.1)$$

where $h = b_1/b_2$ in this case.

The buckling coefficient can also be determined graphically from figure 5.7.1.

If the loading is such as to cause tension of the free edge, the effective width is taken as the full flat width.

5.5 BEAM-COLUMN ELEMENT (1ST APPROXIMATION)

For a beam-column element, the moments at the ends are not uniform. Hence, the stresses at the ends of both the stiffened and unstiffened elements are not equal in both magnitude and direction. This is illustrated in figure 5.5.1 and it should be noted that all the stresses $\sigma_1, \sigma_2, \sigma_3$ and σ_4 can either be tensile or compressive, depending on the end forces. The effective width of such an element is not covered by the design specifications. Therefore, an approximation is made by assuming the element to be a beam element.

5.5.1 STIFFENED ELEMENT

If both σ_1 and σ_3 are compressive, the effective width is determined from Section 5.3.1 treating the element as a beam element and replacing σ_c with the larger of the σ_1 and σ_3. The buckling coefficient is determined from equation (5.3.5)

If either σ_1 or σ_3 is compressive, the effective width is determined from Section 5.3.1 treating the element as a beam element and replacing σ_c with the compressive stress. The buckling coefficient is determined from equation (5.3.5)

If both σ_1 and σ_3 are tensile, the effective width is taken as the full flat width.

In the first two cases, the buckling coefficient can also be determined graphically from figure 5.3.2. If the value is less than 4, then a value of 4 may be used.

5.5.2 UNSTIFFENED ELEMENT

If both σ_2 and σ_4 are compressive, the effective width is determined from Section 5.3.2 and replacing σ_c with the larger of the σ_2 and σ_4. The buckling coefficient is determined from equation (5.4.1)

If either σ_2 or σ_4 is compressive, the effective width is determined from Section 5.3.2 and replacing σ_c with the compressive stress. The buckling coefficient is determined from equation (5.4.1)

If both σ_2 and σ_4 are tensile, the effective width is taken as the full flat width.

In the first two cases, the buckling coefficient can also be determined graphically from figure 5.4.1. If the value is less than 0.425, then a value of 0.425 may be used.

5.6 BEAM-COLUMN ELEMENT (2ND APPROXIMATION)

In the previous section, the computation of the buckling coefficient was based on the assumption that the element is treated as a beam element. In this second approximation, the buckling coefficient is determined by assuming uniform compression.

5.6.1 STIFFENED ELEMENT

If both σ_1 and σ_3 are compressive, the effective width is determined from Section 5.3.1 and replacing σ_c with the larger of the σ_1 and σ_3. The buckling coefficient is determined from equation (5.3.4)

If either σ_1 or σ_3 is compressive, the effective width is determined from Section 5.3.1 and replacing σ_c with the compressive stress. The buckling coefficient is determined from equation (5.3.4)

If both σ_1 and σ_3 are tensile, the effective width is taken as the full flat width.

In the first two cases, the buckling coefficient can also be determined graphically from figure 5.3.1. If the value is less than 4, then a value of 4 may be used.

5.6.2 UNSTIFFENED ELEMENT

If both σ_2 and σ_4 are compressive, the effective width is determined from Section 5.3.2 and replacing σ_c with the larger of the σ_2 and σ_4. The buckling coefficient is determined from equation (5.3.7)

If either σ_2 or σ_4 is compressive, the effective width is determined from Section 5.3.2 and replacing σ_c with the compressive stress. The buckling coefficient is determined from equation (5.3.7)

If both σ_2 and σ_4 are tensile, the effective width is taken as the full flat width.

In the first two cases, the buckling coefficient can also be determined graphically from figure 5.3.1. If the value is less than 0.425, then a value of 0.425 may be used.

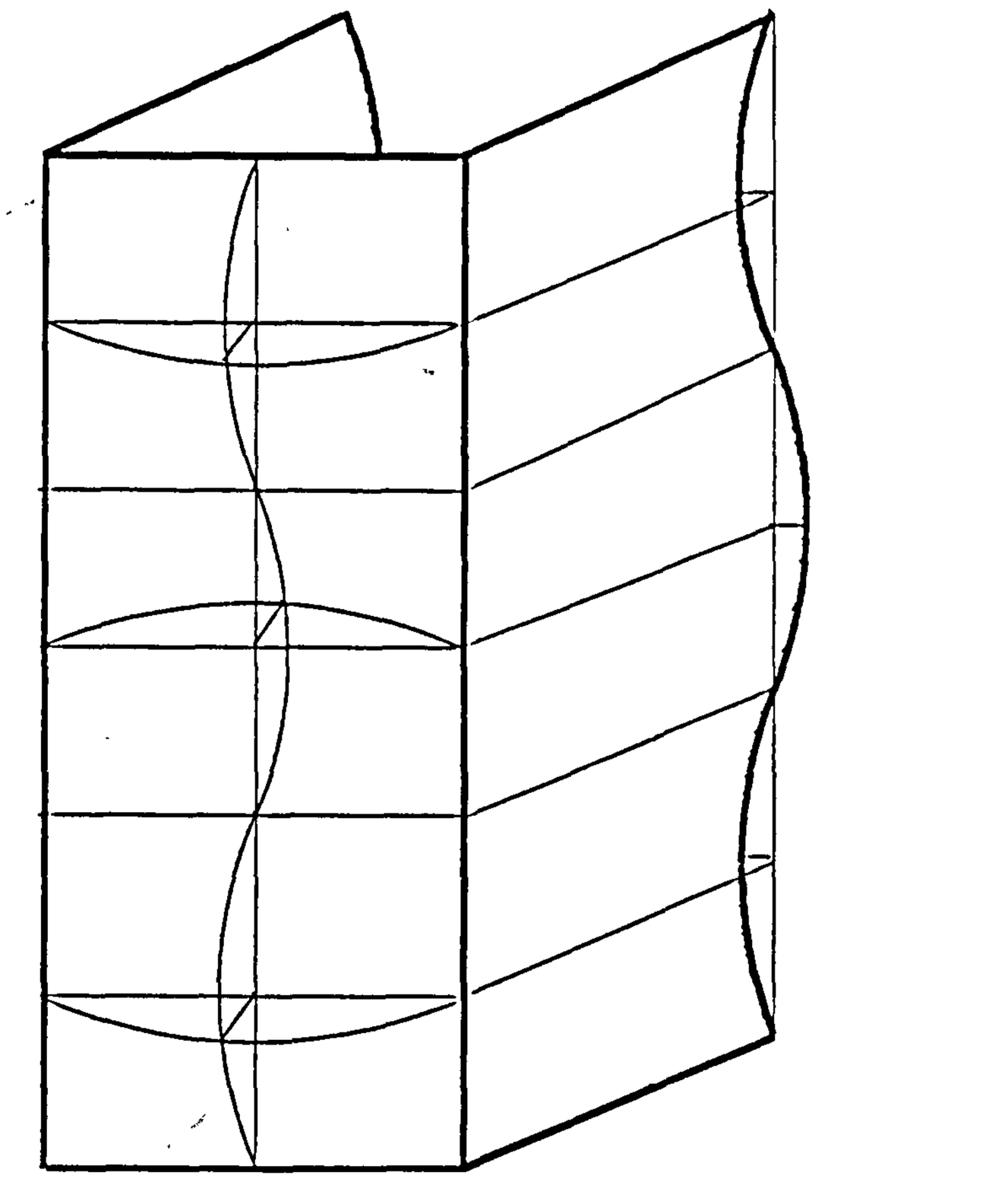

(a)

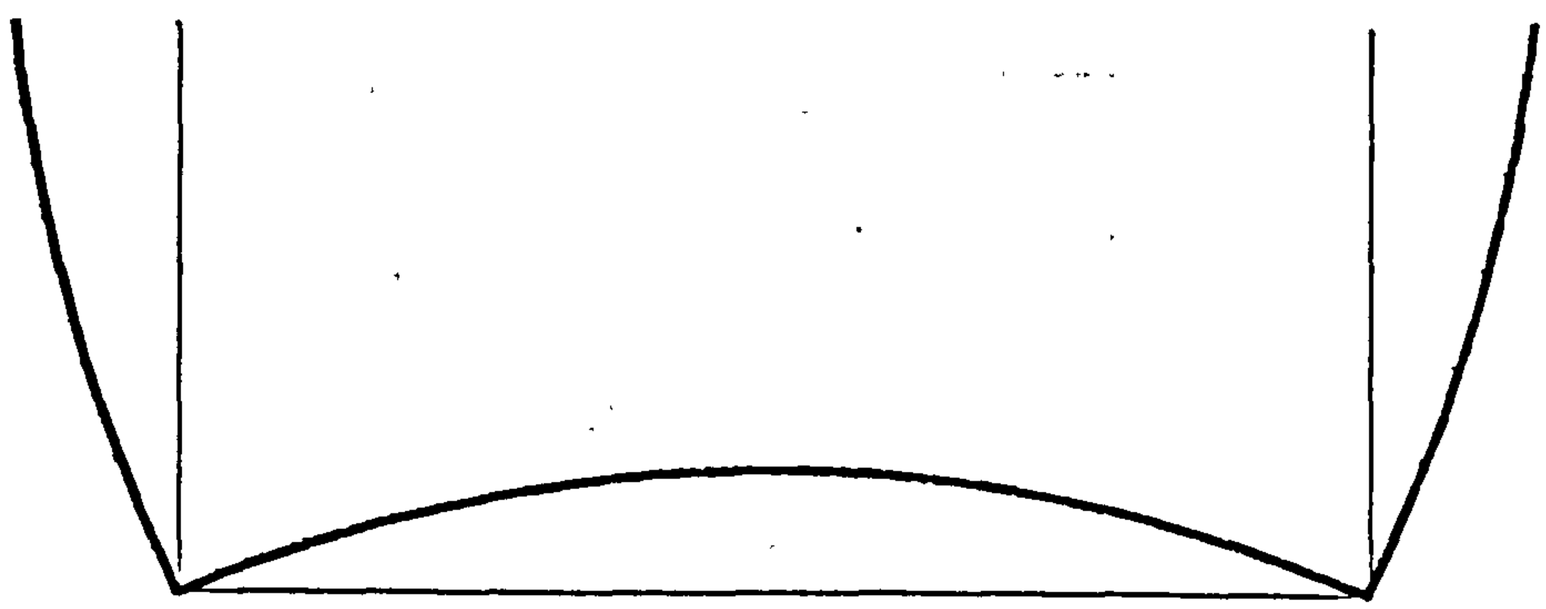

(b)

Fig. 5.1.1

Locally Buckled Plain Channel and Cross Section Shape.

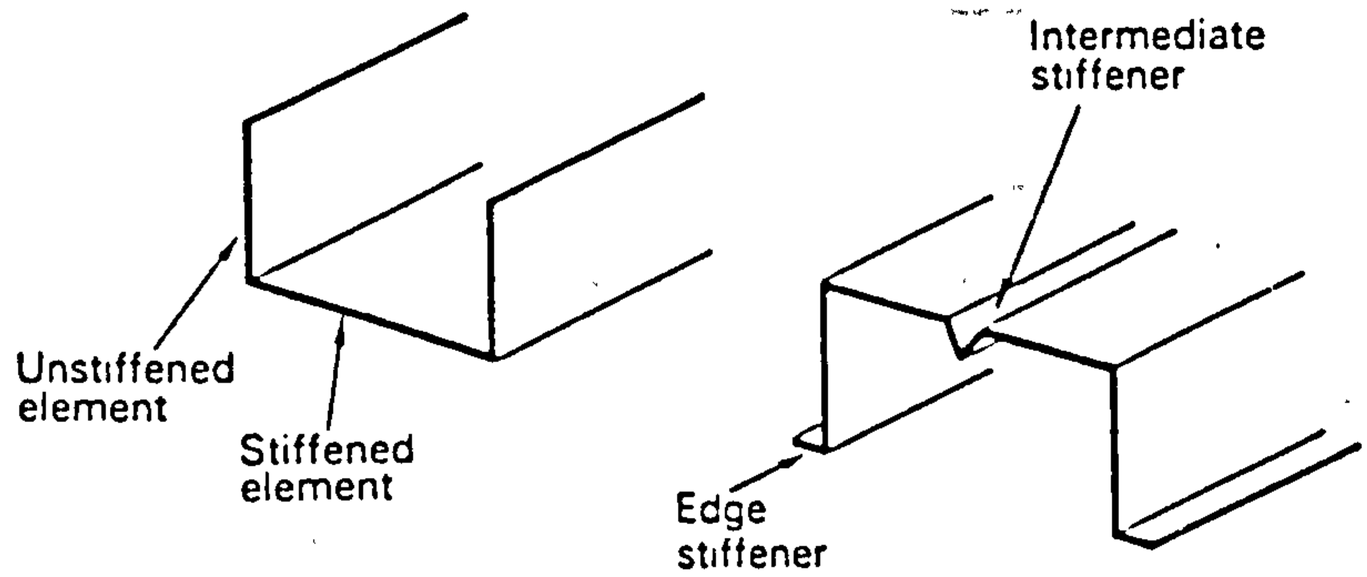

Fig. 5.2.1 Typical Elements of Cold-Formed Sections

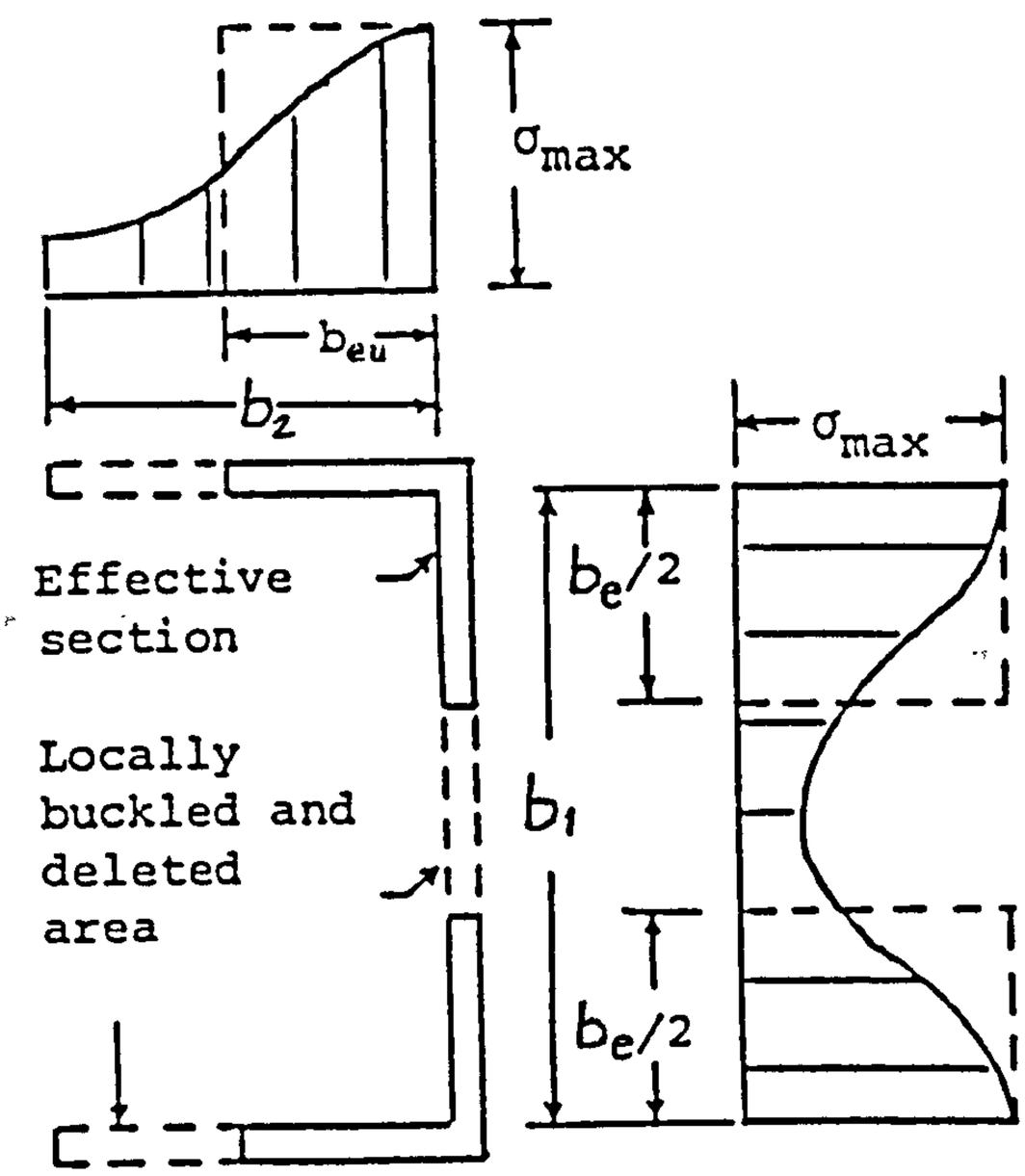

Fig. 5.2.2 Stress Distribution in Locally
Buckled Section and Effective Width Concept

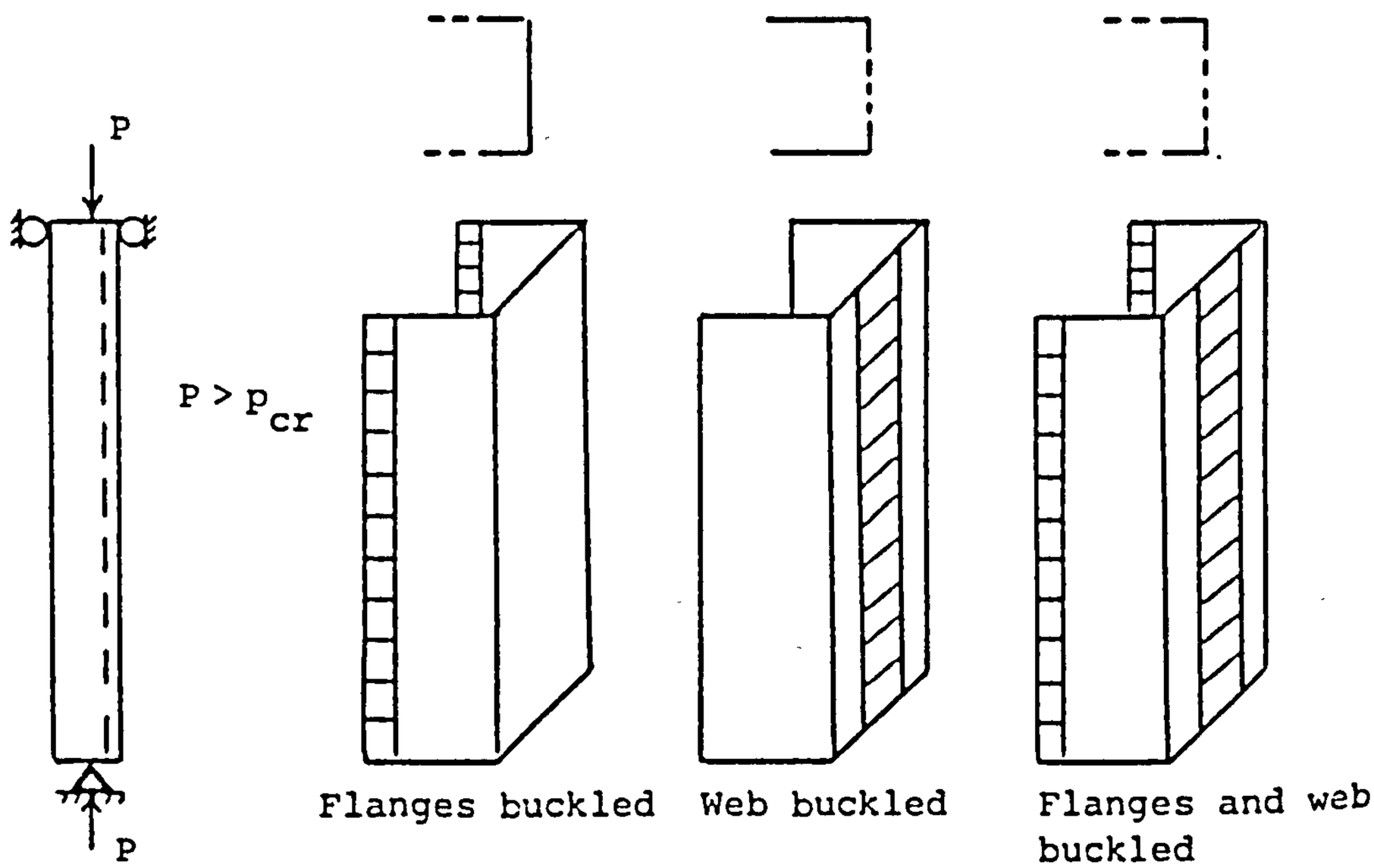

Fig. 5.2.3

Effective Column Section in the Post Local Buckling Range.

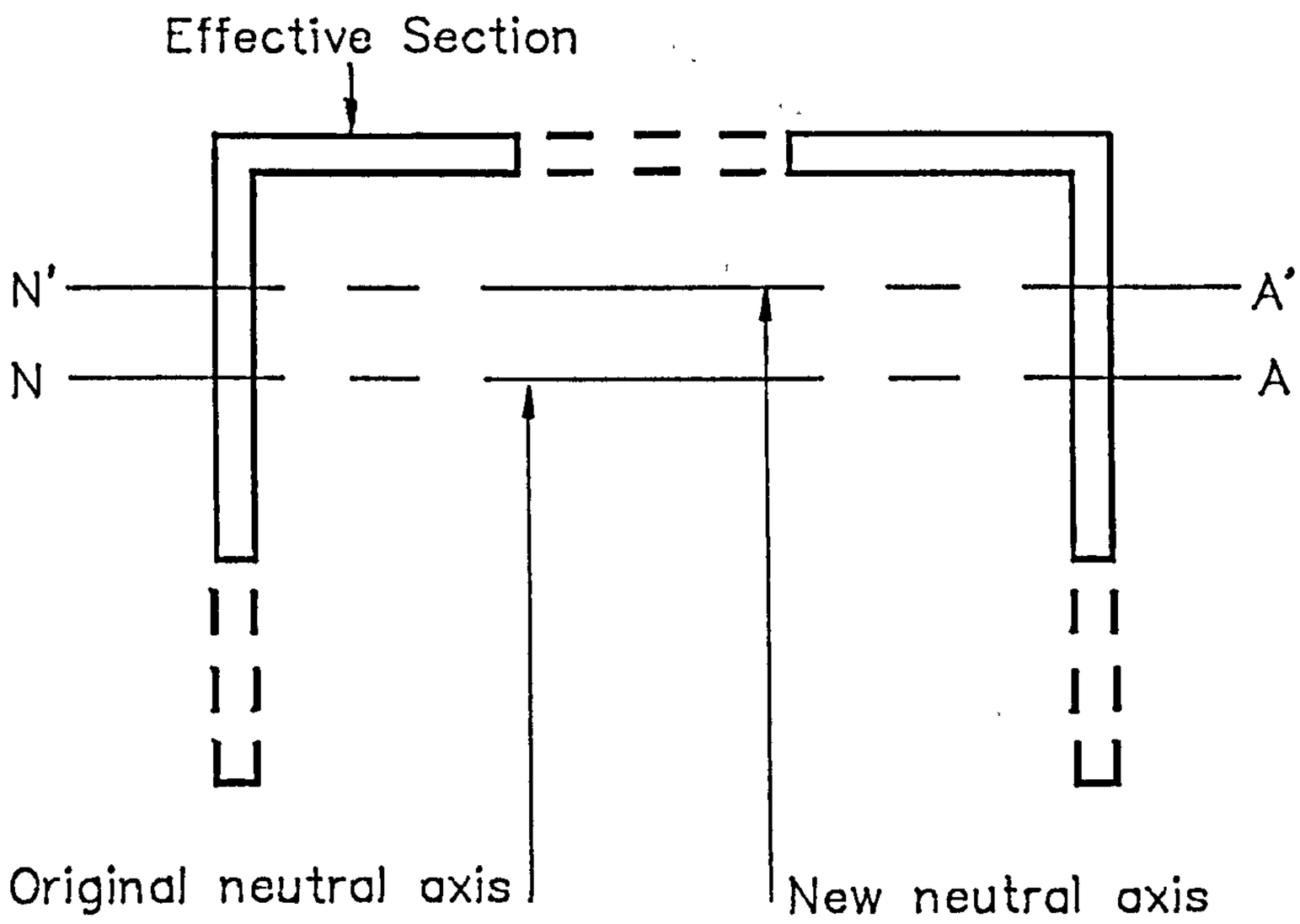

Fig. 5.2.4 Effective Section With New Neutral Axis Position.

K factors for some bending and compression elements

Values for buckling coefficients for elements of some common structural members are plotted in figures 13 to 15 and approximate equations are included to aid calculation. The K factors given refer to the element of width B_1 in all cases and are thus termed K_1. Where K_1 is less than 4 in the case of a stiffened element and 0.425 in the case of an unstiffened element, the value 4 or 0.425 may be used.

In the case of uniformly compressed members the corresponding K factor for elements of width B_2, which is thus termed K_2, may be obtained as follows:

$$K_2 = K_1 h^2 \left(\frac{t_1}{t_2}\right)^2$$

where

$h = B_2/B_1$

t_1, t_2 are the thicknesses of element widths B_1 and B_2 respectively.

Normally t_1 and t_2 are equal, but there are cases where the element has double thickness, e.g. element B_1 in case 3 of figure 13 where $t_1 = 2\,t_2$.

Where K_2 is less than 4 or 0.425 as the case may be then the values 4 or 0.425 may be used.

In the case of beams the K_1 factor refers to the element of width B_1, which is taken as the compression element except in the case of curve 4 in figure 13 and curve 2 in figure 15, in which cases the K_1 factor refers to the tip stress of the unstiffened bending element.

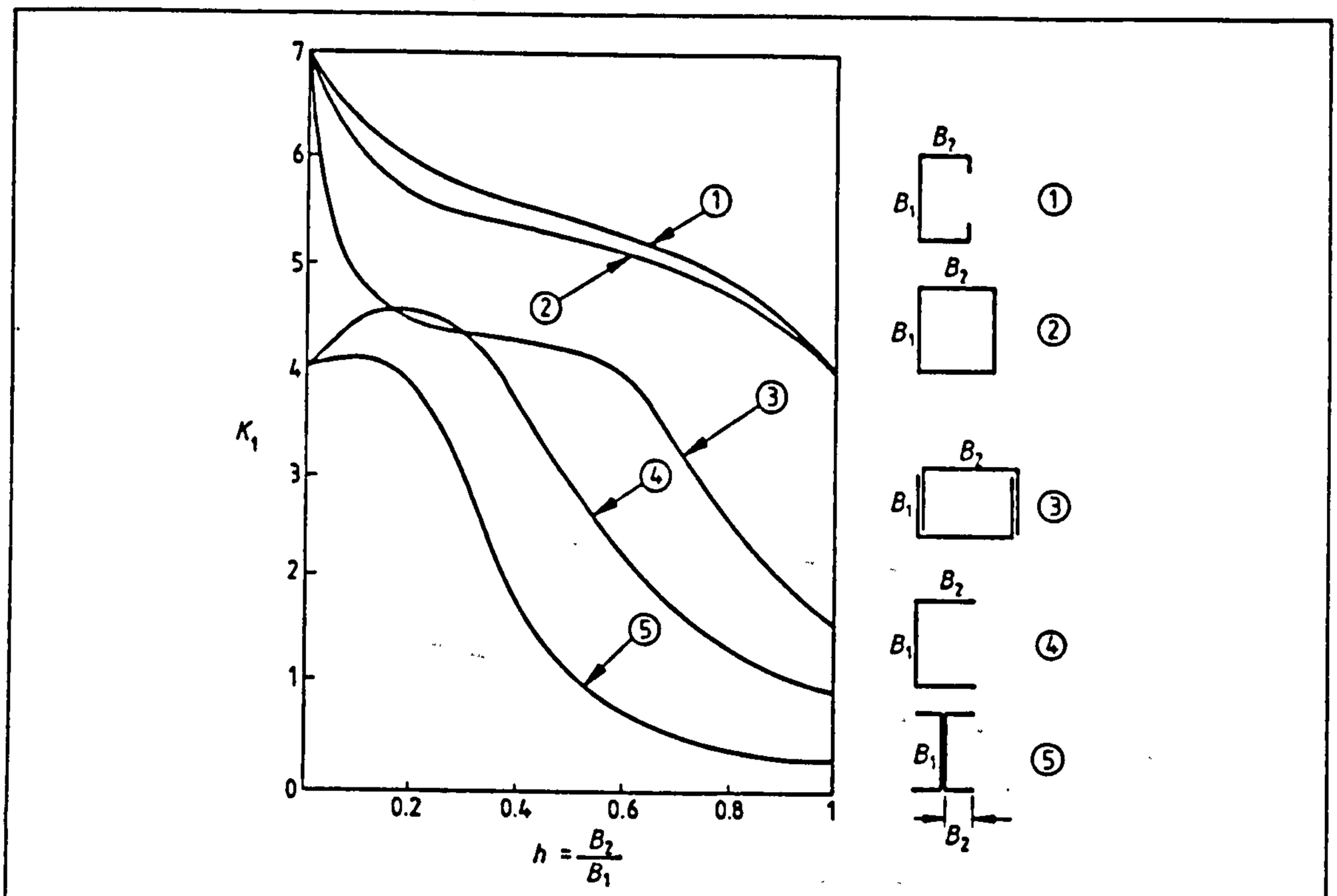

Curve 1 Lipped channel $K_1 \approx 7 - \dfrac{1.8\,h}{0.15 + h} - 1.43\,h^3$

Curve 2 Box with equal thickness sides $K_1 \approx 7 - \dfrac{2\,h}{0.11 + h} - 1.2\,h^3$

Curve 3 Box with unequal thickness sides

$$K_1 \approx 7 - 5.4\,h + 50\,h\,(h - 0.55)\,(h - 0.75)\,(h - 1)$$

Curve 4 Plain channel $K_1 \approx \dfrac{2}{\beta} + \dfrac{2 + 4.8\,h}{\beta^2}$, where $\beta = (1 + 15\,h^3)^{1/2}$

Curve 5 I-section made from two plain channels fixed back to back

$$K_1 \approx \frac{2}{\beta} + \frac{2 + h}{\beta^2}, \text{ where } \beta = (1 + 90\,h^4)^{1/2}$$

Figure 13. *K* factors for uniformly compressed members

Fig. 5.3.1 K Factors for Uniformly Compressed Members

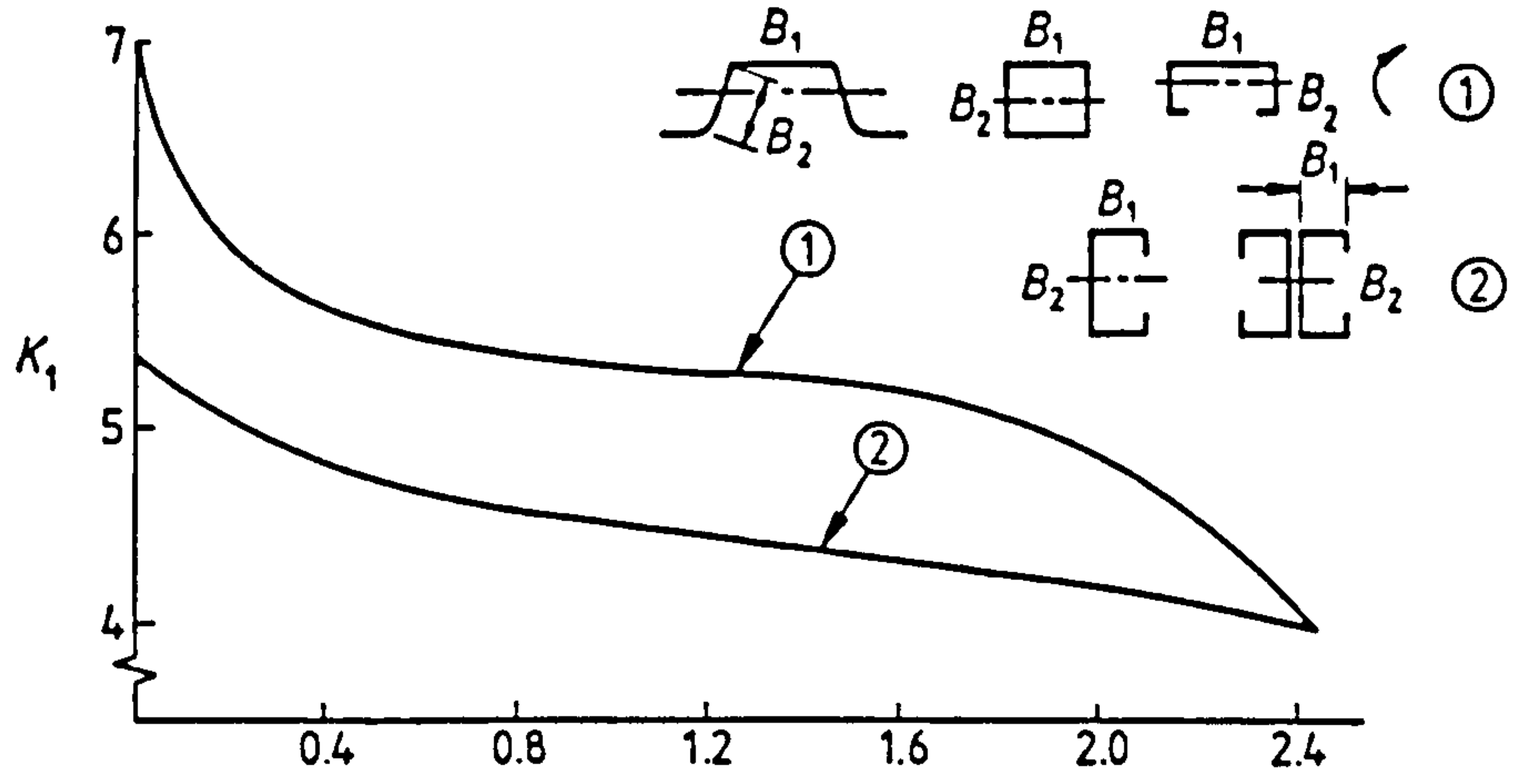

$$h = \frac{B_2}{B_1}$$

Curve 1 Element connection to webs on both edges $K_1 \approx 7 - \dfrac{1.8\,h}{0.15 + h} - 0.091\,h^3$

Curve 2 Element connected to web on one edge and lip on other edge

$$K_1 \approx 5.4 - \frac{1.4\,h}{0.6 + h} - 0.02\,h^3$$

K factors for stiffened compression elements of beams

Fig. 5.3.2

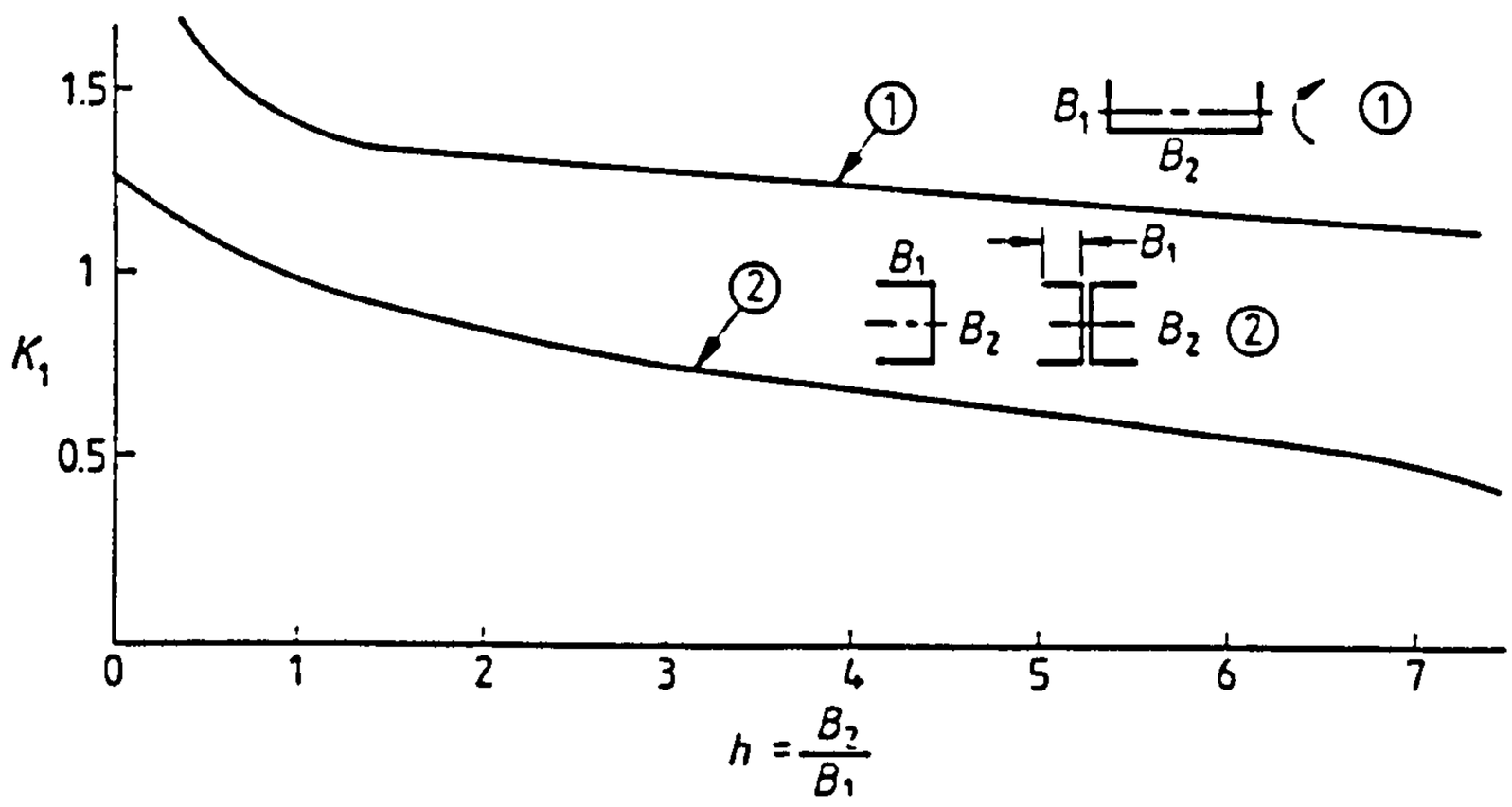

Curve 1 Channel flanges as bending elements $K_1 \approx \dfrac{3.4}{\left(2 + \dfrac{h}{1 + h}\right)}$

Curve 2 Unstiffened element $K_1 \approx 1.28 - \dfrac{0.8\,h}{2 + h} - 0.0025\,h^2$

K factors for unstiffened elements of beams

Fig. 5.4.1

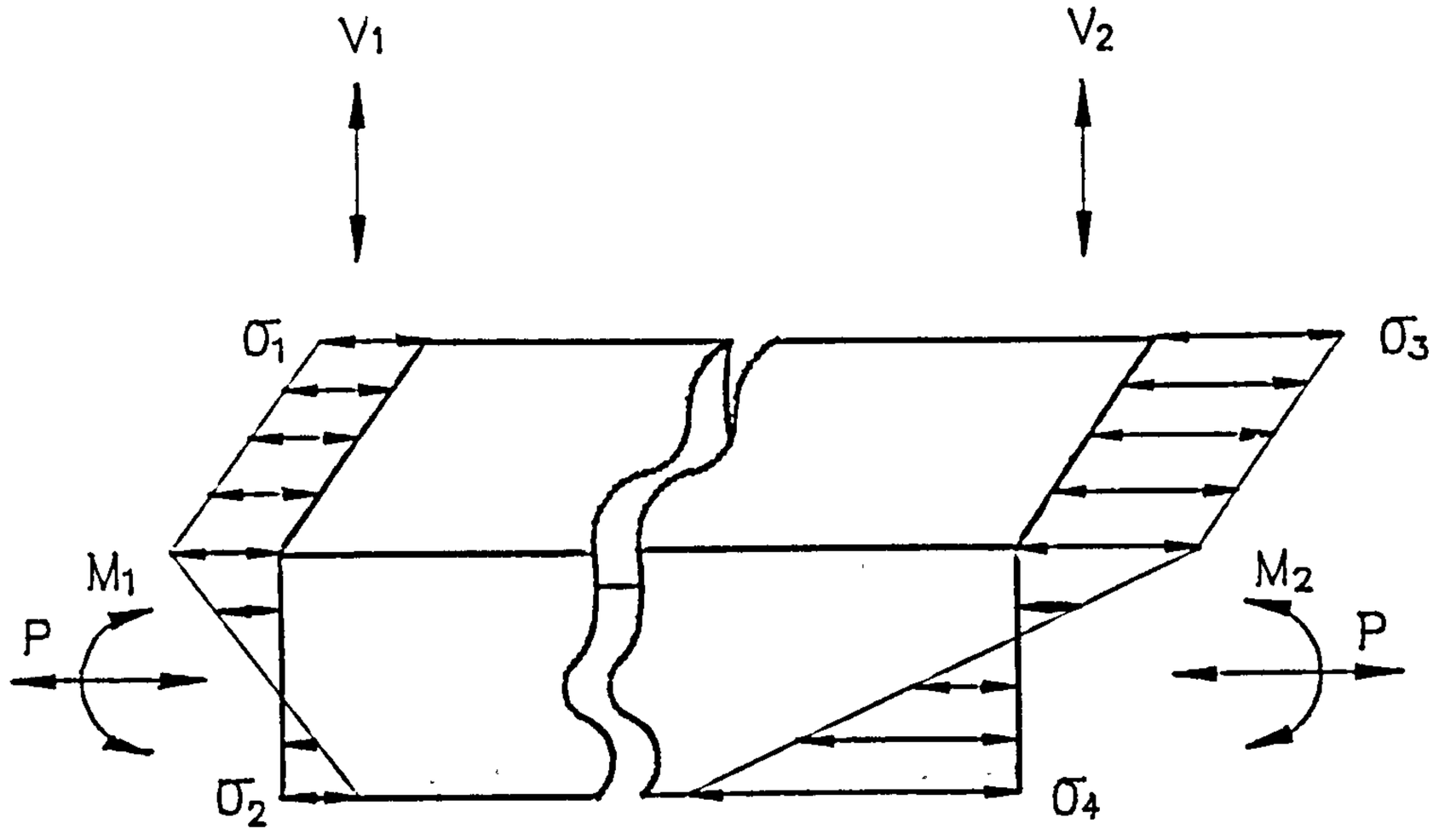

Fig. 5.5.1

Typical Stresses of a Beam–Column.

CHAPTER 6

EVALUATION OF PLASTIC MOMENT

6.1 INTRODUCTION

In the ultimate or collapse load analysis of structural framework, the plastic hinge idealization is often used. When a member is subjected to loading, especially bending, yielding begins at the most stressed section. When full yielding has taken place at a section and unrestrained plastic flow occurs, an idealized plastic hinge is formed. The maximum bending that the section can withstand is the plastic moment. The plastic moment is a geometric property of the section. Both the plastic hinge and moment concepts are idealizations of the true section behaviour. The plastic hinge, which is assumed to occur over an infinitely short length of the member, can undergo rotation while the plastic moment remains constant.

In the derivation of the plastic moment detailed below, the material is assumed to behave in an elastic-perfectly-plastic manner. The usual assumption of small deformation and original plane sections remaining plane are also employed. The effect of shear is neglected and the section is also assumed to be of constant thickness.

In the theoretical critical load analysis detailed in Chapter 9, the computation of the individual member plastic moment is based on the current effective geometry and axial load, if desired. This is to account for the reduced plastic moment capacity of the member due to both local buckling and axial load effects.

6.2 PLASTIC MOMENT WITHOUT AXIAL LOADING

When a plain channel is subjected to bending about the axis parallel to the stiffened element, the stress across the unstiffened element varies linearly until the yield stress is reached. Further increased in the moment due to bending will cause partial plasticity and then finally to full plasticity as illustrated in figure 6.2.1. The direction of the bending moment is shown to cause compression of the free edge of the unstiffened element. As the section is not symmetrical about the neutral axis, this

causes the zero strain axis to move from the centroid at full plasticity. The term zero strain axis is used deliberately to avoid confusion with the neutral axis, which is associated by common usage with the centroid. As the zero strain axis can either lie within the stiffened or unstiffened element, there are two cases to consider.

6.2.1 ZERO STRAIN AXIS WITHIN UNSTIFFENED ELEMENT ($H > t$)

Figure 6.2.1 shows a plain channel section at full plasticity. The zero strain axis lies within the unstiffened element and its position, H is measured from the base of the stiffened element.

From equilibrium of the normal forces,

$$\sigma_y t[2(b_2 - H) - 2(H - t) - b_1] = 0$$

The zero strain axis position is then

$$H = \frac{2(b_2 + t) - b_1}{4} \tag{6.2.1}$$

For $H > t$,

$$2(b_2 + t) - b_1 > 4t \tag{6.2.2}$$

Taking moments about O gives

$$M_p = \sigma_y t\left[(b_2 - H)^2 + (H - t)^2 + b_1\left(H - \frac{t}{2}\right)\right]$$

Substituting of equation (6.2.1) and simplifying result in

$$M_p = \sigma_y Z_p \tag{6.2.3}$$

where Z_p is the plastic section modulus given by :

$$Z_p = t\left(\frac{b_2^2}{2}+\frac{t^2}{2}-\frac{b_1^2}{8}-b_2 t+\frac{b_1 b_2}{2}\right) \tag{6.2.4}$$

Equation (6.2.3) is also valid when the direction of the bending moment is reversed, provided equation (6.2.2) is satisfied, i.e., for $H > t$.

6.2.2 ZERO STRAIN AXIS WITHIN STIFFENED ELEMENT

$(H \leq t)$

Figure 6.2.2 shows the zero strain axis position within the stiffened element, i.e., $H \leq t$, for the bending moment applied in the same direction as before, causing compression at the free edge of the unstiffened element.

From equilibrium,

$$\sigma_y[2t(b_2-t)+b_1(t-H)-b_1 H]=0$$

or

$$H = t\left(\frac{b_2-t}{b_1}+\frac{1}{2}\right) \tag{6.2.5}$$

For $H \leq t$,

$$t\left(\frac{b_2-t}{b_1}+\frac{1}{2}\right)\leq t$$

or

$$\frac{b_2-t}{b_1}\leq\frac{1}{2} \tag{6.2.6}$$

Taking moments about O,

$$M_p = \sigma_y\left[2t(b_2-t)\left(\frac{b_2-t}{2}+t-H\right)+\frac{b_1(t-H)^2}{2}+\frac{b_1 H^2}{2}\right]$$

Substitution of equation (6.2.5) gives

$$M_p = \sigma_y Z_p \tag{6.2.7}$$

where

$$Z_p = t\left(b_2^2 - \frac{b_2^2 t}{b_1} - b_2 t + \frac{2b_2 t^2}{b_1} - \frac{t^3}{b_1} + \frac{b_1 t}{4}\right) \tag{6.2.8}$$

Equation (6.2.7) also applies when the bending moment is reversed, provided equation (6.2.6) is satisfied.

6.3 PLASTIC MOMENT WITH AXIAL LOAD

When an axial load is present in addition to bending moment, the determination of the plastic moment, M_{pa}, is more complex. Furthermore, more different cases have to be considered. This is due to the fact that the axial load can either be compressive or tensile and the bending moment can also be reversed too. For each individual case of loading, the position of the zero strain axis at full plasticity must also be taken into account. In the following evaluation of M_{pa}, the axial load is assumed to act at the centroid of the section.

Before the determination of the full plastic moment, it is necessary to know the position of the centroid, Y, of the cross section. Referring to figure 6.3.1,

$$Y = \frac{\sum A y}{\sum A}$$

From the above equation, the position of the centroid is given by :

$$Y = \frac{b_2^2 - t^2 + \frac{b_1 t}{2}}{2(b_2 - t) + b_1} \tag{6.3.1}$$

6.3.1 COMPRESSIVE AXIAL LOAD AND MOMENT CAUSING COMPRESSION ON FREE EDGE OF UNSTIFFENED ELEMENT

6.3.1.1 ZERO STRAIN AXIS WITHIN UNSTIFFENED ELEMENT ($H > t$)

Figure 6.3.2 shows a fully plasticised section with a compressive axial load and bending moment causing compression above the zero strain axis. The zero strain axis lies within the unstiffened element.

For equilibrium,

$$P = \sigma_y t[2(b_2 - H) - 2(H - t) - b_1]$$

or

$$H = \frac{1}{4}\left[2(b_2 + t) - b_1 - \frac{P}{\sigma_y t}\right] \tag{6.3.2}$$

Note that when there is no axial load, i.e., $P = 0$, equation (6.3.2) is similar to equation (6.2.1), which is for the case without axial load.

For $H > t$, equation (6.3.2) becomes

$$P < \sigma_y t[2(b_2 - t) - b_1] \tag{6.3.3}$$

From summation of moments about O,

$$M_{pa} + P(Y - H) = \sigma_y t\left[(b_2 - H)^2 + (H - t)^2 + b_1\left(H - \frac{t}{2}\right)\right]$$

Simplifying and substitution of equation (6.3.2) give

$$M_{pa}+P(Y-H)=\sigma_y t\left[\frac{b_2^2}{2}+\frac{t^2}{2}-\frac{b_1^2}{8}-b_2 t+\frac{b_1 b_2}{2}\right]+\frac{P^2}{8\sigma_y t} \qquad (6.3.4)$$

By careful examination of equation (6.3.4), it can be noticed that the first term of the right hand side equation is similar to equation (6.2.3), which is the plastic moment, M_p, without axial load. This can be verified by substituting $P=0$ into equation (6.3.4).

From the above,

$$M_{pa}=M_p+\frac{P^2}{8\sigma_y t}-P(Y-H)$$

Substitution of equations (6.3.1) and (6.3.2) leads to

$$M_{pa}=M_p-\frac{P^2}{8\sigma_y t}-\frac{P b_1(b_1-2t)}{4[2(b_2-t)+b_1]}$$

The squash load is given by

$$P_s=\sigma_y t[2(b_2-t)+b_1]$$

Substituting results in

$$M_{pa}=M_p\left\{1-\frac{A^2 t}{8Z_p}\left[B^2+\frac{B\,C}{A^2}\right]\right\} \qquad (6.3.5)$$

where

M_p is from equation (6.2.3)

Z_p is from equation (6.2.4)

$A=2(b_2-t)+b_1$

$B=\dfrac{P}{P_s}$

$C=2b_1(b_1-2t)$

It is interesting to note that when $b_1 \rightarrow 2t$, equation (6.3.5) becomes

$$M_{pa} = M_p(1 - B^2)$$

which is the plastic moment for a rectangular cross section with compressive axial load.

When both the axial load and bending moment are reversed, causing tension above the zero strain axis, it can be easily shown that the plastic moment is similar to that of equation (6.3.5), provided that equation (6.3.3) is satisfied.

6.3.1.2 ZERO STRAIN AXIS WITHIN STIFFENED ELEMENT ($H \leq t$)

Figure 6.3.3 shows the same previous condition discussed except that the position of the zero strain axis now lies within the stiffened element during full plasticity.

From equilibrium,

$$P = \sigma_y[2t(b_2 - t) + b_1(t - H) - b_1 H]$$

or

$$H = t\left(\frac{b_2 - t}{b_1} + \frac{1}{2}\right) - \frac{P}{2\sigma_y b_1} \tag{6.3.6}$$

Again, it can be seen that when $P = 0$, equation (6.3.6) is similar to equation (6.2.5).

For $H \leq t$,

$$t\left(\frac{b_2 - t}{b_1} + \frac{1}{2}\right) - \frac{P}{2\sigma_y b_1} \leq t$$

or

$$P \geq \sigma_y t[2(b_2 - t) - b_1] \tag{6.3.7}$$

Takings moments about O,

$$M_{pa}+P(Y-H)=\sigma_y\left[2t(b_2-t)\left(\frac{b_2-t}{2}+t-H\right)+\frac{b_1(t-H)^2}{2}+\frac{b_1H^2}{2}\right]$$

Substituting equation (6.3.6) and simplifying give

$$M_{pa}+P(Y-H)=M_p+\frac{P^2}{4\sigma_y b_1}$$

where M_p is similar to equation (6.2.7).

As before, when $P=0$, the plastic moment is for the same case without axial load.

Substituting P_s and equation (6.3.6) result in

$$M_{pa}=M_p\{1-\frac{(At)^2}{4Z_p b_1}\left[B^2+\frac{2\,B\,C(b_2-t)^2}{A^2 b_1 t}\right]\} \qquad (6.3.8)$$

where

M_p is from equation (6.2.7)

Z_p is from equation (6.2.8)

$A=2(b_2-t)+b_1$

$B=\frac{P}{P_s}$

$C=2b_1(b_1-2t)$

By observing equation (6.3.7), it can be seen that the plastic moment given by equation (6.3.8) is still valid when $P=P_s$. Hence, by substituting $P=P_s$ into equation (6.3.8),it can be shown that $M_{pa}=0$, i.e., failure is due to squashing.

When $b_2 \rightarrow t$, equation (6.3.8) will become the expression for a rectangular cross section as before.

Similar to the previous case, when both the axial load and bending moment are reversed, thus causing tension above the zero strain axis, equation (6.3.8) is still valid provided that equation (6.3.7) is satisfied.

6.3.2 COMPRESSIVE AXIAL LOAD AND MOMENT CAUSING COMPRESSION ON SUPPORTED EDGE OF UNSTIFFENED ELEMENT

6.3.2.1 ZERO STRAIN AXIS WITHIN UNSTIFFENED ELEMENT ($H > t$)

This case is exactly similar to that of Section 6.3.1.1 except that the direction of the bending moment is reversed. By going through the same procedure, the followings are obtained.

$$H = \frac{1}{4}\left[2(b_2+t) - b_1 + \frac{P}{\sigma_y t}\right] \tag{6.3.9}$$

For $H > t$,

$$P > \sigma_y t[2(t-b_2)+b_1] \tag{6.3.10}$$

Finally,

$$M_{pa} = M_p\left\{1 - \frac{A^2 t}{8Z_p}\left[B^2 - \frac{BC}{A^2}\right]\right\} \tag{6.3.11}$$

where M_p, Z_p, A, B, and C are from equation (6.3.5)

A close examination shows that the above equation can be obtained very easily by changing the sign of P of equations (6.3.2) and (6.3.5). As before, when both the axial load and bending moment are reversed in direction, causing tension on the supported edge of the unstiffened, equation (6.3.11) can be used provided that equation (6.3.10) is satisfied.

6.3.2.2 ZERO STRAIN AXIS WITHIN STIFFENED ELEMENT ($H \leq t$)

By changing the sign of P of equations (6.3.6) and (6.3.8), the following are obtained.

$$H = t\left(\frac{b_2 - t}{b_1} + \frac{1}{2}\right) + \frac{P}{2\sigma_y b_1} \tag{6.3.12}$$

$$P \leq \sigma_y t[2(t - b_2) + b_1] \tag{6.3.13}$$

$$M_{pa} = M_p\{1 - \frac{(At)^2}{4Z_p b_1}\left[B^2 - \frac{2\,B\,C(b_2 - t)^2}{A^2 b_1 t}\right]\} \tag{6.3.14}$$

Equations (6.3.12) and (6.3.14) are also valid when both the axial load and moment are reversed, provided that equation (6.3.13) is satisfied.

A summary of the various plastic moment expressions and their related condition is tabulated and listed in Appendix IV.

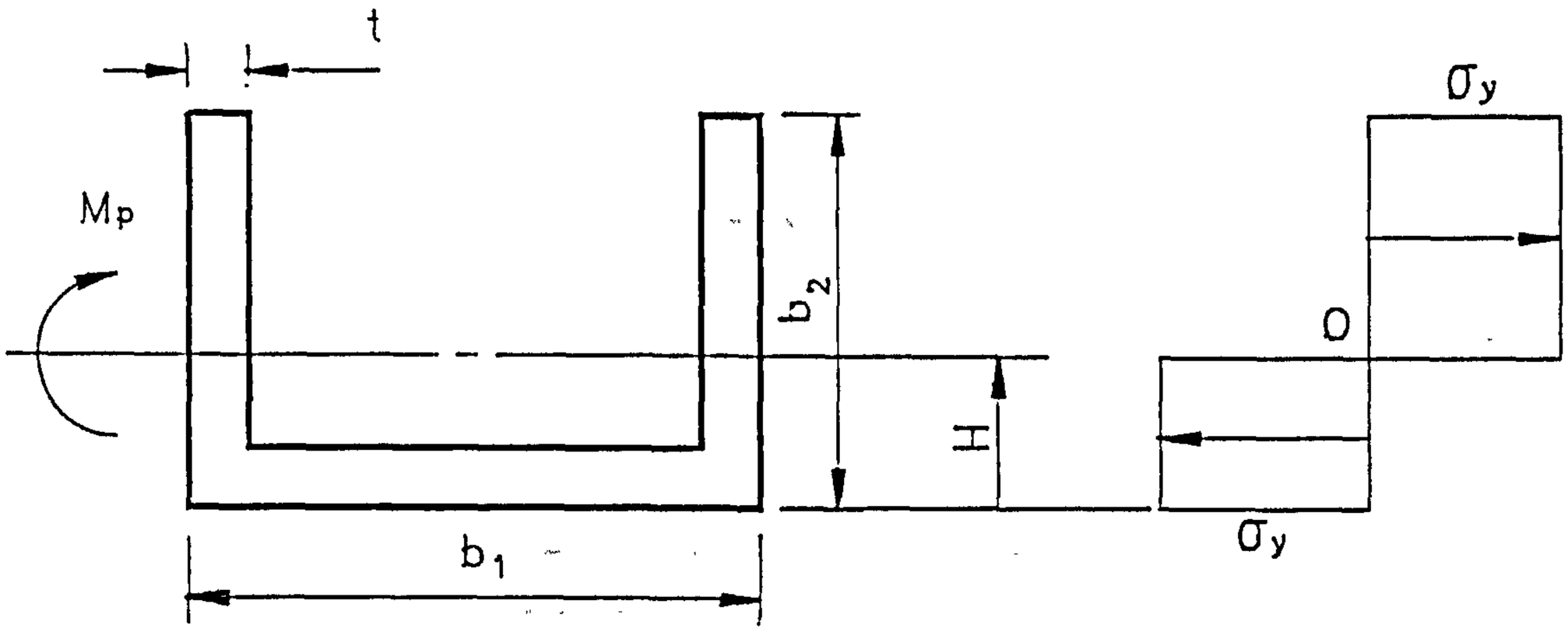

Fig. 6.2.1 Full Plasticity with H>t.

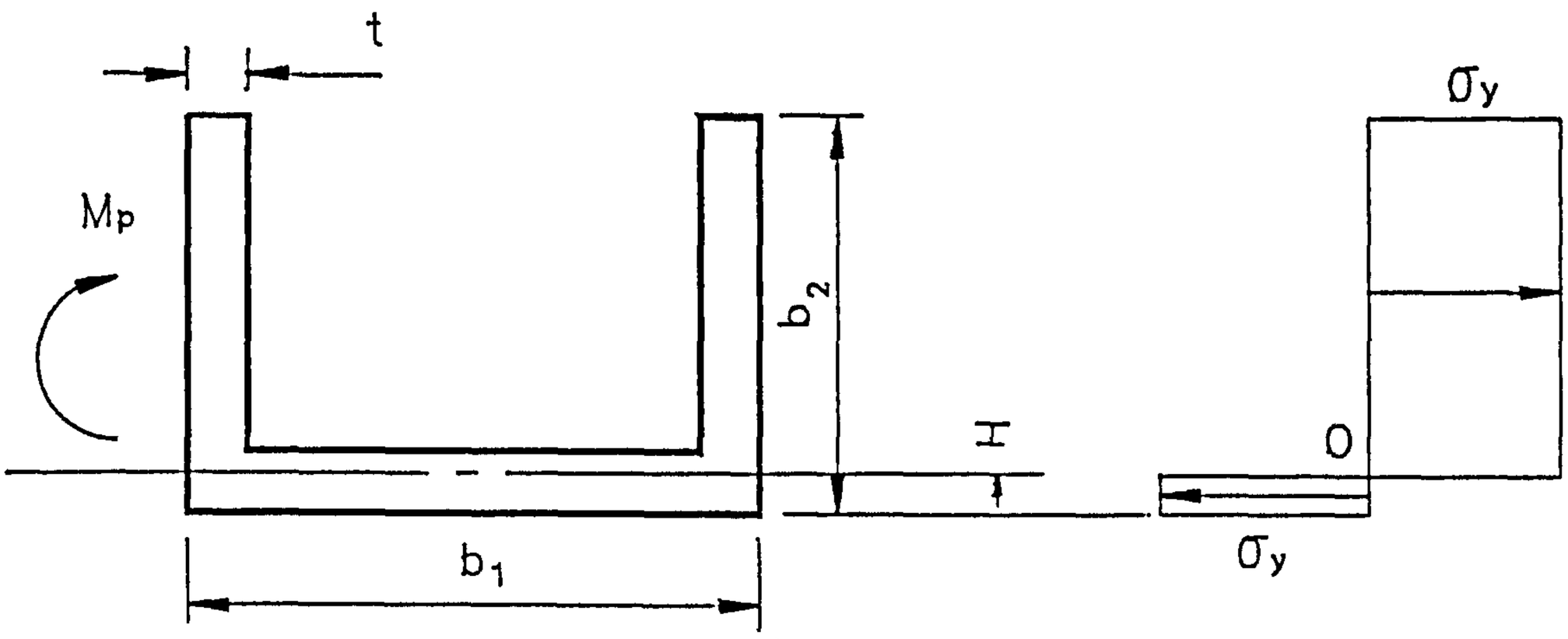

fig. 6.2.2 Full Plasticity with H<=t.

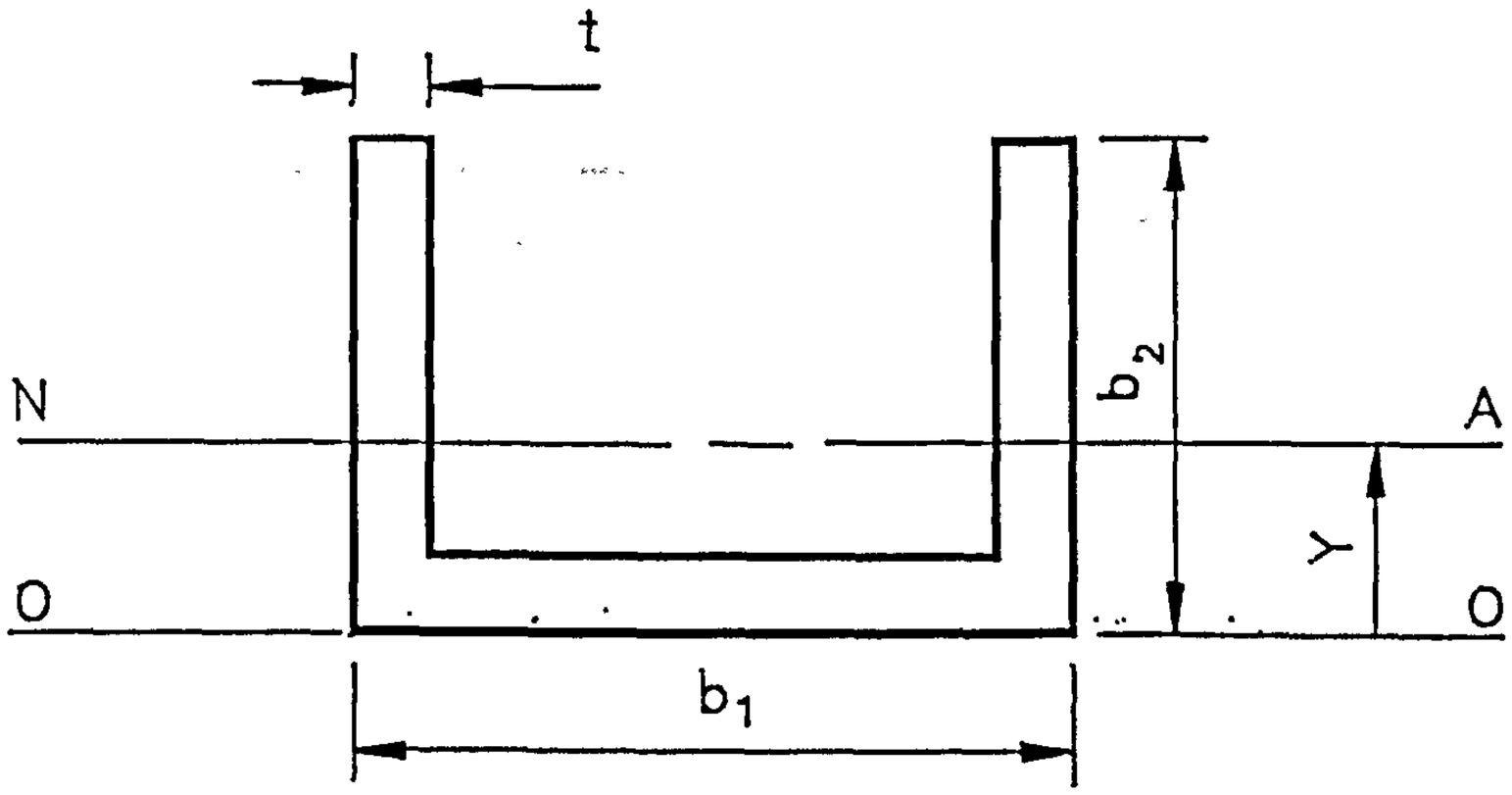

Fig. 6.3.1 Section Geometry.

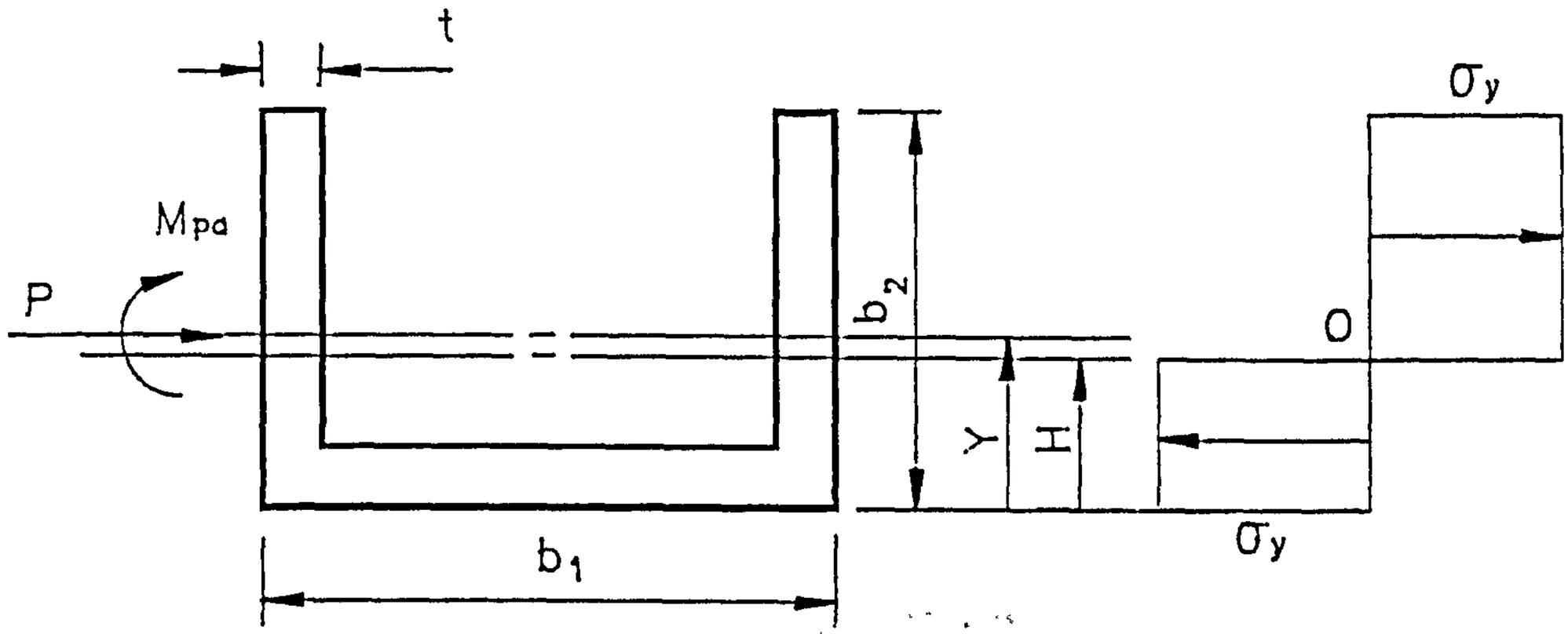

Fig. 6.3.2 Full Plasticity with H>t.

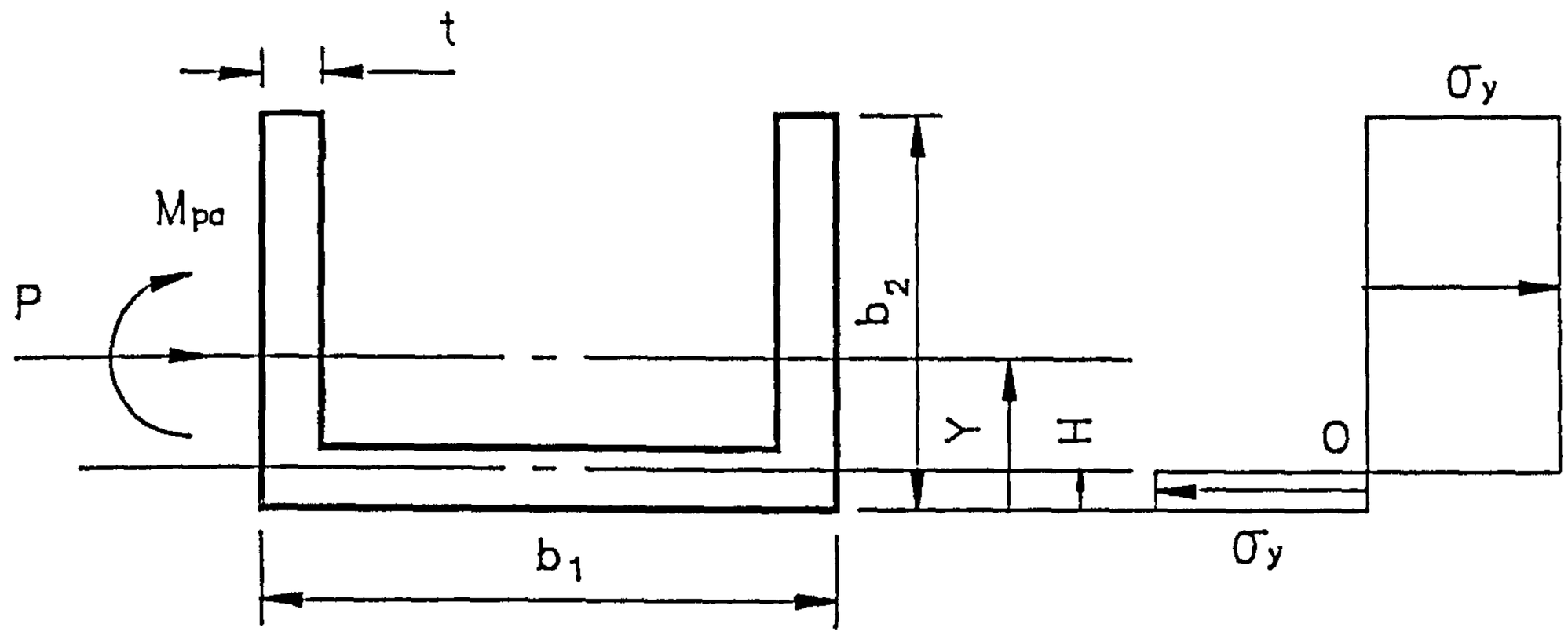

Fig. 6.3.3 Full Plasticity with H<=t.

CHAPTER 7

OTHER CONSIDERATIONS

7.1 INTRODUCTION

Besides local buckling, which is a major phenomenon to be considered in the design and analysis of cold-formed thin-walled structures, the following factors are also included in the theoretical analysis reported herein. These are :

1) Initial imperfections

2) Shortening due to bending

3) Local deformation at the loading point

4) Torsional flexural buckling

This chapter is thus dedicated to the accounting of the above mentioned factors on a single member, separately. The incorporation of the effects into the theoretical analysis is briefly described. A detailed description can be found in Chapter 9.

7.2 INITIAL IMPERFECTIONS

Figure 7.2.1 shows an axially loaded column with one end pinned and the other fully fixed. These boundary conditions are chosen because they closely represent the actual condition of the framework experimental setup. The initial form of imperfection has the approximated deflection of the form :

$$y_o = C_o\left(\sin\frac{\pi x}{L} - \frac{1}{2}\sin\frac{2\pi x}{L}\right) \tag{7.2.1}$$

The additional deflection form is approximated to be :

$$y = C\left(\sin\frac{\pi x}{L} - \frac{1}{2}\sin\frac{2\pi x}{L}\right) \tag{7.2.2}$$

Equation (7.2.2) satisfies the displacement boundary conditions

$$y = 0 \quad \text{at} \quad x = 0 \quad \text{and} \quad x = L$$

Using the Rayleigh Ritz's energy method, the strain energy stored is

$$SE = \int_0^L \frac{EI}{2}\left(\frac{d^2y}{dx^2}\right)^2 dx \tag{7.2.3}$$

Differentiation equation (7.2.2) and performing the integration result in

$$SE = \frac{5EIC^2\pi^4}{4L^3} \tag{7.2.4}$$

The potential energy lost by the load from the imperfect position is

$$PE = \frac{P}{2}\{\int_0^L \left(\frac{dy}{dx} + \frac{dy_o}{dx}\right)^2 dx - \int_0^L \left(\frac{dy_o}{dx}\right)^2 dx\} \tag{7.2.5}$$

Performing the differentiation and integration give

$$PE = \frac{P\pi^2(C^2 + 2CC_o)}{2L} \tag{7.2.6}$$

The change in energy is

$$U = SE - PE \tag{7.2.7}$$

or

$$U = \frac{5EIC^2\pi^4}{4L^3} - \frac{P\pi^2(C^2 + 2CC_o)}{2L} \tag{7.2.8}$$

Differentiating and equating $dU/dC = 0$ result in

$$C = \frac{C_o}{\left(\frac{2.5P_E}{P} - 1\right)} \tag{7.2.9}$$

The axial shortening is given by

$$S_a = \frac{1}{2}\int_0^L \left(\frac{d(y+y_o)}{dx}\right)^2 dx - \frac{1}{2}\int_0^L \left(\frac{dy_o}{dx}\right)^2 dx \qquad (7.2.10)$$

Performing the differentiation and integration give

$$S_a = \frac{1}{2}\left(\frac{\pi}{L}\right)^2 C(C+2C_o)$$

$$= \frac{(\pi C_o)^2}{2L}\left(\frac{1}{\frac{2.5P_E}{P}-1}+2\right) \qquad (7.2.11)$$

In the framework analysis, the computed individual member axial load is used to calculate the axial shortening due to initial imperfections, using equation (7.2.11). In the next iteration, the already computed shortening is "added" to the respective member axial displacement, which will then be used to compute the member end forces. The whole process, which includes other operations, is repeated and finally terminated when convergence at a particular load level is achieved. A detailed step-by-step procedure is given in Chapter 9.

The above method, which uses equation (7.2.11) to account for the member initial imperfection is only employed when the actual member is treated as a single element, i.e., one member one element, as illustrated in figure 7.2.2. This method of node assigning will be called the basic element model from here henceforth for convenience. If the actual member is modelled by two or more elements as illustrated in figure 7.2.3, then initial imperfection is accounted for by specifying the actual imperfect framework geometry during the data input stage of the theoretical analysis. This alternative is adopted because of its simplicity. Furthermore, equation (7.2.11) is only valid for a fully fixed -pinned member. Another reason, which will be discussed in detail in Chapter 9, has to do with the accuracy of the results when local buckling is considered.

7.3 SHORTENING DUE TO BENDING

In addition to the shortening of a member due to the initial imperfections and axial strains in the member, bending also causes axial shortening. This shortening can be significant when the bending moment is relatively large and the flexural stiffness of the member is low.

Shown in figure 7.3.1 is an isolated typical beam-column element of a framework carrying its axial loads, bending moments and associated shear forces. The governing differential equation is

$$\frac{d^2y}{dx^2}+\mu^2 y=\frac{\mu^2}{PL}(M_1+M_2)x-\frac{\mu^2}{P}M_1 \qquad (7.3.1)$$

and the solution is

$$y=A\sin\mu x+B\cos\mu x+\frac{1}{P}\left[\frac{(M_1+M_2)}{L}x-M_1\right] \qquad (7.3.2)$$

Applying the boundary conditions

$y=0$ at $x=0$ and $x=L$ give

$$A=-\left(\frac{M_1\cos\mu L+M_2}{P\sin\mu L}\right)$$

$$B=\frac{M_1}{P}$$

Differentiating equation (7.3.2) gives

$$\frac{dy}{dx}=A\mu\cos\mu x-B\mu\sin\mu x+\frac{(M_1+M_2)}{PL} \qquad (7.3.3)$$

The axial shortening is given by

$$S_b = \frac{1}{2}\int_0^L \left(\frac{dy}{dx}\right)^2 dx$$

Performing the integration results in

$$S_b = \frac{\mu^2 L}{4P^2}\left(\frac{M_1^2 + 2M_1M_2\cos\mu L + M_2^2}{\sin^2\mu L}\right) - \frac{(M_1+M_2)^2}{2P^2L}$$
$$+\frac{\mu\cot\mu L}{4P^2}(M_1^2 + 2M_1M_2\sec\mu L + M_2^2) \qquad (7.3.4)$$

In the case of a tension member, the sign of P in equation (7.3.4) is reversed, and the trigonometric functions must be replaced by the corresponding hyperbolic functions.

The method of incorporating the element axial shortening due to bending into the theoretical framework analysis is similar to that as mentioned in the previous section. However, because of the generality of the derivation, equation (7.3.4) can be used regardless of the number of elements used to model a single member.

7.4 LOCAL DEFORMATION AT LOADING POINT

In the experimental investigation carried out on the framework specimens, the two concentrated loads acting downward on the top beam of the framework was performed through the arrangement illustrated in figure 7.4.1. The load spreader, which consists of a 4 mm thick rectangular steel plate, was used to prevent local stress concentration effects. However, because of the thinness of the framework members, it was observed that local deformation occurred during loading. A typical permanent deformation, which is in the form of a kink, is illustrated in figure 10.7.5 of Chapter 10.

To account for this local deformation, the portion of the beam under the load spreader is assumed to be a rectangular plate simply supported at all edges and subjected to uniform distributed loading. From the theory of plates, the deflection at any point on the rectangular plate is :

$$y = \frac{16W}{\pi^6 D} \sum_{m=1}^{\infty} \sum_{n=1}^{\infty} \frac{\sin\frac{m\pi x}{a} \sin\frac{n\pi y}{b}}{mn\left[\left(\frac{m}{a}\right)^2 + \left(\frac{n}{b}\right)^2\right]^2} \qquad (7.4.1)$$

where

a and b are the dimensions of the sides of the plate.

$m = 1,3,5...$ and $n = 1,3,5....$

By substituting $x = a/2$ and $y = b/2$ and taking only the first term of the series, the deflection at the centre of the plate is :

$$y = \frac{16W}{\pi^6 D\left(\frac{1}{a^2} + \frac{1}{b^2}\right)^2} \qquad (7.4.2)$$

In the framework theoretical analysis, it is assumed that the local deflection at the loading point, computed from equation (7.4.2), does not affect the frame stiffness. Hence, this deflection is added to the deflection of the loading points, only after convergence of each load step.

7.5 TORSIONAL FLEXURAL BUCKLING

For a centrally loaded closed section column, torsional flexural buckling will not occur because of the large torsional rigidity. However, for thin-walled open section, the column may buckle in three possible modes, i.e., flexural, torsional or torsional flexural buckling.

When an open section column buckles in the torsional flexural mode, bending and twisting of the section occur simultaneously. As shown in figure 7.5.1, the section translates u and v in the x and y directions respectively and rotates an angle ϕ about the shear centre.

The equilibrium of a column subjected to an axial load P lends to the following differential equations :

$$EI_x\frac{d^4v}{dz^4}+P\frac{d^2v}{dz^2}-Px_o\frac{d^2\phi}{dz^2}=0 \qquad (7.5.1)$$

$$EI_y\frac{d^4u}{dz^4}+P\frac{d^2u}{dz^2}+Py_o\frac{d^2\phi}{dz^2}=0 \qquad (7.5.2)$$

$$EC_w\frac{d^4\phi}{dz^4}-(GJ-Pr_o^2)\frac{d^2\phi}{dz^2}+Py_o\frac{d^2u}{dz^2}-Px_o\frac{d^2v}{dz^2}=0 \qquad (7.5.3)$$

where

$$J=\frac{1}{3}\Sigma b_i t_i^3$$

$$r_o=\sqrt{r_x^2+r_y^2+x_o^2+y_o^2}$$

and z is the direction along the axis of the member.

Considering the boundary conditions for a member with completely fixed ends,i.e.,

at $z=0$ and L,

$$u=v=\phi=0 \qquad (7.5.4a)$$

$$\frac{du}{dz}=\frac{dv}{dz}=\frac{d\phi}{dz}=0 \qquad (7.5.4b)$$

For a member with hinged ends, i.e., at $z = 0$ and L,

$$u = v = \phi = 0 \tag{7.5.5a}$$

$$\frac{d^2u}{dz^2} = \frac{d^2v}{dz^2} = \frac{d^2\phi}{dz^2} = 0 \tag{7.5.5b}$$

Equations (7.5.1) to (7.5.3) result in the following characteristic equations :

$$r_o^2(P_{cr} - P_x)(P_{cr} - P_y)(P_{cr} - P_z)$$

$$-(P_{cr}y_o)^2(P_{cr} - P_x) - (P_{cr}x_o)^2(P_{cr} - P_y) = 0 \tag{7.5.6}$$

whose roots, P_{cr}, are the three possible buckling loads of the column. The critical buckling load is the smallest value of the roots. The parameters P_x, P_y and P_z have the form, respectively, of the two pure flexural buckling loads about the principal axes and a purely torsional buckling load about the shear centre axis. They are given by

$$P_x = \frac{\pi^2 E I_x}{l^2} \tag{7.5.7a}$$

$$P_y = \frac{\pi^2 E I_y}{l^2} \tag{7.5.7b}$$

$$P_z = \frac{1}{r_o^2}\left(\frac{\pi^2 E C_w}{l^2} + GJ\right) \tag{7.5.7c}$$

For a plain channel section, which is symmetrical about the x axis as illustrated in figure 7.5.2, the distance, y_o, between the shear centre and the centroid in the direction of the y axis is equal to zero. Equation (7.5.6) then reduces to

$$(P_{cr} - P_y)\{r_o^2(P_{cr} - P_x)(P_{cr} - P_z) - (x_o P_{cr})^2\} = 0 \tag{7.5.8}$$

There are again three solutions, one of which is

$$P_{cr} = P_y$$

and represents purely flexural buckling about the y axis. The other two solutions can be obtained by solving the following quadratic equation :

$$r_o^2(P_{cr} - P_x)(P_{cr} - P_z) - (x_o P_{cr})^2 = 0 \qquad (7.5.9)$$

This equation will produce two torsional flexural buckling load. However, the smaller of the two loads is :

$$P_{cr} = \frac{1}{2\omega}\{(P_x + P_z) - \sqrt{(P_x + P_z)^2 - 4\omega P_x P_z} \qquad (7.5.10)$$

where

$$\omega = 1 - \left(\frac{x_o}{r_o}\right)^2$$

This load will always be below P_x and P_z. However, it may be above or below P_y.

Therefore, the section can buckle in either of the two modes, by bending, or in torsional flexural buckling. Which of these two actually occur depends on the dimensions of the section and the effective length, l.

Although equation (7.5.8) can be used to determine the buckling load of a singly symmetric section, the process is rather lengthy and tedious compared to the calculation of the Euler load. Fortunately a simple and efficient procedure using design chart based on analytical and experimental investigations has been developed for plain channel section by Chajes and Winter (7 of Part 2), from which it can be determined whether a section will buckle in the torsional flexural mode. Such a typical chart is shown in figure 7.5.3 for a plain channel.

As indicated in the figure, the buckling domain can be visualised as being composed of three regions. Region 1 is for torsional flexural buckling only. This particular case is characterised by sections for which $I_y > I_x$. When $I_y < I_x$, the section will fail either in region 2 or 3. In region 2, the channel will buckle in either flexural or torsional flexural mode, depending on the specific ratio of b/a and the parameter tl/a^2. For a given channel section and column length, if the value of tl/a^2 is above the $(tl/a^2)_{lim}$ curve, the section will fail in flexural mode. Otherwise, it will fail in torsional flexural buckling mode. In region 3, the section will always fail in the flexural mode regardless of the parameter tl/a^2.

The buckling mode design curves for lipped and plain channels are shown in figure 7.5.4. These curves apply only to compatible end conditions, i.e., equal effective lengths,

$$l_x = l_y = l_z$$

The conditions of restraint existing at the ends of actual columns will, in general, not be compatible. In most cases, however, the values of l_x , l_y and l_z will be fairly near one another. When this is the case, compatible boundary conditions may be assumed to exist without introducing unduly large errors.

In the theoretical framework analysis reported herein, by using the design chart of figure 7.5.4, the particular section is checked to determined whether torsional flexural buckling will occur. If it does, then the phenomenon is accounted for by employing the α factor or length multiplier. This method is also adopted by the BS 5950,Part 5.

Equation (7.5.7 c) may also be written as

$$P_z = \frac{1}{r_o^2}\left(\frac{k\pi^2 EC_w}{l^2} + GJ\right) \qquad (7.5.11)$$

The constant k is dependent on the degree of warping restraint afforded by the end connections of the column. If warping is completely prevented, then the value of k is 4, i.e., the ends of the member are fixed with respect to warping. On the other hand, if warping is completely unrestrained, then the value of k is 1.By using the appropriate value of 4 or 1 for k and using equation (7.5.10) to calculate the torsional flexural buckling load, the α factor can be determined as follows :

For $P_y \leq P_{cr}$,

$$\alpha = 1 \tag{7.5.12}$$

For $P_y > P_{cr}$,

$$\alpha = \sqrt{\frac{P_y}{P_{cr}}} \tag{7.5.13}$$

The α factor obtained is then multiplied by the actual framework column length. Analysis of the framework is then performed based on this factored length.

While the assumption of full warping restraint is undoubtedly unsafe for design purposes, the assumption of zero warping restraint is very conservative in most practical cases. This situation led the BS 5950, Part 5, to incorporate a factor of $k = 2$ in the relevant design analysis. Based on this, α factor for some commonly used sections can be obtained from a design table listed in Appendix V.

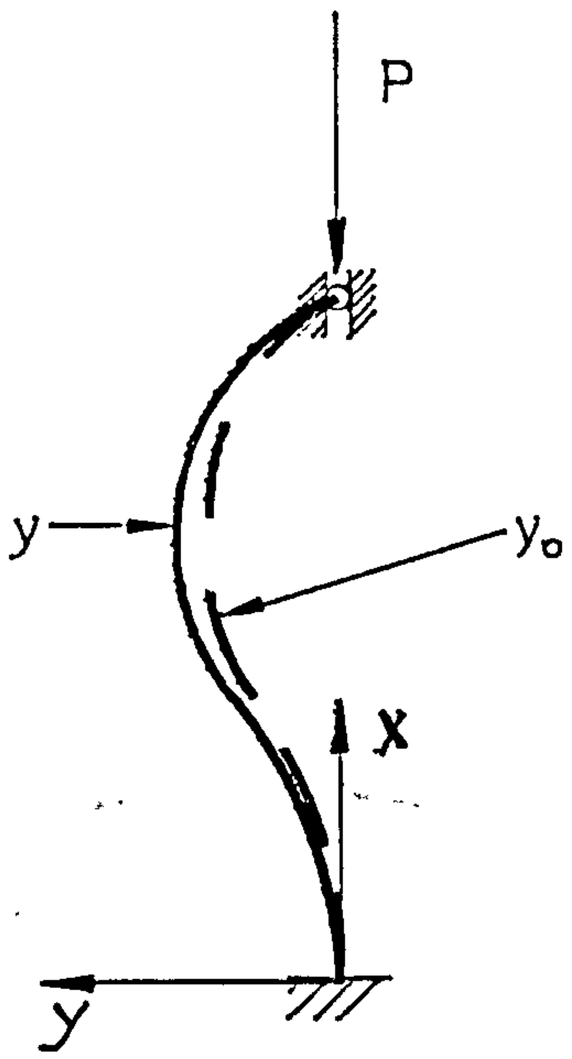

Fig. 7.2.1

Column with Initial

Imperfection

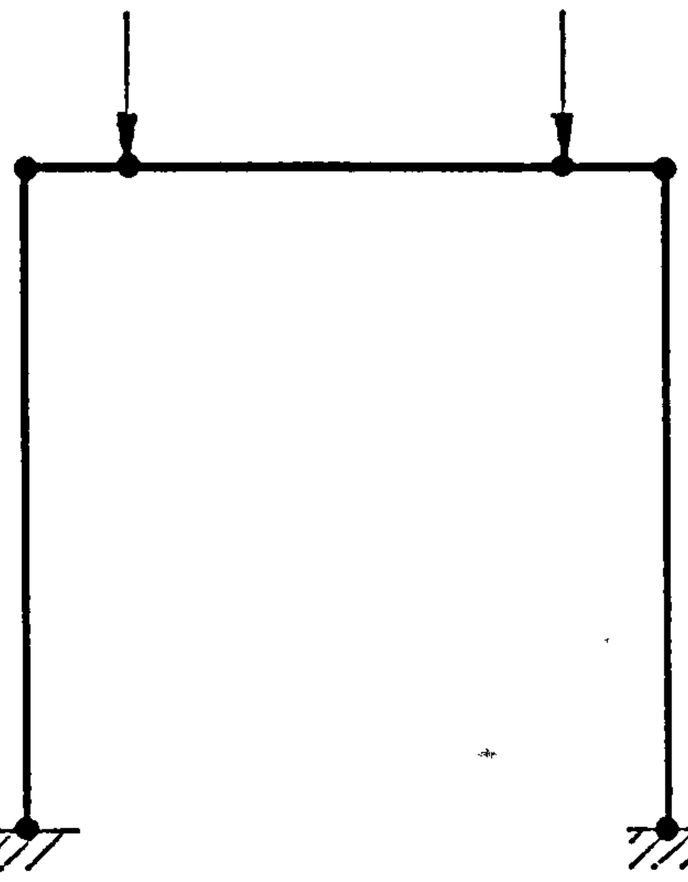

Fig. 7.2.2

Basic Element Node

Assignment.

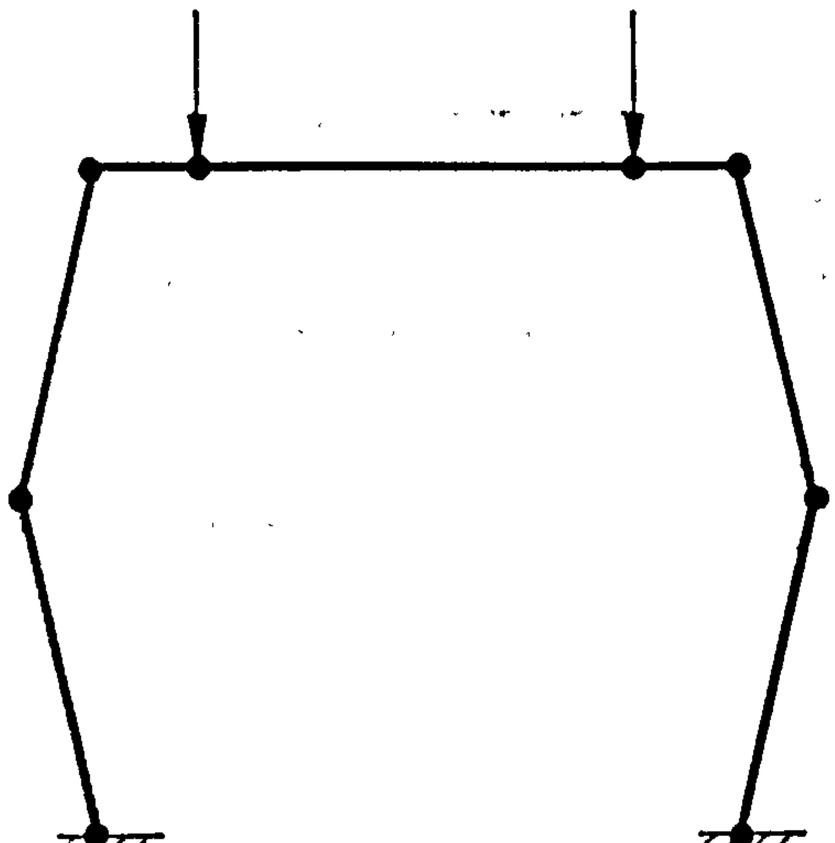

Fig. 7.2.3

Imperfect Framework

Geometry.

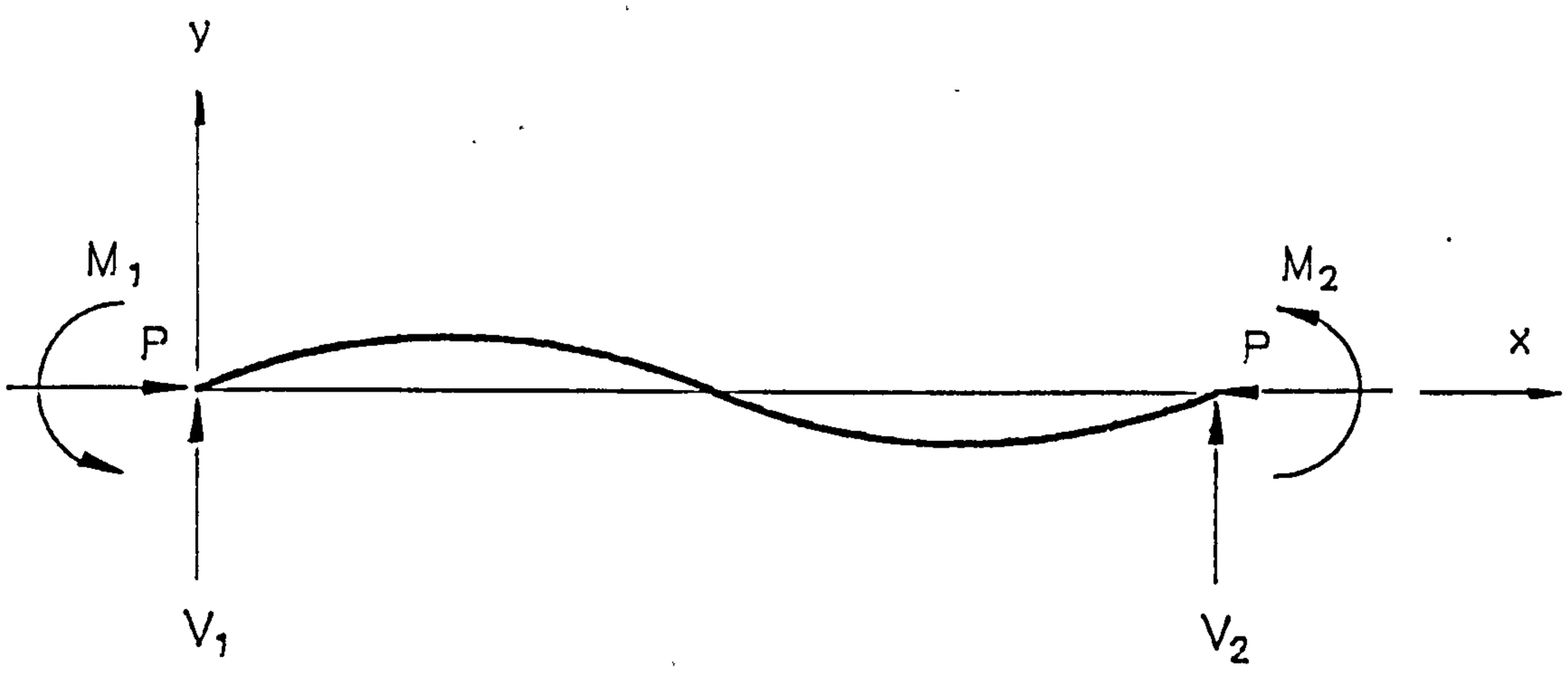

Fig. 7.3.1

Typical Beam–Column Member.

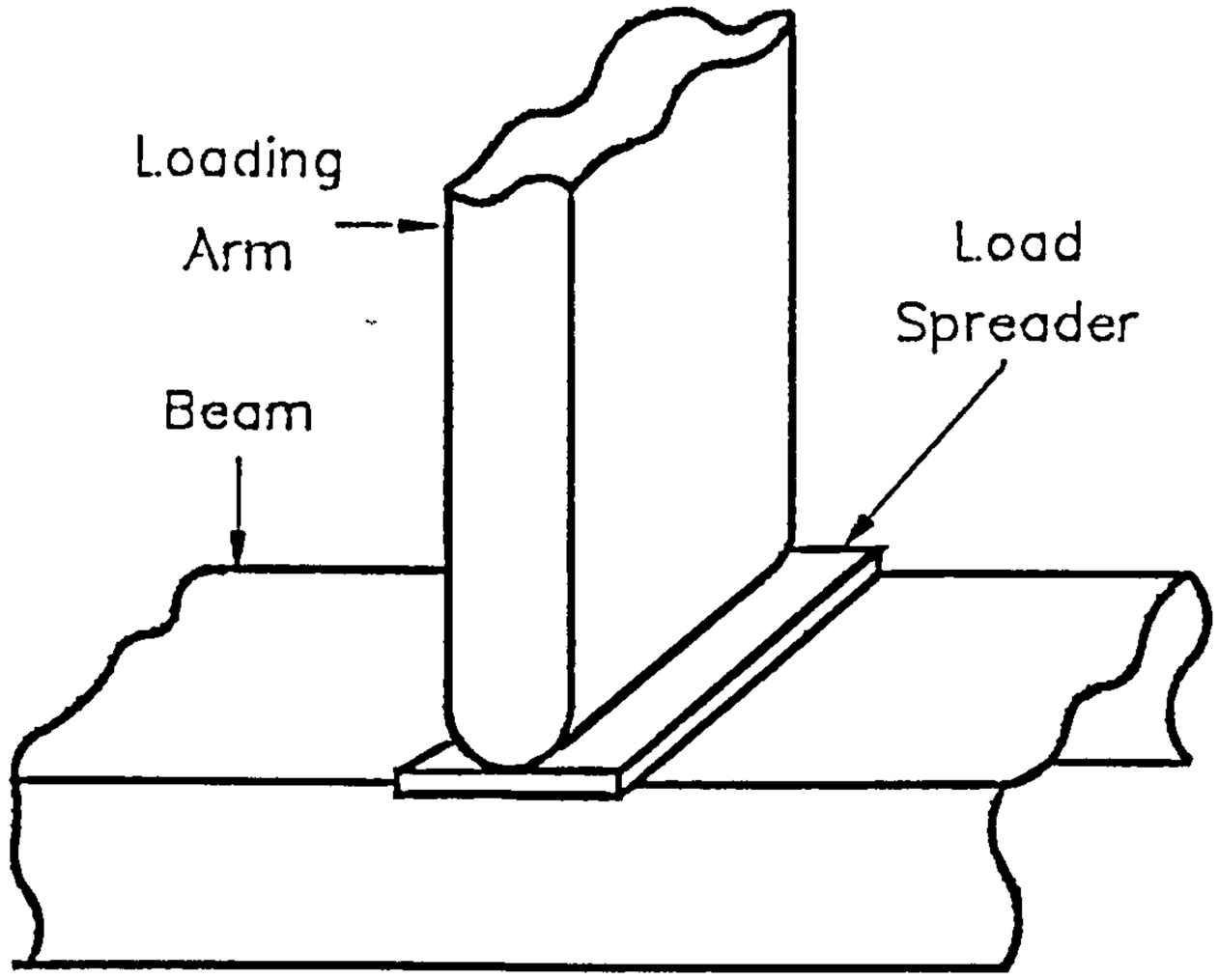

Fig. 7.4.1

Typical Loading on Beam of Framework.

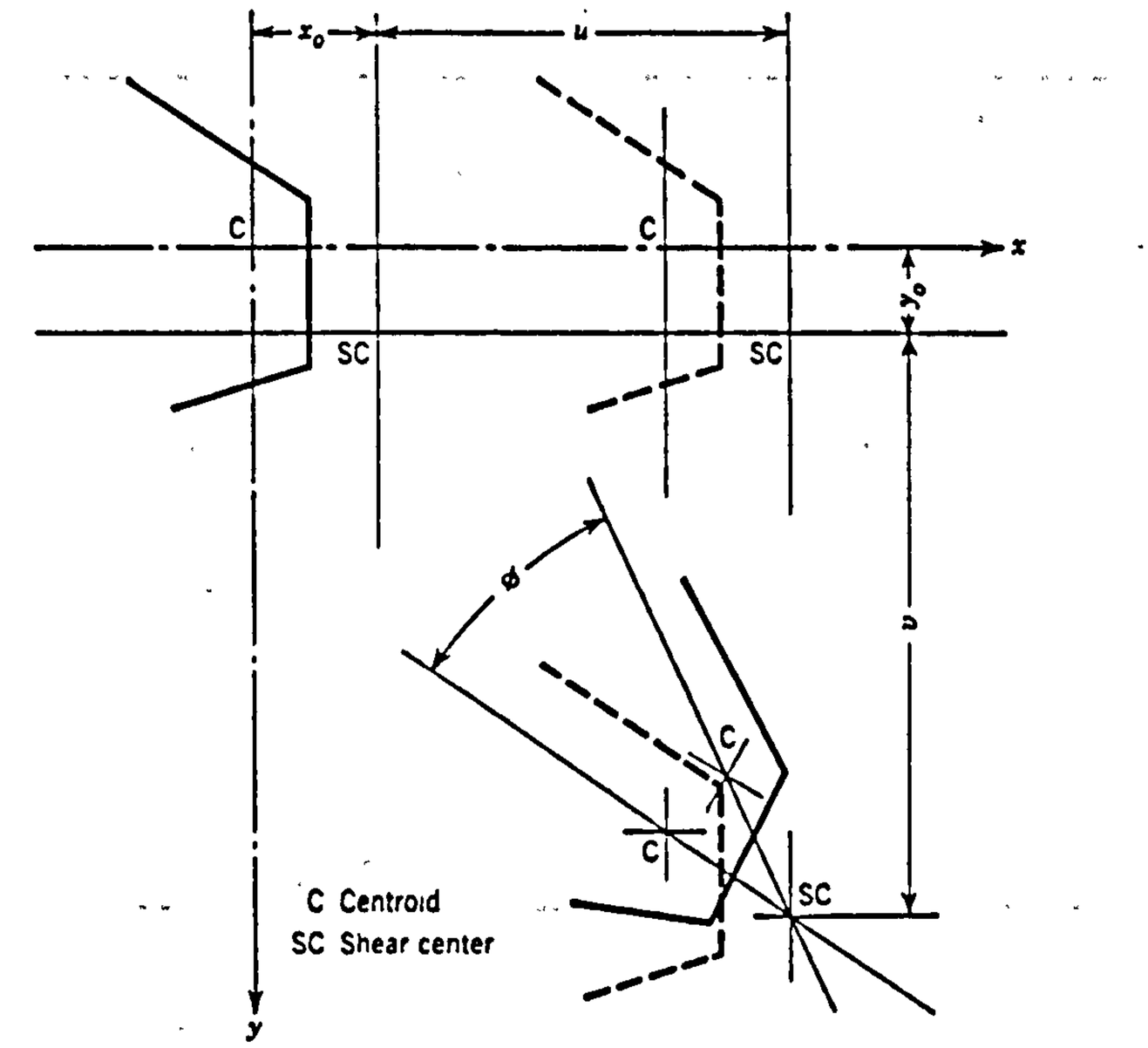

Fig. 7.5.1

Displacement of Section during Torsional Flexural Buckling

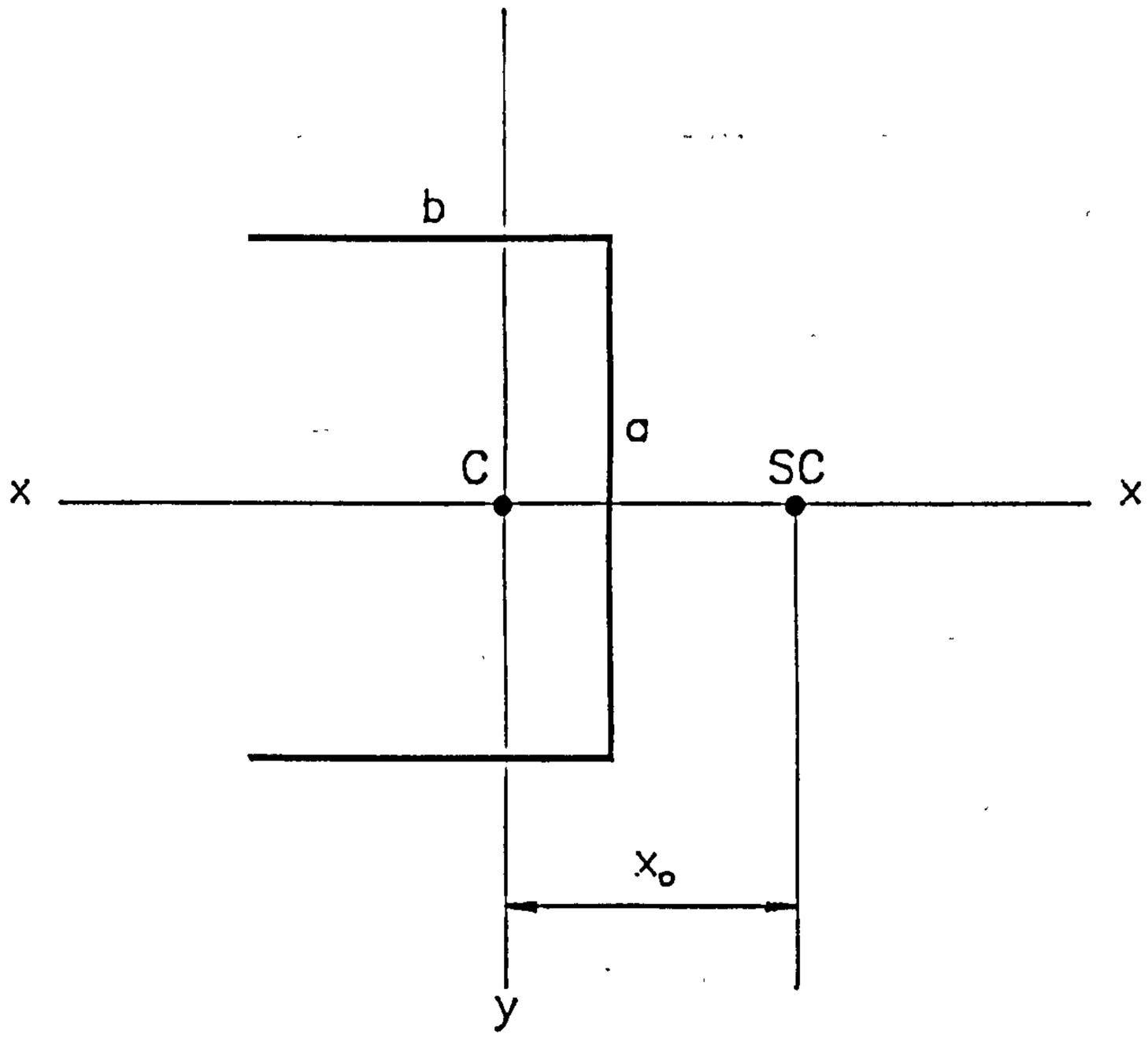

Fig. 7.5.2 Typical C Channel.

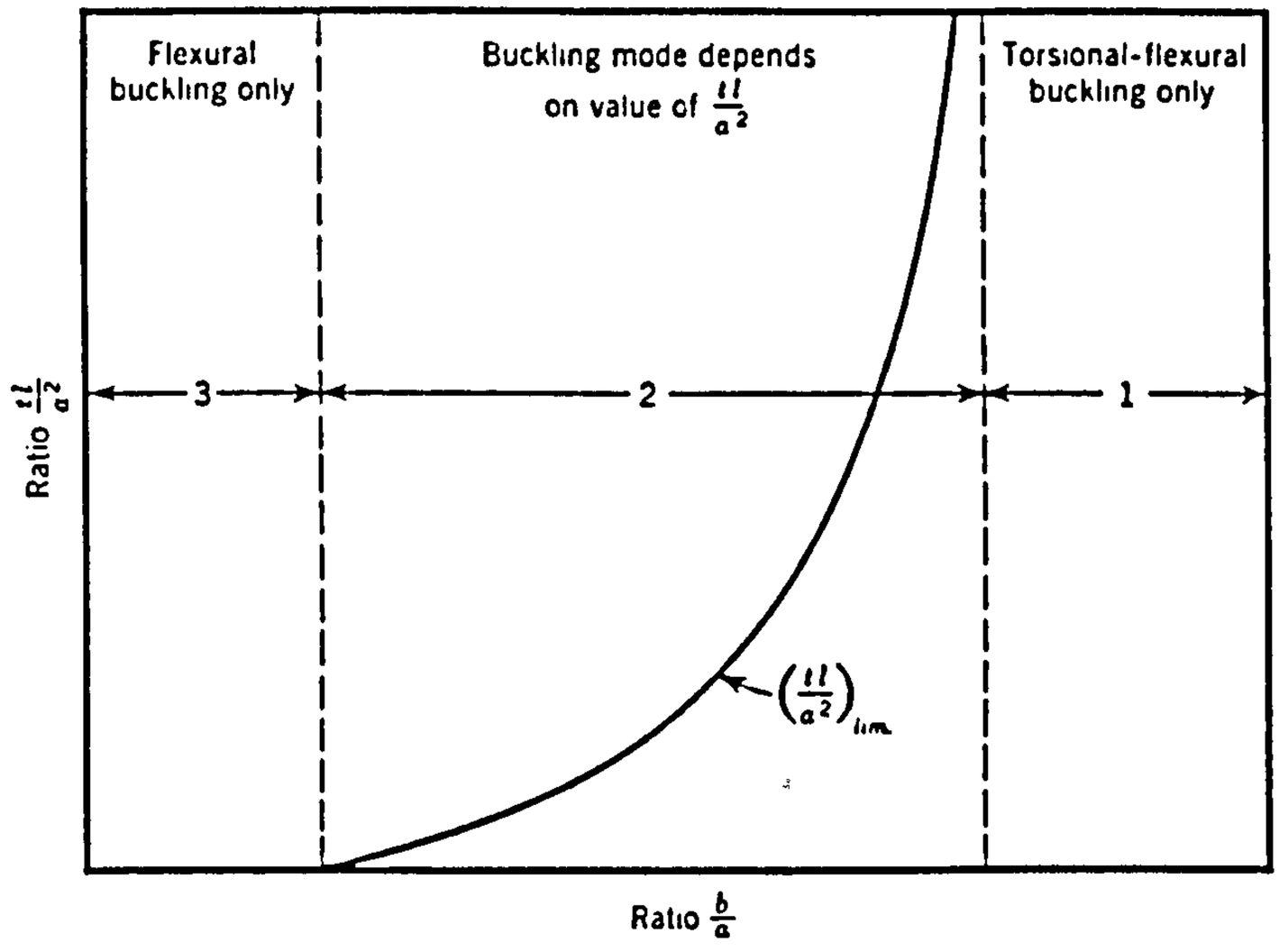

Fig. 7.5.3 Typical Buckling Mode Chart

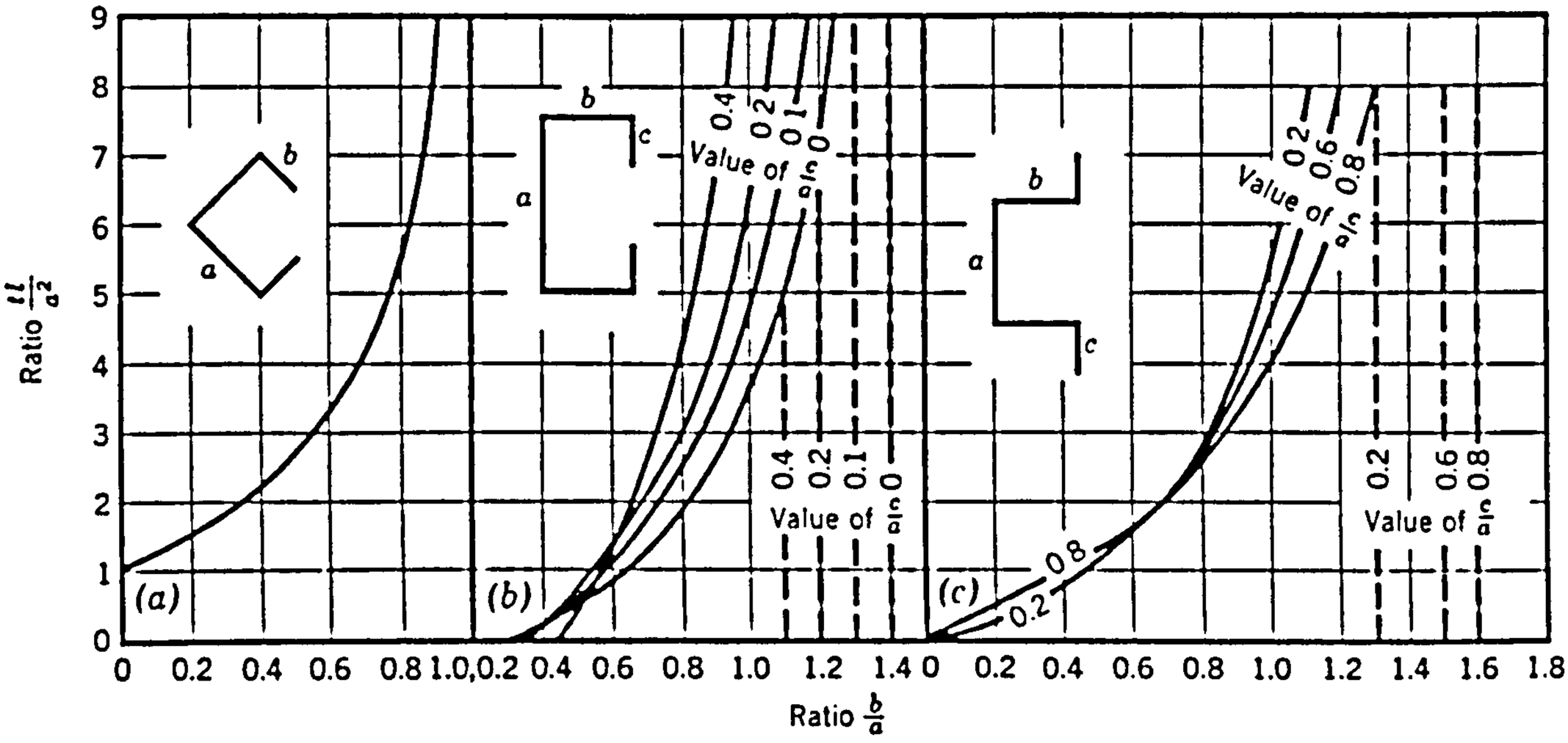

Fig. 7.5.4 Buckling Mode Chart

CHAPTER 8

CONNECTION MOMENT-ROTATION RELATIONSHIP

8.1 INTRODUCTION

In the conventional analysis and design of frameworks, it is customary to represent joint behaviour by idealized joint models. Two of the most commonly used idealized models are the rigid model and the pinned joint model. In the former, it is assumed that the rotational continuity between adjoining members is fully realized. As a result of this assumption, the angle between adjacent members remains virtually unchanged as the framework deforms and the full moment of the beam is transmitted to the column. For the pinned model, it is assumed that the rotational continuity between adjoining members is non-existent. Consequently, no moment is transmitted to the column by the beam.

Although the use of either of the idealized joint behaviour simplifies drastically the analysis and design procedure, the predicted response of the framework may not be realistic as most connections used in actual practice transmit some moment and experience some deformation upon loading. Before an analysis, which accounts for the connection flexibility, can be carried out, it is necessary to know in advance the connection stiffness or moment-rotation behaviour. This chapter is thus devoted to the obtaining of the moment-rotation data of connections experimentally, after which a theoretical model is developed, based on the experimental data, in order to represent the moment-rotation behaviour in an approximate form. The model is then incorporated into the main framework programme to account for the moment-rotation behaviour of the connections.

8.2 CONNECTION EXPERIMENTAL INVESTIGATION

A rather simple experimental test was undertaken in order to obtain the moment-rotation data of individual connection. These data were then used for the theoretical modelling of the connection moment-rotation characteristic. A point that needs special mention regarding the connection tests reported herein is that

although two connections are similar, they are tested individually for their stiffness as long as they are to be used in different frameworks. The overall geometry of the frameworks may be similar but the members (all plain channels) are of different cross sectional geometry. Furthermore, the channels that are used for a connection test are of the same cross sectional geometry as those of the framework that is to be constructed with the same type of connection.

8.2.1 TEST SPECIMENS AND FABRICATION

For economic and simplicity reasons, the type of connection chosen for the frameworks is as shown in figure 8.2.1. In order to acquire a variety of connection stiffnesses and moment-rotation behaviour, the thickness of the connection was varied from 3 mm to 7 mm with an increment of 1 mm.

Four series of connections ,each consisting of five different thickness as mentioned above, were fabricated from mild steel bars. All the 7 mm thick connections were machined to size because they were too thick to form by bending with the equipment available. The rest of the connections were fabricated by bending and then machining to size. A typical series of connections of various thickness is shown in figure 8.2.2. The dimensional details of a typical connection can be found in figure 8.2.3.

A joint model, which consists of the connection and the connecting beam and column is illustrated in figure 8.2.4. The cross sectional dimensions of the connecting beam and column and the respective connection are tabulated and listed in table 8.2.1. From table 10.2.1 of Chapter 10, it can be noted that the cross sectional dimensions of the connecting beam and column of a particular connection are similar to those of the framework that uses that same type of connection.

The beams and columns were fabricated from galvanised steel sheetings, which were initially marked out and cut into strips. The width of the strips were sized to give a corner radius of about two times the thickness of the specimen. Bending of the strips into the final shape was performed on a manual bending machine. Although a few trials were required, the final shape was achieved without much difficulties because of the short length of the specimens.

8.2.2 TEST RIG AND EQUIPMENT

The cantilever type of arrangement was selected for the joint model test because it was a close representation of the exterior column of the actual framework. Furthermore, by using this arrangement, the connection can be subjected to both shear and bending.

The joint model was constructed by bolting the connection onto the respective beam and column specimens as illustrated in figure 8.2.6. During the construction, extra precaution was taken to prevent the connection or connecting members from becoming twisted out of plane. On the other hand, the bolts must be fastened tight enough to prevent any slipping during loading.

The bottom end of the column was then clamped onto the base plate by means of the jigs as illustrated in figure 8.2.7. The base plate was fabricated from a large piece of mild steel plate by machining. Detail drawings of the base plate and jigs are shown in Appendix VI. To prevent horizontal movement, the top end of the column was held in position by a screw rod. As shown in figure 8.2.5, the other end of the screw rod was bolted onto a rigid support stand, which was in turn bolted onto the base plate. As detailed in figure 8.2.8, the rigid support stand was fabricated by welding the angle channel onto the base support.

An eye-bolt was fitted onto the free end of the beam. Loading was achieved by putting weights onto the hanger which was in turn hooked onto the eye-bolt. The vertical deflection of the loaded end of the beam was measured with the means of a 50 mm range dial gauge.

8.2.3 TEST PROCEDURE

The base plate was placed on a strong and flat working bench with a slight overhang to allow the hanging of weights. The already constructed joint model was clamped onto the base plate at the column base. The top end was then held in position with the help of the screw rod and support stand. Precaution was taken to ensure that all nuts were fully tightened, except those at the top of the column. These were only hand-tightened to prevent significant moment from developing during loading. After the weight hanger has been hooked in position, the dial gauge was aligned to measure the vertical deflection of the loading point. Before commencing loading, heavy weights were placed onto the other end of the base plate. The purpose was to prevent any movement of the base plate. Figure 8.2.9 shows the test set-up just before loading.

The joint model was loaded with equal weight at suitable interval and the corresponding deflection was recorded. Recording was carried out only when the dial gauge pointer stopped moving. When it was noticed that the deflection started to become non-linear, smaller weights were used to ensure that the non-linearity could be recorded more accurately. The model was loaded to failure as illustrated in figure 8.2.10.

A total of four series of connections were tested, each series consisting of five connections of thickness, T_c, varying from 3 mm to 7 mm as mentioned earlier. The thickness of the connection can be easily identified by the alphabet designation given. The alphabet "A" represents a connection of thickness 3 mm. Increasing the

connection thickness by 1 mm is represented by the next alphabet "B". Hence, "E" represents a 7 mm thick connection. There are four series because as can be seen from table 8.2.1, there are four different sets of channel (beam and column) cross sectional dimensions. It should be noted that for each individual joint model test, new beam, column and connection were used.

8.2.4 EXPERIMENTAL MOMENT-ROTATION DATA

The experimental deflection of the free end of the beam includes the effects of the connection flexibility and local distortions of the beam and column. To determine the relative change in deflection, the experimentally obtained deflection must be deducted by the deflection when the connection is fully rigid. Hence, as illustrated in figure 8.2.11, the relative change in rotation of the connection at the connecting point is:

$$\phi = \frac{d_{ex} - d_t}{L} \tag{8.2.1}$$

and the corresponding moment is

$$M = P L \tag{8.2.2}$$

where L is the length of the beam in this case.

Thus, once d_t, which is the deflection of the loaded end of the beam when the connection is fully rigid, is known, equations (8.2.1) and (8.2.2) can be used to compute the connection moment-rotation data.

The deflection, d_t, is derived theoretically using simple elastic theory as follows.

The joint model can be represented schematically as illustrated in figure 8.2.12.

The column, which is of length $2L$, is assumed to be fully fixed at C and simply supported at A. The moment, M, due to the applied load at the free end of the beam, acts at B of the column.

From MaCaulay's method, the moment at a distance, x, from A is:

$$M_x = M[x-L]^0 - Vx \tag{8.2.3}$$

From simple beam theory,

$$EI\frac{d^2y}{dx^2} = -M_x \tag{8.2.4}$$

Substituting and integrating give

$$EI\frac{dy}{dx} = \frac{Vx^2}{2} - M[x-L] + A \tag{8.2.5}$$

and

$$Ely = \frac{Vx^3}{6} - \frac{M[x-L]^2}{2} + Ax + B \tag{8.2.6}$$

Applying the boundary conditions

$$y = 0 \quad \text{at} \quad x = 0 \quad \text{and} \quad \frac{dy}{dx} = 0 \quad \text{at} \quad x = 2L$$

to equations (8.2.5) and (8.2.6) results in

$$B = 0 \qquad \text{and} \qquad A = L(M - 2VL)$$

Applying the boundary condition

$$y = 0 \qquad \text{at} \qquad x = 2L$$

and substituting the constants give

$$V = \frac{9M}{16L}$$

Hence, the slope at B is

$$\theta_B = \frac{5ML}{32EI}$$

The deflection at the end of the beam due to column rotation at B is

$$d_r = \theta_B L = \frac{5PL^3}{32EI_c} \tag{8.2.7}$$

The deflection at the end of the beam due to the load P is

$$d_e = \frac{PL^3}{3EI_b} \tag{8.2.8}$$

Therefore, the total deflection at the loading point of the beam when the connection is fully rigid is

$$d_i = d_r + d_e$$

or

$$d_i = \frac{PL^3(15I_b + 32I_c)}{96EI_bI_c} \tag{8.2.9}$$

8.2.5 EXPERIMENTAL RESULTS AND OBSERVATION

Figures 8.2.13 to 8.2.16 show the plot of the applied loads and the corresponding deflections at the free end of the beam for the four series of connection tests respectively. The theoretical deflection, assuming fully rigid connection, obtained from equation (8.2.9) was also plotted.

In the experimental investigation, the top end of the column was held in position by a screw rod. Although the nut was only hand tightened, there will still be some bending moment induced. In the theoretical derivation of the deflection , the top end of the column was assumed to be simply supported. This will result in a larger deflection which will in turn lead to a stiffer connection moment- rotation curve.

From the experimental load-deflection results, the corresponding moment- rotation data, computed from the procedures outlined earlier, were plotted and shown in figures 8.2.17 to 8.2.20 respectively. As expected, the stiffness of the connection increases with respect to the connection thickness. This is due to the increase in flexural rigidity of the connection. The results also show that the moment-rotation relationship of all the connections tested is non-linear. In some cases, this non-linearity begins at a load as low as half the failure load.

A summary of all the joint model test failure mode and observation is tabulated in table 8.2.2. When failure was due purely to full plasticity of the connection, as illustrated in figure 8.2.21, there was no visible distortion of the column except for tests J3-1B and J3-1C. For these two cases, because of the large width-to thickness ratio of the unstiffened element of the column, local distortion of the form shown in figure 8.2.22 was observed. It was also noticed that the column distortion became more obvious when the applied load was increased. The increase in the column distortion was also present when the width-to thickness ratio of the unstiffened element was increased. For the other two failure modes, namely beam failure and the combination of beam and connection failure, distortion of the column was also

observed to occur. For the former failure mode, a plastic hinge formed at the compression portion of the channel immediately after the edge of the connection, where local stress concentration was greatest. Severe local beam distortion was also observed to occur in the vicinity of the bolt, especially in the area next to the column. The edges of the unstiffened element of the beam, towards the column side, bent outwards. All the above observations are shown in figure 8.2.23. The figure also shows the undeformed beam (furthest left on the picture) for the case when failure occurred purely due to connection deformation.

When a combination of both beam and connection deformation was the cause of failure, either the connection or the beam yielded first, depending on their individual strength. When the connection played a more significant role in the failure, partial deformation of the beam was found to have occurred and vice-versa.

The experimental moment-rotation relationship of connections of the same thickness, but connected to different sets of beam and column as tabulated in table 8.2.1, are shown in figures 8.2.24 to 8.2.28. It can be seen that for a connection thickness of 3 mm, the variation in the stiffness is very marginal. This is not true when the connection thickness is increased. In fact, the variation in the connection stiffness was found to increase even more as the connection thickness was further increased. Furthermore, for a particular connection thickness, T_c, the variation becomes larger as the specimen (beam and column) thickness, t, increases. This shows that the moment-rotation behaviour of a particular connection is affected by the local distortion and thickness of the connected members.

In an attempt to justify the above behaviour of the connection, an empirical expression of the form

$$R_o = \left(\frac{9.1811 \times 10^{-5}}{t^3} - 0.002073t - \frac{0.016417}{T_c^3} + \frac{0.016575}{T_c} \right)^{-1} \qquad (8.2.10)$$

was used to compute the initial connection stiffness. The above expression was obtained through curve fitting techniques. The terms associated with t and T_c can be taken as the factors affecting the connection stiffness due to the connected members and connection respectively.

The initial connection stiffness of all the connections tested was computed from equation (8.2.10) and then plotted against the corresponding experimentally obtained initial stiffness. This is shown in figure 8.2.29. If the equation is completely correct, then all the points will lie along the straight line. Nevertheless, it can be seen that the scatter of the points is not very significant. Hence, equation (8.2.10) can be used as a good estimation of the connection initial stiffness, taking into account of the factors attributed by both the connection itself and the connected members.

Figure 8.2.30 shows a plot of the connection stiffness against the thickness of the connected member or specimen. The full lines represent the stiffness calculated from equation (8.2.10). It can be seen that for a particular connection thickness, the stiffness increases with respect to the specimen thickness. The rate of this increase changes from an almost linear to a non-linear form when the connection thickness is increased from 3mm to 7 mm. Furthermore, for a particular specimen thickness, the connection stiffness also increases with respect to its thickness. The greatest increase occurs when the thickest specimen is used.

For the range of connection and specimen thicknesses and the types of connection studied, figure 8.2.30 indicates that the connection stiffness is affected by the thickness of the connection and the connecting members and also the local distortions of the latter. This effect is most prominent when the thickest connection and members were used.

8.3 MODELLING OF CONNECTION MOMENT-ROTATION CURVE.

8.3.1 INTRODUCTION

In the analysis of frameworks with semi-rigid connections, it is necessary to know the connection moment-rotation relationship. Although this relationship can be found experimentally, it is extremely time consuming and costly at times, especially when different and complicated types of connections are to be used in the framework. The main purpose of connection modelling is thus to obtain the connection moment-rotation relationship using a theoretically derived standardized model. However, it should be pointed out that , if possible, the theoretical model obtained should only be applied to connections working under the same experimental conditions from which the model was initially derived.

8.3.2 THEORETICAL MODELLING

Although the modelling of the connection moment-rotation behaviour is of significant importance, the procedure adopted here is only an approximate one because it is beyond the scope of the this research to perform an extensive study on the connection behaviour independently.

The theoretical model reported herein is based entirely on the experimental moment-rotation data obtained. For a given moment-rotation curve of a connection, the stiffness, R, at a particular moment, M, can be expressed in the form

$$R = R_o - CM \tag{8.3.1}$$

Substituting the inverse of the connection factor

$$R = \frac{M}{\phi}$$

into equation (8.3.1) results in

$$M = \frac{\phi R_o}{1 + C\phi} \tag{8.3.2}$$

By feeding the experimentally obtained moment and corresponding relative angle change into a curve fitting programme, the constants R_o and C can be obtained. Although R_o, which is the initial connection stiffness, can be calculated from the experimental data directly, the value obtained from the curve fitting technique results in a better curve fit. These constants are then substituted back into equation (8.3.2) and the approximate moments are computed using the corresponding experimental relative angle change values. The experimental and modelled moment-rotation curves are then plotted and compared as illustrated in figures 8.3.1 to 8.3.20. The constants obtained from the curve fitting technique for the respective connections are shown in table 8.3.1. It should be mentioned that the moment of equation (8.3.1) must be in *Nmm* and the computed stiffness is in *Nmm/rad*.

Although equation (8.3.2) is used to model the connection moment-rotation curve, equation (8.3.1) represents the secant stiffness directly and depends only on the moment at the connection. This expression is implemented into the framework analysis computer programme. At each load level, the calculated moment at the connection is substituted into the model equation to compute the connection stiffness which will in turn be used to compute the coefficients of the element matrix. This procedure is repeated at every load level. Hence, the full moment-rotation relationship of the connection is taken into account in the framework analysis with the use of equation (8.3.1).

8.3.3 COMPARISON OF THEORETICAL MODEL AND EXPERIMENTAL RESULTS.

The individual connection experimental and modelled moment-rotation curves are plotted and shown in figures 8.3.1 to 8.3.20. It can be seen that the theoretical model represents the connection moment-rotation relationship rather well in all cases

Although still considered as acceptable, figure 8.3.13 illustrates one of the "worst" representation of the model. The connection stiffness below and above a moment of about 11.5 *KNmm* is slightly over and under estimated respectively. Since equation (8.3.1) represents the secant stiffness of the connection corresponding to a particular moment, the error in the connection stiffness will be amplified when the moment is below 11.5 *KNmm*. This means that a higher connection stiffness than actual is used for computation. When the moment is above 11.5 *KNmm*, the higher secant stiffness from equation (8.3.1) is compensated by the under estimation of the theoretical model.

The error in the representation of the connection stiffness mentioned above is due to the approximate theoretical model employed. There are other factors that may also affect the experimentally obtained moment-rotation data. One of these is the assumption of the boundary condition as in the case of the assumed simply supported top end of the column. Other significant factors not considered are local buckling of the members and panel zone deformation.

Having said that, it is assumed that for practical purpose, the theoretical model derived herein represents the connection moment-rotation relationship within engineering accuracy.

8.4 CONCLUSIONS

Due to the constraint of time and cost, a rather simple but reliable method was employed to determine the moment-rotation relationship of the various connections studied. An approximate and standardized theoretical model was developed and used to represent the connection behaviour. For the particular type of connections investigated and also within the range of the connection and members geometries, the following are concluded.

1) The flexibility of all the connections investigated was found to be between the two extreme idealized cases normally assumed, i.e., fully pinned or fully fixed. All the connections exhibited a non-linear moment-rotation relationship.

2) The moment-rotation curve of a particular connection is affected by the local distortions of the connected members. The degree of variation increases with both the thickness of the connection and the connecting members.

3) It has been demonstrated that the standardized theoretical model represented the experimentally obtained connection moment-rotation curves rather accurately.

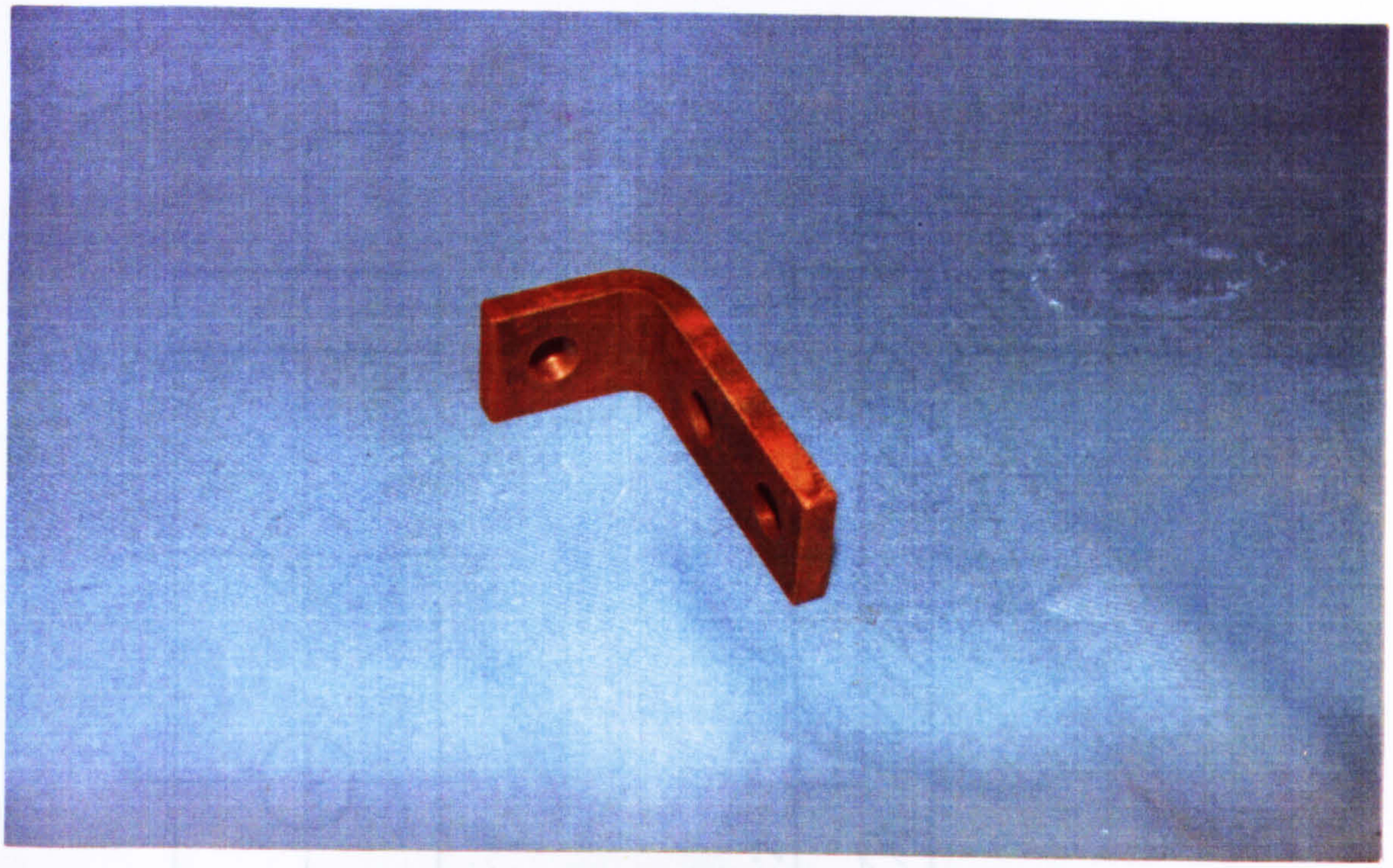

Fig. 8.2.1 A Typical Connection

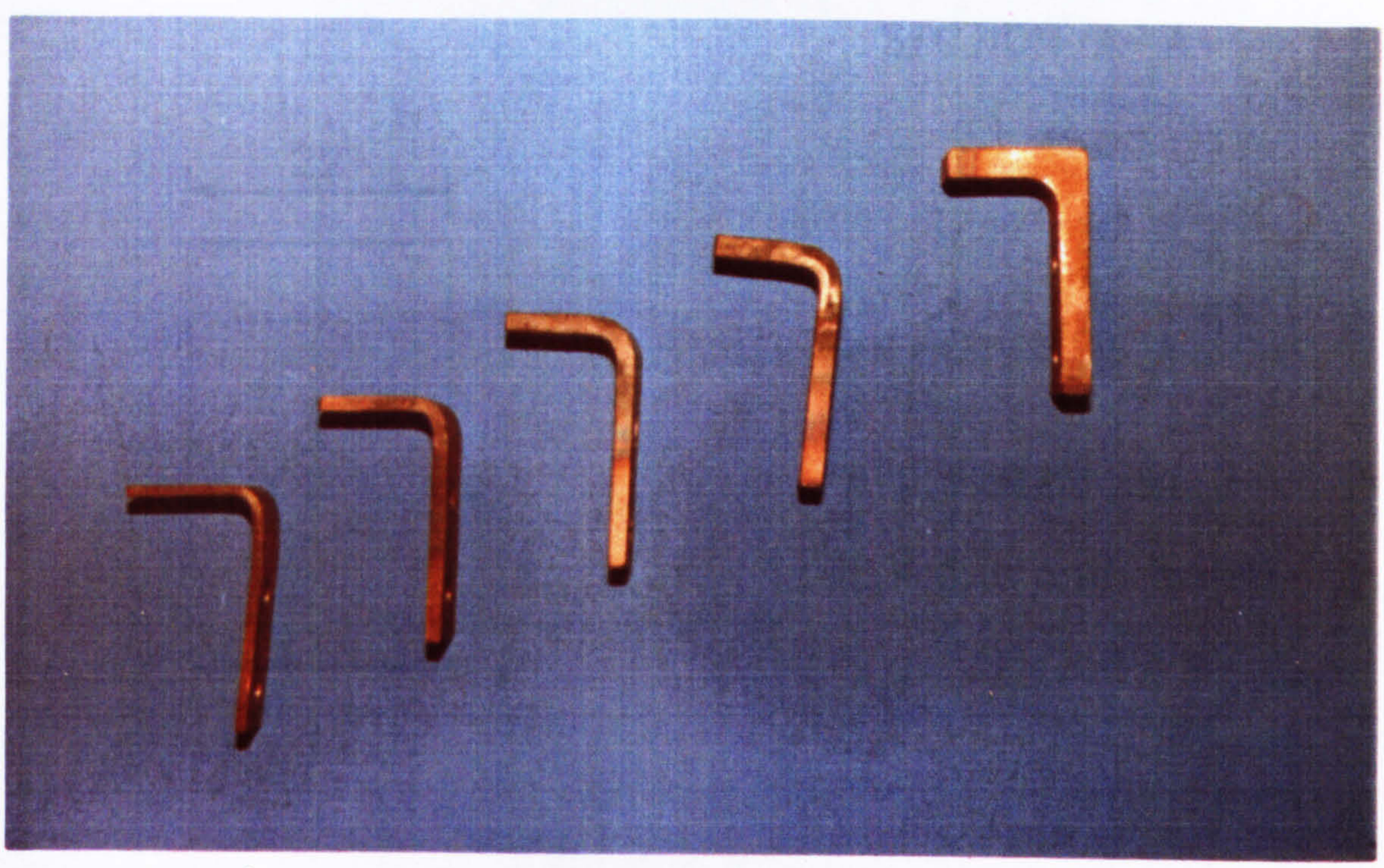

Fig. 8.2.2 Connections of Various Thickness

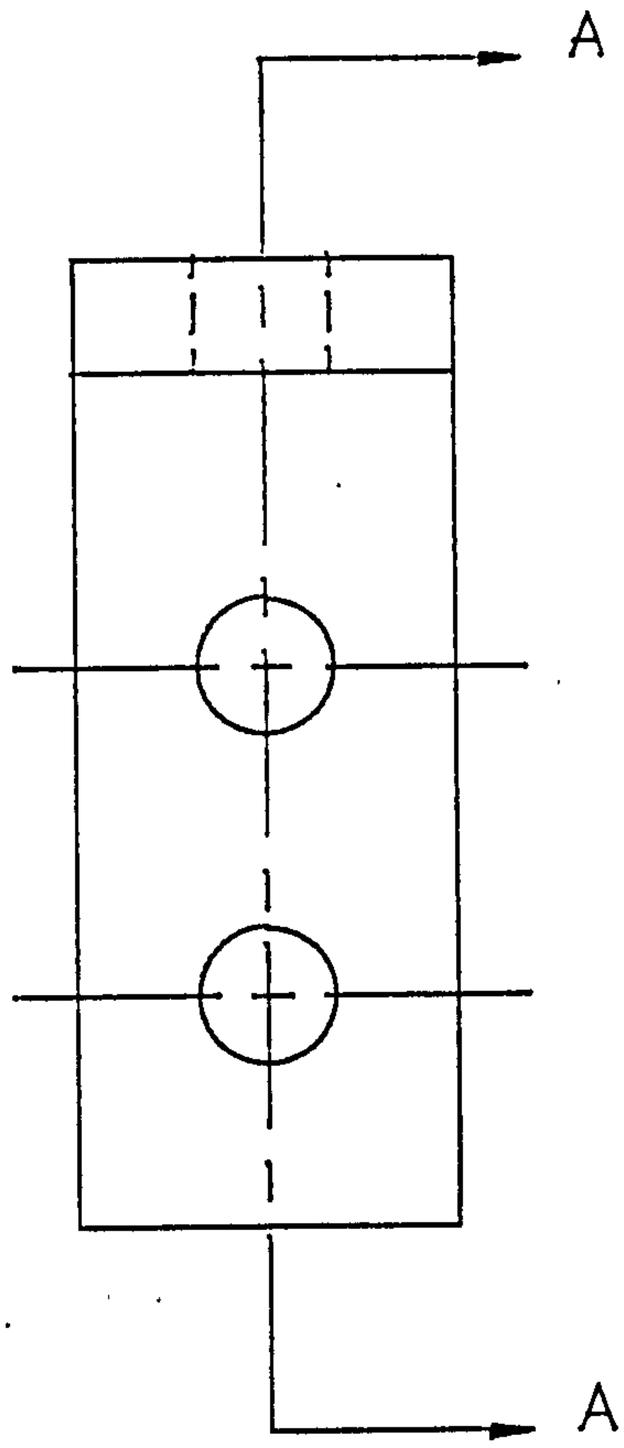

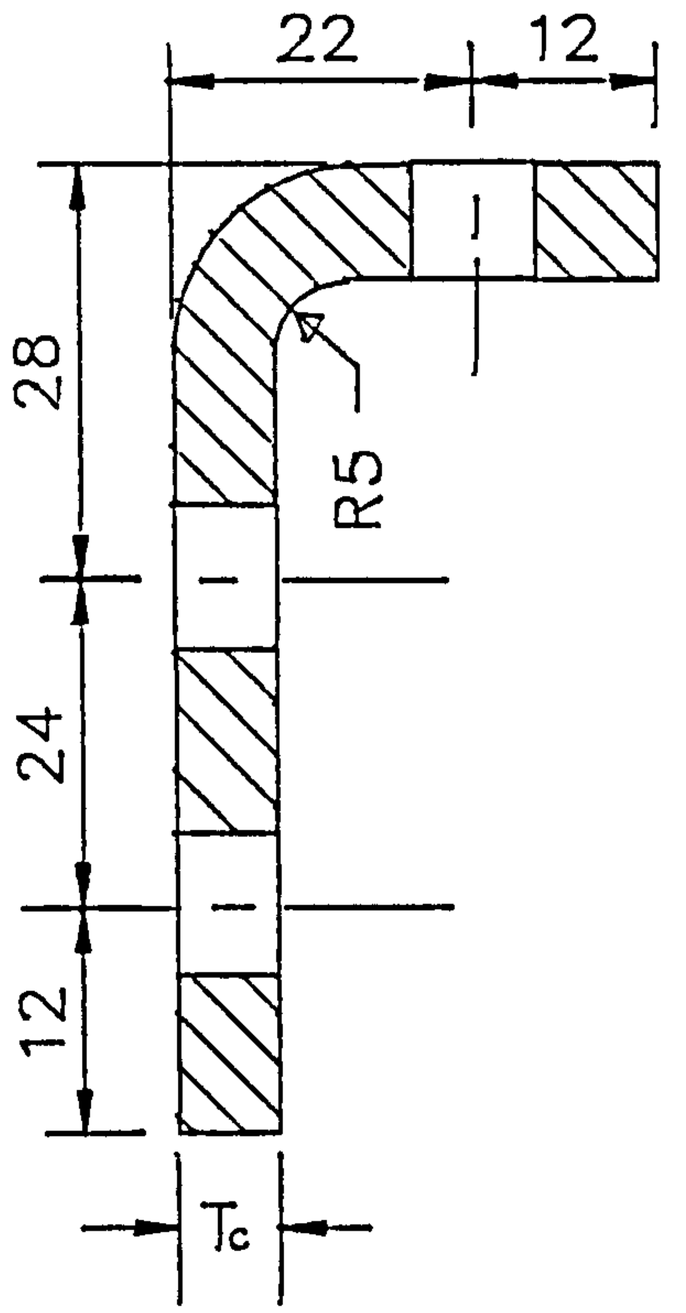

SECTION A–A

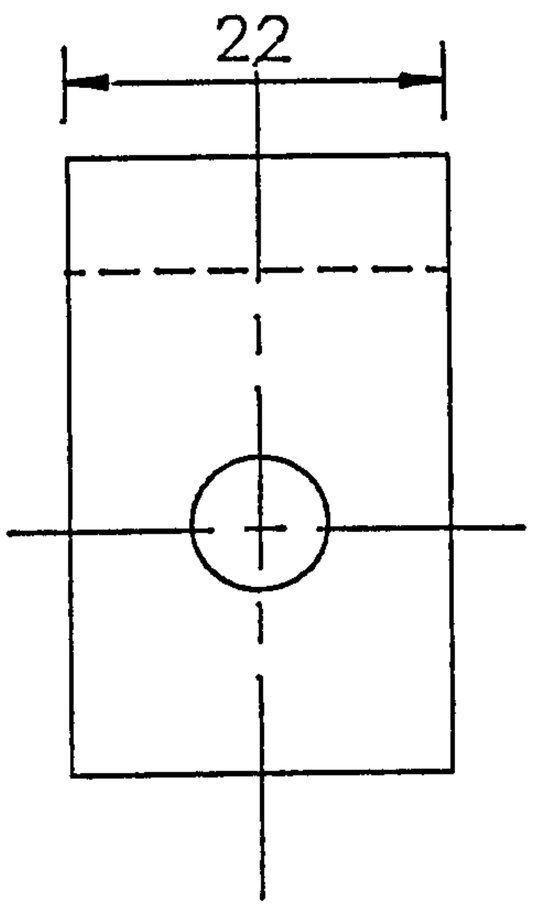

ALL HOLES Ø9

Tc=3,4,5,6 and 7 mm

Fig. 8.2.3 Connection Dimensions.

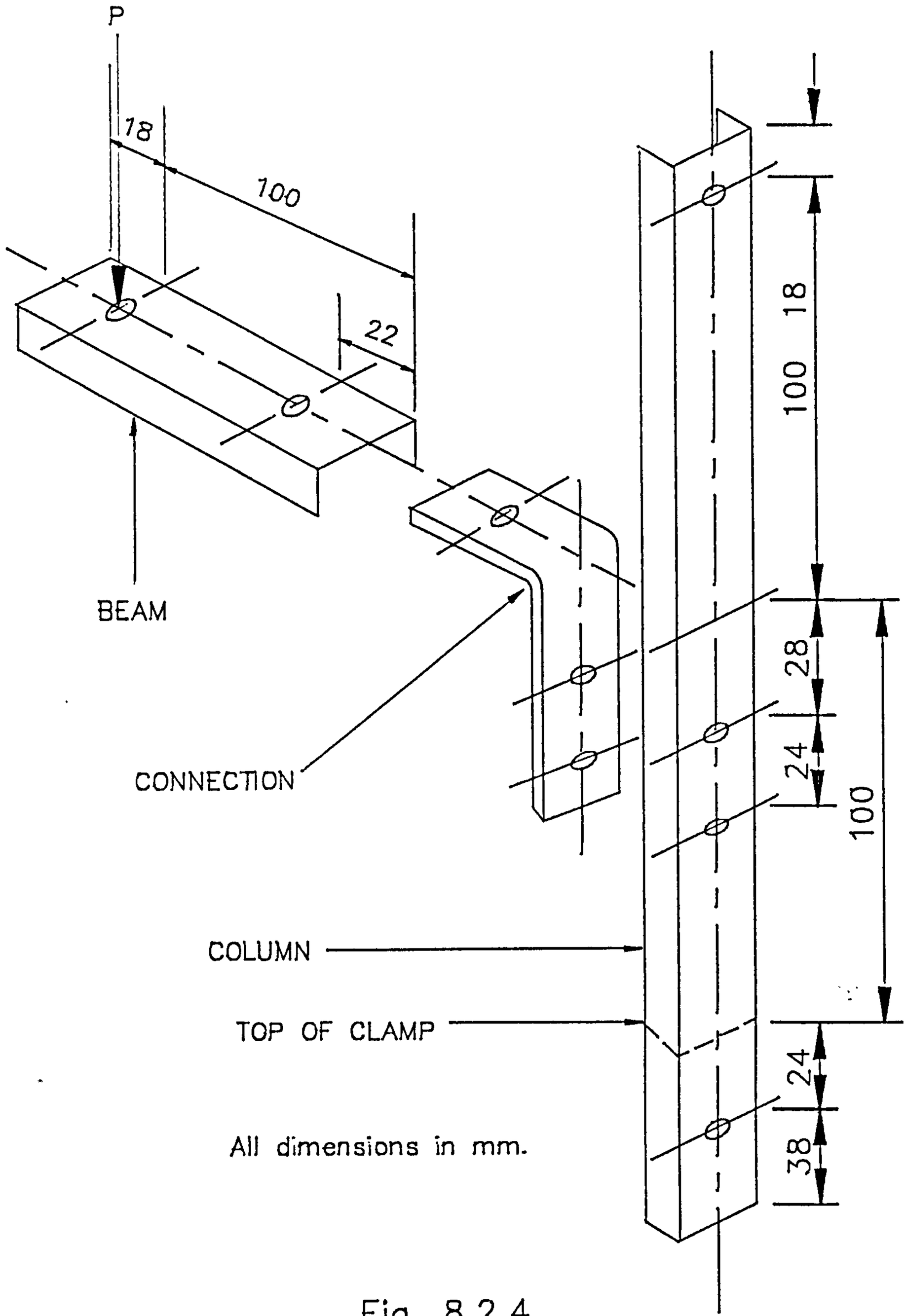

Fig. 8.2.4

COLUMN AND BEAM DETAILS FOR CONNECTION TEST

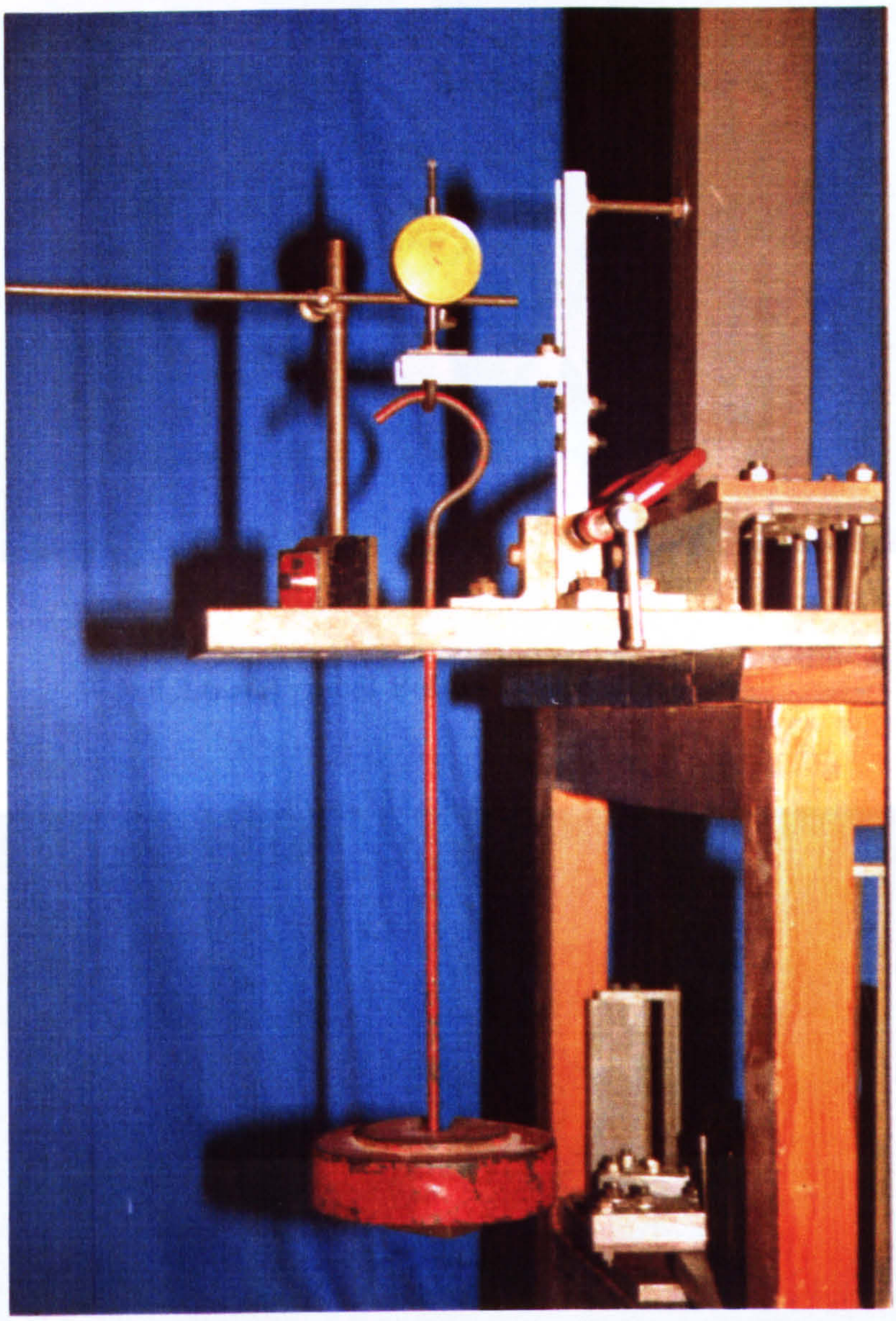

Fig. 8.2.5 Cantilever Type Arrangement

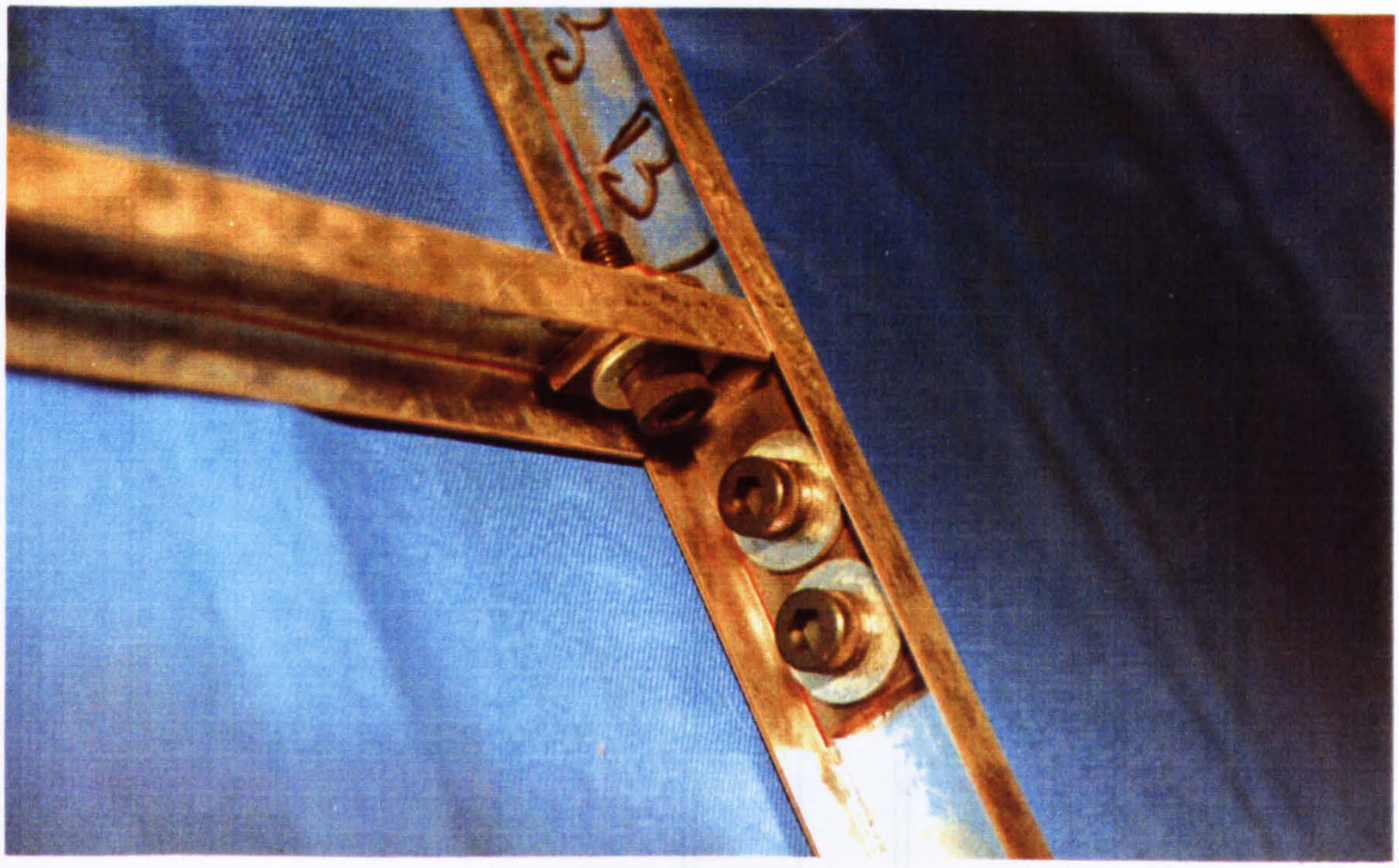

Fig. 8.2.6 A Typical Bolted Connection

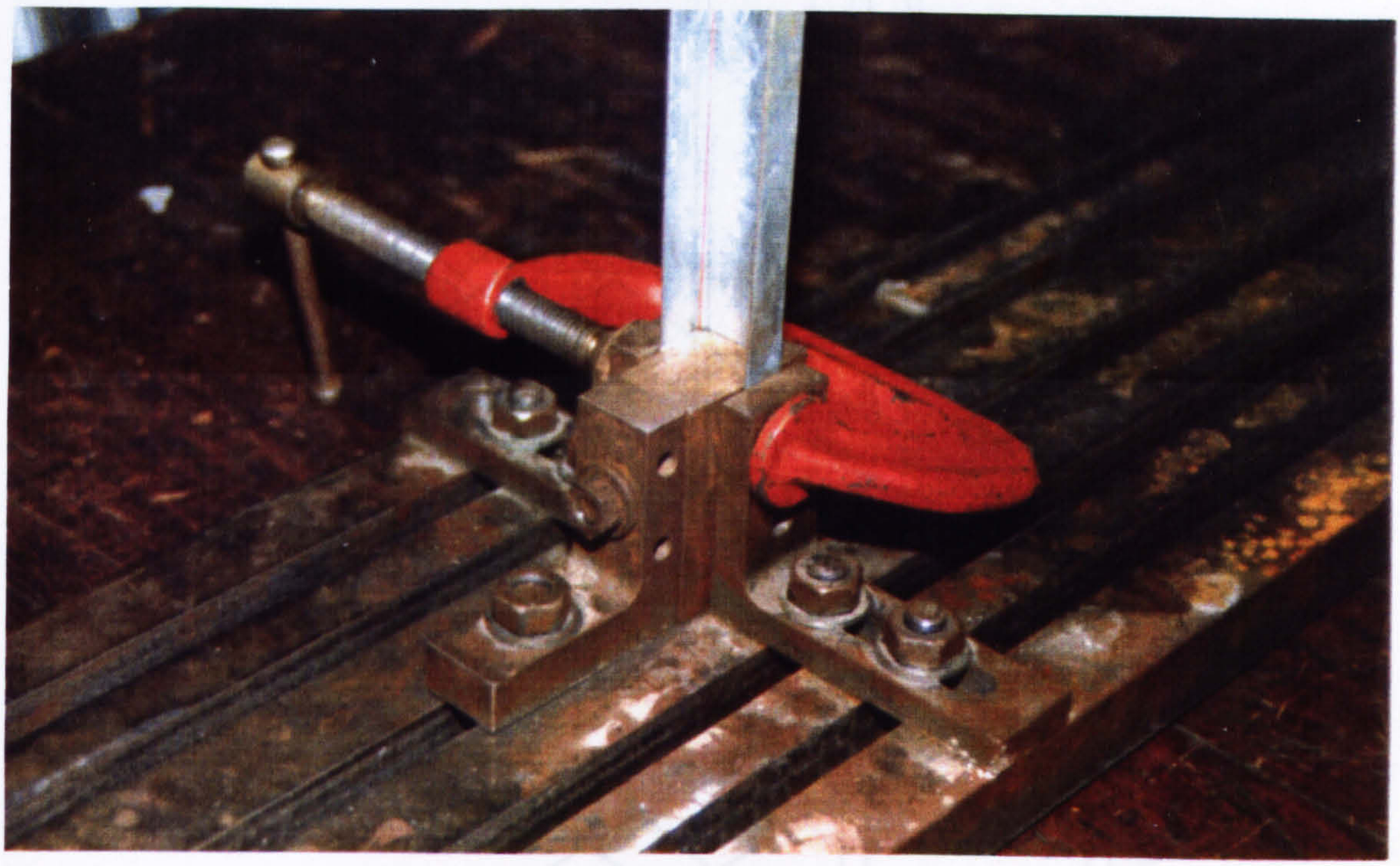

Fig. 8.2.7 Clamped End of Column

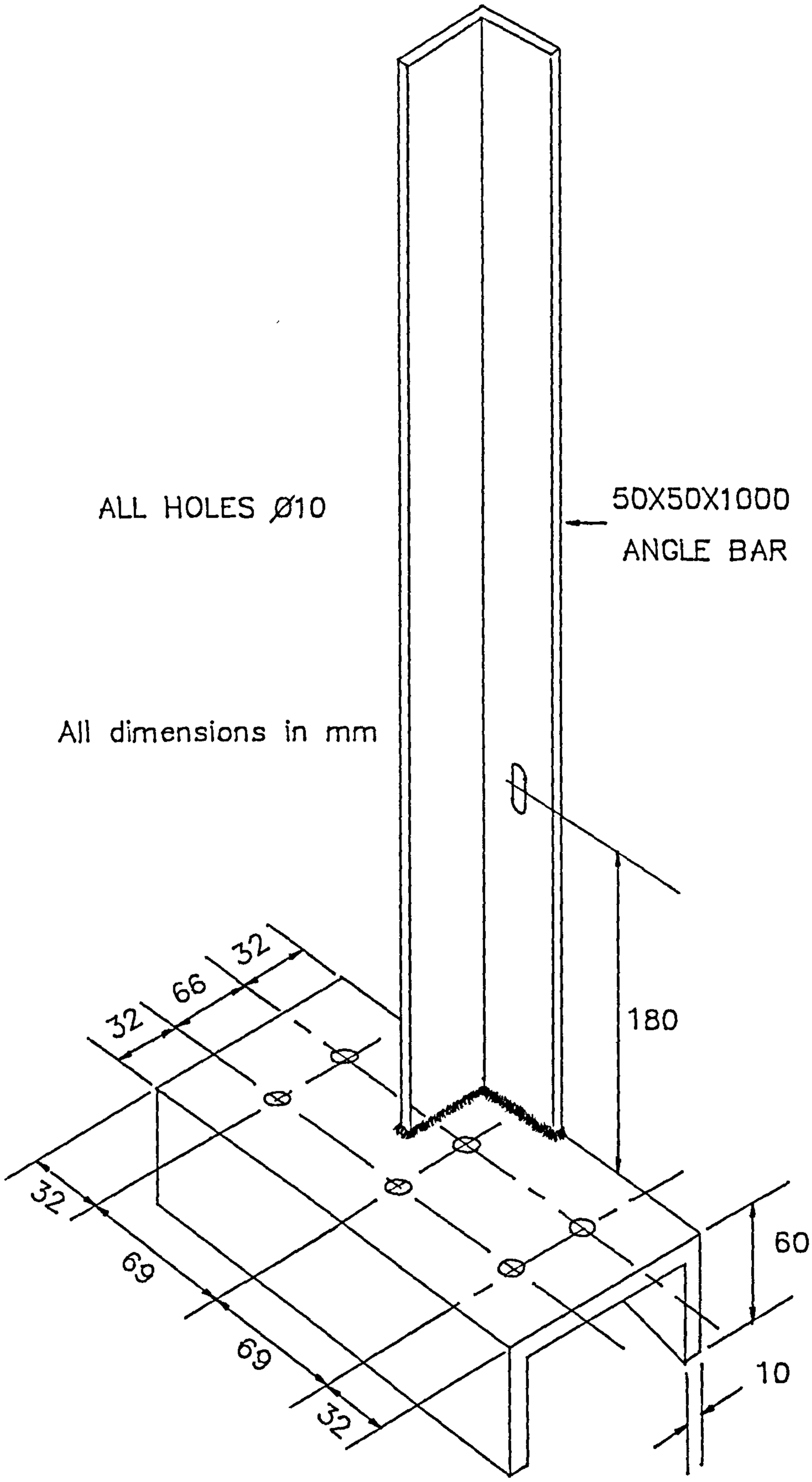

Fig. 8.2.8 Rigid Support Stand

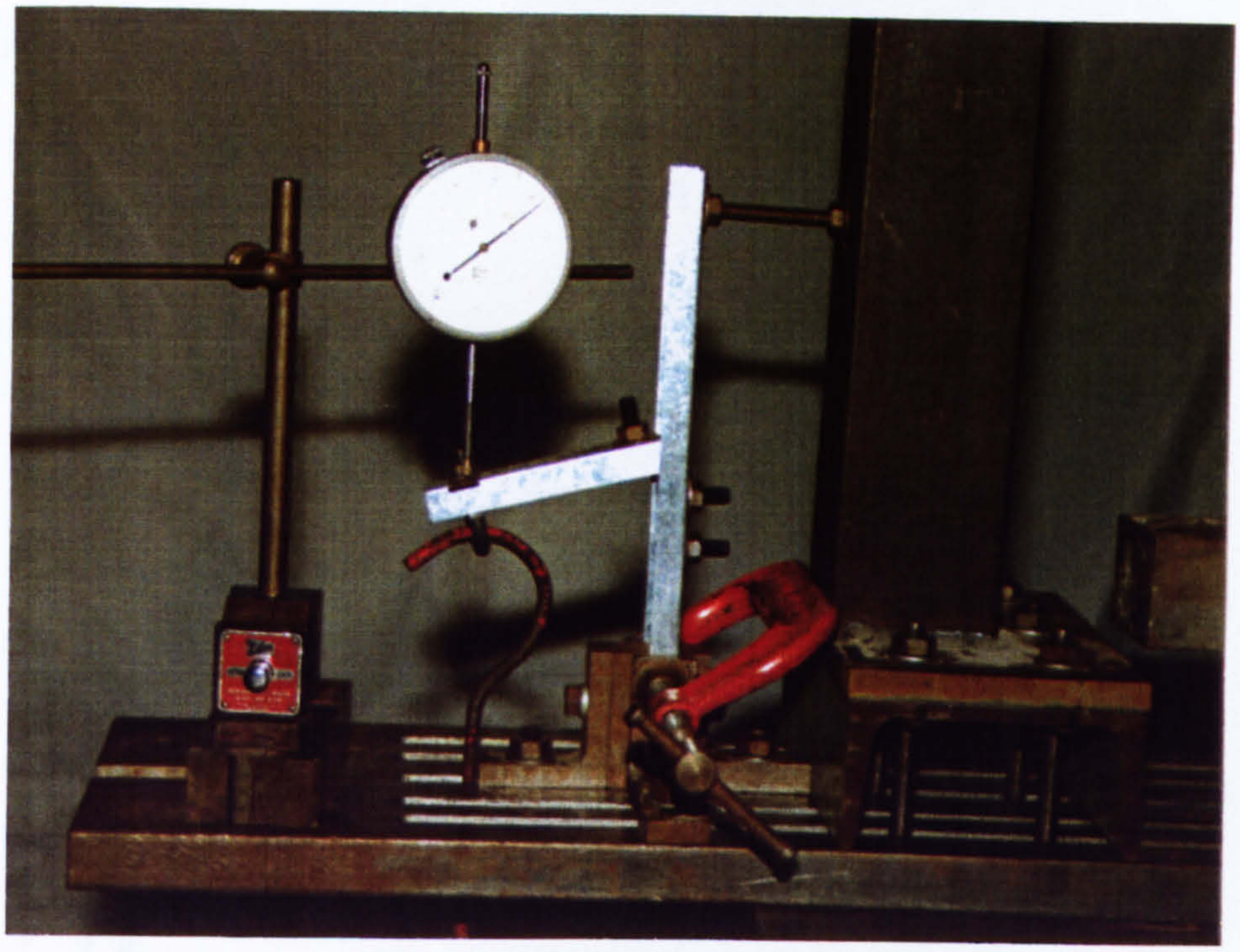

Fig. 8.2.10 Typical Joint Model at Failure

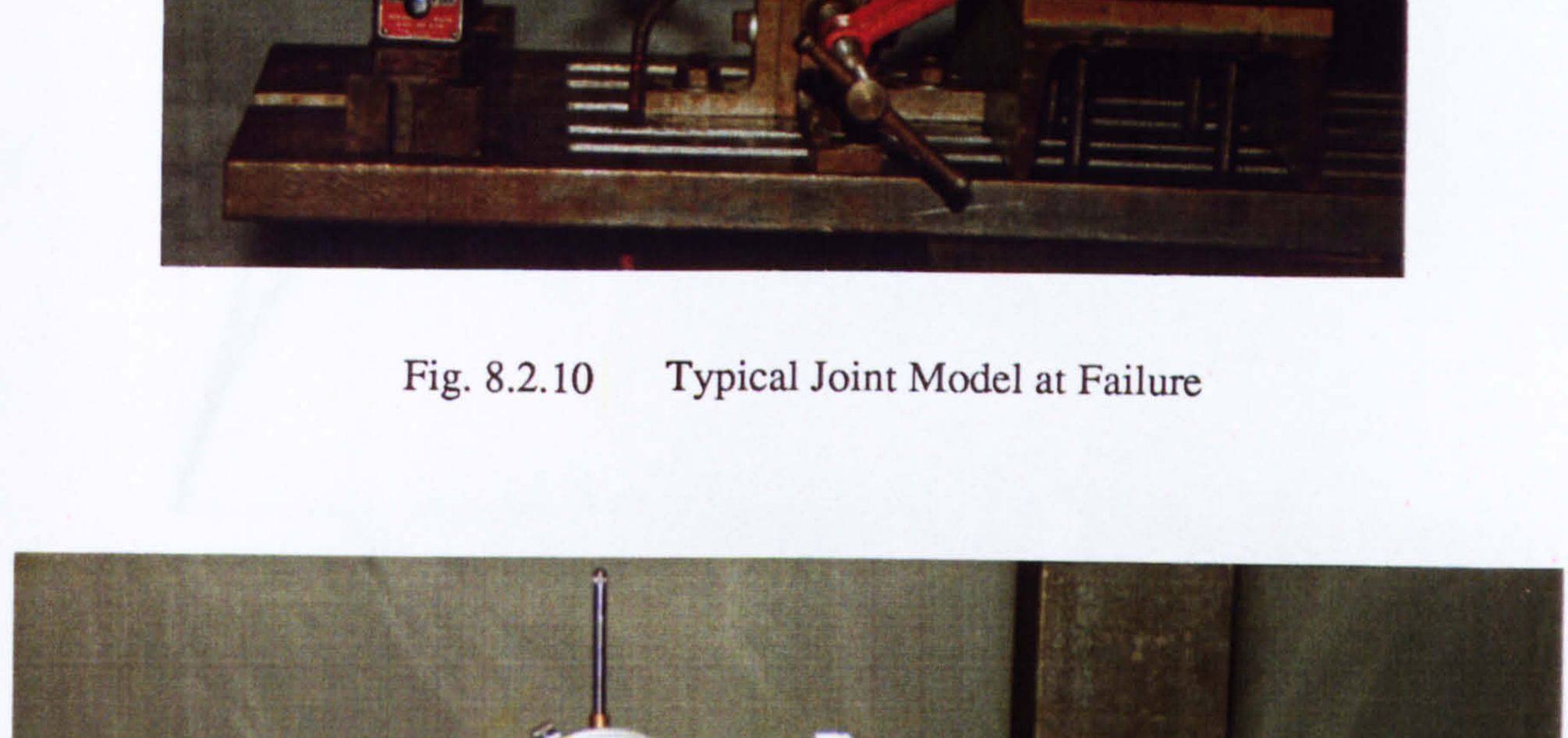

Fig. 8.2.9 Joint Model Test Setup Before Loading

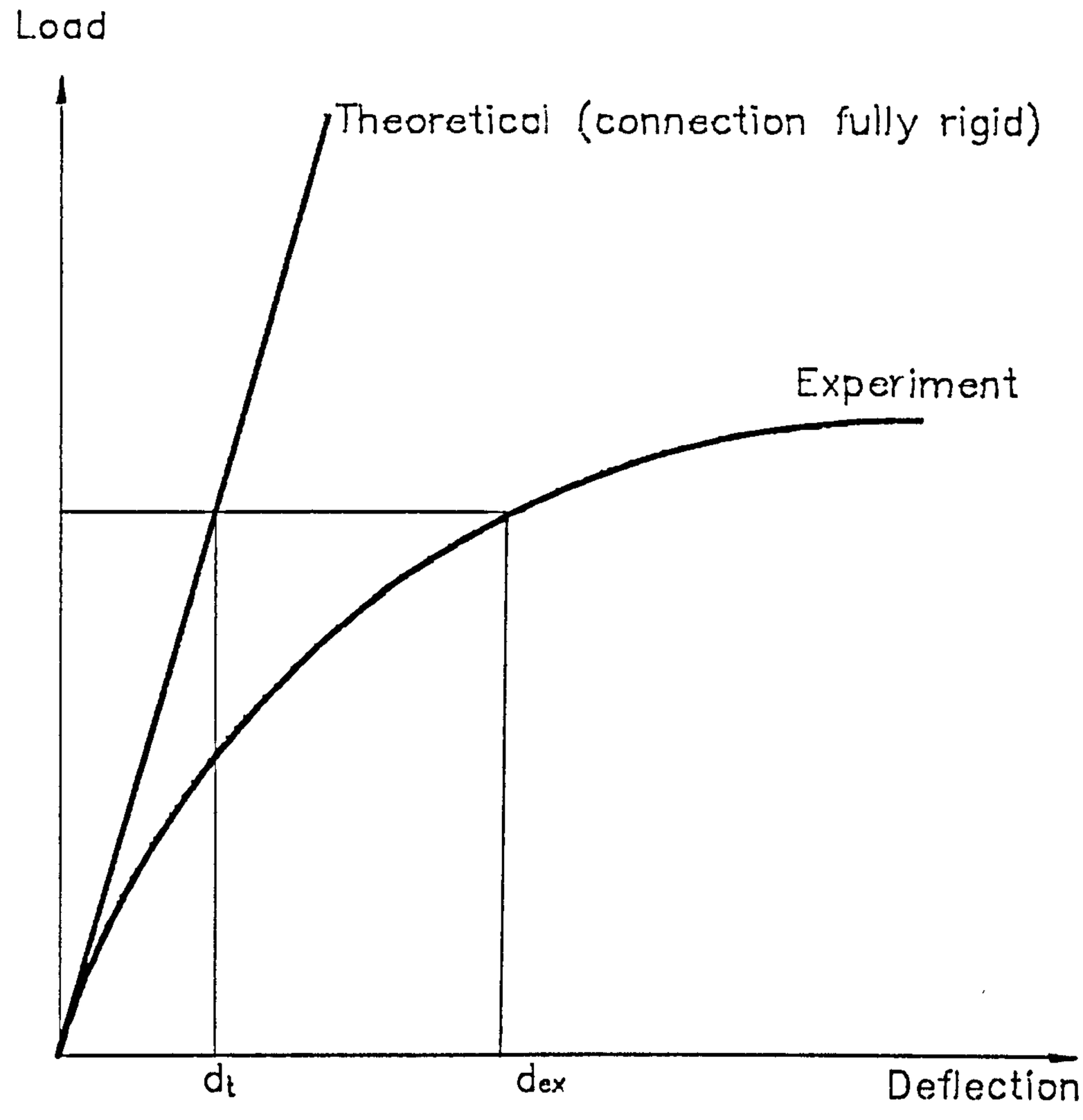

Fig. 8.2.11 Typical Joint Model Load/Deflection Plot.

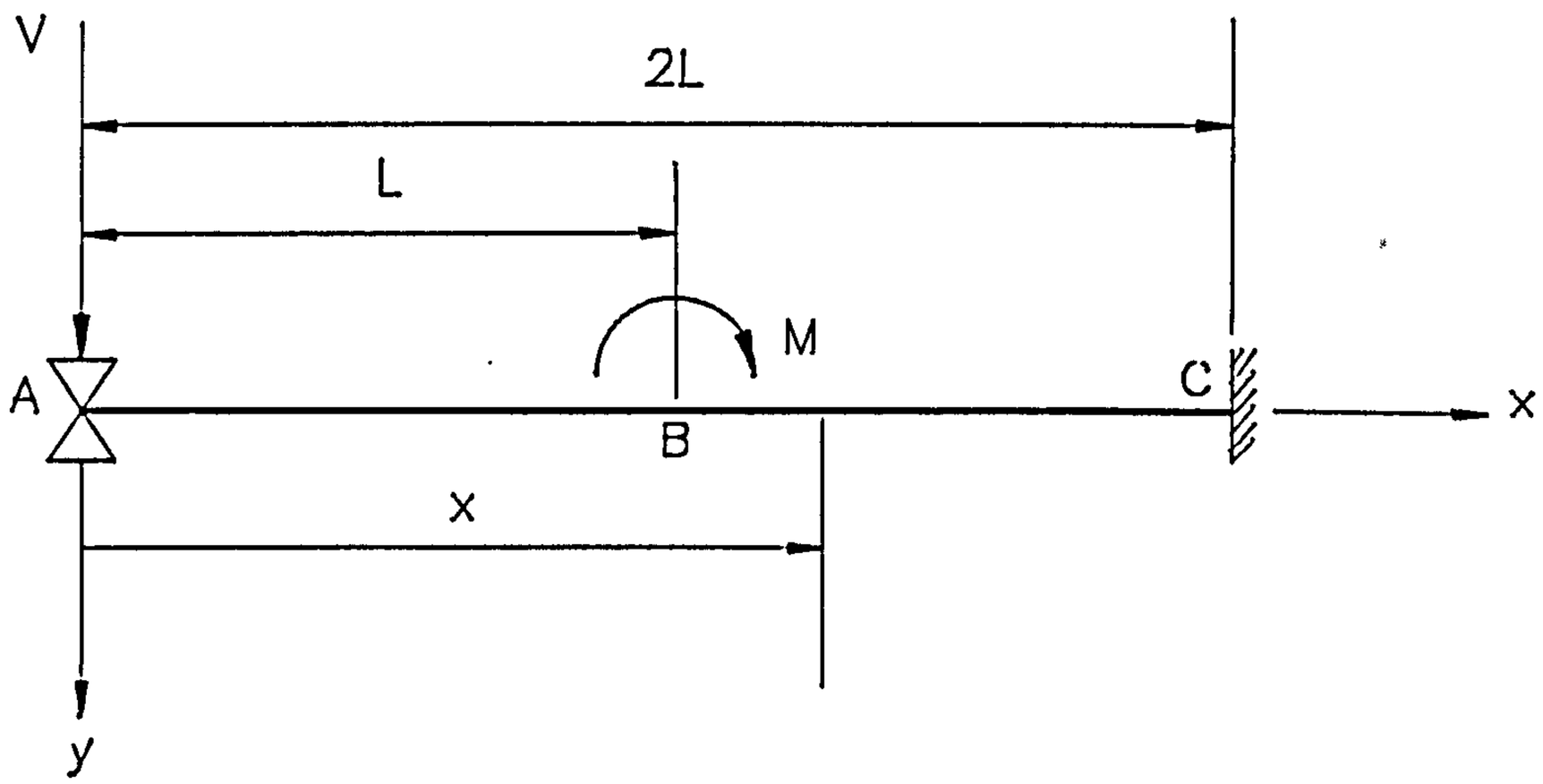

Fig. 8.2.12 Schematic Drawing of Joint Model Test.

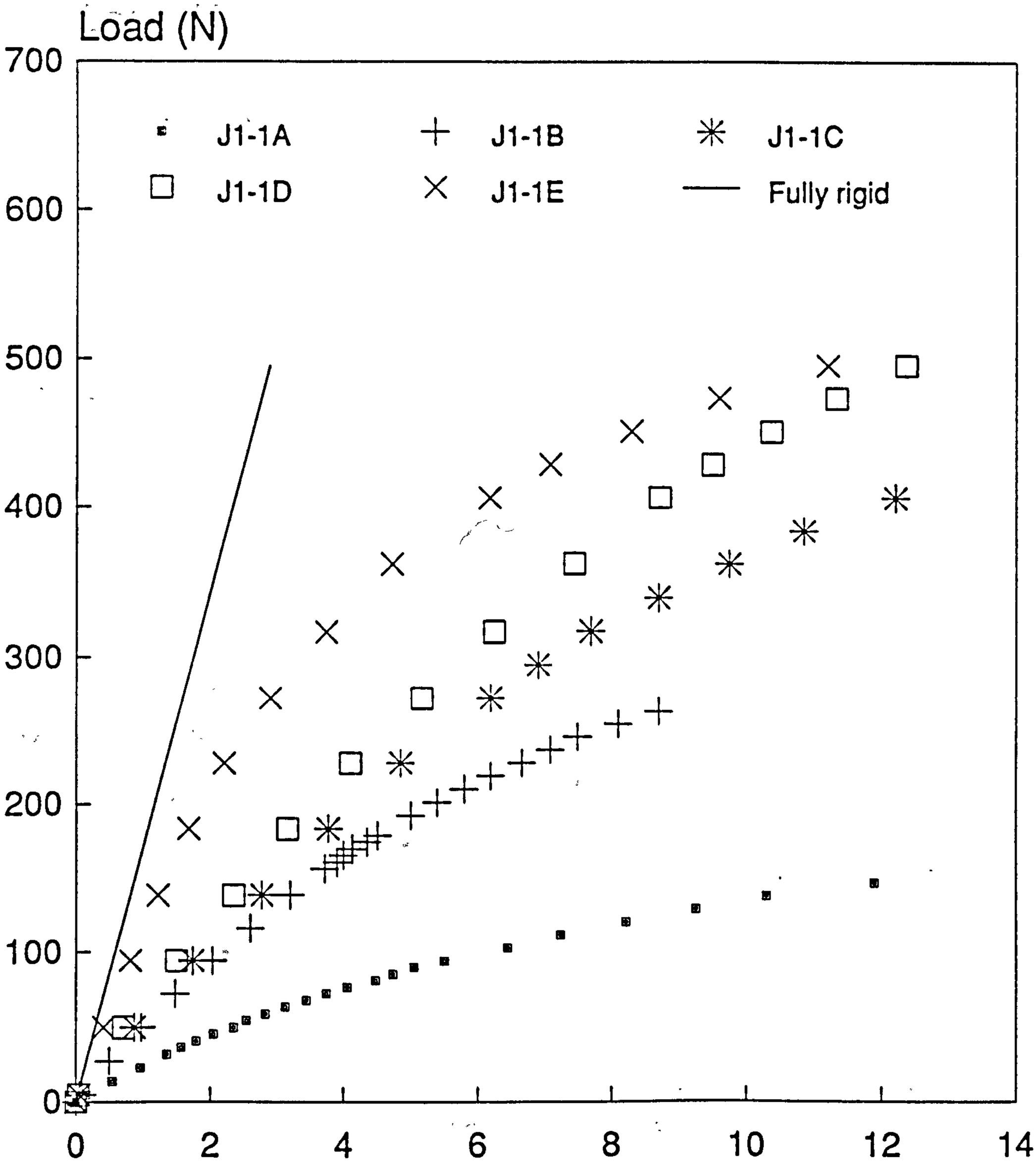

Fig.8.2.13 Connection J1-1A to E Load/Displacement plot

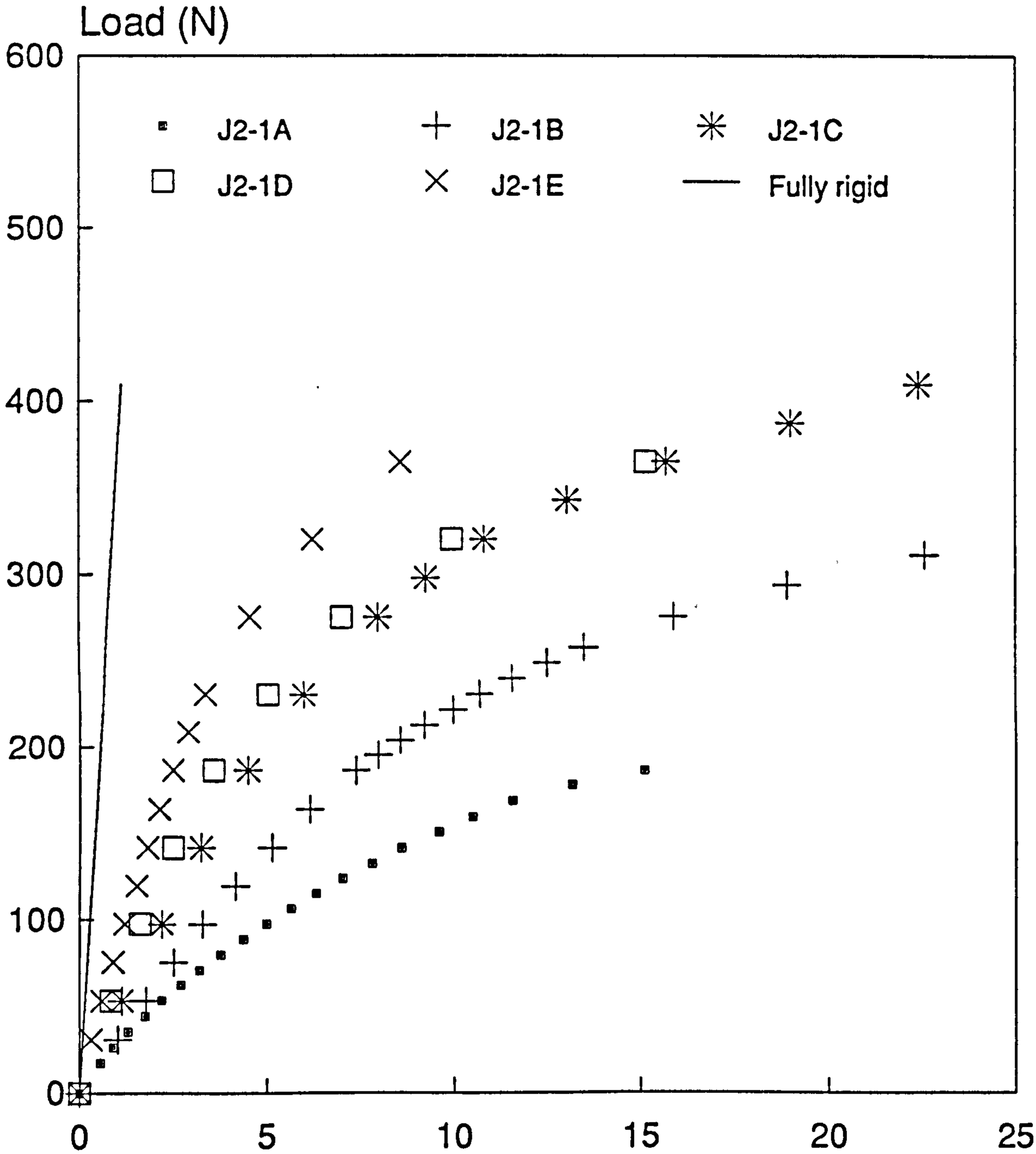

Fig.8.2.14 Connection J2-1A to E Load/Displacement plot

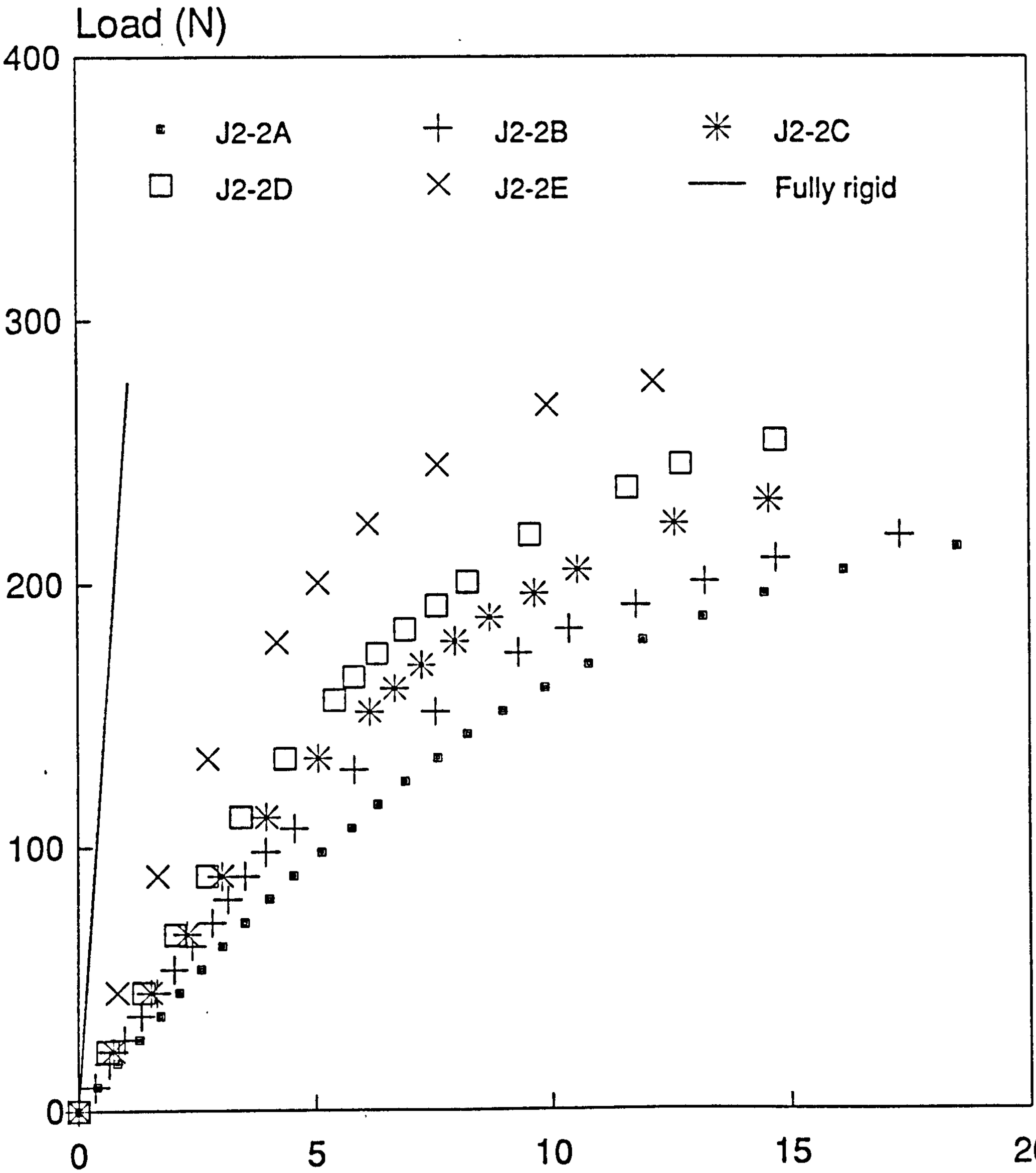

Fig.8.2.15 Connection J2-2A to E Load/Displacement plot

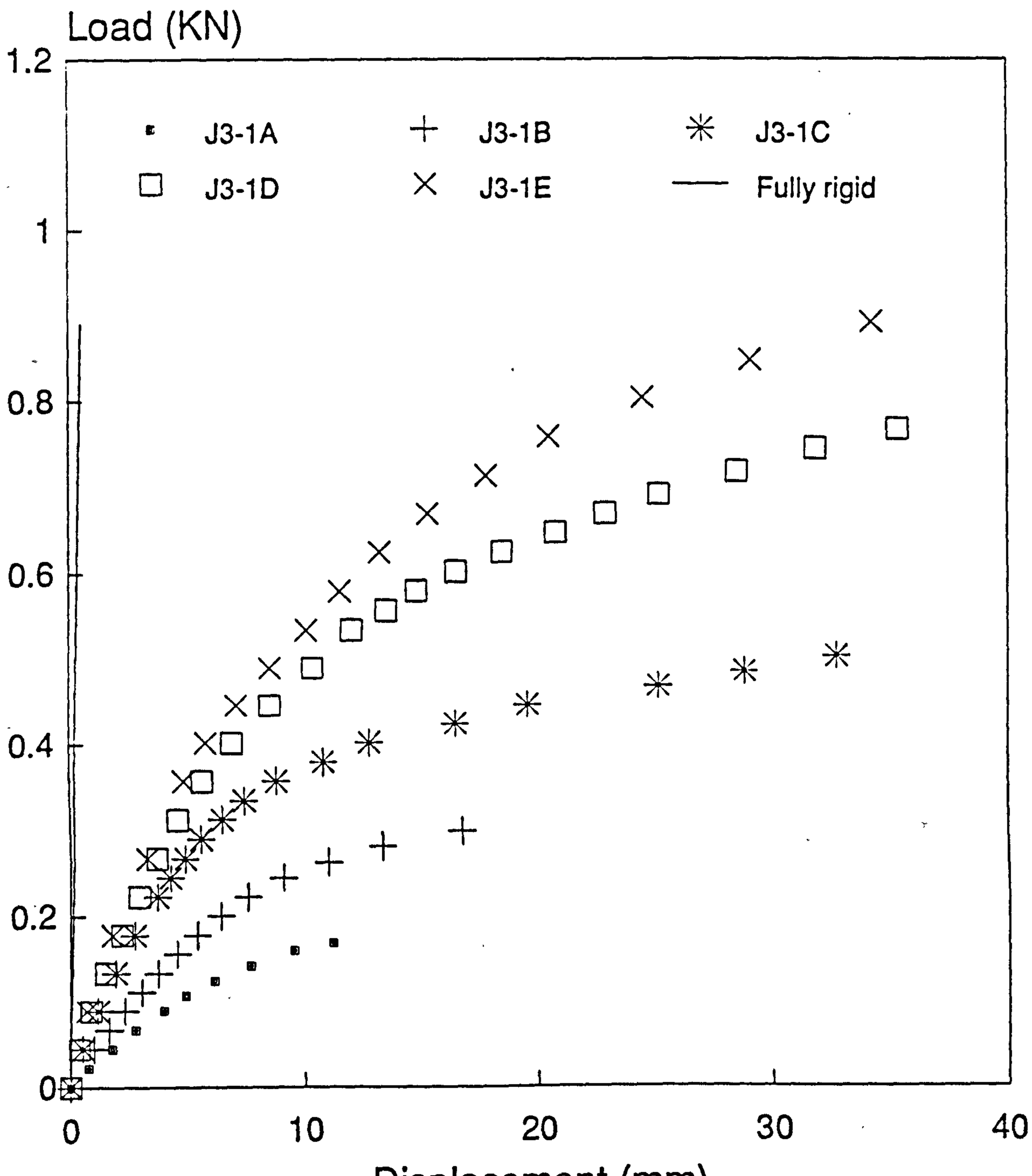

Fig.8.2.16 Connection J3-1A to E Load/Displacement plot

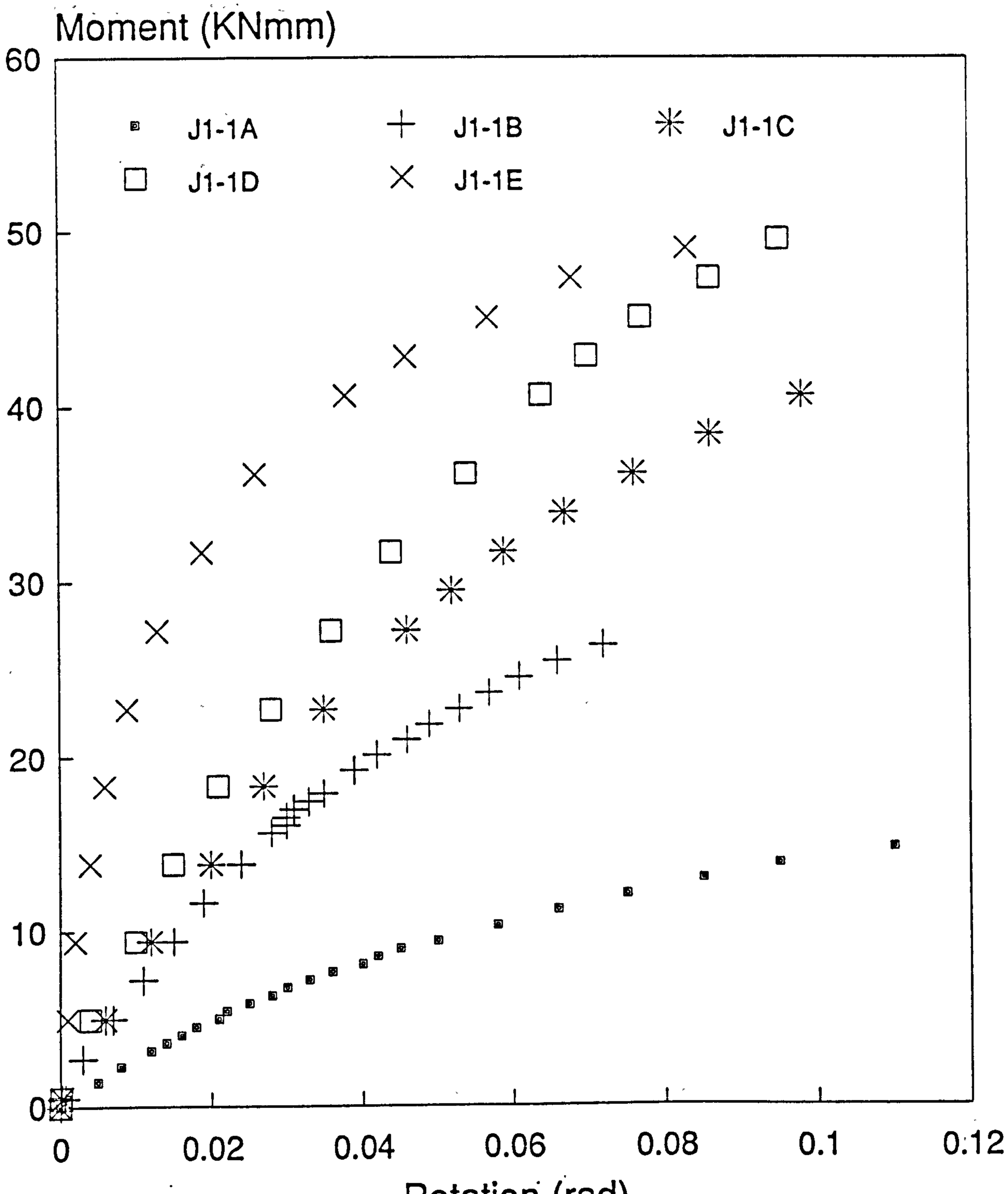

Fig.8.2.17 Connection J1-1A to E experimental plot

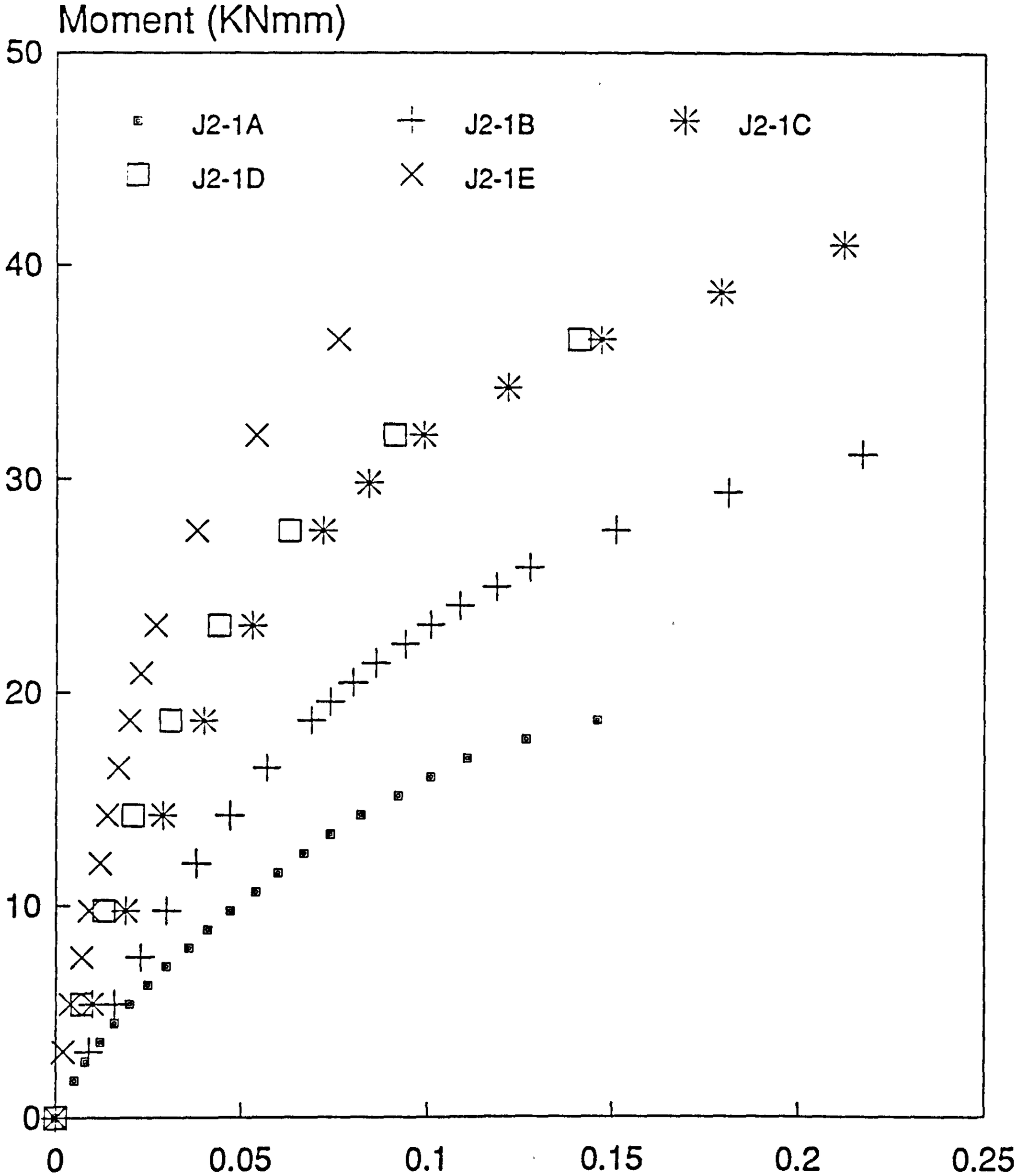

Fig.8.2.18 Connection J2-1A to E experimental plot

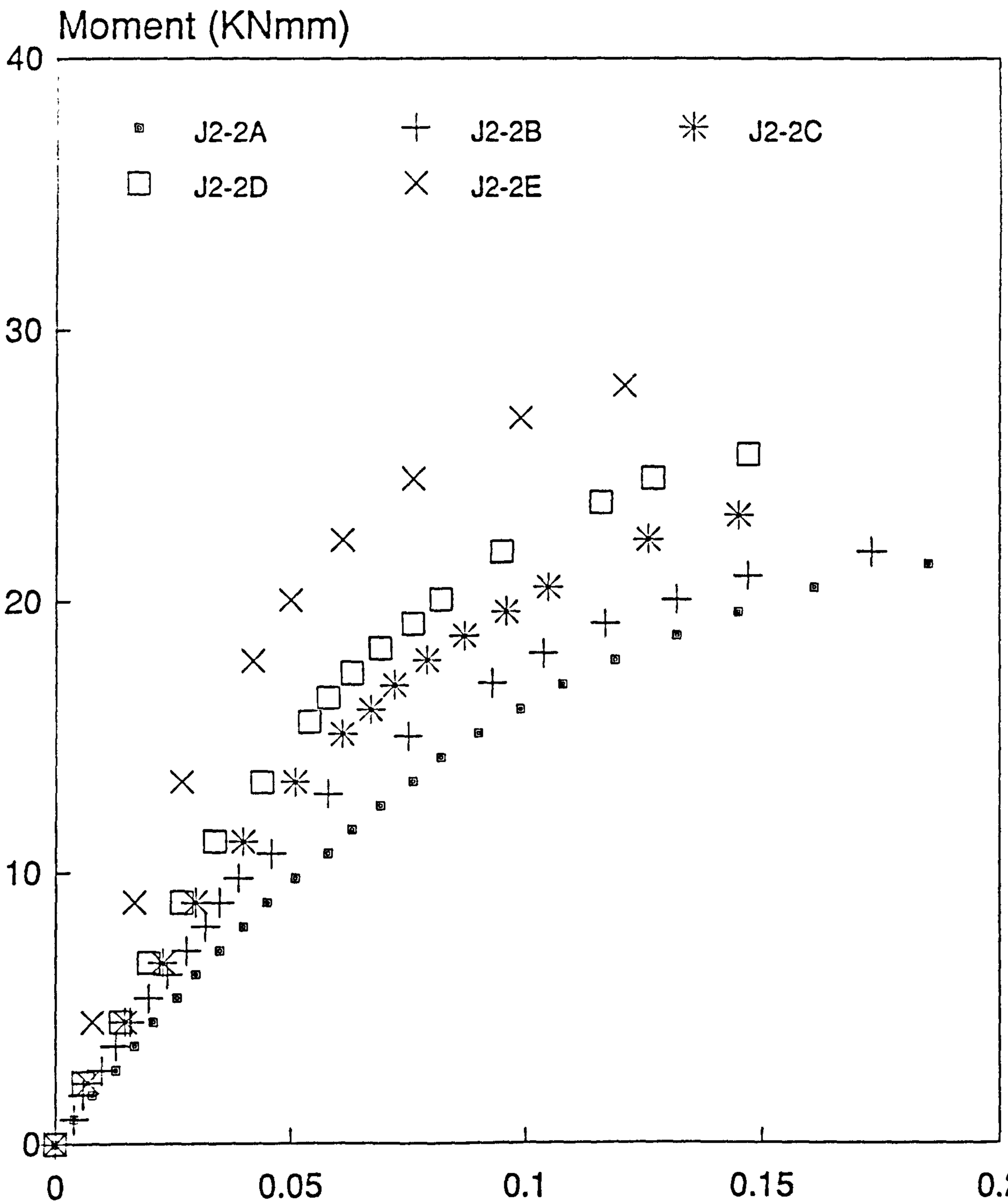

Fig.8.2.19 Connection J2-2A to E experimental plot

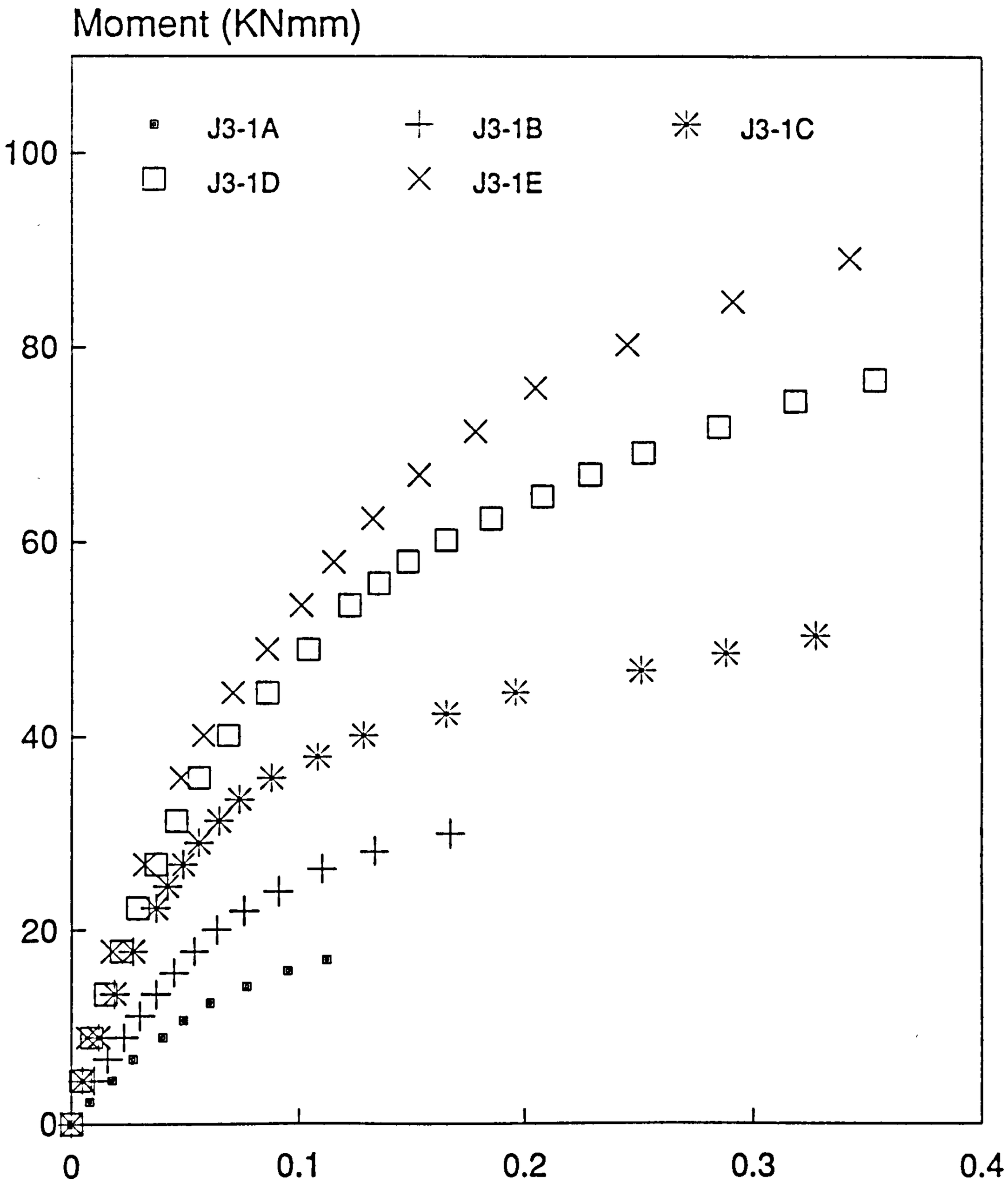

Fig.8.2.20 Connection J3-1A to E experimental plot

Fig. 8.2.21
Connection Failure

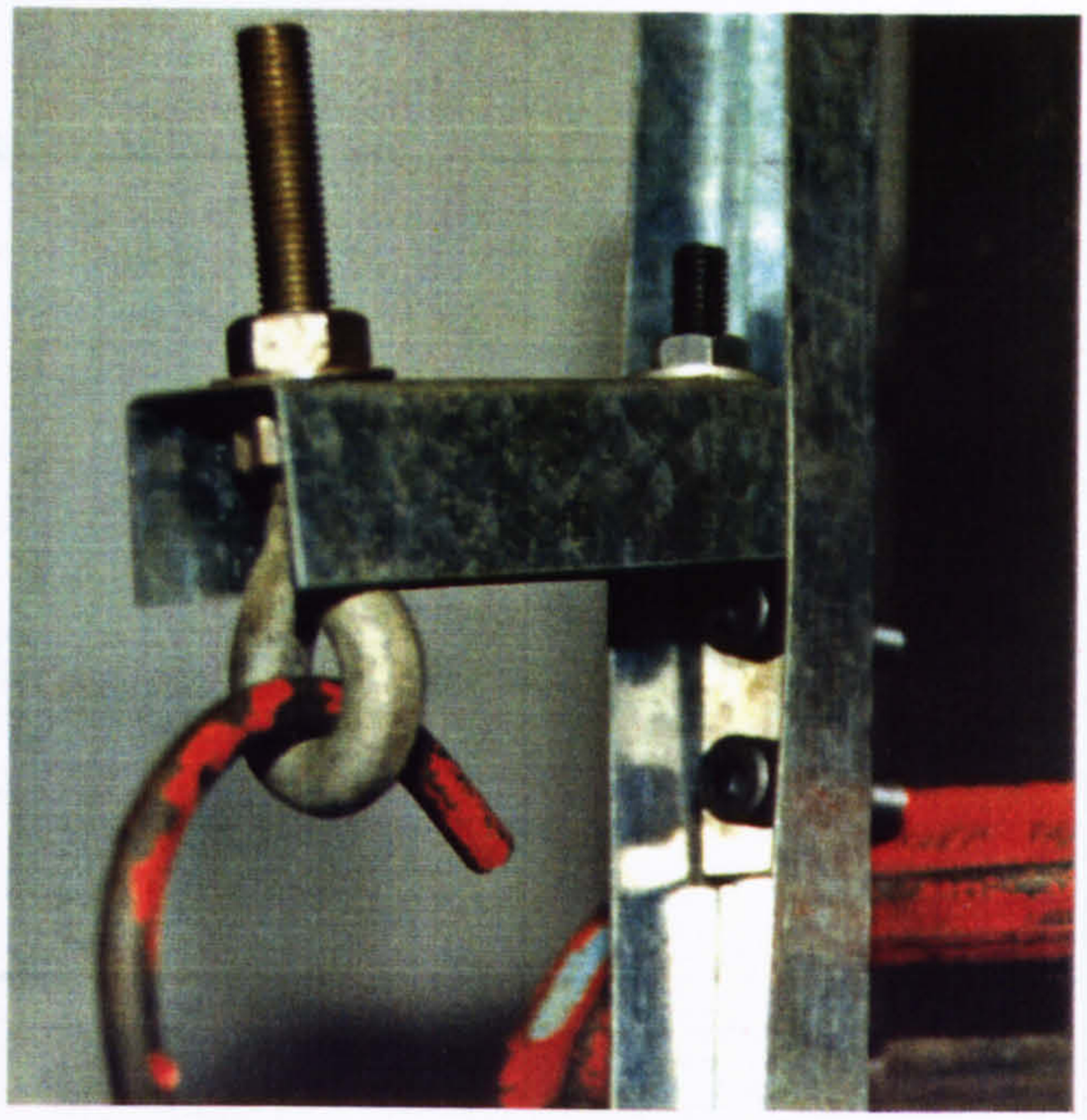

Fig. 8.2.22
Column Local Distortions

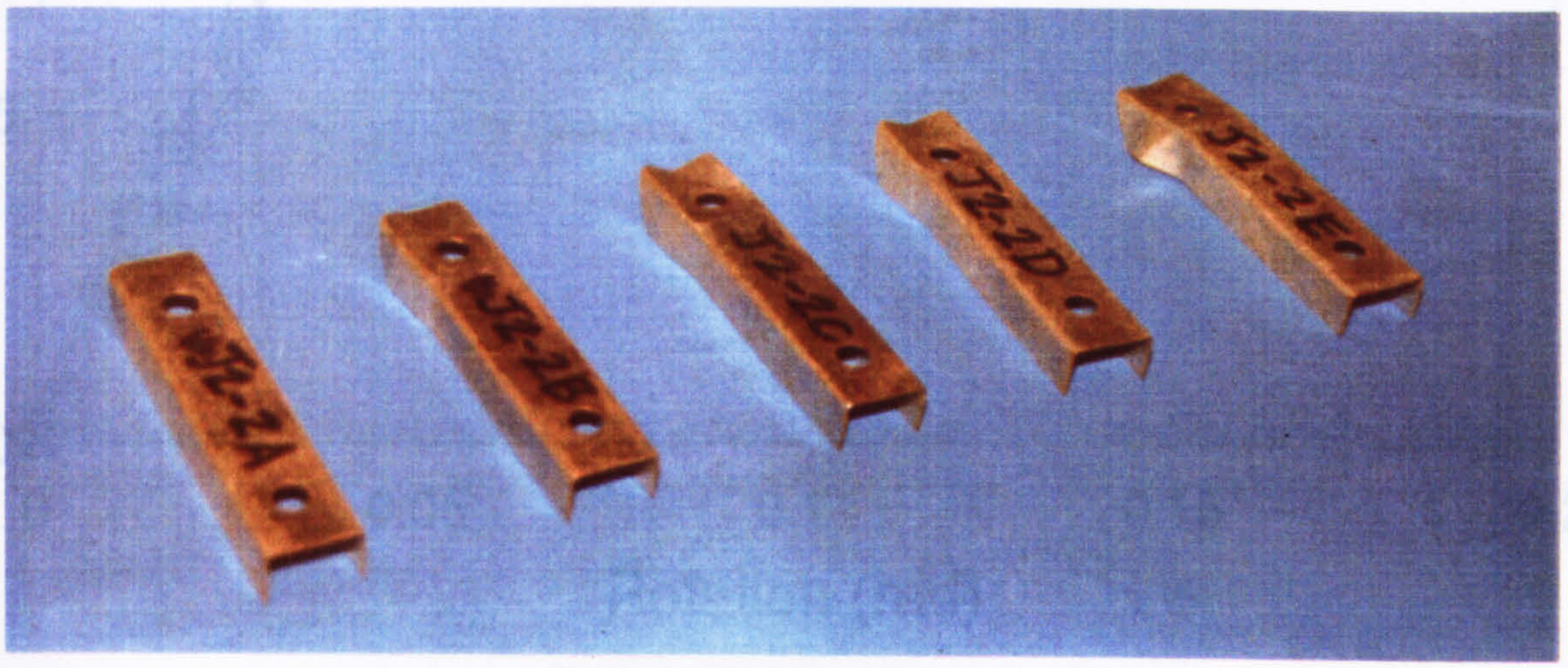

Fig. 8.2.23
Beam Local Distortions

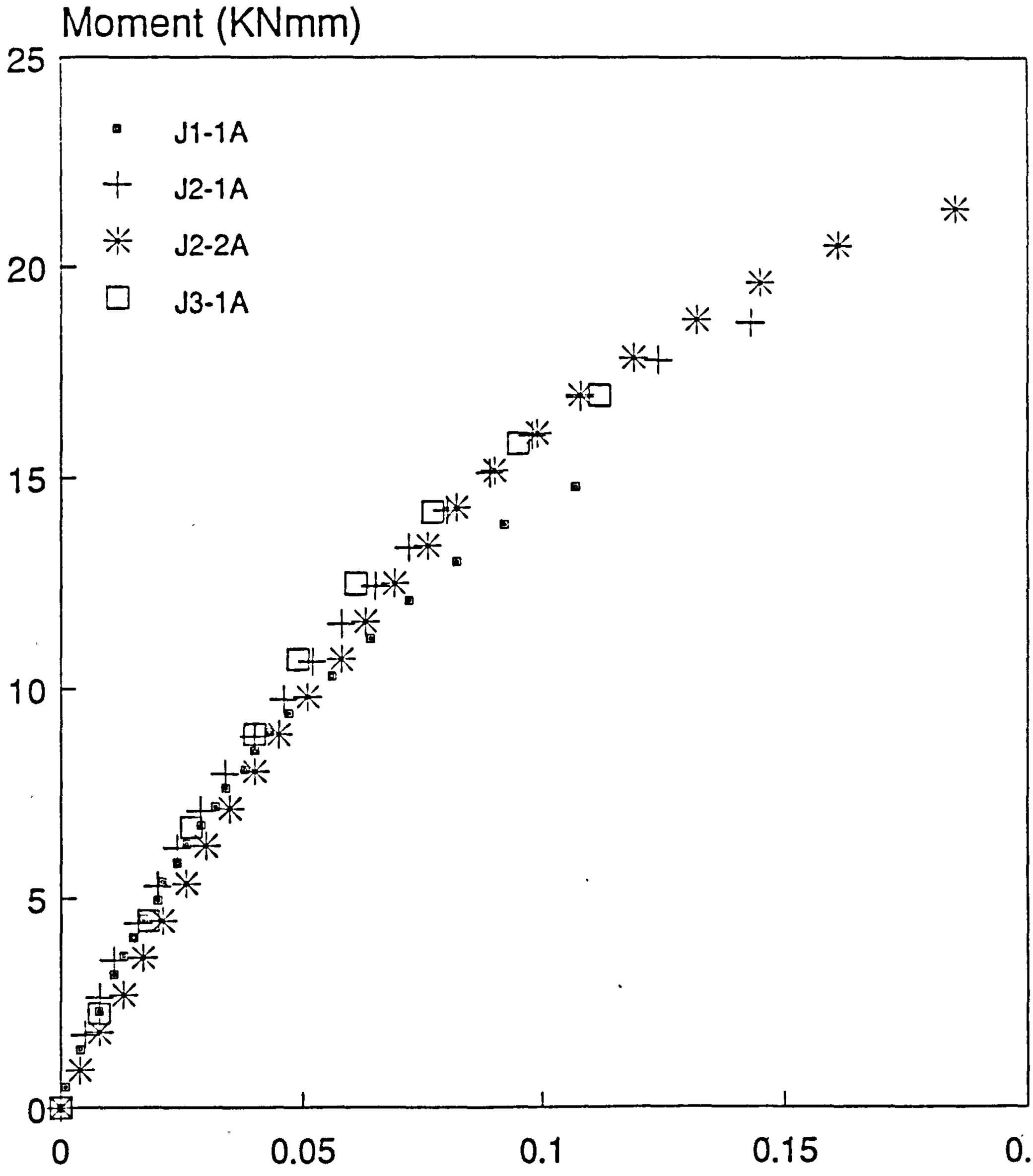

Fig. 8.2.24 Type "A" Connection (Tc=3mm)

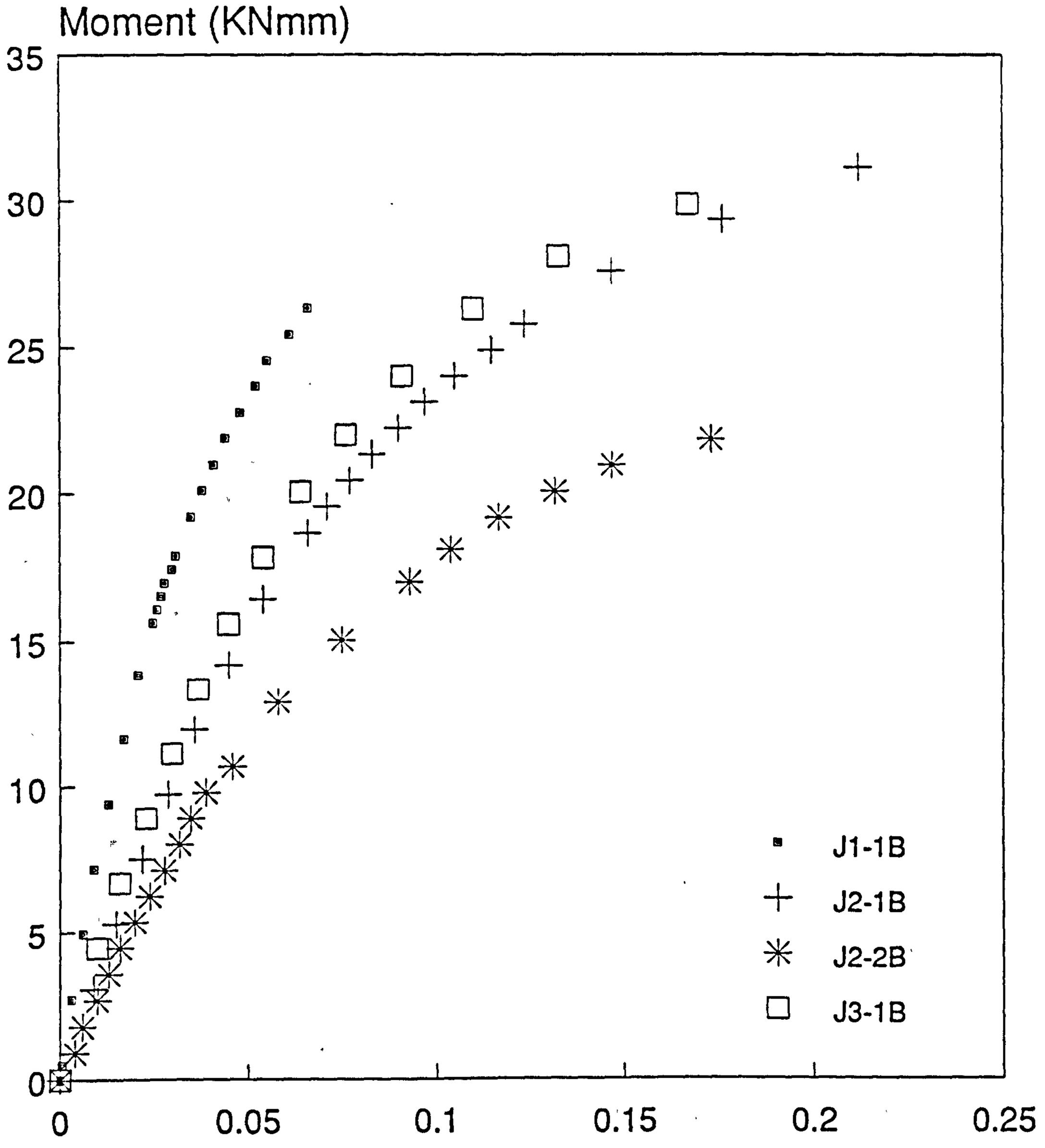

Fig. 8.2.25 Type "B" Connection (Tc=4mm)

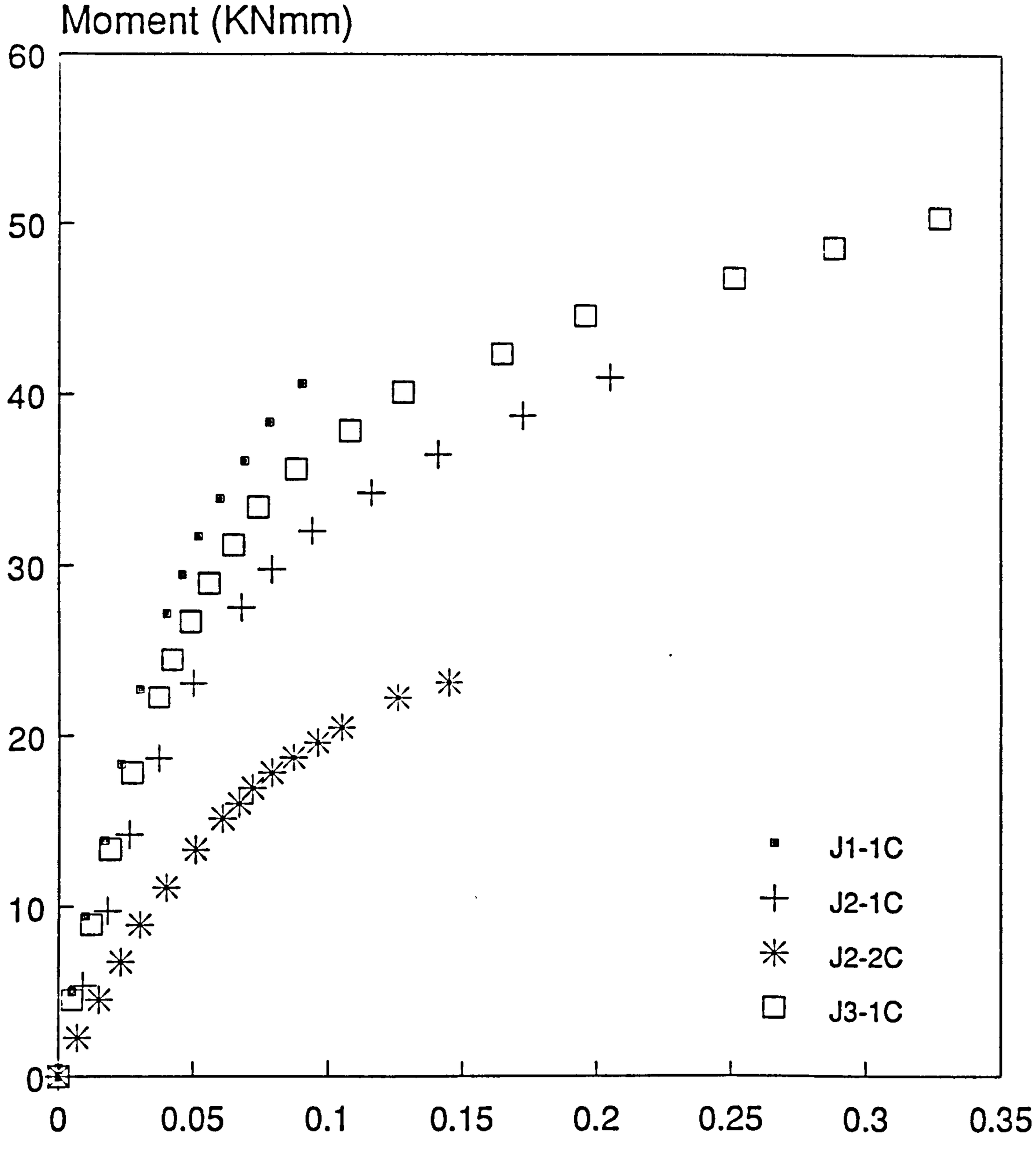

Fig. 8.2.26 Type "C" Connection (Tc=5mm)

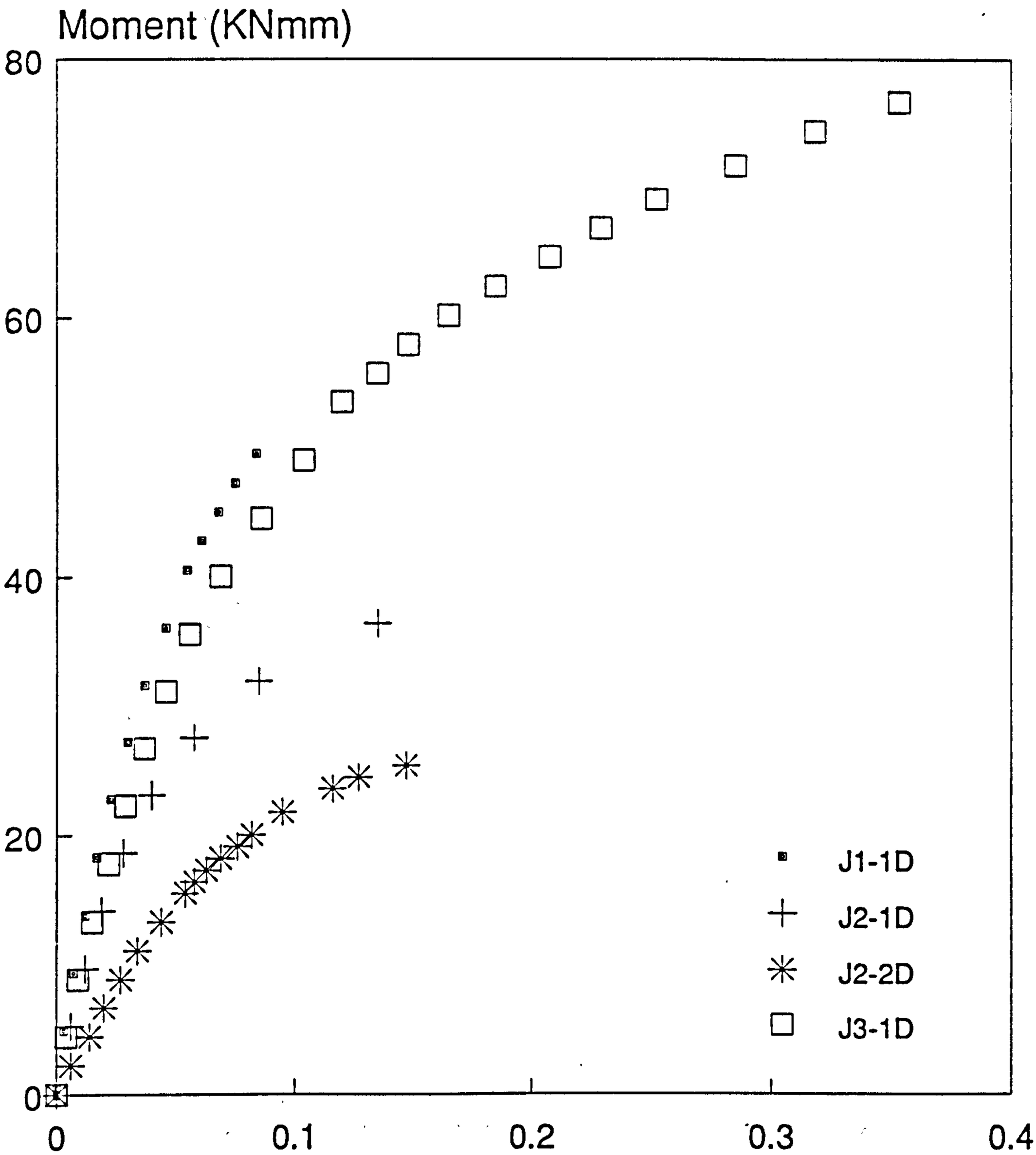

Fig. 8.2.27 Type "D" Connection (Tc=6mm)

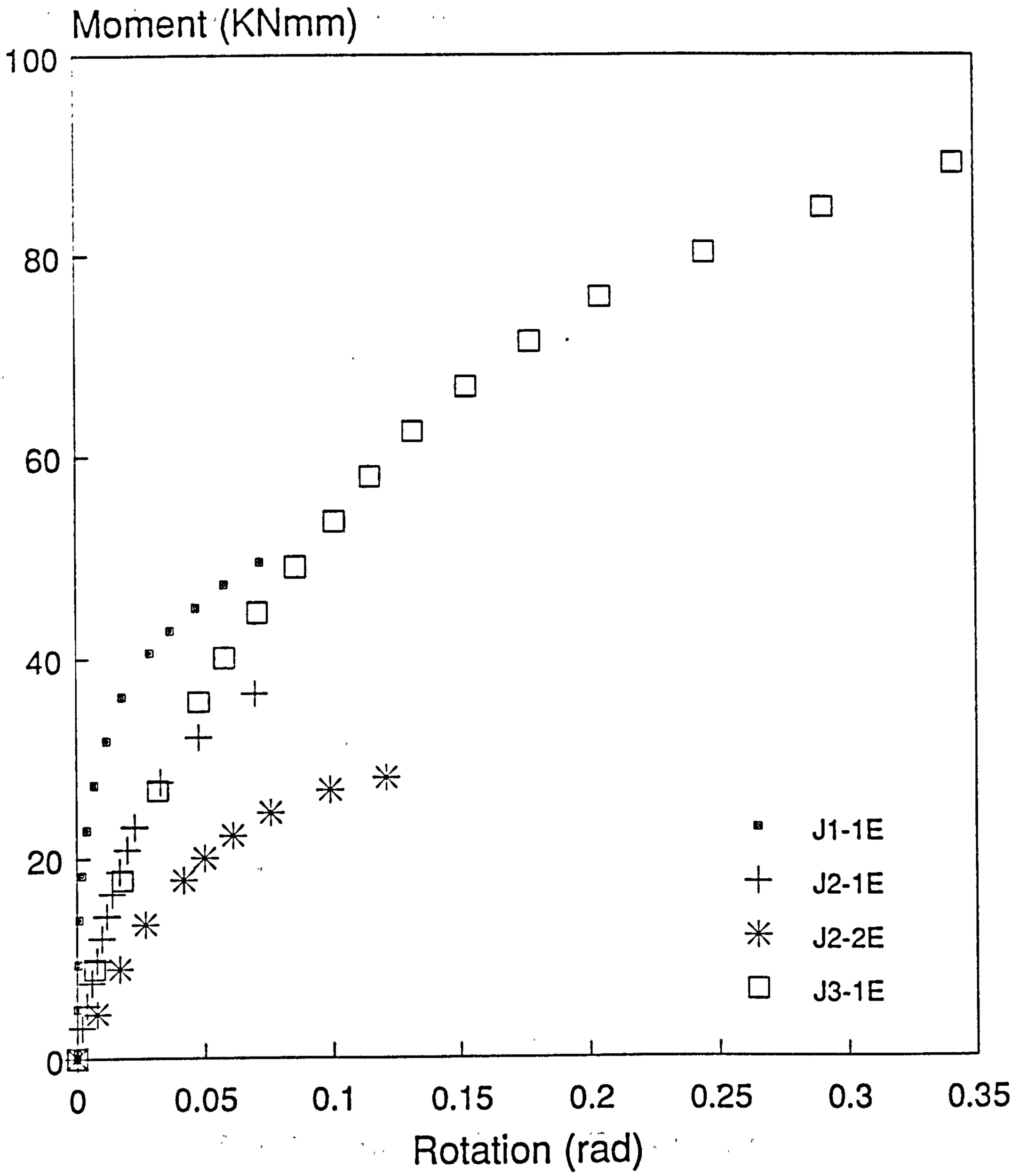

Fig. 8.2.28 Type "E" Connection (Tc=7mm)

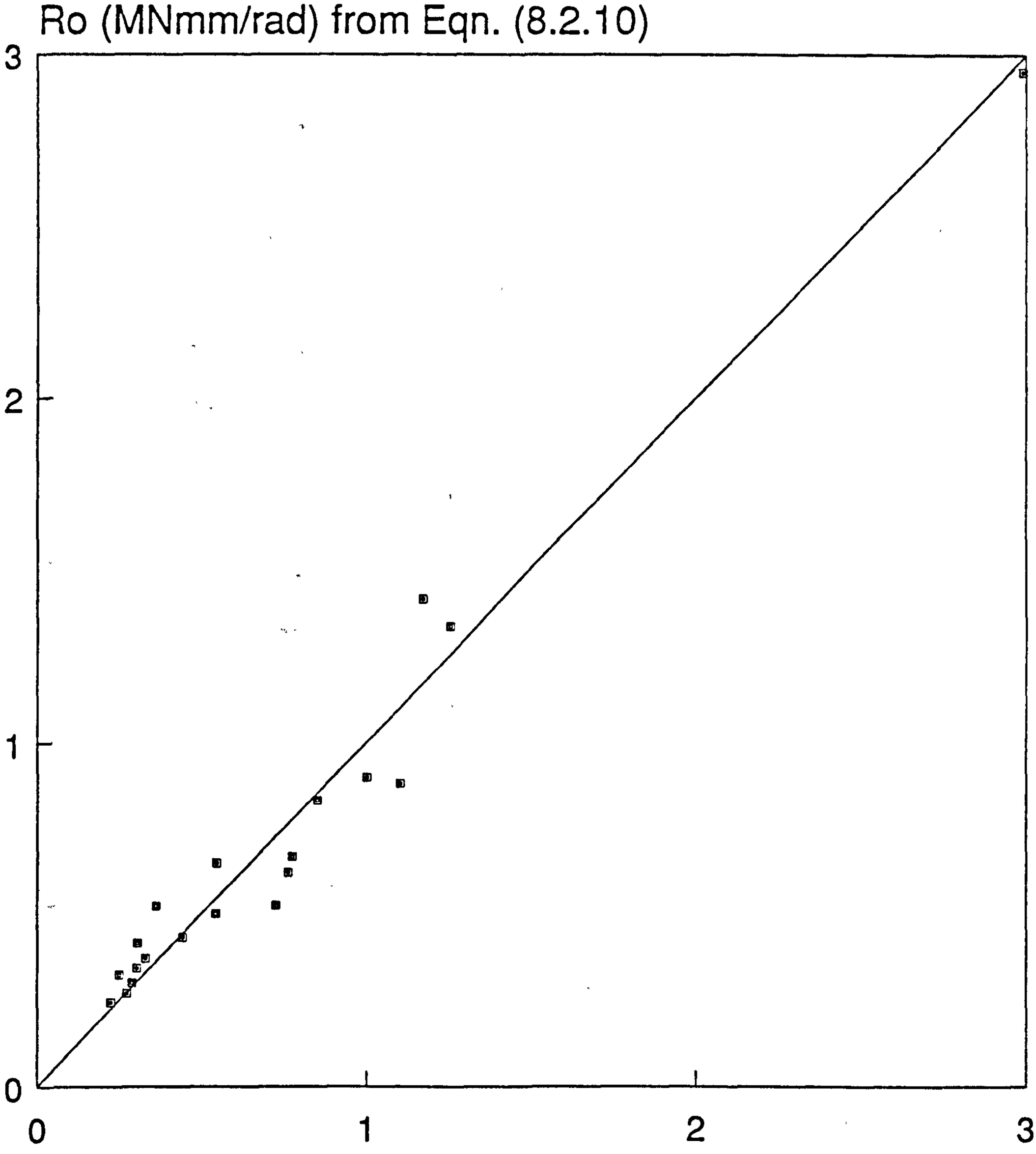

Fig. 8.2.29 Accuracy of Eqn. (8.2.10)

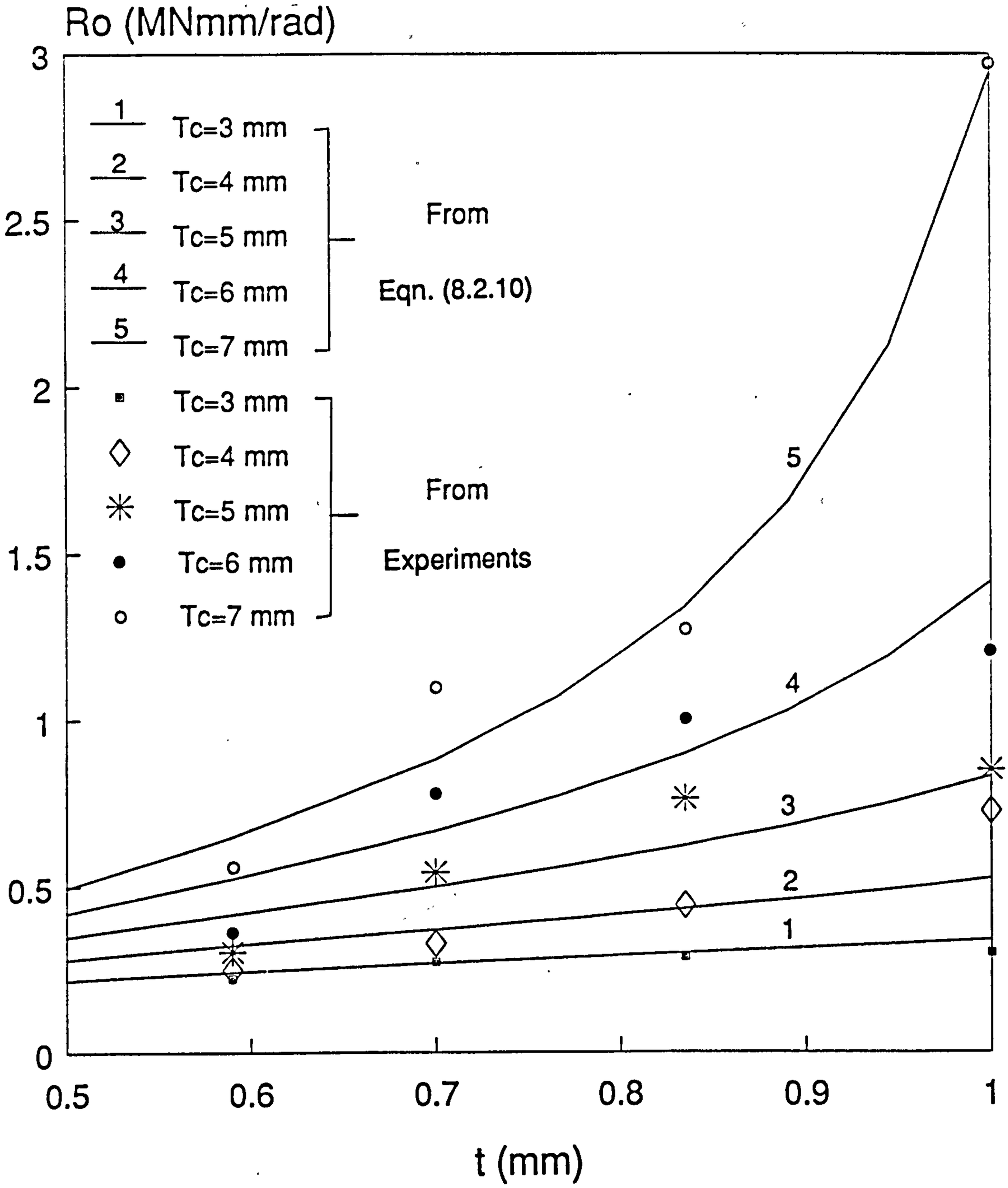

Fig. 8.2.30 Effects of Tc and t on Ro

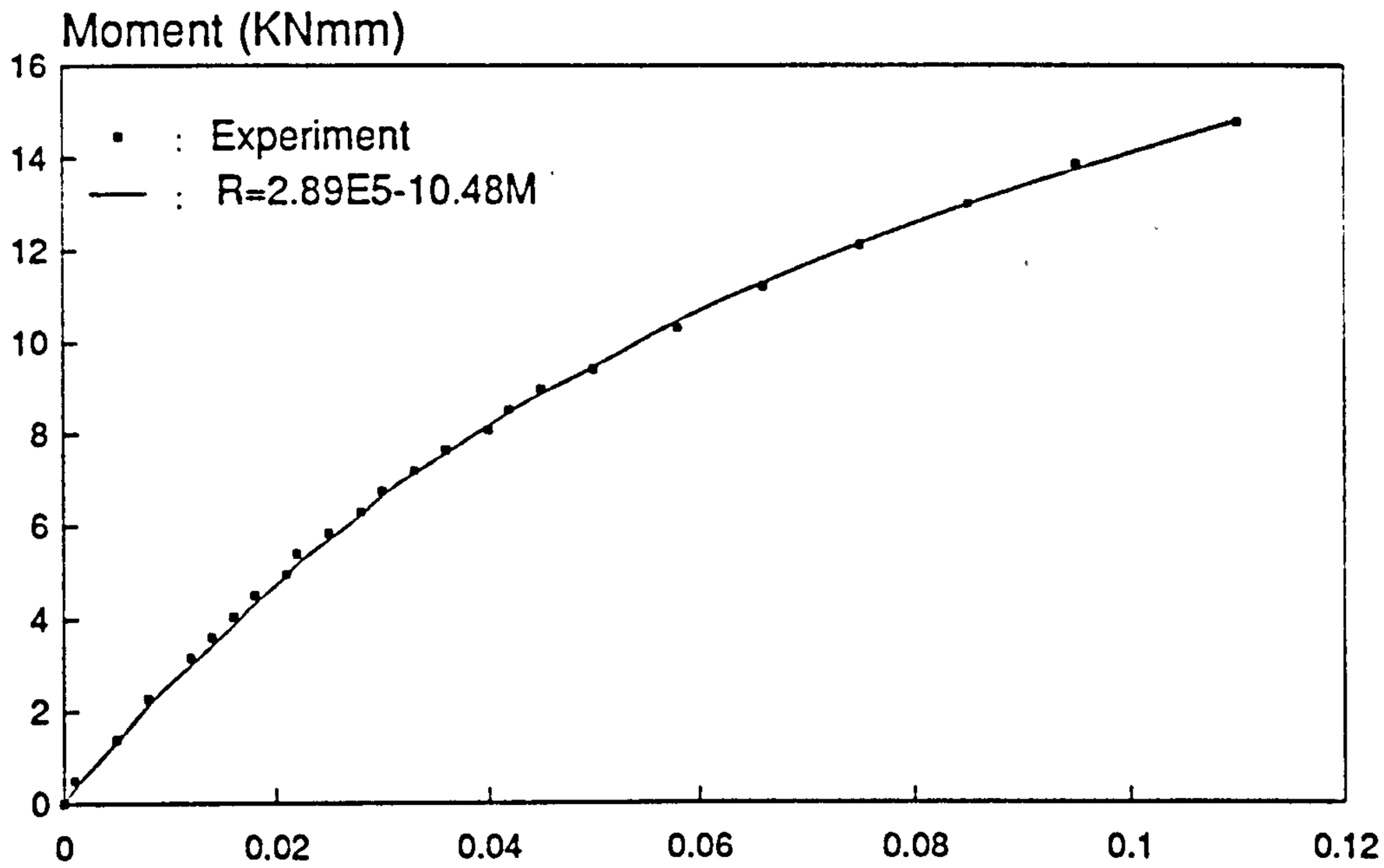

Fig.8.3.1 Connection J1-1A Moment/Rotation plot

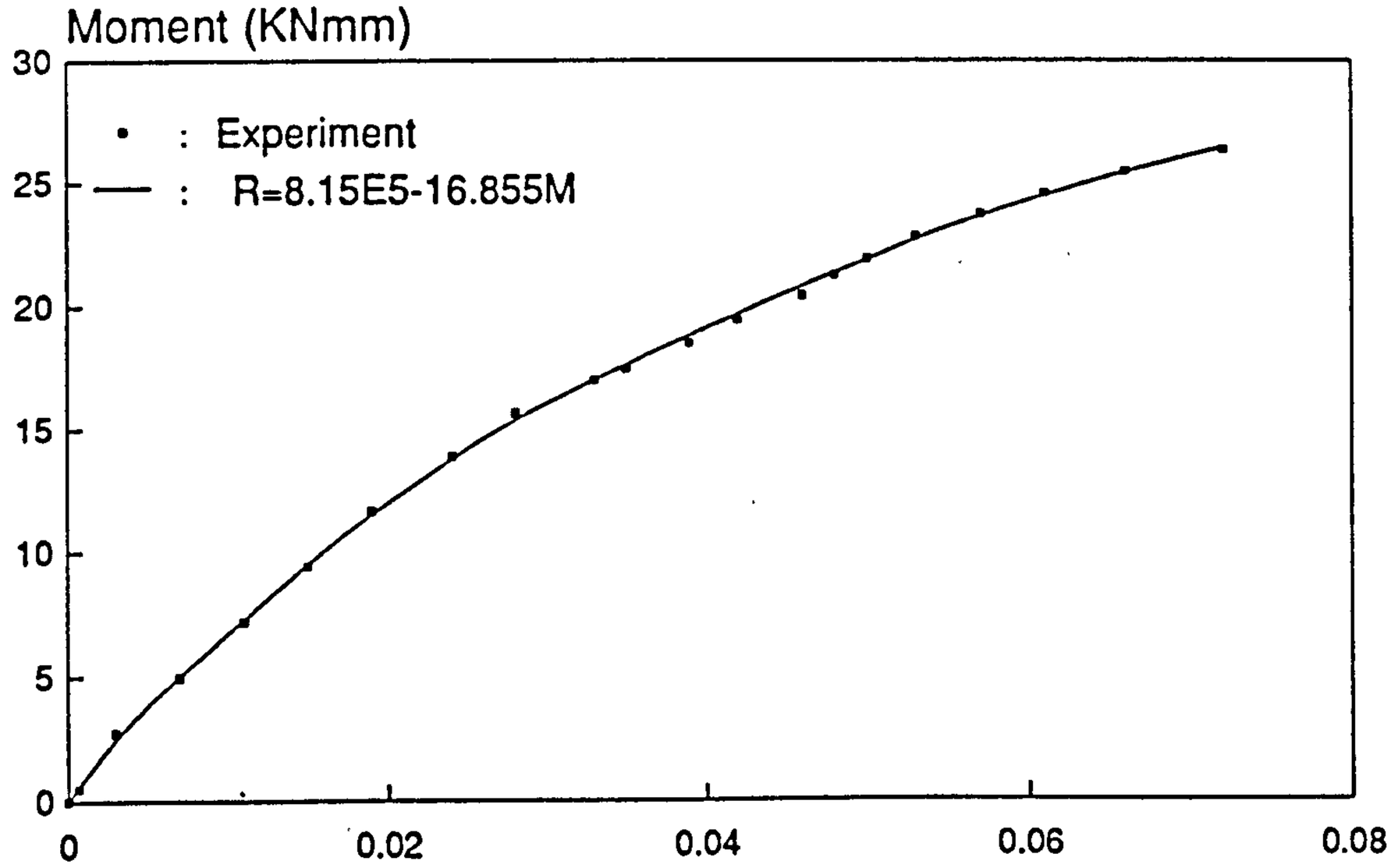

Fig.8.3.2 Connection J1-1B Moment/Rotation plot

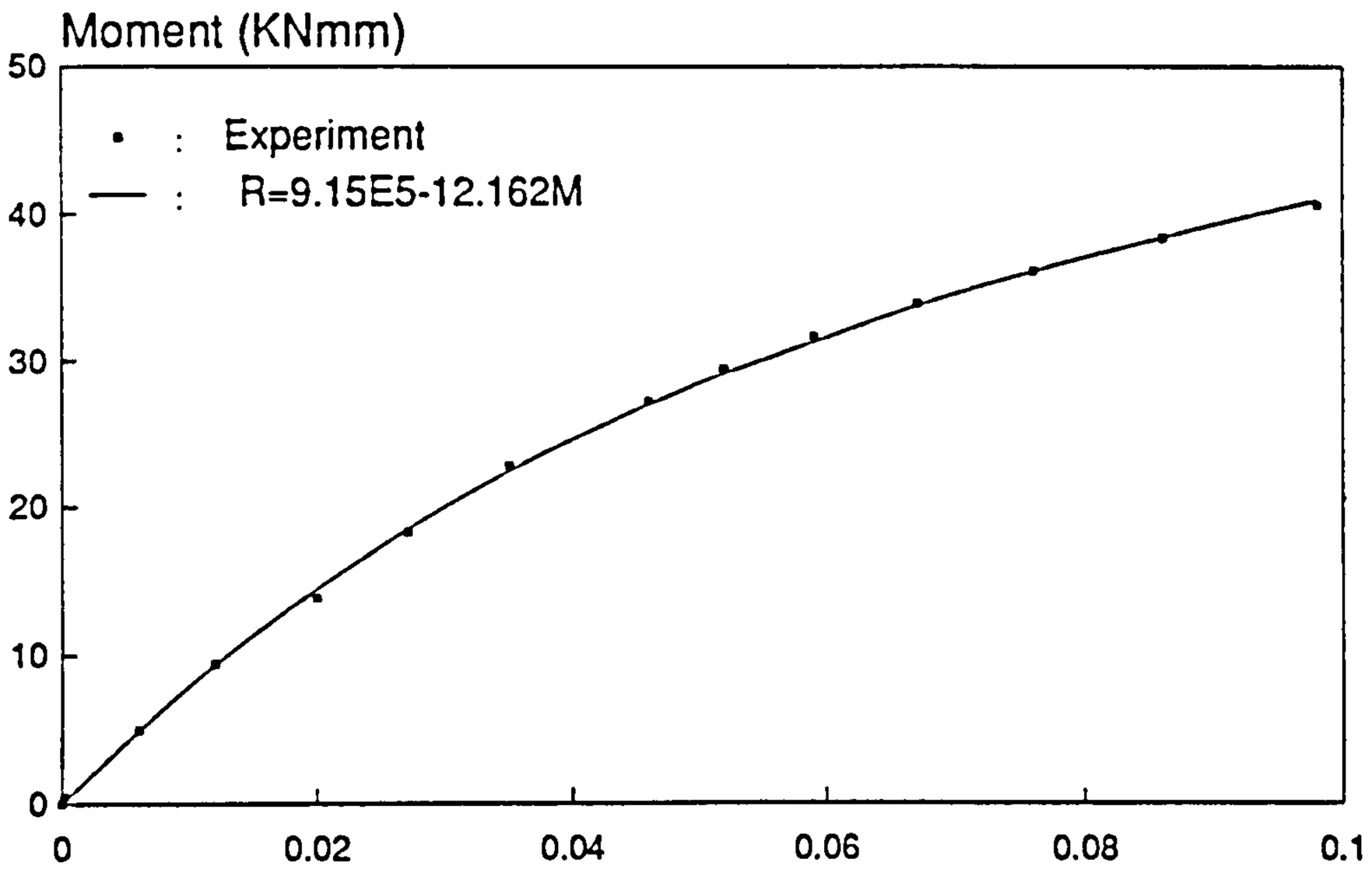

Fig.8.3.3 Connection J1-1C Moment/Rotation plot

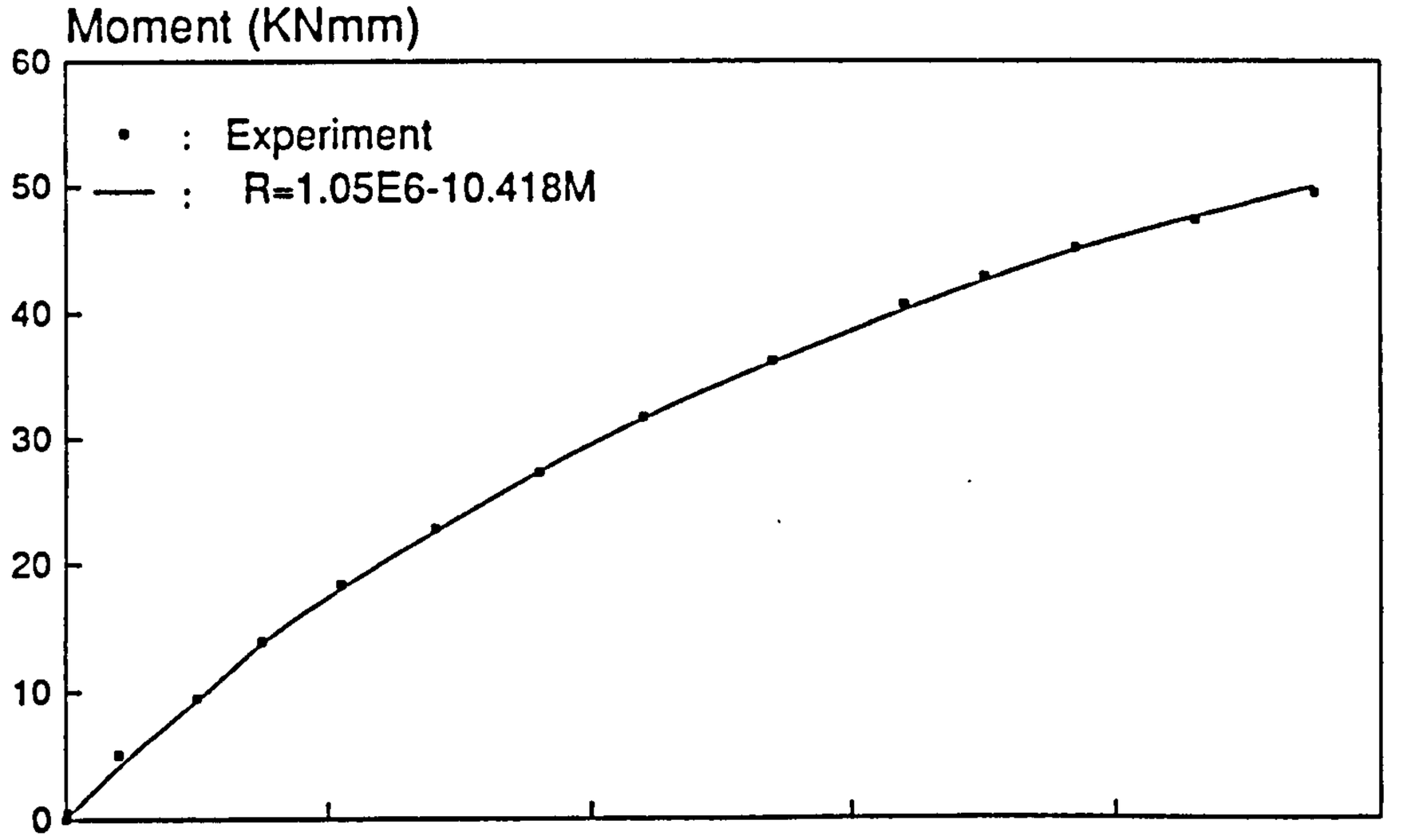

Fig.8.3.4 Connection J1-1D Moment/Rotation plot

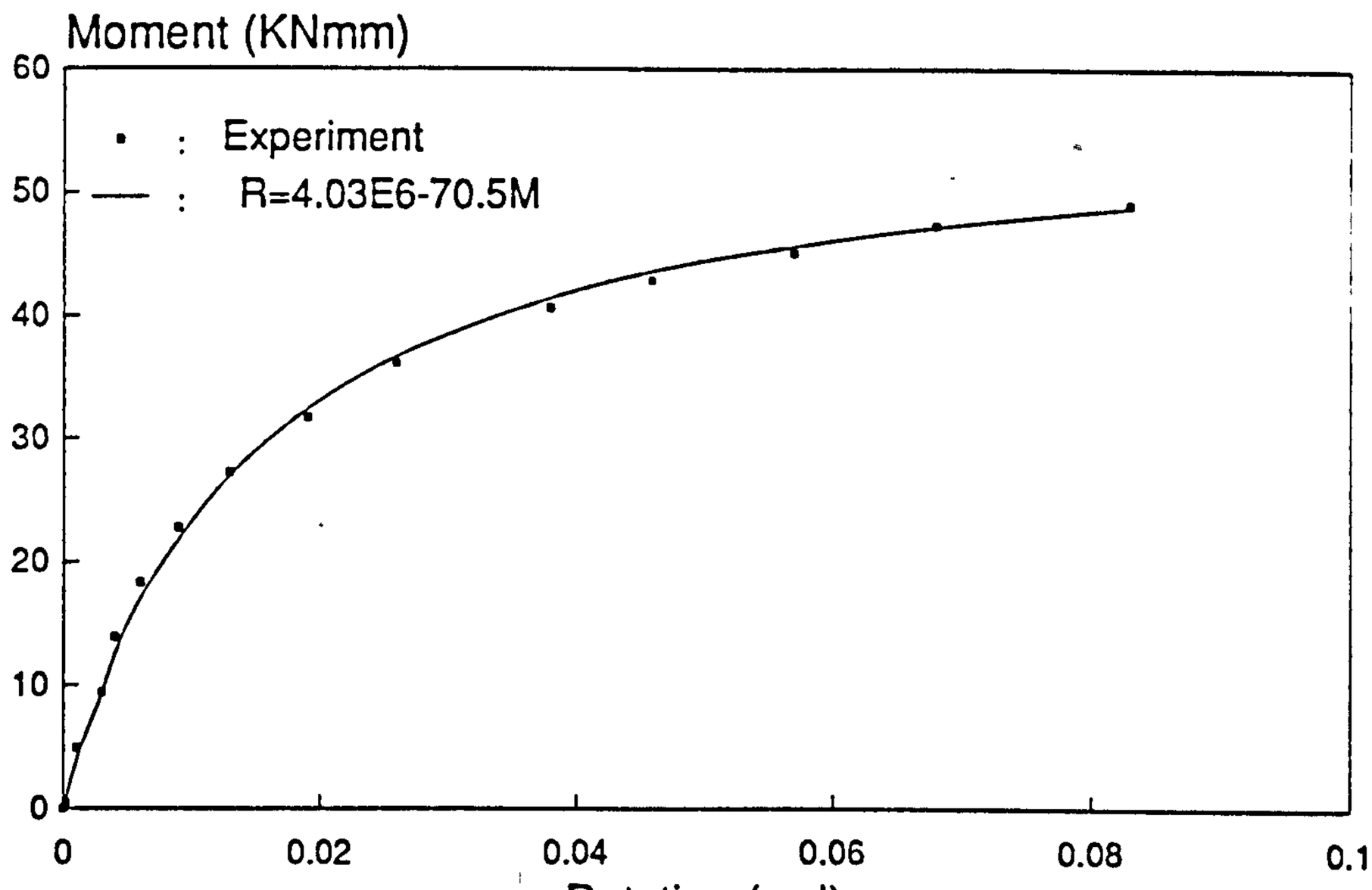

Fig.8.3.5 Connection J1-1E Moment/Rotation plot

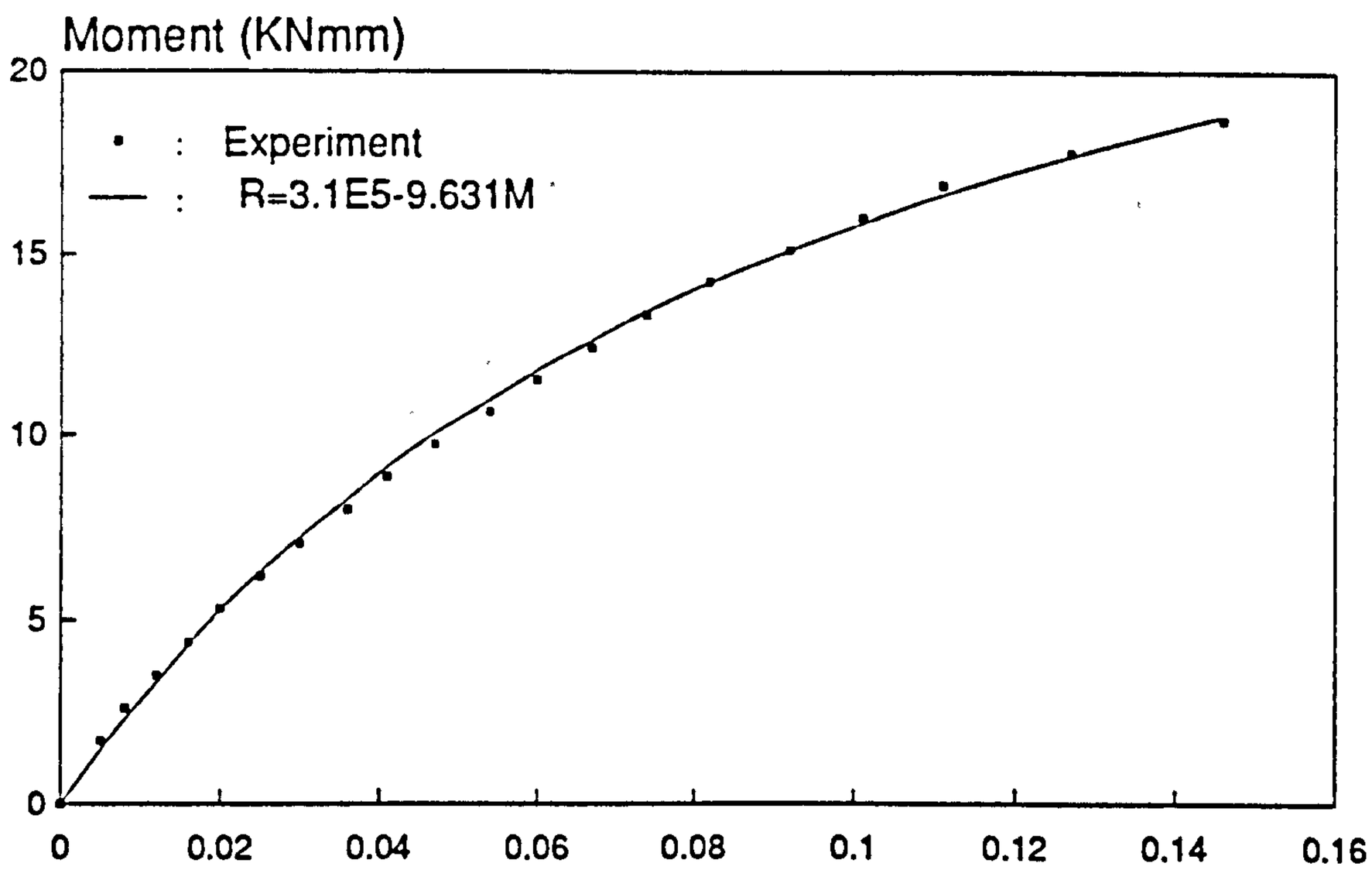

Fig.8.3.6 Connection J2-1A Moment/Rotation plot

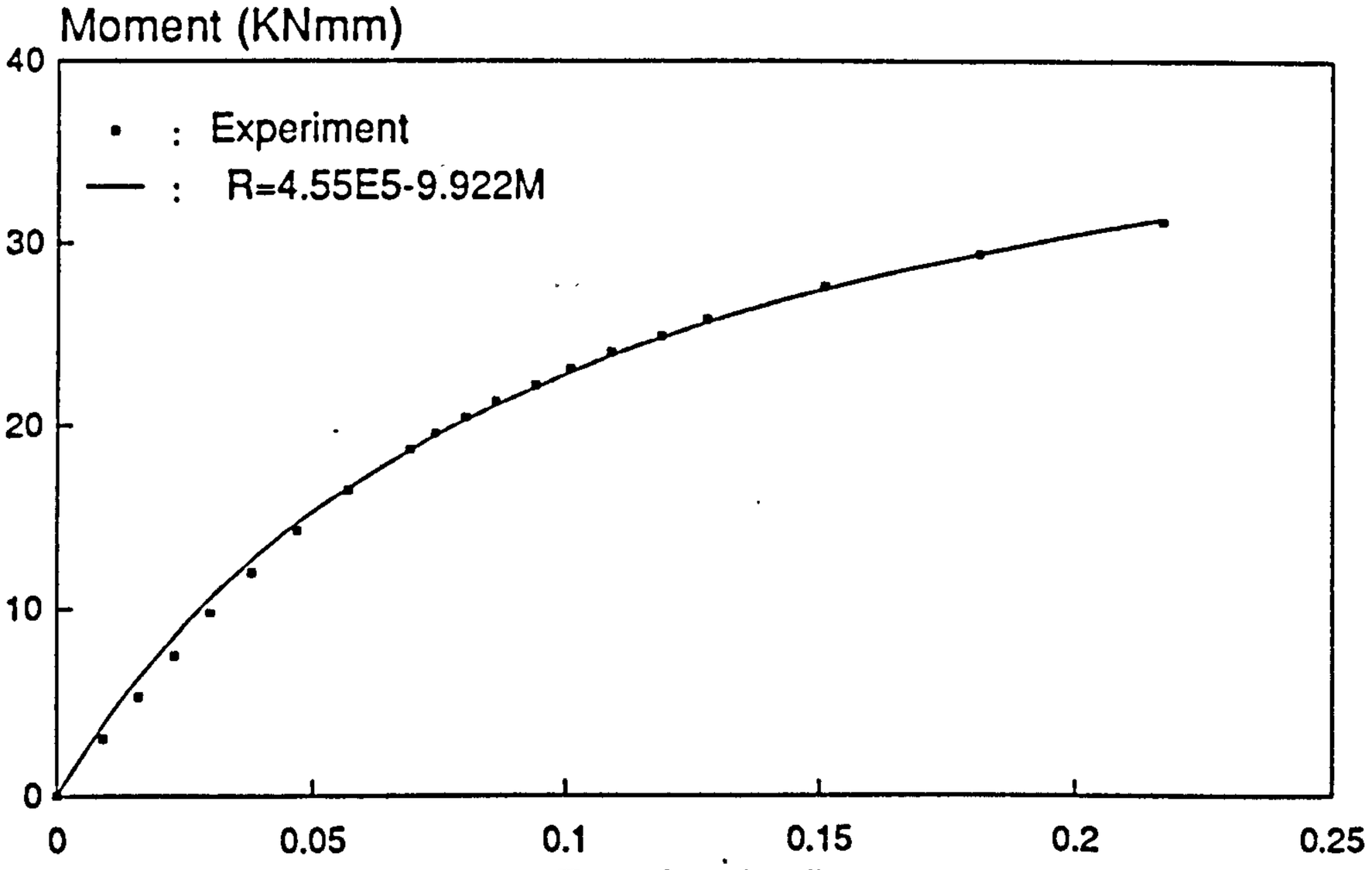

Fig.8.3.7 Connection J2-1B Moment/Rotation plot

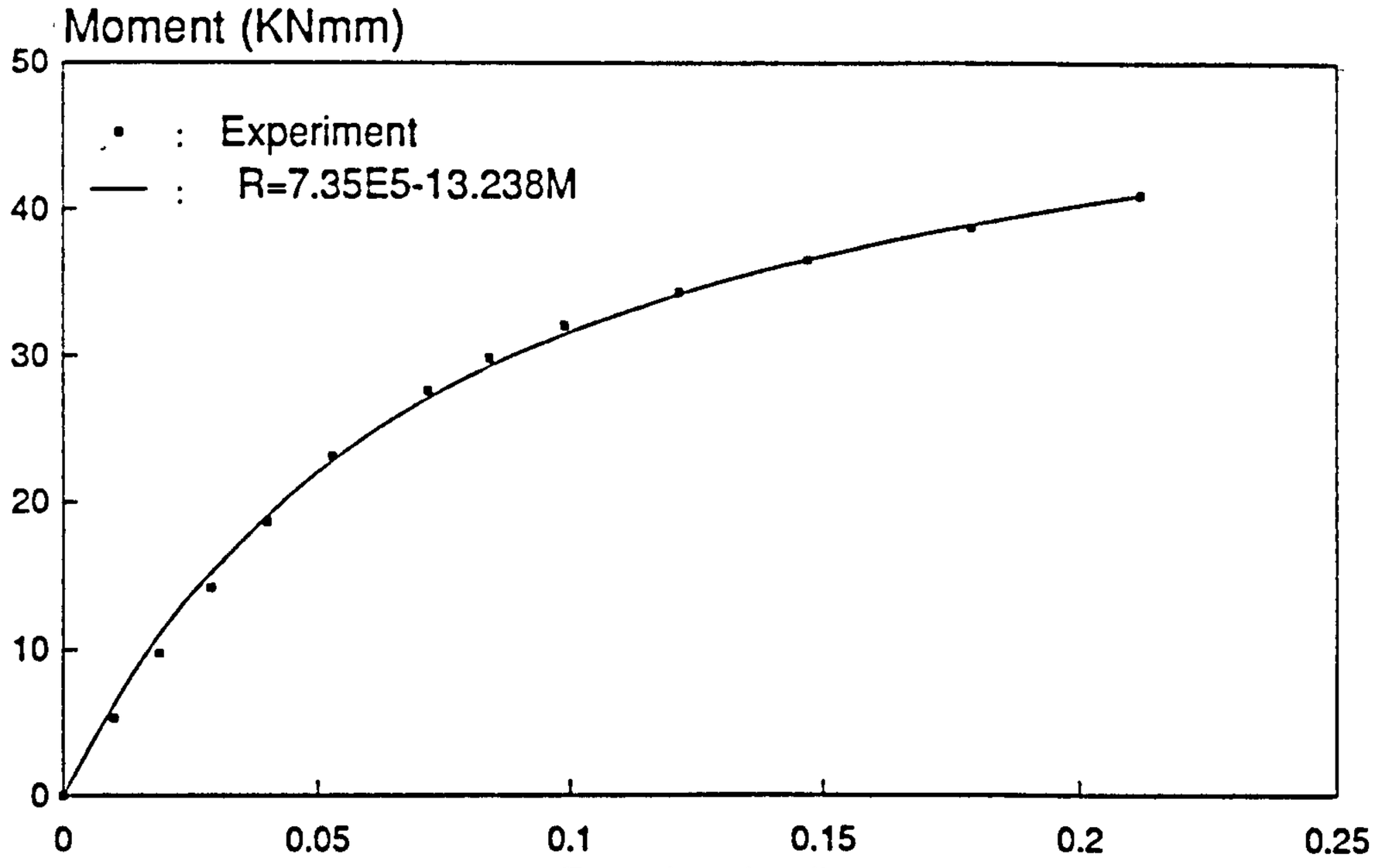

Fig.8.3.8 Connection J2-1C Moment/Rotation plot

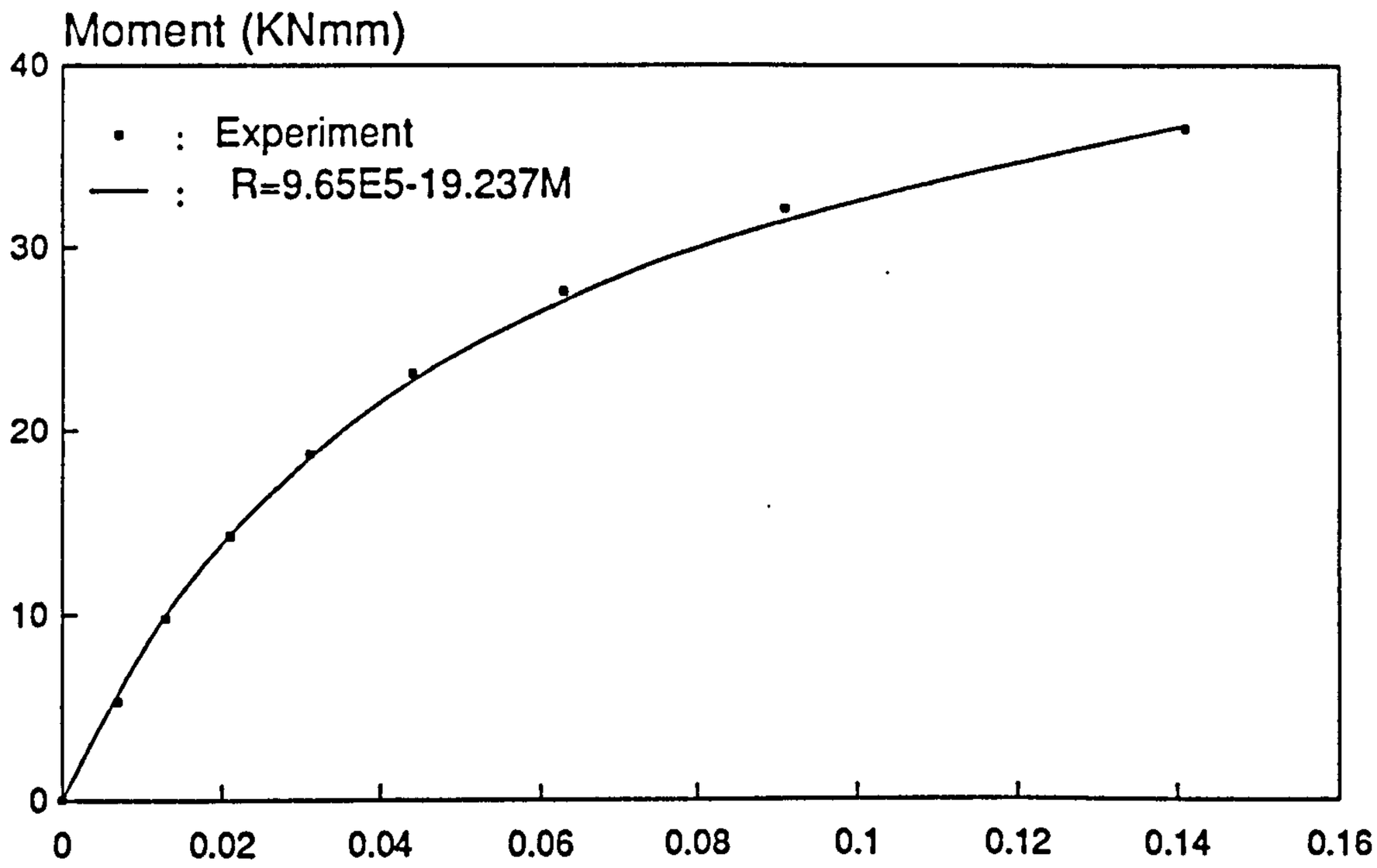

Fig.8.3.9 Connection J2-1D Moment/Rotation plot

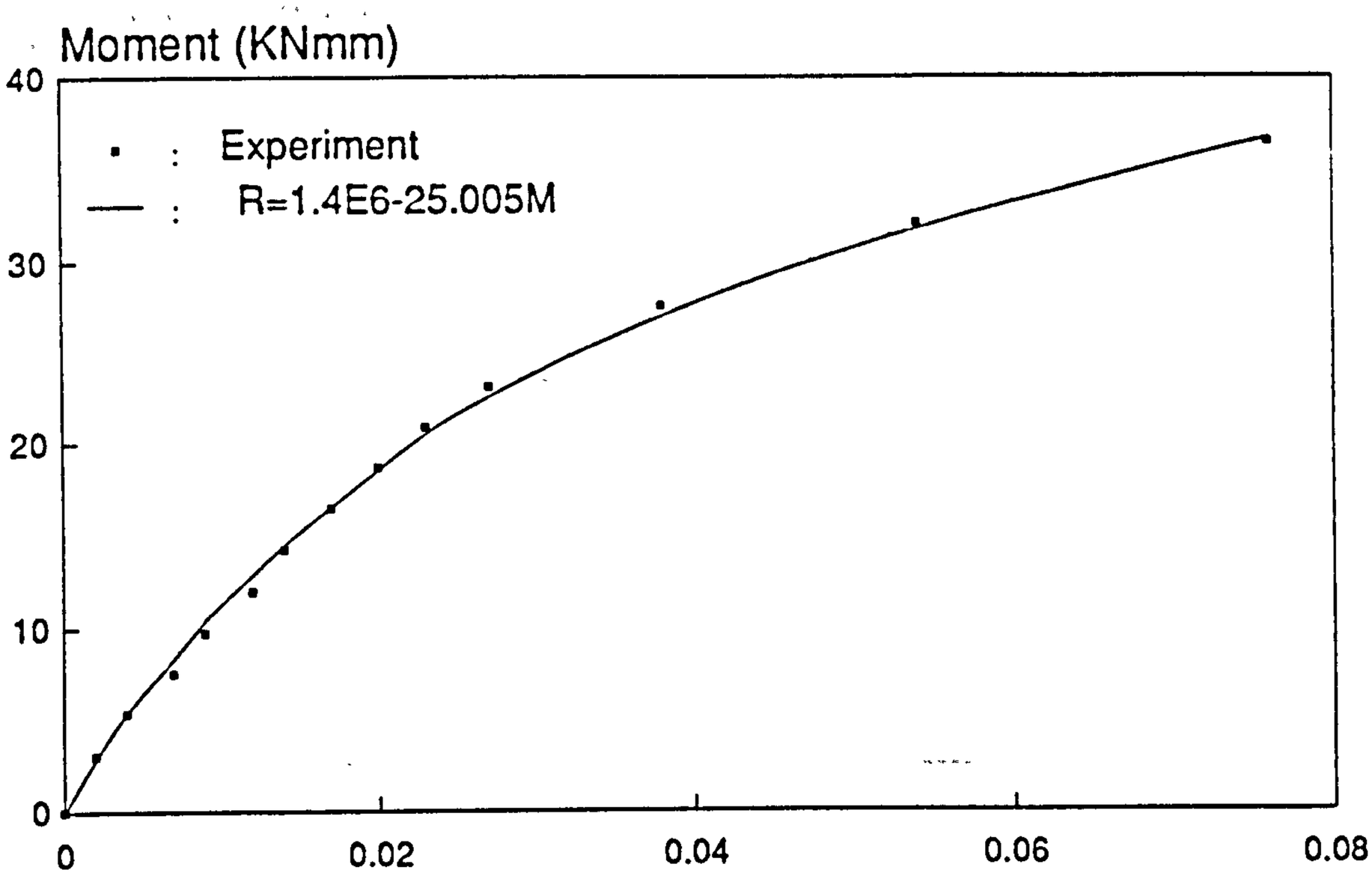

Fig.8.3.10 Connection J2-1E Moment/Rotation plot

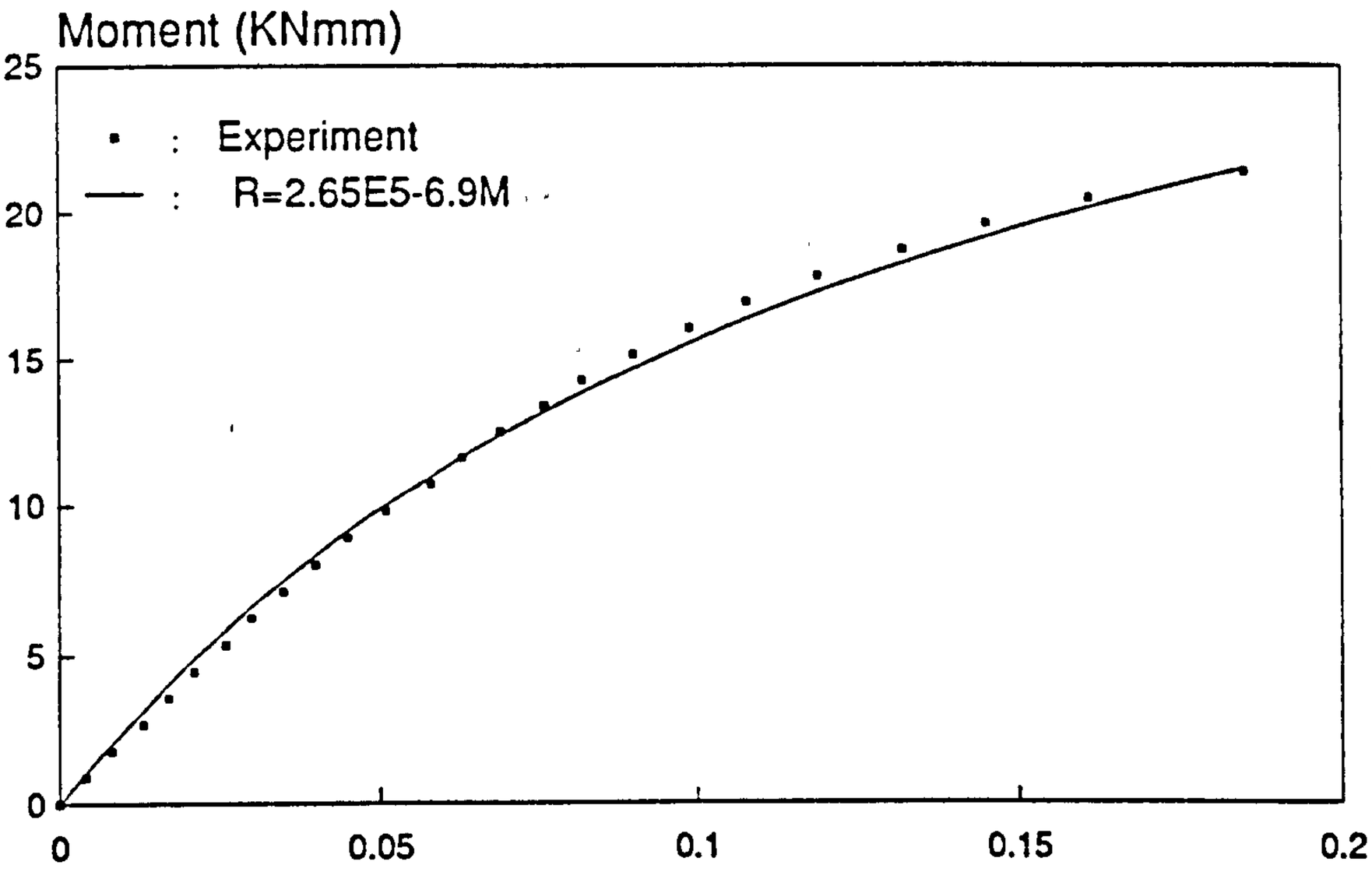

Fig.8.3.11 Connection J2-2A Moment/Rotation plot

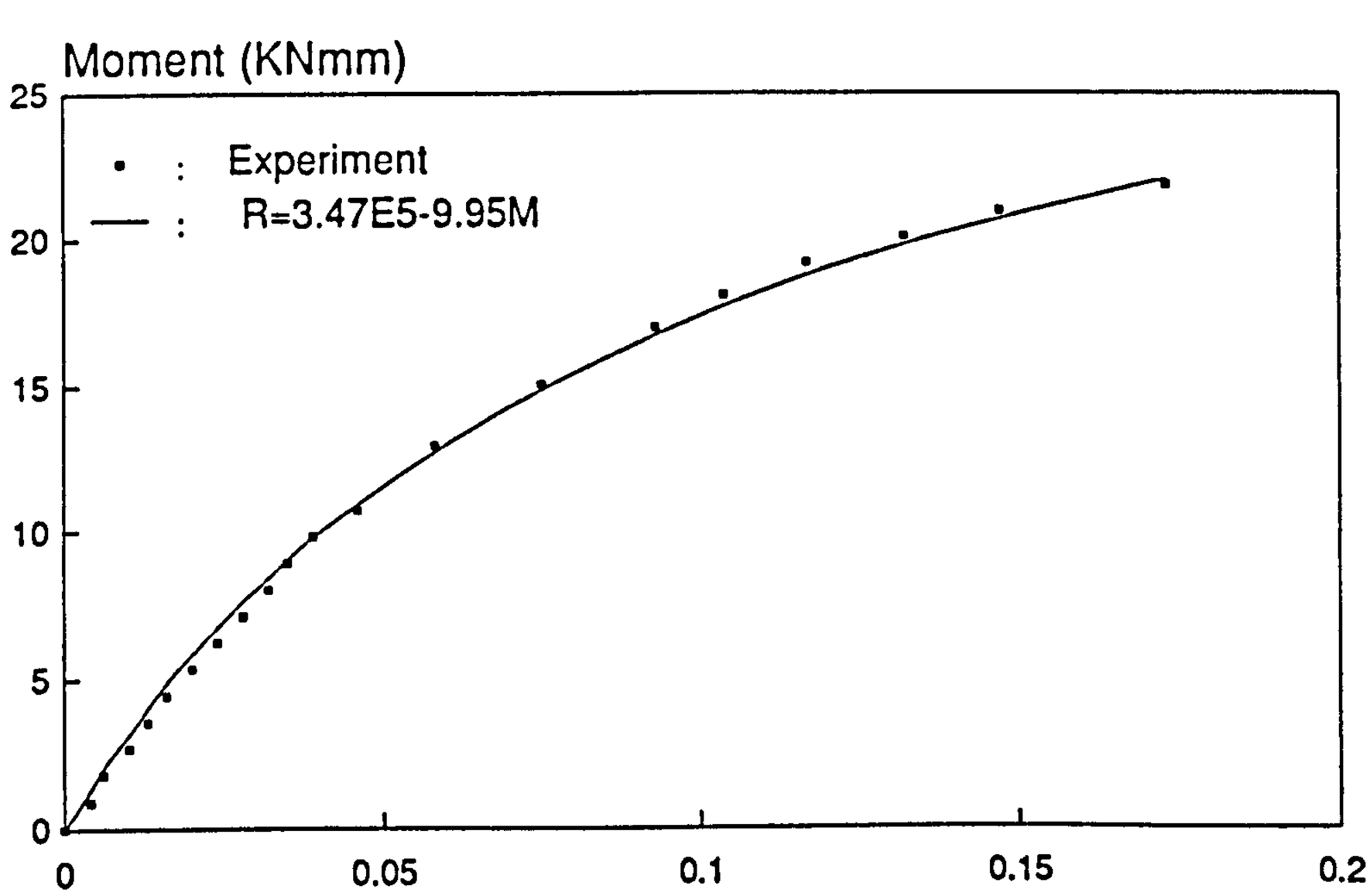

Fig.8.3.12 Connection J2-2B Moment/Rotation plot

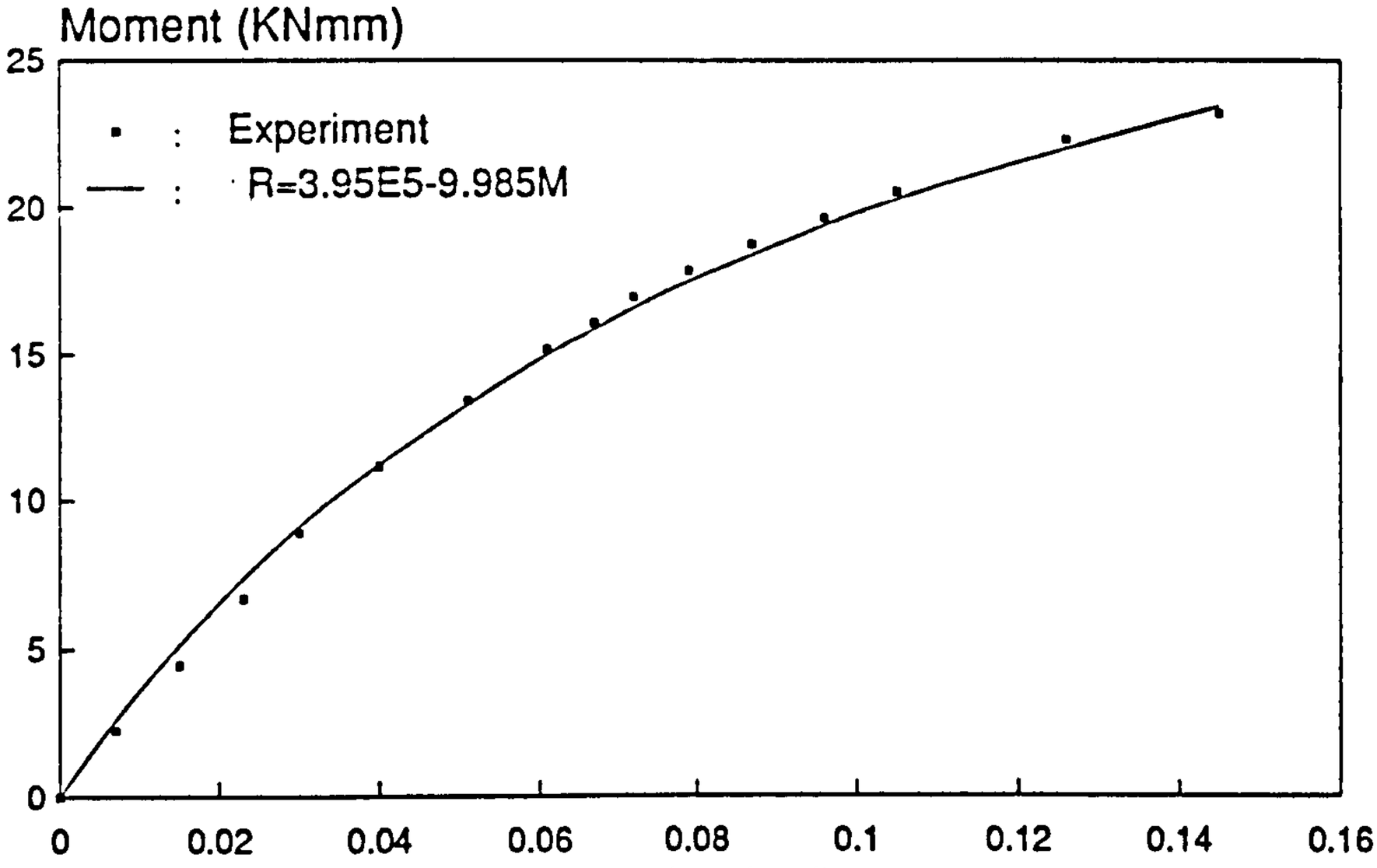

Fig.8.3.13 Connection J2-2C Moment/Rotation plot

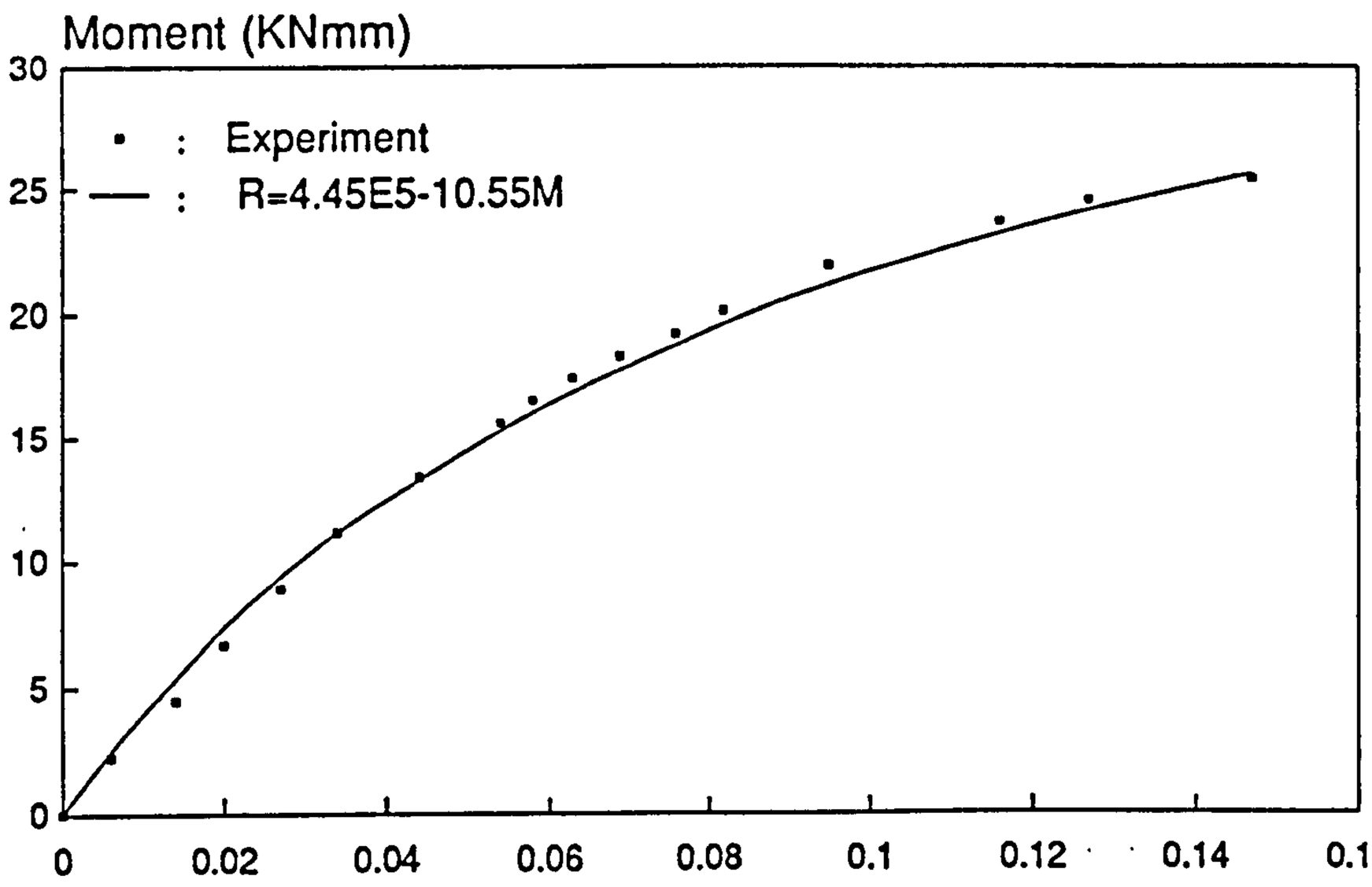

Fig.8.3.14 Connection J2-2D Moment/Rotation plot

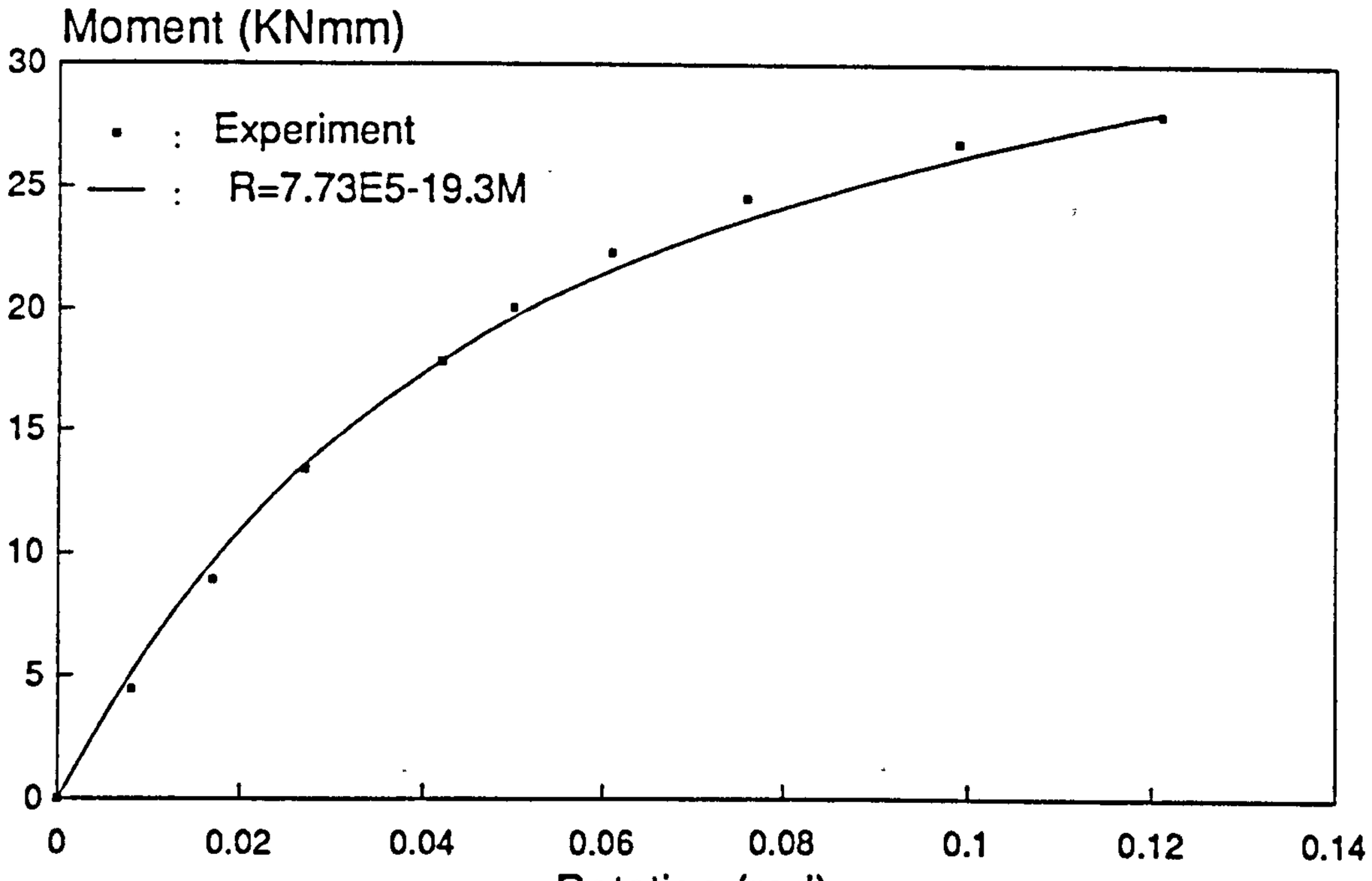

Fig.8.3.15 Connection J2-2E Moment/Rotation plot

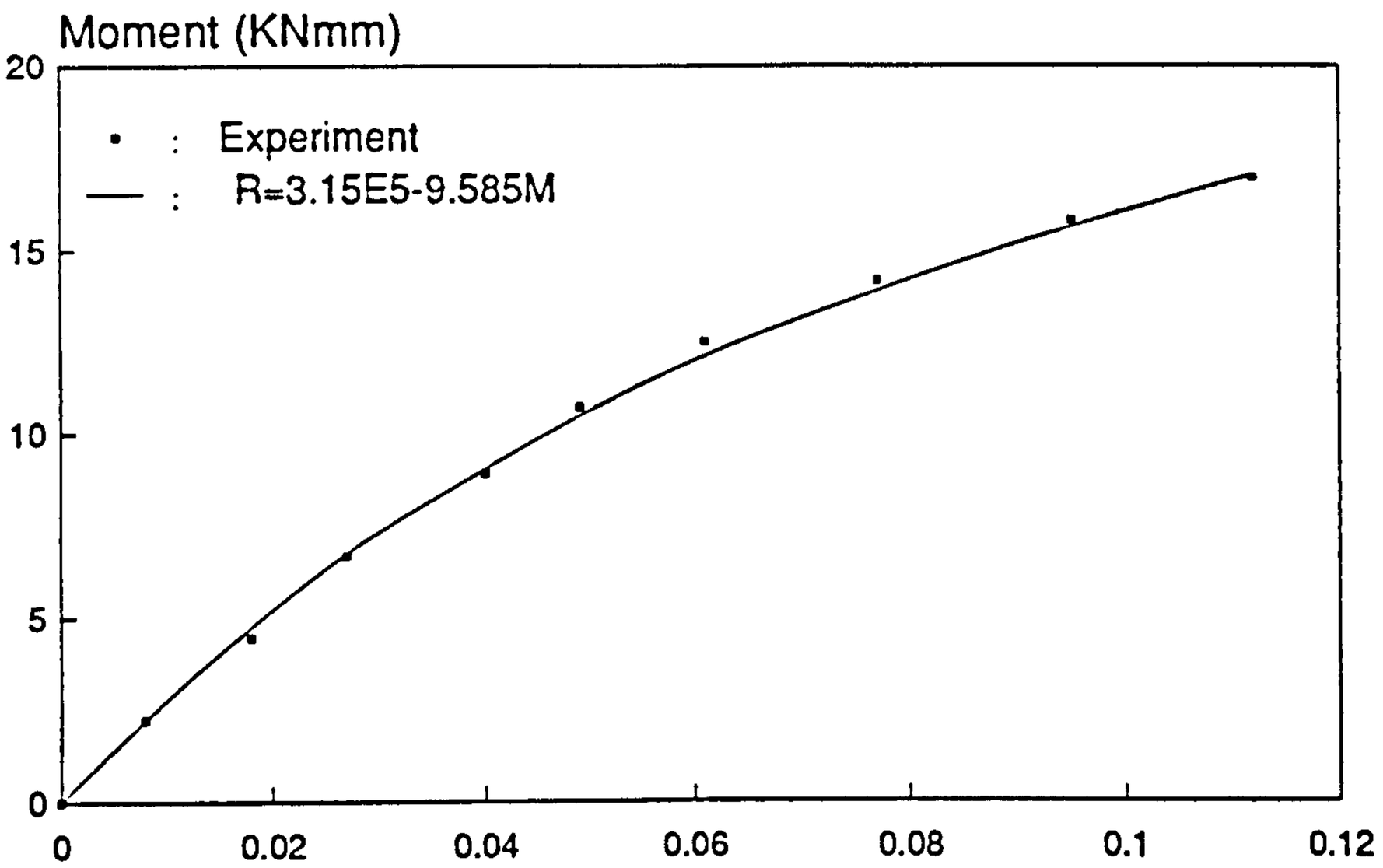

Fig.8.3.16 Connection J3-1A Moment/Rotation plot

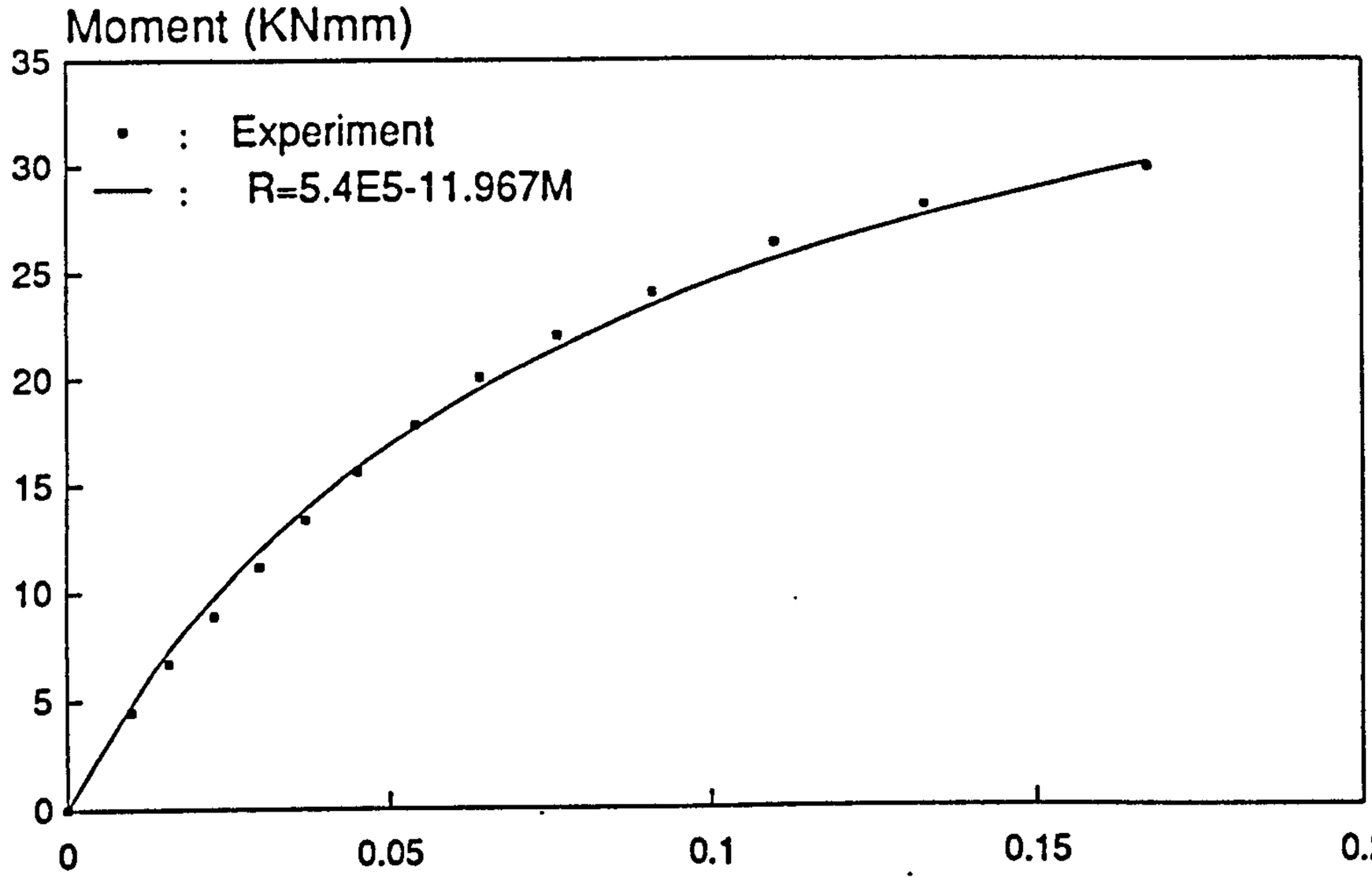

Fig.8.3.17 Connection J3-1B Moment/Rotation plot

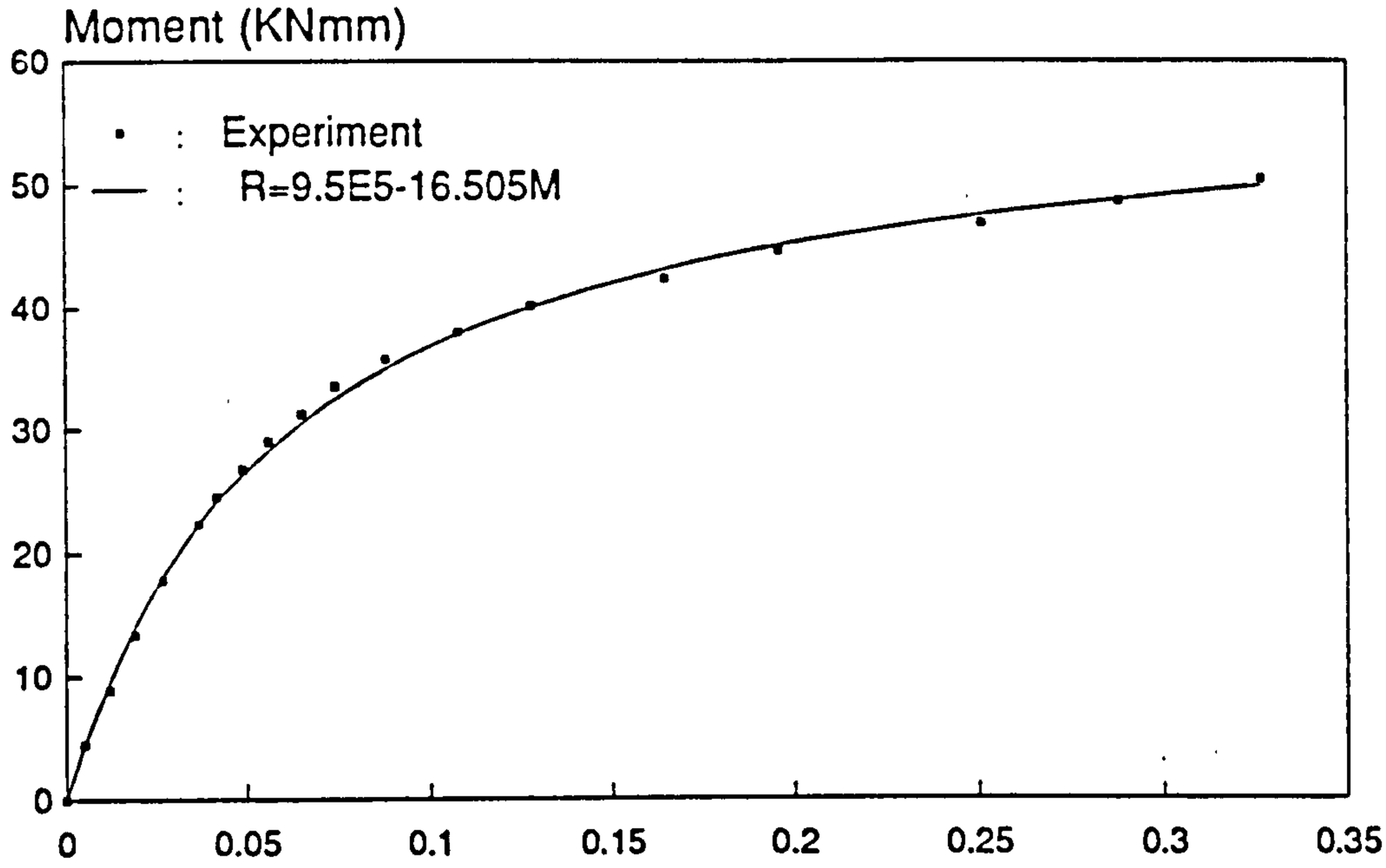

Fig.8.3.18 Connection J3-1C Moment/Rotation plot

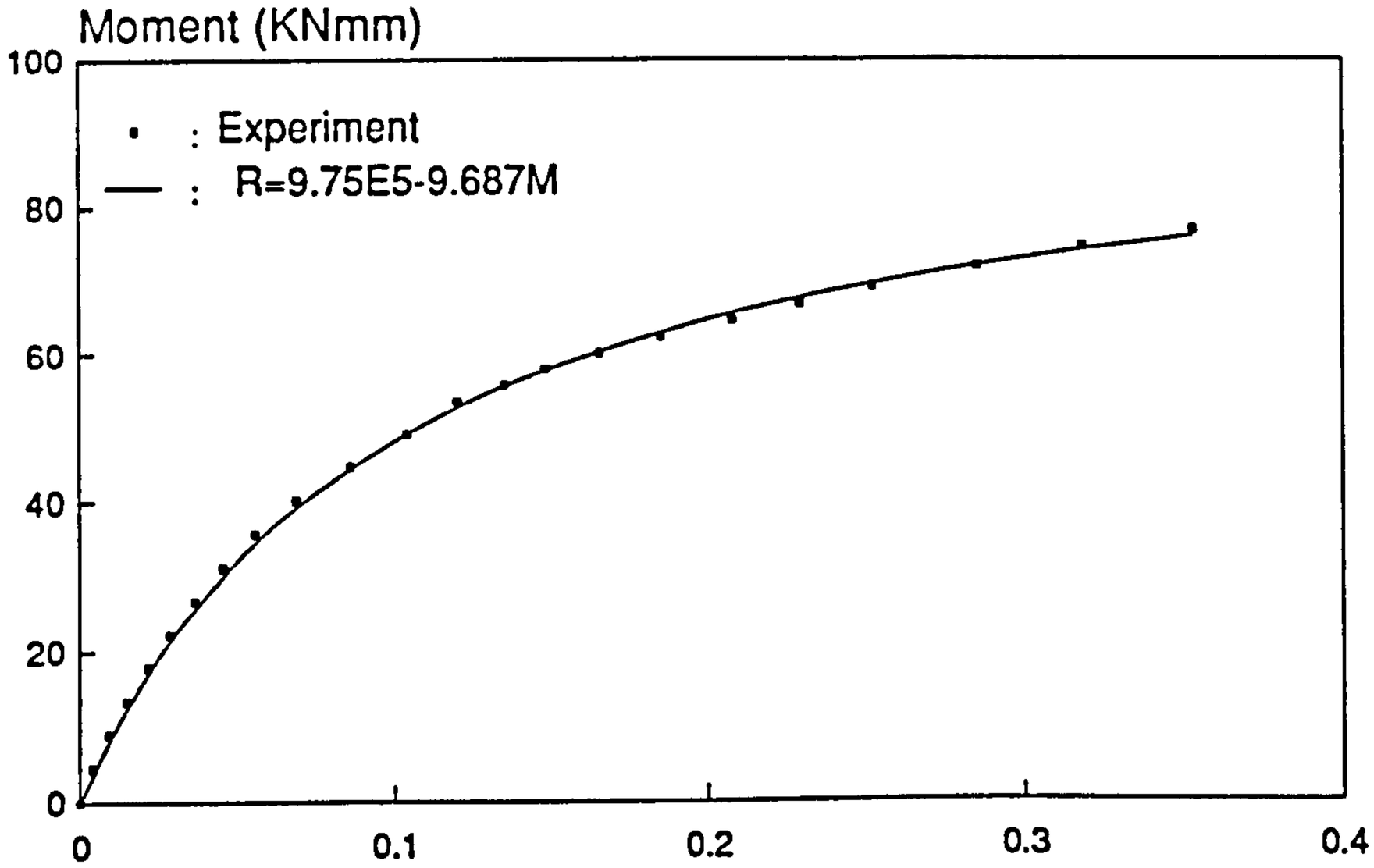

Fig.8.3.19 Connection J3-1D Moment/Rotation plot

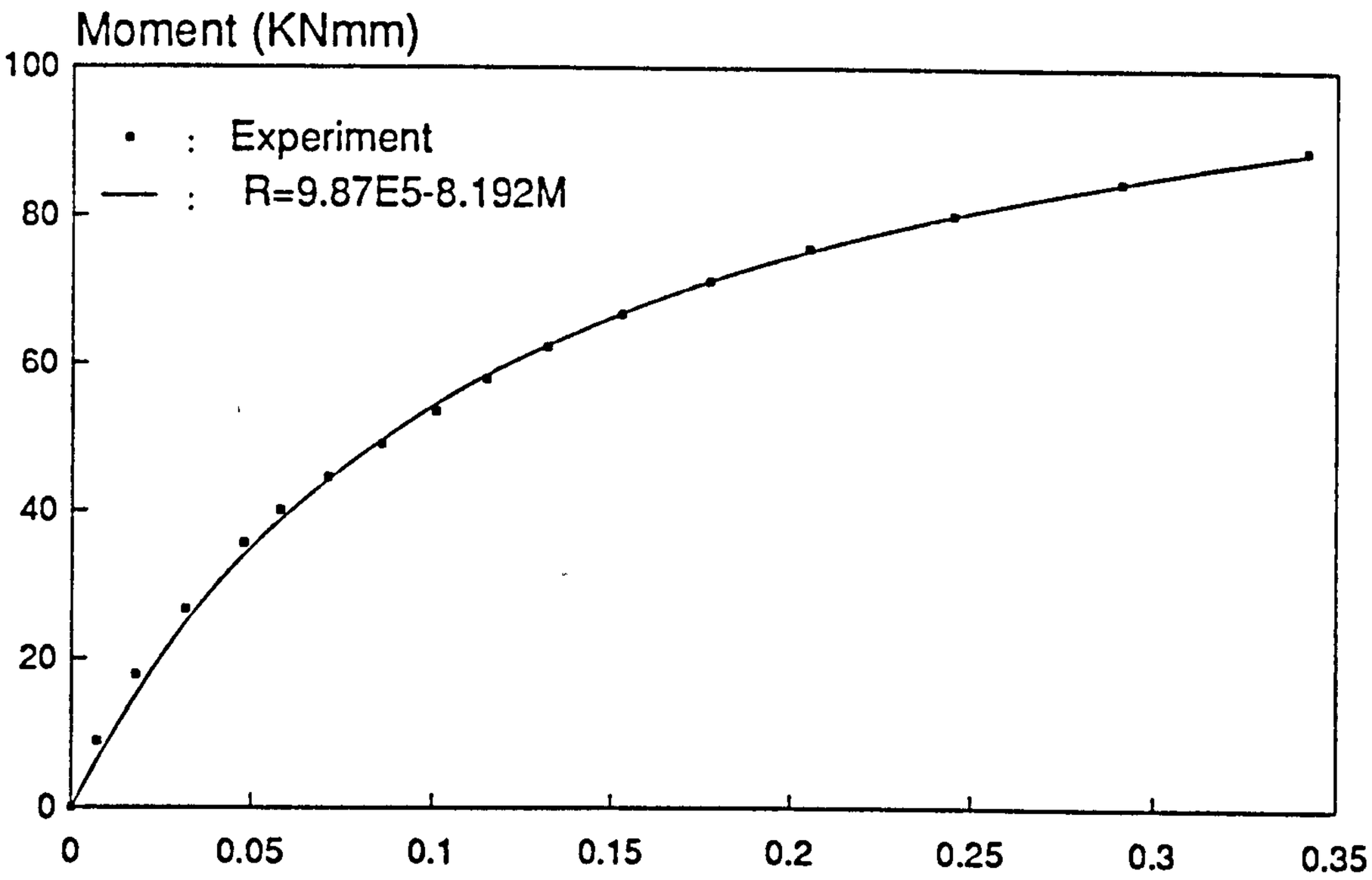

Fig.8.3.20 Connection J3-1E Moment/Rotation plot

Joint Model	T_c	Column b_1	Column b_2	Beam b_1	Beam b_2	t
J1-1A	3	29	14	27	14	1.000
J1-1B	4	29	14	27	14	1.000
J1-1C	5	29	14	27	14	1.000
J1-1D	6	29	14	27	14	1.000
J1-1E	7	29	14	27	14	1.000
J2-1A	3	27	15	25	15	0.700
J2-1B	4	27	15	25	15	0.700
J2-1C	5	27	15	25	15	0.700
J2-1D	6	27	15	25	15	0.700
J2-1E	7	27	15	25	15	0.700
J2-2A	3	28	15	25	15	0.590
J2-2B	4	28	15	25	15	0.590
J2-2C	5	28	15	25	15	0.590
J2-2D	6	28	15	25	15	0.590
J2-2E	7	28	15	25	15	0.590
J3-1A	3	27	25	25	25	0.835
J3-1B	4	27	25	25	25	0.835
J3-1C	5	27	25	25	25	0.835
J3-1D	6	27	25	25	25	0.835
J3-1E	7	27	25	25	25	0.835

All units in *mm*

Table 8.2.1 Connection and Connected Members Sectional Dimensions

Joint Model	T_c (*mm*)	Failure Mode	Distortion *
J1-1A	3	C	No
J1-1B	4	B+C	Yes
J1-1C	5	B+C	Yes
J1-1D	6	B	Yes
J1-1E	7	B	Yes
J2-1A	3	C	No
J2-1B	4	B+C	Yes
J2-1C	5	B	Yes
J2-1D	6	B	Yes
J2-1E	7	B	Yes
J2-2A	3	C	No
J2-2B	4	B+C	Yes
J2-2C	5	B	Yes
J2-2D	6	B	Yes
J2-2E	7	B	Yes
J3-1A	3	C	No
J3-1B	4	C	Yes
J3-1C	5	C	Yes
J3-1D	6	B+C	Yes
J3-1E	7	B	Yes

B : Beam failure as shown in Fig. 8.2.23

C : Connection failure as shown in Fig. 8.2.21

B+C : Combination of beam and connection failure.

* : Local distortion of unstiffened element of column as shown in Fig. 8.2.22

Table 8.2.2 Joint Model Test Failure Mode

Joint Model	T_c (mm)	R_0 ($\times 10^5 Nmm/rad$)	C (rad^{-1})
J1-1A	3	2.89	10.480
J1-1B	4	8.15	16.855
J1-1C	5	9.15	12.162
J1-1D	6	10.5	10.418
J1-1E	7	40.3	70.500
J2-1A	3	3.10	9.631
J2-1B	4	4.55	9.922
J2-1C	5	7.35	13.238
J2-1D	6	9.65	19.237
J2-1E	7	14.0	25.005
J2-2A	3	2.65	6.900
J2-2B	4	3.47	9.950
J2-2C	5	3.95	9.985
J2-2D	6	4.45	10.55
J2-2E	7	7.73	19.30
J3-1A	3	3.15	9.585
J3-1B	4	5.40	11.967
J3-1C	5	9.50	16.505
J3-1D	6	9.75	9.687
J3-1E	7	9.87	8.192

Table 8.3.1 Connection Modelling Parameters

CHAPTER 9

THEORETICAL ANALYSIS PROCEDURE

9.1 ELASTIC INSTABILITY ANALYSIS

The stiffness matrix method of analysis as discussed in Chapter 2 leads to an equation which relates the load, stiffness and resultant nodal displacements of a framework, i.e.,

$$\mathbf{P} = \mathbf{K}\ \mathbf{D} \qquad (2.5.1)$$

The above equation can be rewritten as

$$\mathbf{D} = \mathbf{K}^{-1}\ \mathbf{P} \qquad (9.1.1)$$

Providing **K** is non-singular, its inverse exists. Equation (9.1.1) can then be used to determine the framework nodal displacements. When the axial force is neglected or well below the Euler load, the element stiffness coefficients derived in Chapter 3 can be used to compute the element end forces or displacements.

In Chapter 4, it has been shown that the element stiffness matrices are dependent on the axial forces, which are in turn functions of the applied loads. Equation (2.5.1) can thus be rewritten as

$$\mathbf{P} = \mathbf{K}(\mathbf{P})\ \mathbf{D} \qquad (9.1.2)$$

Strictly speaking, the structure stiffness coefficients are also a function of the cross sectional area and second moment of area of the respective elements when local buckling is taken into account. However, since the computation of the effective cross section properties depends on the stresses, which in turn depend on the axial load, equation (9.1.2) may be written as it is, generally.

In order to obtain the critical load factor, λ_c , to cause elastic instability, equation (9.1.2) can be expressed in the form

$$\lambda \mathbf{P} = \mathbf{K}(\lambda \mathbf{P})\ \mathbf{D} \qquad (9.1.3)$$

The use of $\mathbf{K}(\lambda \mathbf{P})$ implies that $\mathbf{K}$ is a function of the applied load $\lambda \mathbf{P}$. Equation (9.1.3) is thus non-linear due to the axial load and local buckling of the members. Even if the latter is excluded in the analysis, the effect of the axial load alone will still result in equation (9.1.3) being non-linear.

To determine the elastic critical load factor, the problem is performed using a doubly iterative process as illustrated in figure 9.4.1. The value of λ is increased in a step-by-step manner and at each load level the singularity of $\mathbf{K}(\lambda \mathbf{P})$ is checked. At each load level, an inner iteration is performed to find the correct values of the various element axial forces and effective cross sectional properties, if local buckling is considered. Equation (9.1.3) is solved repeatedly until a consistent set of displacements is obtained. In this analysis, complete convergence is assumed to have been achieved when the proportionate change in the determinant of $\mathbf{K}(\lambda \mathbf{P})$ is less than 0.1%, which is rather reasonable in practice. As soon as a load factor for $\mathbf{K}(\lambda \mathbf{P})$ becomes singular, it is known that the critical load has been reached. The singularity of $\mathbf{K}(\lambda \mathbf{P})$ is equivalent to the structure stiffness being zero. The test used to detect singularity is to the determinant of the structure stiffness matrix, which should be positive until singularity when it becomes zero. In practice, exact singularity cannot be achieved and the sign of the determinant becomes negative, corresponding to a state of singularity.

9.2 COLLAPSE LOAD ANALYSIS

In the elastic instability analysis, it is assumed that the stresses in the members of the structure remain linearly elastic throughout the entire loading range and there is no yielding of the material. This method of analysis, although useful as a guide or reference, becomes increasingly less valid as the material of the members is

pushed past the limit of proportionality in the stress-strain curve. At actual collapse, large regions of the structure may be inelastic. Hence, a purely elastic analysis is insufficient.

In the collapse load analysis, it is assumed that the material of the members behaves in an elastic-perfectly-plastic manner so that plastic hinges can develop wherever the bending moment reaches the plastic moment capacity. It is further assumed that the hinge is concentrated to a point and spread of yielding is neglected.

The elastic analysis of the previous section is modified to cater for plastic effects as follows. Repeated analyses are performed at a series of gradually increasing load factors. At each load level, the plastic moment at the nodes of respective elements are calculated after convergence using the relevant plastic moment expressions derived in Chapter 6. If local buckling is considered, then the effective cross sectional properties are used. The nodal bending moments are then compared with the computed plastic moments of the respective elements in a systematic manner. When a bending moment is found to have reached the plastic moment level, a plastic hinge is formed. The individual element stiffness matrix involved is modified to maintain the moment at the hinge at a constant level, and to allow continuous rotation, and the loading is increased again. Hence, the development of hinges is traced with increasing load. At each stage, the singularity of the structure stiffness is checked, until eventually, singularity is reached.

In the check for the formation of plastic hinges, a tolerance of ±5% is given. This means that a hinge will develop when

$$0.95M_p \le M \le 1.05M_p \qquad (9.1.4)$$

The reason behind this is because of the difficulty in achieving a condition whereby the bending moment is exactly equal to the plastic moment. At times, even a very small increase in load leads to a substantial increase in the bending moment.

9.3 NOTES ON ANALYSIS

9.3.1 SNAGS

In using the sign of the determinant to check for the critical load, the following points need to be observed.

1) If the determinant of the stiffness matrix $\mathbf{K}(\lambda \mathbf{P})$ of order $n \times n$ is expanded, a polynomial of the nth order in $\lambda \mathbf{P}$ is obtained. There are, therefore, n possible values of $\lambda \mathbf{P}$ for which $\mathbf{K}(\lambda \mathbf{P})$ is singular. In general, only the smallest value of λ_c is of interest but there may be other values close by as illustrated in figure 9.3.1.If the initial value of λ used is too near the first critical value, or the increment used is too large, there is a danger that the lowest λ_c will be missed altogether. From figure 9.3.1, it can be seen that the third smallest value of λ_c might be picked up as the smallest (point T). There seems no way of predicting in advance the form of the curve. The only safe solution is to keep the initial value of λ low and the increment small.

2) The determinant of a matrix is particularly sensitive to the magnitude of the terms of the matrix. For instance, an alteration in the magnitude of the terms by a factor of 100 (by a change of units used for instance) would alter the determinant by a factor of 100^n for a n by n matrix. This could well take the determinant outside the range of positive numbers which a computer can hold. To remove this difficulty, scaling of the matrix is carried out and this is discussed in detail in Appendix I.

3) As equation (9.3.1) approaches singularity, it becomes increasingly ill-conditioned and convergence is extremely difficult. A counter is used to check the number of iterations and when a preset value is exceeded, the critical load is assumed to have been reached. The error evolved will be small and acceptable in engineering practice.

9.3.2 FRAME ELEMENT CONFIGURATION

In the theoretical analysis of the framework , the members of the framework are modelled using elements. The various framework element configuration for the double and single storey frameworks are shown in figures 9.3.2 and 9.3.3 respectively. From figures 9.3.2a and 9.3.3a, the frameworks are modelled using the minimum or basic number of elements. For these frameworks, the initial imperfections are accounted for by using the expressions derived in Chapter 7. For frameworks where the number of elements are greater than the basic number of elements, for instance 14 or 18 elements as illustrated in figures 9.3.2b and 9.3.2c respectively, initial imperfections are accounted for directly by using the actual framework geometry during analysis.

Although increasing the number of elements increases the computation time, an advantage to be gained is that the results obtained will be more accurate when local buckling is considered in the analysis. As the moments at the ends of a beam-column element are normally not uniform, the element end stresses, which are used to calculate the effective widths using the effective width concept, are also not uniform. This will result in a non-prismatic element if the effective width concept is followed strictly. However, as mentioned in Chapter 5, the largest of the compressive stress is used to compute the effective width. This will lead to a smaller effective width as illustrated in figure 9.3.4b. On the other hand, the use of more elements will

induce less errors. This is illustrated in figure 9.3.4a, where three elements are used. Hence, by increasing the number of elements, a closer representation of the actual effective element can be achieved

9.4 DESCRIPTION OF COMPUTER FLOW CHART

The theoretical analysis was written into a computer programme, the flow chart of which is shown in figure 9.4.1. Listed below is a step-by-step description of the flow chart.

1) There is an option of performing an elastic critical load analysis or collapse load analysis.

2) The data input consists of the following :

   a) Number of nodes.

   b) Number of elements.

   c) Nodal coordinates.

   d) Element material properties, element section geometry, element number and nodal designations.

   e) Boundary conditions.

   f) Initial applied loads.

   g) Connection theoretical model constants.

   h) Initial load factor (LF), the increment to be applied to it (INC) and the accuracy in the final results (ACC).

   i) Amplitude of initial imperfections (only when the basic number of elements are used)

3) The analysis can be performed with or without local buckling. For the former, either the first or second approximation method can be used.

4) N is used to count the number of loading cycles. The axial forces in the elements are generally unknown before the analysis begins and are all assumed to be zero. Initial guesses might be read in as input data but this is unlikely to reduce the computing time.

5) The loading cycle is increased by one. As the axial forces at each load level are initially only known approximately, a number of solutions, counted by I, are performed.

6) Individual element stiffness matrix in the structure axes system is formed. The stiffness coefficients are calculated using the current effective geometry (if local buckling is considered), connection stiffness and the axial forces of the respective elements

7) The element stiffness matrices are assembled to form the overall stiffness of the structure.

8) The determinant, DET2, of the reduced structure stiffness matrix is calculated.

9) If DET2 is singular, and if the load cycle is one, it means that the initial applied load is too high or some unrealistic data was used. The analysis is terminated and returned to the step 2. If the load cycle is greater than one, then the critical load has been reached. An accuracy check is then performed to decide if better accuracy is required. If the desired accuracy is achieved, the critical load is given and from there, there is an option of performing another analysis or terminating the programme. The load is decreased and the process repeated if the desired accuracy is not obtained.

10) The structure load vector is formed if DET2 is not singular.

11) The nodal displacements are computed using the Choleski Triangular Decomposition method as detailed in Appendix I.

12) The shortenings due to both initial imperfections and bending are "added" to the respective nodal displacements.

13) Element nodal forces are computed.

14) The shortening due to initial imperfections and bending are calculated using the current element effective section properties if local buckling is accounted for. In steps 12 and 14, the shortening due to initial imperfections is only activated when the basic number of elements is used. If more elements are used, initial imperfections are taken care of by the actual framework geometry input.

15) Nodal stresses are calculated, again using the current effective section geometries if local buckling is considered.

16) If there is local buckling, the effective widths computed are used to determine the new effective section properties of each element.

17) The repetition of the analysis performed at each load level is terminated when the terms of the assembled stiffness matrix converge to a steady state at successive cycles. DET2 is used as a convenient quantity, whose value depends on the stiffness coefficients. If DET2 has reached a steady state, it is likely that the stiffness coefficients of the matrix have done so i.e., convergence of individual displacements. When the loading approaches the critical level, the assembled stiffness matrix becomes increasingly ill-conditioned and successive values of DET2 may vary widely. In this case, the repeated analysis is terminated at $I = 200$, i.e., if local buckling is considered. With no local buckling, the termination is at $I = 10$.

18) If a collapse load analysis is performed, the nodal plastic moment of individual element end nodes is calculated and compared against the respective nodal

moment. When $M > 1.05M_p$, the load is decreased and the analysis repeated till the required tolerance is met. For an elastic critical load analysis, the load is increased after convergence and the analysis repeated till the critical load is reached.

19) For semi-rigid connections, the stiffness changes with each load level according to the end moment. This change is accounted for with the use of equation (8.3.1) of Chapter 8. This step is only activated when a collapse load analysis is required. For the elastic instability analysis, the stiffness of the connection is assumed constant throughout and takes the value of the initial tangent stiffness obtained from the curve fitting technique.

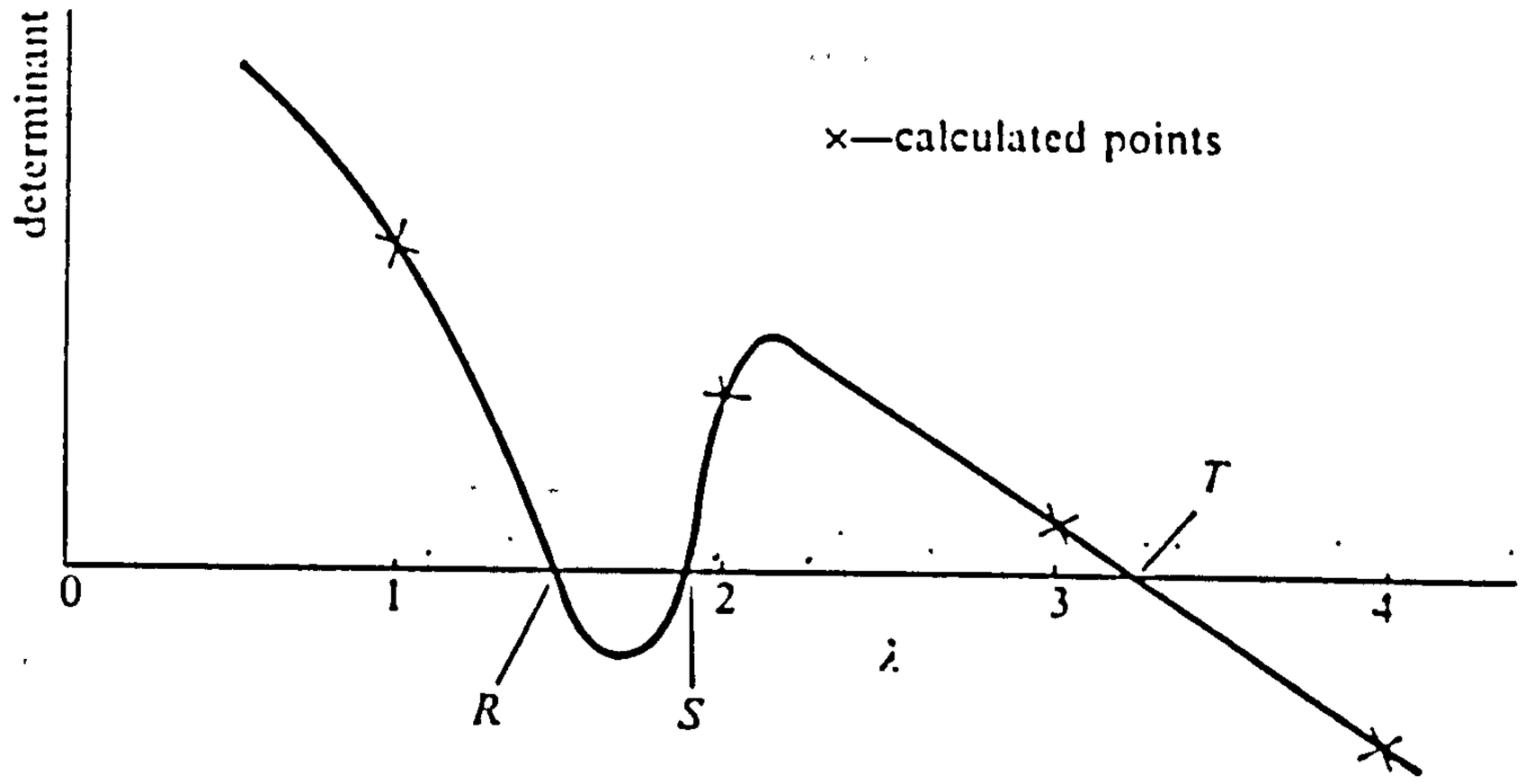

Fig. 9.3.1 Possible λ_c Values

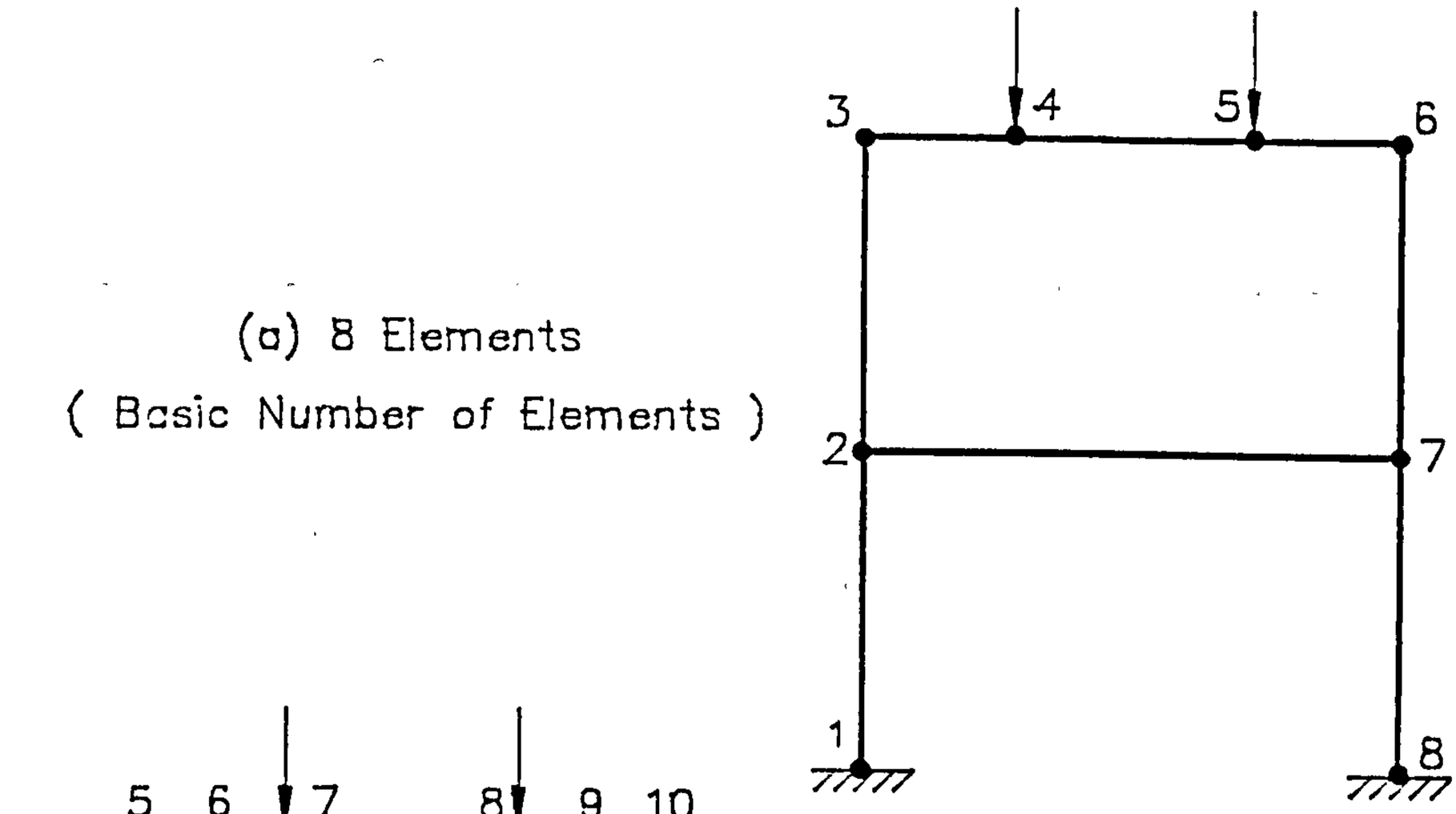

(a) 8 Elements

(Basic Number of Elements)

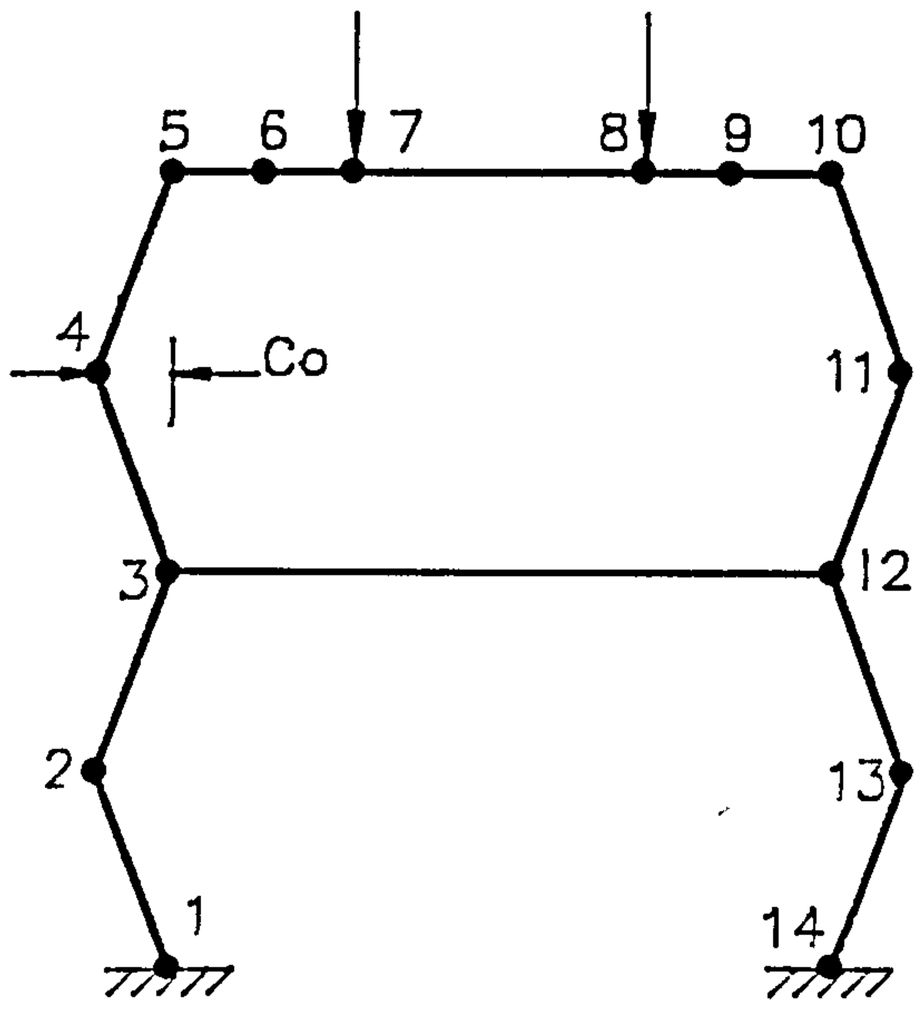

(b) 14 Elements

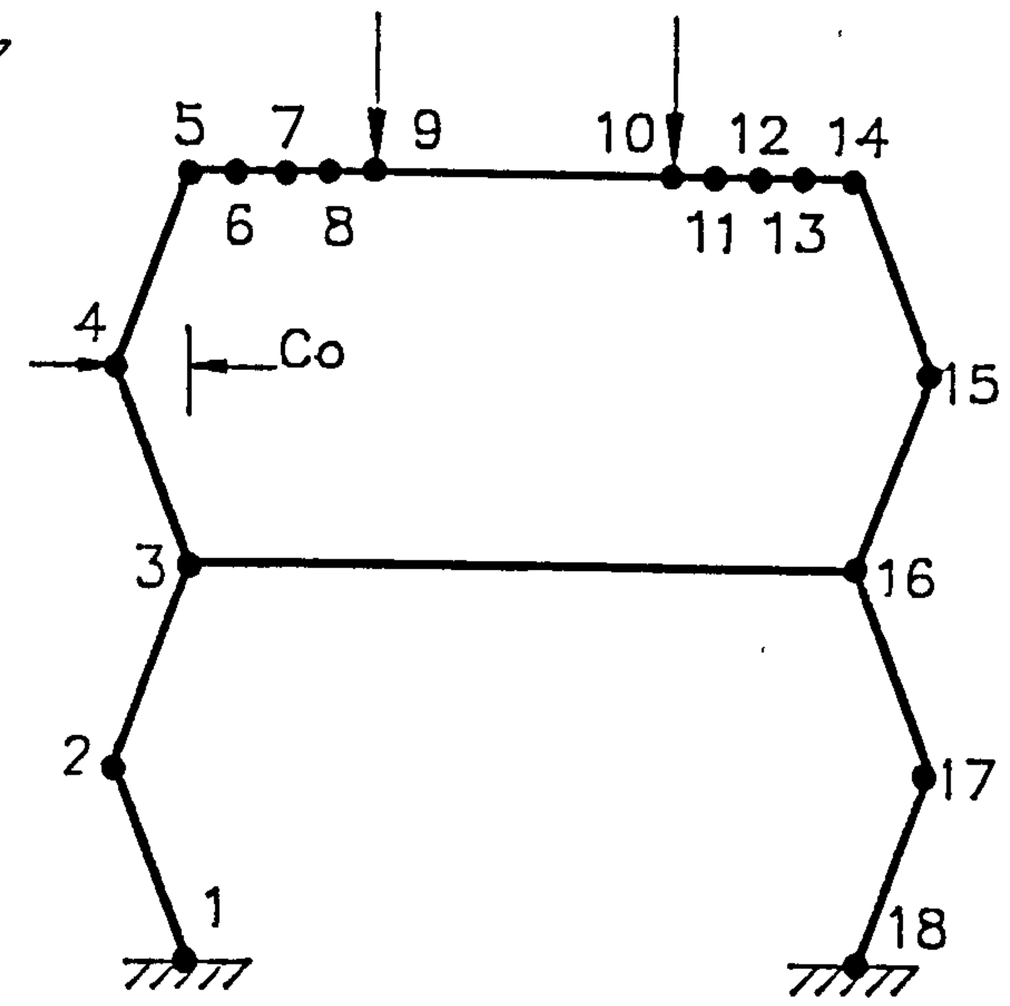

(c) 18 Elements

Fig. 9.3.2

Various Element Configuration for Double Storey Framework.

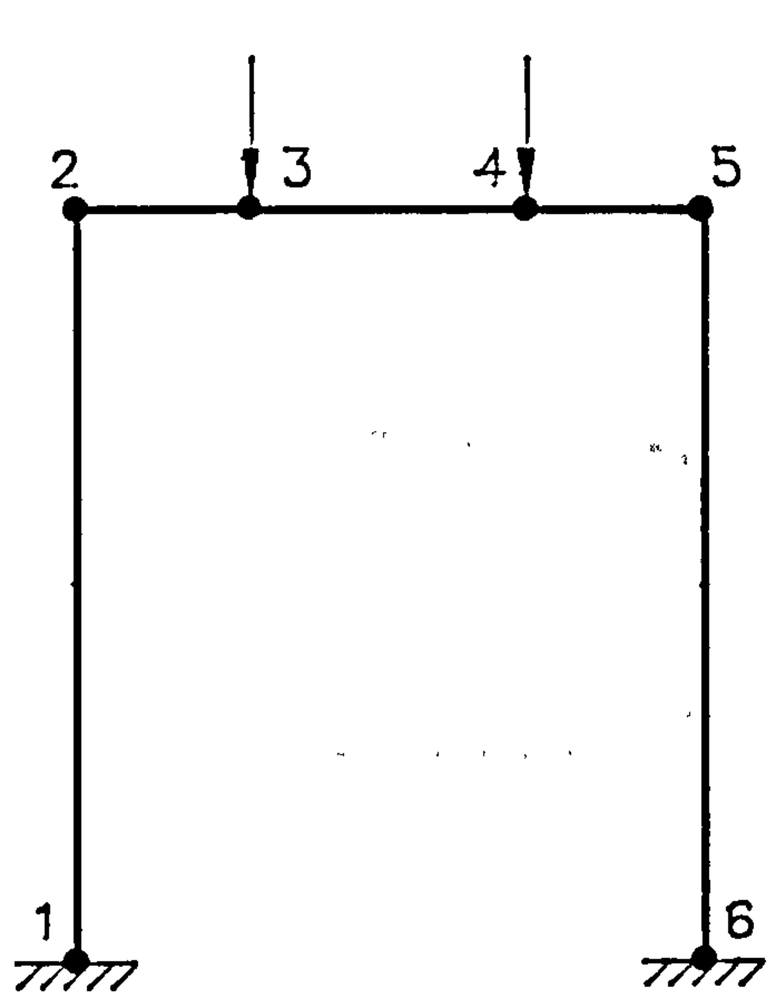

(a) 5 Elements

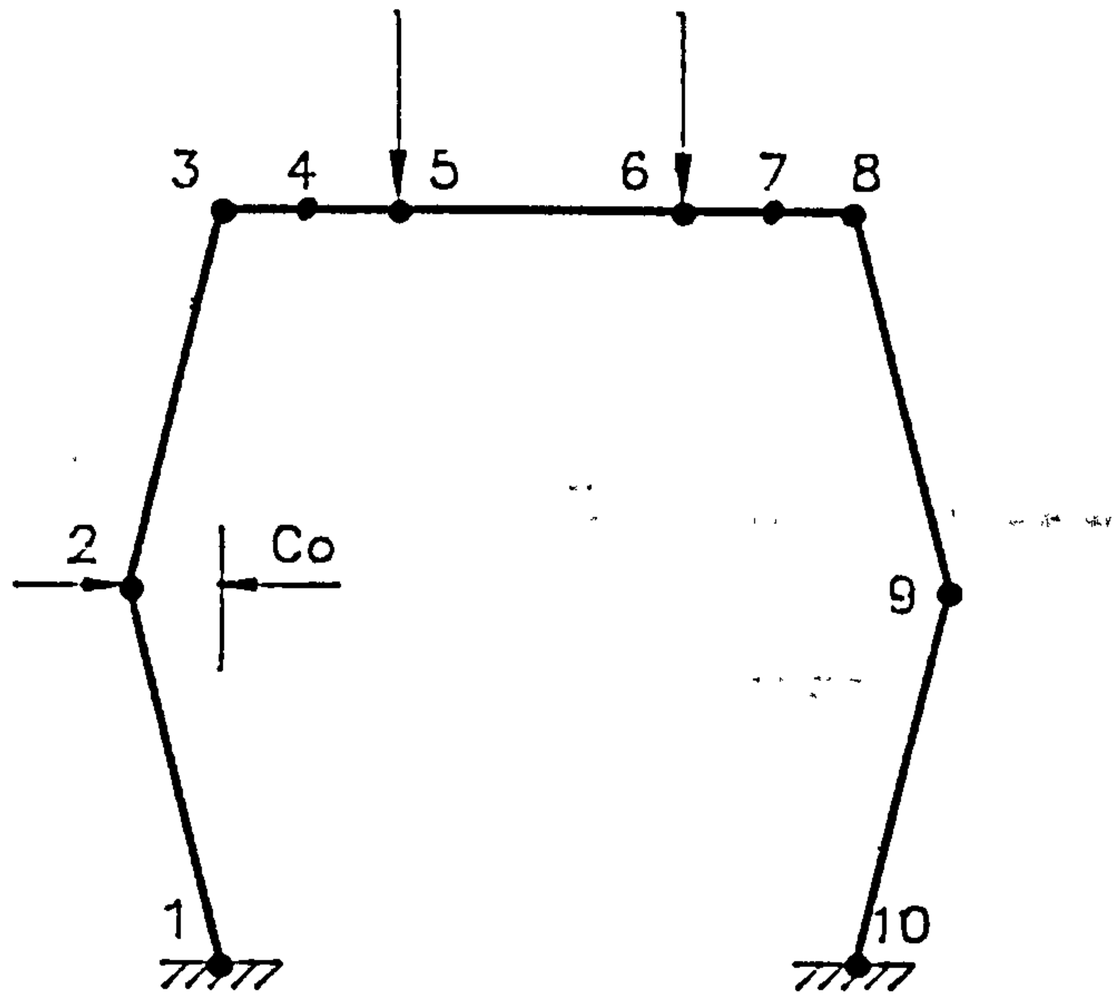

(b) 9 Elements

(Basic Number of Elements)

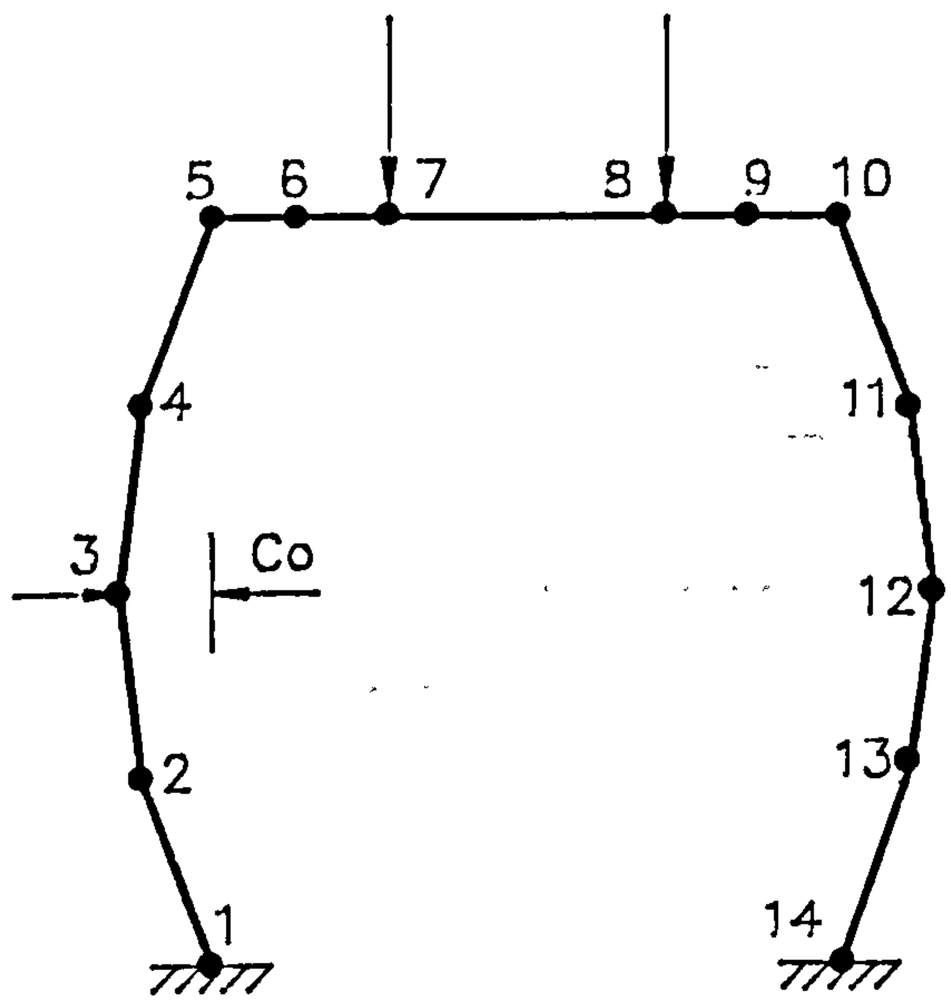

(c) 13 Elements

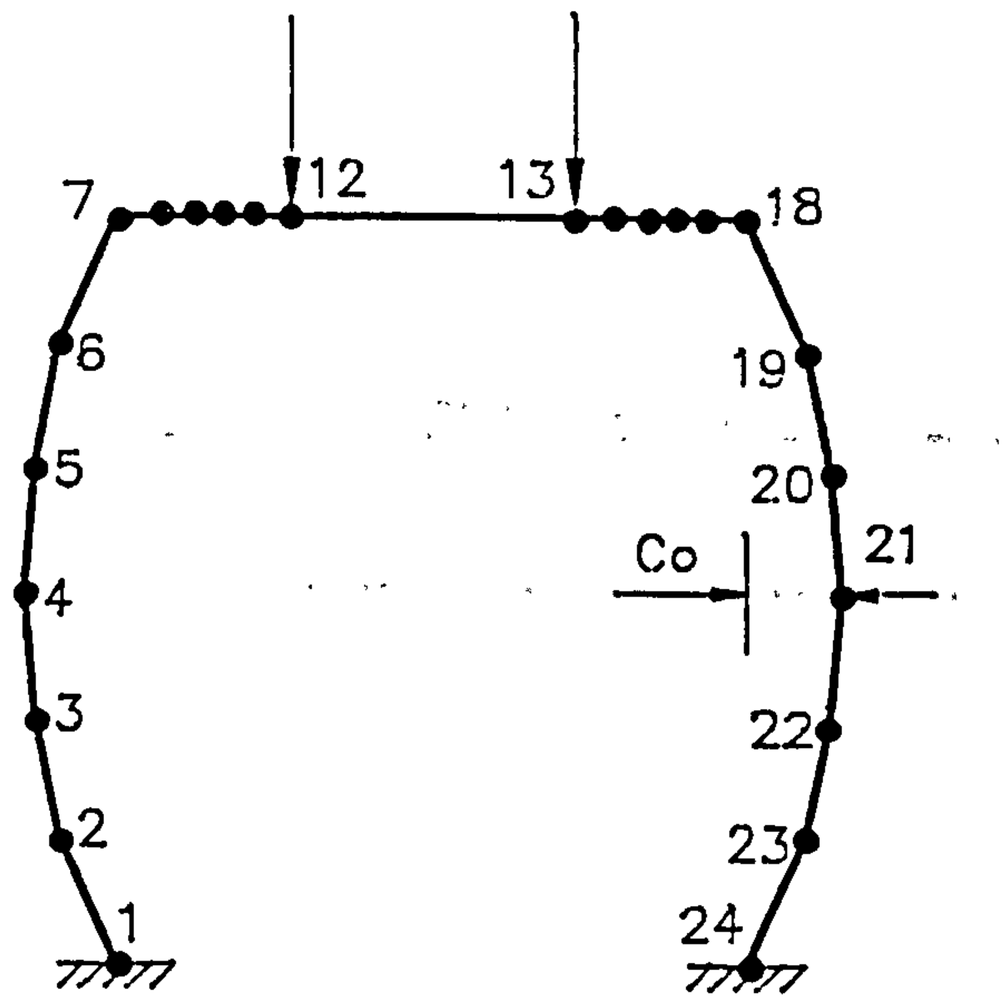

(d) 23 Elements

Fig. 9.3.3 a,b,c,d

Various Element Configuration for Single Storey Framework.

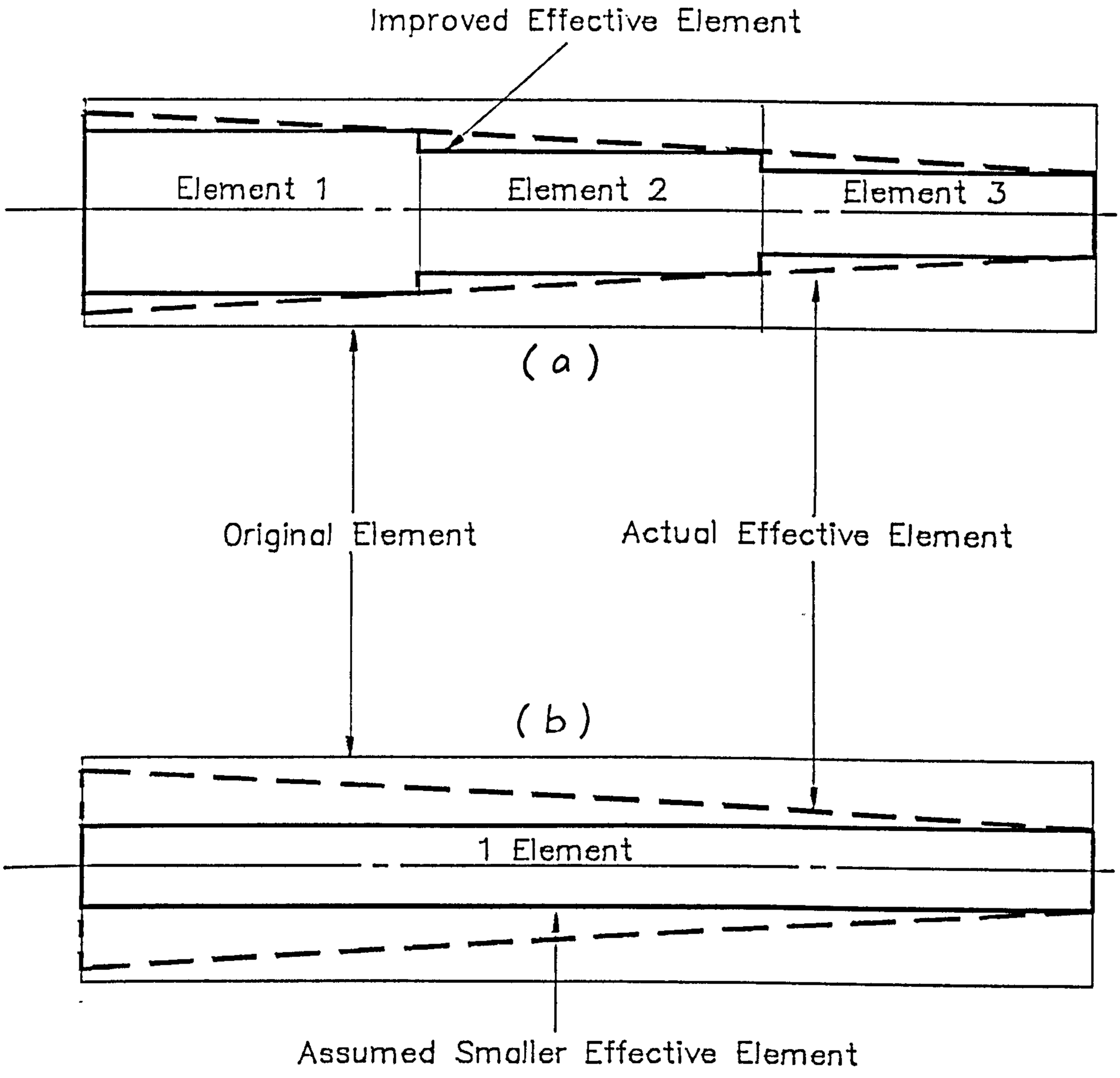

Fig. 9.3.4

Comparison of Effective Widths Using 3 Elements

and 1 Element

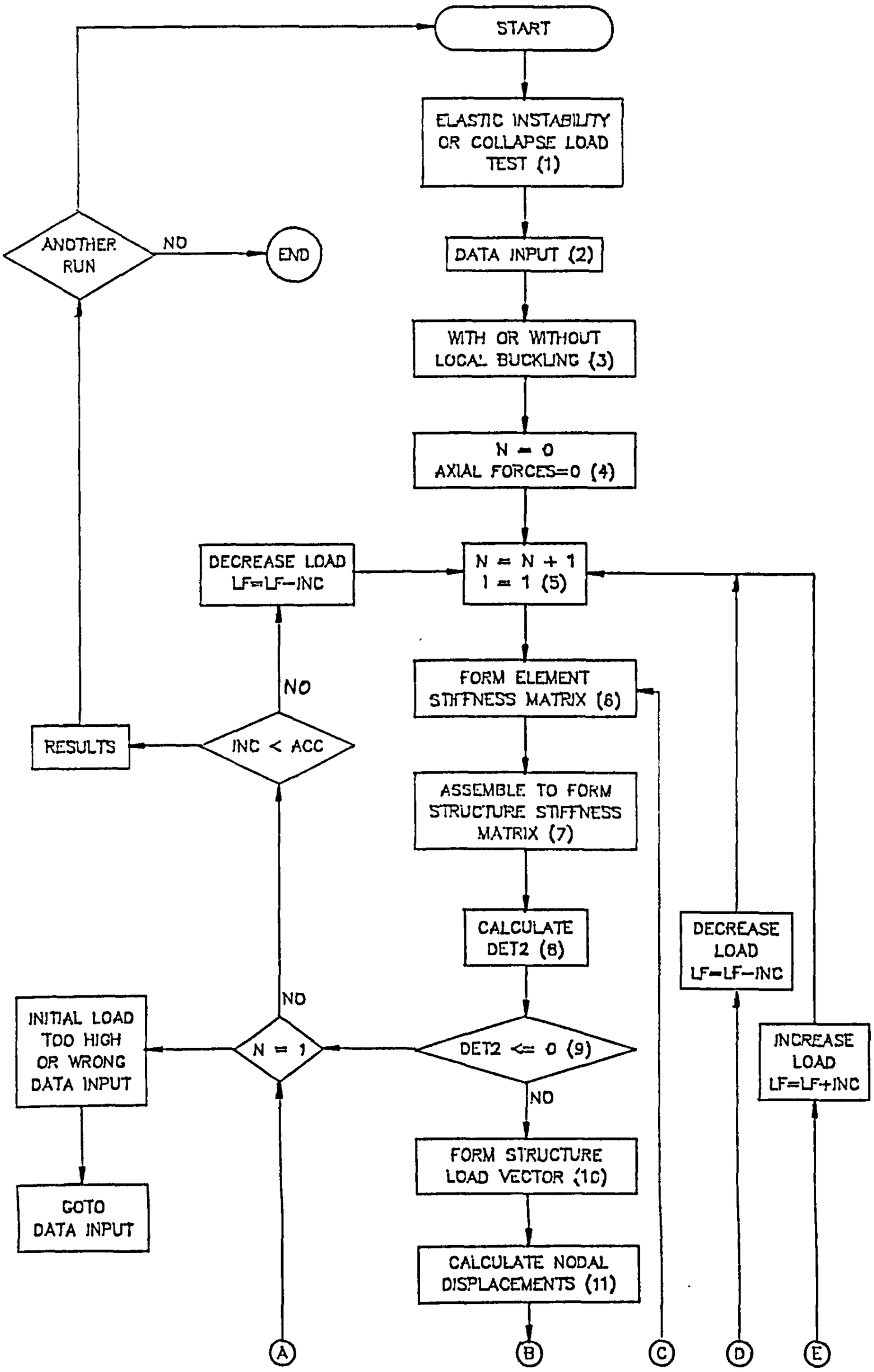

Fig. 9.4.1 Computer Flow Chart.

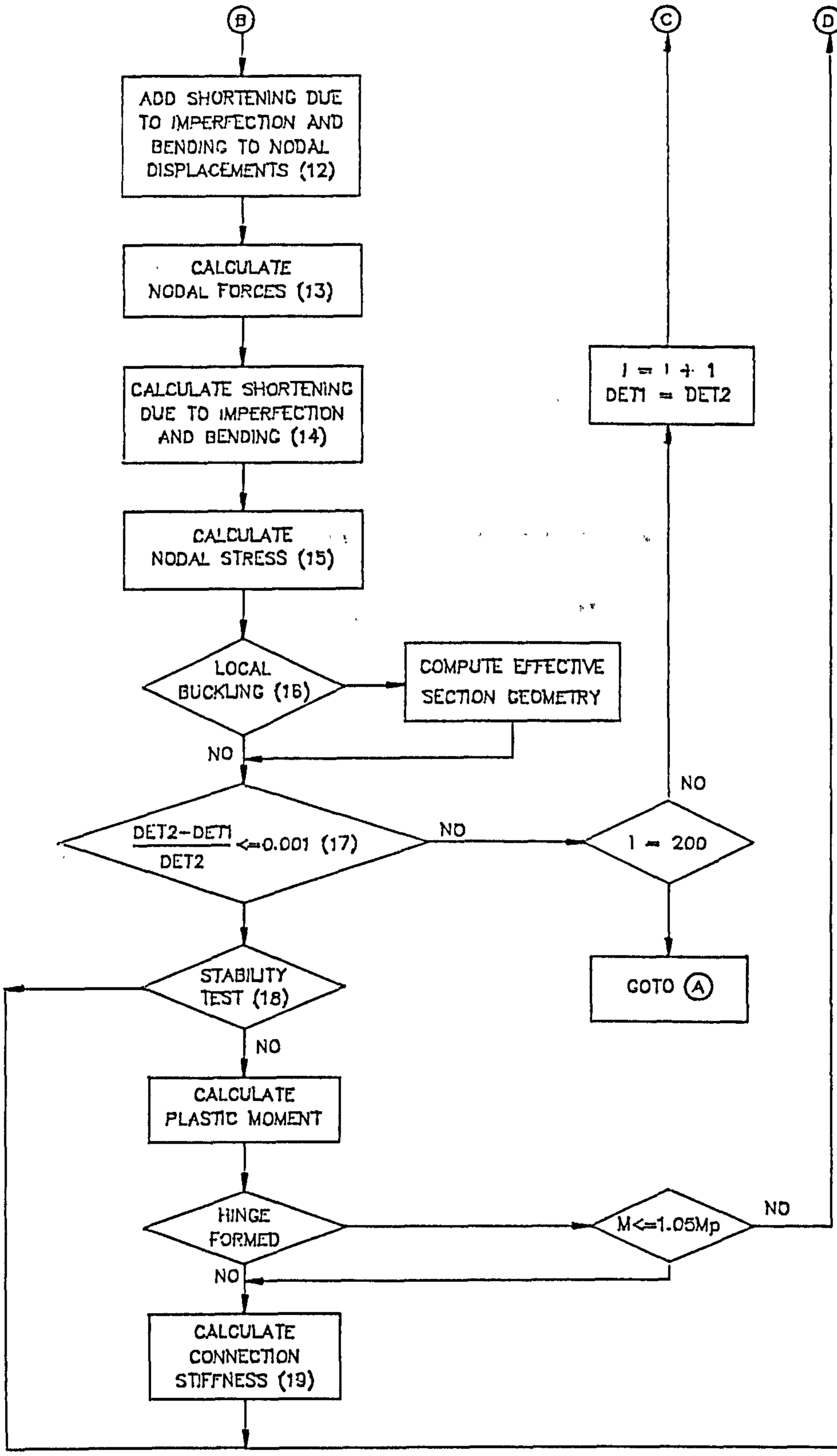
B
ADD SHORTENING DUE TO IMPERFECTION AND BENDING TO NODAL DISPLACEMENTS (12)
CALCULATE NODAL FORCES (13)
CALCULATE SHORTENING DUE TO IMPERFECTION AND BENDING (14)
CALCULATE NODAL STRESS (15)
LOCAL BUCKLING (16)
COMPUTE EFFECTIVE SECTION GEOMETRY
NO
DET2-DET1 / DET2 <=0.001 (17)
NO
STABILITY TEST (18)
NO
CALCULATE PLASTIC MOMENT
HINGE FORMED
NO
CALCULATE CONNECTION STIFFNESS (19)
C
D
E
I = I + 1
DET1 = DET2
NO
I = 200
GOTO A
M<=1.05Mp
NO

CHAPTER 10

FRAMEWORK EXPERIMENTAL INVESTIGATION

10.1 OBJECTS OF INVESTIGATION

An intensive experimental investigation was undertaken in order to obtain information on the behaviour of cold-formed thin-walled single and double storey frameworks, under concentrated loadings on the beam. The beams are connected to the column with semi-rigid connections. Theoretical solutions obtained from the analysis described in Chapter 9 were used to compare with the experimental results obtained. The main objects of the investigation are as follows:

1) To obtain experimental values of the load to cause collapse of the frameworks.
2) To examine the load-displacement behaviour at the loading point of the frameworks at all stages of loading.
3) To observe the growth and formation of plastic hinges and local buckles during loading.

10.2 TEST SPECIMENS AND FABRICATION

A total of six series of frameworks, half of which were single storey and the other half double storey, were tested to collapse. Each series consisted of five frameworks, all of which were constructed with similar plain channel members. However, the connections for each framework in a series were of different thickness or stiffness. A complete table showing all the frameworks with their respective connection type and members cross sectional geometry is listed in table 10.2.1. As shown in the table, a particular framework can be recognised by the specific designation given. The relevance of the designation is illustrated below with an example:

F 1 - 1 A

The first letter "F" means that it is a framework test. The number after the first alphabet refers to the members cross sectional geometry as detailed in table 10.2.1. Frameworks F1-2A to F1-2E were supposed to have been constructed with members of cross sectional geometry similar to those of frameworks F1-1A to F1-1E, but because of fabrication, there were slight discrepancy. If the second number is "1" then the framework is *double* storey. "2" refers to a *single* storey framework. The last letter indicates the thickness of the connection and this was already explained in Chapter 8.

The framework overall and members dimension is shown in figure 10.2.1. The dimensions apply to all the frameworks. However, for a single storey framework, the lower beam and two holes located about mid height of each column do not apply.

The members were fabricated from flat galvanised steel sheetings. Flat strips were cut to the correct size from the sheetings. The width of the strips was sized to give a corner radius of about twice the thickness of the respective specimen. Before marking out, it was ensured that the same sheeting, which was used earlier for fabricating the connecting members of the connection during the joint model test, was used for fabricating the framework members which were of the same cross sectional geometry as the connecting members of the connection.

The holes on the strips were drilled before bending was carried out. Because of the thinness of the material, it was much easier to drill about ten strips at a time. To prevent deformation around the hole, which was to be drilled, due to the twisting action of the drill, clamps were positioned as close to the hole as possible. The burrs around the drilled holes were then filed away to facilitate the bending process.

For the beams, cold bending on a manual bending machine was relatively easy because of the short length. On the other hand, forming the columns posed some

difficulties because of the length and several trials were necessary. This accounted for the slight difference in the cross sectional geometry. Because of the 25 mm width of the unstiffened elements of the columns of framework series F3-1 and F3-2, bending was carried out on a very simple and old bending machine. In addition to the length of the columns, many problems were encountered during bending. As a result, besides the lack of straightness, sinuisoidal camber or out of plane distortion of the unstiffened element were inevitable. These are illustrated in figure 10.2.2 and the average lack of straightness and camber are listed in table 10.2.2.

The final frameworks were constructed by bolting the beams and columns to the respective connections. A typical fully constructed framework is illustrated in figure 10.5.2. Because of the length of the columns causing the framework to be rather flimsy, and the possibility of the connections slipping out of position, extra precautions were undertaken to prevent the framework from becoming twisted out of plane during the construction.

10.3 DESIGN OF BOLTED CONNECTION

The bolted connections used in the frameworks were designed in accordance with BS 5950, Part 5. Based on a bolt diameter, d, of 8 mm, the procedures outlined in the specification were checked and detailed below.

From figure 10.2.1, the pitch or distance between the centres of adjacent bolts in the line of stress is $3d$. The minimum distance between the centre of the bolt and the edge is $2.75d$.

The shear capacity of a bolt is

$$P_{sh} = p_s A \qquad (10.3.1)$$

From table 11 of BS 5950, Part 5, p_s is 160 N/mm^2 for grade 4.6 bolt.

Therefore

$$P_{sh} = 8.042\ KN$$

As washers were used under both the bolt head and the nut, the bearing capacity for each bolt in the line of force is

$$P_{bs} = 2.1 d t \sigma_y \qquad (10.3.2)$$

To be on the safe side, the smallest product of $t\sigma_y$ of framework series F2-2 was taken from table 10.2.1. This results in

$$P_{bs} = 3.132\ KN$$

From table 11.1 of Chapter 11, the maximum theoretical collapse load acting on one loading point of the beam is 5.3 KN for framework F3-1E. As this load was obtained without consideration of local buckling, it will be conservative. Since there are two bolts connecting the connection to the top end of the column, the shear and bearing load on each bolt is 2.65 KN, which is less than the calculated shear or bearing capacity.

10.4 MATERIAL PROPERTIES

In order to obtain the yield stress of the material of the members used for the construction of the frameworks, four tensile coupons were produced from each piece of sheeting of different thicknesses and then tested in accordance with BS 18, Part 3. A typical tensile coupon is shown in figure 10.4.1.

The tensile test was carried out on the Tinius Olsen electro-mechanical testing machine, a description of which will be given later. An electronic extensometer was attached over a 50 mm gauge length of the coupon in order to measure the

strain. The load-strain curve was automatically plotted onto the recorder of the testing machine. For a material that depicts a sharp yielding stress-strain curve, the yield point is defined by the level at which the curve becomes horizontal. The yield point for a gradual yielding curve is determined by the offset method with 0.2% proof stress as specified by the specification. The average values of the yield stress of each thickness of the sheetings used are tabulated as below :

t (mm)	σ_y (N/mm^2)
0.590	316
0.700	295
0.835	298
1.000	295*

* 0.2% proof stress

As it is known that the Young's modulus, E, and the Poisson's ratio, ν, varied very little in commercial grade mild steel, these values assumed in the theoretical analyses are :

$$E = 205\,KN/mm^2 \qquad \nu = 0.3$$

10.5 TEST RIG AND EQUIPMENT

The test rig was designed to provide a fully fixed condition for the base of the framework. Moreover, it was also designed so that it could be used on the Tinius Olsen testing machine.

The test rig consists of a base plate and two sets of fixture. The detail drawings of these are shown in Appendix VI. The base plate and one set of fixture were used

during the joint model experimental investigation. The base plate was designed with the thought of future use. The slot at each end of the base plate is for bolting down onto the Tinius Olsen machine. The five slots running along the length of the base plate are for the sliding of the fixtures along the plate. The fixtures can also be bolted onto the base plate through the slots. Another purpose of the slots is that columns of bigger cross section, not necessarily only plain channel, can be accomodated and clamped onto the base plate. Each set of fixture consists of four jigs as shown in figure 8.2.7 of Chapter 8. The figure also shows how the fully fixed condition can be achieved.

Loading of the framework was achieved by the setup shown in figure 10.5.1. The loading bar was attached onto the machine crosshead by means of a large bolt. The purpose of the spacer was to facilitate bolting of the loading arm onto the loading bar. The tip of the loading arms was rounded off and load spreaders were used to prevent local stress concentration at the loading points.

The vertical deflection at the loaded point of the framework was measured with a deflectometer, which was placed on a support as shown in figure 10.5.2. The support was clamped onto the rod of the machine. The deflectometer has a maximum measuring range of about 50 mm. The measured deflection, together with the corresponding load, were plotted onto the machine recorder automatically.

The Tinius Olsen electro-mechanical testing machine was used to provide the loading in the framework experimental investigation. The machine is equipped with four load ranges and has a maximum capacity of 200,000 lbf. The crosshead of the machine can be raised and lowered by means of the four screws as shown in figure 10.5.2. These screws are synchronised to rotate in opposite directions which effectively eliminate any torsional effects on the test framework.

Figure 10.5.3 shows the machine load indicator and control unit. The range selector switch changes the capacity of the indicating system and the value of each scale division. Zeroing of the appropriate zeroing knobs correspond to the required load range.

The rate of loading is electronically controlled by the speed controller dial. The unit is used for plotting the load-deflection curve automatically during loading. The rotation of the recorder drum is in direct proportion to the measured deflection while the recorder pen moves across the drum in direct proportion to the applied load.

10.6 TEST PROCEDURE

Firstly, the loading arms were bolted onto the loading bar. Using the slot on the loading arm and the various holes along the loading bar, the loading arms were adjusted to give the correct distance between the tips of the loading arms. The whole assembly was then bolted centrally onto the machine crosshead as shown in figure 10.5.1. The bolt was only hand tightened because finer adjustments would be required later.

The base plate was bolted onto the rails of the machine working surface. The framework to be tested was then supported to stand on the base plate in a position such that the tips of the loading arms were in line with the markings (for loading) on the beam. The lower ends of the columns were then clamped using the fixtures as shown in figure 8.2.7. Before clamping, a beam, which is of the same length as the one used on the framework, was placed between the two lower ends of the column. This was to ensure that the top and bottom distance between the columns was equal.

The erected framework was checked to ensure that it was standing upright and erect. This was done by looking at the framework from the side. Corrections could be accomplished by loosening the base plate from the machine rails and inserting flat

pieces of metal plates in the correct position between the base plate and the rails. In some cases, several repetition of the above procedure were required before the framework was upright and erect.

The loading setup, which was only hand tightened initially, was adjusted till the tips of the loading arms were exactly in line with the markings on the beam and at the same time square with the framework. Checking was carried out by looking at the framework from both the front and the side.

Before loading, the load spreaders were placed in position on the beam. The load indicator and recorder pen were zeroed and the deflectometer was set up in position and adjusted such that the full range could be used. The framework was given an initial loading of about one third of the predicted collapse load. The purpose was to remove any slack present in the system. The framework was unloaded to zero load and the recorder pen was readjusted back to zero. Figure 10.5.2 shows a framework just before the actual loading. Loading was carried out gradually till the framework collapsed. The full load-deflection was automatically plotted on the machine recorder.

10.7 EXPERIMENTAL RESULTS AND OBSERVATION

From the framework experimental investigation, four different failure modes were observed. These are illustrated schematically in figure 10.7.1, which also shows the location and order of hinge formation. For frameworks with a dashed line, which represents a beam, the failure mode associated is applicable to both single and double storey frameworks.

Table 10.7.1 lists the failure mode of all the frameworks tested. It can be seen that , including framework F3-1B, all the frameworks with the thinnest connection, type A, failed in mode I. After the simultaneous formation of hinges at the loading points, further increase in load resulted in the failure of the connections. At this point, a

mechanism was formed and the framework collapsed. Framework F3-1B also failed in mode I because of the lower flexural stiffness of the connection, compared to that of the column. An actual typical mode I failure is illustrated in figure 10.7.2 and a magnified picture of the hinge formation at the loading points of the beam and the full plastic deformation of the connections is shown in figure 10.7.3.

For mode II failure, full plastic deformation occurred at the loading points initially. Further increase in the load resulted in the formation of hinges at the top end of the columns. This is due to the fact that by using stiffer connections, the bending moment along the beam is more distributed. Hence, the hinges at the loading points will occur at a *higher* load compared to the same framework with connections of lower stiffness. However, although the bending moment at the ends of the loaded beam is higher, the connections did not fail because of the higher moment capacity due to the increase in thickness. The reduction of the column's moment capacity due to the rather large compressive axial load and local buckling, if any, will cause the top end of the column to plasticise. The location of the hinges on the column was observed to have occurred just after the edge of the connection due to local stress concentration. A typical mode II failure is illustrated in figure 10.7.4. The hinges at the loading points of the beam and column can be seen from figure 10.7.5.

The two types of failure mode discussed above are symmetrical. Failure mode III is an unsymmetrical case. This manner of failure could be due to several factors. The connections or columns might be of slightly different geometrical dimensions. During the framework construction and testing setup, unsymmetry could have been introduced. For the three cases with mode III failure as shown in table 10.7.1, the hinges at the loading points formed almost simultaneously, followed by the formation of the third hinge at the column nearest the first hinge formed at the beam. At this stage, the framework collapsed. An example of mode III failure is illustrated in figure 10.7.6 and the middle framework of figure 10.7.7, which also shows the

collapsed frameworks of series F3-1. Notice that whatever the failure mode, the lower beam was virtually undeformed. This was true for all double storey frameworks, regardless of the failure mode.

For framework series F3-2, except for framework F3-2A which failed in mode I, the rest of the frameworks were observed to fail in mode IV. As with all the other failure modes, except mode III, the initial set of hinges formed at the loaded points simultaneously. Because of the cross sectional geometry and length of the column, torsional flexural buckling occurred upon further increase in applied load. The framework finally failed in a twisted manner as illustrated in figures 10.7.8 and 10.7.9.

The experimental load-displacement plots of the six series of framework, the details of which are tabulated and shown in table 10.2.1, are shown in figures 10.7.10 to 10.7.15. The load represents the loading at one loaded point of the beam and the displacement is the corresponding vertical deflection at that point.

From fig 10.7.10, it is shown that the framework stiffness increases with respect to the thickness or stiffness of the respective connections used. This is also true for the rest of the series of tests. For frameworks that failed in mode I, there is considerable increase in deflection or decrease in framework stiffness after the formation of the first set of hinges at the beam. This may be attributed to the low moment-rotation behaviour of the connections. For framework F1-1B, the drop in framework stiffness was due to the partial deformation of the top connections. Frameworks F3-1C, F2-2C and F2-2D , all of which failed in mode III, exhibited a sudden drop in stiffness because of the low plastic reserve of the columns. For framework series F3-2, except for framework F3-2A, the stiffness between the formation of hinges at the beam and final failure could not be compared because of the torsional flexural effect. For frameworks that failed purely in mode II with no other side effects, there was very little reserve strength left in the framework

after formation of the first set of hinges at the beam and total collapsed occurred rather suddenly. From table 10.7.1, it is shown that the collapse load increases with respect to the connection stiffness up to a point. When connection type E was used, the collapse load reduces. The experimental plots for these series, as shown in figures 10.7.10, 10.7.11 and 10.7.13, exhibit a very similar pattern in both stiffness and collapse load. On the other hand, framework series F3-1 indicated an increase in the collapse load with respect to the increase in connection stiffness and framework F3-1E gave the highest collapse load. Although the unsymmetrical failure of frameworks F2-2C and F2-2D prevented a definite comparison, an estimation of the values of the collapse load shown in table 10.7.1 seemed to indicate the similarity with the former collapse load-connection stiffness behaviour discussed earlier. The results of framework series F1-2 and F3-2 cannot be discussed conclusively due to the significant out of plane distortion of the framework and torsional flexural effects respectively.

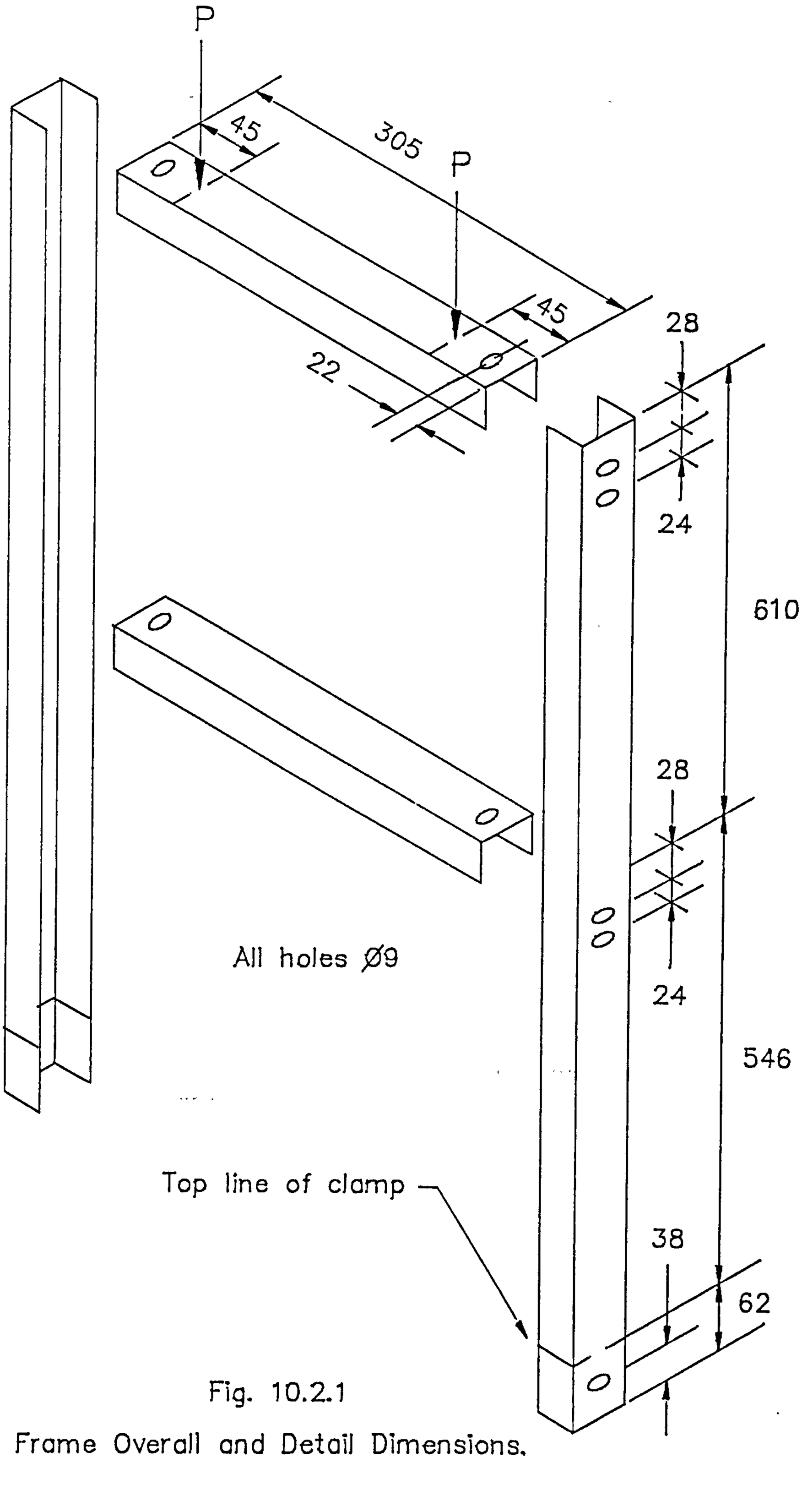

Fig. 10.2.1

Frame Overall and Detail Dimensions.

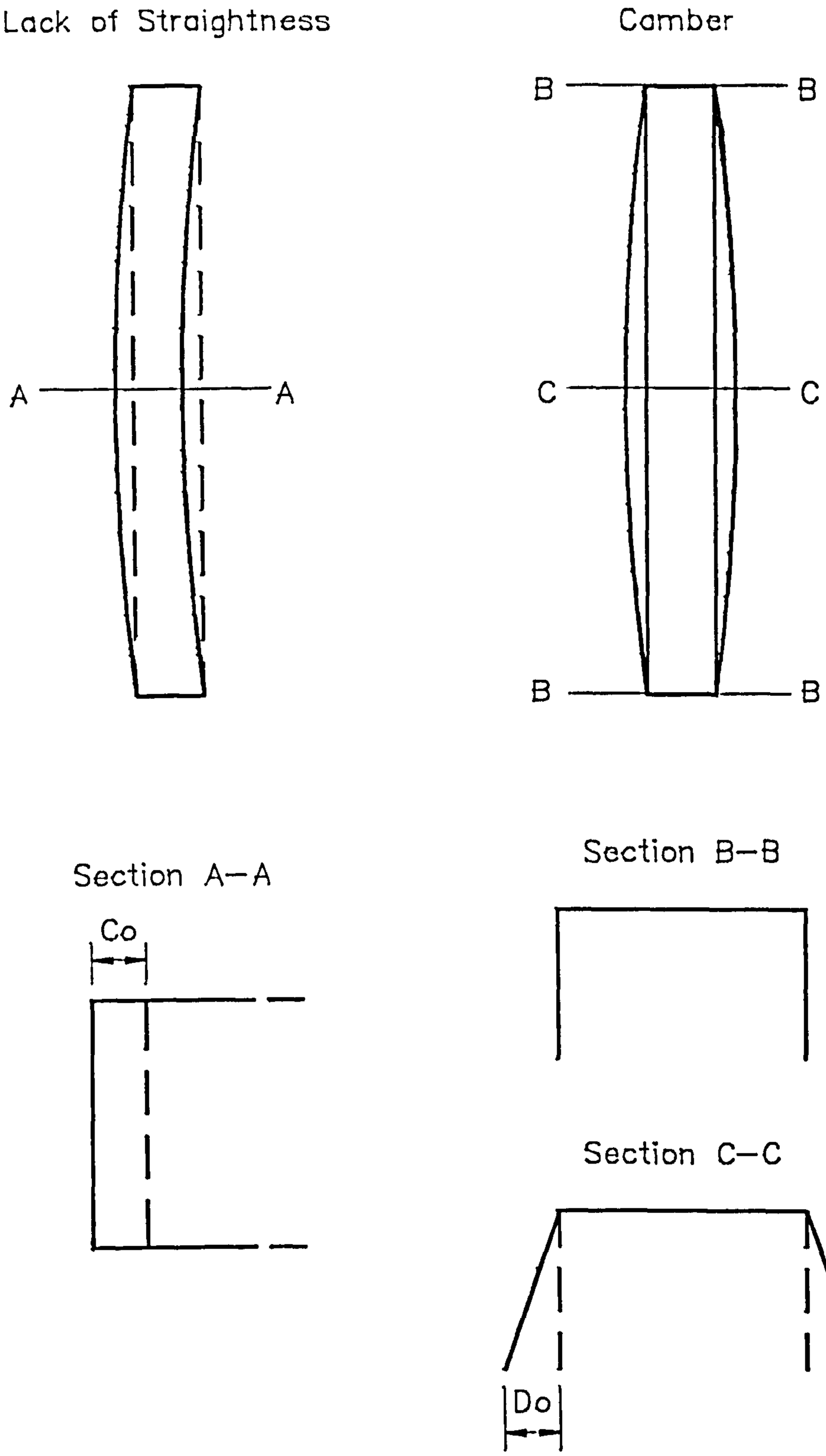

Fig. 10.2.2
Column Initial Imperfections.

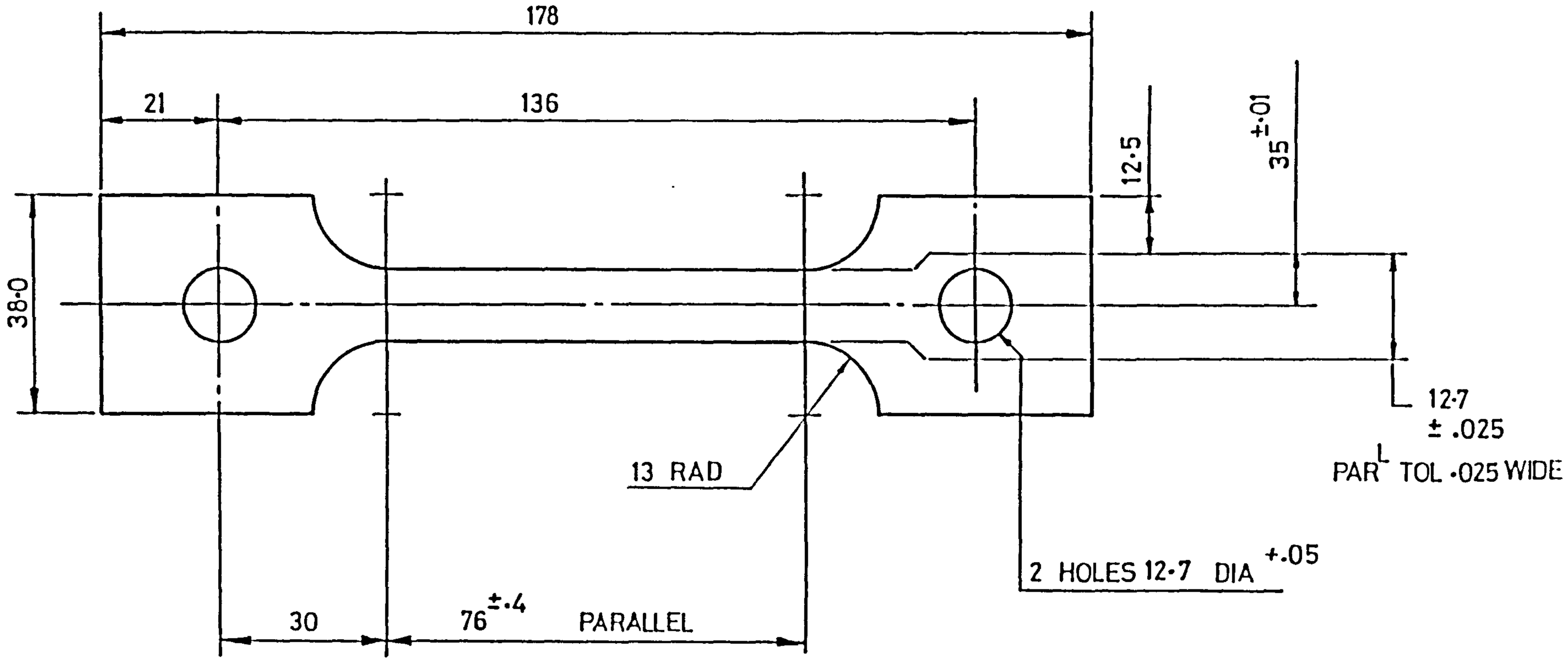

NOTES G.L. CONTOUR ON BOTH SIDES TO BE

1. EXACTLY SAME AND FINISH EXACTLY OPPOSITE EACH OTHER
2. 12·7 REAMED HOLES MUST LIE ON ℄ OF PARALLEL GAUGE LENGTH

DIM. UNIT M.M

PLATE THICKNESS UPTO 10

Fig. 10.4.1 Typical Tensile Coupon

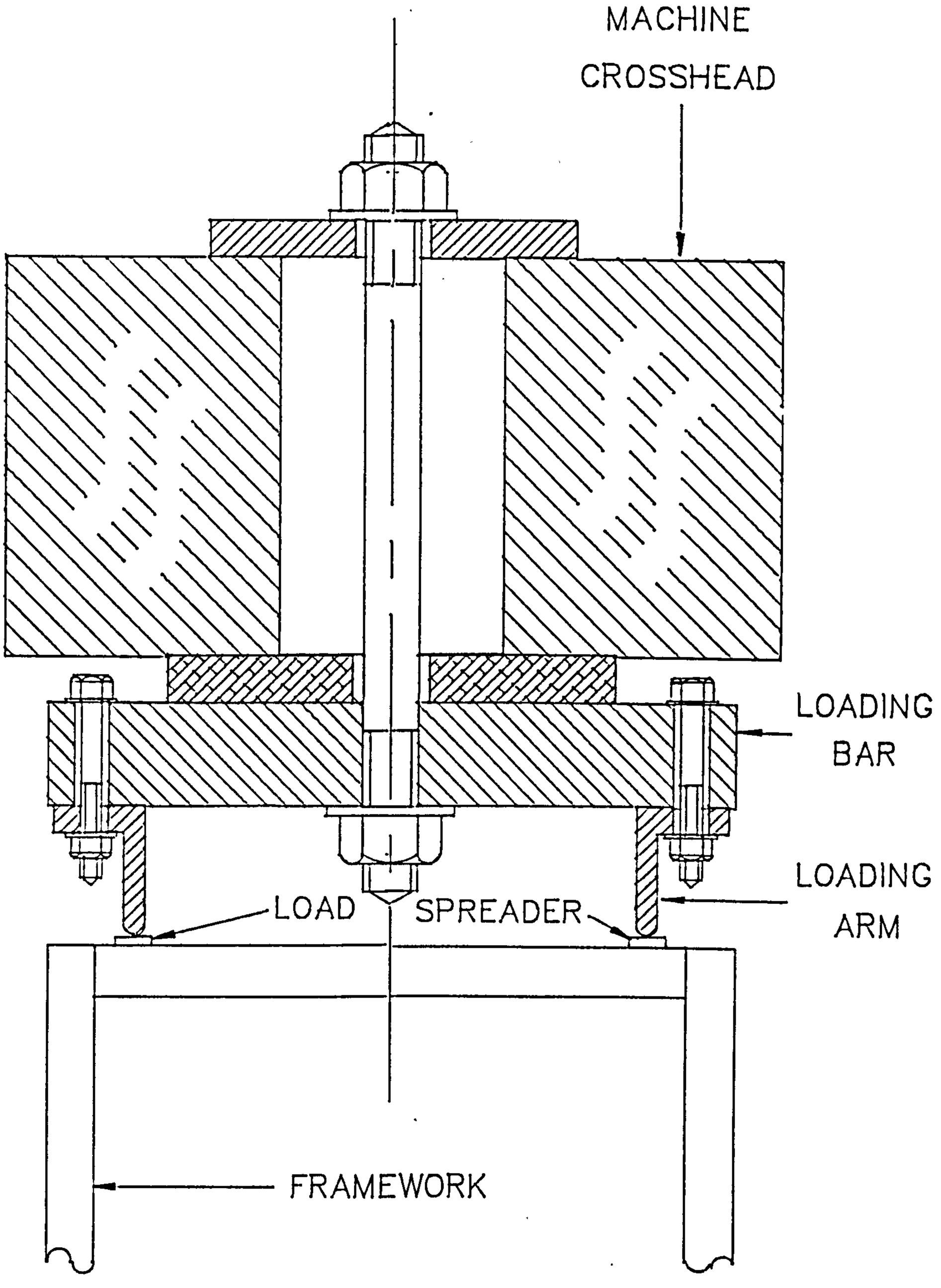

FRAME LOADING SETUP DETAILS

Fig. 10.5.1

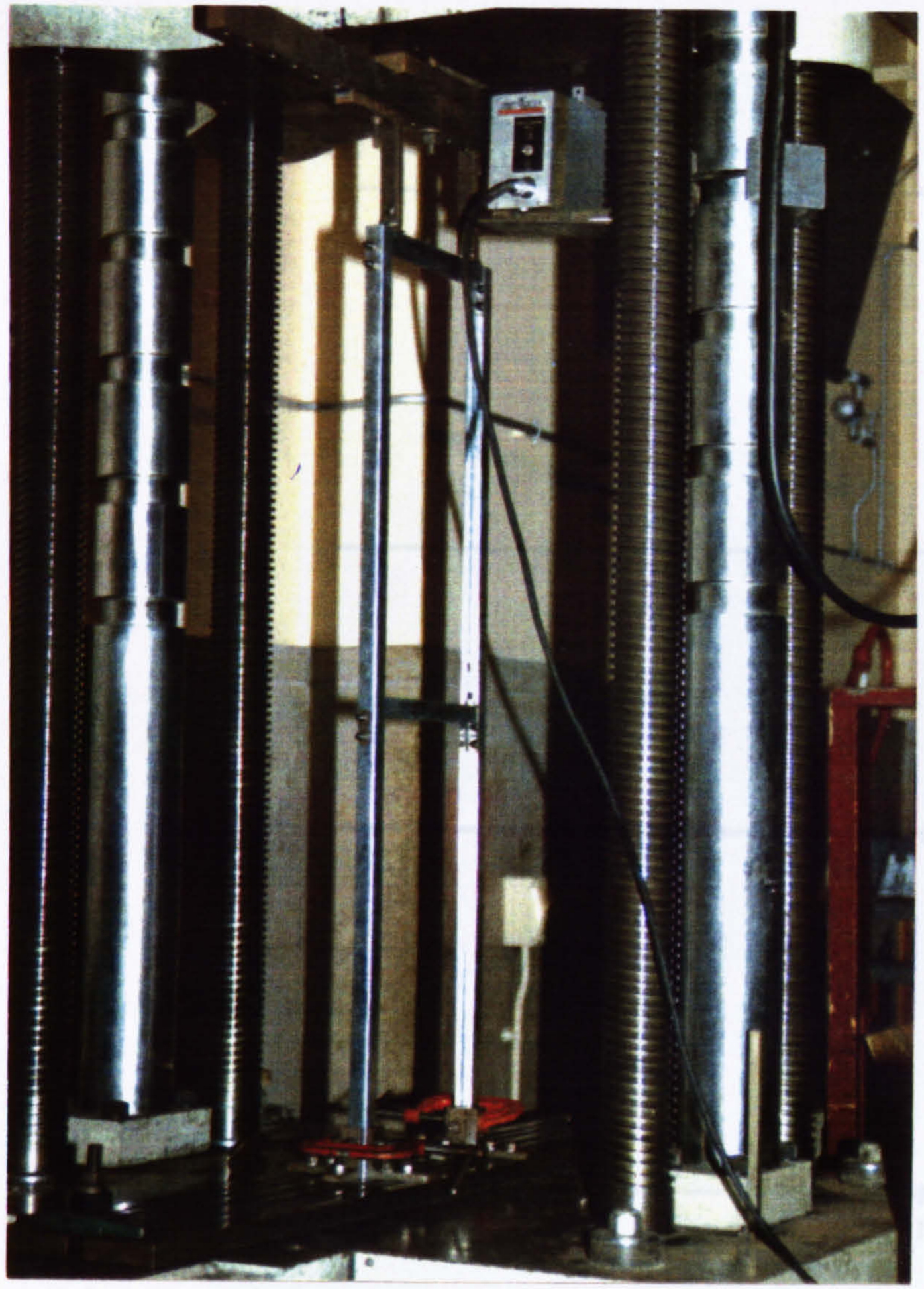

Fig. 10.5.2 Test Setup Before Loading

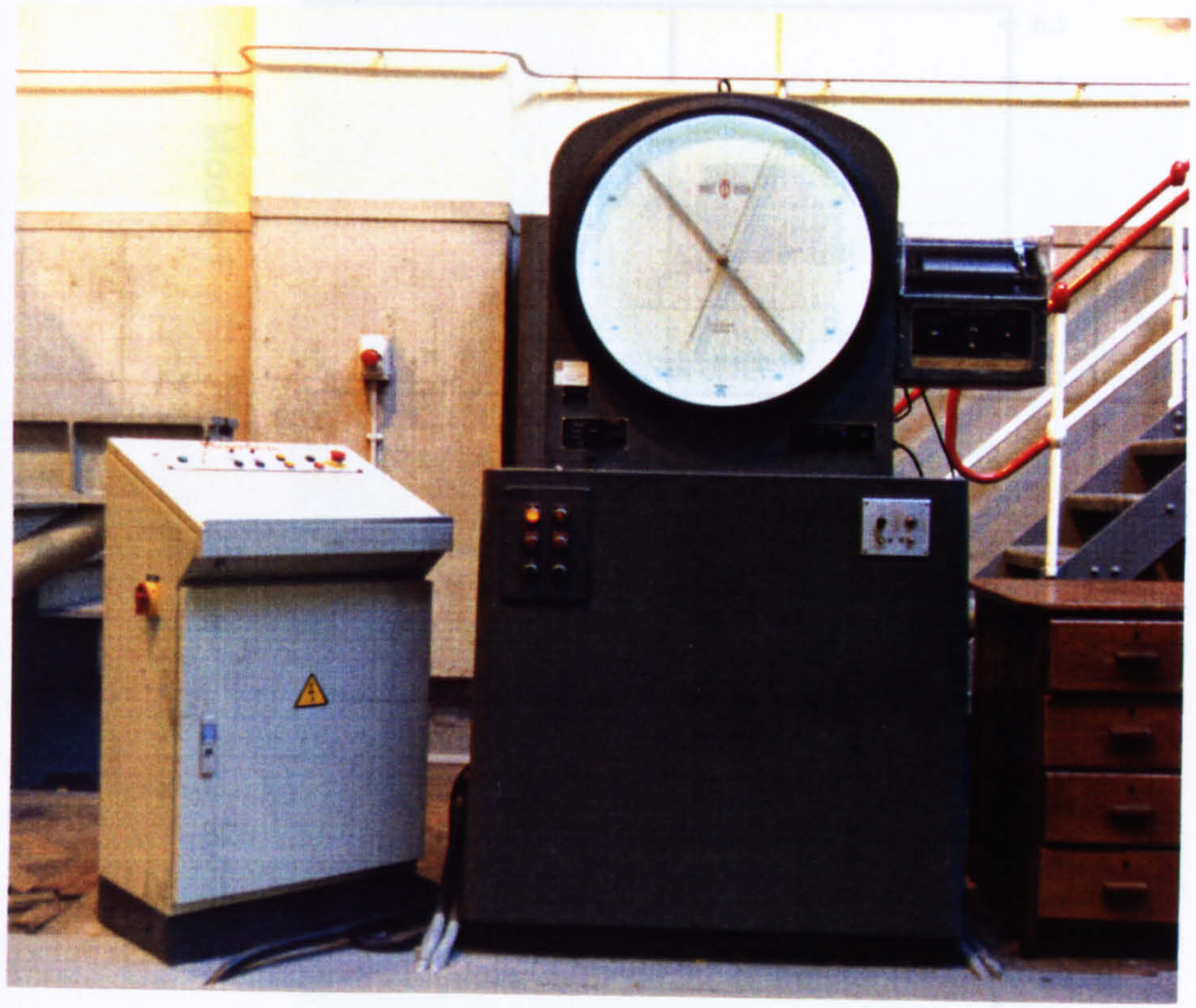

Fig. 10.5.3 Tinius Olsen Machine Load Indicator and Control Unit

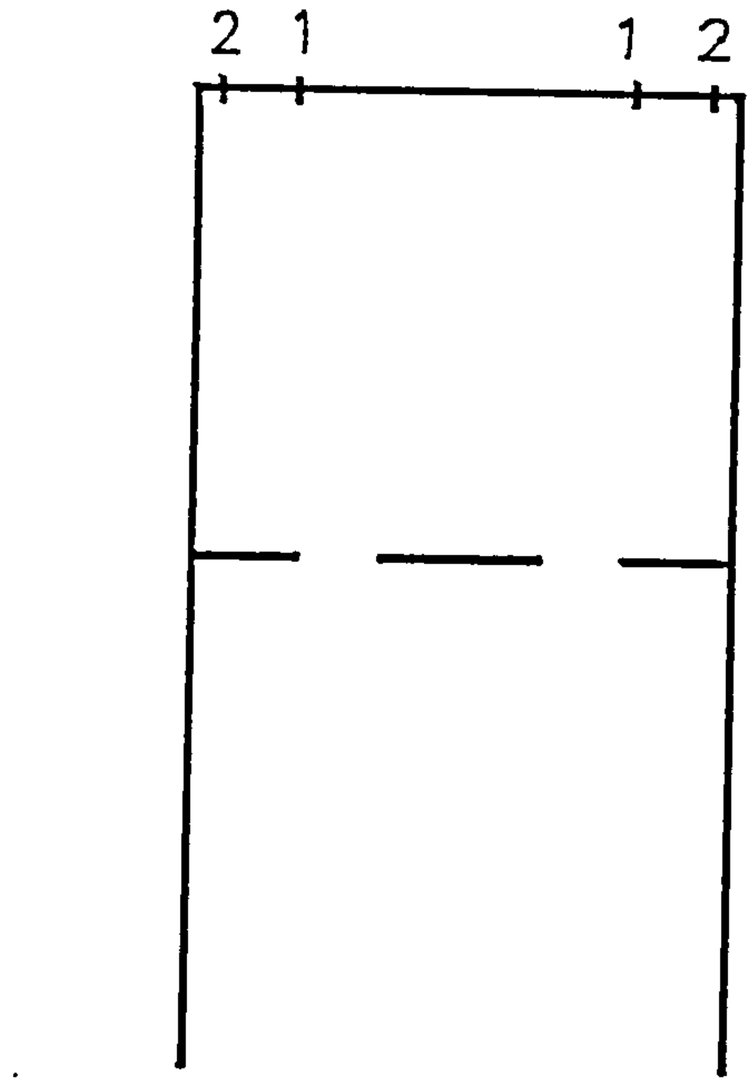

Mode I

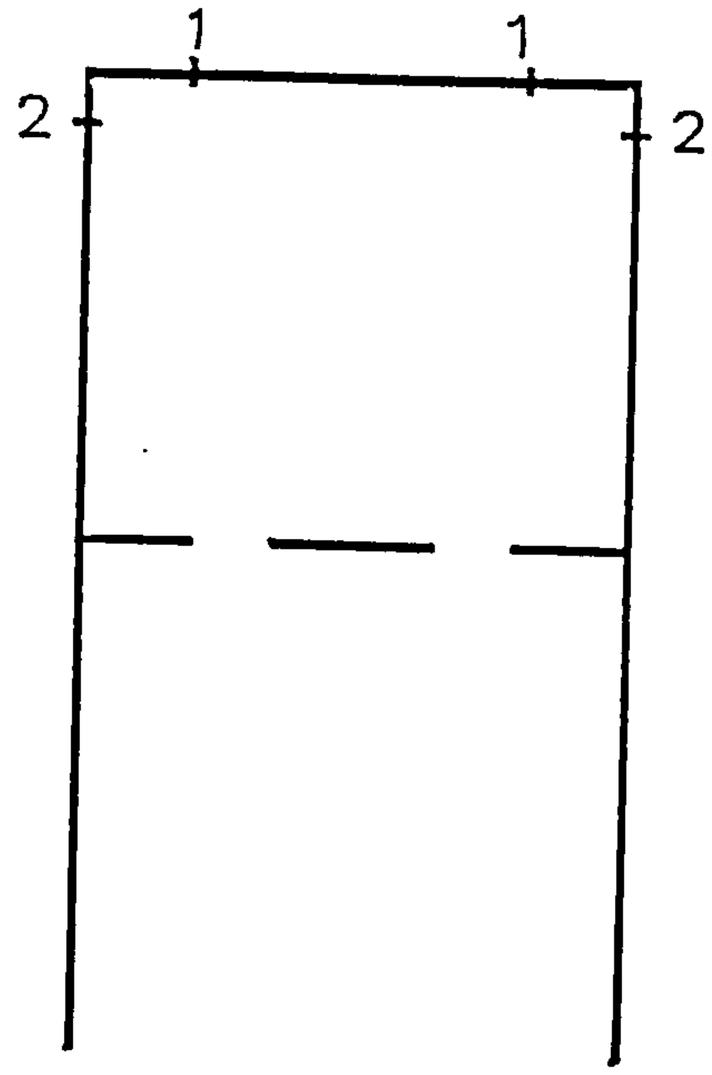

Mode II

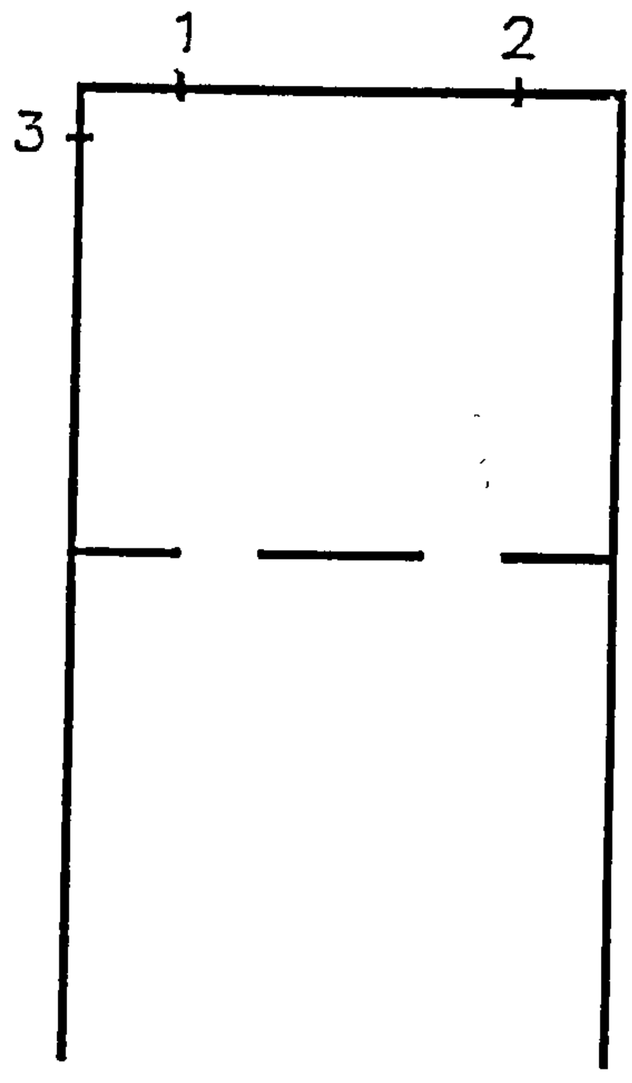

Mode III

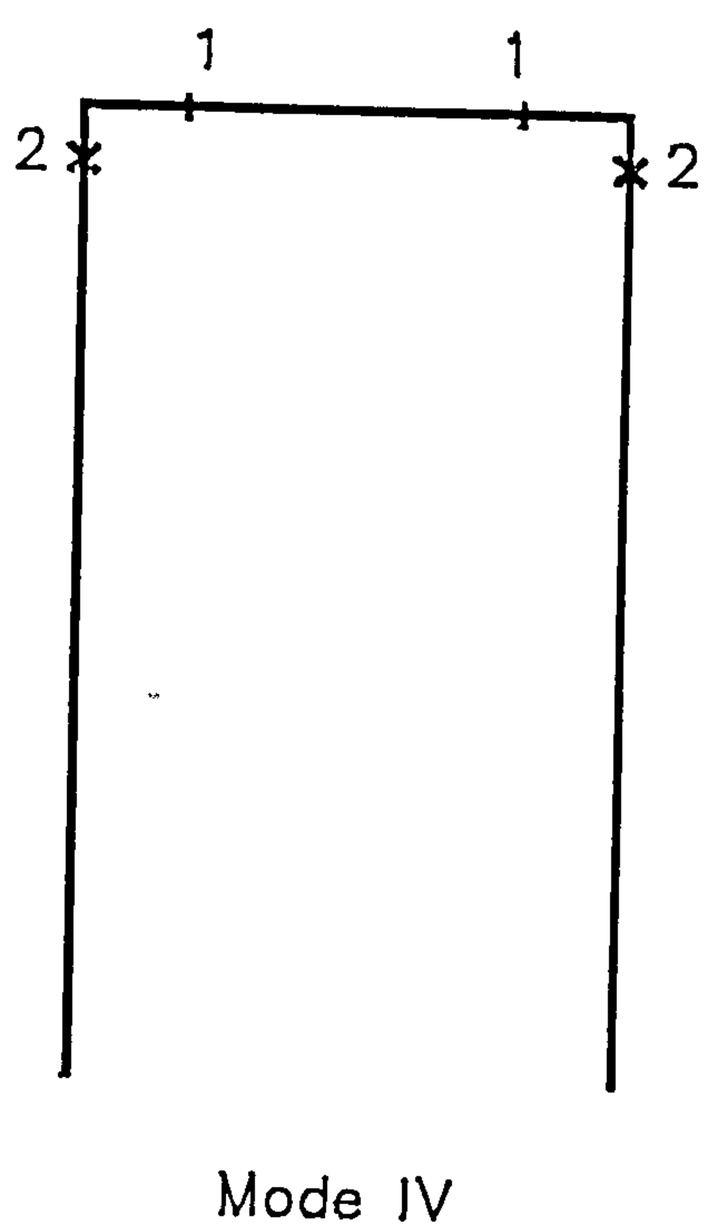

Mode IV

Fig. 10.7.1

Various Framework Failure Mode.

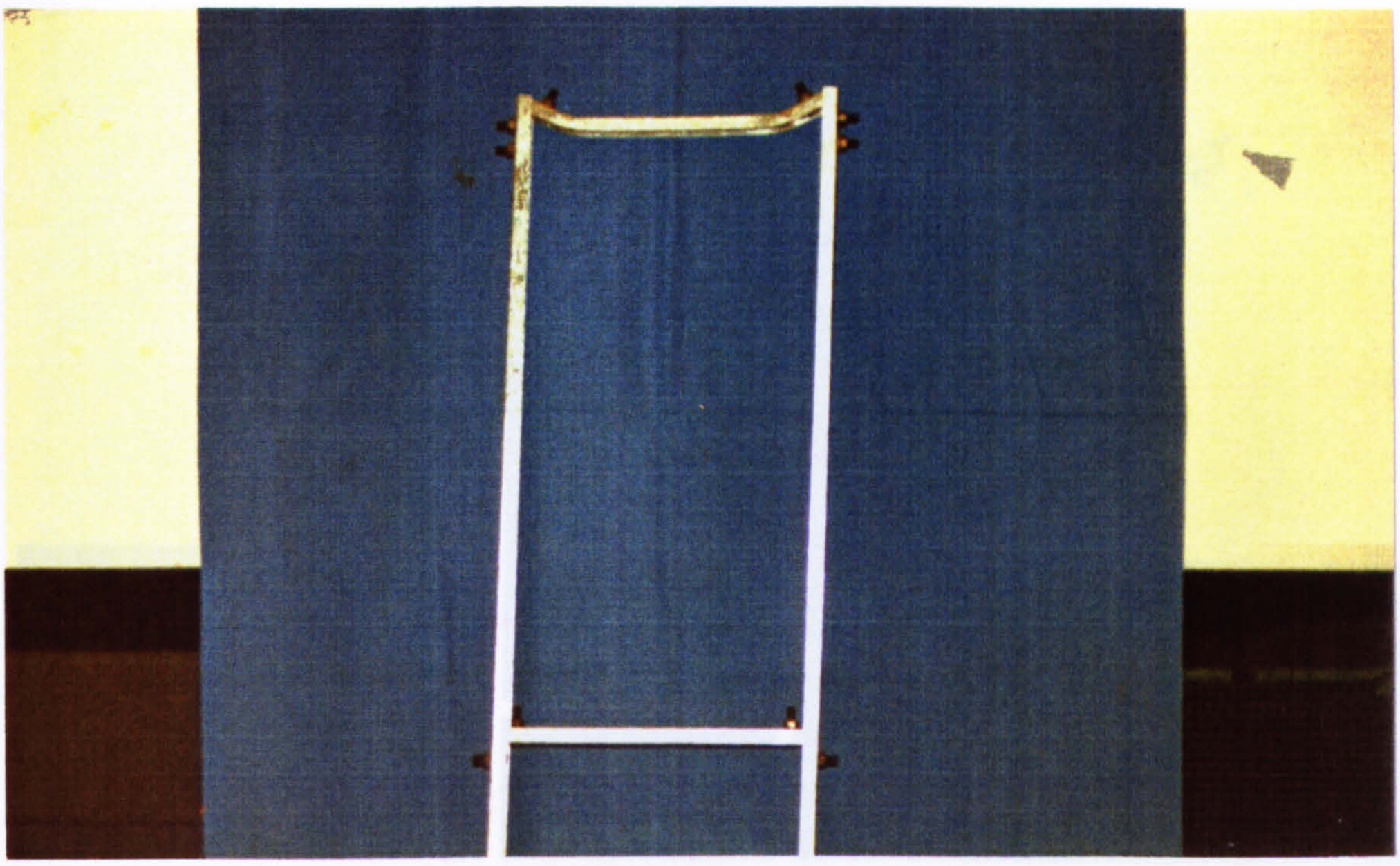

Fig. 10.7.2 Mode I Failure

Fig. 10.7.3 Hinge Formation at Beam and Connections

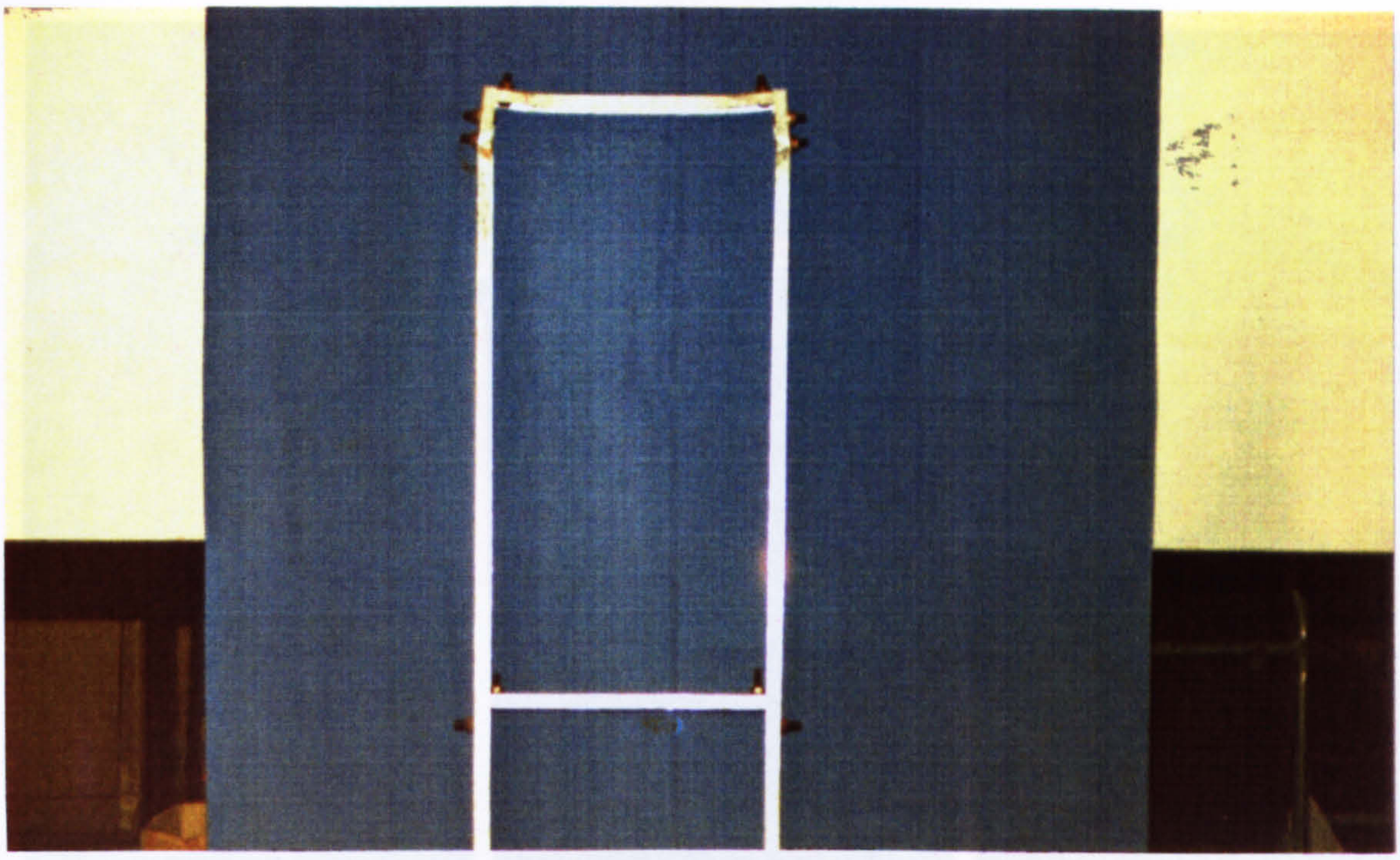

Fig. 10.7.4 Mode II Failure

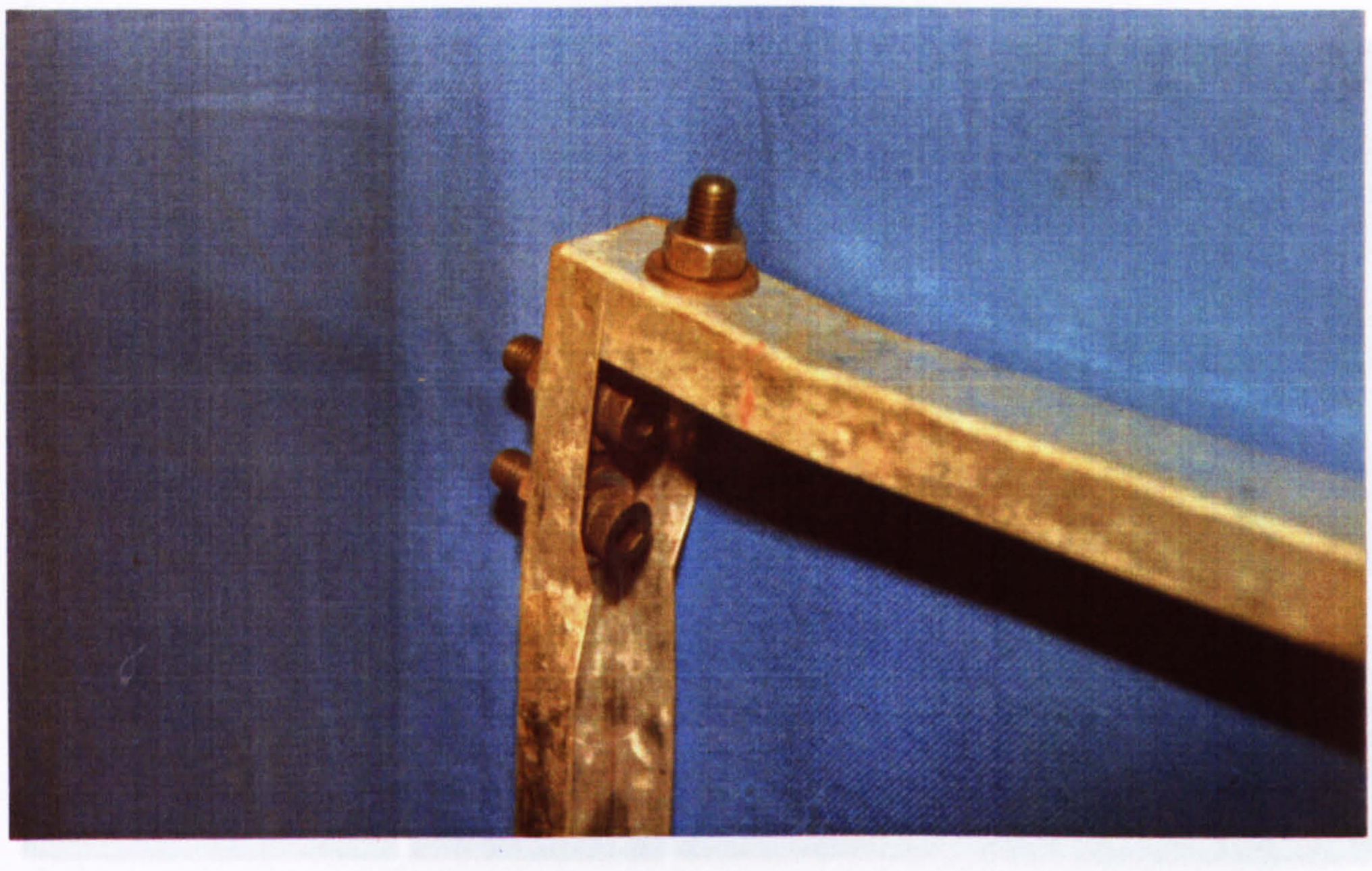

Fig. 10.7.5 Hinge Formation at Beam and Column

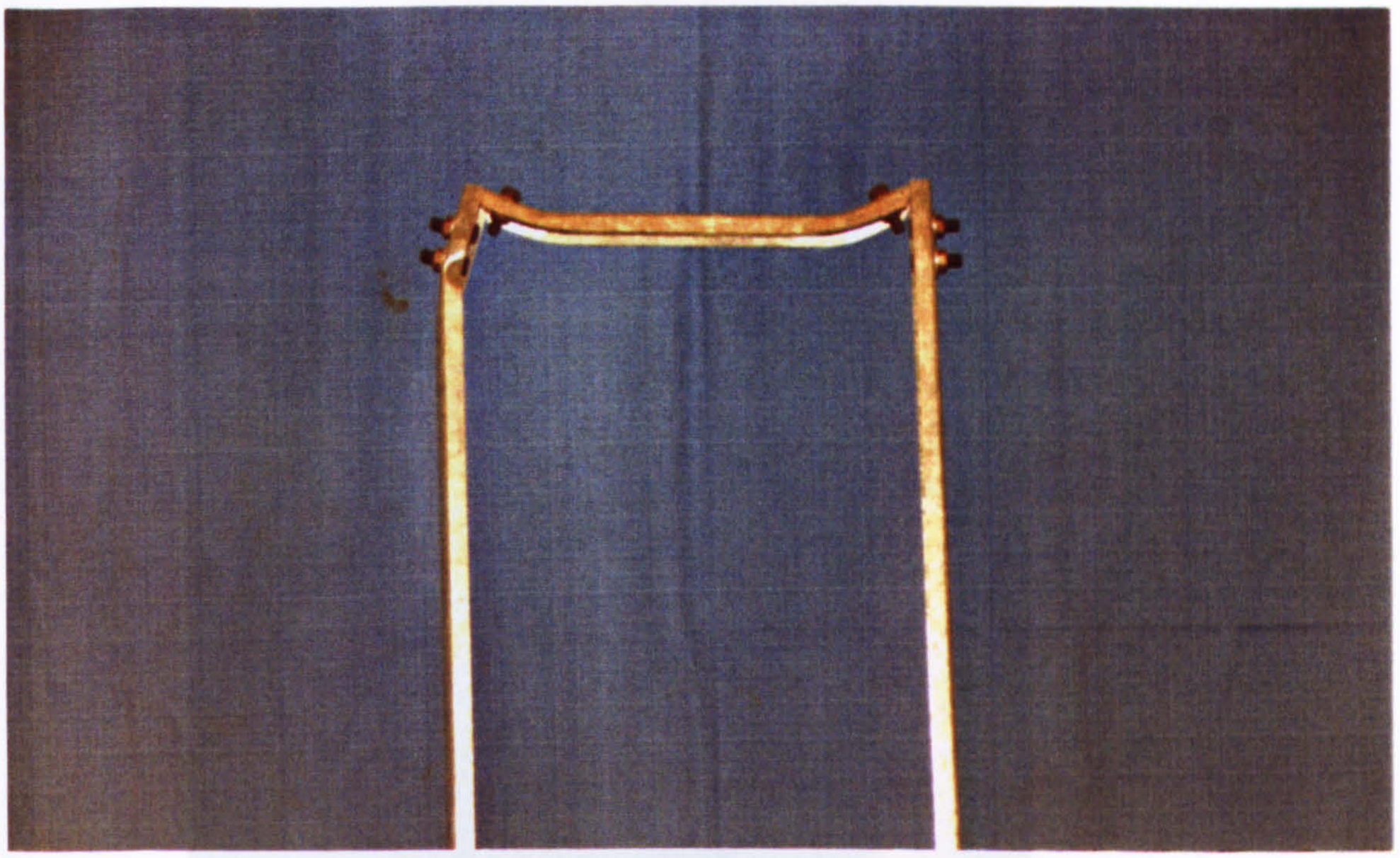

Fig. 10.7.6 Mode III Failure

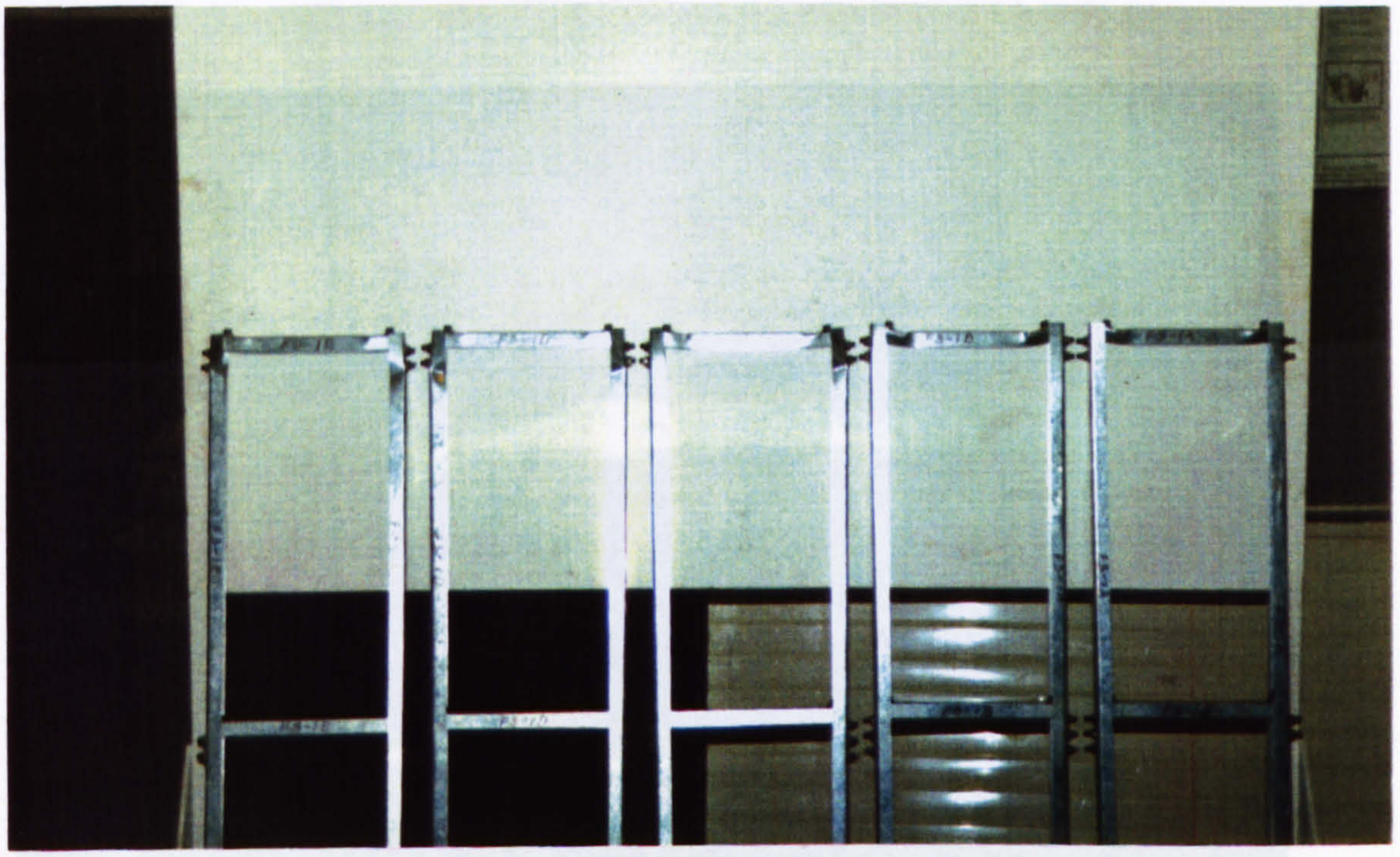

Fig. 10.7.7 Collapsed Frameworks

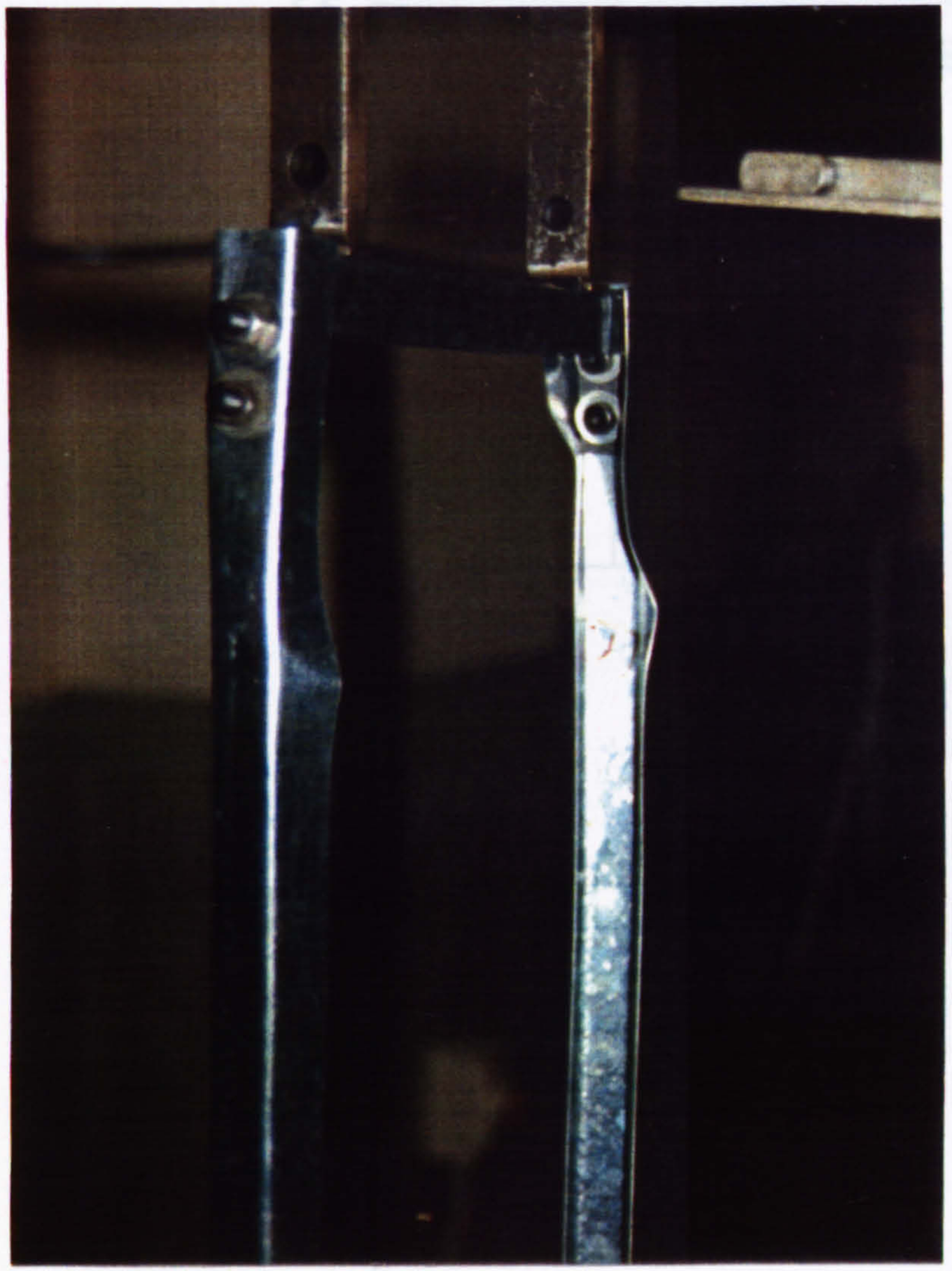

Fig. 10.7.8 Mode IV Failure

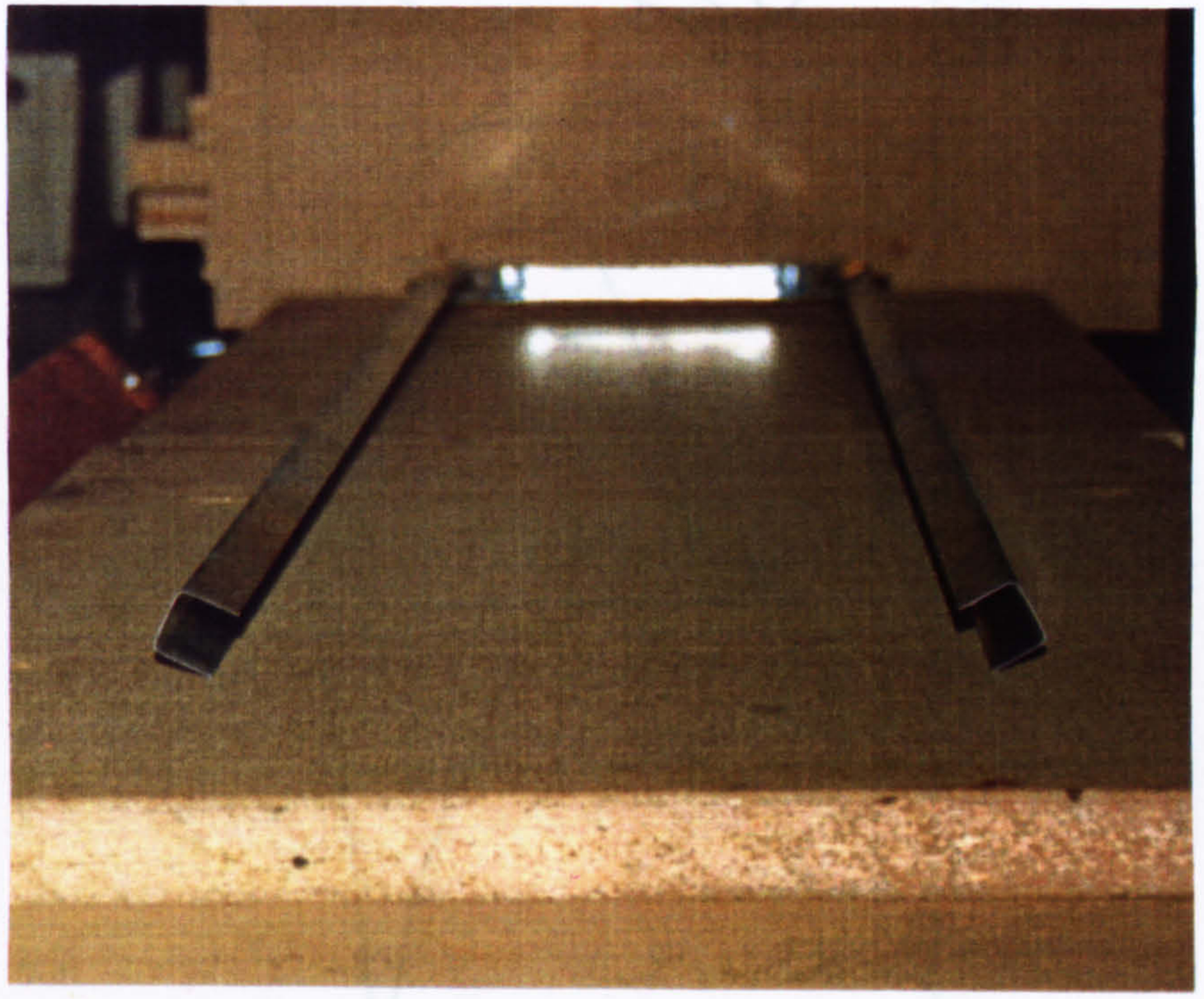

Fig. 10.7.9 Twisting of Columns

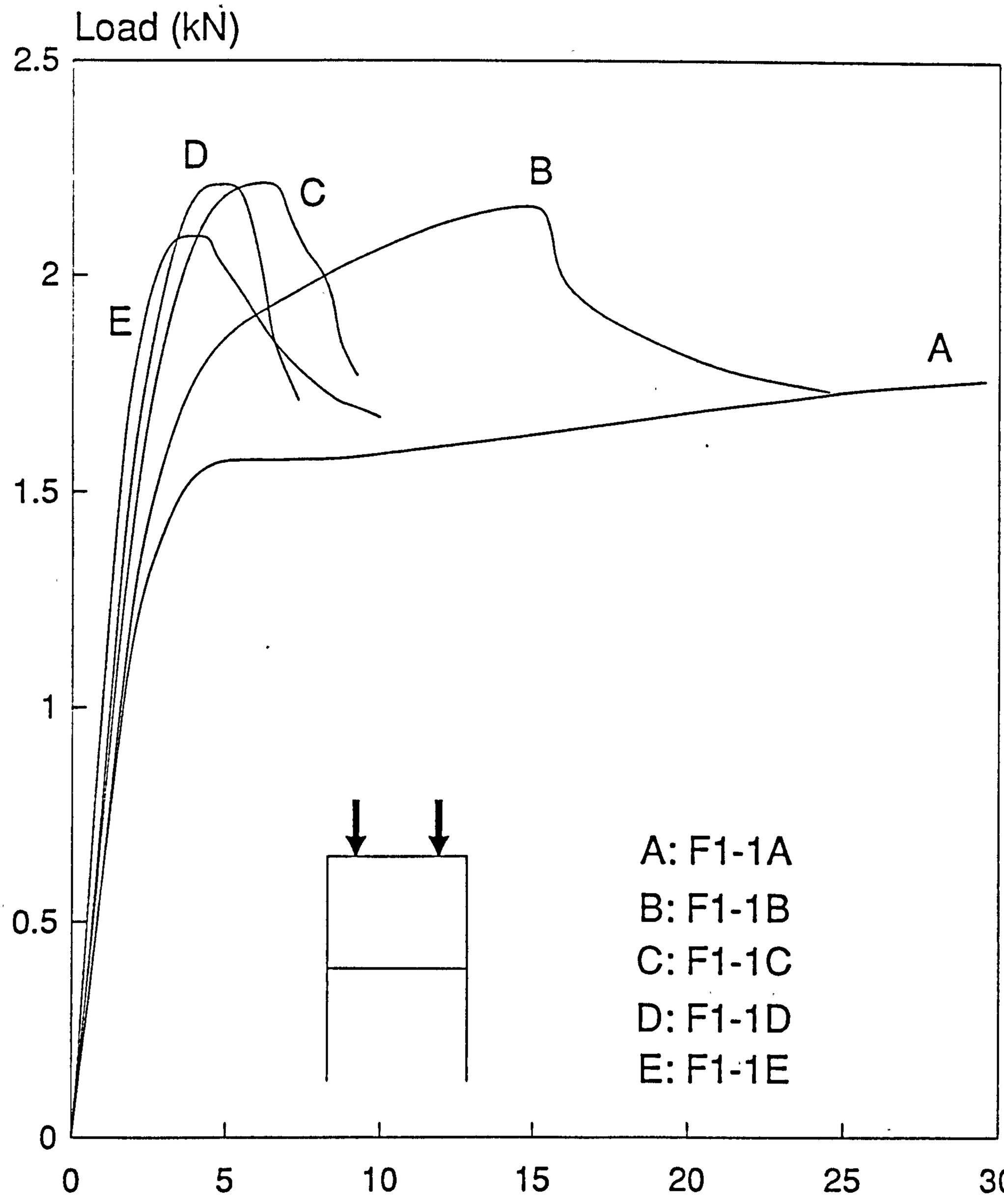

Fig.10.7.10 Frame F1-1A to E experimental plot

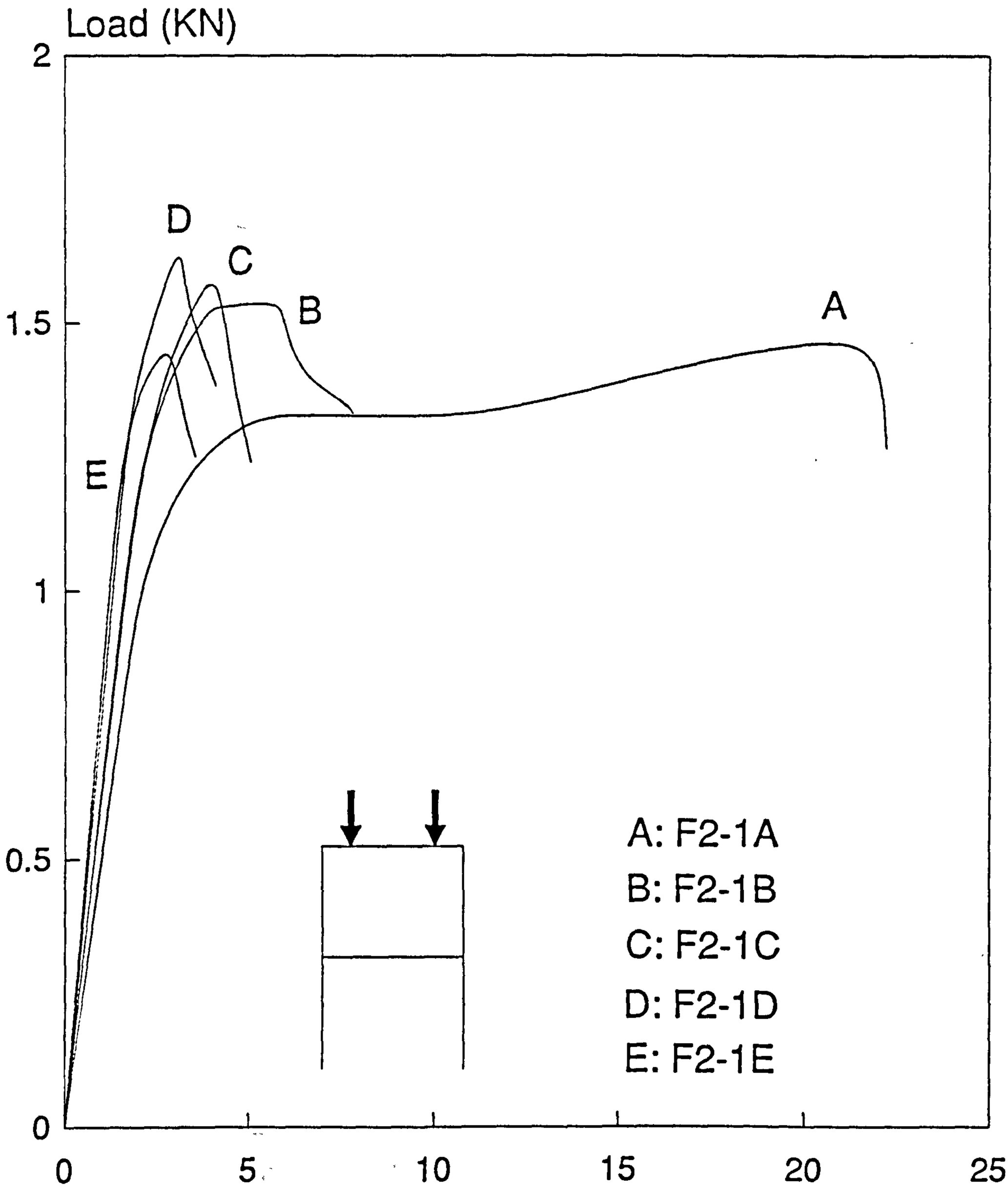

Fig.10.7.11 Frame F2-1A to E experimental plot

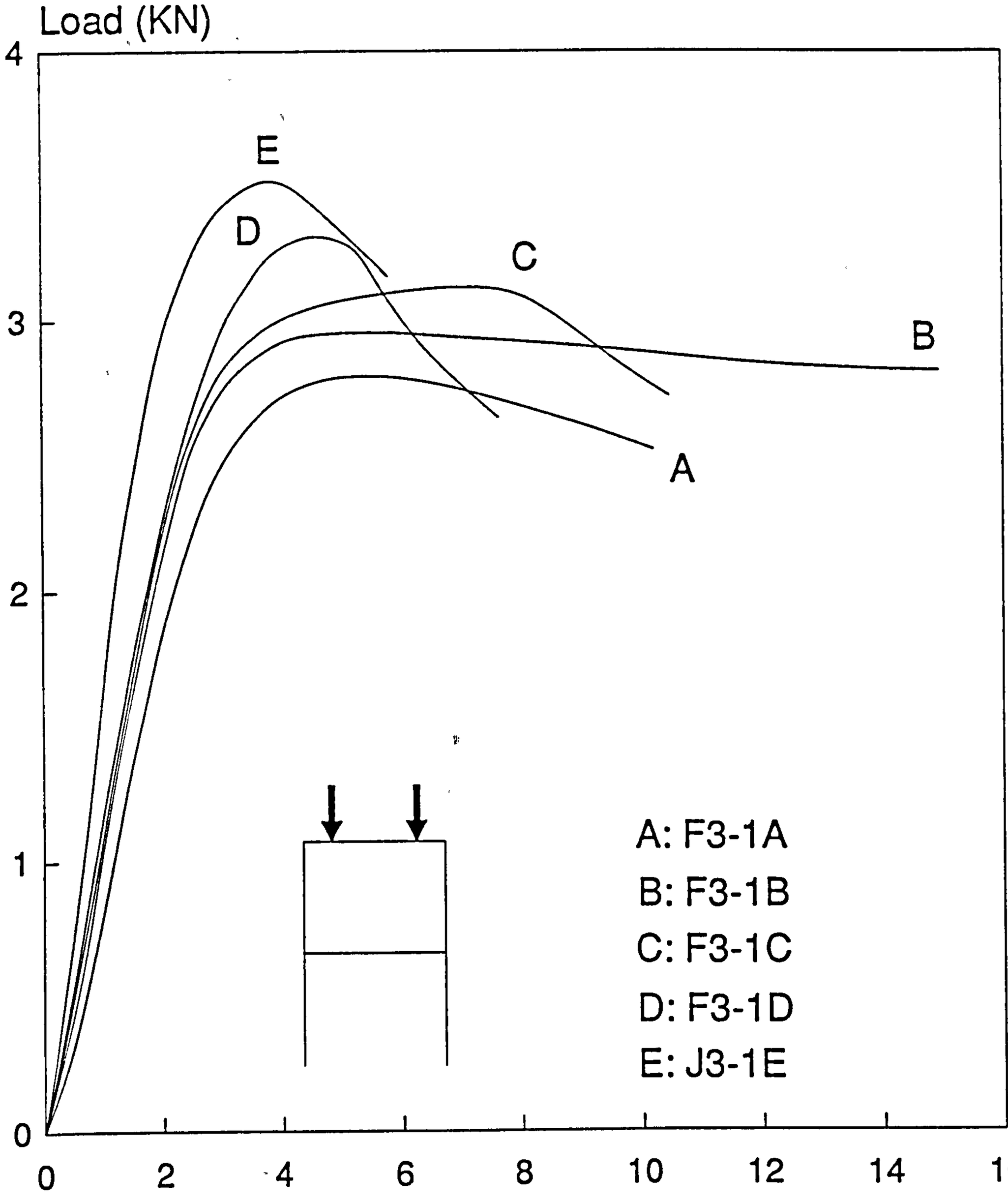

Fig.10.7.12 Frame F3-1A to E experimental plot

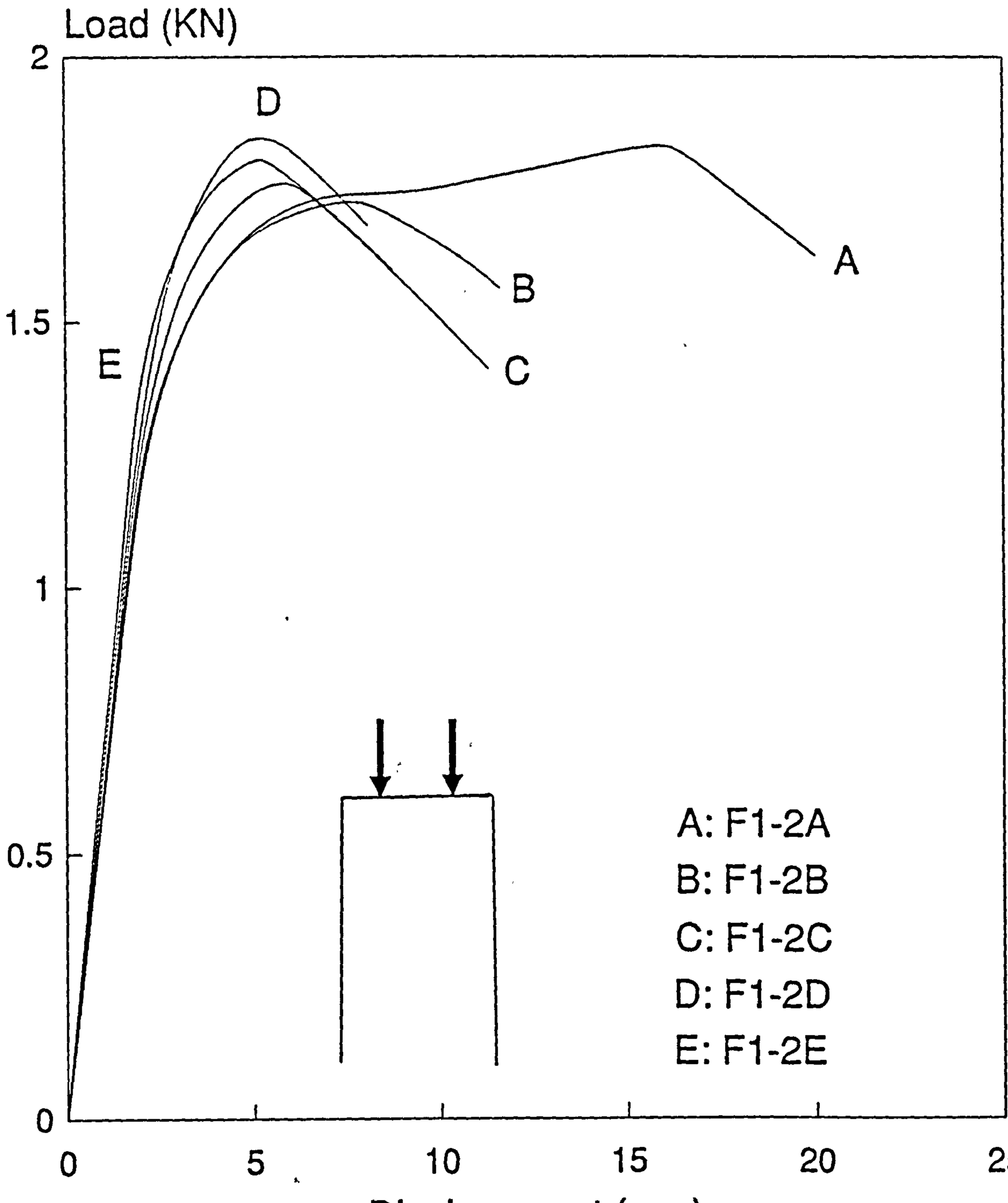

Fig.10.7.13 Frame F1-2A to E experimental plot

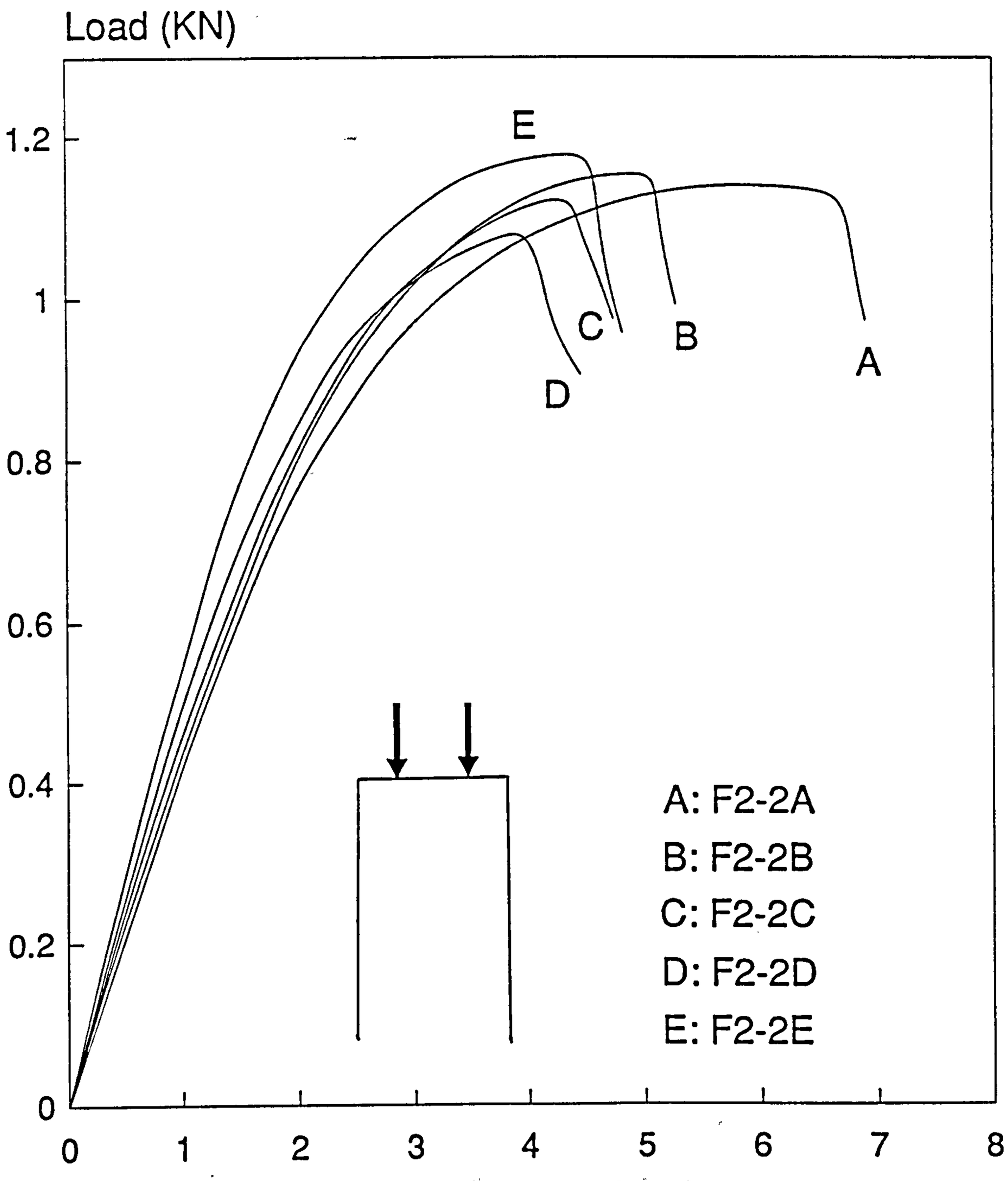

Fig.10.7.14 Frame F2-2A to E experimental plot

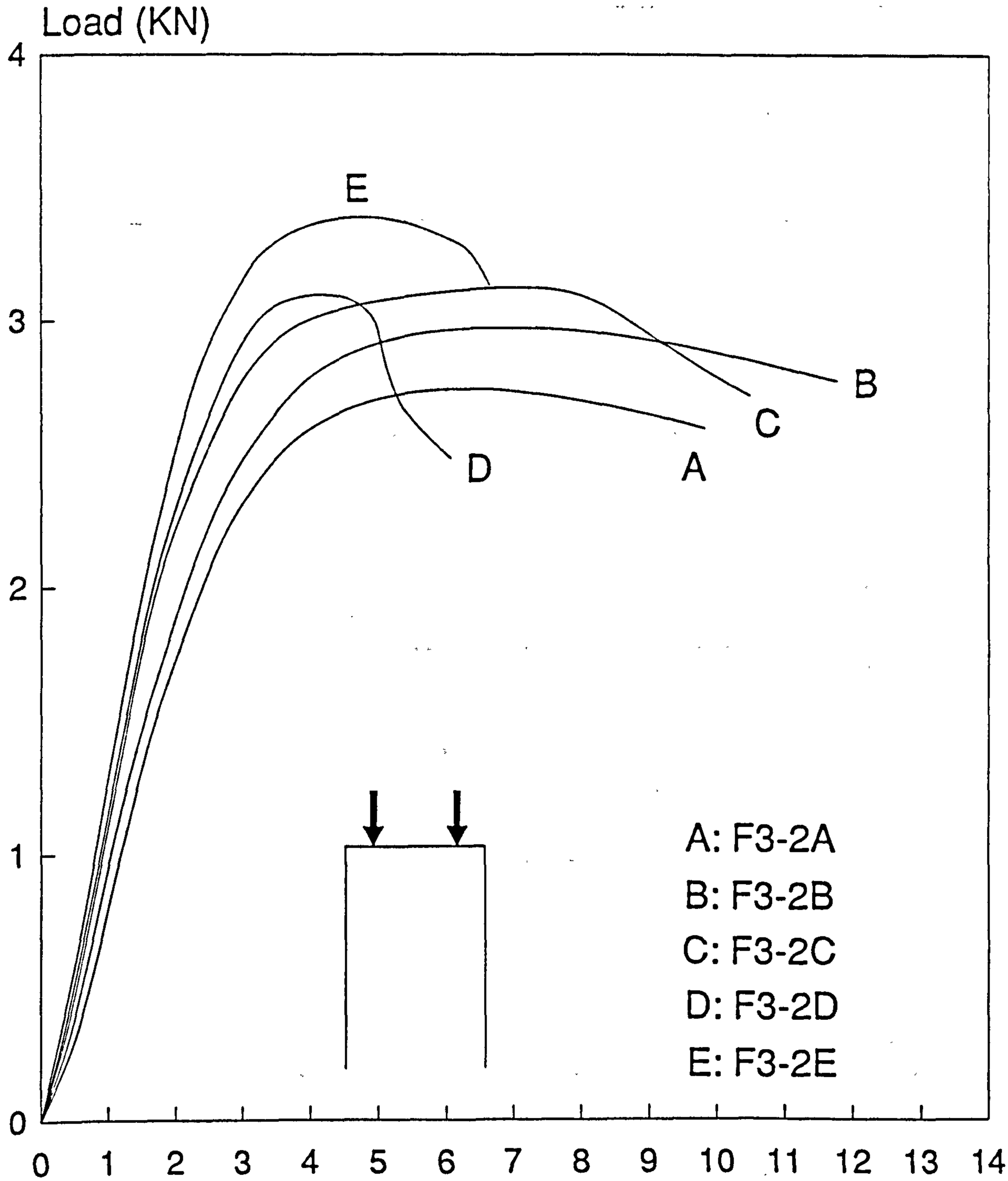

Fig.10.7.15 Frame F3-2A to E experimental plot

Framework No.	Column b_1	Column b_2	Beam b_1	Beam b_2	t	Connection Type	σ_y (N/mm^2)
F1-1A	29	14	27	14	1.000	J1-1A	295
F1-1B	29	14	27	14	1.000	J1-1B	295
F1-1C	29	14	27	14	1.000	J1-1C	295
F1-1D	29	14	27	14	1.000	J1-1D	295
F1-1E	29	14	27	14	1.000	J1-1E	295
F1-2A	29	14	27	14	1.000	J1-1A	295
F1-2B	29	13	27	13	1.000	J1-1B	295
F1-2C	29	13	27	13	1.000	J1-1C	295
F1-2D	29	13	27	13	1.000	J1-1D	295
F1-2E	29	13	27	13	1.000	J1-1E	295
F2-1A	27	15	25	15	0.700	J2-1A	295
F2-1B	27	15	25	15	0.700	J2-1B	295
F2-1C	27	15	25	15	0.700	J2-1C	295
F2-1D	27	15	25	15	0.700	J2-1D	295
F2-1E	27	15	25	15	0.700	J2-1E	295
F2-2A	28	14	25	15	0.590	J2-2A	316
F2-2B	28	14	25	15	0.590	J2-2B	316
F2-2C	28	14	25	15	0.590	J2-2C	316
F2-2D	28	14	25	15	0.590	J2-2D	316
F2-2E	28	15	25	15	0.590	J2-2E	316
F3-1A	27	25	25	25	0.835	J3-1A	298
F3-1B	27	25	25	25	0.835	J3-1B	298
F3-1C	27	25	25	25	0.835	J3-1C	298
F3-1D	27	25	25	25	0.835	J3-1D	298
F3-1E	27	26	25	25	0.835	J3-1E	298
F3-2A	27	25	25	25	0.835	J3-1A	298
F3-2B	27	25	25	25	0.835	J3-1B	298
F3-2C	27	25	25	25	0.835	J3-1C	298
F3-2D	27	25	25	25	0.835	J3-1D	298
F3-2E	27	25	25	25	0.835	J3-1E	298

All dimensions in *mm* unless otherwise stated.

Table 10.2.1 Frameworks with Their Respective Connections and Member Details

Framework No.	$C_o(mm)$	$D_o(mm)$
F1-1A	0.1	negligible
F1-1B	0.1	
F1-1C	0.3	
F1-1D	0.3	
F1-1E	0.1	
F1-2A	0.5	negligible
F1-2B	0.2	
F1-2C	0.2	
F1-2D	0.2	
F1-2E	0.1	
F2-1A	0.1	negligible
F2-1B	0.1	
F2-1C	0.5	
F2-1D	0.1	
F2-1E	1.0	
F2-2A	1.0	negligible
F2-2B	1.5	
F2-2C	1.0	
F2-2D	1.0	
F2-2E	0.5	
F3-1A	3.0	2.5
F3-1B	2.5	2.5
F3-1C	3.0	3.0
F3-1D	1.5	3.0
F3-1E	2.0	2.5
F3-2A	4.0	3.0
F3-2B	3.0	3.0
F3-2C	4.0	2.5
F3-2D	3.0	2.5
F3-2E	2.0	3.0

Table 10.2.2 Initial Imperfection Amplitude of Columns

Framework No.	P_{ex} (*KN*)	Failure Mode
F1-1A	1.800	I
F1-1B	2.149	II#
F1-1C	2.184	II
F1-1D	2.184	II
F1-1E	2.064	II
F1-2A	1.833	I
F1-2B	1.703	II*
F1-2C	1.743	II*
F1-2D	1.833	II*
F1-2E	1.784	II
F2-1A	1.449	I
F2-1B	1.516	II
F2-1C	1.551	II
F2-1D	1.603	II
F2-1E	1.420	II
F2-2A	1.128	I
F2-2B	1.146	II
F2-2C	1.113	III
F2-2D	1.068	III
F2-2E	1.163	II
F3-1A	2.765	I
F3-1B	2.916	I
F3-1C	3.088	III
F3-1D	3.277	II
F3-1E	3.478	II
F3-2A	2.716	I
F3-2B	2.943	IV
F3-2C	3.153	IV
F3-2D	3.057	IV*
F3-2E	3.456	IV

Partial deformation of top connections.

* Significant twisting of framework.

Table 10.7.1 Various Framework Failure Modes

CHAPTER 11

EXPERIMENTAL RESULTS

AND

COMPARISON WITH THEORY

The results of the framework experimental investigation are shown graphically and numerically, and compared, where relevant, with the theoretical predictions. Before discussing the results, some explanation of the abbreviations used in the graphs and tables are necessary and they are as follows :

LB: Local buckling.

LB (BE) N ele: Local buckling is accounted for using the first approximation method, i.e., treating the element as a beam element (see Section 5.5 of Chapter 5). The framework is modelled using N elements. The various element configuration of the framework can be found in figures 9.3.2 and 9.3.3 of Chapter 9.

LB (CE) N ele: As above but treating local buckling using the second approximation method, i.e., assuming uniform compression (see Section 5.6 of Chapter 5).

LB (CE2) N ele: As above but the actual length is multiplied by the α factor to account for torsional flexural buckling as detailed in Section 7.5 of Chapter 7.

The experimental and various theoretical predictions of the load- displacement results for individual framework are shown in figures 11.1 to 11.30. In all the load-displacement plots, the y and x axes represent the load at one of the loading point and the corresponding vertical displacement of that point respectively.

Beginning with framework series F1-1, it can be seen from figure 11.1, for framework F1-1A, that although curve 4 gives the best fit, the other curves also represent the experimental result rather well. The theoretical prediction obtained by treating local buckling using the first approximation method is almost the same as that for no local buckling. This is so because for the cross sectional geometry of the members, there is very little local buckling. However, by using the second

approximation method to account for local buckling, a smaller effective width will be obtained. This resulted in the formation of hinges at the loading points of the beam at a lower load. From this point onwards, the frame stiffness is reduced and failure occurred at a slightly lower load. For framework F1-1B, it can again be observed from figure 11.2 that the difference between curves 1,2 and 3 is marginal. However, the displacement at failure is about 75% higher than that of the experiment. This is due to the partial deformation of the top connections. As before, treating local buckling assuming uniform compression for the elements resulted in a slightly lower collapse load. The use of the second approximation method for local buckling underestimated the collapse load for frameworks F1-1C and F1-1D, as illustrated in figures 11.3 and 11.4 respectively. The framework stiffness after the simultaneous formation of hinges at the top beam is also lower. For both the frameworks, curve 1,2 and 3 represent the experimental result better than curve 4. Like the above case, there is only a slight difference between curves 1,2 and 3. Although still acceptable, curves 1,2 and 3 predicted a higher collapse load for framework F1-1E as shown in figure 11.5. Curve 4 agrees with the experimental result rather well and gives a better prediction of the collapse load.

Because of the full flat width-to-thickness ratio of both the stiffened and unstiffened elements of the members, especially the latter, the theoretical prediction with no local buckling over estimated the collapse load for all the frameworks of series F2-1, as illustrated in figures 11.6 to 11.10. This over estimation averages to about 20%. When the basic number of elements are used to model the framework and the first approximation method is employed to treat local buckling, the average over estimation drops to about 4%. Increasing the numberof elements to 18 brought this figure up to about 18%. Although increasing the number of elements gives a more correct analysis, a higher collapse load, compared to the analysis using the basic number of elements, is obtained because as mentioned in Chapter 5, the maximum compressive stress of the element is used to compute the effective width. Hence,

for a member consisting four elements and with a linearly varying stress, the effective width is computed for each element using the maximum compressive stress in that element. This will result in the member comprising of four elements, each being prismatic but with different cross sectional properties. On the other hand, for the same member subjected to the same loading as above and modelled by a single element, using the maximum compressive stress to compute the effective width will result in a prismatic element with a cross section property that is equal to the smallest of the four elements of the first case. Therefore, the overall framework stiffness is reduced and this will lead to a lower failure load for the basic number of element analysis.

As explained earlier, for the same number of elements, in this case 18, using the second approximation method to treat local buckling will lead to a lower collapse load compared to when the first approximation method was used. This phenomenon is demonstrated by curve 4 of figures 11.6 to 11.10. For framework F2-1C and F2-1D, besides giving a lower collapse load, the stiffness after formation of the first set of hinges at the top beam is very much lower compared to the experimental results. Hence, for framework series F2-1, although predicting an accurate collapse, curve 4 underestimates the stiffness at higher loads. Having said that, curve 2, which represents the basic number of elements analysis, also gives a rather reasonable representation of the experimental results generally.

For framework series F3-1, the difference between curves 1 and 2 is very significant as illustrated in figures 11.11 to 11.15, due to the effects of local buckling. This effect caused the first set of hinges at the loaded beam to occur at a load of about 30% lower than when no local buckling was considered. For the same reason, the collapse load predicted by curve 2 dropped drastically to a value closer to the experimental collapse load. However, the displacement at collapse is over estimated and for framework F3-1A, this over prediction amounts to about 400%. As

explained before, using the more correct model of 18 elements resulted in a higher collapse load compared to the 8 element analysis. Except for framework F3-1E, using the second approximation method for local buckling did not produce a good enough collapse load prediction as indicated by curve 4.

By adopting the procedures outlined in Section 7.5 of Chapter 7, it was found that for the column length and cross sectional geometry, torsional flexural buckling is the critical mode for the columns of the F3-1 framework series. Hence, by multiplying the appropriate α factors, which were obtained assuming no warping restraint, to the actual column lengths and using them for analysis, the theoretical prediction obtained is represented by curve 5 of figures 11.11 to 11.15. It can be seen that for all the frameworks, a closer agreement with the experimental results is obtained. This is attributed to the overall reduction of the framework stiffness. In a general sense, although curve 5 has a better agreement compared with the experimental results, the collapse load predicted by curve 2 is slightly better.

The various theoretical predictions for individual framework of framework series F1-2, as illustrated in figures 11.16 to 11.20, is rather similar to those of framework series F1-1 respectively. The reason behind this is due to the almost similar members cross sectional geometry, in which there is very little local buckling. With the exception of framework F1-2A, curve 4 indicates only a marginal reduction in the collapse load for the rest of the frameworks. On the whole, any of the four curves can be used to represent the experimental results.

Similar to framework series F2-1, the large width-to thickness ratio of the elements of the members of series F2-2 frameworks caused a considerable reduction in collapse load compared to the no local buckling analysis, as illustrated in figures 11.21 to 11.25. Again, it is shown that increasing the number of elements from 5 to 13 for the same method of treating local buckling increases the predicted collapse load. When the second approximation method was used, the agreement in both

stiffness and load between curve 4 and the experimental result is improved. Figure 11.22 shows the results of seven different theoretical predictions. As before, curve 1 gives the highest stiffness and load prediction. From curves 2 and 3, it is again observed that increasing the number of elements will give a more correct but higher load prediction. Increasing the number of elements from 9 to 13 resulted in very little difference in the theoretical prediction. When the second approximation method of treating local buckling was employed, the same behaviour can also be observed as illustrated by curves 5,6 and 7. Considering the negligible difference between curves 6 and 7, it was hence decided that 13 and 18 elements are accurate enough to model the single and double storey framework respectively. Figure 11.22 also shows an important feature, i.e., the difference in the theoretical predictions obtained by using the first and second method to treat local buckling. This difference is clearly indicated by comparing curves 3 and 5 or curves 4 and 6. There is quite a significant variation in the collapse load, and the load required to cause formation of the first set of hinges on the beam and the stiffness thereafter.

For framework series F3-2, the various theoretical predictions for individual framework, as shown in figures 11.26 to 11.30, are more or less similar to those of framework series F3-1. To avoid repetition, only the main features will be mentioned. Except for framework F3-2E, curve 5 (with torsional flexural buckling included) over estimated the collapse load rather significantly. The prediction using the basic number of elements actually gave the best load prediction. However, the displacement at failure is rather high compared to the experiment.

Figure 11.28 shows the effects of excluding the torsional flexural buckling in the analysis. The best agreement between the theoretical and experimental results is reflected by the analysis which employs the second approximation method to treat local buckling. However, both the stiffness and collapse load are nowhere near the experimental result. The effects of considering torsional flexural buckling is shown

in figure 11.28a. For curves 4 and 6, the α factors were obtained assuming full warping restraint at the ends of the column. This will produce an α factor that is smaller compared to the case when no warping restraint is assumed. The resulting outcome can be seen very obviously by comparing curves 4 and 5 or curves 6 and 7. There is a significant reduction in both the stiffness and collapse load when assuming no warping restraint. Also shown, increasing the number of elements from 13 to 23 did not improve the prediction significantly. In fact, the improvement is so little that it can be ignored. Figure 11.28a also shows that curve 5 can be used as an approximate prediction when there is torsional flexural buckling of the column.

Although the comparisons between the various theoretical and experimental failure loads have been discussed, they were only touched upon briefly. The following gives a more specific comparison. The average values mentioned below were computed from table 11.3, which tabulates the ratio of the various theoretical collapse load to the experimental collapse load. These loads are in turn tabulated and shown in tables 11.1 and 11.2.

The various predicted and experimental collapse loads for framework series F1-1 are plotted against the connection initial stiffness of the respective framework as shown in figure 11.31. As expected, the analysis without local buckling gave the greatest average difference of about 7%. On the other hand, using the second method to account for local buckling resulted in the best prediction. Except for framework F1-1A, where the prediction was exact, the collapse load for the rest of the framework were in fact slightly underestimated. The average under estimation is only about 1.5%. A point worth mentioning is that both the experiment and the theoretical prediction indicated a reduction in the collapse load when the most stiff connections, type E, were used.

The phenomenon just mentioned is also true for framework series F2-1 as illustrated in figure 11.32. On an average basis, the prediction given by the basic number of element analysis is around 4% higher. This is only marginally better than the 5% obtained from the analysis using 18 elements and the second approximation method to treat local buckling. Without local buckling, the predicted average over estimation is about 20%.

For framework series F3-1, because of the greater tendency for the members to buckle locally, the analysis without local buckling over predicted by 42% on average. This error is reduced to about 8% when torsional flexural buckling of the column is accounted for. Not surprisingly, the use of the basic number of elements model resulted in an over prediction of about only 1.5%. From figure 11.33, the experimental results indicate an increase in the collapse load for framework with the thickest connection, i.e., F3-1E. This behaviour is in contrast with that of framework series F1-1 and F2-1.

Illustrated in figure 11.34 and mentioned in Chapter 10, the reduction in the experimental failure load for frameworks F1-2B, F1-2C and F1-2D compared to F1-2A was due to the severe out of plane distortion or twisting of the framework during testing. Nevertheless, the experimental collapse load for F1-2E, when compared to framework F1-2A, seems to indicate that the reduction of the collapse load when the thickest connection is used is possible. Due to the low full flat width-to-thickness ratios, the average over prediction of the collapse load from the no local buckling, 5 and 13 elements theoretical predictions are 12.6%, 10.3% and 6.9% respectively.

As illustrated in figure 11.35 for framework series F2-2, the unsymmetrical mode of failure resulted in a reduction of the experimental failure load for frameworks F2-2C and F2-2D. Hence, it is not possible to ascertain experimentally whether there is a drop in failure load when the thickest connections were used. However,

all the various theoretical results showed a very slight increase in the collapse load for framework F2-2E compared to F2-2D. The computed average over prediction in the collapse load are 40%, 7.4% and 0.3% for the no local buckling, 5 and 13 elements theoretical analysis respectively.

For framework series F3-2, where failure was affected by torsional flexural buckling of the columns, except for framework F3-2A which failed in mode I, figure 11.36 shows that the no local buckling collapse loads are very much higher then the experimental results. These errors average to about 41%. Because of the conservativeness resulting from the basic number of elements model, the average over prediction of about 3% is much better than the 11% obtained from the analysis considering torsional flexural buckling of the columns.

In order to study the effects of initial imperfection on the behaviour of the frameworks, theoretical analyses were performed for framework F2-2B. This framework was chosen because there is significant local buckling of the members. Furthermore, the stiffness of the connections used is approximately between fully fixed and fully pinned. Moreover, the framework collapsed purely in mode II without any other significant or noticeable unaccounted effects. In the theoretical analysis, the framework was modelled using 13 elements. Loading of the framework was similar as before. Besides initial imperfection, the analysis was carried out with (using the first approximation method) and without consideration of local buckling. For the latter, the loads at one of the loading point and the corresponding vertical deflections are plotted and shown in figure 11.37. The initial imperfection is expressed as a ratio of the column length. From the figure, it is shown that as the initial imperfection is increased, both the stiffness and collapse load reduce drastically. The reserve strength of the framework also decreases rather significantly after the simultaneous formation of hinges at the loading points. When local buckling was considered, effects similar to the above were indicated as illustrated

in figure 11.38. However, for the same degree of initial imperfection, a lower stiffness and collapse load are obtained. The reduction in the collapse load can be seen more clearly from figure 11.39, which shows the reduction in collapse load with respect to the increase in initial imperfection from the two cases of analysis. Table 11.4 shows the percentage change in collapse load for the various degree of initial imperfection when local buckling was considered. It varies non-linearly, as illustrated in figure 11.40, from about 16% to 38% when the initial imperfection ratio is increase from zero to 5% respectively.

The discussion now concentrates on the elastic critical loads of the frameworks studied. As pointed out in Chapter 10, for this analysis, the stresses in the material of the framework are assumed to be remain linearly elastic throughout the loading range and there is no yielding of the material. As such, the stiffness of the connections are assumed to be constant and takes the value of their initial stiffness respectively. As before, the analyses were carried out with (using the first approximation method) and without the consideration of local buckling.

The elastic critical load, referred to as the critical load from here henceforth for convenience, obtained for the six series of framework studied are plotted against the respective connection initial stiffness as shown in figures 11.41 to 11.46. These figures show that without local buckling, the critical load increases non-linearly with respect to the connection initial stiffness. From fully pinned to a stiffness of about 10 *KNmm/rad*, the rate of increase is very low and almost constant in some cases. When the connection stiffness is further increased to about 10 *MNmm/rad*, the critical load increases non-linearly till a point where the increase is almost negligible. In fact, after about 100 *MNmm/rad*, the critical load remains constant.

When local buckling was considered, depending on the local buckling potential of the members, the variation of the critical load against the connection stiffness is rather different. Firstly, considering the double storey frameworks, it can be seen

from figures 11.41, 11.43 and 11.45 that the critical load decreases when the connection stiffness is increased. For a particular connection stiffness, the amount of reduction in the critical load compared to without local buckling is different for each framework. This behaviour is illustrated in a clearer manner in figure 11.47, which shows the percentage reduction in the critical load, compared to the no local buckling case, plotted against the connection stiffness for the double storey frameworks. It is rather obvious that as the local buckling potential of the members of the framework increases, the percentage reduction in the critical load increases non-linearly with respect to the connection stiffness.

Another interesting comparison can be made from figure 11.48, which shows the percentage change in the critical load compared to the critical load with fully pinned connections, plotted against the connection stiffness. The negative sign on the y axis indicates a reduction in the critical load. The purpose of this plot is to show, in a clearer form, the variation of the reduction of the critical load of the double storey framework series when the connection stiffness is increased.

For the single storey framework series, figures 11.42, 11.44 and 11.46 show that, compared to the no local buckling case, there is a reduction in the critical load for a particular connection stiffness. To compare this reduction, figure 11.49 is used. Similar to the double storey framework series, the percentage reduction in the critical load increases in a non-linear fashion with respect to the connection stiffness. For a particular connection stiffness, when the local buckling potential of the members of the framework is higher, the percentage reduction in the critical load is also higher.

As to the variation of the critical load with the connection stiffness, figure 11.42 shows that instead of decreasing, the critical load increases very slowly when the connection stiffness in increased. This is due to the very slight local buckling of the members of the framework. On the other hand, for framework series F2-2 and

F3-2, figures 11.44 and 11.46 respectively show that as the connection stiffness is increased, the critical load reduces very slowly up to a certain connection stiffness. After that, there is a very small increase till a point where the critical load remains constant with further increase in the connection stiffness. This behaviour can be studied more clearly from figure 11.50, which, as in the double storey framework series, shows the percentage change in the critical load compared to that when fully pinned connections are used, plotted against the connection stiffness. An interesting behaviour noted is that depending on the local buckling potential, the critical load of the framework can either increase or decrease and then increase again as the connection stiffness increases.

In order to confirm the behaviour just mentioned, further theoretical analyses were carried out on a series of framework having the cross sectional geometry as shown in table 11.7. Except for these dimensions, which apply to both the beam and the columns, and the same yield stress assumed for all the frameworks, everything else remained unchange. The stiffened element width is kept constant but that of the unstiffened element is varied. The purpose of this is to vary the local potential of the members of the frameworks. As before, the critical load obtained were plotted against the connection stiffness as shown in figures 11.51 to 11.57. The critical load for no local buckling increases non-linearly with respect to the connection stiffness as before. With the consideration of local buckling, except for framework F10-5-1 where there is no local buckling of the members, there is a reduction of the critical load for a particular connection stiffness. This reduction is shown in figure 11.58. It can be seen that the pattern of the reduction of the critical load is similar to that of both the single and double storey framework series discussed earlier. As to the variation of the change in the critical load, compared to when fully pinned connections were used, with the stiffness, figure 11.59 indicates that the interesting behaviour discussed earlier is true. For framework 10-5-1, the critical load increases with respect to the connection stiffness. Framework F10-10-1, whose

members have very little local buckling potential, exhibits the same behaviour. However, for frameworks F10-14-1, F10-16-1, F10-18-1 and F10-20-1, the critical load decreases initially and then starts increasing at a certain connection stiffness. As for framework F10-30-1, whose members have the greatest local buckling potential, there is no increase in the critical load when the connection stiffness is increased. This behaviour did not occur in any of the original frameworks studied. However, from this theoretical investigation, it has been demonstrated that the variation of the critical load with the connection stiffness depends on the local buckling potential of the members of the framework.

The final part of this discussion will focus on the comparison of the elastic critical loads with the experimentally obtained failure loads of the original frameworks studied. These loads are tabulated as shown in table 11.10. The fifth column compares the critical load of the no local buckling case with that of the local buckling case. This comparison has been dealt with earlier and will not be repeated here. The ratio of the critical load without local buckling to the experimental failure load is given in the sixth column. Due to local buckling, the critical load is always higher than the experimental value. Except for framework series F1-2, the average over prediction is greater than 100%. However, when local buckling was considered, the critical load reduces rather drastically, especially for those frameworks with members of high local buckling potential. For framework series F2-2, the maximum average over prediction of the analysis is only about 13%, which is rather good. The reason for this low value is because of the cross sectional geometry of the members, which gives the framework the lowest overall stiffness compared to the other framework series. Hence, elastic instability will occur at a lower load. Moreover, the rather high local buckling potential of the members resulted in a further reduction of the critical load.

In order to have an overall picture of the load-displacement curves of the elastic instability and collapse load analyses compared with the experimental results, framework F2-2A was chosen as an example. Because of the rather low elastic critical loads, a more proportional plot can be obtained and this is illustrated in figure 11.60. As expected, curve 1 gives the highest predicted load. Surprising as it may seem, curve 3, which was obtained from the collapse load analysis without consideration of local buckling, resulted in a higher failure load compared to curve 2. To compare the various stiffness, a magnified plot is shown in figure 11.61. It can be seen that curve 1 predicted the highest stiffness because of the constant initial connection stiffness assumed. Curve 2, due to the local buckling effect, indicated a rather significant reduction of the stiffness. The use of the theoretical connection moment-rotation behaviour resulted in a further drop in the stiffness as indicated by curve 3. Curves 4 and 5, which are almost identical, gave the lowest stiffness.

OPTIMUM ANALYSIS PARAMETERS

From the various theoretical predictions as illustrated in figures 11.31 to 11.36 and tables 11.1 to 11.3, the analysis which uses the second approximation method to treat local buckling combined with a sufficient number of elements, 13 and 18 for the single and double storey frameworks respectively, produces the best results when compared to the experiments. However, when torsional flexural buckling of the columns is critical, the effective length multiplier must be used, as in the case of framework series F3-1 and F3-2.

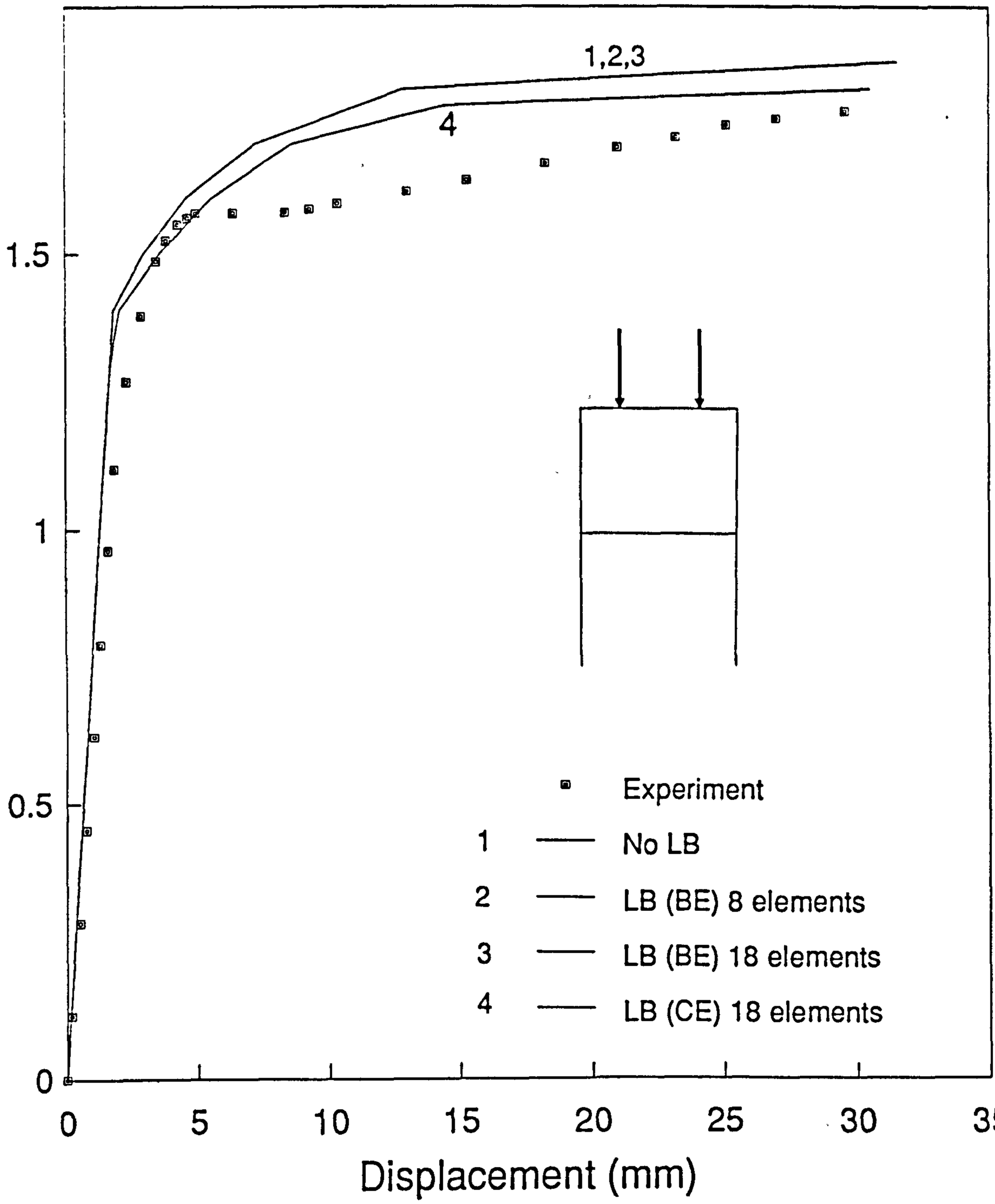

Fig.11.1 Frame F1-1A Load/Displacement plot

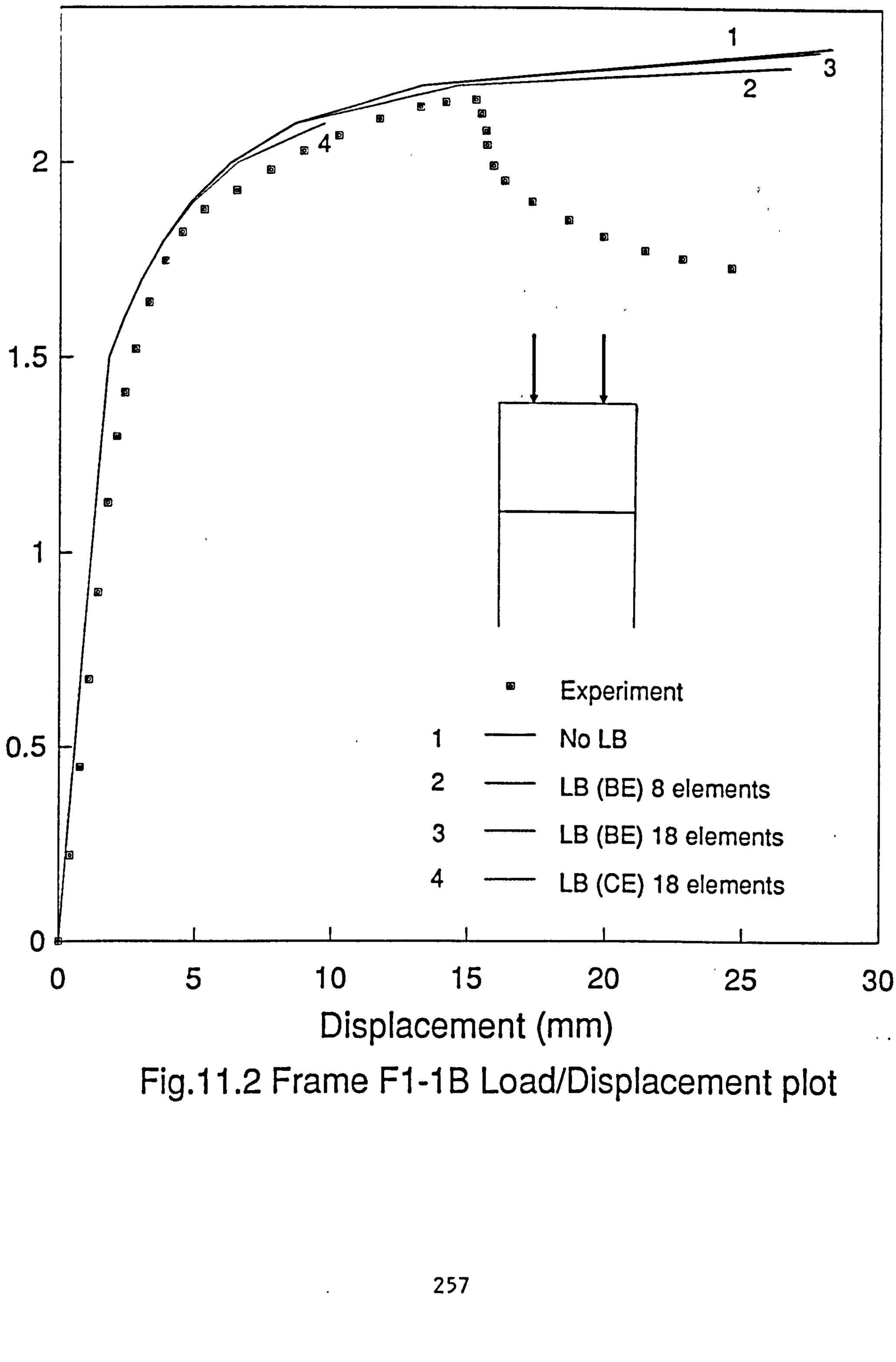

Fig.11.2 Frame F1-1B Load/Displacement plot

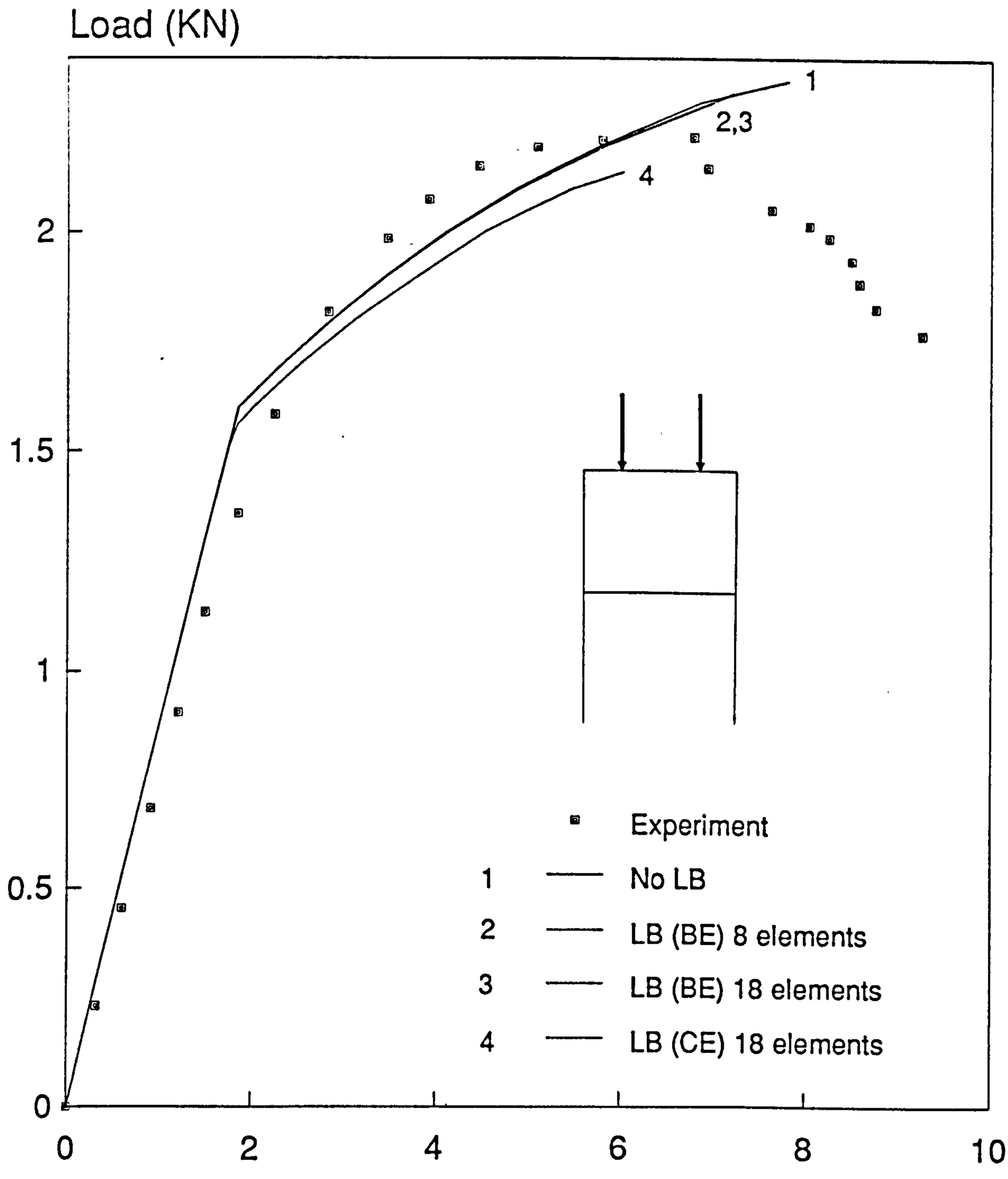

Fig.11.3 Frame F1-1C Load/Displacement plot

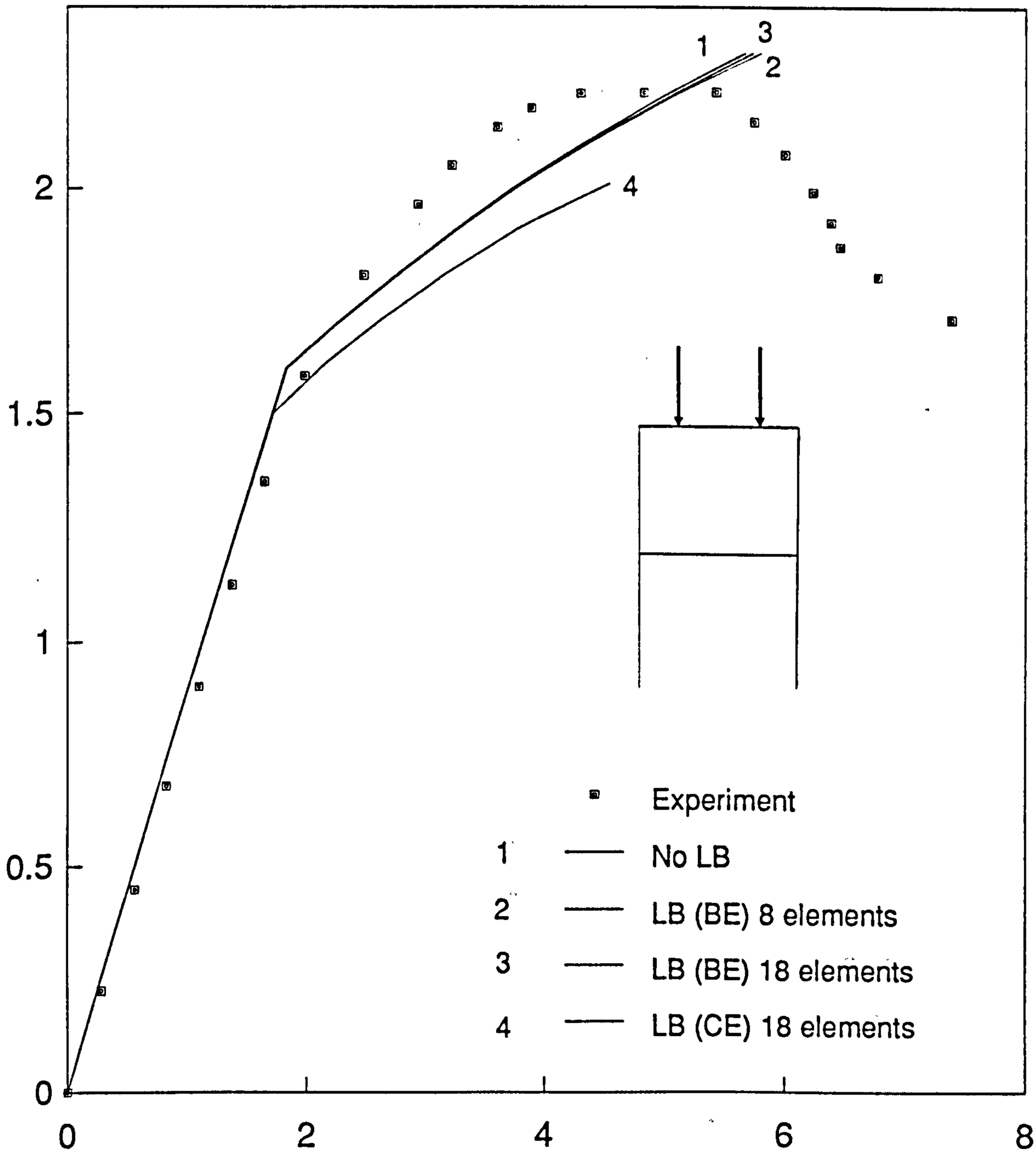

Fig.11.4 Frame F1-1D Load/Displacement plot

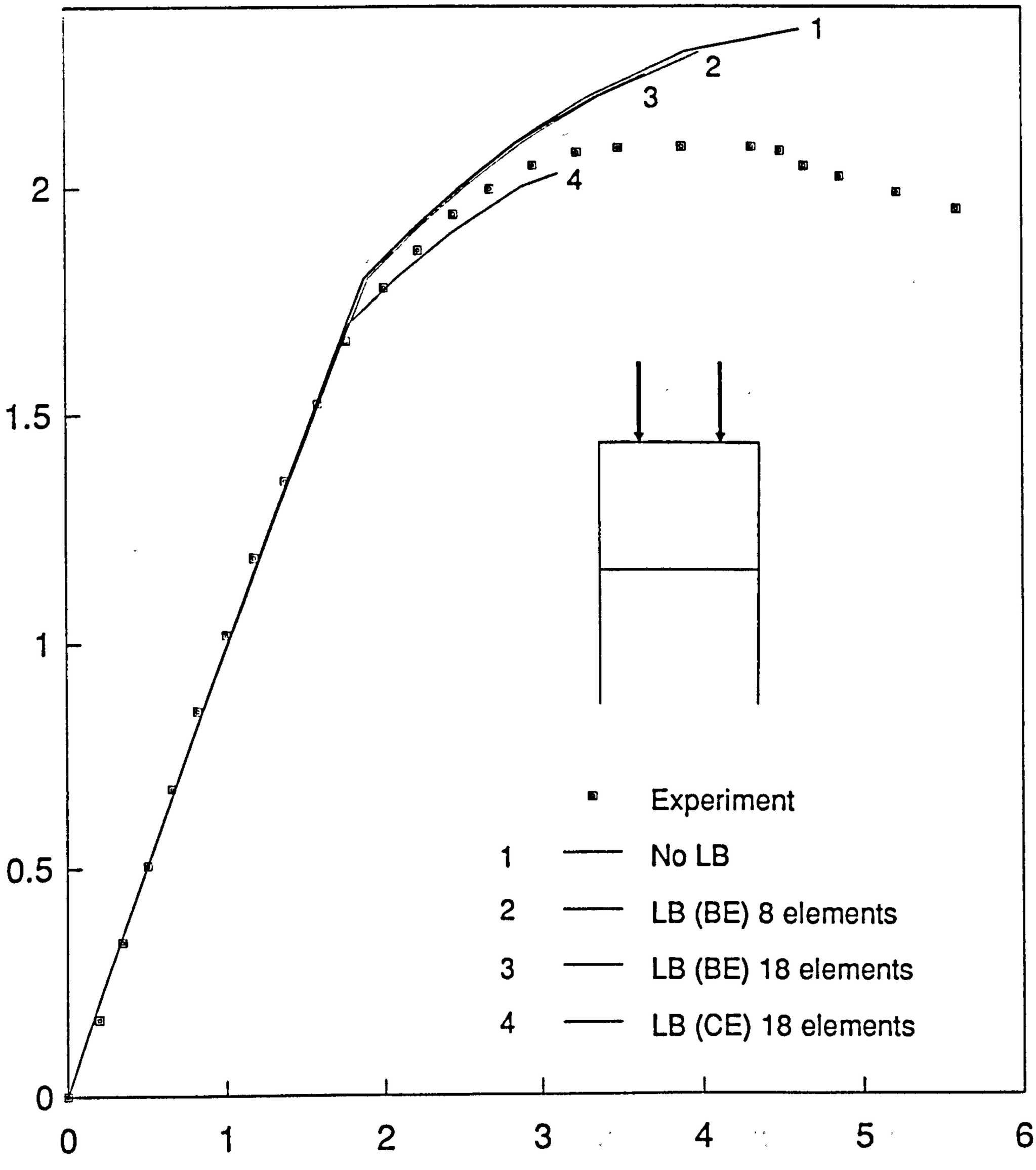

Fig.11.5 Frame F1-1E Load/Displacement plot

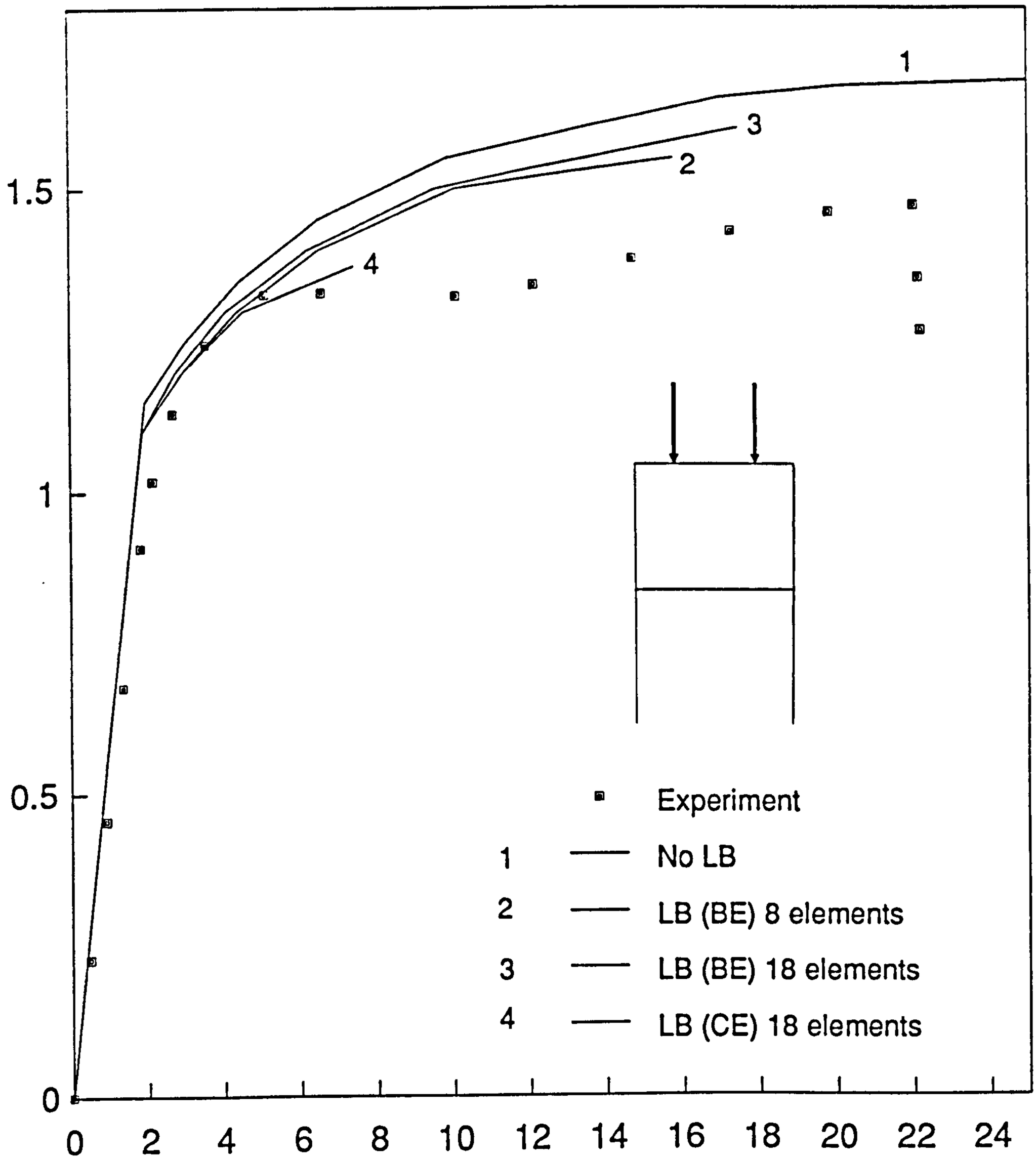

Fig.11.6 Frame F2-1A Load/Displacement plot

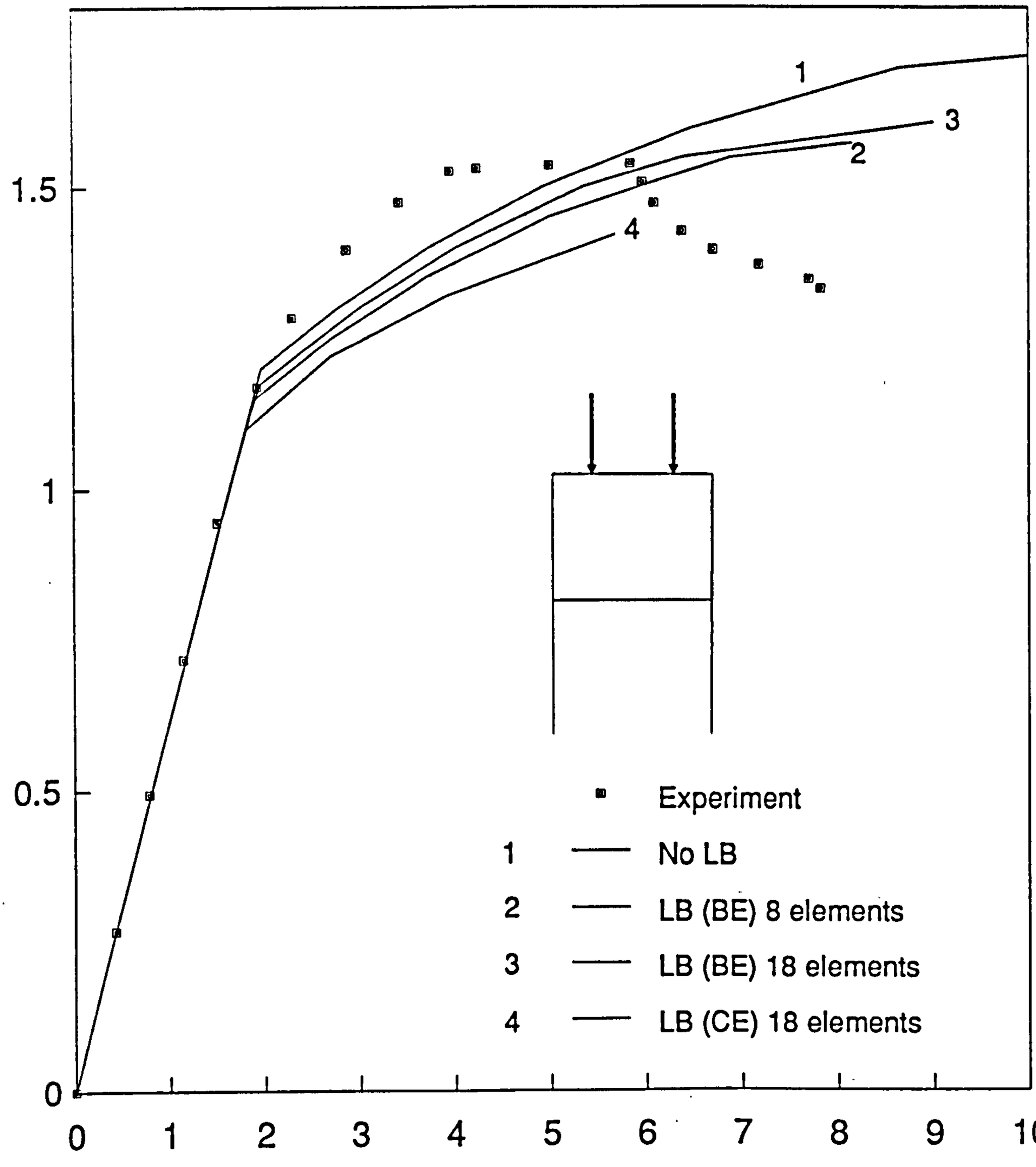

Fig.11.7 Frame F2-1B Load/Displacement plot

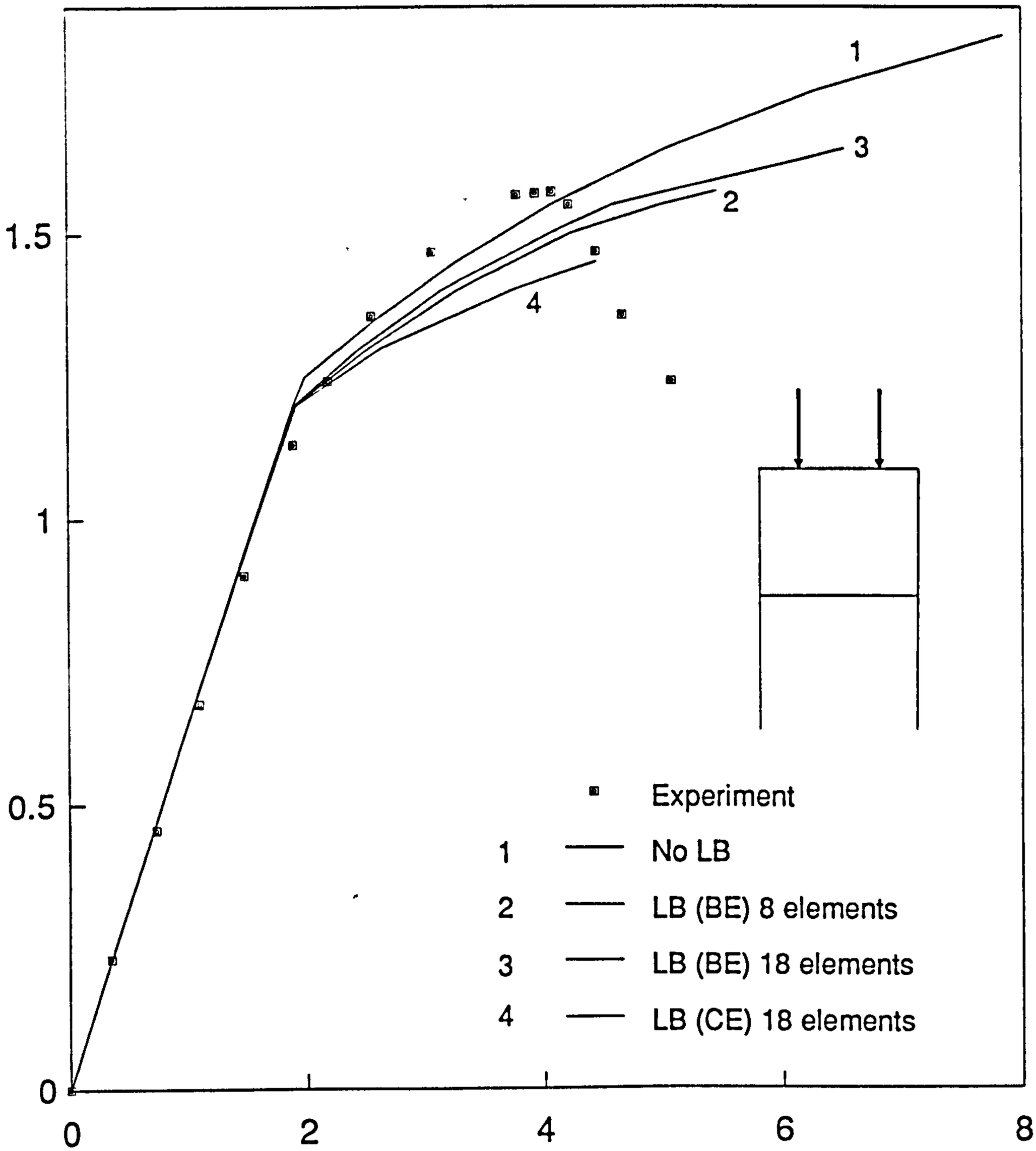

Fig.11.8 Frame F2-1C Load/Displacement plot

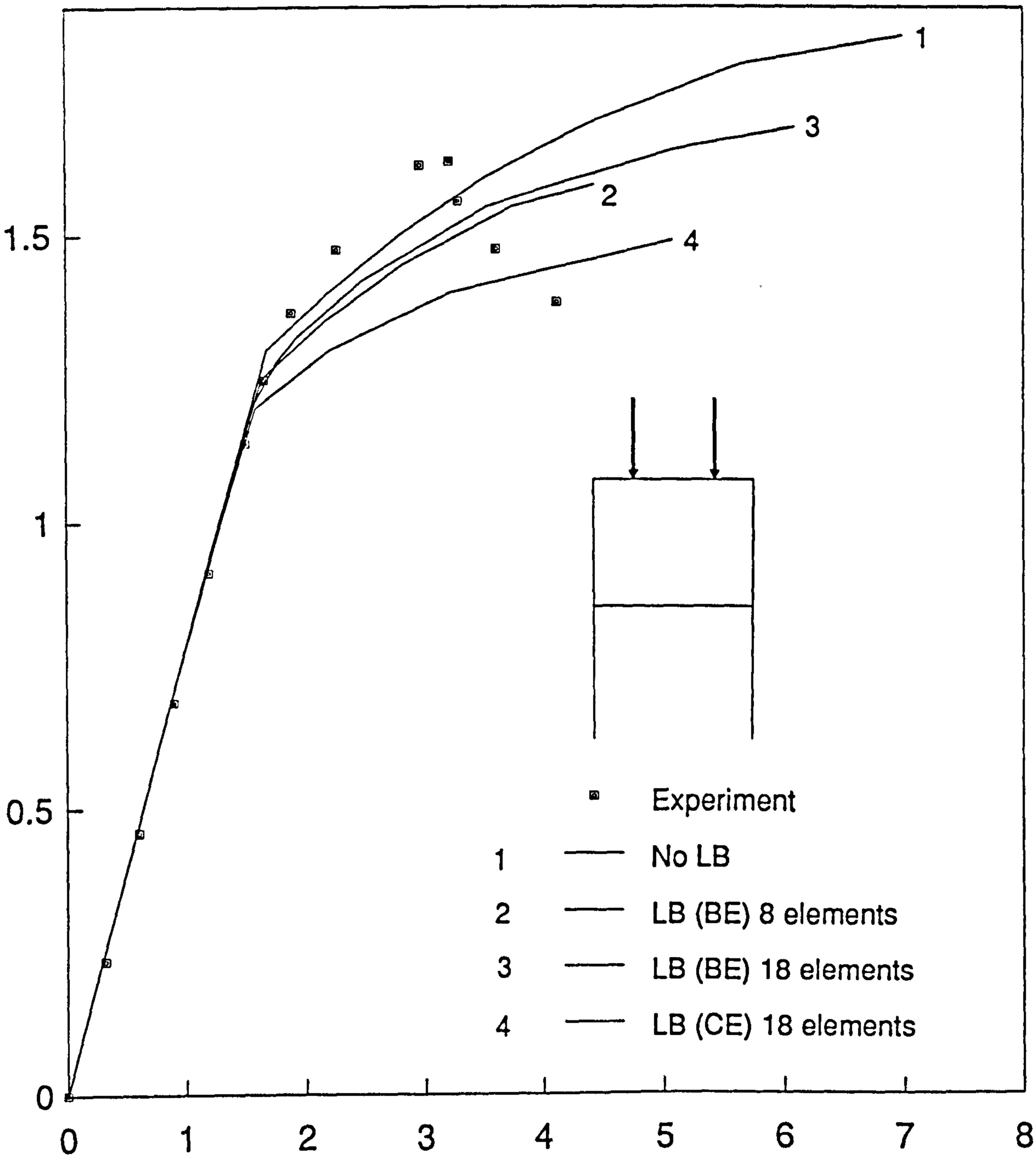

Fig.11.9 Frame F2-1D Load/Displacement plot

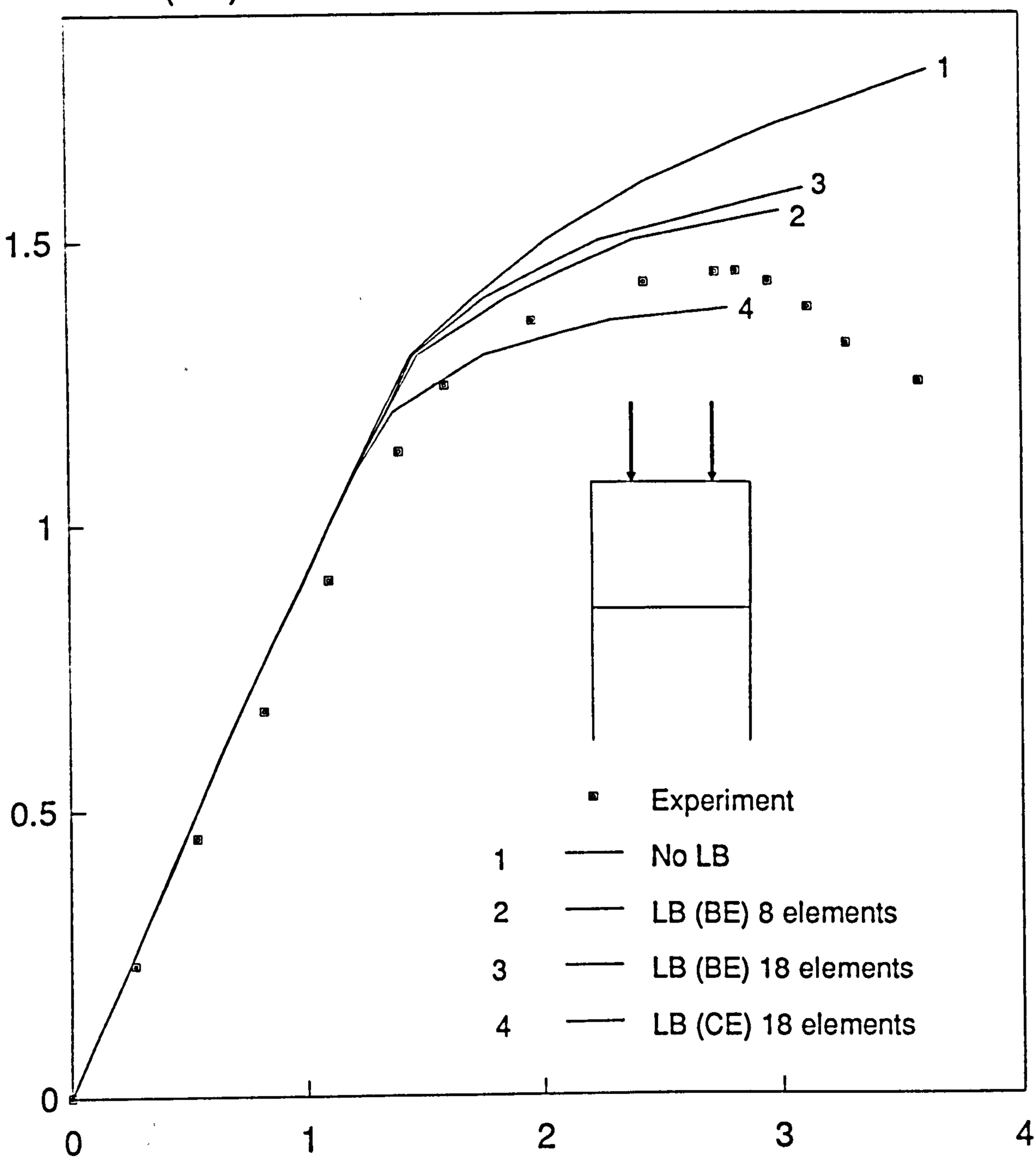

Fig.11.10 Frame F2-1E Load/Displacement plot

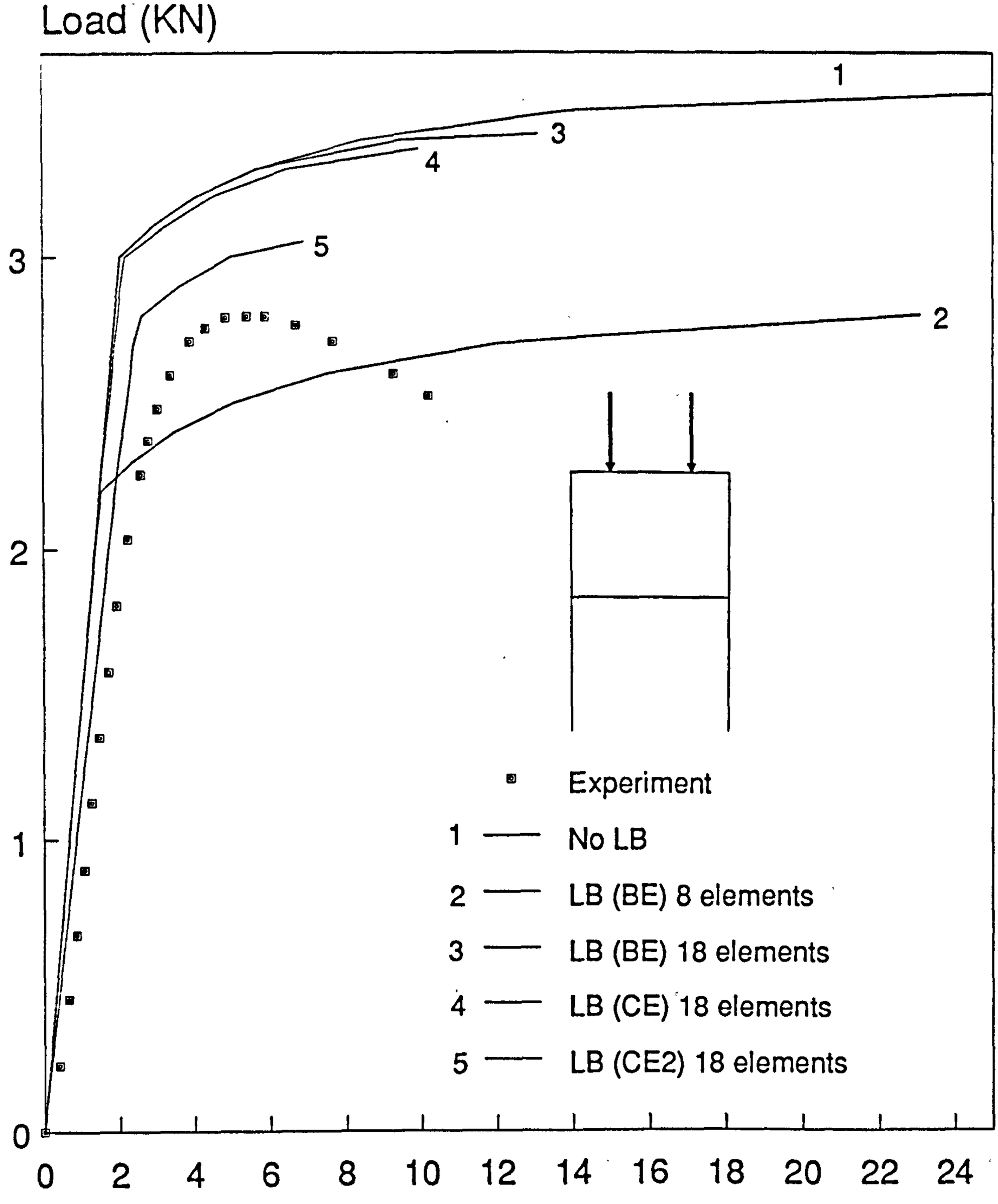

Fig.11.11 Frame F3-1A Load/Displacement plot

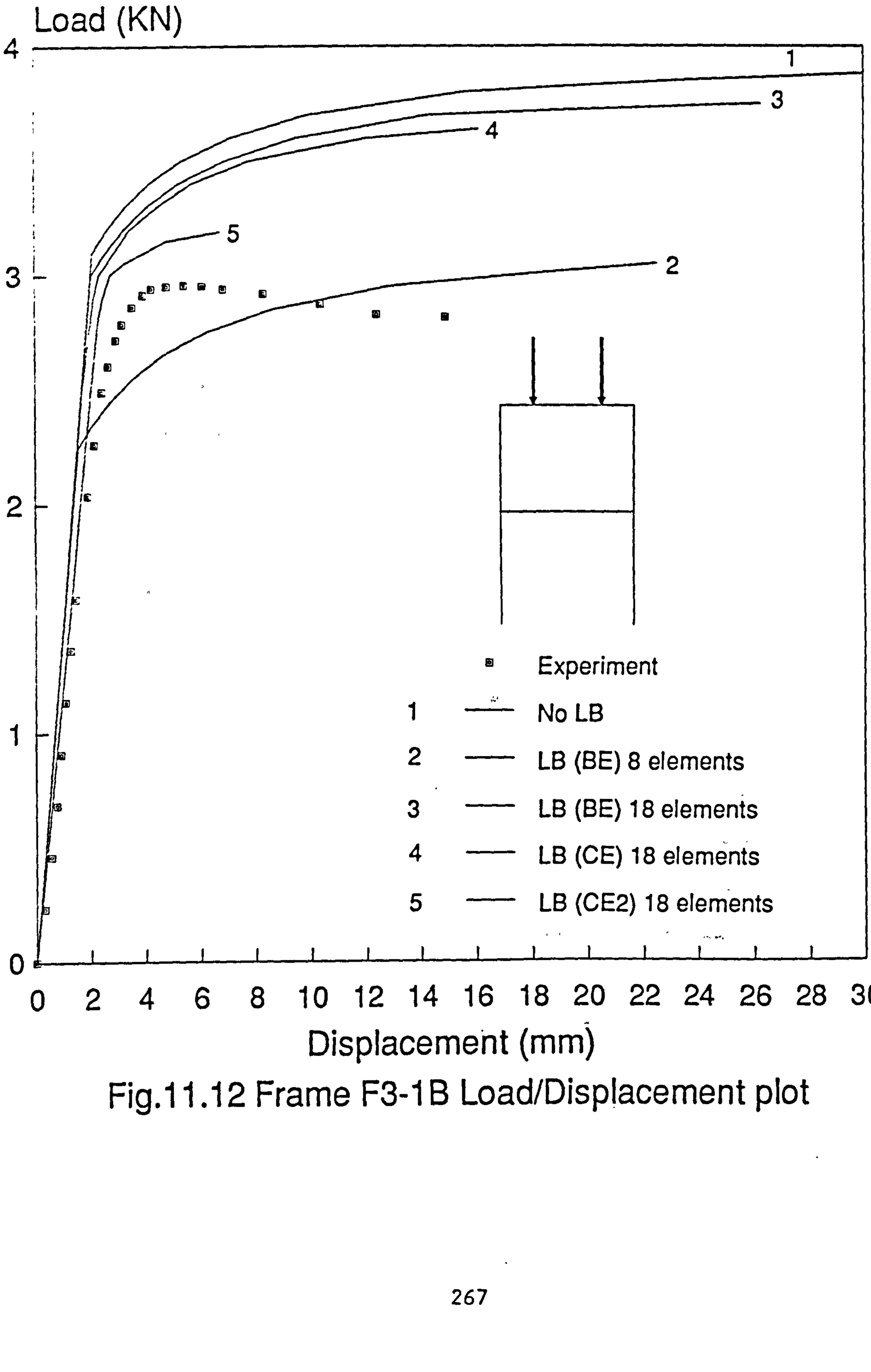

Fig.11.12 Frame F3-1B Load/Displacement plot

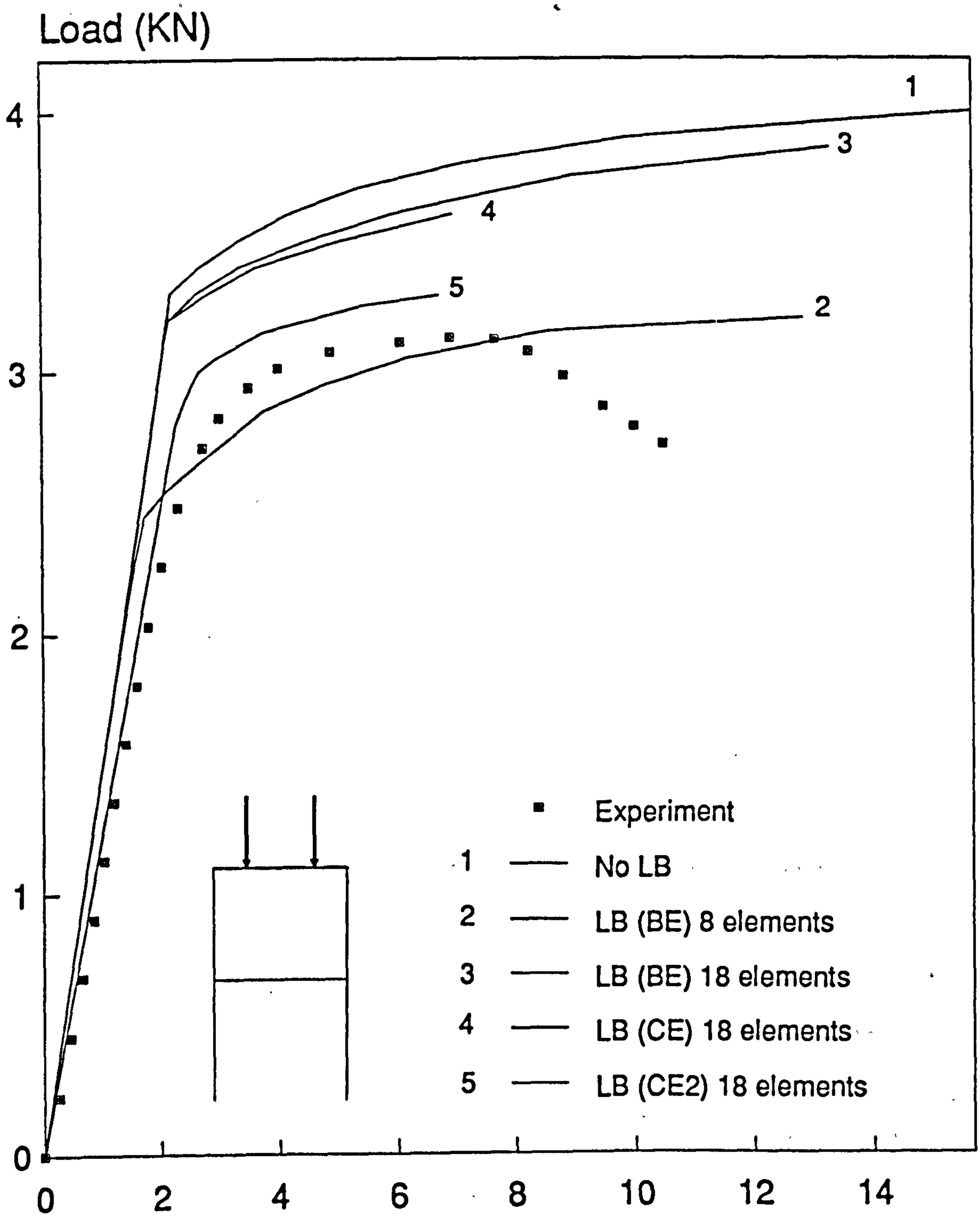

Fig.11.13 Frame F3-1C Load/Displacement plot

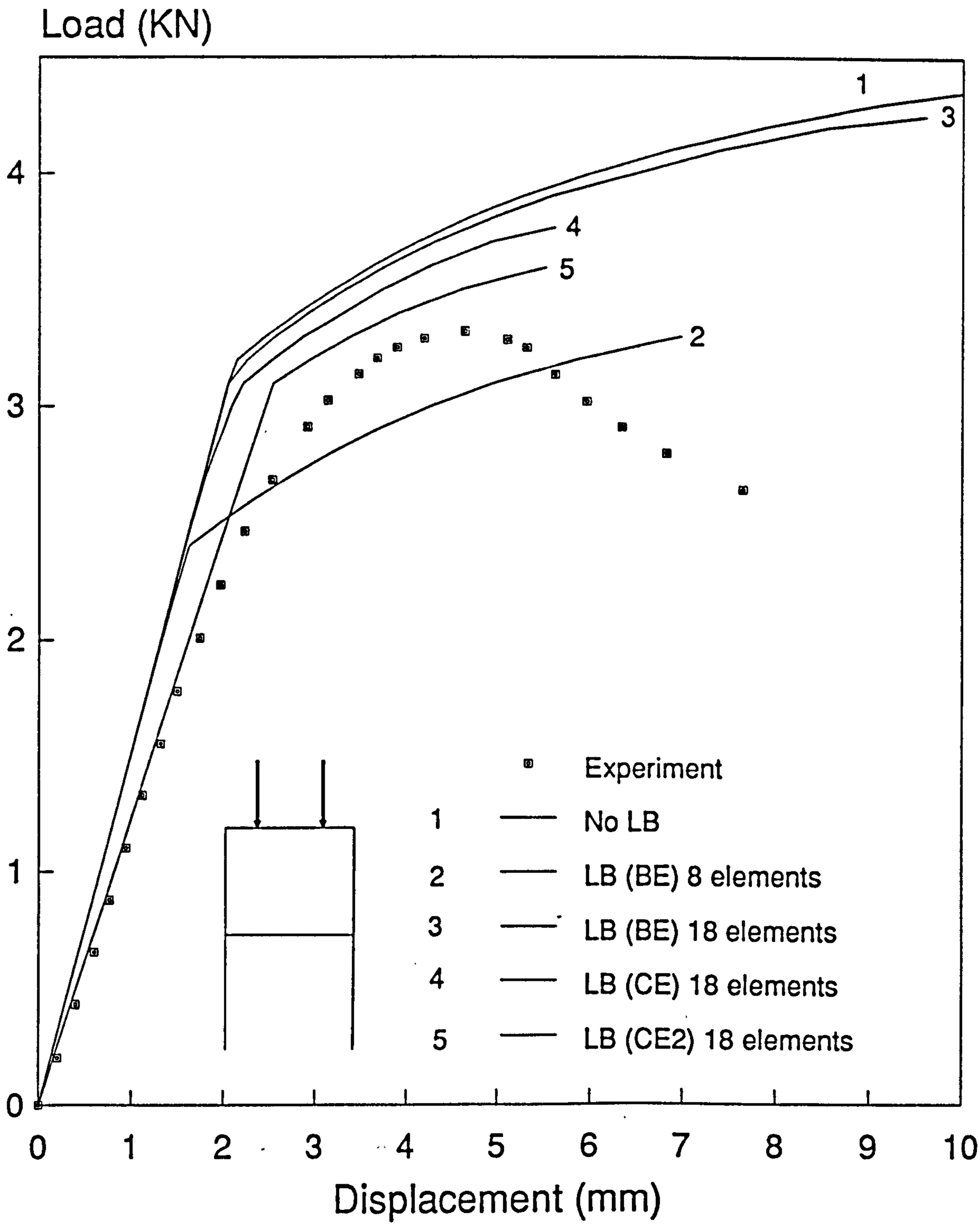

Fig.11.14 Frame F3-1D Load/Displacement plot

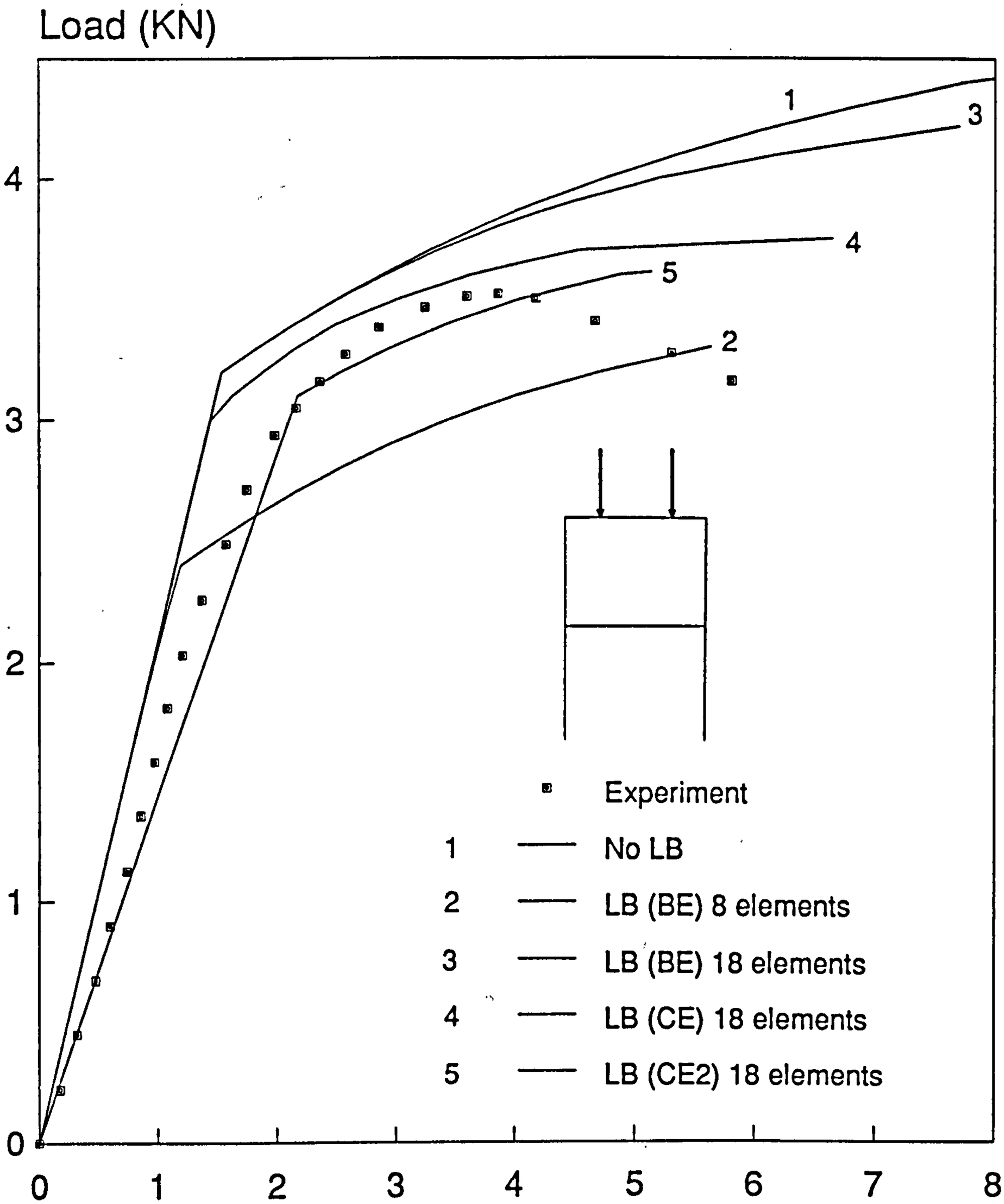

Fig.11.15 Frame F3-1E Load/Displacement plot

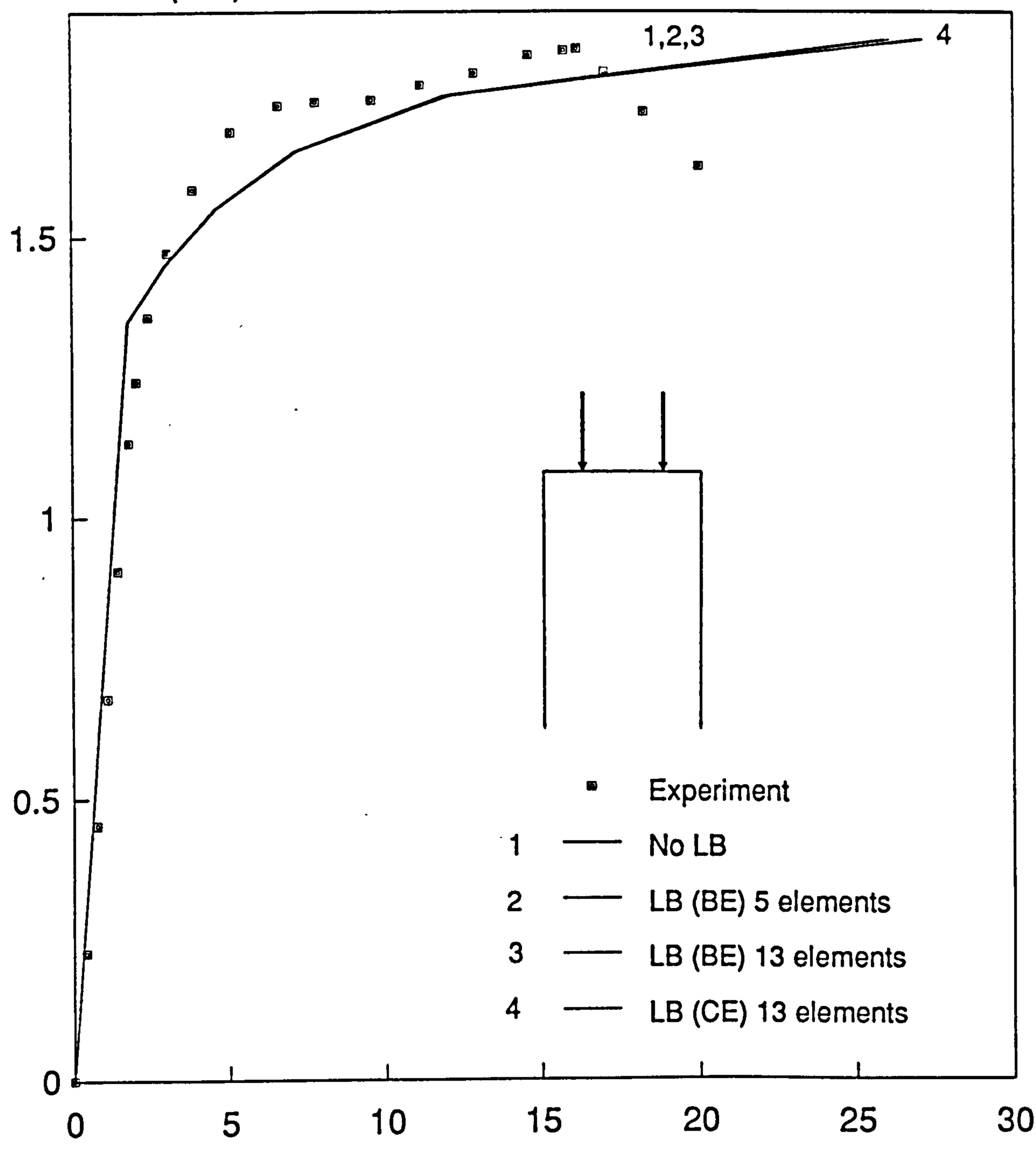

Fig.11.16 Frame F1-2A Load/Displacement plot

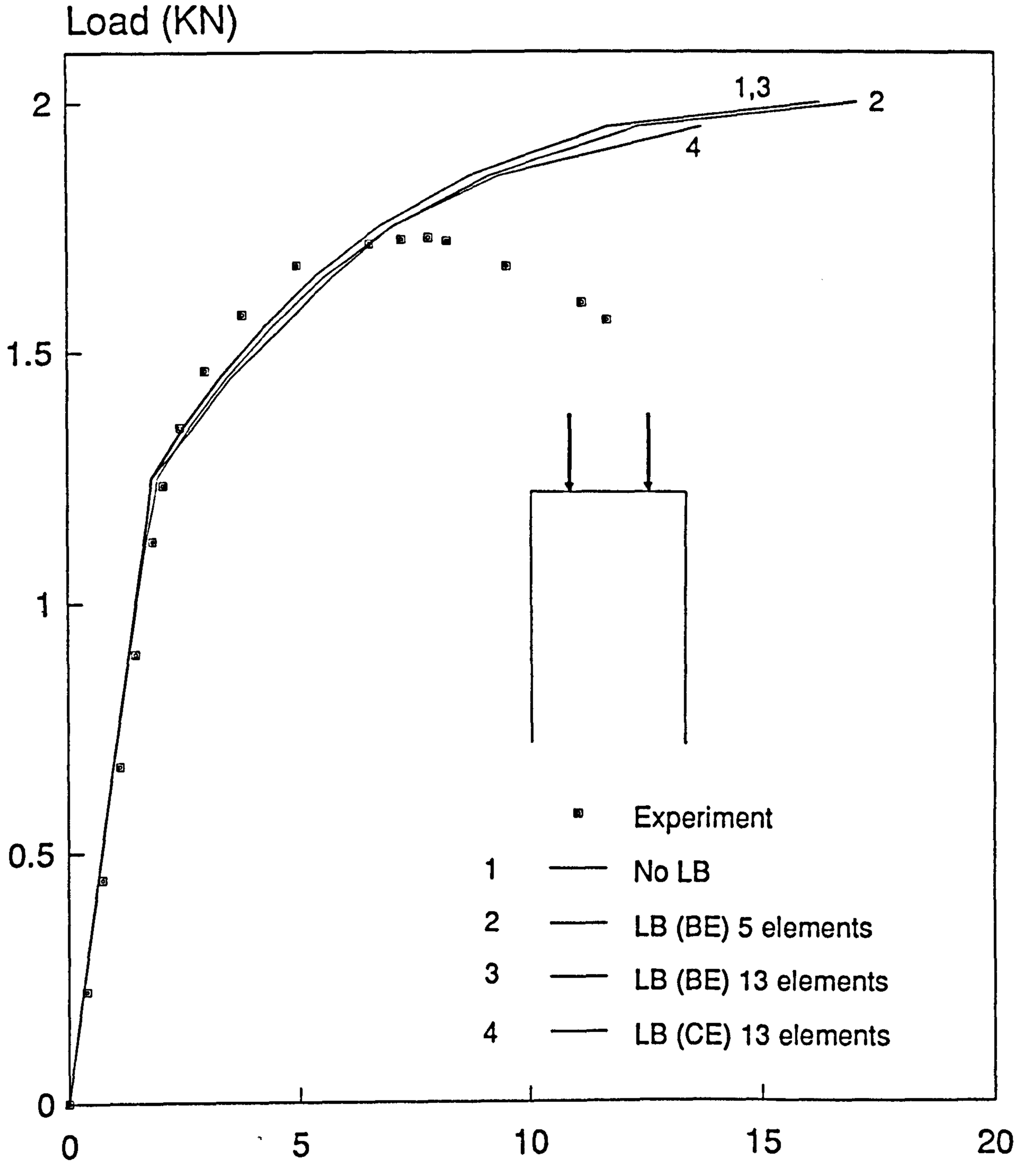

Fig.11.17 Frame F1-2B Load/Displacement plot

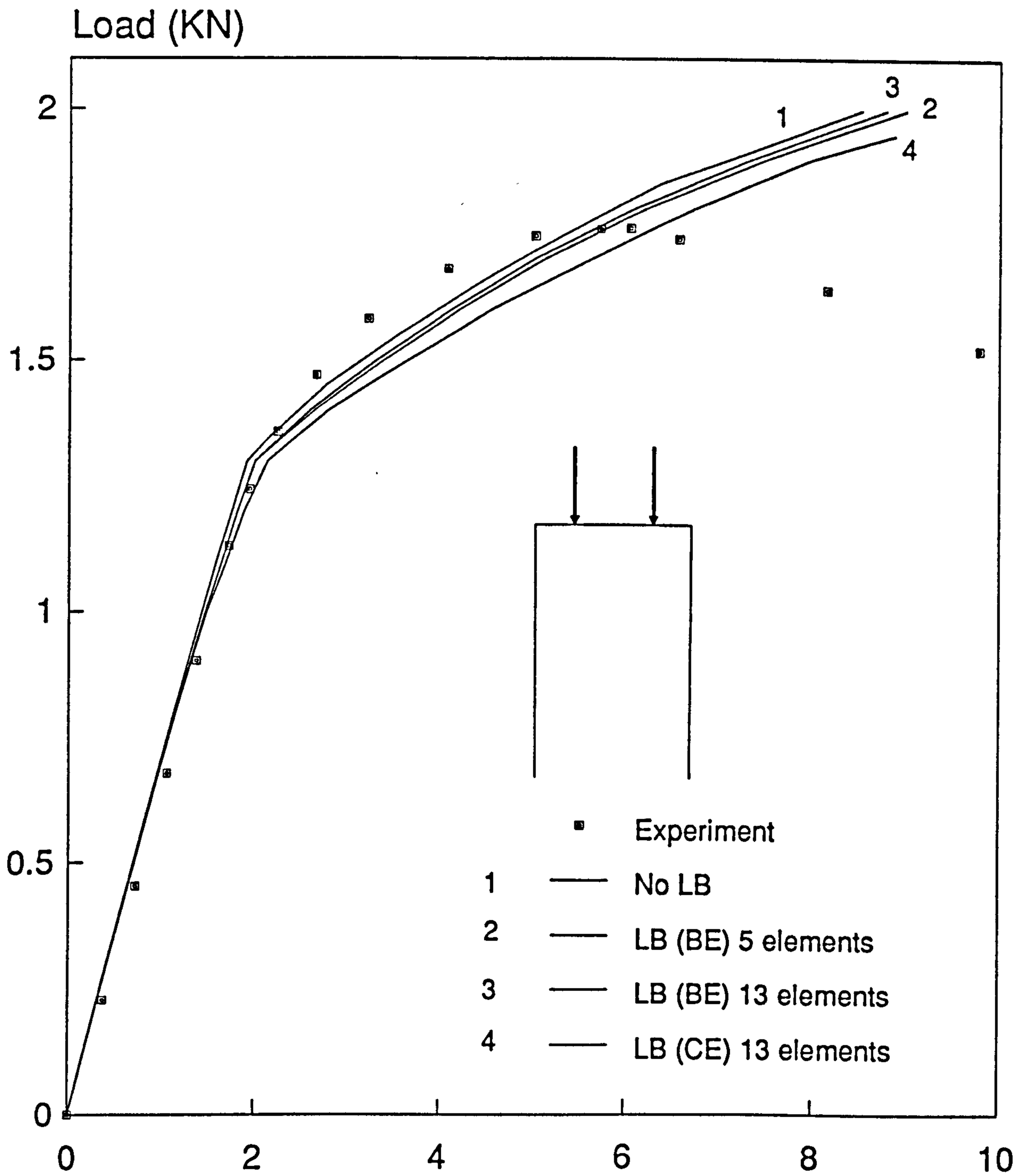

Fig.11.18 Frame F1-2C Load/Displacement plot

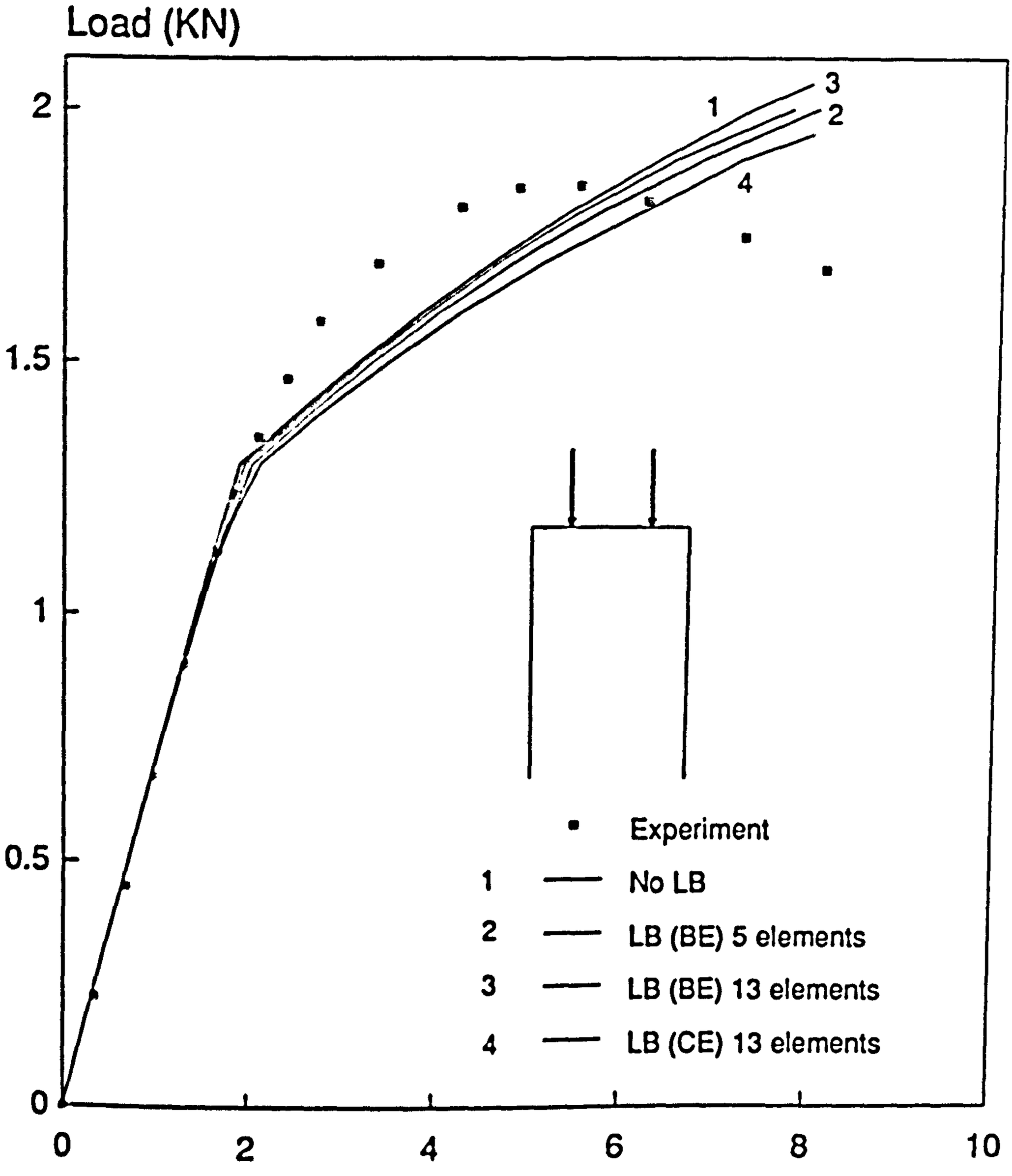

Fig.11.19 Frame F1-2D Load/Displacement plot

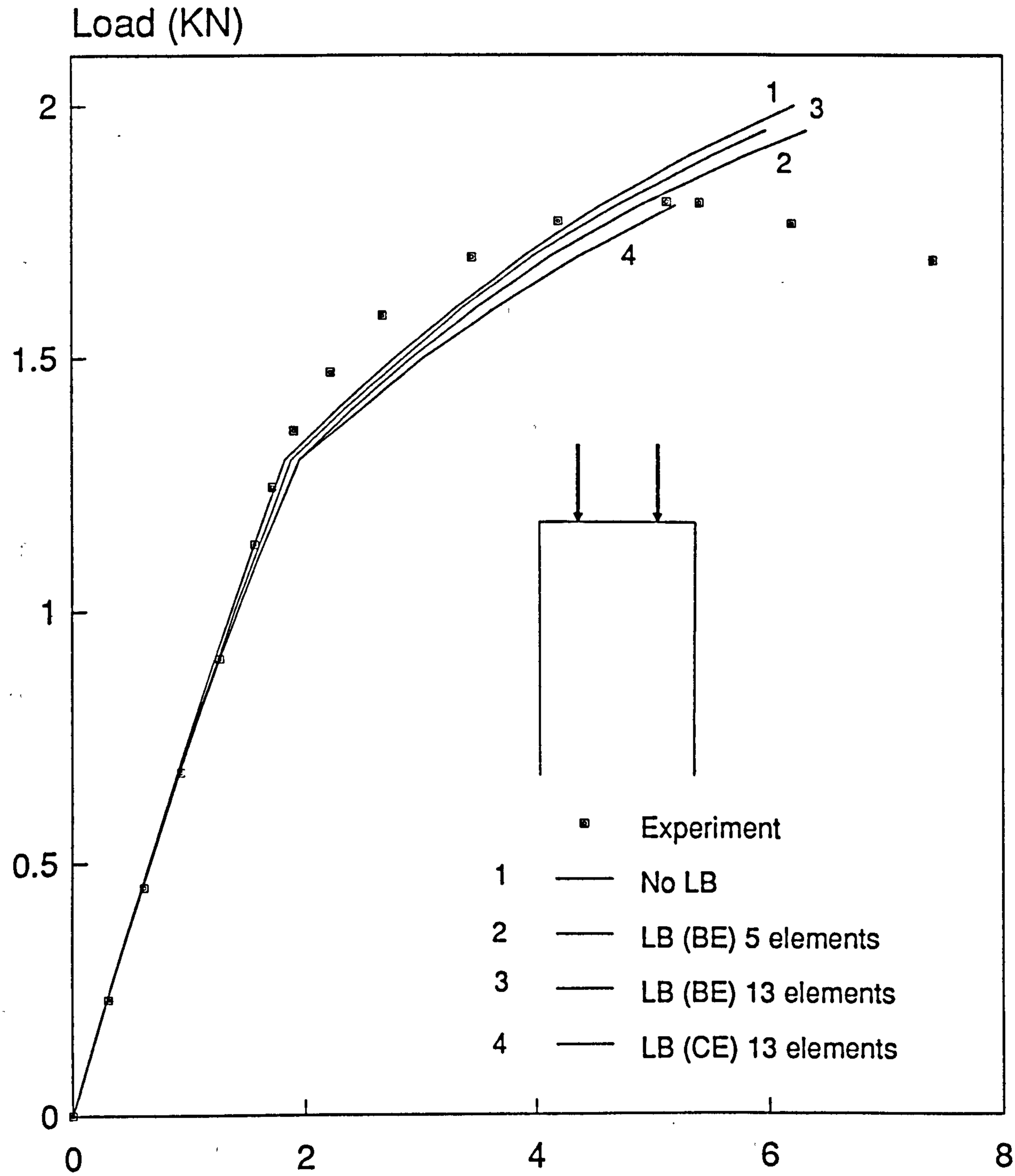

Fig.11.20 Frame F1-2E Load/Displacement plot

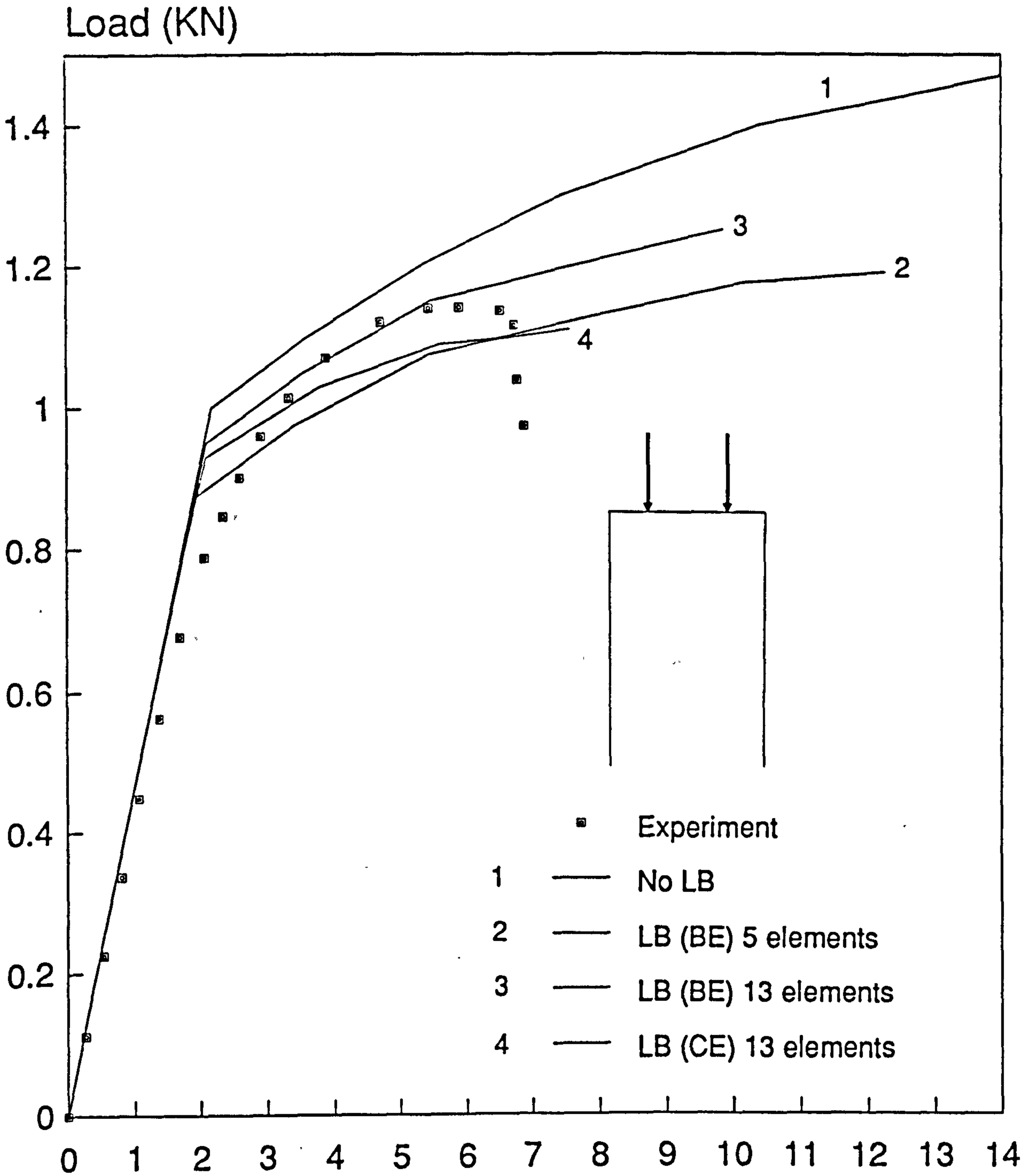

Fig.11.21 Frame F2-2A Load/Displacement plot

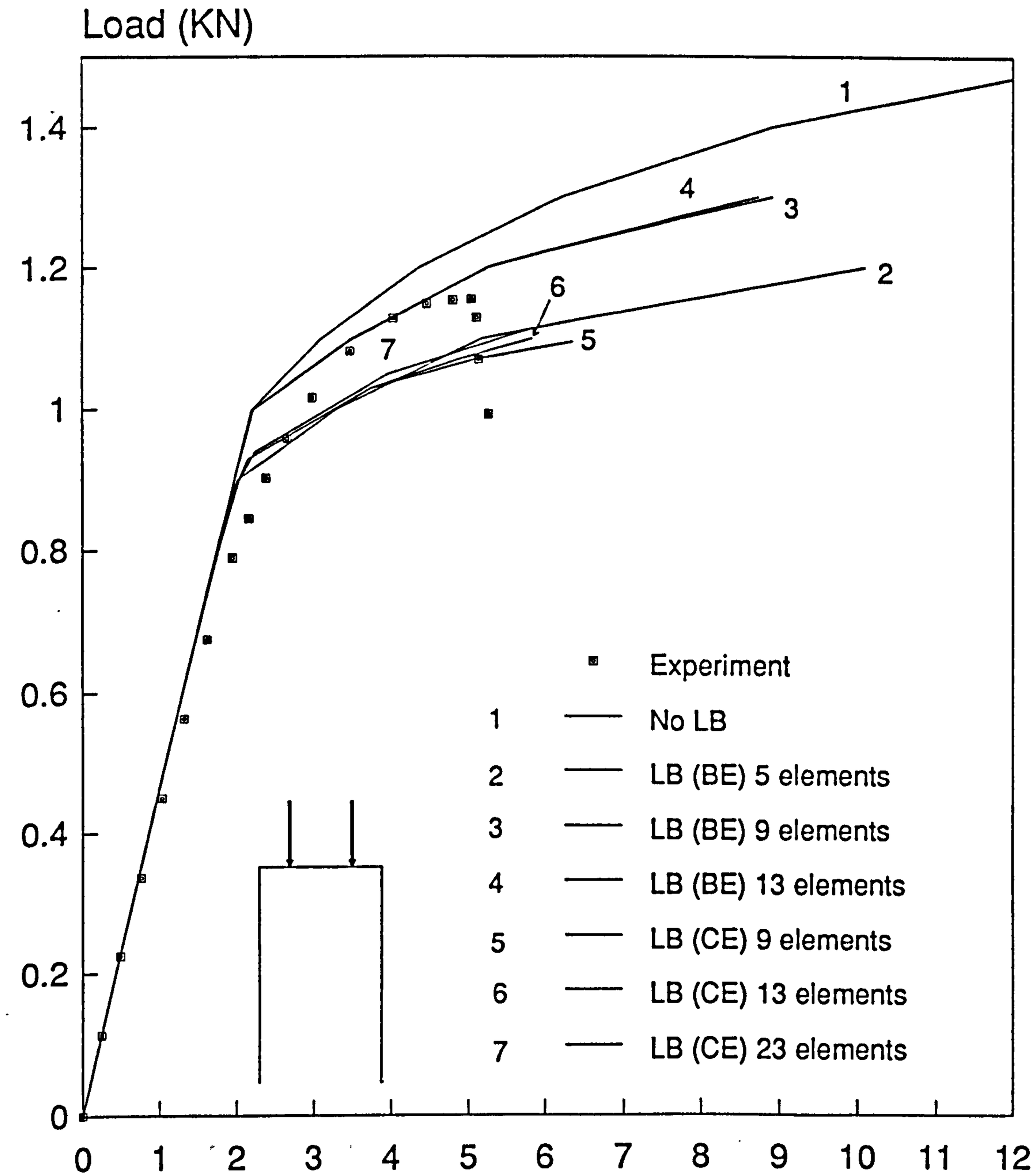

Fig.11.22 Frame F2-2B Load/Displacement plot

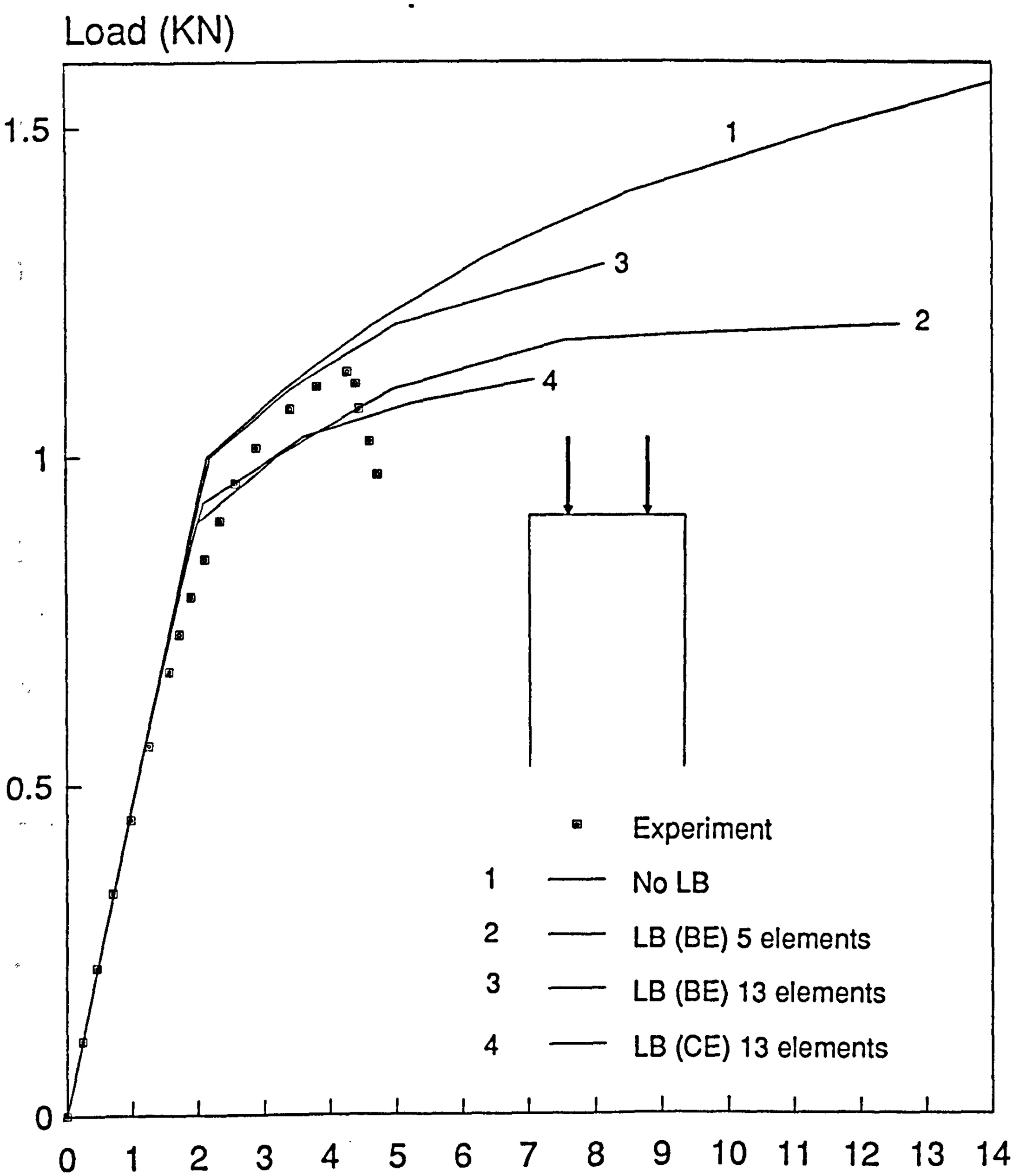

Fig.11.23 Frame F2-2C Load/Displacement plot

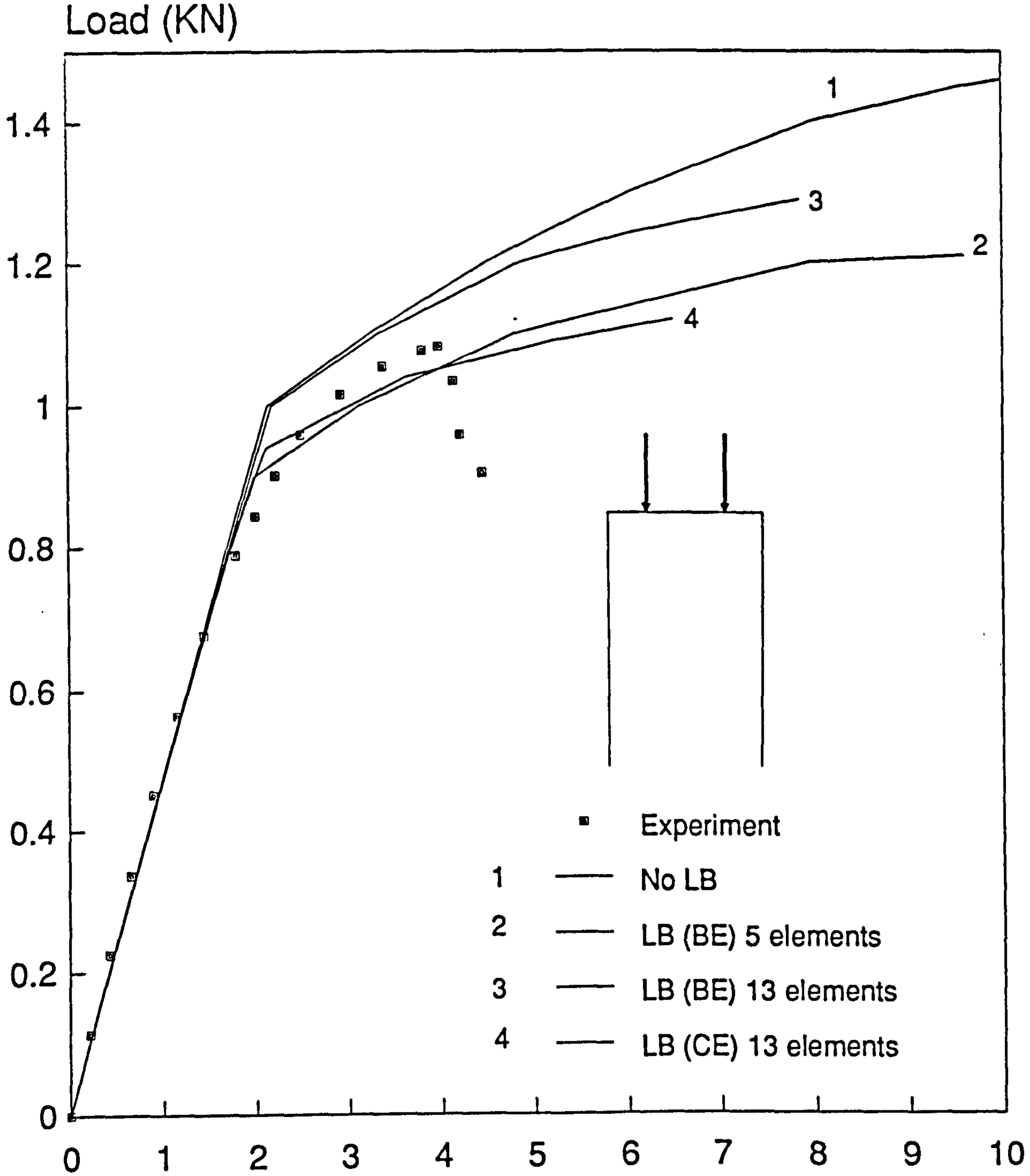

Fig.11.24 Frame F2-2D Load/Displacement plot

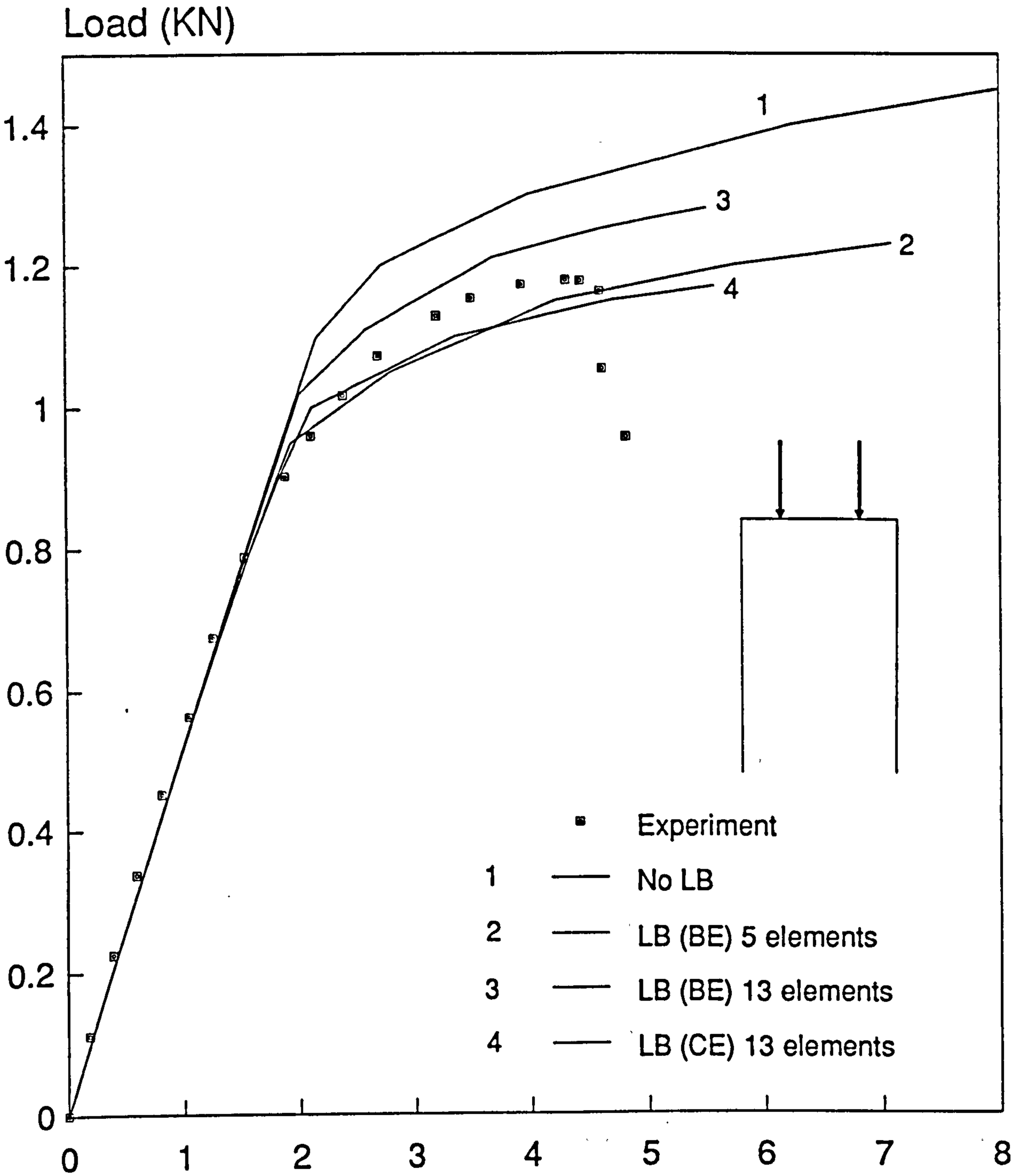

Fig.11.25 Frame F2-2E Load/Displacement plot

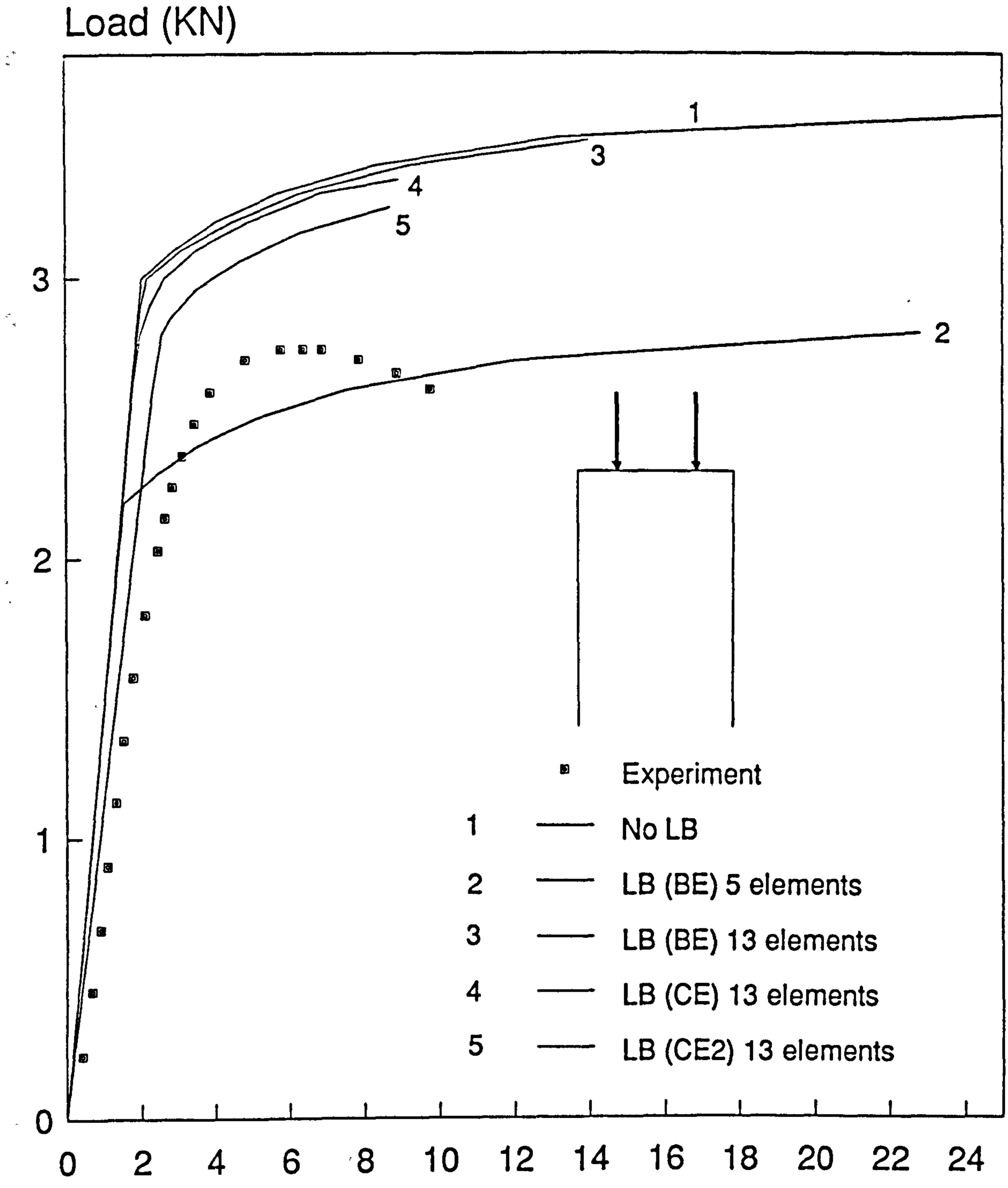

Fig.11.26 Frame F3-2A Load/Displacement plot

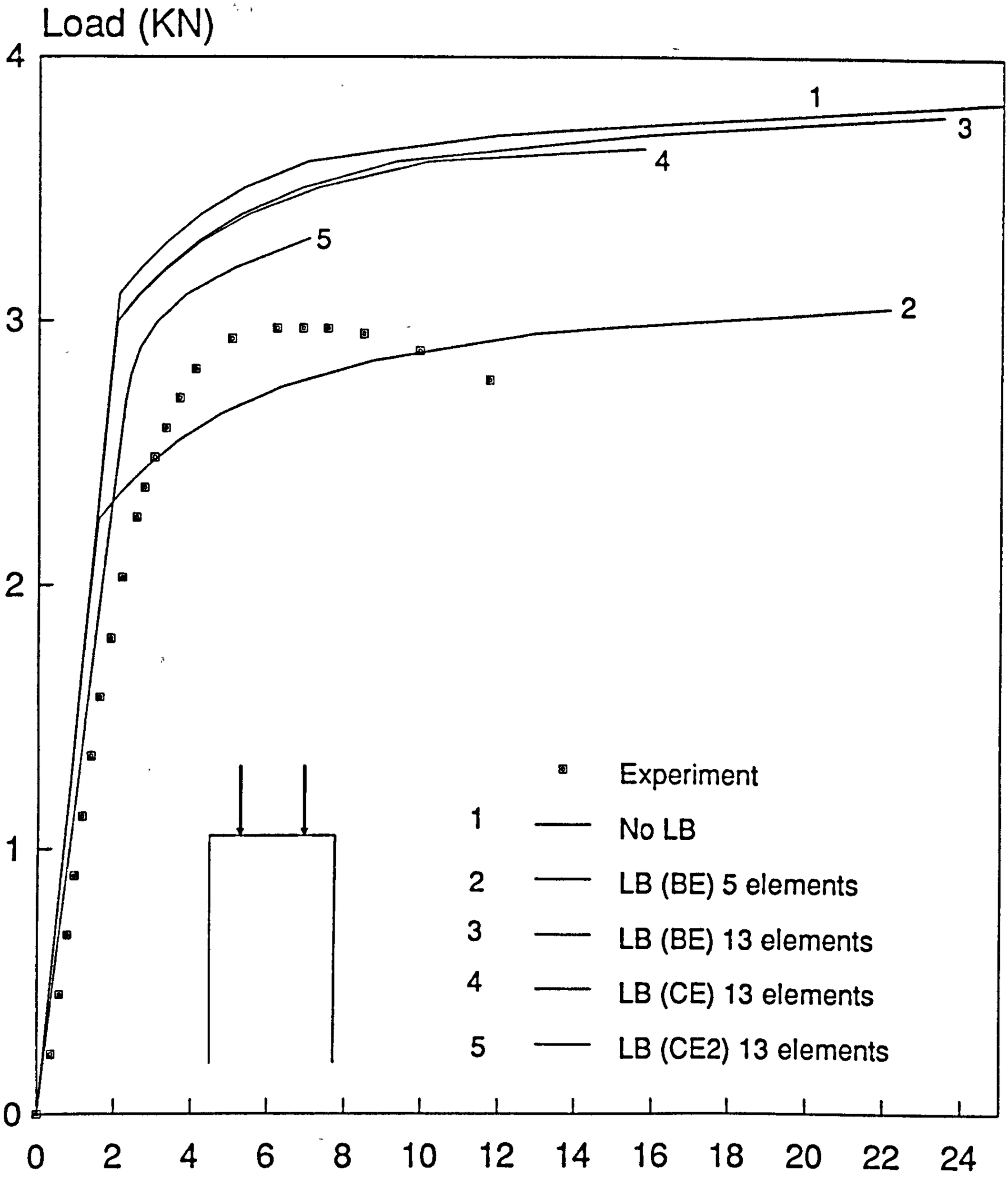

Fig.11.27 Frame F3-2B Load/Displacement plot

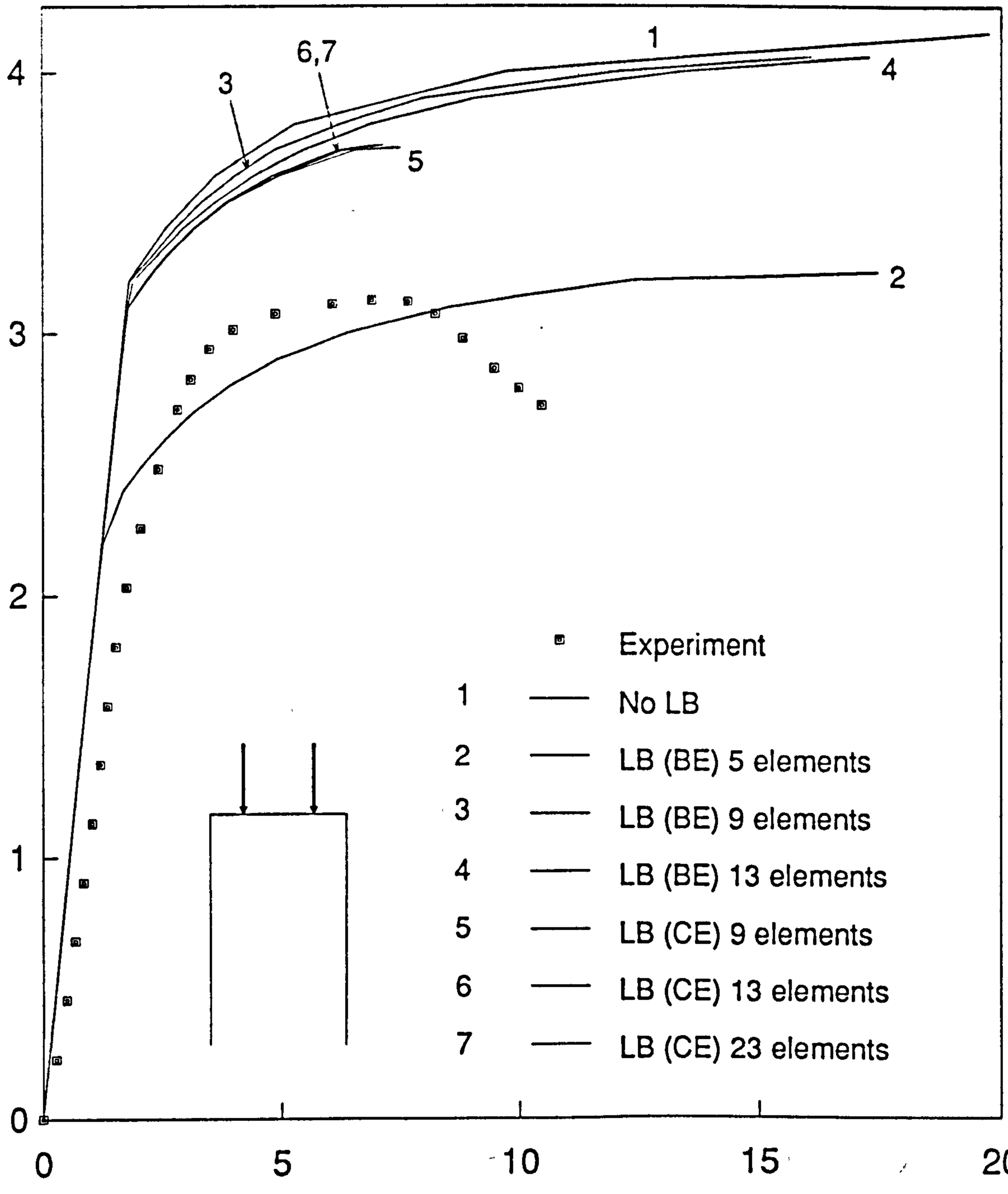

Fig.11.28 Frame F3-2C Load/Displacement plot

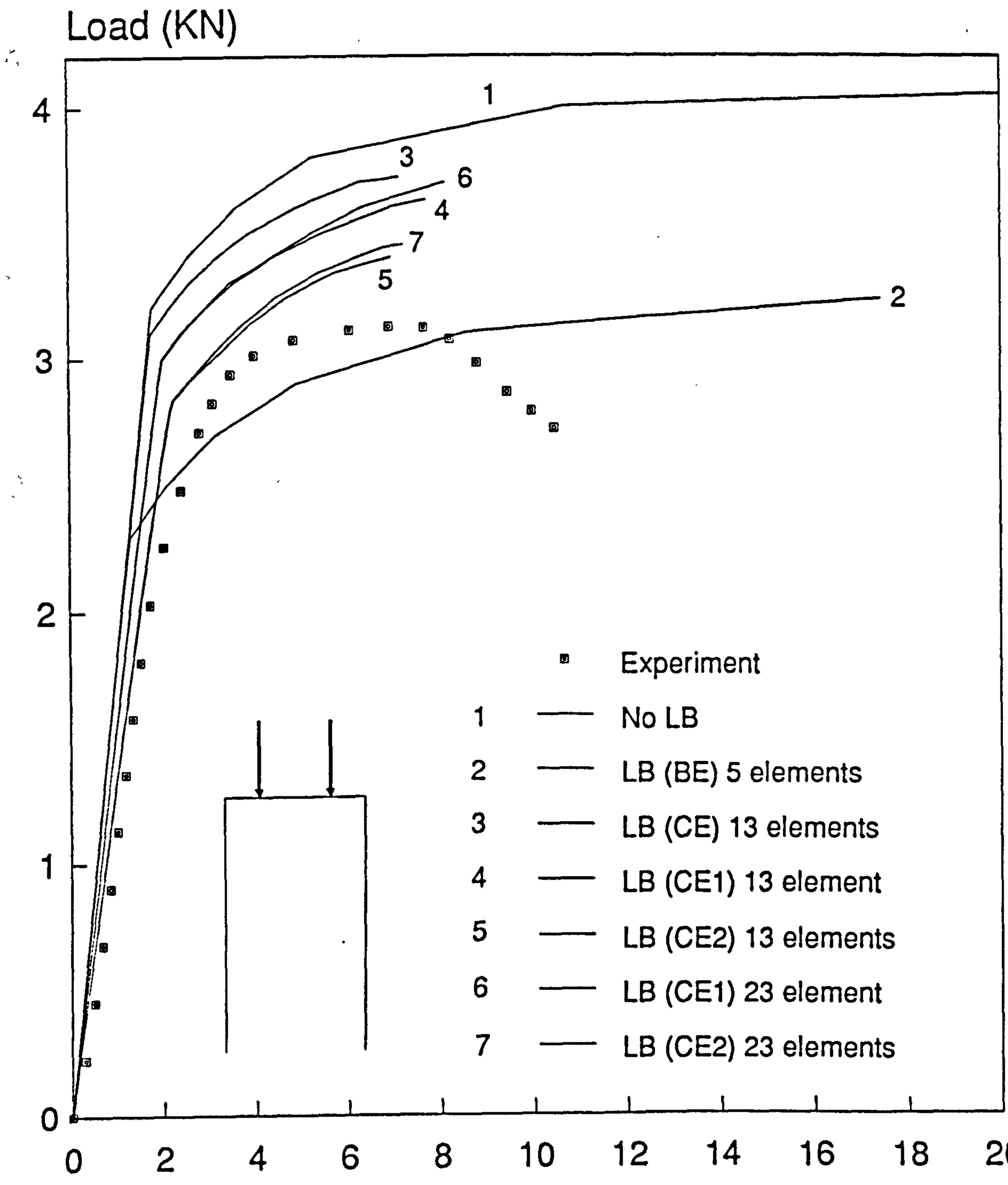

Fig.11.28a Frame F3-2C Load/Displacement plot

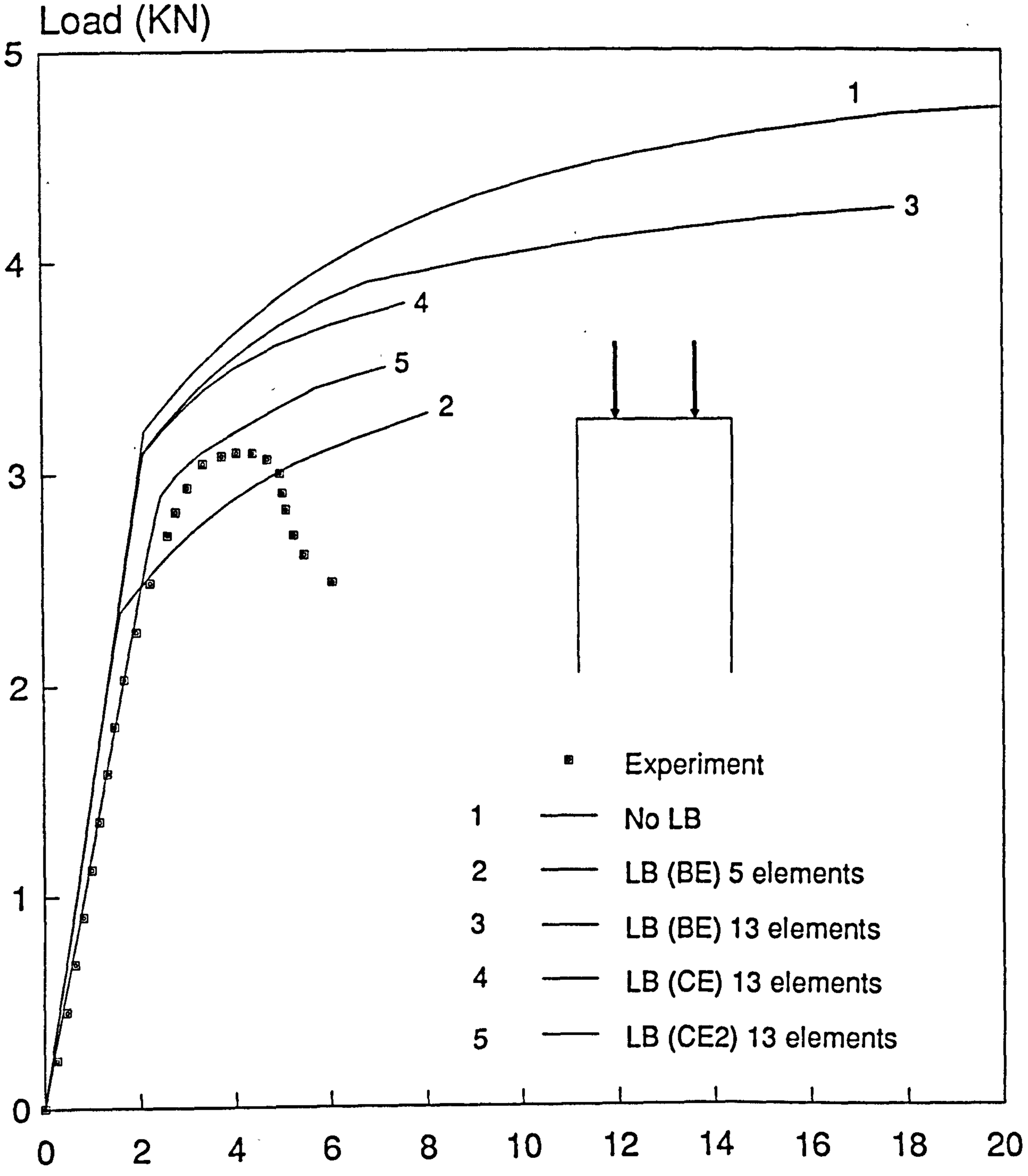

Fig.11.29 Frame F3-2D Load/Displacement plot

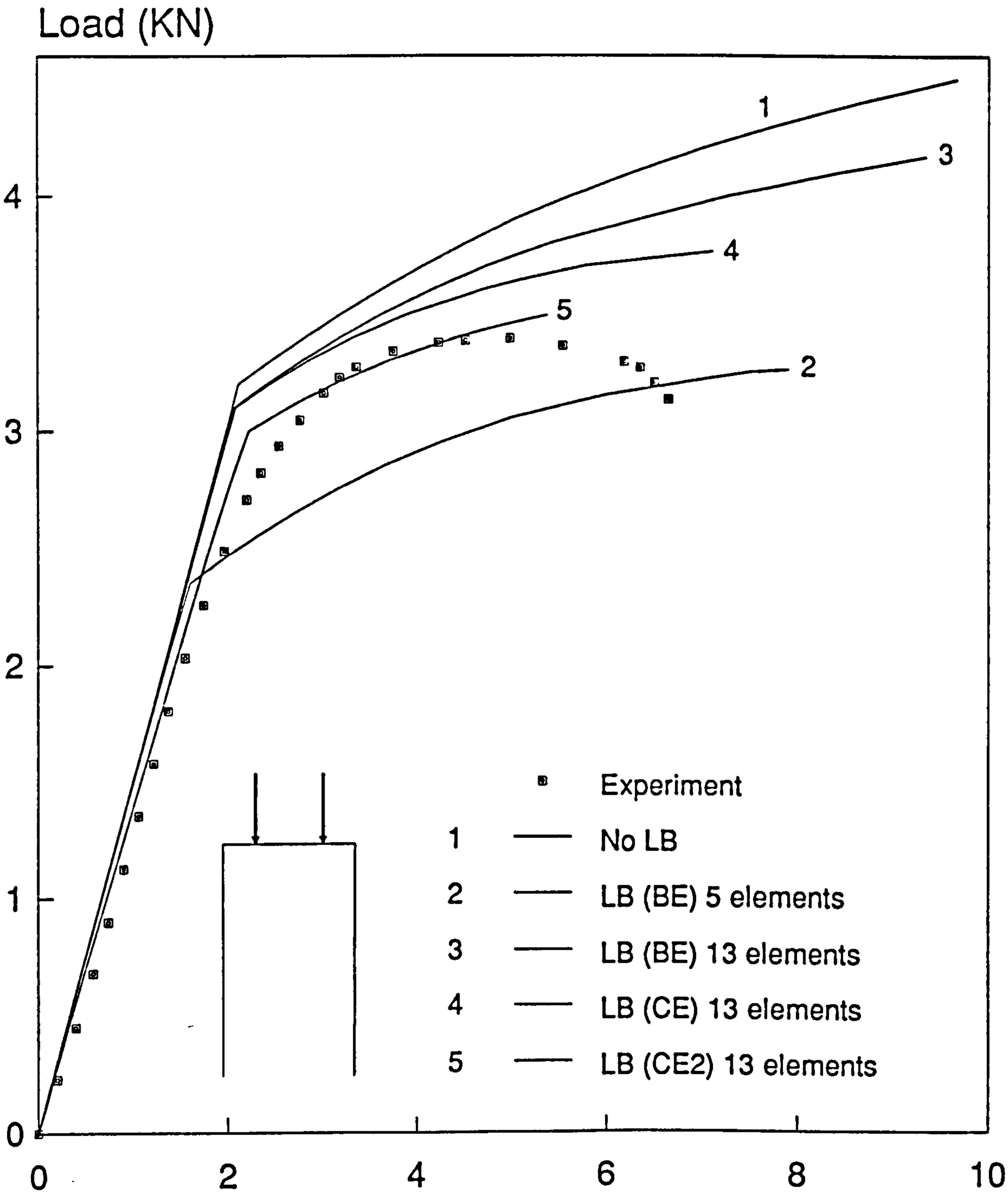

Fig.11.30 Frame F3-2E Load/Displacement plot

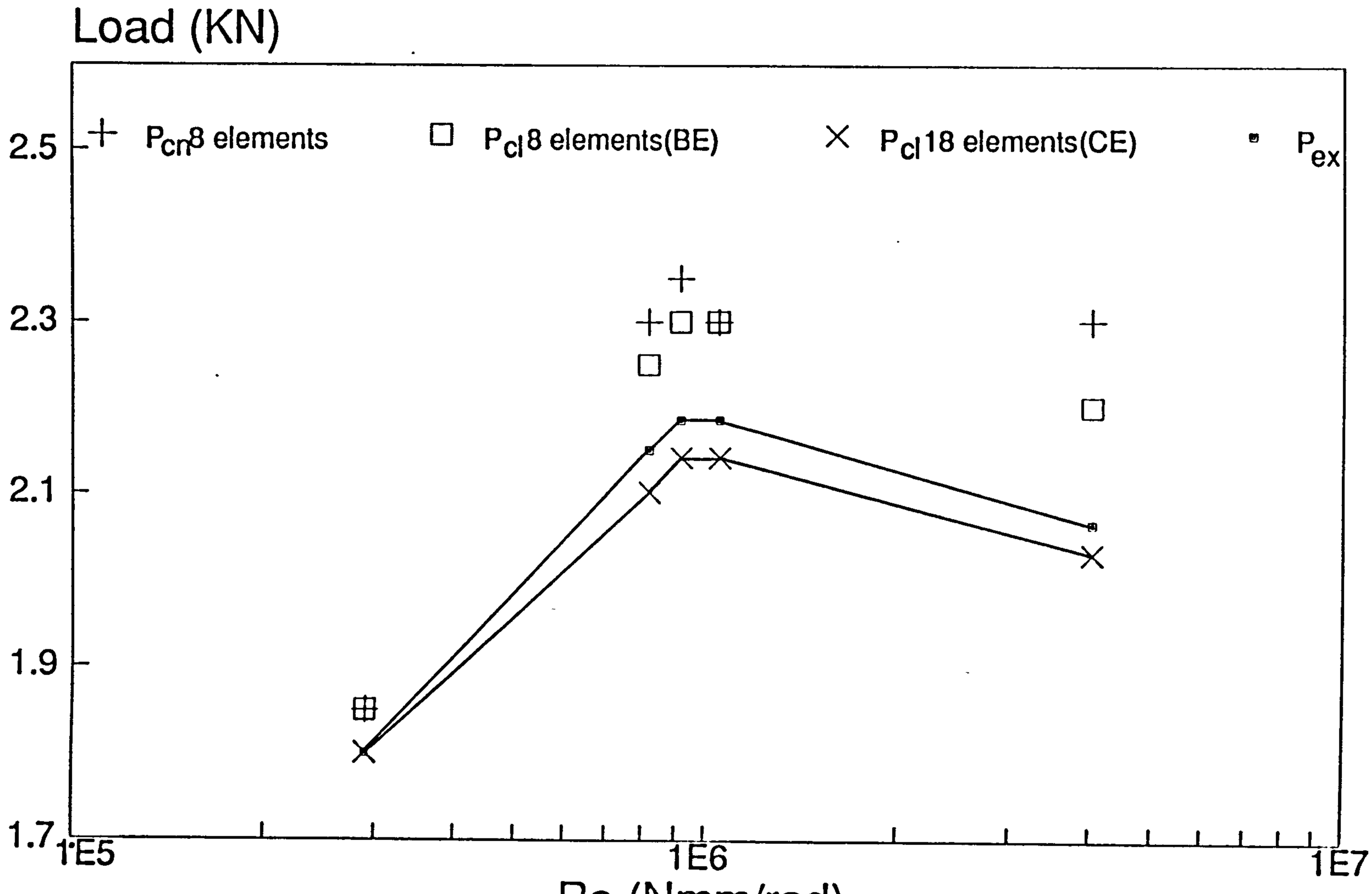

Fig.11.31 Frame F1-1 various Load/Connection Stiffness plot

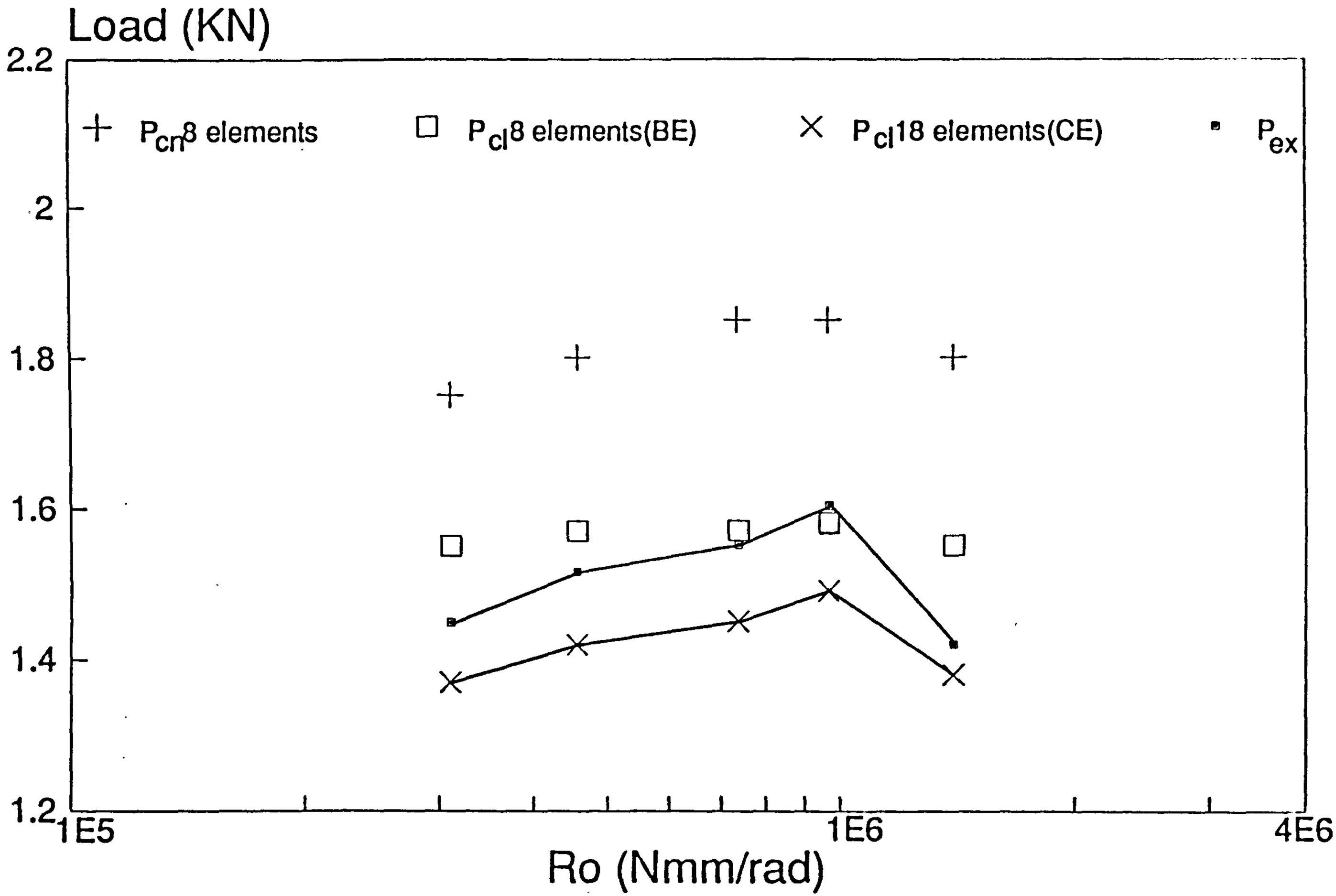

Fig.11.32 Frame F2-1 various Load/Connection Stiffness plot

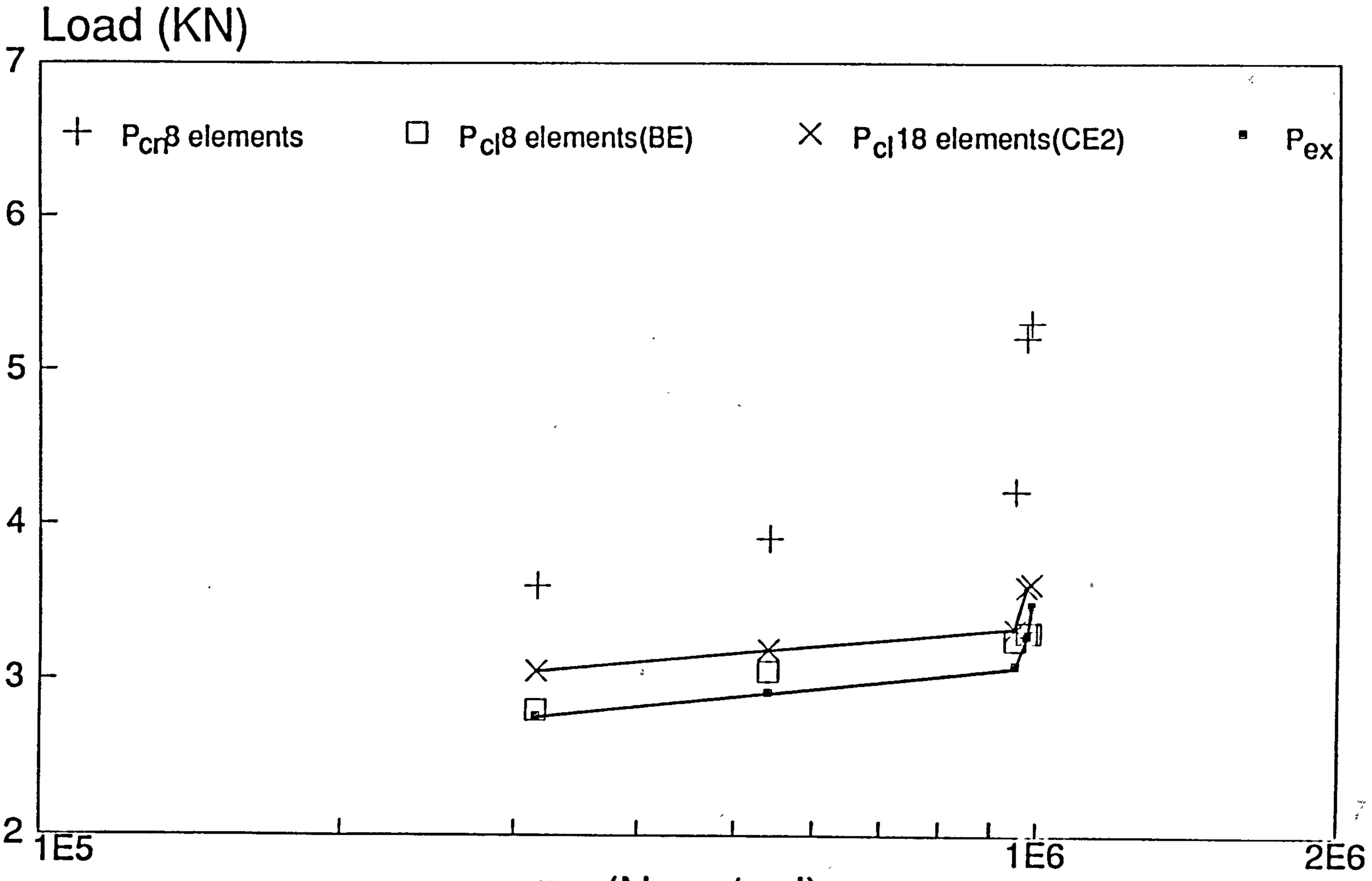

Fig.11.33 Frame F3-1 various Load/Connection Stiffness plot

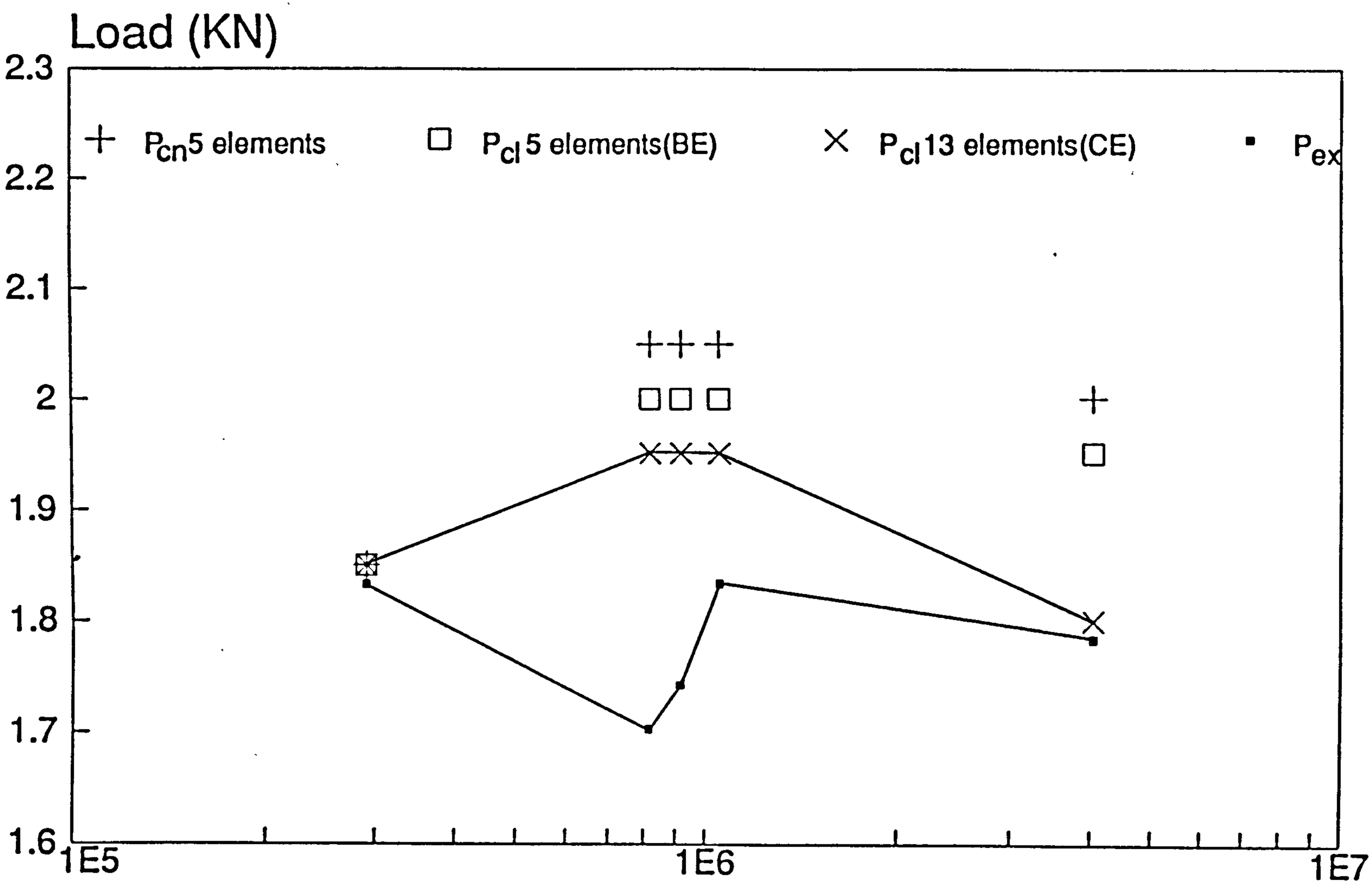

Fig.11.34 Frame F1-2 various Load/Connection Stiffness plot

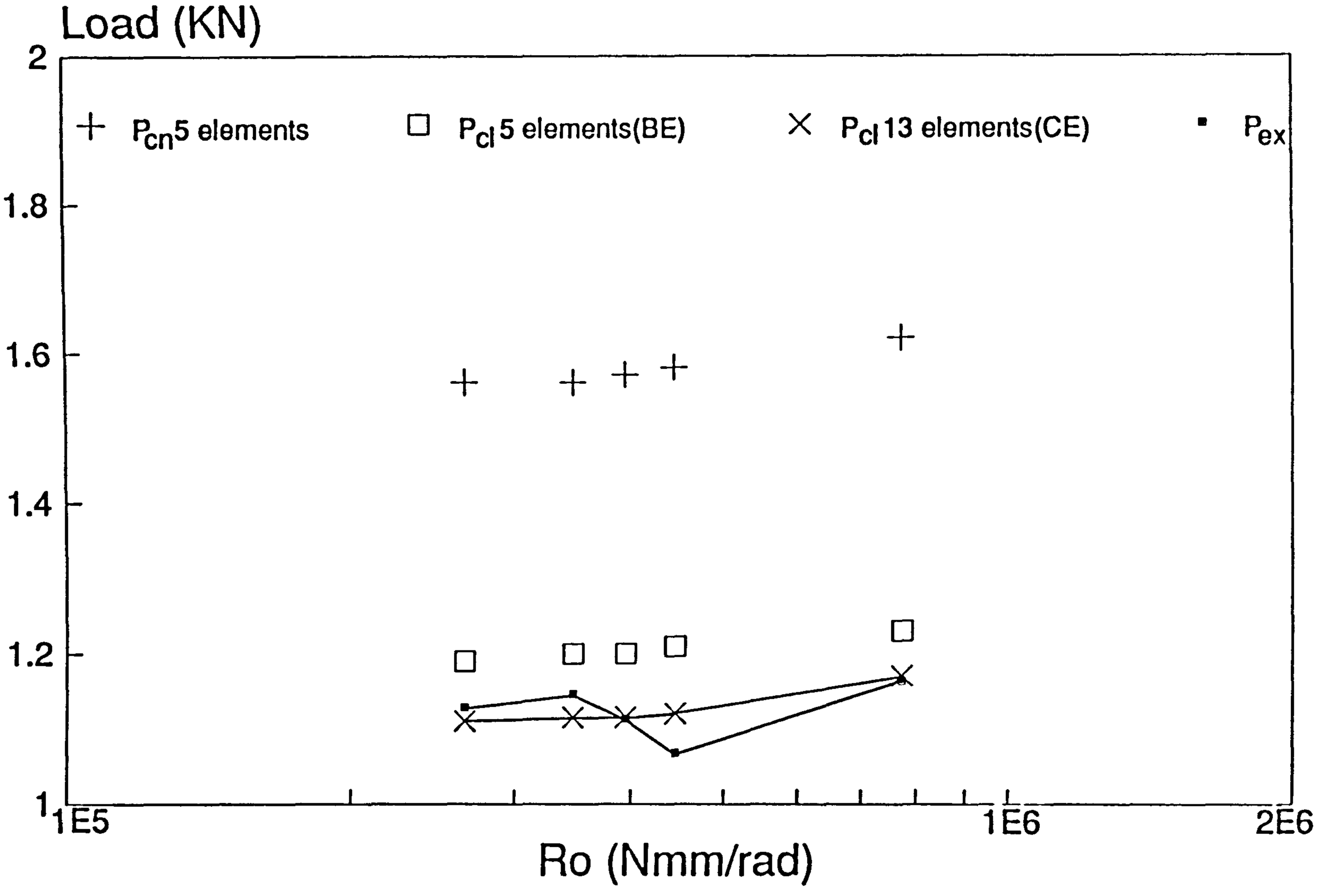

Fig.11.35 Frame F2-2 various Load/Connection Stiffness plot

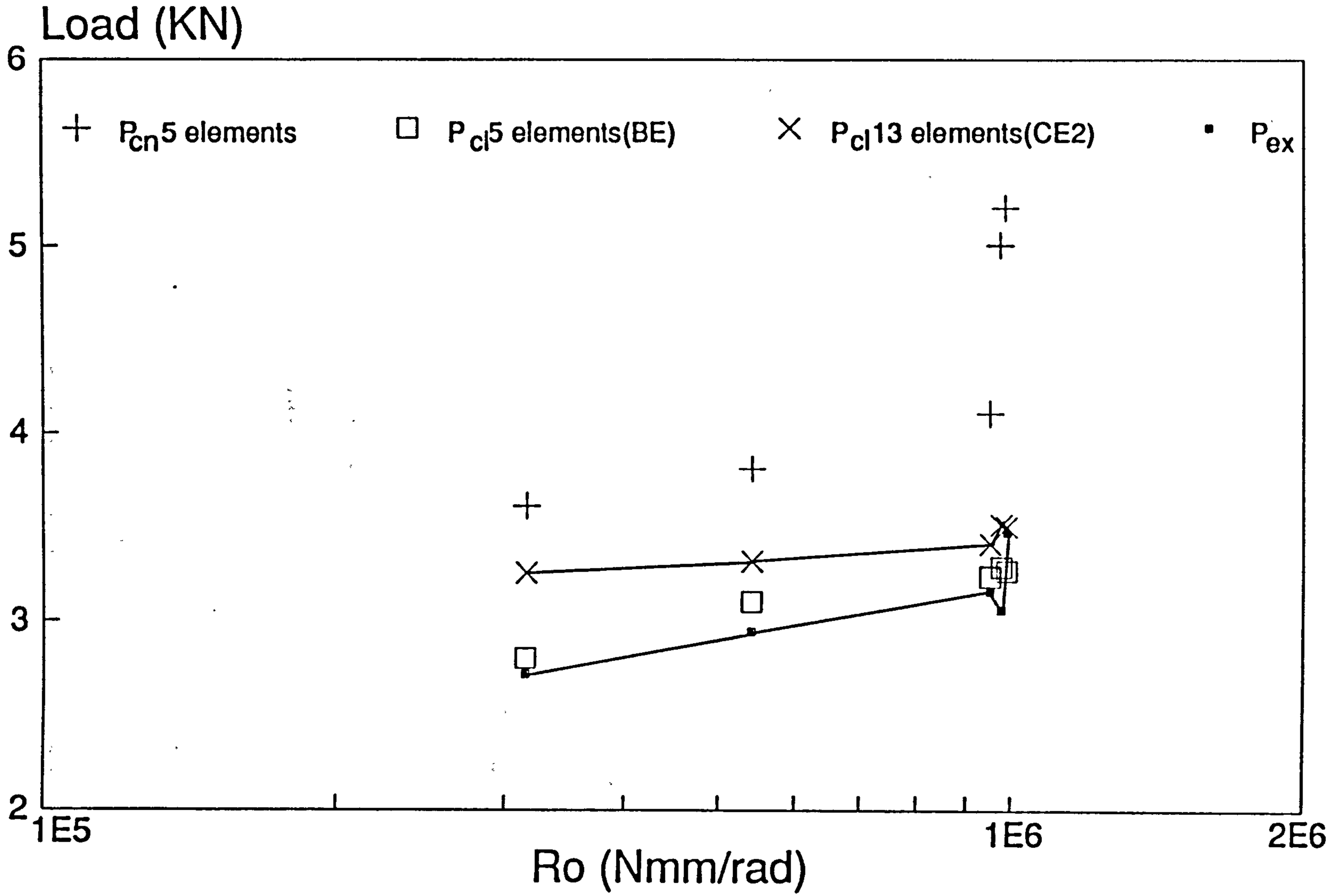

Fig.11.36 Frame F3-2 various Load/Connection Stiffness plot

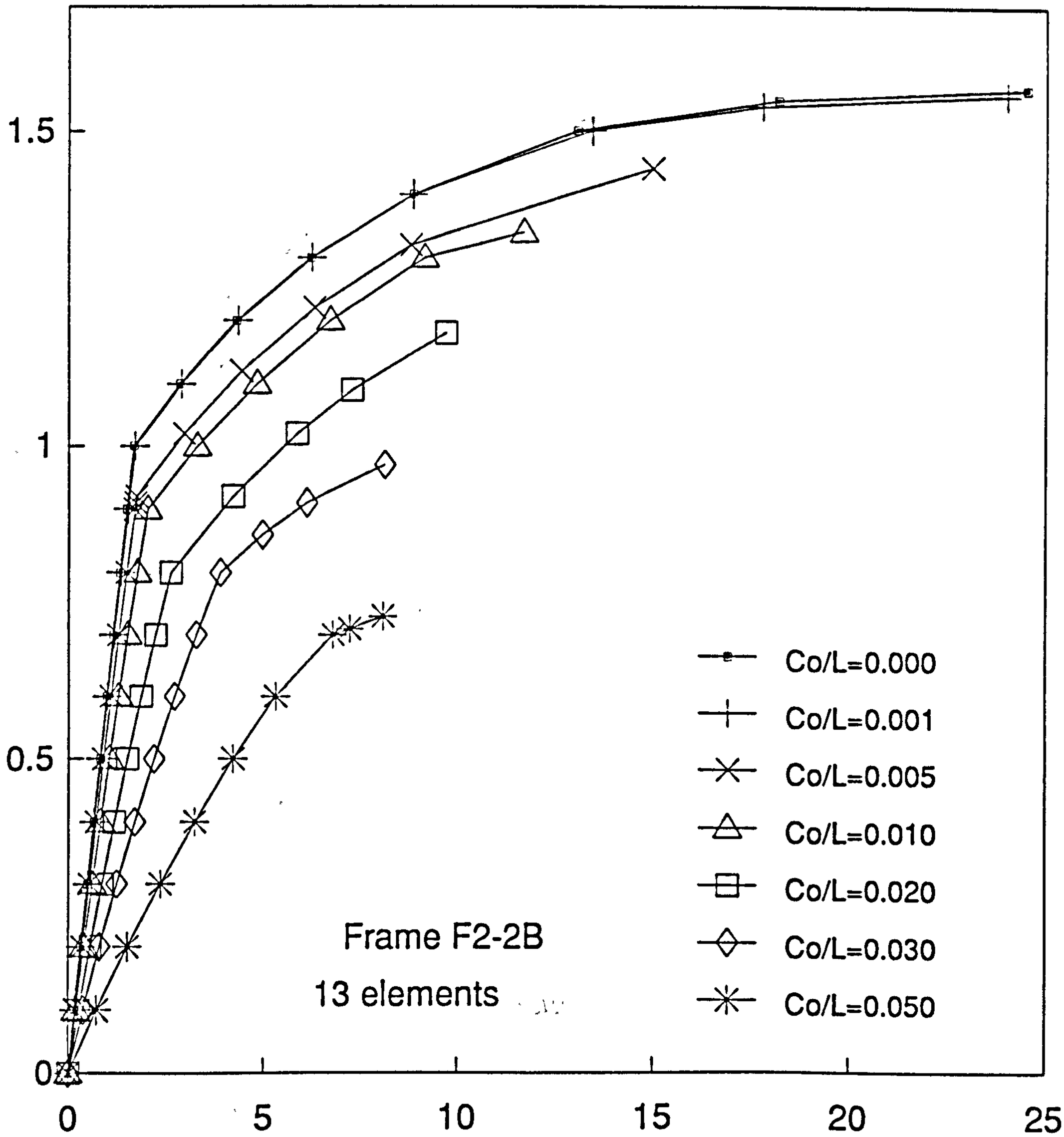

Fig.11.37 Effects of imperfection without local buckling

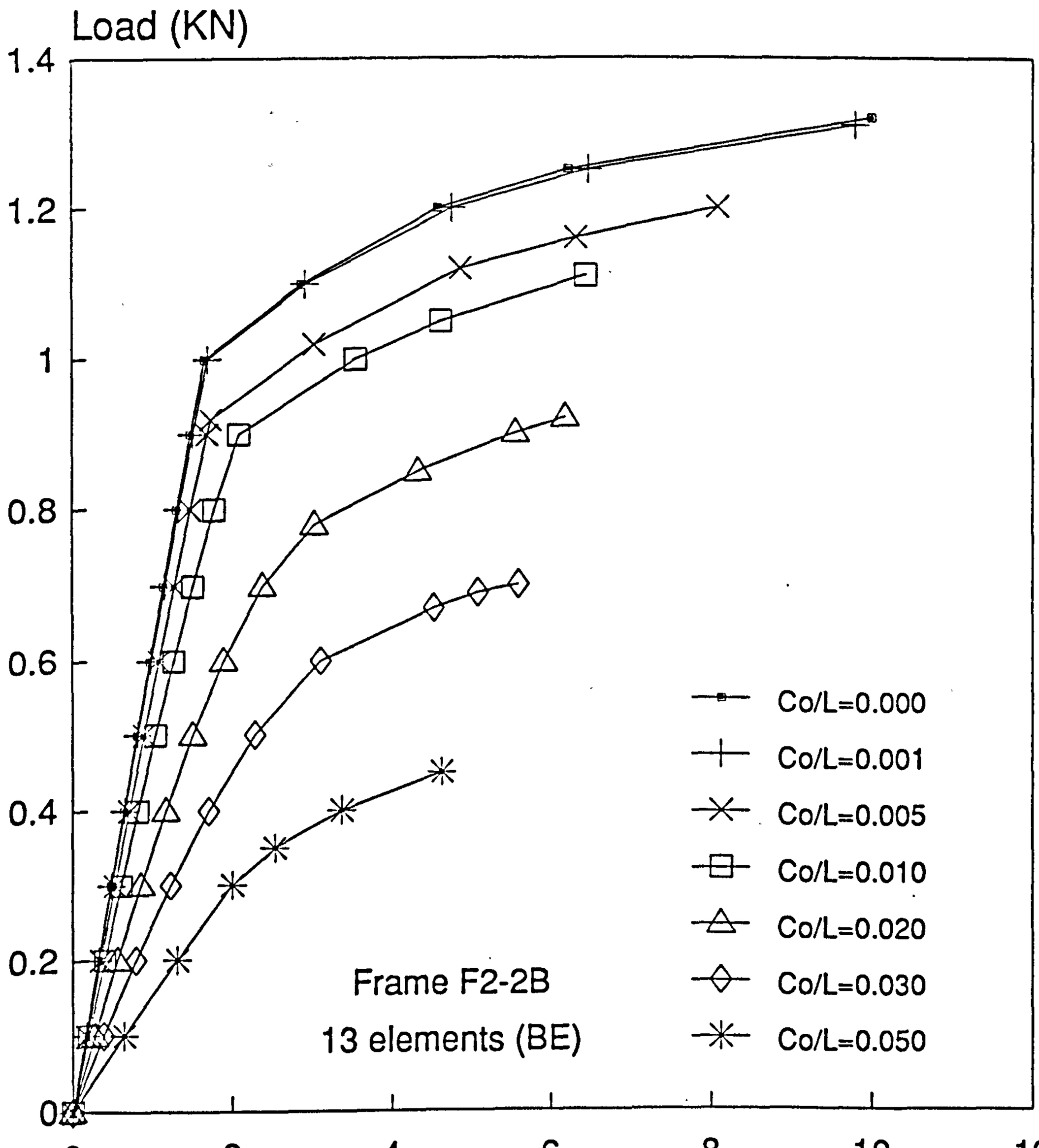

Fig.11.38 Effects of imperfection with local buckling

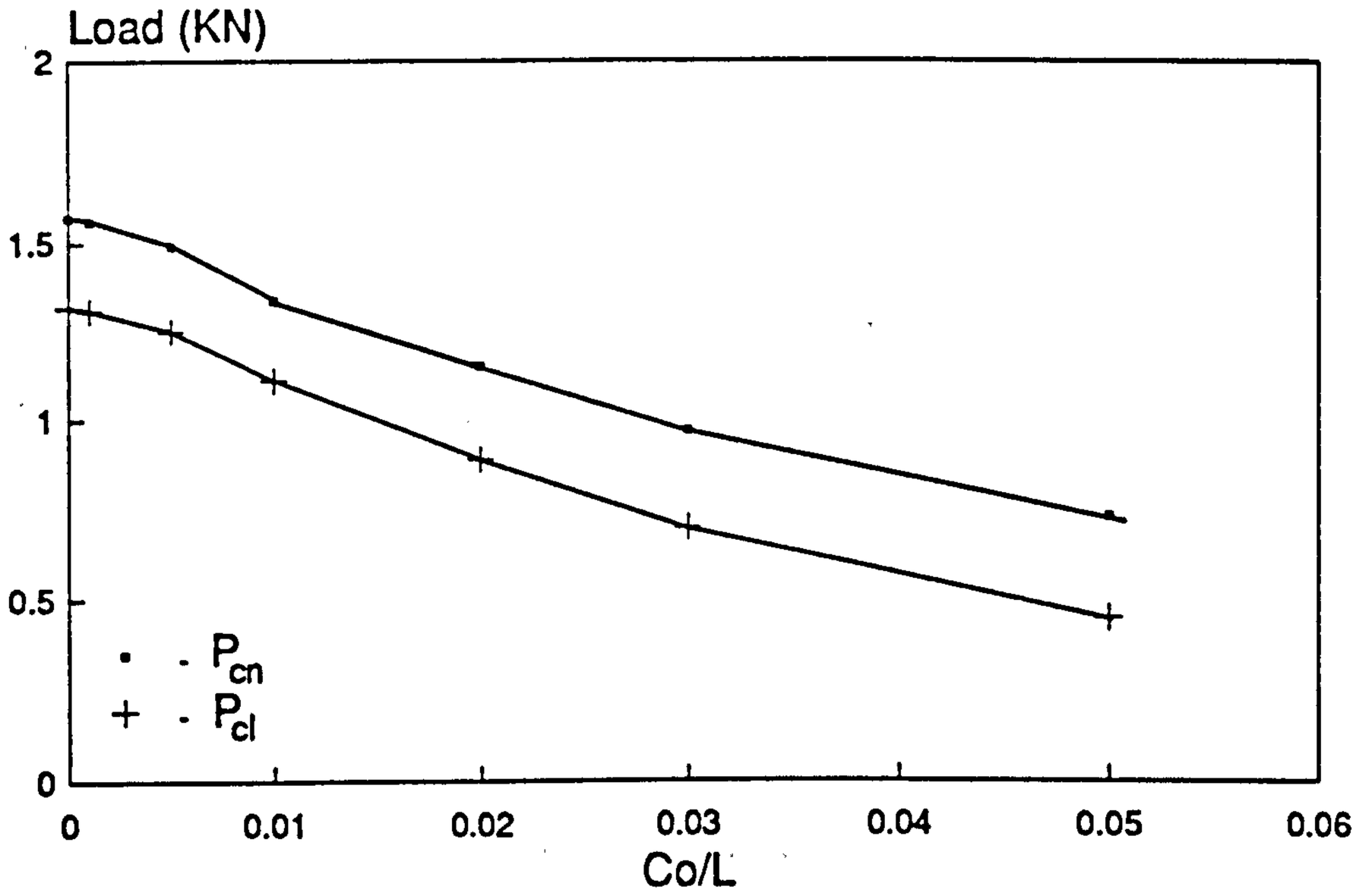

Fig.11.39 Effects of imperfection

$$(P_{cn}-P_{cl})100/P_{cn} \quad (\%)$$

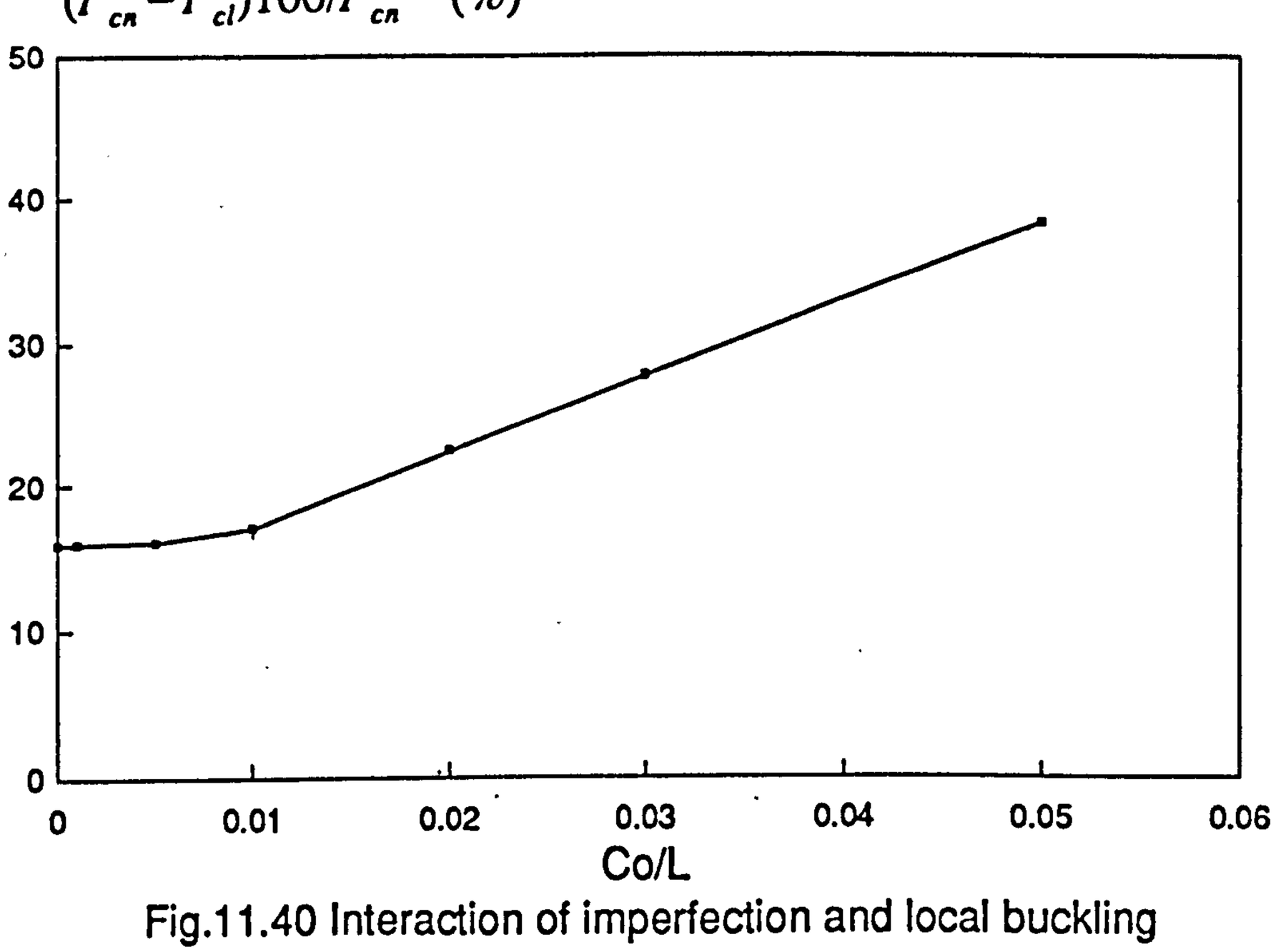

Fig.11.40 Interaction of imperfection and local buckling

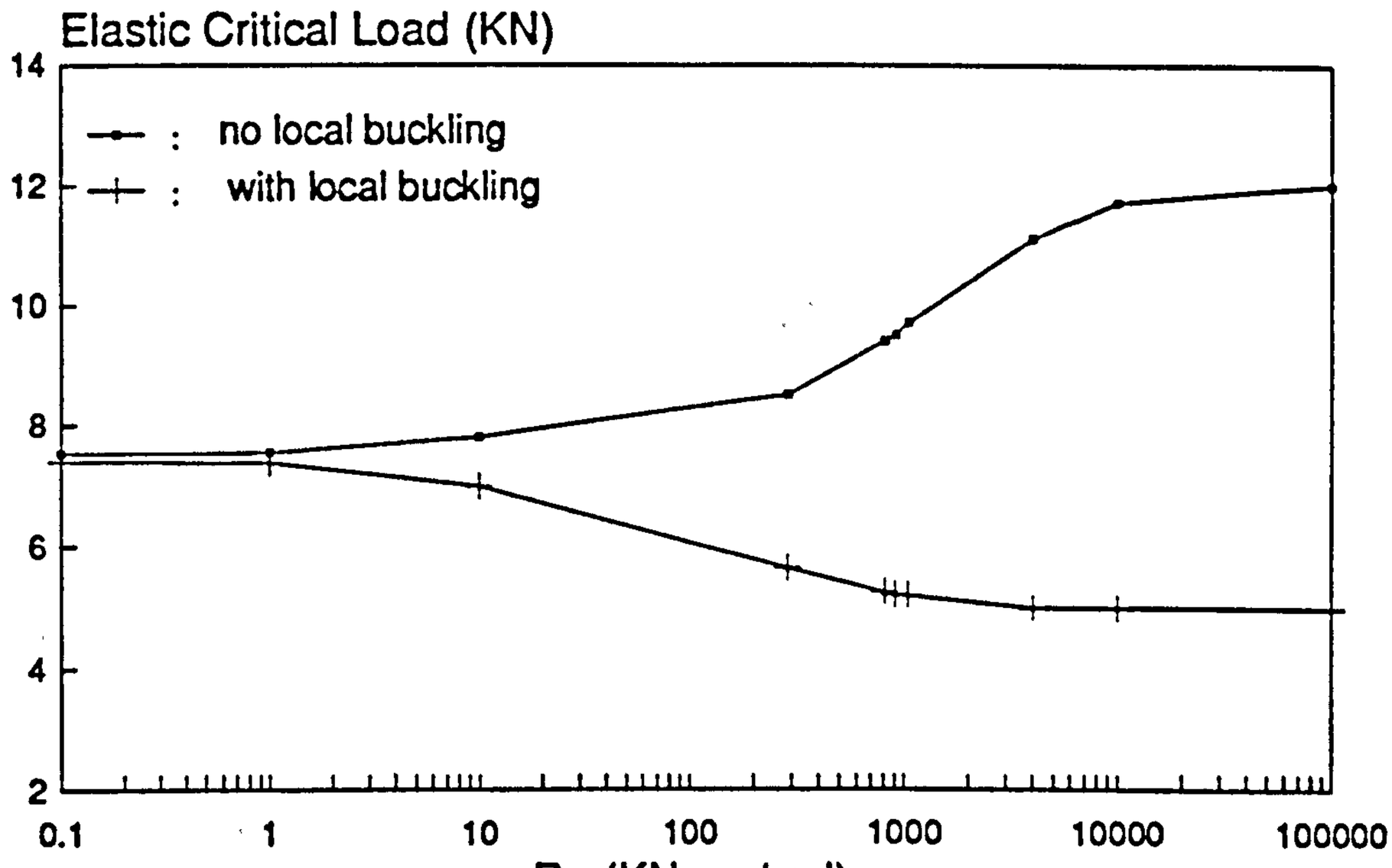

Fig.11.41 Frame F1-1A to E Load/Connection Stiffness plot

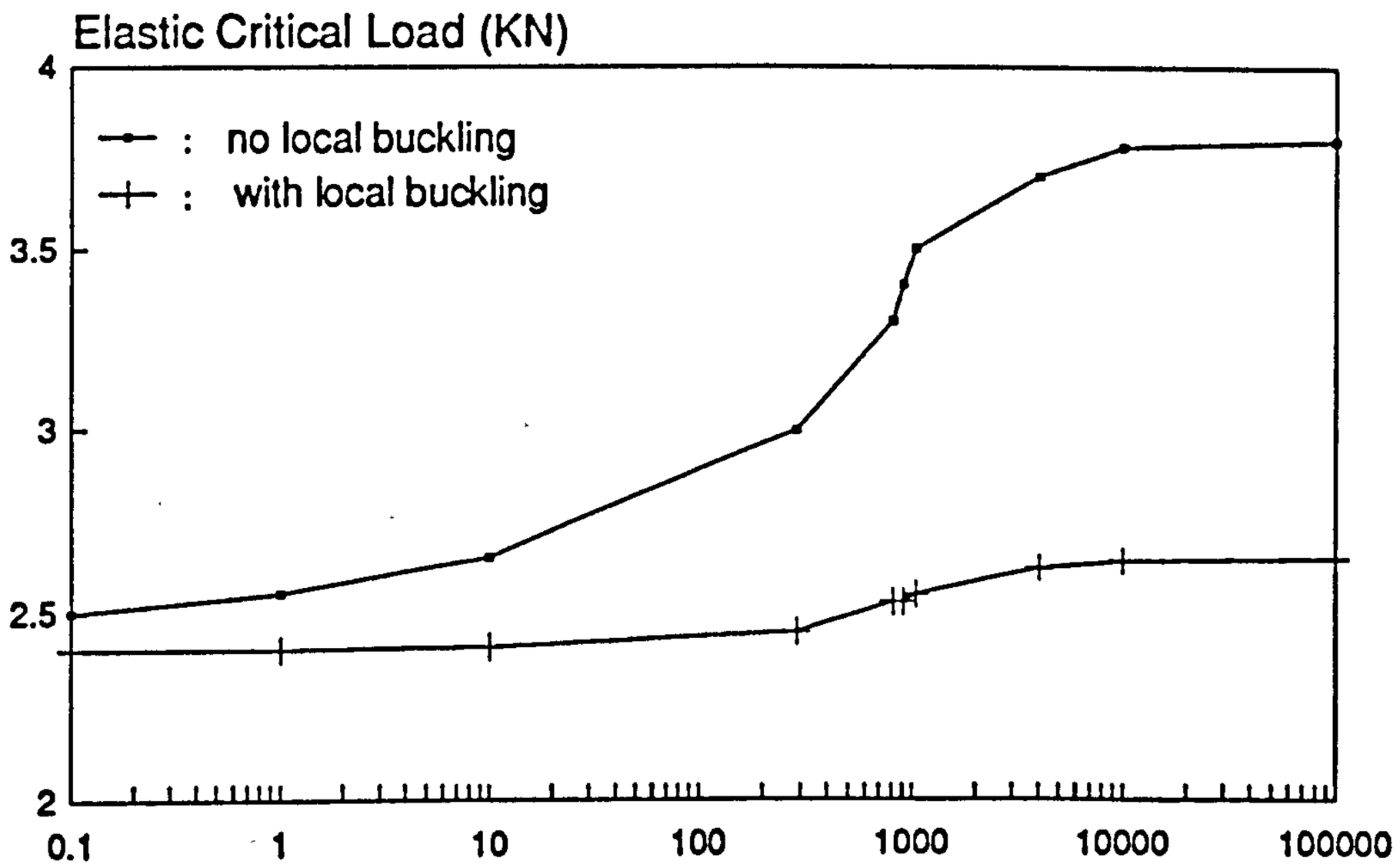

Fig.11.42 Frame F1-2A to E Load/Connection Stiffness plot

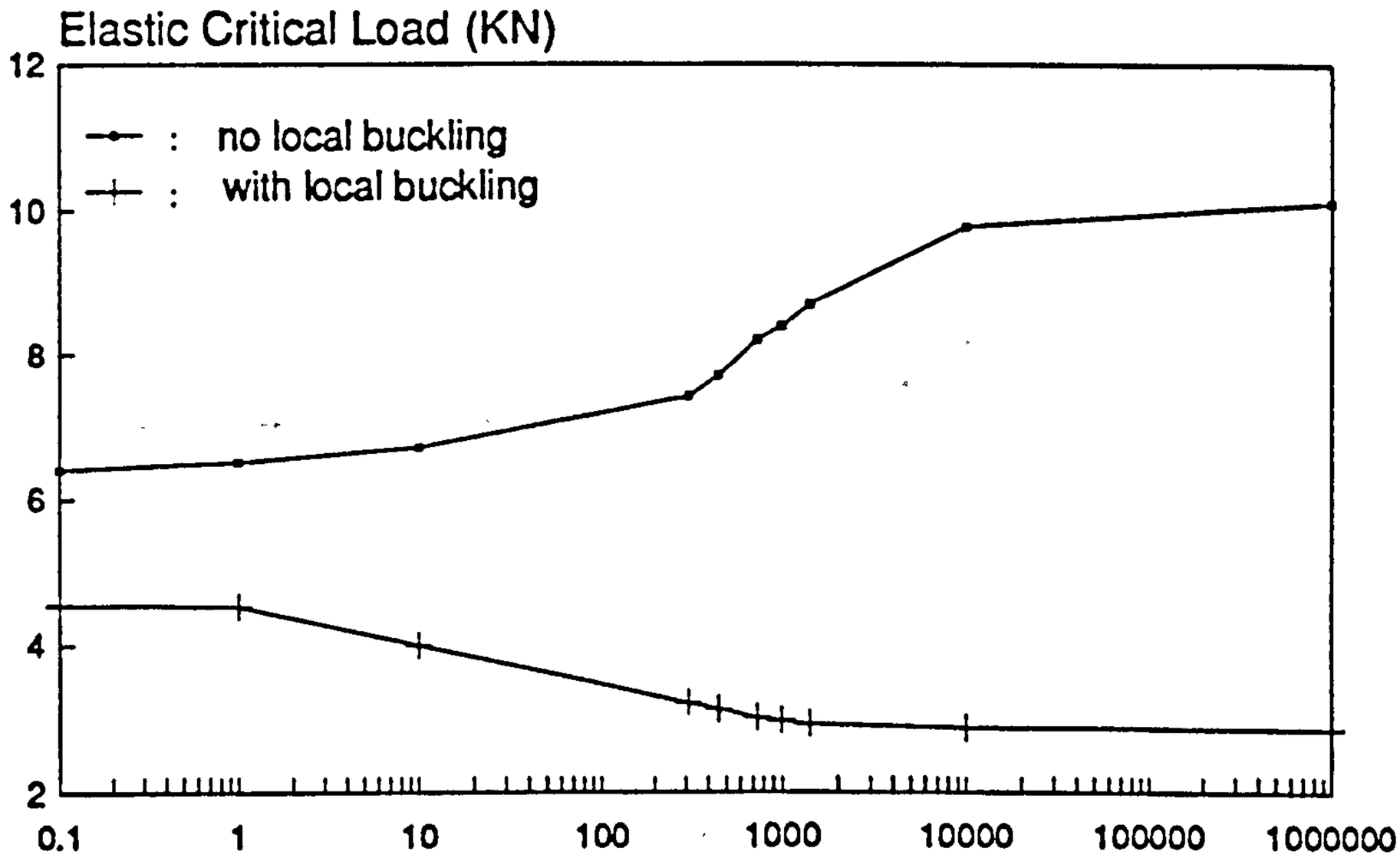

Fig.11.43 Frame F2-1A to E Load/Connection Stiffness plot

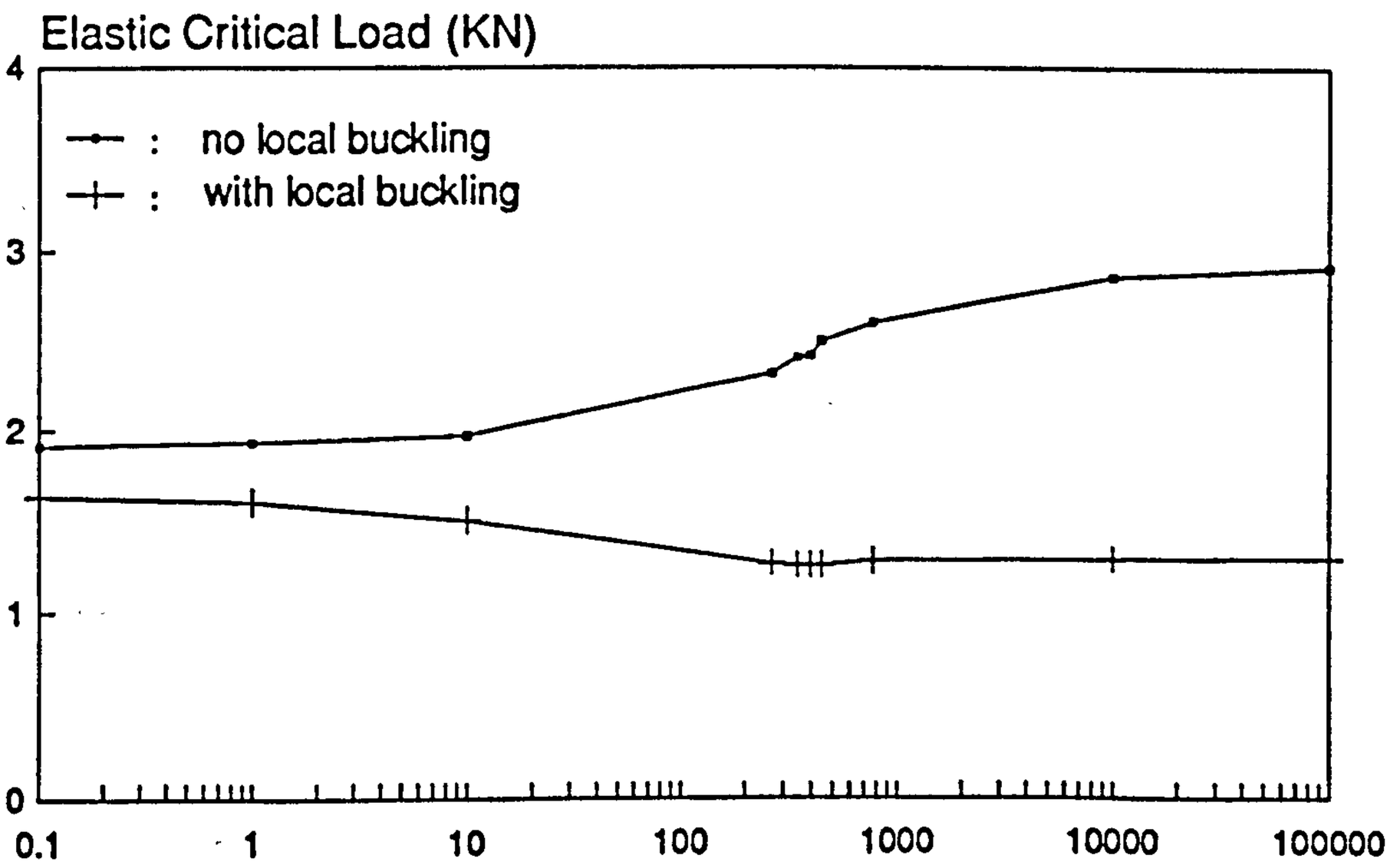

Fig.11.44 Frame F2-2A to E Load/Connection Stiffness plot

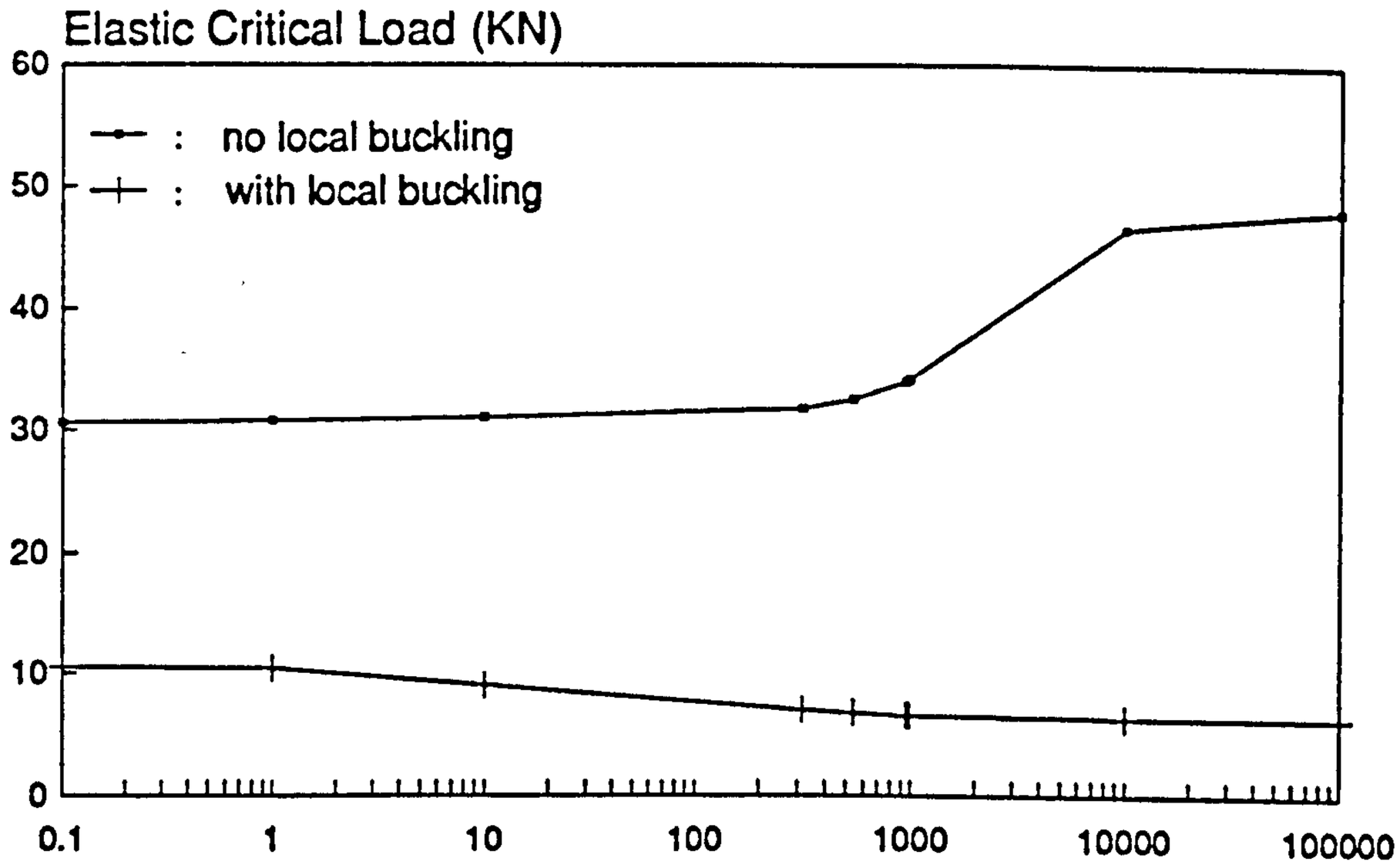

Fig.11.45 Frame F3-1A to E Load/Connection Stiffness plot

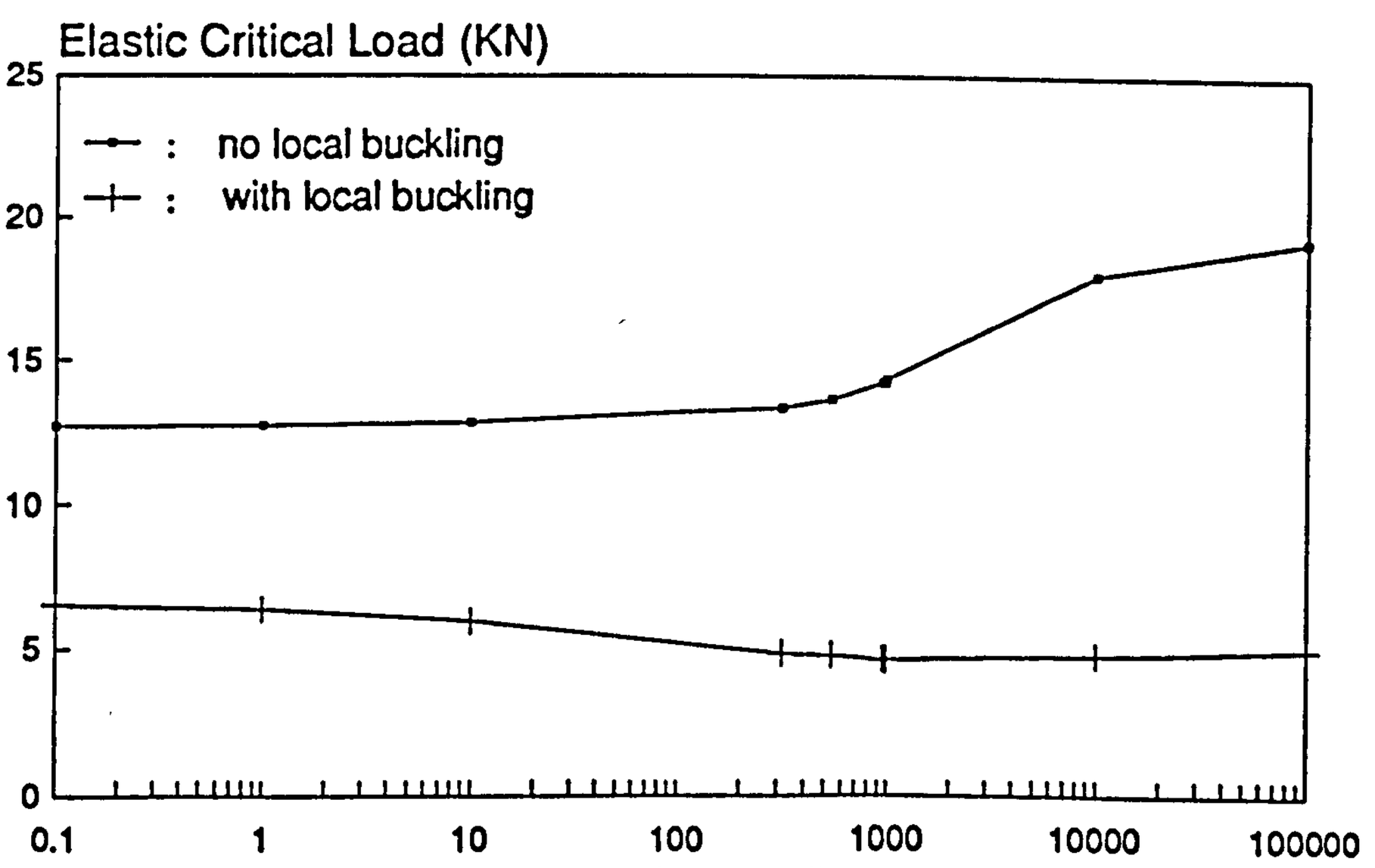

Fig.11.46 Frame F3-2A to E Load/Connection Stiffness plot

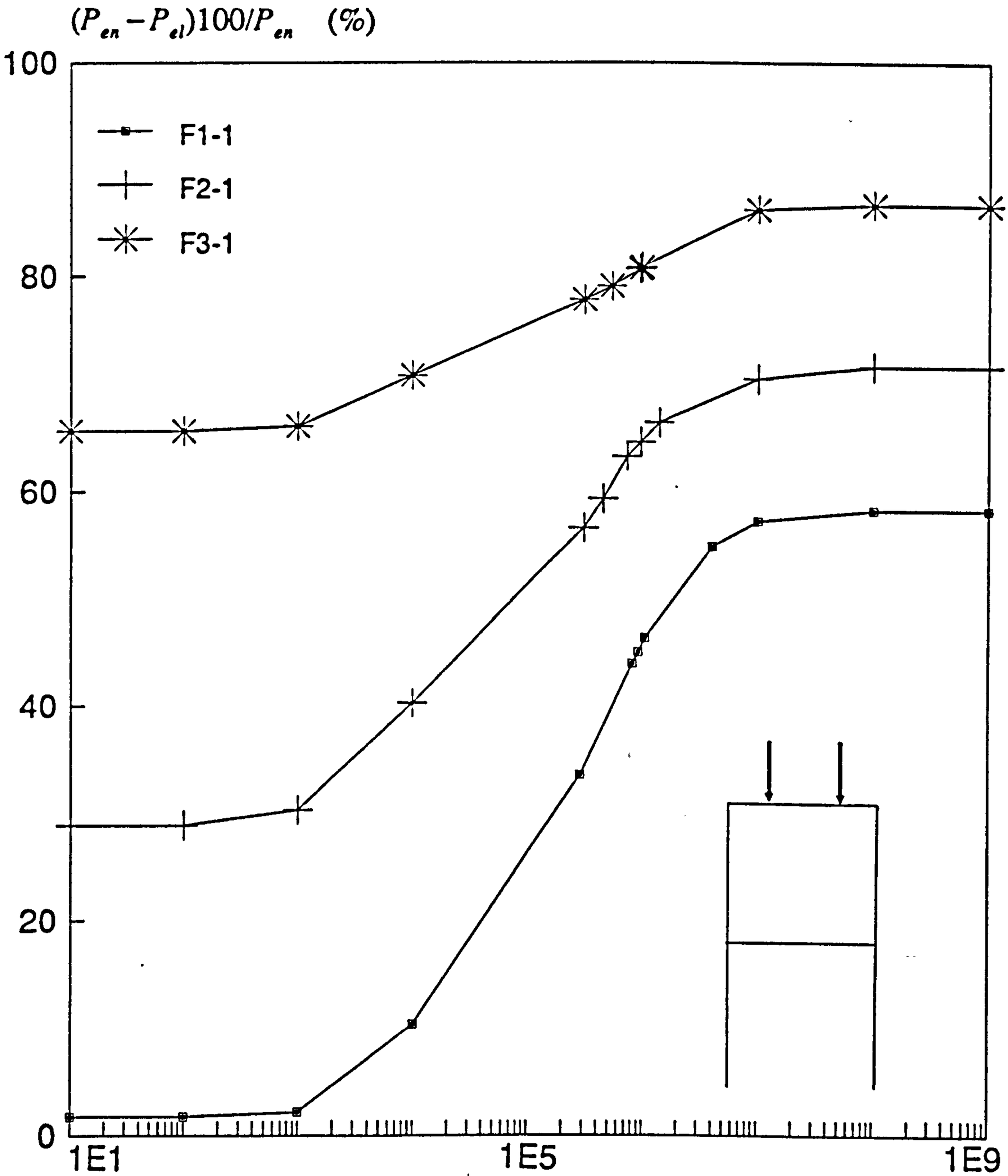

Fig.11.47 Effects of local buckling on elastic critical load

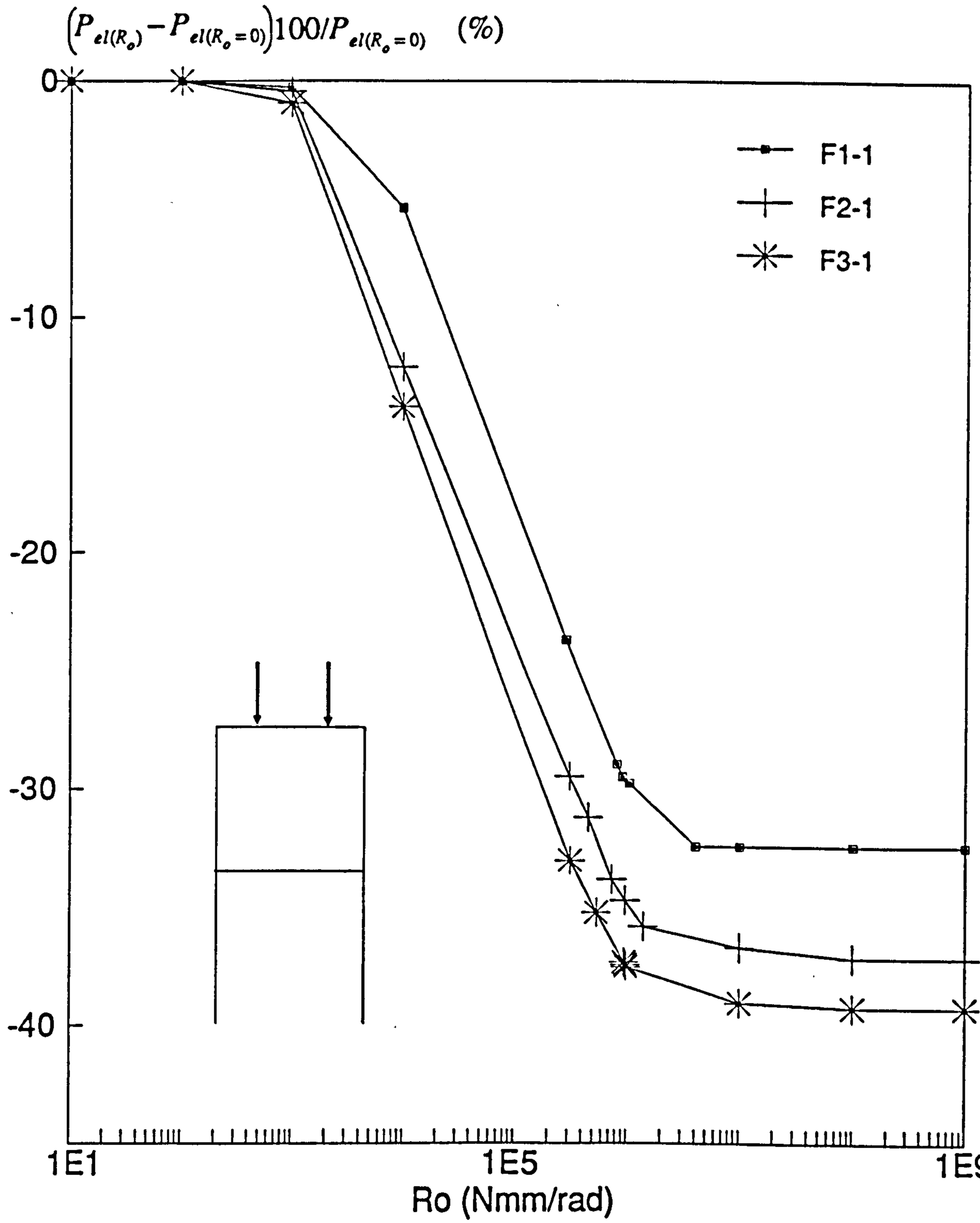

Fig.11.48 Change in elastic critical load with stiffness

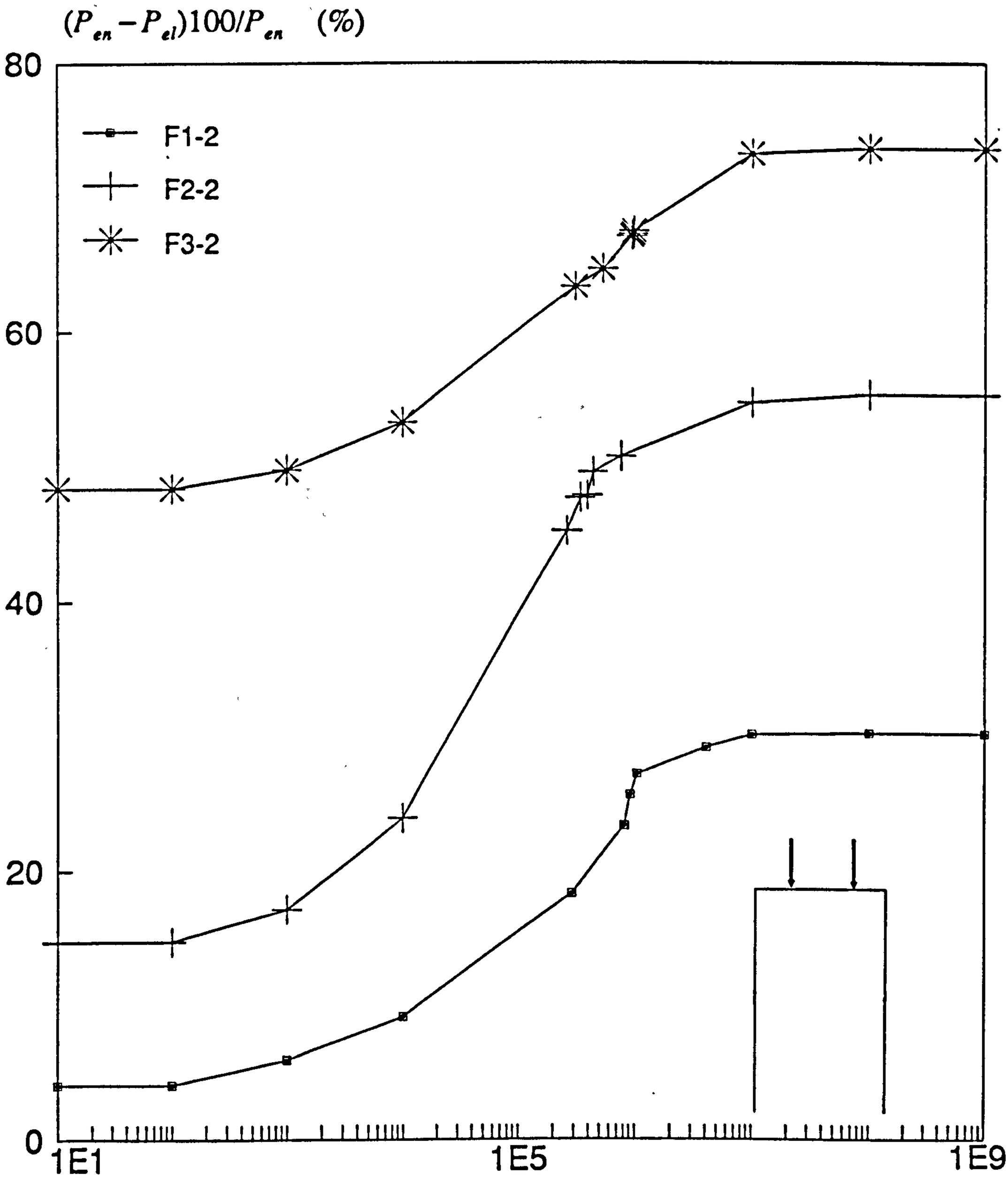

Fig.11.49 Effects of local buckling on elastic critical load

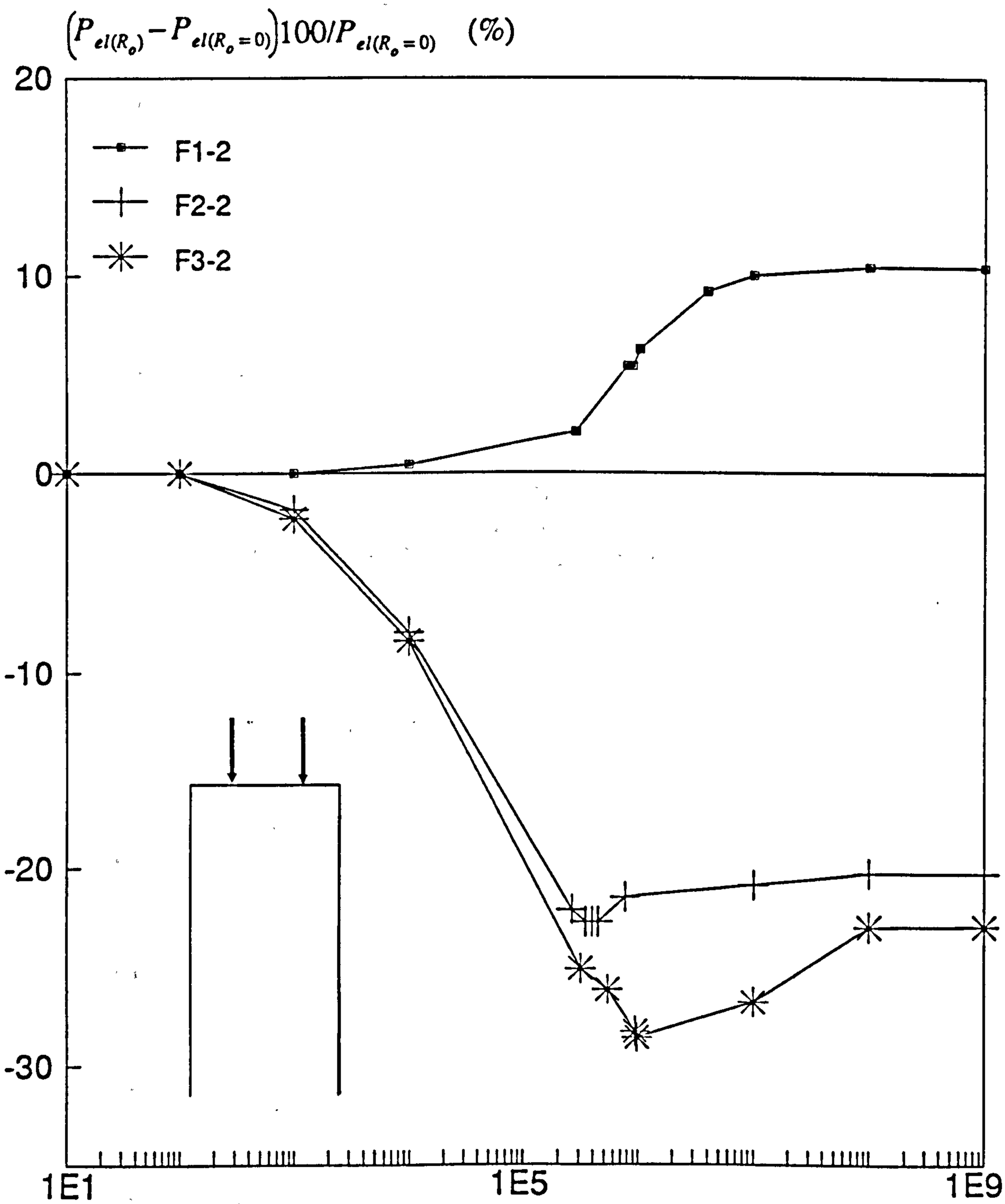

Fig.11.50 Change in elastic critical load with stiffness

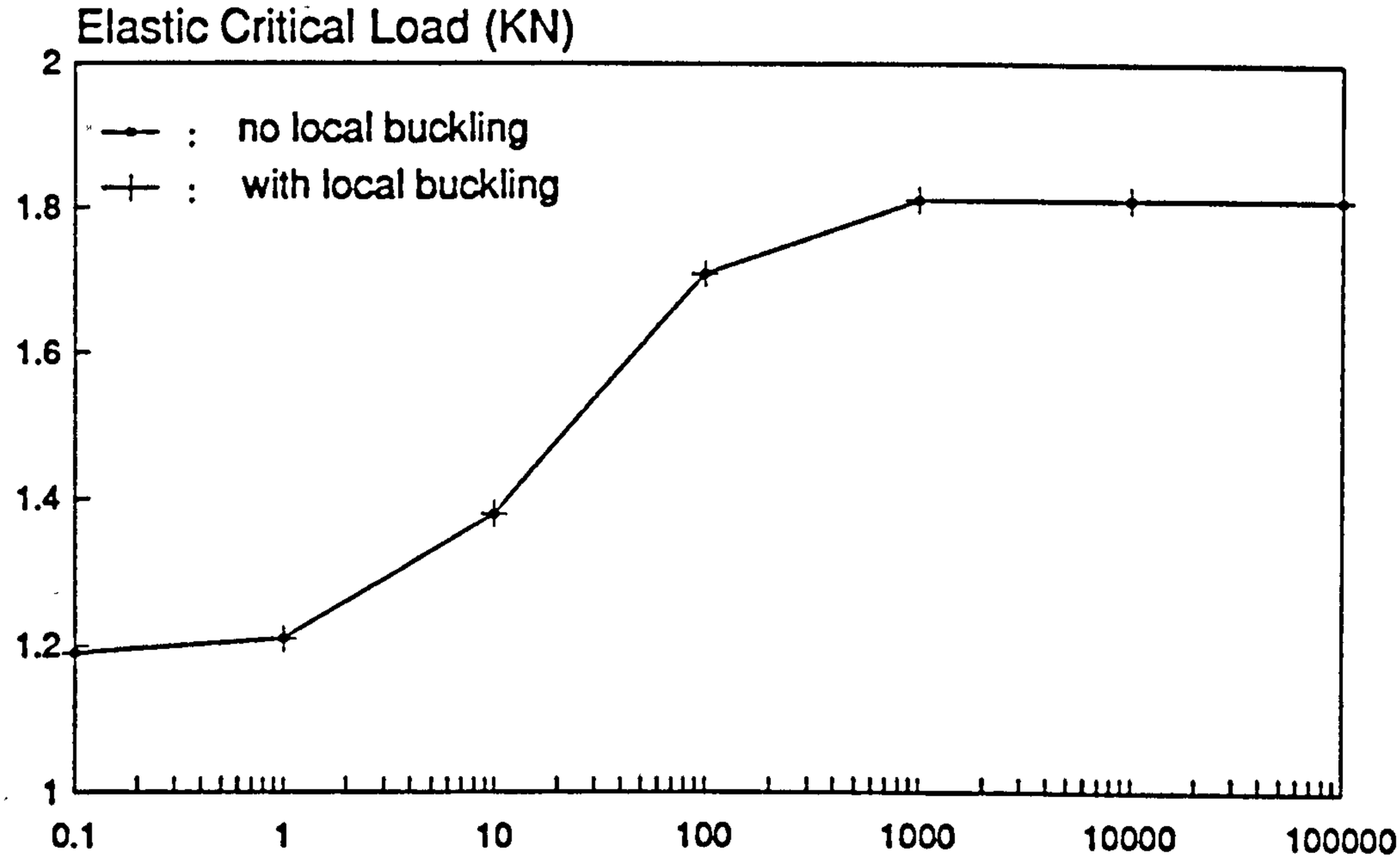

Fig.11.51 Frame F10-5-1 Load/Connection Stiffness plot

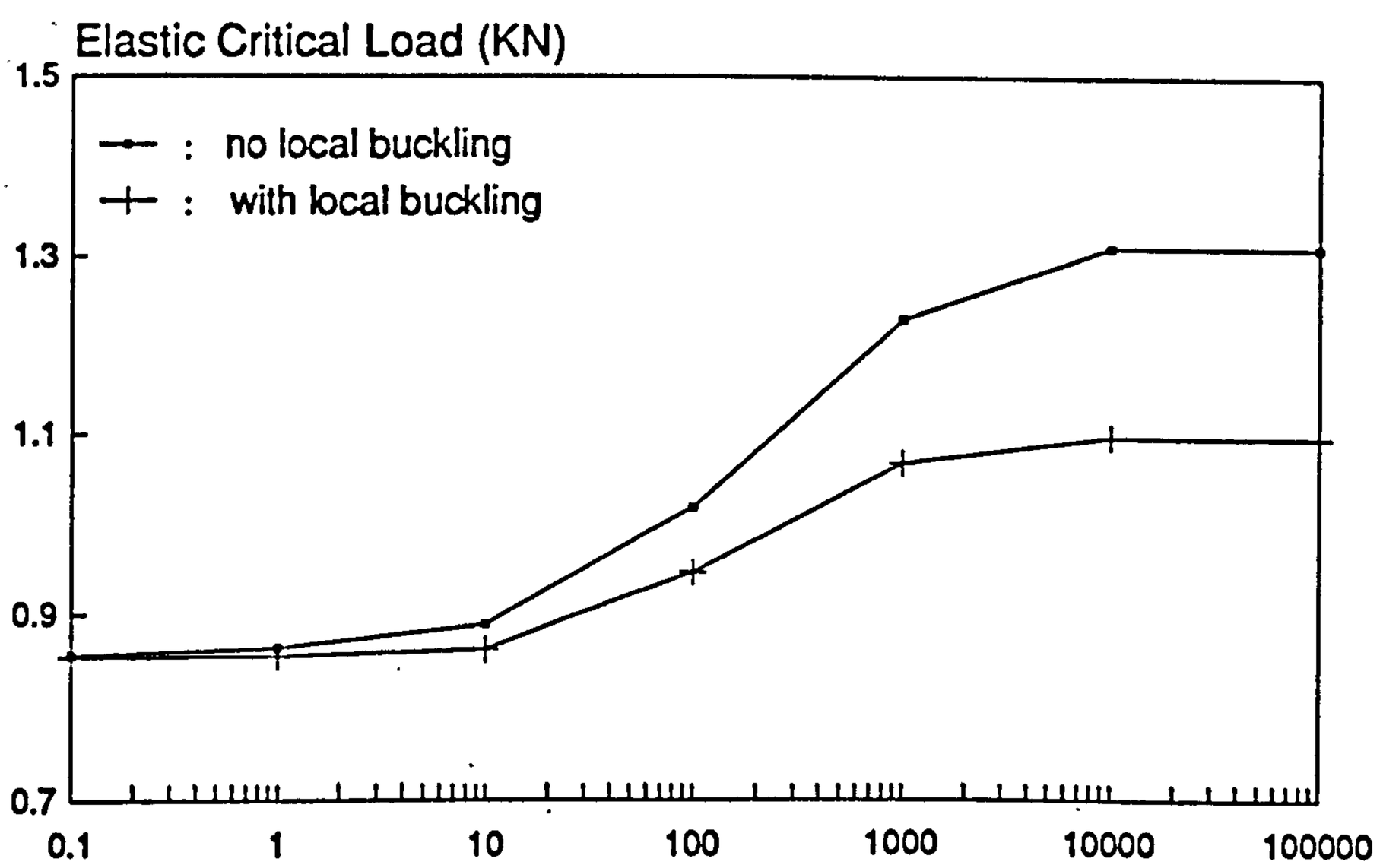

Fig.11.52 Frame F10-10-1 Load/Connection Stiffness plot

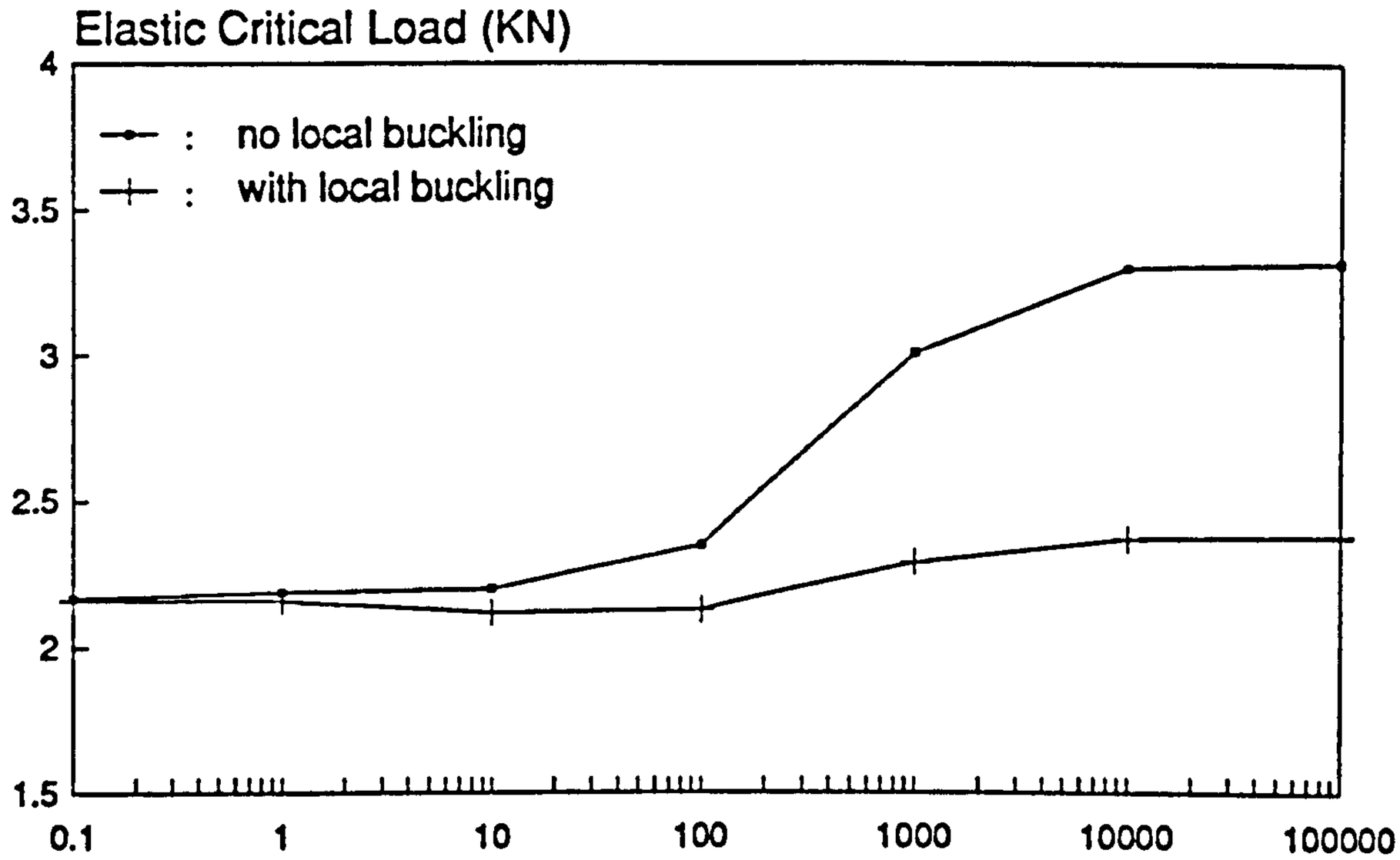

Fig.11.53 Frame F10-14-1 Load/Connection Stiffness plot

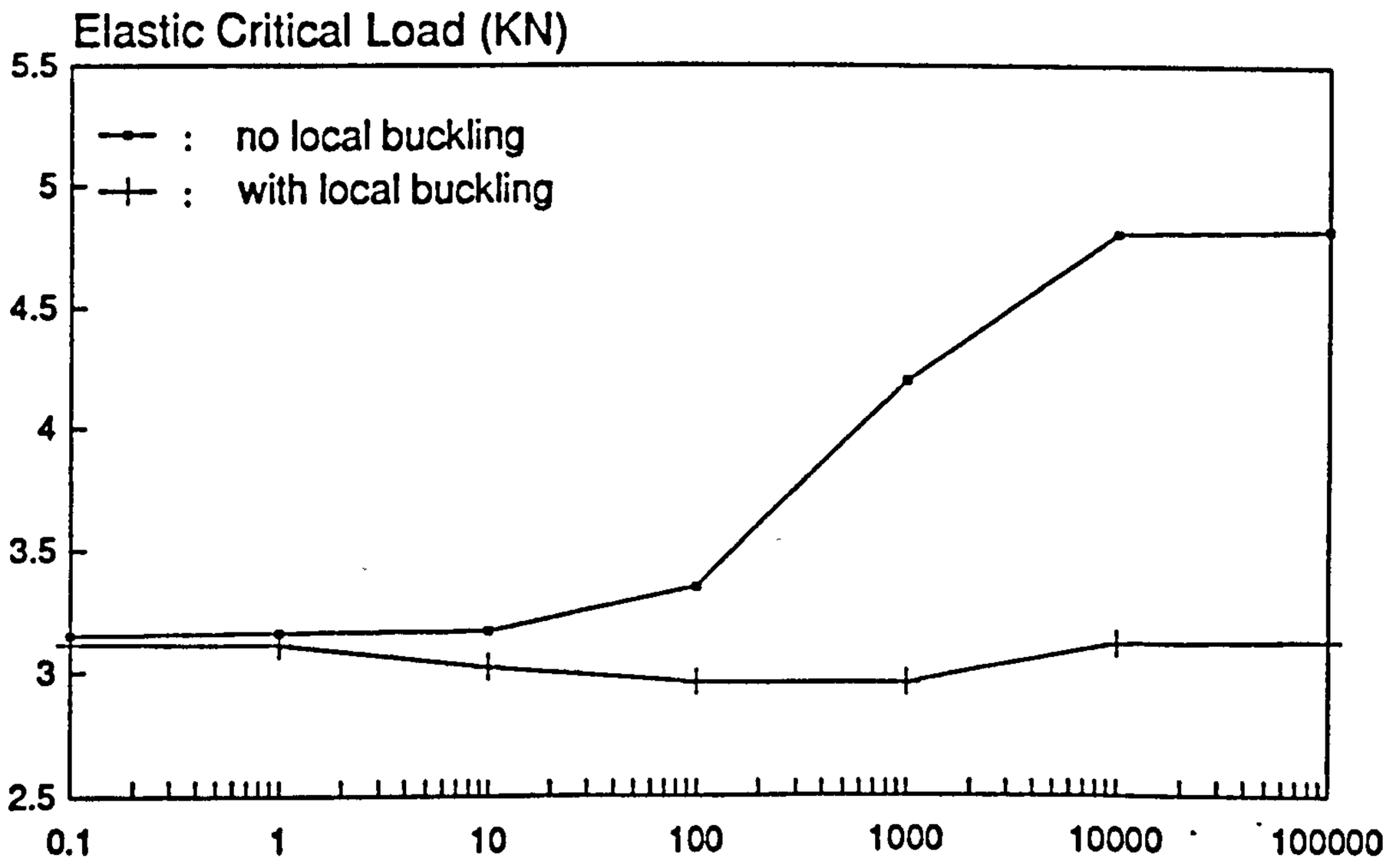

Fig.11.54 Frame F10-16-1 Load/Connection Stiffness plot

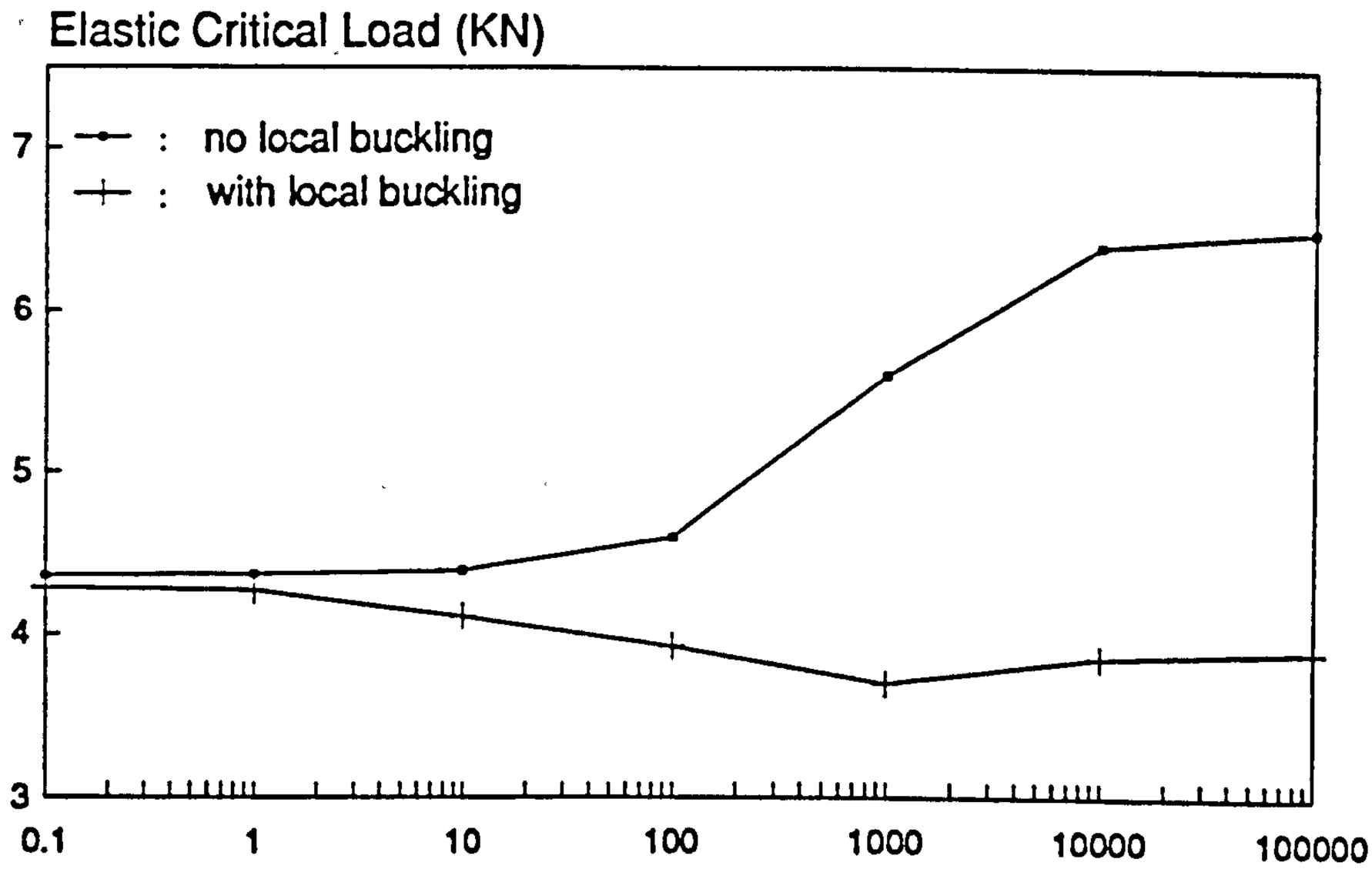

Fig.11.55 Frame F10-18-1 Load/Connection Stiffness plot

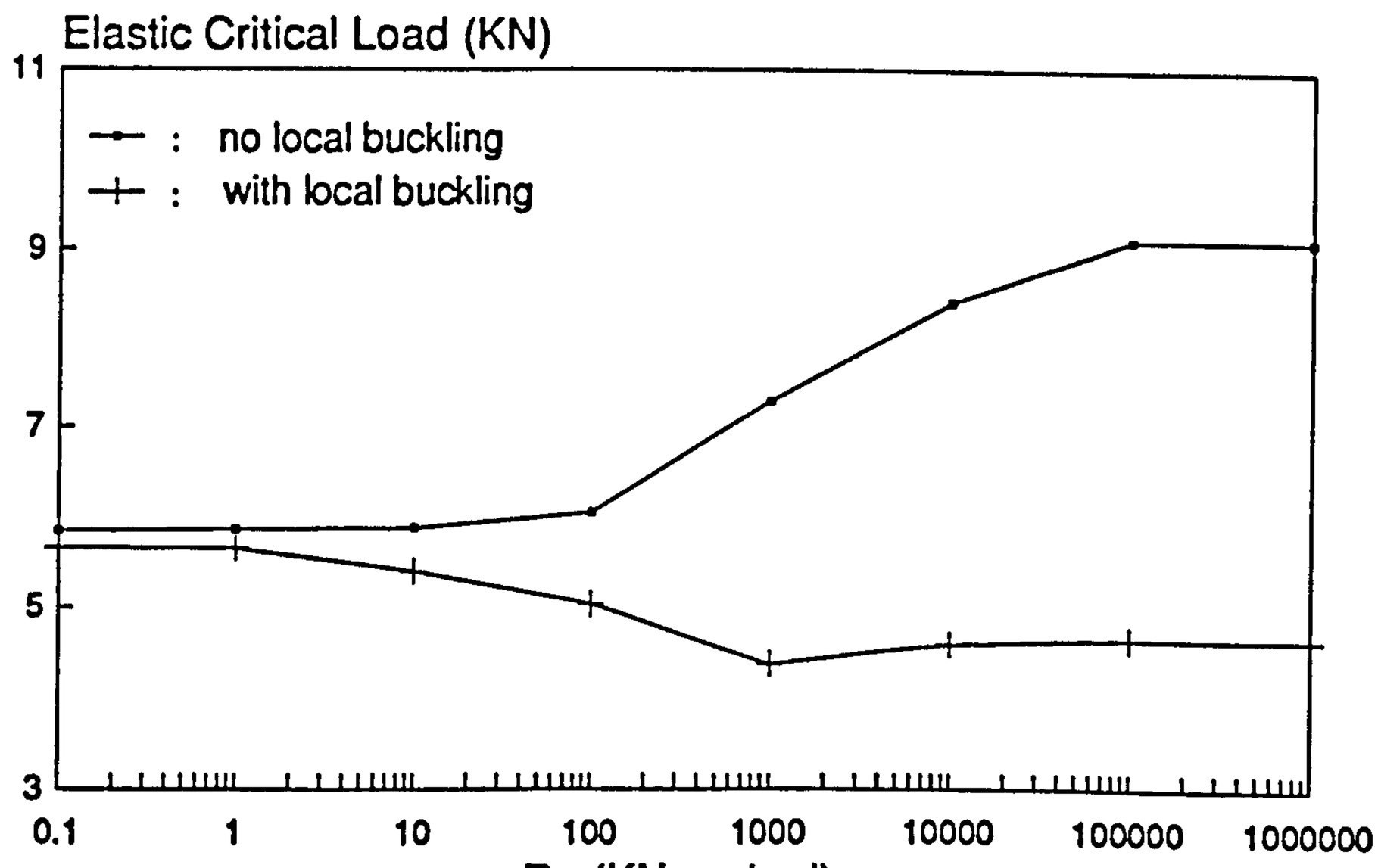

Fig.11.56 Frame F10-20-1 Load/Connection Stiffness plot

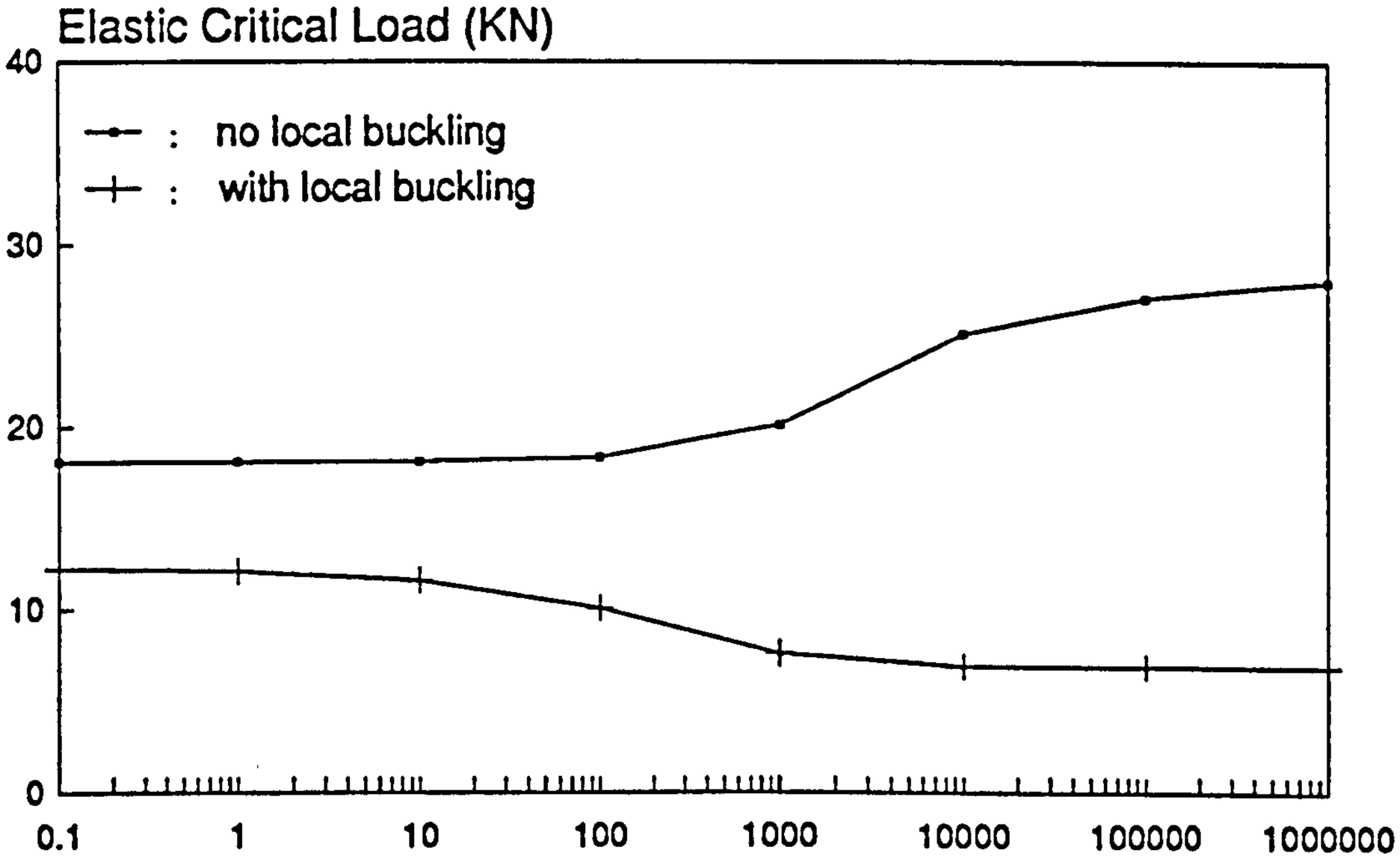

Fig.11.57 Frame F10-30-1 Load/Connection Stiffness plot

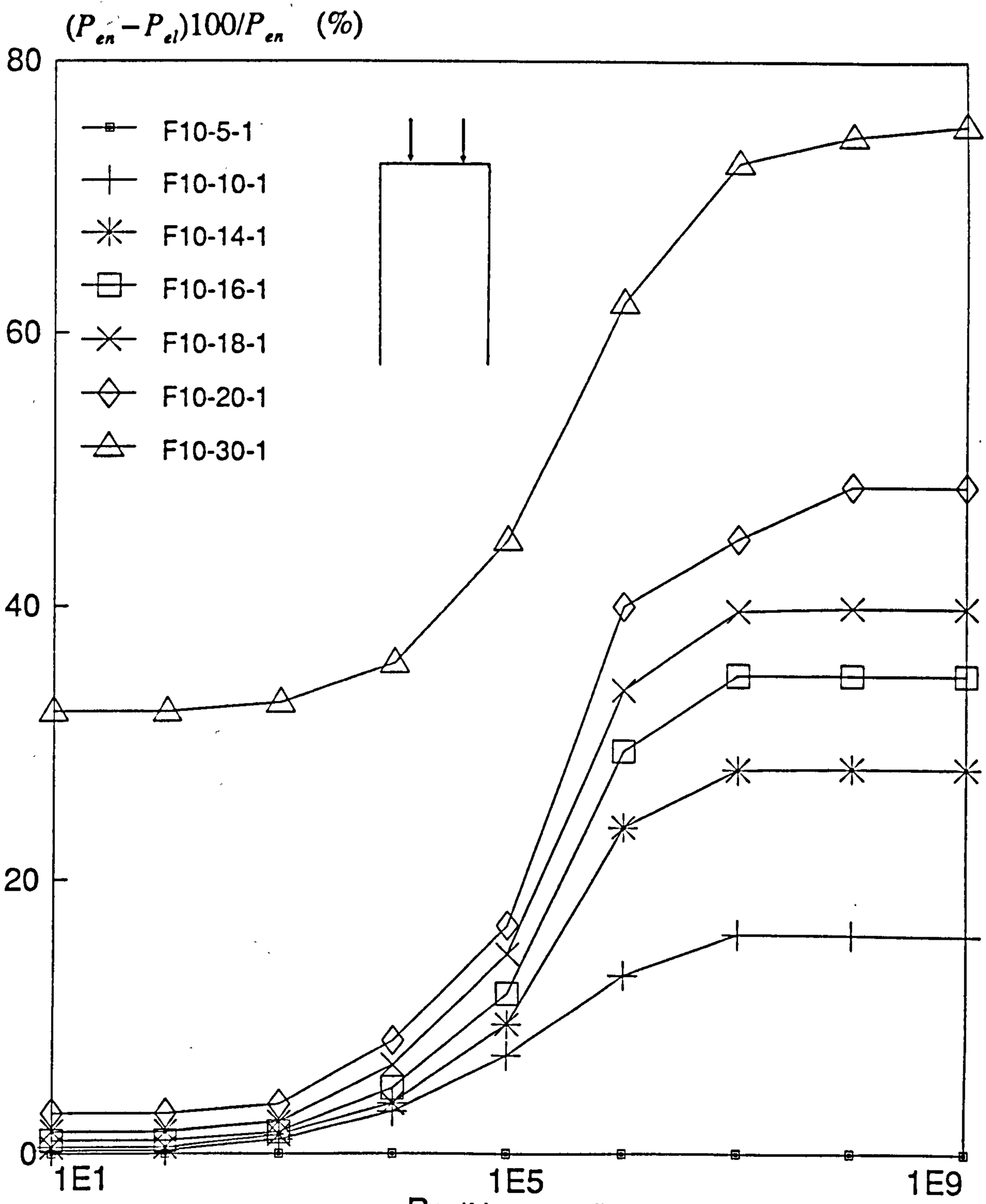

Fig.11.58 Effects of local buckling on elastic critical load

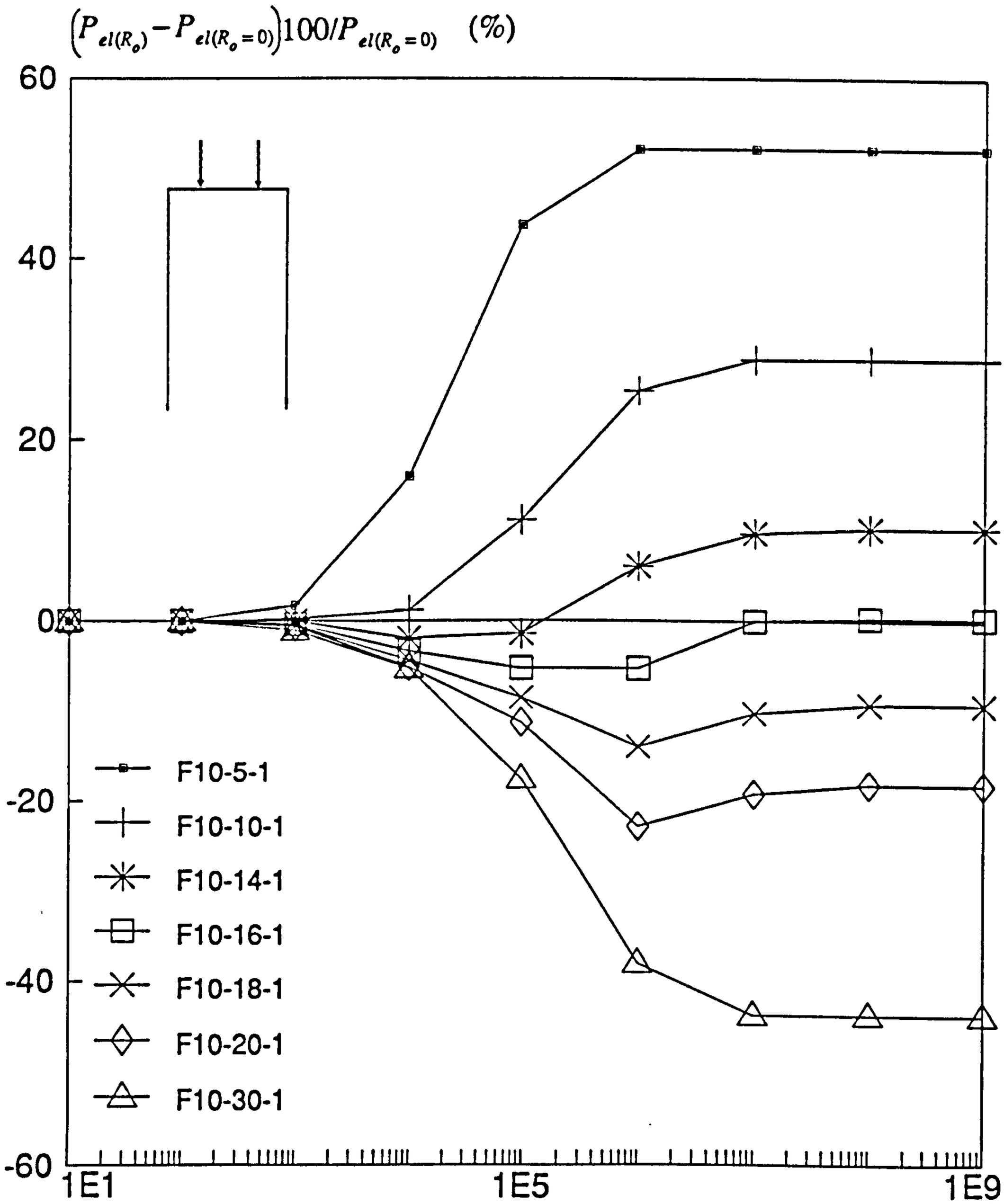

Fig.11.59 Change in elastic critical load with stiffness

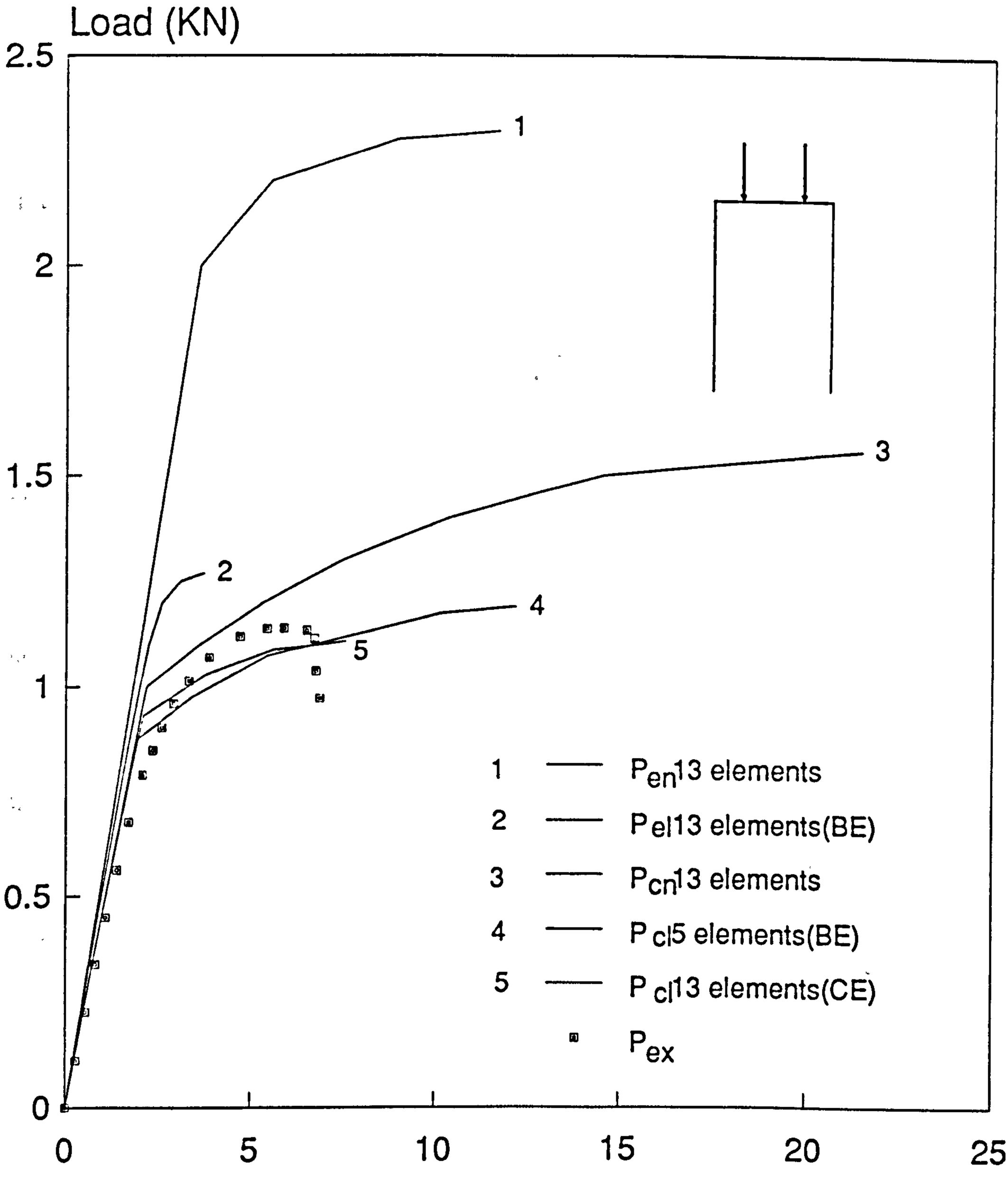

Fig.11.60 Frame F2-2A Load/Displacement plot

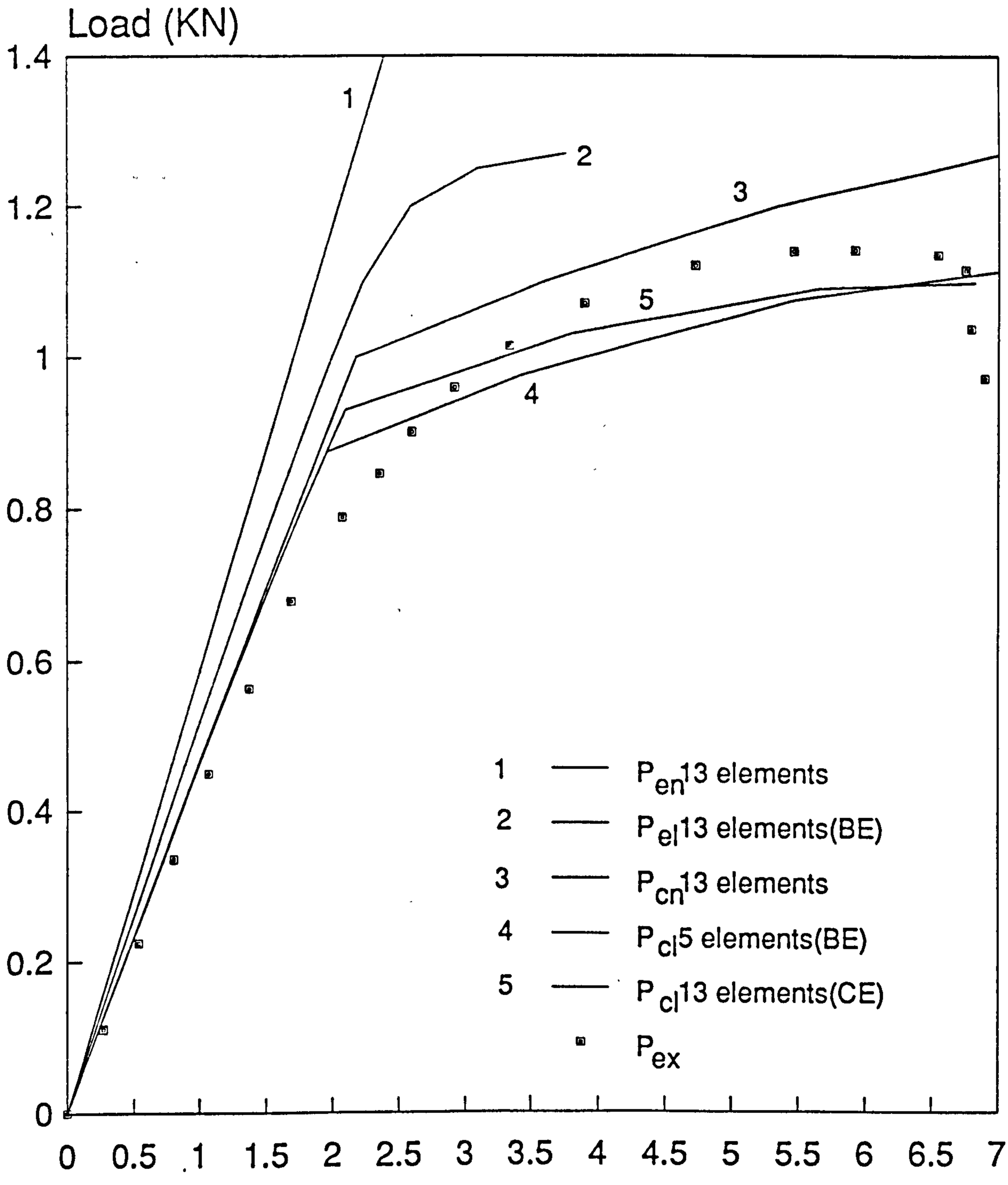

Fig.11.61 Expanded plot of Fig.11.60

Framework No.	A	B	C	D	E	F	Z
	P_{cn} 8 ele	P_{cl} 8 ele (BE)	P_{cl} 18 ele (BE)	P_{cl} 14 ele (CE)	P_{cl} 18 ele (CE)	P_{cl} 18 ele (CE2)	P_{ex}
F3-1A	3.60	2.80	3.42	3.37	3.37	3.05	2.765
F3-1B	3.90	3.05	3.80	3.64	3.64	3.19	2.916
F3-1C	4.20	3.25	3.94	3.68	3.68	3.32	3.088
F3-1D	5.20	3.30	4.25	3.76	3.76	3.59	3.277
F3-1E	5.30	3.30	4.22	3.75	3.75	3.61	3.478
F1-1A	1.85	1.85	1.85	1.80	1.80	-	1.800
F1-1B	2.30	2.25	2.29	2.10	2.10	-	2.149
F1-1C	2.35	2.30	2.32	2.14	2.14	-	2.184
F1-1D	2.30	2.30	2.30	2.14	2.14	-	2.184
F1-1E	2.30	2.20	2.25	2.03	2.03	-	2.064
F2-1A	1.75	1.55	1.60	1.37	1.37	-	1.449
F2-1B	1.80	1.57	1.61	1.42	1.42	-	1.516
F2-1C	1.85	1.57	1.65	1.45	1.45	-	1.551
F2-1D	1.85	1.58	1.69	1.49	1.49	-	1.603
F2-1E	1.80	1.55	1.59	1.38	1.38	-	1.420

All units in *KN*

Table 11.1 Experimental and Various Theoretical Collapse Loads

Frame No.	A	B	C	D	E	F	G	H	Z
	P_{cn} 5 ele	P_{cl} 5 ele (BE)	P_{cl} 13 ele (BE)	P_{cl} 9 ele (CE)	P_{cl} 13 ele (CE)	P_{cl} 13 ele (CE2)	P_{cl} 9 ele (BE)	P_{cl} 23 ele (CE)	P_{ex}
F1-2A	1.85	1.85	1.85	1.85	1.85	-	-	-	1.833
F1-2B	2.05	2.00	2.00	1.95	1.95	-	-	-	1.703
F1-2C	2.05	2.00	2.00	1.95	1.95	-	-	-	1.743
F1-2D	2.05	2.00	2.00	1.95	1.95	-	-	-	1.833
F1-2E	2.00	1.95	1.95	1.80	1.80	-	-	-	1.784
F2-2A	1.56	1.19	1.25	1.110	1.110	-	-	-	1.128
F2-2B	1.56	1.20	1.30	1.095	1.095	-	1.30	1.115	1.146
F2-2C	1.57	1.20	1.29	1.115	1.115	-	-	-	1.113
F2-2D	1.58	1.21	1.29	1.120	1.120	-	-	-	1.068
F2-2E	1.62	1.23	1.28	1.170	1.170	-	-	-	1.163
F3-2A	3.60	2.80	3.49	3.35	3.35	3.25	-	-	2.716
F3-2B	3.80	3.10	3.78	3.65	3.65	3.31	-	-	2.943
F3-2C	4.10	3.23	4.06	3.72	3.72	3.40	4.06	3.73	3.153
F3-2D	5.00	3.28	4.25	3.80	3.80	3.50	-	-	3.057
F3-2E	5.20	3.26	4.17	3.76	3.76	3.49	-	-	3.456

All units in *KN*

Table 11.2 Experimental and Various Theoretical Collapse Loads

Frame No.	A/Z	B/Z	C/Z	D/Z	F/Z	G/Z	H/Z
F1-1A	1.028	1.028	1.028	1.000	-	-	-
F1-1B	1.070	1.047	1.066	0.977	-	-	-
F1-1C	1.076	1.053	1.062	0.980	-	-	-
F1-1D	1.053	1.053	1.053	0.980	-	-	-
F1-1E	1.114	1.066	1.090	0.984	-	-	-
F2-1A	1.208	1.070	1.104	0.946	-	-	-
F2-1B	1.187	1.036	1.062	0.937	-	-	-
F2-1C	1.193	1.012	1.064	0.935	-	-	-
F2-1D	1.154	0.986	1.054	0.930	-	-	-
F2-1E	1.268	1.092	1.120	0.972	-	-	-
F3-1A	1.302	1.013	1.237	1.219	1.103	-	-
F3-1B	1.338	1.046	1.303	1.248	1.094	-	-
F3-1C	1.360	1.053	1.276	1.192	1.075	-	-
F3-1D	1.587	1.007	1.297	1.147	1.096	-	-
F3-1E	1.524	0.949	1.213	1.078	1.038	-	-
F1-2A	1.009	1.009	1.009	1.009	-	-	-
F1-2B	1.204	1.174	1.174	1.145	-	-	-
F1-2C	1.176	1.147	1.147	1.119	-	-	-
F1-2D	1.118	1.091	1.091	1.064	-	-	-
F1-2E	1.121	1.093	1.093	1.009	-	-	-
F2-2A	1.383	1.055	1.108	0.984	-	-	-
F2-2B	1.316	1.047	1.134	0.956	-	1.134	0.973
F2-2C	1.411	1.078	1.159	1.002	-	-	-
F2-2D	1.479	1.133	1.208	1.049	-	-	-
F2-2E	1.393	1.058	1.101	1.006	-	-	-
F3-2A	1.325	1.031	1.285	1.233	1.197	-	-
F3-2B	1.291	1.053	1.284	1.240	1.125	-	-
F3-2C	1.300	1.024	1.288	1.180	1.078	1.288	1.183
F3-2D	1.636	1.073	1.390	1.243	1.145	-	-
F3-2E	1.505	0.943	1.207	1.088	1.010	-	-

This table is to be read in conjunction with tables 11.1 and 11.2.

Table 11.3 Comparison of Theoretical and Experimental Failure Loads.

$\frac{C_o}{L}$	P_{cn} (KN)	P_{cl} (KN)	$\frac{P_{cn}-P_{cl}}{P_{cn}}\times 100$
0.000	1.57	1.32	15.92
0.001	1.56	1.31	16.03
0.005	1.49	1.25	16.11
0.010	1.34	1.11	17.16
0.020	1.15	0.89	22.61
0.030	0.97	0.70	27.84
0.050	0.73	0.45	38.36

Table 11.4 Effects of Initial Imperfection.

$R_\bullet$ (*Nmm/rad*)	P_{en} (*KN*)	P_{el} (*KN*)	$\frac{P_{en}-P_{el}}{P_{en}}\times 100$	$\frac{P_{el(R_\bullet)}-P_{el(R_\bullet=0)}}{P_{el(R_\bullet=0)}}\times 100$
Framework Series F1-2				
0.0000	2.50	2.40	4.00	0.00
1.00E2	2.50	2.40	4.00	0.00
1.00E3	2.55	2.40	5.88	0.00
1.00E4	2.65	2.41	9.06	0.42
2.89E5	3.00	2.45	18.33	2.08
8.15E5	3.30	2.53	23.33	5.42
9.15E5	3.40	2.53	25.59	5.42
1.05E6	3.50	2.55	27.14	6.25
4.03E6	3.70	2.62	29.19	9.17
1.00E7	3.78	2.64	30.16	10.00
1.00E8	3.80	2.65	30.26	10.42
1.0E20	3.80	2.65	30.26	10.42
Framework Series F2-2				
0.0000	1.91	1.63	14.66	0.00
1.00E2	1.91	1.63	14.66	0.00
1.00E3	1.93	1.60	17.10	-1.84
1.00E4	1.97	1.50	23.86	-7.98
2.65E5	2.32	1.27	45.26	-22.09
3.47E5	2.41	1.26	47.72	-22.70
3.95E5	2.42	1.26	47.93	-22.70
4.45E6	2.50	1.26	49.60	-22.70
7.73E6	2.60	1.28	50.77	-21.47
1.00E7	2.85	1.29	54.74	-20.86
1.00E8	2.91	1.30	55.33	-20.25
1.0E20	2.91	1.30	55.33	-20.25
Framework Series F3-2				
0.000	12.70	6.55	48.43	0.00
1.00E2	12.70	6.55	48.43	0.00
1.00E3	12.75	6.40	49.80	-2.29
1.00E4	12.85	6.00	53.31	-8.40
3.15E5	13.40	4.91	63.36	-25.04
5.40E5	13.70	4.84	64.67	-26.11
9.50E5	14.30	4.70	67.13	-28.24
9.75E5	14.30	4.68	67.27	-28.55
9.87E5	14.40	4.68	67.50	-28.55
1.00E7	18.00	4.80	73.33	-26.72
1.00E8	19.20	5.05	73.70	-22.90
1.0E20	19.20	5.05	73.70	-22.90

Table 11.5 Elastic Critical Loads for Single Storey Frameworks

R_e (*Nmm/rad*)	P_{en} (*KN*)	P_{el} (*KN*)	$\frac{P_{en}-P_{el}}{P_{en}}\times 100$	$\frac{P_{el(R_e)}-P_{el(R_e=0)}}{P_{el(R_e=0)}}\times 100$
Framework Series F1-1				
0.0000	7.53	7.40	1.730	0.00
1.00E2	7.53	7.40	1.730	0.00
1.00E3	7.54	7.38	2.120	-0.270
1.00E4	7.80	7.00	10.26	-5.410
2.89E5	8.50	5.65	33.55	-23.65
8.15E5	9.40	5.26	44.04	-28.92
9.15E5	9.50	5.22	45.05	-29.46
1.05E6	9.70	5.20	46.39	-29.73
4.03E6	11.1	5.00	54.95	-32.43
1.00E7	11.7	5.00	57.26	-32.43
1.00E8	12.0	5.00	58.33	-32.43
1.0E20	12.0	5.00	58.33	-32.43
Framework Series F2-1				
0.0000	6.40	4.55	28.91	0.00
1.00E2	6.40	4.55	28.91	0.00
1.00E3	6.50	4.53	30.31	-0.44
1.00E4	6.70	4.00	40.30	-12.09
3.10E5	7.40	3.21	56.62	-29.45
4.55E5	7.70	3.13	59.35	-31.21
7.35E5	8.20	3.01	63.29	-33.85
9.65E6	8.40	2.97	64.64	-34.73
1.40E6	8.70	2.92	66.44	-35.82
1.00E7	9.77	2.88	70.52	-36.70
1.00E8	10.1	2.86	71.68	-37.14
1.0E20	10.1	2.86	71.68	-37.14
Framework Series F3-1				
0.0000	30.6	10.5	65.69	0.00
1.00E2	30.6	10.5	65.69	0.00
1.00E3	30.7	10.4	66.12	-0.95
1.00E4	31.0	9.05	70.81	-13.81
3.15E5	31.7	7.03	77.82	-33.05
5.40E5	32.5	6.80	79.08	-35.24
9.50E5	34.0	6.58	80.65	-37.33
9.75E5	34.1	6.57	80.73	-37.43
9.87E5	34.2	6.56	80.82	-37.52
1.00E7	46.5	6.40	86.24	-39.05
1.00E8	48.0	6.38	86.71	-39.24
1.0E20	48.0	6.38	86.71	-39.24

Table 11.6 Elastic Critical Loads for Double Storey Frameworks

Framework Number	b_2 (mm)	$\frac{b_1}{t}$	$\frac{b_2}{t}$
F10-5-1	5	10	5
F10-10-1	10	10	10
F10-14-1	14	10	14
F10-16-1	16	10	16
F10-18-1	18	10	18
F10-20-1	20	10	20
F10-30-1	30	10	30

Table 11.7 Members Cross Sectional Dimensions

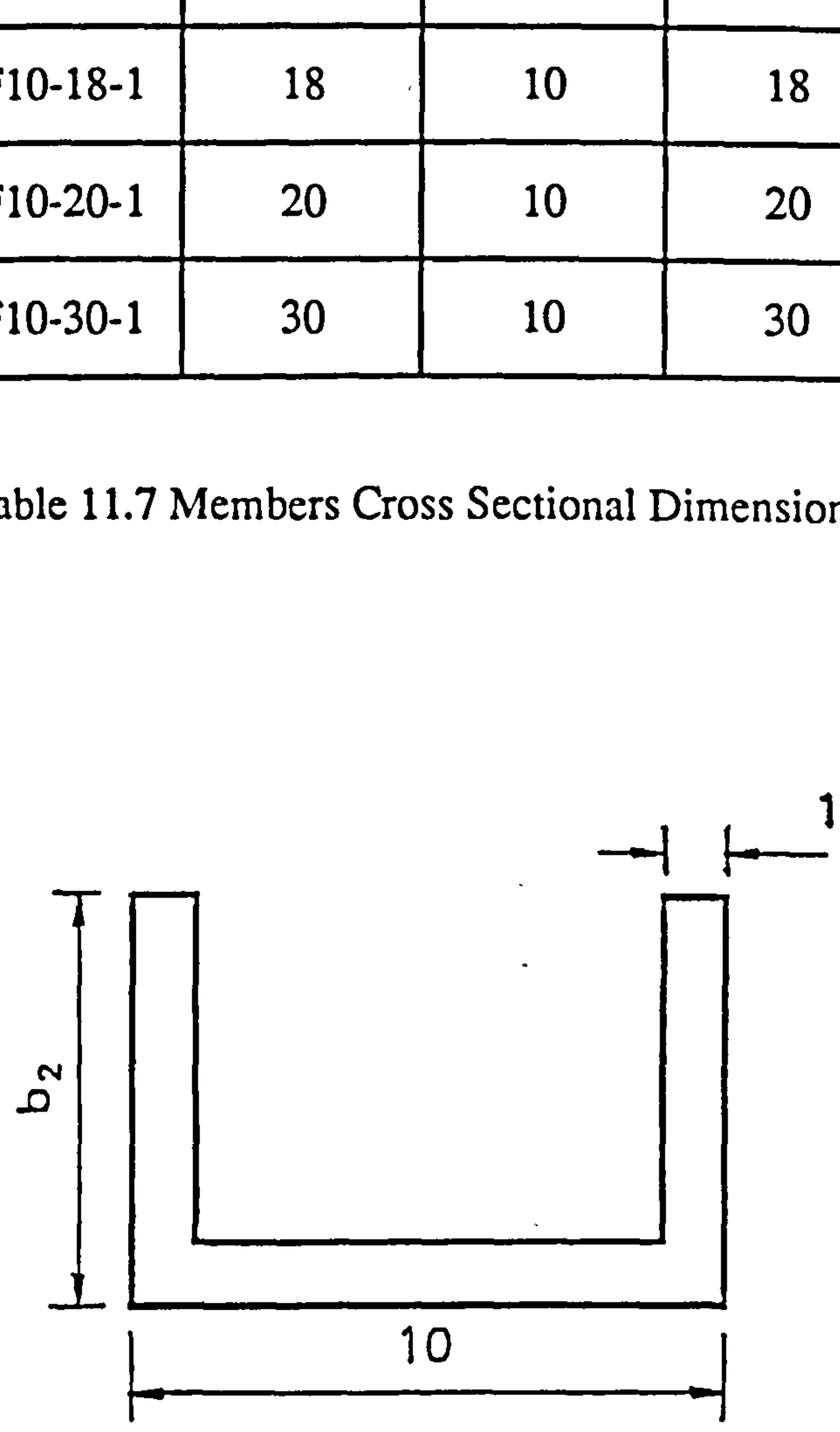

$\sigma_y = 280\ N/mm^2$

$R_\bullet$ (*Nmm/rad*)	P_{en} (*KN*)	P_{el} (*KN*)	$\frac{P_{en}-P_{el}}{P_{en}}\times 100$	$\frac{P_{el(R_\bullet)}-P_{el(R_\bullet=0)}}{P_{el(R_\bullet=0)}}\times 100$
Framework Series F10-5-1				
0	1.19	1.19	0.00	0.000
1E3	1.21	1.21	0.00	1.680
1E4	1.38	1.38	0.00	15.97
1E5	1.71	1.71	0.00	43.70
1E6	1.81	1.81	0.00	52.10
1E20	1.81	1.81	0.00	52.10
Framework Series F10-10-1				
0	0.855	0.853	0.230	0.000
1E3	0.863	0.854	1.040	0.230
1E4	0.890	0.863	3.030	1.170
1E5	1.020	0.948	7.060	11.14
1E6	1.230	1.070	13.01	25.44
1E7	1.310	1.100	16.03	28.96
1E20	1.310	1.100	16.03	28.96
Framework Series F10-14-1				
0	2.17	2.16	0.460	0.00
1E3	2.19	2.16	1.370	0.00
1E4	2.20	2.12	3.640	-1.85
1E5	2.35	2.13	9.360	-1.39
1E6	3.01	2.29	23.92	6.02
1E7	3.30	2.37	28.18	9.72
1E8	3.32	2.38	28.31	10.19
1E20	3.32	2.38	28.31	10.19
Framework Series F10-16-1				
0	3.15	3.12	0.950	0.00
1E3	3.16	3.11	1.580	-0.32
1E4	3.17	3.02	4.730	-3.21
1E5	3.35	2.96	11.64	-5.13
1E6	4.20	2.96	29.52	-5.13
1E7	4.80	3.12	35.00	0.00
1E8	4.82	3.13	35.06	0.32
1E20	4.82	3.13	35.06	0.32

Table 11.8 Elastic Critical Loads

R_o (*Nmm/rad*)	P_{en} (*KN*)	P_{el} (*KN*)	$\frac{P_{en}-P_{el}}{P_{en}}\times 100$	$\frac{P_{el(R_o)}-P_{el(R_o=0)}}{P_{el(R_o=0)}}\times 100$
Framework Series F10-18-1				
0	4.36	4.29	1.610	0.00
1E3	4.37	4.27	2.290	-0.470
1E4	4.39	4.11	6.380	-4.200
1E5	4.60	3.93	14.57	-8.390
1E6	5.60	3.70	33.93	-13.75
1E7	6.40	3.86	39.69	-10.02
1E8	6.50	3.90	40.00	-9.090
1E20	6.50	3.90	40.00	-9.090
Framework Series F10-20-1				
0	5.84	5.67	2.910	0.00
1E3	5.85	5.64	3.590	-0.530
1E4	5.87	5.39	8.180	-4.940
1E5	6.05	5.04	16.69	-11.11
1E6	7.30	4.38	40.00	-22.75
1E7	8.40	4.59	45.36	-19.05
1E8	9.10	4.65	48.90	-17.99
1E20	9.10	4.65	48.90	-17.99
Framework Series F10-30-1				
0	18.08	12.22	32.41	0.00
1E3	18.08	12.10	33.08	-0.980
1E4	18.11	11.60	35.95	-5.080
1E5	18.30	10.09	44.86	-17.46
1E6	20.10	7.60	62.19	-37.87
1E7	25.10	6.90	72.51	-43.61
1E8	27.10	6.90	75.36	-43.61
1E20	28.00	6.90	75.36	-43.61

Table 11.9 Elastic Critical Loads

Frame No.	P_{en} (KN)	P_{el} (KN)	P_{ex} (KN)	$\frac{P_{en}}{P_{el}}$	$\frac{P_{en}}{P_{ex}}$	$\frac{P_{el}}{P_{ex}}$
F1-1A	8.50	5.65	1.800	1.504	4.722	3.139
F1-1B	9.40	5.26	2.149	1.787	4.374	2.448
F1-1C	9.50	5.22	2.184	1.820	4.350	2.390
F1-1D	9.70	5.20	2.184	1.865	4.441	2.381
F1-1E	11.1	5.00	2.064	2.220	5.441	2.422
F2-1A	7.40	3.21	1.449	2.305	5.107	2.215
F2-1B	7.70	3.13	1.516	2.460	5.079	2.065
F2-1C	8.20	3.01	1.551	2.724	5.287	1.941
F2-1D	8.40	2.97	1.063	2.828	5.240	1.853
F2-1E	8.70	2.92	1.420	2.979	6.127	2.056
F3-1A	31.7	7.03	2.765	4.509	11.46	2.542
F3-1B	32.5	6.80	2.916	4.779	11.15	2.332
F3-1C	34.0	6.58	3.088	5.167	11.01	2.131
F3-1D	34.1	6.57	3.277	5.190	10.41	2.005
F3-1E	34.2	6.56	3.478	5.213	9.833	1.886
F1-2A	3.00	2.45	1.833	1.224	1.637	1.337
F1-2B	3.30	2.53	1.703	1.304	1.938	1.486
F1-2C	3.40	2.53	1.743	1.344	1.951	1.452
F1-2D	3.50	2.55	1.833	1.373	1.909	1.391
F1-2E	3.70	2.62	1.784	1.412	2.074	1.469
F2-2A	2.32	1.27	1.128	1.827	2.057	1.126
F2-2B	2.41	1.26	1.146	1.913	2.103	1.100
F2-2C	2.42	1.26	1.113	1.921	2.174	1.132
F2-2D	2.50	1.26	1.068	1.984	2.341	1.180
F2-2E	2.60	1.28	1.163	2.031	2.236	1.101
F3-2A	13.4	4.91	2.716	2.729	4.934	1.808
F3-2B	13.7	4.84	2.943	2.831	4.655	1.645
F3-2C	14.3	4.70	3.153	3.043	4.535	1.491
F3-2D	14.3	4.68	3.057	3.056	4.678	1.531
F3-2E	14.4	4.68	3.456	3.077	4.167	1.354

Table 11.10 Elastic Critical and Experimental Loads

CHAPTER 12

SUMMARY AND CONCLUSIONS

12.1 GENERAL SUMMARY

The theoretical standardized model developed has been demonstrated to represent the full moment-rotation behaviour of the connections studied rather accurately. The experimental data has revealed that the same type of connection, when connected to a different set of connecting members of varying cross sectional dimensions, exhibited different moment-rotation behaviour. This difference has been shown to vary according to the thickness of both the members and the connection. Justification of this behaviour has been achieved through the use of an empirical expression.

For the frameworks, the theoretical analysis using an optimum number of elements and the second approximation method to account for local buckling, has been demonstrated to predict very accurate collapse load. The optimum number of elements for the single and double storey frameworks are 13 and 18 respectively. For frameworks where torsional flexural buckling of the column is critical, it has been shown that incorporating the α factors into the above analysis yielded rather accurate collapse load. The simple plastic method employed in the theoretical analysis resulted in good prediction of the hinge formation. In all the predictions, the order and load at which hinges formed agreed very well with the experiments, except for cases where unsymmetrical failure or out of plane distortion occurred.

From the framework experimental investigation, it was found that when very flexible connections were used, the plastic deformation of the connections played a vital part in the rather gradual collapse of the framework. For frameworks with stiffer connections, collapse was rather sudden due the eventual formation of hinges at the columns. Except for a few frameworks which failed unsymmetrically or with severe twisting, the results obtained were generally satisfactory.

12.2 SUGGESTIONS FOR FUTURE WORK

In the theoretical analysis, the consideration of local buckling has been confined to plain channel subjected to compression and bending about the unsymmetrical axis. Modifications can be carried out to include bending about the symmetrical axis and also to cater for other cross sections.

Although more complex and complicated, lateral buckling of beam can be incorporated into the analysis. This inclusion will further ease the difficulties faced when extending the analysis to cater for space frameworks.

Standard connections for hot-rolled members have been extensively researched over the years. Relatively few experimental investigation has been carried out to determine the moment-rotation relationship of connections used in the cold-formed thin-walled structures.

12.3 CONCLUSIONS

1) The theoretical standardized model developed for the connections represent the full moment-rotation behaviour rather accurately.

2) A connection, when connected to a different set of members, exhibits different moment-rotation behaviour. This difference vary according to the thickness of both the connection and the connecting members.

3) The moment-rotation relationship of all the connections studied are found to be non-linear.

4) The behaviour of semi-rigid framework composed of cold-formed thin-walled members is influenced to a large extent by the connection stiffness and the local buckling potential of the members.

5) The treatment of local buckling using the second approximation method combined with the optimum number of elements used to model the framework predicts accurate collapse load when there is no torsional flexural buckling of the columns.

6) When incorporated into the above analysis, the length multiplier used to account for torsional flexural buckling of the columns yields rather accurate collapse load.

7) For a member with a varying stress along its length, more elements should be used to model the member.

8) The simple plastic method employed gives good prediction of the order and load at which the hinges form.

9) Although rightfully wrong, modelling the framework with the basic number of elements combined with the first approximation method of accounting for local buckling has been demonstrated to yield rather accurate collapse load. This method of analysis can be used as an estimation of the collapse load.

BIBLIOGRAPHY

PART 1

1. LU, L. W.

" A Survey of Literature on the Stability of Frames," Welding Research Council Bulletin, No. 18, Sept. 1962.

2. BLEICH, F.

" Der Knickfestigkeit Elastischer Stabverbindungen," Der Eisenbau, No. 10, 1919.

3. BLEICH, F.

" Buckling Strength of Metal Structures," Mcgraw Hill, Inc., 1952.

4. MERCHANT, W.

" Critical Loads of Tall Building Frames - Part I," The Structural Engineer, Vol. 33, No. 3, Mar. 1955.

5. SMITH, R. B. L. and MERCHANT, W.

" Critical Loads of Tall Building Frames - Part II," The Structural Engineer, Vol. 34, No. 8, Aug. 1956.

6. BOWLES, R. E. and MERCHANT, W.

" Critical Loads of Tall Building Frames - Part III," The Structural Engineer, Vol. 34, No. 9, Sept. 1956.

7. BOWLES, R. E. and MERCHANT, W.

" Critical Loads of Tall Building Frames - Part IV," The Structural Engineer, Vol. 36, No. 6, June 1958.

8. LUNDQUIST, E. E.

" Principle of Moment Distribution Method Applied to Stability of Structural Members," Proc. Fifth Int. Congress of Applied Mechanics, 1938.

9. HOFF, N. J.

" Stable and Unstable Equilibrium of Plane Frameworks," J. of Aero. Sci., Vol. 8, No. 3, Jan. 1941.

10. HOFF, N. J.

"The Proportioning of Aircraft Frameworks," J. of Aero. Sci., Vol. 8, No. 8, June 1941.

11. HOFF, N. J.

" Stress Analysis of Aircraft Frameworks," J. of Royal Aero. Soc., Vol. 45, No. 367, July 1941.

12. MASUR, E. F. and CUKURS, A.

" Lateral Buckling of Plane Frameworks," Proc. A.S.C.E., Vol. 83, No. EM 1, Jan. 1957.

13. LIVESLEY, R. K. and CHANDLER, D. B.

" Stability Functions for Structural Frameworks," Manchester University Press, 1956.

14. ZWEIG, A.

" Buckling Analysis of One Storey Frame," J. of Struct. Div., A.S.C.E., Vol. 94, No. ST 9, Sept. 1968.

15. PORTER, D. M.

" Elastic Stability of Symmetrical Single Bay Frames," J. of Struct. Div., A.S.C.E., Vol. 96, No. ST 8, Aug. 1970.

16. KORN, A.

" Bounding of Frame Buckling," J. of Struct. Div., A.S.C.E., Vol. 96, No. ST 8, Aug. 1970.

17. ZWEIG, A.

" Force Method for Frame Buckling Analysis," J. of Struct. Eng., A.S.C.E., Vol. 110, No. 8, Aug. 1984.

18. GALLAGHER, R. H. and PADLOG, J.

" Discrete Element Approach to Structural Analysis," A.I.A.A., 1, 1963.

19. BESKOS, D.E.

" Framework Stability by Finite Element Method," J. of Struct. Div., A.S.C.E., Vol. 103, No. ST 11, Nov. 1977.

20. LONG, Z.F.

" A High Precision Element for Frame Buckling Analysis," Recent Research Advances and their Applications to Design, Part 1, Ed. Hadjin, N. and Sekulovic, M., Proc. of the Int. Conf. on Steel Structures, Budva, Yugoslavia, 1986

21. CHWALLA, E.

" Die Stabilitaet Lotrecht Belasteter Rechteckrahmen," Der Bauingenieur, No. 19, 1938.

22. MASUR, E. F., CHANG, I. C. and DONELL, L. H.

" Stability of Frames in the Presence of Primary Bending Moments," Proc. A.S.C.E., Vol. 87, No. EM4, Aug. 1961.

23. LU, L. W.

" Stability of Elastic and Partially Plastic Frames," Ph.D. Dissertation, Lehigh University, USA, 1960.

24. MOSES, F.

" Inelastic Frame Buckling," J. of Struct. Div., A.S.C.E., Vol. 90, No. ST 6, Dec. 1964.

25. HARTZ, B.J.
" Matrix Formulation of Structural Stability Problems," J. of Struct. Div., A.S.C.E., Vol. 91, No. ST 6, Dec. 1965.

26. KRUEGER, R. C., HEINS, C. P. and SCHELLING, D. A.
" Design Program for Multi-Storey Structures," Computers and Structures, Vol. 7, 1977.

27. CONNOR, J. J., LOGCHER, R. D. and CHAN, S.C.
" Non-Linear Analysis of Elastic Framed Structures," J. of Struct. Div., A.S.C.E., Vol. 94, No. ST 6, June 1968.

28. AWADALLA, E. S.
" Elastic Critical Loads on Multi-Storey Rigid Frames," J. of Struct. Eng., A.S.C.E., Vol. 109, No. 5, May 1983.

29. CHU, K. H. and RAMPETSREITER R. H.
" Large Deflection Buckling of Space Frames," J. of Struct. Div., A.S.C.E., Vol. 98, No. ST 12, Dec. 1972.

30. TORIDIS, T. G. and KHOZEIMEH, K.
" Computer Analysis of Rigid Frames," Computers and Structures, Vol. 1, 1971.

31. MAHENDRA, J. S.
" The Analysis of Non-Linear Three Dimensional Frames," Computers and Structures, Vol. 2, 1972.

32. RANKOVIC, S. and KANJERIC, C.
" The Critical Value of Plane Frames with a Non-Linear Stress-Strain Relationship Exceeding the Proportionality Limit," Recent Research

Advances and their Applications to Design, Part 1, Ed. Hadjin, N. and Sekulovic, M., Proc. of the Int. Conf. on Steel Structures, Budva, Yugoslavia, 1986

33. SIMITSES, G.J. and GIRI, J.
" Asymmetrical Loaded Portal Frames," Computers and Structures, Vol. 19, No. 4, 1984.

34. SIMITSES, J.G., VLAHINOS, A. S. and SIMITSES, G. J.
" Stability Analysis of a Semi-Rigid Connected Simple Frame," J. of Constr. Steel Research, Vol. 2, No. 3, Sept. 1982.

35. AKKOUSH, E. A., TORIDIS, T. G., KHOZEIMEH, K. and HUANG, H. K.
" Bifurcation, Pre- and Post-Buckling Analysis of Frame Structures," Computers and Structures, Vol. 8, 1978.

36. REMSETH, S.N.
" Non-Linear Static and Dynamic Analysis of Framed Structures," Computers and Structures, Vol. 10, 1979.

37. WEN, R.K. and RAHIMZADEH, J.
" Non-Linear Elastic Frame Analysis by Finite Element," J. of Struct. Eng., A.S.C.E., Vol. 109, No. 8, Aug 1983.

38. SCHOLZ, H.
" Approximate P-Delta Method for Rigid Steel Sway Frames in Load and Resistance Factor Design," Recent Research Advances and their Applications to Design, Part 1, Ed. Hadjin, N. and Sekulovic, M., Proc. of the Int. Conf. on Steel Structures, Budva, Yugoslavia, 1986

39. KANCHANALAI, T.

" A Study on the Design of Columns in Unbraced Steel Frames," Recent Research Advances and their Applications to Design, Part 1, Ed. Hadjin, N. and Sekulovic, M., Proc. of the Int. Conf. on Steel Structures, Budva, Yugoslavia, 1986

40. GAIOTTI, R. and SMITH, B. S.

" P-Delta Analysis of Building Structures," J. of Struct. Eng., A.S.C.E., Vol. 115, No. 4, Apr. 1989.

41. EKHANDE, S. G., SELVAPPALAM, M. and MADUGULA, M. K. S.

" Stability Functions for Three Dimensional Beam-Columns," J. of Struct. Eng., A.S.C.E., Vol. 115, No. 2, Feb. 1989.

42. MERCHANT, W.

" The Failure Load of Rigid Jointed Frameworks as Influence by Stability," The Structural Engineer, Vol. 32, No. 7, July 1954.

43. MERCHANT, W., RASHID, C. A., BOLTON, A. and SALEM, A. H.

" The Behaviour of Unclad Frames," Fithieth Anniversary Conf., The Inst. of Struct. Engrs., 1958.

44. LOW, M. W.

" Some Model Tests on Multi-Storey Rigid Steel Frames," Proc. Inst. of Civil Engrs., No. 13, July 1959.

45. SALEM, A.

" Structural Frameworks," Ph.D. Dissertation, University of Manchester, UK, 1958.

46. YEN, Y. C., LU, L. W. and DRISCOLL, G. C. Jr.
"Tests on Stability of Steel Frames," Welding Research Council Bulletin, No. 81, Sept. 1962.

47. MORRIS, G. A. and FENVES, S. J.
" Elastic-Plastic Analysis of Frameworks," J. of Struct. Div., A.S.C.E., Vol. 96, No. ST 5, May 1970.

48. KORN, A. and GALAMBOS, T. V.
" Behaviour of Elastic-Plastic Frames," J. of Struct. Div., A.S.C.E., Vol. 94, No. ST 5, May 1968.

49. WOOD, R. H.
" Effective Lengths of Columns in Multi-Storey Buildings - Part 1, 2, 3," The Structural Engineer, Vol. 52, No. 7-9, July-Sept. 1974.

50. CHI, K. S. and LIN, T. H.
" Slope Deflection Method for Elastic-Plastic Multi-Storey Frames," Int. J. of Solids and Structures, Vol. 13, 1977.

51. KASSIMALI, A.
" Large Deformation Analysis of Elastic-Plastic Frames,"J. of Struct. Eng., A.S.C.E., Vol. 109, No. 8, Aug 1983.

52. McIVOR, I. K., WINEMAN, A. S. and WANG, H. C.
" Plastic Collapse of General Frames," Int. J. of Solids and Structures, Vol. 13, 1977.

53. WANG, S. T.
" Non-Linear Analysis of Locally Buckled Thin-Walled Structures," Proc. Int. Conf. on Computational Methods in Non-Linear Mechanics, Austin, Texas, USA, 1974.

54. WINTER, G.

" Commentary on the Specification for the Design of Cold-Formed Steel Structural Members," A.I.S.I., New York, USA, 1970.

55. WANG, S. T. and BLANDFORD, G.E.

" Stability Analysis of Locally Buckled Frames," Recent Research and Developments in Cold-Form Steel Structures-Vol. 1, Ed. Yu, W. W. and Senne, J. H., Fourth Int. Specialty Conf. on Cold-Formed Structures, Univ. of Missouri-Rolla, USA, June 1978.

56. WANG, S. T., ERRERA, S. J. and WINTER, G.

" Behaviour of Cold-Rolled Stainless Steel Members," J. of Struct. Div., A.S.C.E., Vol. 101, No. ST 11, Nov. 1975.

57. BAIGENT, A. H. and HANCOCK, G. J.

" The Behaviour of Portal Frames Composed of Cold-Formed Members," Thin-Walled Structures-Recent Technical Advances and Trends in Design, Research and Construction, Ed. Rhodes, J and Walker, A. C., Int. Conf. at the Univ. of Strathclyde, Glasgow, UK, Apr. 1979.

58. BAIGENT, A. H. and HANCOCK, G. J.

" Structural Analysis of Assemblages of Thin-Walled Members," J. of Engineering Structures, Vol. 4, Part 3, 1982.

59. BAIGENT, A. H. and HANCOCK, G. J.

" The Stiffness and Strength of Portal Frames Composed of Cold-Formed Members," Civ. Eng. Trans., Inst. of Engrs., Australia, Vol. CE24, Part 3, 1982.

60. BAIGENT, A. H. and HANCOCK, G. J.

" The Strength of Cold-Formed Portal Frames," Recent Research and

Developments in Cold-Form Steel Design and Construction, Ed. Yu, W. W. and Senne, J. H., Sixth Int. Specialty Conf. on Cold-Formed Structures, Univ. of Missouri-Rolla, USA, Nov. 1982.

61. HANCOCK, G. J.
" Portal Frames Composed of Cold-Formed Channel and Z-Secitons," Steel Framed Structures - Stability and Strength, Ed. Narayanan, R., 1985.

62. VACHARAJITTIPHAN, P. and TRAHAIR, N. S.
" Analysis of Lateral Buckling in Plane Frames," J. of Struct. Div., A.S.C.E., Vol. 101, No. ST 7, July 1975.

63. NETHERCOT, D. A.
" Torsional-Flexural Buckling Effects in Portal Frames," J. of Struct. Div., A.S.C.E., Vol. 100, No. ST 9, Sept. 1974.

64. BARSOUM, R. S. and GALLAGHER, R. H.
" Finite Element Analysis of Torsional and Torsional Flexural Stability Problems," Int. J. for Numerical Methods in Eng., Vol. 2, 1970.

65. ALWIS, W. A. M. and USAMI, T.
" Elastic Lateral Torsional Buckling of Unbraced and Braced Planar Frames," Computers and Structures, Vol. 10, 1979.

66. WILSON, W. M. and MOORE, H. F.
" Tests to Determine the Rigidity of Riveted Joints of Steel Structures," Univ. of Illinois, Eng. Expt. Stn., Bulletin No. 104, Urbana, USA, Dec. 1917.

67. DEPT. of SCIENTIFIC and INDUSTRIAL RESEARCH

" First, Second and Final Report of the Steel Structures Research Committee," Her Majesty's Stationery Office, 1931, 1934, 1936.

68. RATHBUN, J. C.

" Elastic Properties of Riveted Connections," Proc. A.S.C.E., Vol. 61, Jan. 1935.

69. LOTHERS, J. E.

" Elastic Restraint Equations for Semi-Rigid Connections," Trans. A.S.C.E., Vol. 116, Paper No. 2437, 1951.

70. MUNSE, W. H., BELL, W. G. and CHESSON, E.

" behaviour of Riveted and Bolted Beam-to-Column Connections," J. of Struct. Div., A.S.C.E., Vol. 97, No. ST 3, Aug. 1959.

71. SOMMER, W. H.

"Behaviour of Welded Header Plate Connections," Masters Thesis, Univ. of Toronto, Canada, 1969.

72. ROMSTAD, K. M. and SUBRAMANIAN, C. V.

" Analysis of Frames with Partial Connection Rigidity," J. of Struct. Div., A.S.C.E., Vol. 96, No. ST 11, Nov. 1970.

73. FRYE, M. J. and MORRIS, G. A.

" Analysis of Flexibly Connected Steel Frames," Canadian J. of Civ. Eng., Vol. 2, 1975.

74. JONES, S. W., KIRBY, P. A. and NETHERCOT, D. A.

" The Analysis of Frames with Semi-Rigid Connections - A State of Art Report," Dept. of Civil and Struct. Eng., Univ. of Sheffield, UK, Jan 1979

75. JONES, S. W., KIRBY, P. A. and NETHERCOT, D. A.
" Effects of Semi-Rigid Connections on Steel Column Strength," J. of Constr. Steel Research, Vol. 1, Part 1, Sept. 1980.

76. JONES, S. W., KIRBY, P. A. and NETHERCOT, D. A.
" Modelling of Semi-Rigid Connection Behaviour and its Influence on Steel Column Behaviour," Joints in Structural Steelwork, Ed. Howlett, J. H., Jenkins, W. M. and Stainsby, R., 1981.

77. JONES, S. W., KIRBY, P. A. and NETHERCOT, D. A.
" Columns with Semi-Rigid Joints," J. of Struct. Div., A.S.C.E., Vol. 108, No. ST 2, Feb. 1982.

78. RICHARD, R. M., GILLETT, P. E., KRIEGH, J. D. and LEWIS, B. A.
" The Analysis and Design of Single Plate Framing Connections," Engineering Journal, A.I.S.C., Vol. 17, No. 2, 2nd. Quarter, 1980.

79. HUANG, J. S. and CHEN, W. F.
" Steel Beam-to-Column Moment Connections," Preliminary Print No. 1920 - National Struct. Eng. Meeting, A.S.C.E., San Francisco, California, USA, Apr. 1973.

80. REGEC, J. E., HUANG, J. S. and CHEN, W. F.
" Test of a Fully Welded Beam-to-Column Connection," Welding Research Council Bulletin, No. 188, Oct. 1973.

81. STANDIG, K. F., RENTSCHLER, G. P. and CHEN, W. F.
" Tests of Bolted Beam-to-Column Flange Moment Connections," Welding Research Council Bulletin, No. 218, Aug. 1976.

82. ACKROYD, M. H. and GERSTLE, K. H.
" Behaviour of Type 2 Steel Frames," J. of Struct. Div., A.S.C.E., Vol. 108, No. ST 7, July 1982.

83. COLSON, A. L. and LOUVEAU. J. M.
" Connections Incidence on the Inelastic Behaviour of Steel Structures," Euromech Colloquium No. 174, Oct. 1983.

84. ANG, K. M. and MORRIS, G. A.
" Analysis of 3 Dimensional Frames with Flexible Beam-Column Connections," Canadian J. of Civil Eng., Vol. 11, No. 2, 1984.

85. RAMBERG, W. and OSGOOD, W. R.
" Description of Stress-Strain Curve by 3 Parameters," N.A.C.A. Technical Report No.902, 1943.

86. YEE, Y. L.
" Prediction of Non-Linear Behaviour of End-Plate Eave Connections," Ph.D. Dissertation, Monash Univ. of Australia, Nov. 1984.

87. NETHERCOT, D. A.
" Utilisation of Experimentally Obtained Connection Data in Assessing the Performance of Steel Frames," Proc. of A.S.C.E. Convention on Connection Flexibility and Steel Frames, Detroit, Michigan, USA, Ed. Chen, W. F., Oct.1985

88. KRISHNAMURTHY, N. and BATTLES, L. D.
" Rigidity of Bolted Seated Beam Connections by Finite Element," Proc. Int. Conf. on Finite Element Methods in Eng., Coimbature, India, Dec. 1974.

89. KRISHNAMURTHY, N.
" Modelling and Prediction of Steel Bolted Connection Behaviour," Computers and Structures, Vol. 11, No. 1-2, Feb. 1980.

90. MAXWELL, S. W., JENKINS, W. M. and HOWLETT, J. H.
" A Theoretical Approach to the Analysis of Connection Behaviour," Joints in Structural Steelwork, Ed. Howlett, J. H., Jenkins, W. M. and Stainsby, R., 1981.

91. JENKINS, W. M., TONG, C. S. and PRESCOTT, A. T.
" Moment-Transmittig End Plate Connections in Steel Construction and a Proposed Basis for Flush End Plate Design," The Structural Engineer, Vol. 64A, No. 5, May 1986.

92. KUKRETI, A. R., MURRAY, T. M. and ABOLMAALI, A.
"End Plate Connection Moment-Rotation Relationship," Joint Flexibility in Steel Frames, Ed. Chen, W. F., 1987.

93. LUI, E. M. and CHEN, W. F.
" Joint Flexibility in Steel Frames," Proc. of A.S.C.E. Convention on Connection Flexibility and Steel Frames, Detroit, Michigan, USA, Ed. Chen, W. F., Oct.1985

94. KISHI, N. and CHEN, W. F.
" Steel Connection Data Bank Program," CE-STR-86-18, School of Civ. Eng., Purdue Univ., W. Lafayette, Indiana, USA, 1986.

95. KISHI, N. and CHEN, W. F.
" Data Base of Steel Beam-to Column Connection," CE-STR-86-26, School of Civ. Eng., Purdue Univ.,W. Lafayette, Indiana, USA, 1986.

96. KISHI, N. and CHEN, W. F.

" Moment-Rotation Relation of Top and Seat Angle Connections," CE-STR-87-4, School of Civ. Eng., Purdue Univ.,W. Lafayette, Indiana, USA, 1987.

97. KISHI, N. and CHEN, W. F.

" Moment-Rotation Relation of Top and Seat Angle with Double Web Angle Connections," CE-STR-87-16, School of Civ. Eng., Purdue Univ.,W. Lafayette, Indiana, USA, 1987. (Proc. of the State of the Art Workshop on Connections and Behaviour, Strength and Design of Steel Structures, Ed. Bjorhove, R., Brozzetti, J. and Colson, A., Ecole Normale Superieure de Cahan, France, May 1987.)

98. KISHI, N. Et Al.

"Moment-Rotation Relation of Single/Double Web Angle Connections," CE-STR-87-18, School of Civ. Eng., Purdue Univ.,W. Lafayette, Indiana, USA, 1987. (Proc. of the State of the Art Workshop on Connections and Behaviour, Strength and Design of Steel Structures, Ed. Bjorhove, R., Brozzetti, J. and Colson, A., Ecole Normale Superieure de Cahan, France, May 1987.)

99. RICHARD, R. M. and ABBOTT, B. J.

" Versatile Elastic-Plastic Stress-Strain Formula," J. of Eng. Mechs. Div., A.S.C.E., Vol. 101, No. EM4, Aug. 1975.

100. MORRIS, G. A. and PACKER, J. S.

" Beam-to-Column Connections in Steel Frames," Canadian J. of Civil Eng., Vol. 14, Part 1, 1987.

101. TSCHEMMERNEGG, F. and HUNTER, C.
" The Design of Structural Steel Frames Under Consideration of the Non-Linear Behaviour of Joints," J. of Constr. Steel Research, Vol. 11, 1988.

102. PIPPARD, A. J. S. and BAKER, J. F.
"The Analysis of Engineering Structures," Third Edition, Edward Arnold (Publishers) Ltd., London, UK, 1957.

103. BAKER, J. F.
" The Steel Skeleton, Vol. 1-Elastic Behaviour and Design," Cambridge Univ. Press, Reprint, 1960.

104. JOHNSTON, B. G. and MOUNT, E. H.
" Analysis of Building Frames with Semi-Rigid Connections," Trans. A.S.C.E., Vol. 107, Paper No. 2152, 1942.

105. STEWART, R. W.
" Analysis of Frames with Elastic Joints," Trans. A.S.C.E., Vol. 114, 1947.

106. MAUGH, L. C.
" Comments on Semi-Rigid Connections in Steel Frames," I.A.B.S.E. Final Report, Sixth Congress, 1960.

107. LIGHTFOOT, E. and BAKER, A. R.
"The Analysis of Steel Frames with Elastic Beam-Column Connections," Golden Jubilee Congress - Symposium on the Design of High Buildings, Hong Kong Univ. Press, Hong Kong, 1961.

108. MONFORTON, G. R. and WU. T. S.
" Matrix Analysis of Semi-Rigidly Connected Frames," J. of Struct. Div., A.S.C.E., Vol. 89, No. ST 6, Dec. 1963.

109. LIVESLEY, R. K.
" Matrix Methods of Structural Analysis," Pergamom Press Ltd., 1964.

110. GERE, J. M. and WEAVER, W. Jr.
" Analysis of Framed Structures," D. Van Nostrand, Princeton, 1965.

111. LIGHTFOOT, E. and LE MESSURIER, A. P.
" Elastic Analysis of Frameworks with Elastic Connections," J. of Struct. Div., A.S.C.E., Vol. 100, No. ST 6, June 1974.

112. MONCARZ, P. D. and GERSTLE, K. H.
" Steel Frames with Non-Linear Connections,"J. of Struct. Div., A.S.C.E., Vol. 107, No. ST 8, Aug. 1981.

113. STELMACK, T. W., MARLEY, M. J. and GERSTLE, K. H.
" Analysis and Tests of Flexibly Connected Steel Frames," J. of Struct. Eng., A.S.C.E., Vol. 112, No. 7, July 1986.

114. GERSTLE, K. H.
" Flexibly Connected Steel Frames," Steel Framed Structures-Stability and Strength, Ed. Narayanan, R., 1985.

115. ACKROYD, M. H. and GERSTLE, K. H.
" Elastic Stability of Flexibly Connected Frames," J. of Struct. Eng., A.S.C.E., Vol. 109, No. 1, Jan. 1983.

116. ACKROYD, M. H. and GERSTLE, K. H.
" Strength of Flexibly Connected Steel Frames," J. of Engineering Structures, Vol. 5, Part 1, Jan. 1983.

117. MELCHERS, R. E. and YEE, Y. L.
" Deflection of Frames with Bolted End Plate Connections," Proc. of Metal Structures Conf., Brisbane, Australia, May 1983.

118. SIMITSES, G. J., SWISSHELM, J. D. and VLAHINOS, A. S.
"Flexibly-Jointed Unbraced Portal Frames," J. of Constr. Steel Research, Vol. 4, No. 1, 1984.

119. SIMITSES, G. J. and VLAHINOS, A. S.
" Stability Analysis of a Semi-Rigidly Connected Simple Frame," J. of Constr. Steel Research, Vol. 2, No. 3, Sept. 1982.

120. SIMITSES, G. J. and VLAHINOS, A. S.
" Elastic Stability of Rigidly and Semi-Rigidly Connected Unbraced Frames," Steel Framed Structures - Stability and Strength, Ed. Narayanan, R., 1985.

121. SIMITSES, G. J. and MOHAMED, S. E.
" Non-Linear Analysis of Gabled Frames Under Static Loads," J. of Constr. Steel Research, Vol. 12, 1989.

122. POGGI, C. and ZANDONINI, R.
"Behaviour and Strength of Steel Frames with Semi-Rigid Connections," Proc. of A.S.C.E. Convention on Connection Flexibility and Steel Frames, Detroit, Michigan, USA, Ed. Chen, W. F., Oct.1985.

123. YU, C. H. and SHANMUGAM, N. E.
" Stability of Frames with Semi-Rigid Joints," Computers and Structures, Vol. 23, No. 5, 1986.

124. LUI, E. M. and CHEN, W. F.
" Analysis and Behaviour of Flexibly-Jointed Frames," J. of Engineering Structures, Vol. 8, Part 2, Apr. 1986.

125. LUI, E. M. and CHEN, W. F.
" Steel Frame Analysis with Flexible Joints," Joint Flexibility in Steel Frames, Ed. Chen, W. F., 1987.

126. LUI, E. M. and CHEN, W. F.
" Effects of Joint Flexibility on the Behaviour of Steel Frames," Computers and Structures, Vol. 26, No. 5, 1987.

127. CHEN, W. F. and CHOU, S. P.
" Inelastic Analysis of Steel Braced Frames with Flexible Joints," Int. J. of Solids and Structures., Vol. 23, No. 5, 1987.

128. AMERICAN INSTITUTE OF STEEL CONSTRUCTION.
" Load and Resistance Factor Design Specification for Structural Steel Buildings," Chicago, Illinois, USA, Nov. 1986.

129. DRISCOLL, G. C.
" Elastic-Plastic Analysis of Top and Seat Angle Connections," Joint Flexibility in Steel Frames, Ed. Chen, W. F., 1987.

130. GOTO, Y. and CHEN, W. F.
' On the Computer-Based Design Analysis for the Flexibly Jointed Frames," Joint Flexibility in Steel Frames, Ed. Chen, W. F., 1987.

131. ACKROYD, M. H.

"Design of Flexibly-Connected Unbraced Steel Building Frames," Joint Flexibility in Steel Frames, Ed. Chen, W. F., 1987.

132. JASPART, J. P.

"Extending of the Merchant-Rankine Formula for the Assessment of the Ultimate Load of Frames with Semi-Rigid Joints," J. of Constr. Steel Research, Vol. 11, 1988.

133. KATO, B., CHEN, W. F. and NAKAO, M.

" Effects of Joint-Panel Shear Deformation on Frames," J. of Constr. Steel Research, Vol. 10, 1988.

134. POPOV, E. P

" Panel Zone Flexibility in Seismic Moment Joints," Joint Flexibility in Steel Frames, Ed. Chen, W. F., 1987.

135. KRAWINKLER, H and MOHASSEB, S.

" Effects of Panel Zone Deformations on Seismic Response," Joint Flexibility in Steel Frames, Ed. Chen, W. F., 1987.

BIBLIOGRAPHY

PART 2

1. ALLEN, H. G. and BULSON, P. S.

" Background to Buckling," Mcgraw-Hill, Inc., 1980.

2. BHATT, P.

" Programming the Matrix Analysis of Skeletal Structures," Ellis Horwood Ltd., 1986.

3. BRYAN, E. R. and ZADANFARROKH, F.

" Bearing Strength of Bolted Connections in Cold-Formed Steel," Dept. of Civil Eng., Univ. of Salford, UK, July 1989.

4. BRITISH STANDARD INSTITUTION

" British Standard 5950 : Part 5. Code of Practice for Design of Cold-Formed Sections," The Structural Use of Steelwork in Building, 1987.

5. BOTMAN, M. and BESSELING, J. F.

" The Effective Width in the Plastic Range of Flat Plates Under Compression," National Luchtvaartlaboratorium, National Aero. Research Inst., Report S445, Armsterdam, The Netherlands, 1954.

6. BRYAN, E. R. and ZADANFARROKH, F.

" Report on the Bearing Strength of Bolted Connections in Cold-Formed Steel Sections - Conclusions," Dept. of Civil Eng., Univ. of Salford, UK, Feb. 1990.

7. CHAJES, A and WINTER, G.

" Torsional Flexural Buckling of Thin-Walled Members," J. of Struct. Div., A.S.C.E., Vol. 91, No. ST4, Aug. 1965.

8. *CHONG, K. P. and MATLOCK, R. B.*

" Light Gage Steel Bolted Connections Without Washers,: J. of Struct. Div., A.S.C.E., Vol. 101, No. ST7, July 1975.

9. DAVIDS, A. J. and HANCOCK, G. J.

" Non-Linear Elastic Response of Locally Buckled Thin-Walled Beam-Columns," Thin-Walled Structures, Vol. 5, No. 3, 1987.

10. DAWE, J. L. and KULAK, G. L.

" Local Buckling Behaviour of Beam-Columns," J. of Struct. Eng., A.S.C.E., Vol. 112, No. 11, Nov. 1986.

11. DEWOLF, J. T.

" Local Buckling in Channel Columns," Proc. Third Int. Specialty Conf. on Cold-Formed Steel Structures, Research and Developments in Cold-Formed Steel Design and Construction- Vol. 1, University of Missourri-Rolla, USA, Ed. Yu, W. W. and Senne, J. H., Nov. 1975.

12. DEWOLF, J. T., PEKOZ, T. and WINTER, G.

" Local and Overall Buckling of Cold-Formed Members," J. of Struct. Div., A.S.C.E., Vol. 100, No. ST10, Oct. 1974.

13. DHALLA, A. K., ERRERA, S. J. and WINTER, G.

" Connections in Thin Low-Conductivity Steels," J. of Struct. Div., A.S.C.E., Vol. 97, No. ST10, Oct. 1971.

14. GHOBARAH, A. A. and TSO, W. K.

" Overall and Local Buckling of Channel Columns," J. of Eng. Mechs. Div., A.S.C.E., Vol. 95, No. EM2, Apr. 1969.

15. GILCHRIST, R. T. and CHONG, K. P.
" Thin Light Gage Bolted Connections Without Washers'" J. of Struct. Div., A.S.C.E., Vol. 105, No. ST1, Jan. 1979.

16. HARRISON, H. B.
" Computer Methods in Structural Analysis," Prentice Hall Inc., Englewood Cliffs, N. J., 1973.

17. HEYMAN, J.
" Plastic Design of Frames - 2 : Applications," Cambridge Univ. Press, 1971.

18. HOLZER, S. M.
" Computer Analysis of Structures - Matrix Structural Analysis Structured Programming," Elsevier Sci. Publishers, 1985.

19. JOHNSON, D. L.
" Connections in Cold-Formed Construction," The Canadian Soc. for Civil Eng., Conf. Proc. of Cold-Formed Steel Structures, Apr. 1980.

20. KAM, T. Y. and LEE, F. S.
" Non-Linear Analysis of Steel Plane Frames with Initial Imperfections," Computers and Structures, Vol. 23, No. 4, 1986.

21. LOTHERS, J. E.
" Advanced Design in Structural Steel," Prentice Hall Inc., Englewood Cliffs, N. J., 1960.

22. LOUGHLAN, J. and UPADHYA, A. R.
" Locally Imperfect Plain Channel Columns," Behaviour of Thin- Walled Structures, Ed. Rhodes, J. and Spence, J., Elsevier Applied Sci. Publishers, 1984.

23. LOUGHLAN, J., RHODES, J. and HARVEY, J. M.
" Bolted Connections in Thin-Walled Steel Sections Using High Tensile Bolts," Univ. of Strathclyde, Glasgow, UK, 1973.

24. MOY, S. S. J.
" Plastic Methods for Steel and Concrete Structures," Macmillan, London, UK, 1981.

25. MURRAY, N. W.
" Introduction to the Theory of Thin-Walled Structures," Clarendon Press, Oxford, London, UK, 1986.

26. NEAL, B. G.
"The Plastic Methods of Structural Analysis," Third Edition (S.I.), Chapman and Hall Ltd., 1977.

27. POPOWICH, D. W.
" Tension Capacity of Bolted Connections in Light Gage Cold- Formed Steel," Ph.D. Dissertation, Cornell Univ., USA, 1969.

28. PRZEMIENIECKI, J. S.
" Theory of Matrix Structural Analysis," Mcgraw Hill, Inc., 1968.

29. RHODES, J.
" Effective Widths in Plate Buckling," Developments in Thin-Walled Structures - 1," Ed. Rhodes, J and Walker, A. C., Elsevier Applied Science Publishers, 1982.

30. RHODES, J.
" Behaviour of Thin-Walled Channel Sections in Bending," Dynamics of Structures, Ed. Roesset, J. M., 1987.

31. RHODES, J. and HARVEY, J. M.

" The Local Instability of Thin-Walled Sections Under Combined Compression and Bending," Proc. Third Int. Specialty Conf. on Cold-Formed Steel Structures, Research and Developments in Cold-Formed Steel Design and Construction- Vol. 1, University of Missourri-Rolla, USA, Ed. Yu, W. W. and Senne, J. H., Nov. 1975.

32. RHODES, J. and HARVEY, J. M.

" Plain Channel Section Struts in Compression and Bending Beyond the Local Buckling Load," Int. J. of Mech. Sci., Vol. 18, 1976.

33. RHODES, J. and HARVEY, J. M.

" Interaction Behaviour of Plain Channel Columns Under Concentric or Eccentric Loading," Preliminary Report, Second Int. Colloquium on the Stability of Steel Structure, Apr. 1977.

34. RHODES, J. and WALKER, A. C.

" Current Problems in the Design of Cold-Formed Steel Sections," An Offprint from Aspects of the Analysis of Plate Structures, Ed. Dawe, D. J., Horsington, R. W., Kamtekar, A. G. and Little, G. H., Clarendon Press, Oxford, UK, 1985.

35. ROORDA, J

" Stability of Structures with Small Imperfections," J. of Eng. Mechs. Div., A.S.C.E., Vol. 91, No. EM1, Feb. 1965.

36. STARK, J. M. B. and TOMA, A. W.

" Connections in Thin-Walled Structures," Developments in Thin-Walled Structures - 1, Ed. Rhodes, J. and Walker, A. C., Elsevier Applied Sci. Publishers, 1982.

37. VON KARMAN T., SECHLER, E. E. and DONNELL, L. H.
" The Strength of Thin Plates in Compression," Trans. A.S.M.E., 54, 1932.

38. WALKER, A. C.
" Design and Analysis of Cold-Formed Sections," Intertext Books, London, UK, 1975.

39. WANG, S. T. and PAO, H. Y.
" Stability Analysis of Locally Buckled Singly Symmetric Columns," Thin-Walled Structures - Recent Technical Advances and Trends in Design, Research and Construction, Ed. Rhodes, J and Walker, A.C., Int. Conf. at the Univ. of Strathclyde, Glasgow, UK, Apr., 1979.

40. WANG, S. T. and PAO, H. Y.
" Torsional Flexural Buckling of Locally Buckled Columns," Computers and Structures, Vol. 11, No.1-2, Feb. 1980.

41. WANG, S. T. and TIEN, Y. L.
" Post Local Buckling Behaviour of Thin-Walled Columns," Proc. Second Int. Specialty Conf. on Cold-Formed Steel Structures, Research and Developments in Cold-Formed Steel Design and Construction, University of Missourri-Rolla, USA, Ed. Yu, W. W. and Senne, J. H., 1973.

42. WINTER, G.
" Strength of Thin Steel Compression Flanges," Trans. A.S.C.E., Vol. 112, Paper No. 2305, 1947.

43. WINTER, G.

"Light Gage steel Connections with High Strength, High Torqued Bolts," Publication of the I.A.B.S.E., Vol. 16, 1956.

44. WINTER, G.

" Tests on Bolted Connections in Light Gage Steel," J. of Struct. Div., A.S.C.E., Vol. 82, No. ST2, Mar. 1956.

45. WINTER, G.

" Thin-Walled Structures -Theoretical Solutions and Test Results," Preliminary Publication of the Eighth Congress, I.A.B.S.E., 1968.

46. WINTER, G., LANSING, W. and MCCALLEY, R. B.

" Four Papers on the Performance of Thin-Walled Steel Structures," Cornell Univ. Eng. Expt. Stn., Reprint No. 33, Nov. 1950.

47. WITTRICK, W. H. and WILLIAMS, F. W.

" Initial Buckling of Channels in Compression," J. of Eng. Mechs. Div., A.S.C.E., Vol. 97, No. EM3, June 1971.

48. YU, W. W.

" Cold-Formed Steel Structures - Design Analysis Construction," Mcgraw Hill, Inc., 1973.

49. YU, W. W. and MOSBY, R. L.

" Bolted Connections in Cold-Formed Steel Structures," University of Missouri-Rolla, Missouri, USA, Jan 1981.

APPENDICES

APPENDIX I

CHOLESKI TRIANGULAR DECOMPOSITION

I CHOLESKI TRIANGULAR DECOMPOSITION

Any square matrix **A** may be factorized or decomposed in the form :

$$\mathbf{A} = \mathbf{L}\ \mathbf{U} \tag{I.1}$$

where **L** and **U** are the lower and upper triangular matrices and in the particular case of a symmetric matrix it can be arranged that

$$\mathbf{U} = \mathbf{L}^T \tag{I.2}$$

and

$$\mathbf{A} = \mathbf{L}\ \mathbf{L}^T \tag{I.3}$$

The matrix **L** is unique for any given **A** and the leading diagonal terms are all positive if **A** is positive definite. The decomposition may be summarized as follows :

$$\mathbf{A} = \mathbf{L}\ \mathbf{L}^T \tag{I.3}$$

and

$$\mathbf{A} = \mathbf{A}^T \tag{I.4}$$

or

$$\begin{bmatrix} a_{11} & a_{12} & \cdot & \cdot & \cdot & a_{1n} \\ a_{21} & a_{22} & \cdot & \cdot & \cdot & \\ \cdot & & \cdot & & & \\ \cdot & & & \cdot & & \\ \cdot & & & & \cdot & \\ a_{n1} & & & & & a_{nn} \end{bmatrix} = \begin{bmatrix} l_{11} & & & & & \\ l_{21} & l_{22} & & & & \\ l_{31} & l_{32} & l_{33} & & & \\ \cdot & & & \cdot & & \\ \cdot & & & & \cdot & \\ l_{n1} & & & & & l_{nn} \end{bmatrix} \begin{bmatrix} l_{11} & l_{21} & l_{31} & \cdot & \cdot & l_{n1} \\ & l_{22} & l_{32} & & & \\ & & l_{33} & & & \\ & & & \cdot & & \\ & & & & \cdot & \\ & & & & & l_{nn} \end{bmatrix}$$

Multiplying,

first row by first column:

$$l_{11} = \sqrt{a_{11}}$$

second row by first column:

$$l_{21} = \frac{a_{21}}{l_{11}}$$

third row by first column:

$$l_{31} = \frac{a_{31}}{l_{11}}$$

or ith row by first column:

$$l_{i1} = \frac{a_{i1}}{l_{11}}$$

Similarly,

second row by second column:

$$l_{22} = \sqrt{a_{22} - l_{21}^2}$$

third row by second column:

$$l_{32} = \frac{(a_{32} - l_{31} l_{21})}{l_{22}}$$

or ith row by second column:

$$l_{i2} = \frac{(a_{i2} - l_{i1} l_{21})}{l_{22}}$$

From these examples the general term may be deduced as :

$$l_{ii} = \sqrt{\left(a_{ii} - \sum_{m=1}^{m=i-1} l_{im}^2\right)} \qquad (I.5)$$

and

$$l_{ij} = \frac{\left(a_{ij} - \sum_{m=1}^{m=j-1} l_{im} l_{jm}\right)}{l_{jj}} \qquad (i > j) \qquad (I.6)$$

It can be seen from these results that no term in A is used more than once and that one use is to obtained the l term in the same position, and therefore the storage locations in A can be overwritten by the values of l as each is obtained. No additional storage is therefore required for $\mathbf{L}$ or $\mathbf{L}^T$. A computer flow chart for the decomposition is given in figure I.1.

The solution process applied to a structures stiffness matrix, which is both symmetric and positive definite is :

$$\mathbf{P} = \mathbf{K}\ \mathbf{D} \qquad (I.7)$$

$$= \mathbf{L}\ \mathbf{L}^T\ \mathbf{D} \qquad (I.8)$$

where $\mathbf{f} = \mathbf{L}^T\ \mathbf{D}$

Or written in full :

$$\begin{bmatrix} P_1 \\ P_2 \\ P_3 \\ . \\ . \\ P_n \end{bmatrix} = \begin{bmatrix} l_{11} & & & & & \\ l_{21} & l_{22} & & & & \\ l_{31} & l_{32} & l_{33} & & & \\ . & & & . & & \\ . & & & & . & \\ l_{n1} & . & . & . & . & l_{nn} \end{bmatrix} \begin{bmatrix} f_1 \\ f_2 \\ f_3 \\ . \\ . \\ f_n \end{bmatrix} \qquad (I.9)$$

The new unknowns **f** can now be solved by forward substitution, for:

$$f_1 = \frac{P_1}{l_{11}}$$

$$f_2 = \frac{(P_2 - f_1 l_{21})}{l_{22}}$$

$$f_3 = \frac{(P_3 - f_1 l_{31} - f_2 l_{32})}{l_{33}} \qquad (I.10)$$

.....etc

The values of **f** are obtained in order and can be stored in the vector **P** as each of the original values stored there is used only once. The next step is the back substitution :

$$\mathbf{f} = \mathbf{L}^T \mathbf{D} \qquad (I.11)$$

This may be written in full as :

$$\begin{bmatrix} f_1 \\ f_2 \\ f_3 \\ . \\ f_{n-1} \\ f_n \end{bmatrix} = \begin{bmatrix} l_{11} & l_{21} & l_{31} & . & . & l_{n1} \\ & l_{22} & l_{23} & & & l_{n2} \\ & & l_{33} & & & l_{n3} \\ & & & . & & . \\ & & & & l_{n-1,n-1} & l_{n,n-1} \\ & & & & & l_{nn} \end{bmatrix} \begin{bmatrix} d_1 \\ d_2 \\ d_3 \\ . \\ d_{n-1} \\ d_n \end{bmatrix} \qquad (I.12)$$

Hence

$$d_n = \frac{f_n}{l_{nn}}$$

$$d_{n-1} = \frac{(f_{n-1} - l_{n,n-1} d_n)}{l_{n-1,n-1}} \qquad (I.13)$$

.....etc

The values of the unknown displacements **D** are found from bottom to top, and can be placed in the vector **f** as they are calculated. Computer flow charts for the forward and back substitution are shown if figures I.2 and I.3 respectively.

When the decomposition of **K** is carried out it may be found that the terms vary greatly in size. It is good practice to scale the matrix, and a suitable technique is to pre- and post-multiply **K** by the diagonal matrix $\mathbf{E}^{-1/2}$, whose terms are the inverse of the square root of the diagonal terms of **K**. This reduces all leading diagonal terms of **K** to unity.

Thus

$$(\mathbf{E}^{-1/2}\,\mathbf{K}\,\mathbf{E}^{-1/2})\,\mathbf{E}^{+1/2}\,\mathbf{D} = \mathbf{E}^{-1/2}\,\mathbf{P} \qquad (I.14)$$

where the terms $\mathbf{E}^{+1/2}$ are the square roots of the diagonal terms of **K**. The unknowns solved for are $\mathbf{E}^{+1/2}\mathbf{D}$ and hence the required **D** is obtained by pre-multiplying once more by $\mathbf{E}^{-1/2}$. Although $\mathbf{E}^{-1/2}$ is a square matrix, little additional storage is required as the terms may be stored in a vector.

Notes on figure I.1

The right hand loop calculates leading diagonal terms of **L** (equation (*I*.5)) while the left hand loop calculates the off diagonal terms (equation (*I*.6)).

Once calculated, the terms of **L** are stored in **K**. Some of the terms of **K** remain in the upper triangular part, but they may be left there as these positions are not used in the forward or back substitution.

Notes on figure I.2

The pattern is seen in equation (*I*.10).

Once calculated, the *f* values (*I*.10) are stored in **P**.

Notes on figure I.3

The pattern is seen in equation (*I*.13).

Once calculated, the unknowns **D** are stored in **P**.

Matrix to be decomposed is **K** of order N.

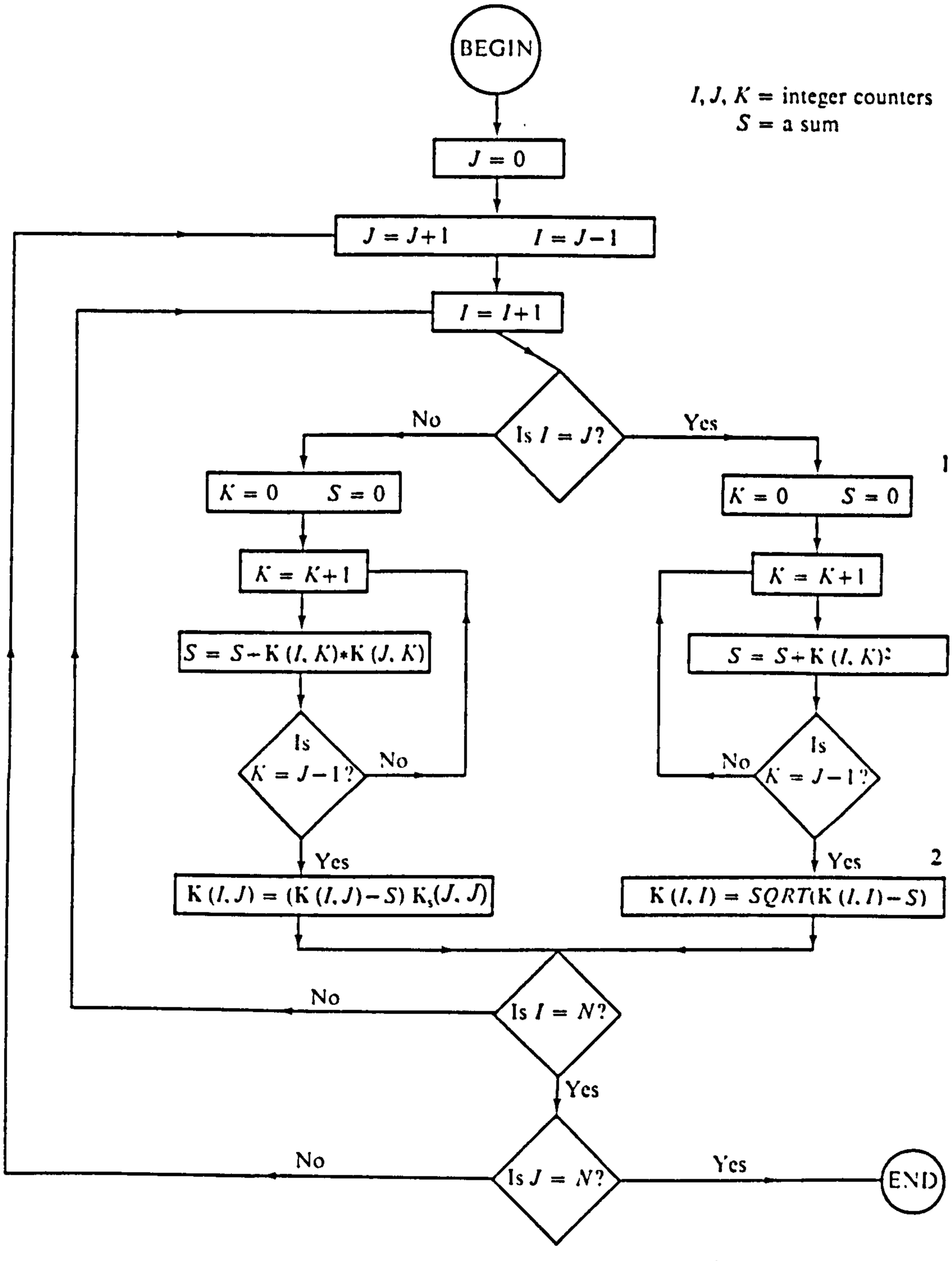

I, J, K = integer counters
S = a sum

Fig. I.1 Flow Chart for Choleski Decomposition.

The equation to be solved is **KD=** **P** and the matrix **K** now holds the lower triangular matrix **L.**

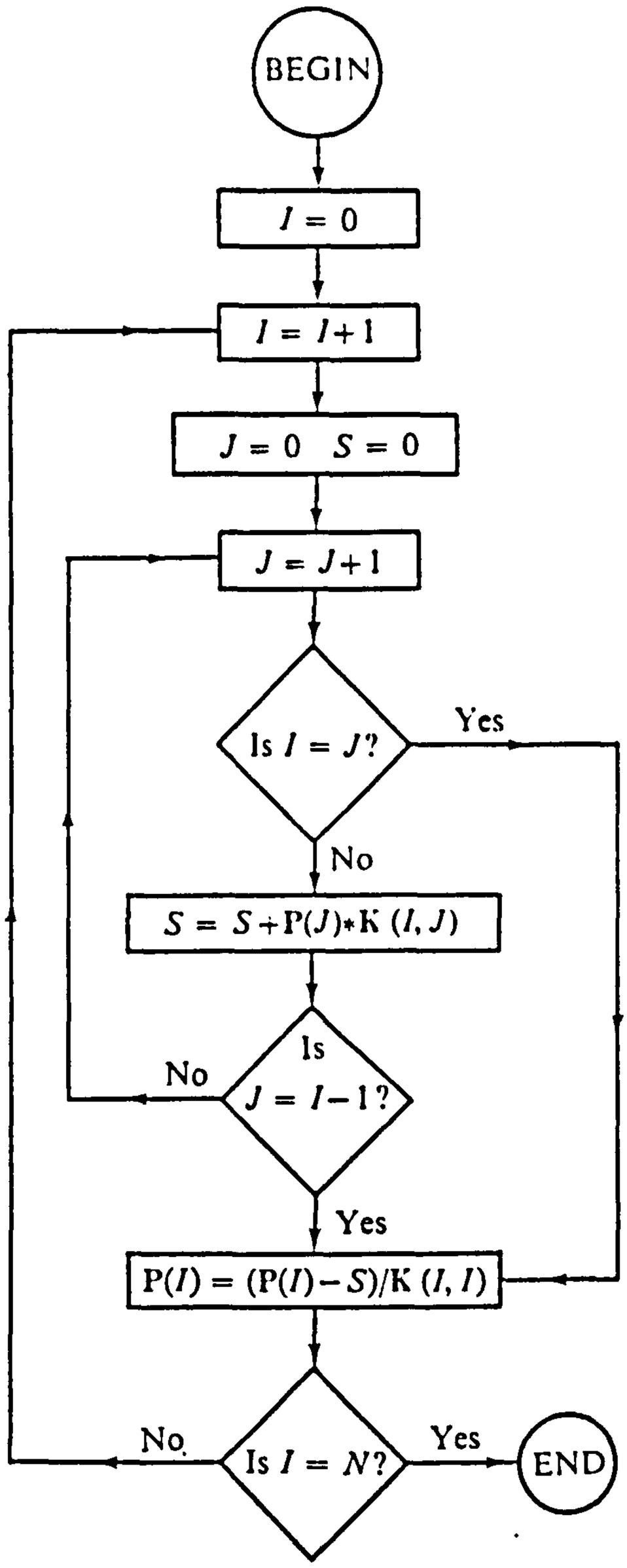

Fig. I.2 Flow Chart for Forward Substitution.

The lower triangular matrix **L** is stored in **K** and the intermediate values of f are stored in **P**.

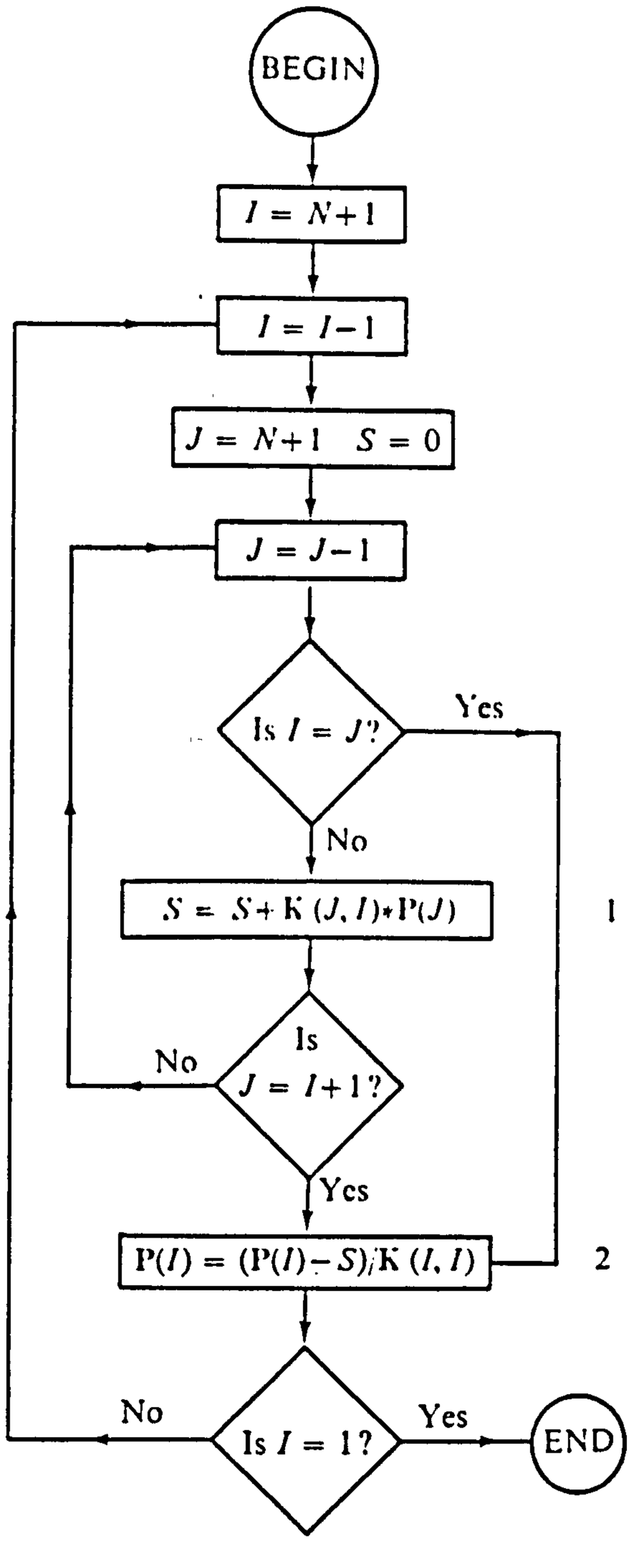

Fig. I.3 Flow Chart for Back Substitution.

APPENDIX II

CASTIGLIANO'S THEOREM

OF

STRAIN ENERGY

II CASTIGLIANO'S THEOREM OF STRAIN ENERGY

In a linear elastic structure subjected to loads $P_1 \cdots P_n$ the corresponding displacements will be of the form :

$$d_1 = f_{11}P_1 + f_{12}P_2 + f_{13}P_3 + f_{1n}P_n \qquad (II.1)$$

where f_{mn} is a flexibility influence coefficient. In such a structure, it is shown in Appendix III that

$$f_{mn} = f_{nm} \qquad (II.2)$$

Now the work done by each applied load is $\frac{1}{2}Pd$ and hence

$$SE = \frac{1}{2}\mathrm{PD} = \sum_1^n \frac{1}{2}Pd$$

$$= \frac{1}{2}P_1(f_{11}P_1 + f_{12}P_2 + f_{13}P_3 \cdots f_{1n}P_n)$$

$$+ \frac{1}{2}P_2(f_{21}P_1 + f_{22}P_2 + f_{23}P_3 \cdots f_{2n}P_n)$$

$$+ \frac{1}{2}P_3(f_{31}P_1 + f_{32}P_2 + f_{33}P_3 \cdots f_{3n}P_n)$$

$$+ \frac{1}{2}P_n(f_{n1}P_1 + f_{n2}P_2 + f_{n3}P_3 \cdots f_{nn}P_n)$$

$$= \frac{1}{2}(f_{11}P_1^2 + f_{22}P_2^2 \cdots f_{nn}P_n^2) + (f_{12}P_1P_2 \cdots f_{1n}P_1P_n)$$

$$+ (f_{23}P_2P_3 \cdots f_{2n}P_2P_n) \cdots \text{etc} \qquad (II.3)$$

in which the first bracket term arises from the leading diagonal of the flexibility matrix, the second from the reciprocal terms containing P_1 , and the third from reciprocal terms which do not contain P_1 .

The rate at which SE increases with P_1 is given by differentiating equation (II.3) with respect to P_1 and, since the loads are independent variables (any reactions have done no work), and since the flexibility coefficients are properties of the structure alone,

$$\frac{\partial SE}{\partial P_1} = f_{11}P_1 + f_{12}P_2 + f_{13}P_3 \cdots f_{1n}P_n = d_1 \qquad (II.4)$$

Similarly

$$\frac{\partial SE}{\partial P_2} = d_2 \cdots \text{etc}$$

and

$$\frac{\partial SE}{\partial P_n} = d_n \qquad (II.5)$$

APPENDIX III

BETTI-MAXWELL'S THEOREM

III.1 BETTI'S THEOREM

Consider a linearly elastic structure subjected to two force system represented by matrices $\mathbf{P}_A$ and $\mathbf{P}_B$ respectively. The displacements due to system $\mathbf{P}_A$ alone will be represented by $\mathbf{D}_A$, and those due to $\mathbf{P}_B$ alone by $\mathbf{D}_B$. If the system $\mathbf{P}_A$ is applied first followed by the system $\mathbf{P}_B$, the work done by external forces is given by

$$WD_{A,B} = \frac{1}{2}\mathbf{P}_A\mathbf{D}_A + \frac{1}{2}\mathbf{P}_B\mathbf{D}_B + \mathbf{P}_A\mathbf{D}_B \qquad (III.1)$$

where the subscript A,B with WD indicates the sequence of application of the load systems. If the sequence is reversed, the work done by external forces becomes

$$WD_{B,A} = \frac{1}{2}\mathbf{P}_B\mathbf{D}_B + \frac{1}{2}\mathbf{P}_A\mathbf{D}_A + \mathbf{P}_B\mathbf{D}_A \qquad (III.2)$$

In both instances, work is stored as elastic strain energy SE_i and the amount of energy so stored must be the same, since the final deformed configuration in a linear system must be independent of the sequence of load application. Therefore

$$SE_i = WD_{A,B} = WD_{B,A} \qquad (III.3)$$

from which it follows that

$$\mathbf{P}_A\mathbf{D}_B = \mathbf{P}_B\mathbf{D}_A \qquad (III.4)$$

Equation (III.4) is usually referred to as the reciprocal theorem of Betti, which states that "the work done by the system of forces $\mathbf{P}_A$ over the displacements $\mathbf{D}_B$ is equal to the work done by the system of forces $\mathbf{P}_B$ over the displacements $\mathbf{D}_A$, where $\mathbf{D}_A$ and $\mathbf{D}_B$ are the displacements due to $\mathbf{P}_A$ and $\mathbf{P}_B$ respectively."

III.2 MAXWELL'S RECIPROCAL THEOREM

If systems of forces $\mathbf{P}_A$ and $\mathbf{P}_B$ used in Betti's theorem consist each of one force, for example, P_1 and P_2, applied at two different locations, then equation (III.4) becomes

$$[P_1 \quad 0]\begin{bmatrix} f_{12} & P_2 \\ f_{22} & P_2 \end{bmatrix} = [0 \quad P_1]\begin{bmatrix} f_{11} & P_1 \\ f_{21} & P_1 \end{bmatrix} \tag{III.5}$$

where f_{ij} is the displacement in the $i$the direction due to a unit force in the jth direction. After multiplying out matrices in equation (III.5), it follows that

$$f_{12} = f_{21} \tag{III.6}$$

or, in general

$$f_{ij} = f_{ji} \tag{III.7}$$

The results expressed by equation (III.7) is the well-known Maxwell reciprocal theorem. It represents the reciprocal relationship for the influence coefficients which form the elements of flexibility matrices. Thus all flexibility matrices, and hence stiffness matrices, must be symmetric for linear structures.

APPENDIX IV

SUMMARY

OF

PLASTIC MOMENT

IV PLASTIC MOMENT

The following are to be read in conjunction with figure IV.1 and table IV.1.

Zero strain axis position:

$$H_1 = \frac{1}{4}[2(b_2 + t) - b_1]$$

$$H_2 = t\left[\frac{b_2 - t}{b_1} + \frac{1}{2}\right]$$

$$H_3 = H_1 - \frac{P}{4\sigma_y t}$$

$$H_4 = H_2 - \frac{P}{2\sigma_y b_1}$$

$$H_5 = H_1 + \frac{P}{4\sigma_y t}$$

$$H_6 = H_2 + \frac{P}{2\sigma_y b_1}$$

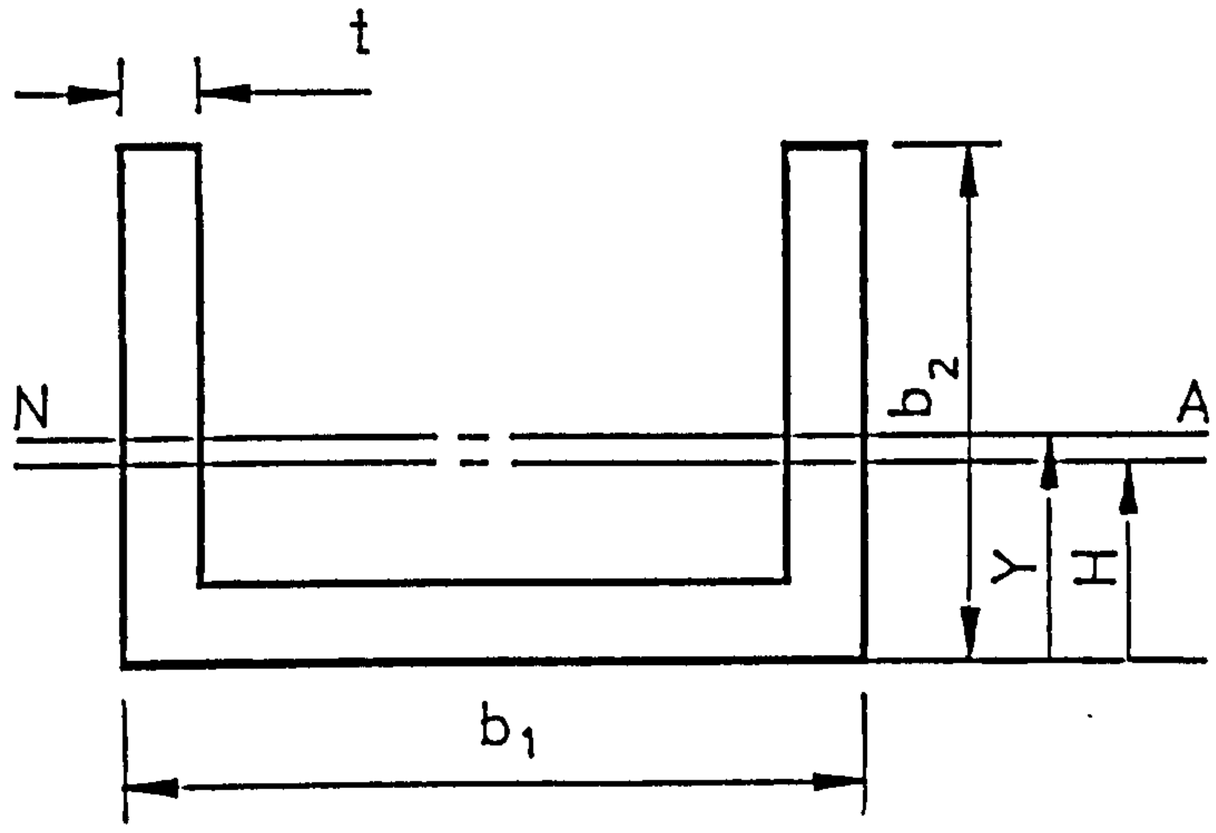

Fig. IV.1

Centroid position:

$$Y = \frac{b_2^2 - t^2 + \frac{b_1 t}{2}}{2(b_2 - t) + b_1}$$

Plastic Moment:

$$M_{p1} = \sigma_y Z_{p1}$$

where

$$Z_{p1} = t\left(\frac{b_2^2}{2} + \frac{t^2}{2} - \frac{b_1^2}{8} - b_2 t + \frac{b_1 b_2}{2}\right)$$

$$M_{p2} = \sigma_y Z_{p2}$$

where

$$Z_{p2} = t\left(b_2^2 - \frac{b_2^2 t}{b_1} - b_2 t + \frac{2b_2 t^2}{b_1} - \frac{t^3}{b_1} + \frac{b_1 t}{4}\right)$$

$$M_{p3} = M_{p1}\left[1 - \frac{A^2 t}{8Z_{p1}}\left(B^2 + \frac{BC}{A^2}\right)\right]$$

where

$$A = 2(b_2 - t) + b_1$$

$$B = \frac{P}{P_s}$$

$$P_s = \sigma_y t A$$

$$C = 2b_1(b_1 - 2t)$$

$$M_{p4} = M_{p2}\left[1 - \frac{(At)^2}{4Z_{p2}b_1}\left(B^2 + \frac{2BCF}{A^2}\right)\right]$$

where

$$F = \frac{(b_2 - t)^2}{b_1 t}$$

$$M_{p5} = M_{p1}\left[1 - \frac{A^2 t}{8Z_{p1}}\left(B^2 - \frac{BC}{A^2}\right)\right]$$

$$M_{p6} = M_{p2}\left[1 - \frac{(At)^2}{4Z_{p2}b_1}\left(B^2 - \frac{2BCF}{A^2}\right)\right]$$

Axial load:

$$P_3 = \sigma_y t[2(b_2 - t) - b_1]$$

$$P_5 = \sigma_y t[2(t - b_2) + b_1]$$

Type of Loading	H	Condition	Axial Load	M_p
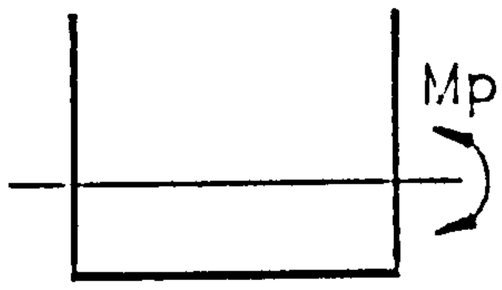	H_1 H_2	$H_1 > t$ $H_2 \leq t$	- -	M_{p1} M_{p2}
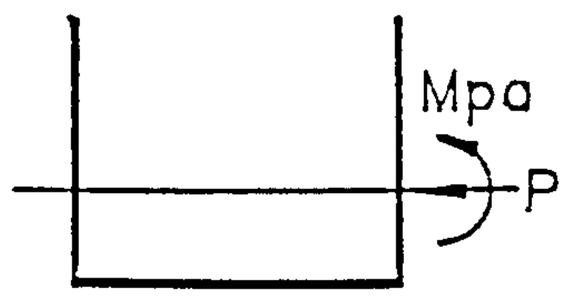	H_3 H_4	$H_3 > t$ $H_4 \leq t$	$P < P_3$ $P \geq P_3$	M_{p3} M_{p4}
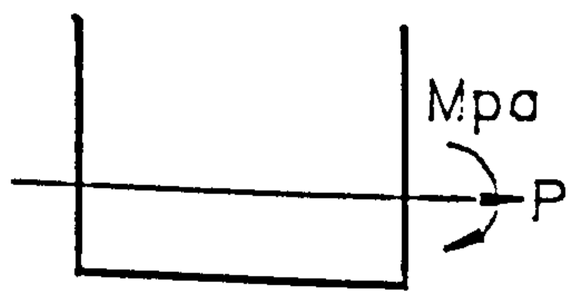	H_3 H_4	$H_3 > t$ $H_4 \leq t$	$P < P_3$ $P \geq P_3$	M_{p3} M_{p4}
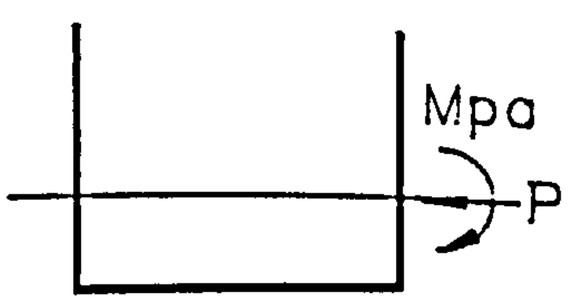	H_5 H_6	$H_5 > t$ $H_6 \leq t$	$P > P_5$ $P \leq P_5$	M_{p5} M_{p6}
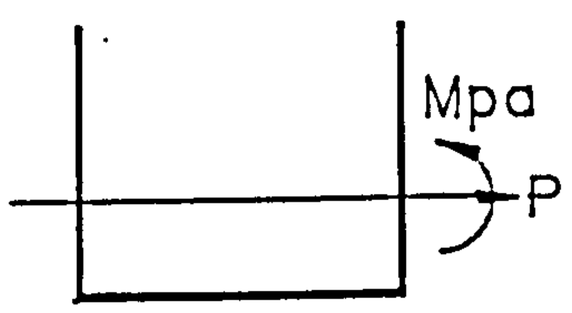	H_5 H_6	$H_5 > t$ $H_6 \leq t$	$P > P_5$ $P \leq P_5$	M_{p5} M_{p6}

Table IV.1 Summary of Plastic Moment

APPENDIX V

α FACTORS FOR MEMBERS IN COMPRESSION

α factors for members in compression															
Section	$L/r_{min} \times t/B$														
	D/B	2	3	4	5	6	7	8	9	10	11	12	13	14	15
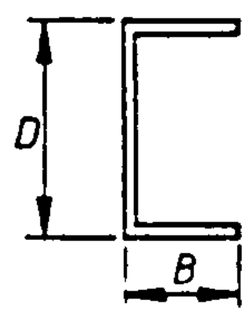	1.75	1.02	1.00												
	1.50	1.15	1.11	1.06	1.02	1.00									
	1.25	1.33	1.27	1.21	1.14	1.08	1.02	1.00							
	1.00	1.60	1.51	1.41	1.31	1.23	1.15	1.09	1.04	1.00					
	0.75	2.04	1.87	1.70	1.56	1.45	1.36	1.30	1.24	1.20	1.17	1.14	1.12	1.10	1.09
	0.50	2.14	1.95	1.77	1.62	1.51	1.41	1.34	1.28	1.24	1.20	1.18	1.15	1.13	1.12
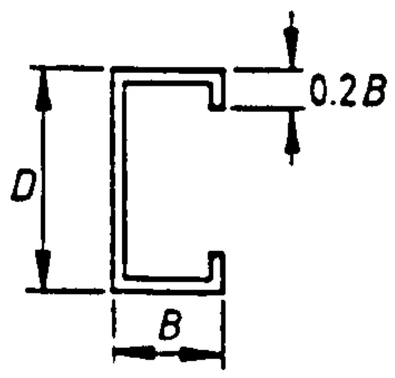	1.75	1.08	1.06	1.03	1.00										
	1.50	1.21	1.18	1.14	1.10	1.06	1.02	1.00							
	1.25	1.39	1.35	1.30	1.24	1.18	1.13	1.08	1.04	1.00					
	1.00	1.65	1.58	1.51	1.43	1.36	1.30	1.24	1.19	1.15	1.11	1.08	1.06	1.04	1.02
	0.75	1.81	1.73	1.65	1.57	1.49	1.42	1.36	1.31	1.27	1.24	1.21	1.18	1.16	1.14
	0.50	1.67	1.62	1.56	1.50	1.45	1.39	1.34	1.30	1.27	1.24	1.21	1.19	1.17	1.15
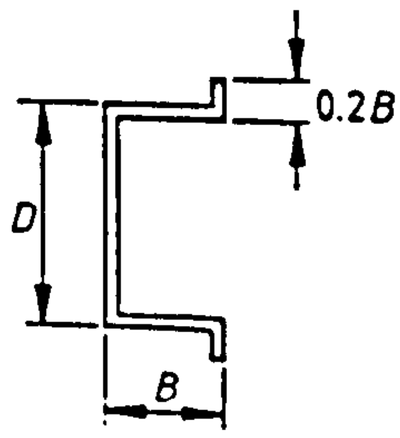	2.25	1.01	1.00												
	2.00	1.11	1.08	1.05	1.01	1.00									
	1.75	1.23	1.20	1.15	1.10	1.05	1.00								
	1.50	1.40	1.35	1.28	1.22	1.15	1.08	1.03	1.00						
	1.25	1.64	1.55	1.46	1.36	1.27	1.19	1.12	1.06	1.01	1.00				
	1.00	1.98	1.83	1.68	1.55	1.43	1.33	1.25	1.18	1.13	1.09	1.05	1.02	1.00	
	0.75	2.39	2.15	1.93	1.74	1.60	1.49	1.40	1.33	1.28	1.24	1.20	1.18	1.15	1.14
	0.50	2.37	2.13	1.91	1.73	1.59	1.48	1.40	1.33	1.28	1.24	1.20	1.18	1.15	1.14
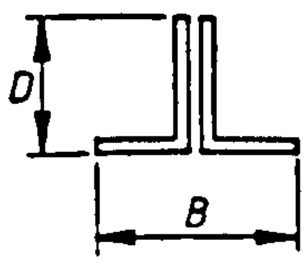	0.25	1.10	1.00												
	0.33	1.12	1.00												
	0.50	1.33	1.00												
	0.75	1.80	1.34	1.17	1.10	1.06	1.05	1.03	1.03	1.02	1.02	1.01	1.01	1.01	1.01
	1.00	2.30	1.64	1.36	1.22	1.14	1.10	1.08	1.06	1.05	1.04	1.03	1.03	1.02	1.02
	1.33	3.05	2.11	1.68	1.44	1.30	1.22	1.16	1.13	1.10	1.08	1.07	1.06	1.05	1.04
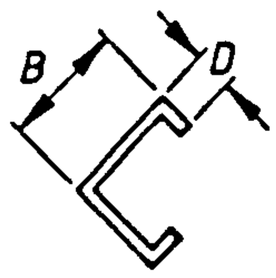	0.00	2.55	1.72	1.31	1.07	1.00									
	0.20	2.15	1.72	1.41	1.20	1.04	1.00								
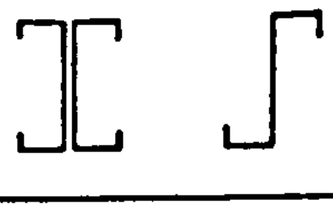	α = 1 For all geometries														

Table V.1 α Factors for Members in Compression

APPENDIX VI

TEST RIG DRAWINGS

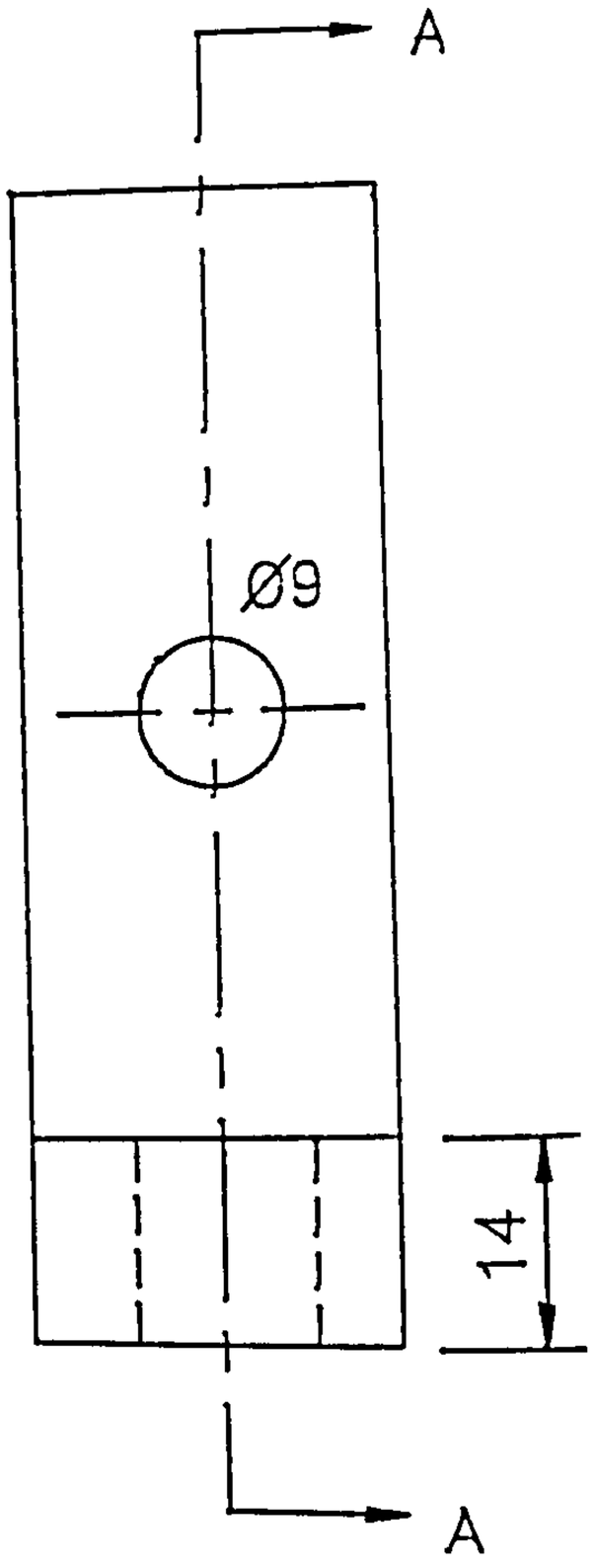

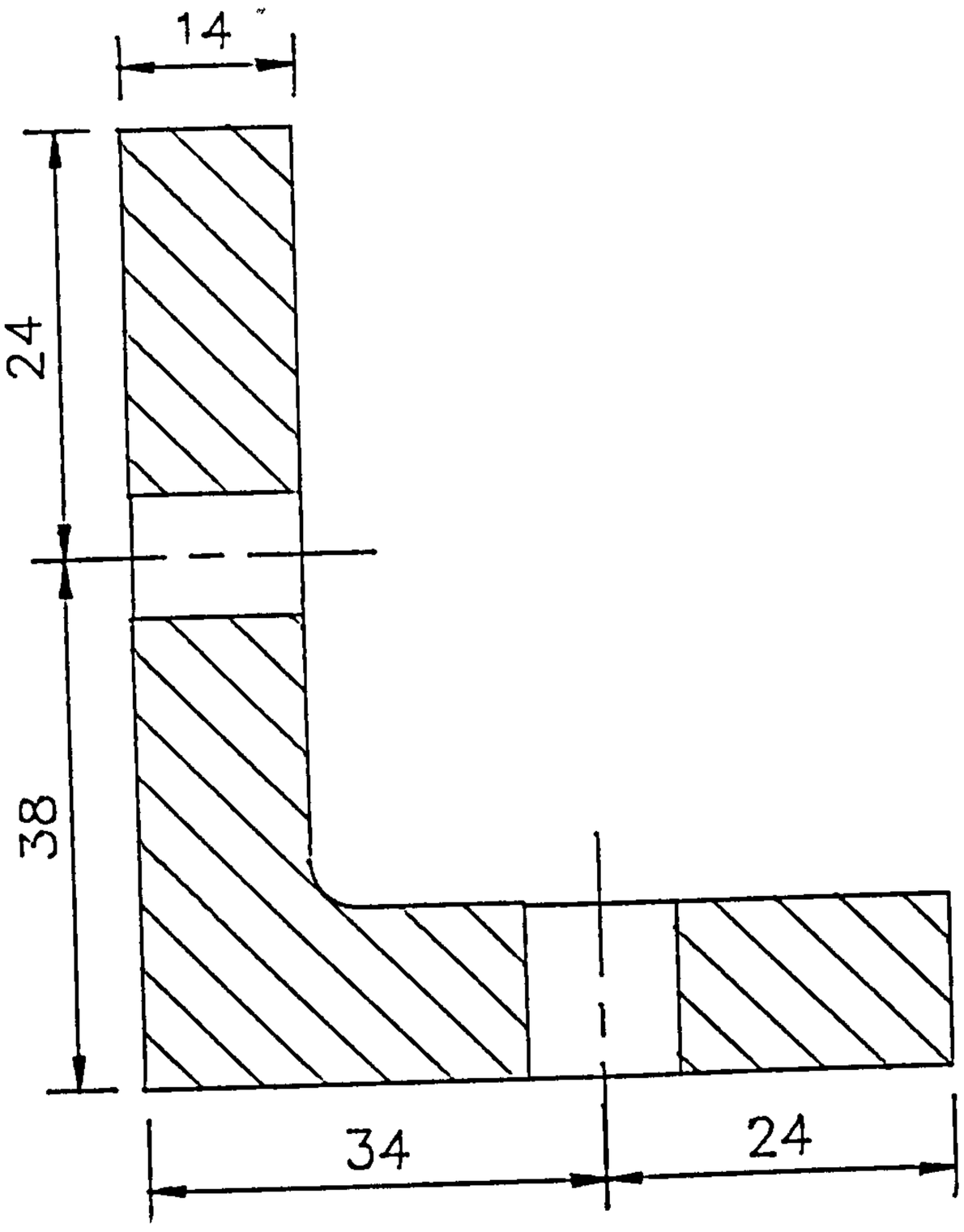

SECTION A–A

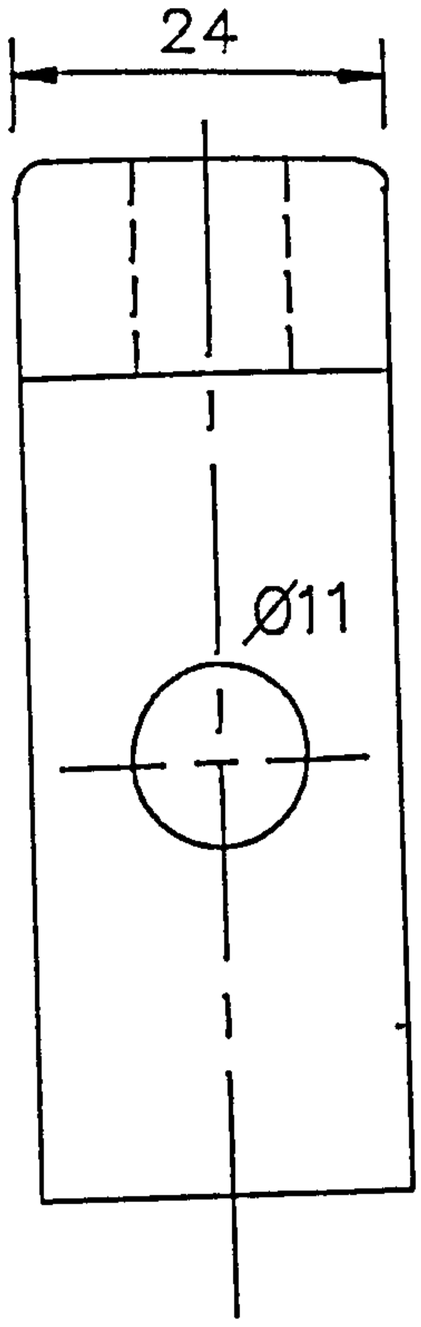

All dimensions in mm

2 OFF

Fig. VI.1

PART NO.1

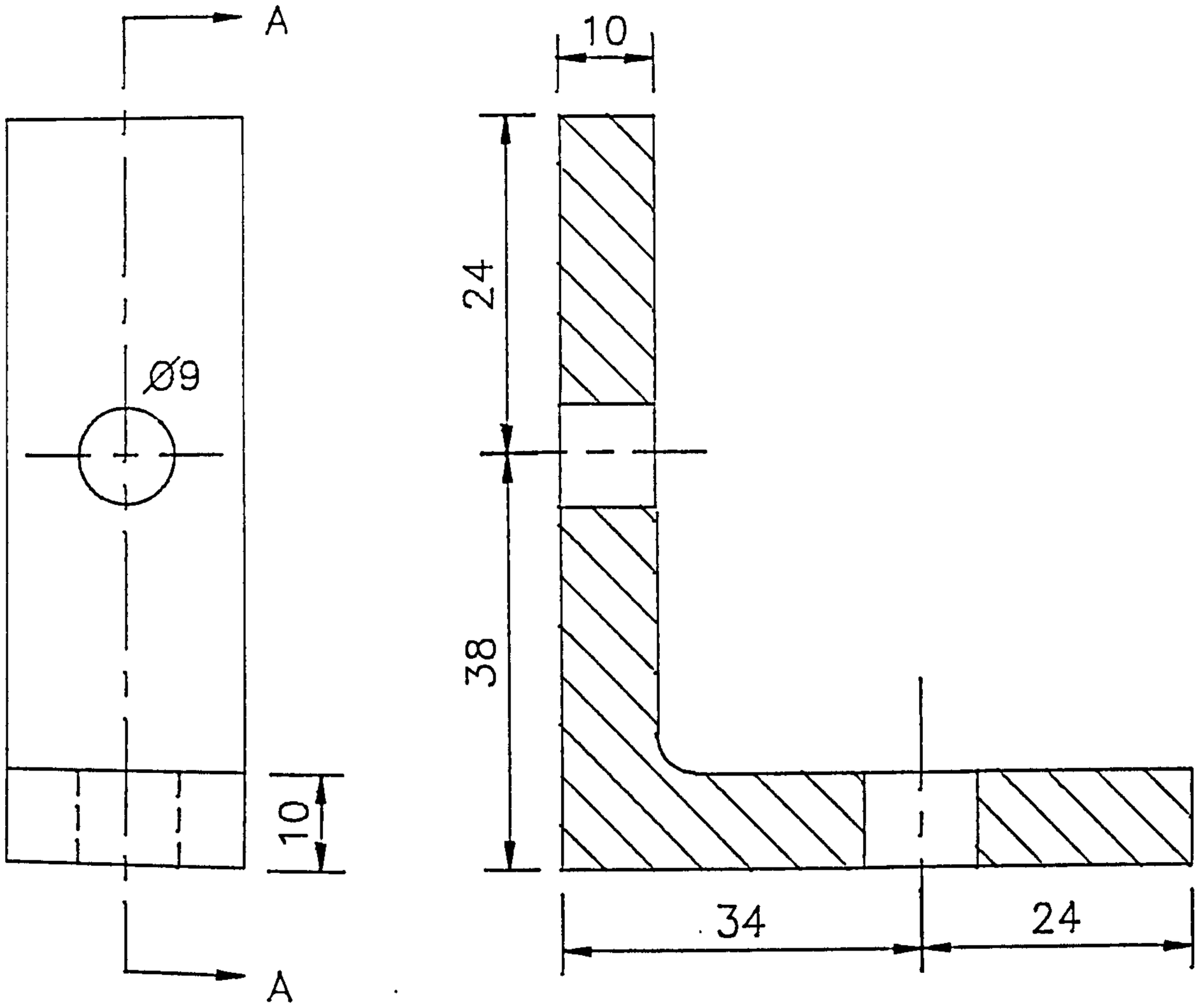

SECTION A–A

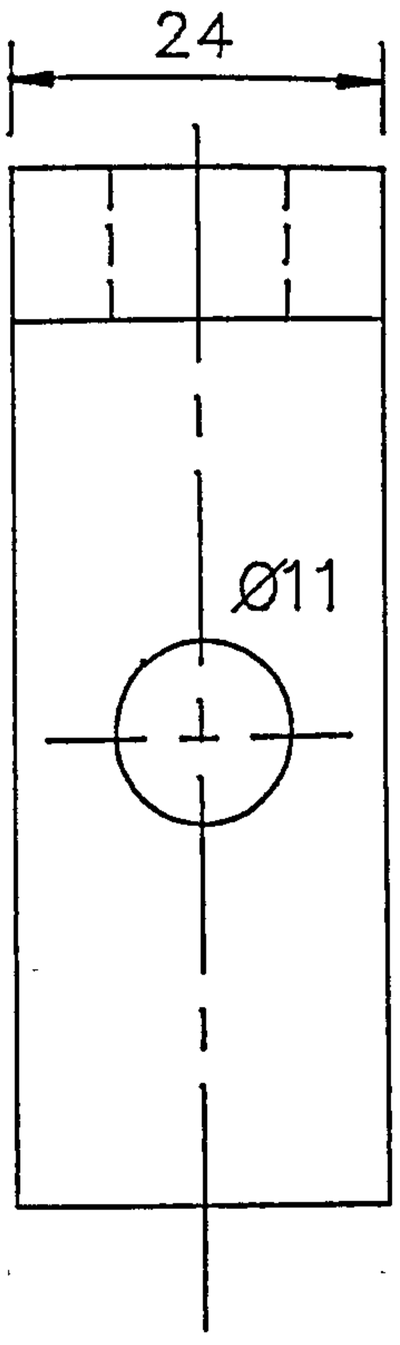

All dimensions in mm

2 OFF

Fig. VI.2

PART NO.2

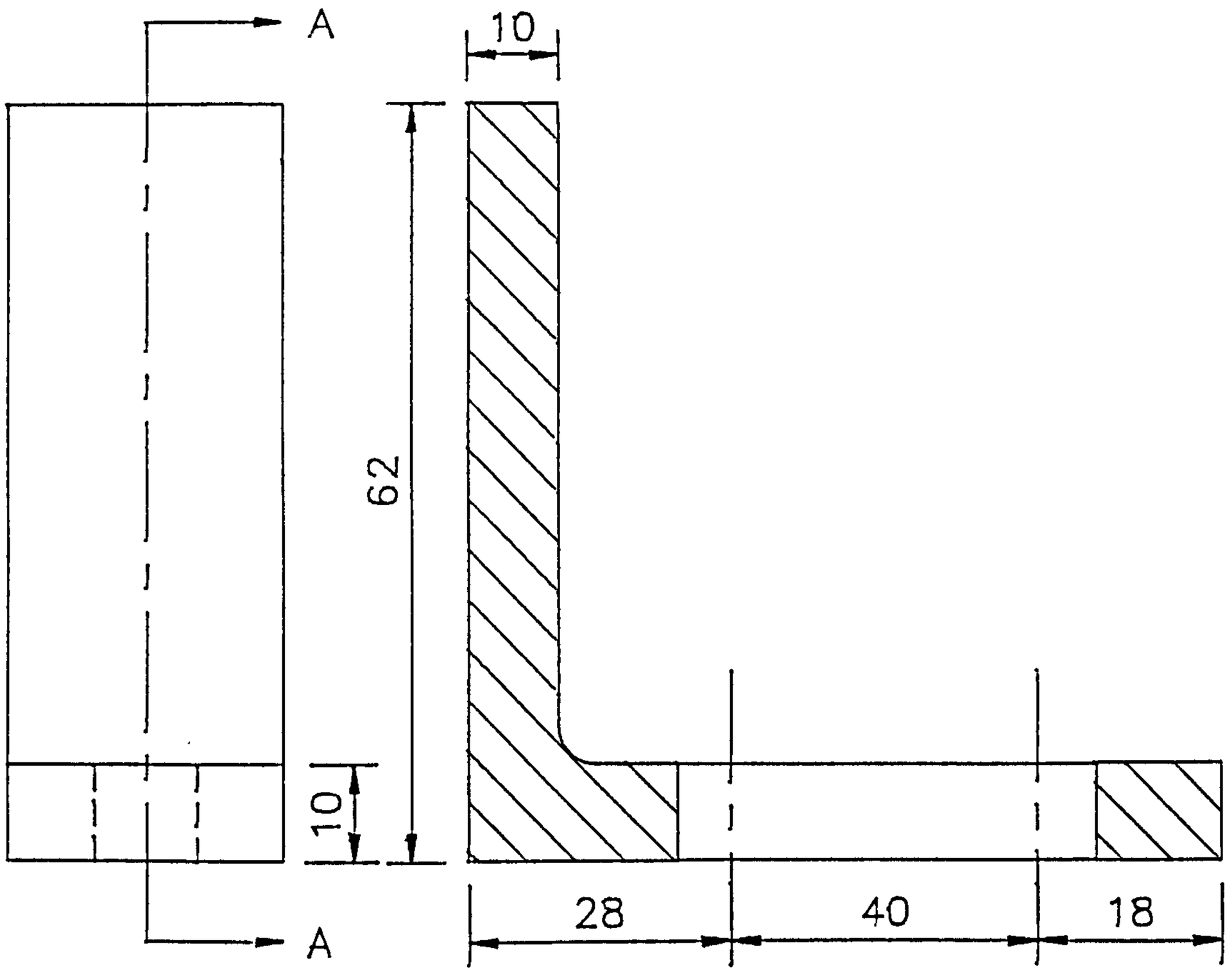

SECTION A–A

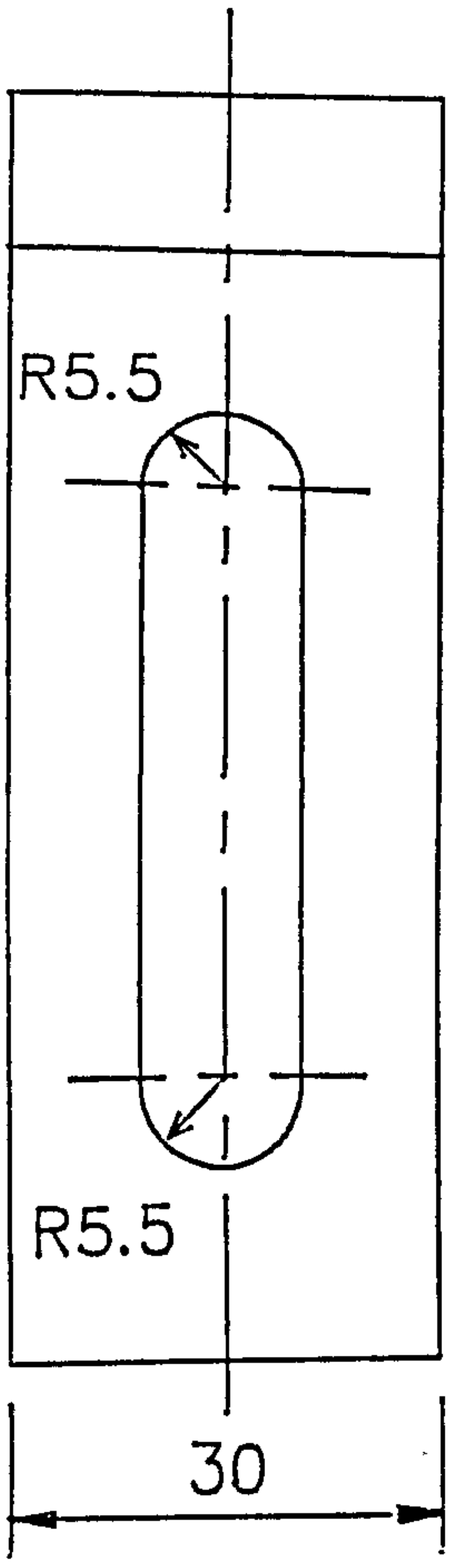

All dimensions in mm

4 OFF

Fig. VI.3

PART NO.3

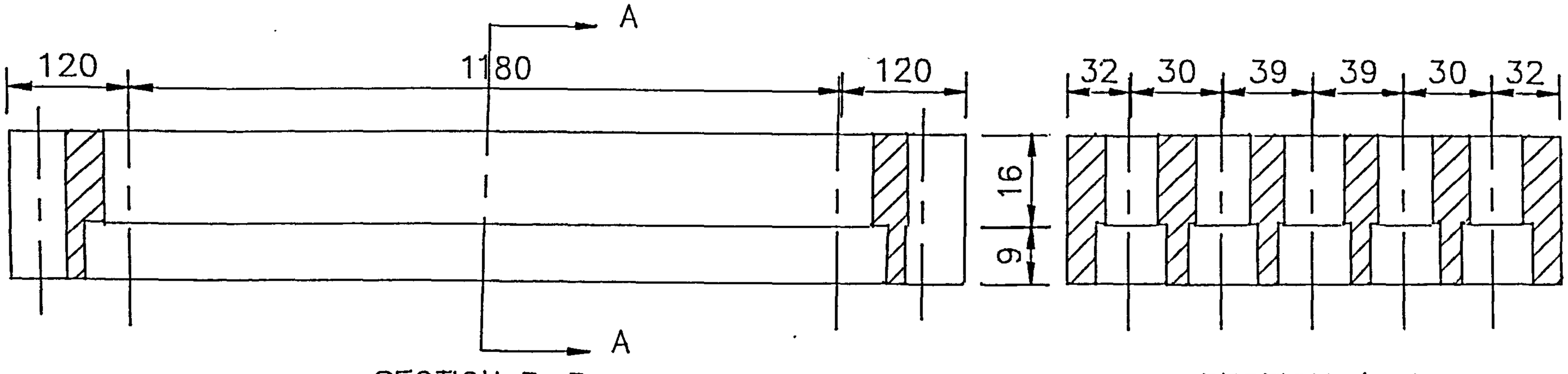

SECTION B–B

SECTION A–A

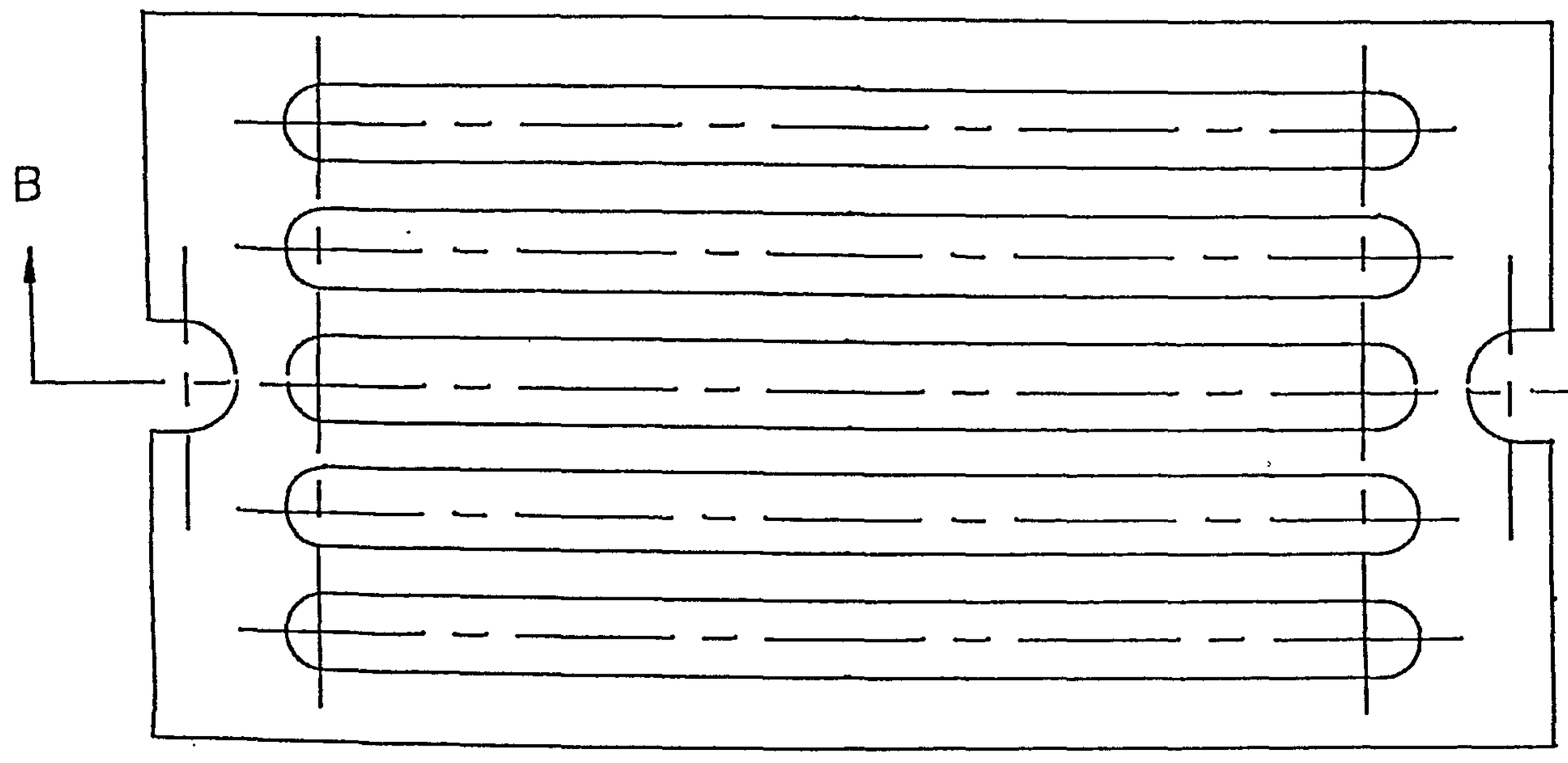

ALL TOP SLOTS WIDTH 11

ALL BOTTOM SLOTS WIDTH 16

ALL DIMENSIONS IN MM

FIG. VI.4 PART NO.4 BASE PLATE